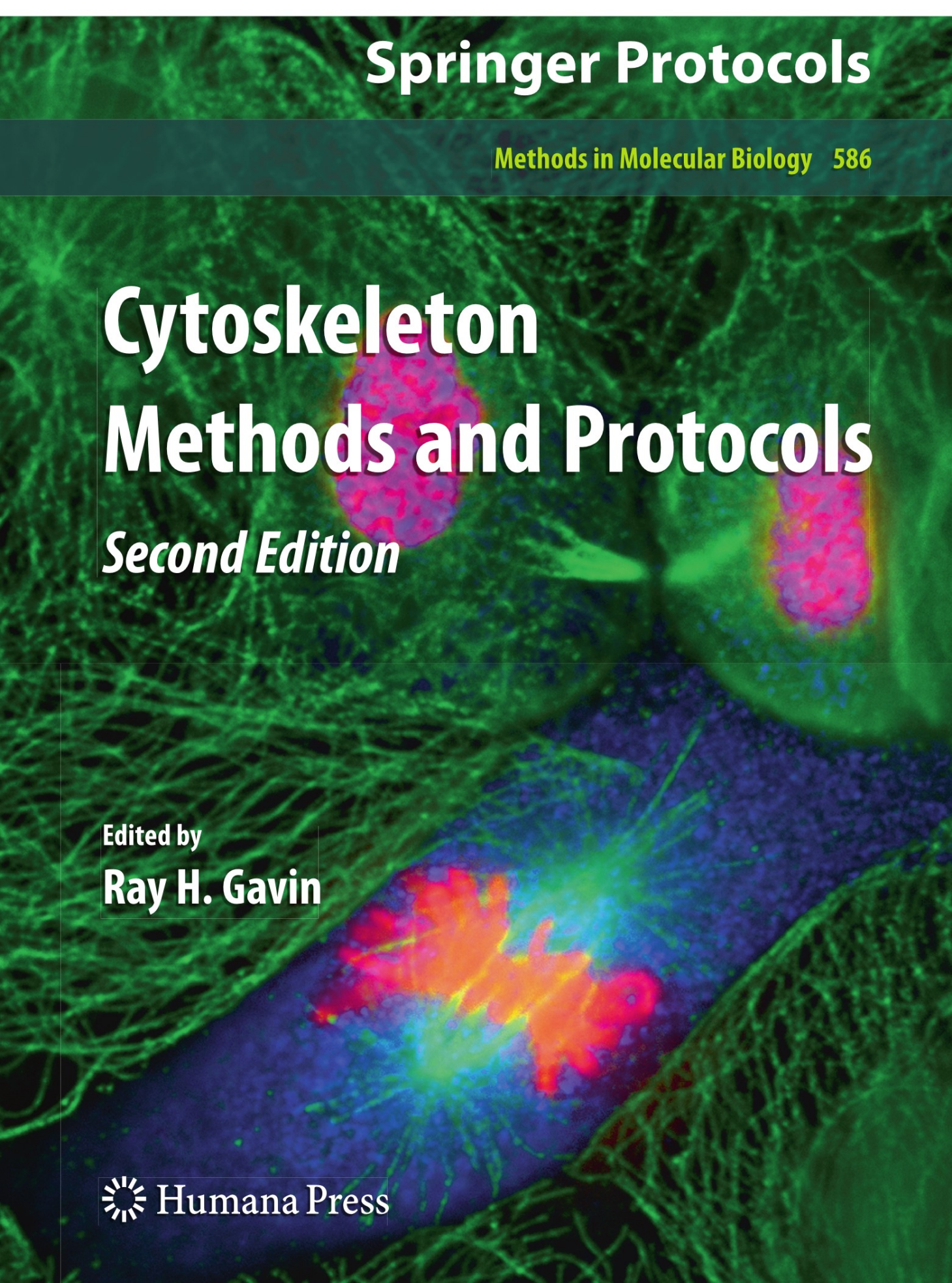
Springer Protocols
Methods in Molecular Biology 586
Cytoskeleton Methods and Protocols
Second Edition
Edited by
Ray H. Gavin
Humana Press

METHODS IN MOLECULAR BIOLOGY™

Series Editor
John M. Walker
School of Life Sciences
University of Hertfordshire
Hatfield, Hertfordshire, AL10 9AB, UK

For other titles published in this series, go to
www.springer.com/series/7651

Cytoskeleton Methods and Protocols

Edited by

Ray H. Gavin

Brooklyn College of The City University of New York, Brooklyn, NY, USA

Humana Press

Editor
R.H. Gavin
Brooklyn College of The City University of New York
Brooklyn, NY
USA
rhgavin@brooklyn.cuny.edu

ISSN 1064-3745 e-ISSN 1940-6029
ISBN 978-1-60761-375-6 e-ISBN 978-1-60761-376-3
DOI 10.1007/978-1-60761-376-3
Springer New York Dordrecht Heidelberg London

Library of Congress Control Number: 2009930645

© Humana Press, a part of Springer Science+Business Media, LLC 2009
All rights reserved. This work may not be translated or copied in whole or in part without the written permission of the publisher (Humana Press, c/o Springer Science+Business Media, LLC, 233 Spring Street, New York, NY 10013, USA), except for brief excerpts in connection with reviews or scholarly analysis. Use in connection with any form of information storage and retrieval, electronic adaptation, computer software, or by similar or dissimilar methodology now known or hereafter developed is forbidden.
The use in this publication of trade names, trademarks, service marks, and similar terms, even if they are not identified as such, is not to be taken as an expression of opinion as to whether or not they are subject to proprietary rights.
While the advice and information in this book are believed to be true and accurate at the date of going to press, neither the authors nor the editors nor the publisher can accept any legal responsibility for any errors or omissions that may be made. The publisher makes no warranty, express or implied, with respect to the material contained herein.

Cover illustration: The cover illustration shows a field of dividing and non-dividing Xenopus tissue culture cells stained for microtubules (green), DNA (red), and a soluble protein that accumulates in nuclei during interphase and distributes throughout the cytoplasm during mitosis (blue). In the mitotic cell near the center of the image, the highly condensed chromosomes are aligned on the mitotic spindle, the elaborate macromolecular machine that is responsible for moving sister chromatids apart during cell division. Prominent in the two cells just below it are the remnants of the mitotic spindle (named the midbody) that persists as the daughter cells finish cytokinesis and enter the next interphase. Microtubules in the non-dividing cells at the periphery of the image are longer and are arranged in a radial pattern around a single centrosome in each cell (not shown; please note that the nuclei of these cells are also not visible in this image). Photo courtesy Christiane Wiese and Adam Steinberg

Printed on acid-free paper

Humana is part of Springer Science+Business Media (www.springer.com)

Preface

In the 10 years since the publication of the first edition of *Cytoskeleton Methods and Protocols*, advances in fluorescent labeling, optics, and sample preparation have significantly improved the imaging capability of microscopy. Techniques for live-cell imaging, advances in software for the analysis of cell and organelle motility, and proteomics for assessing potential interaction of cytoskeleton components contribute to the arsenal of improved tools for cytoskeleton research. We continue to refine our understanding of the cytoskeleton as a dynamic synergy of components.

The second edition of *Cytoskeleton Methods and Protocols* reflects many of the recent technological advances in experimental tools for cytoskeleton research with emphasis on animal, plant, protist, and fungal model systems. New chapters describe methods for live-cell imaging, fluorescence microscopy, electron microscopy, analysis of cell and organelle motility, isolation of cytoskeleton components, and proteomics. Each chapter contains up-to-date protocols organized in a step-by-step format that is useful for established and novice investigators. A notes section provides a troubleshooting guide and often contains unpublished technical information.

I thank John Walker for carefully reviewing initial drafts of manuscripts. More than 50 internationally renowned experts in their fields contributed to *Cytoskeleton Methods and Protocols*, and I thank all of them.

Brooklyn, NY ***Ray H. Gavin***

Contents

Preface v
Contributors ix

PART I LIVE – CELL IMAGING OF THE CYTOSKELETON

1 High Resolution Multimode Light Microscopy of Cell Migration: Long-Term Imaging and Analysis 3
Torsten Wöllert and George M. Langford

2 Imaging the Cytoskeleton in Live *Xenopus laevis* Embryos 23
Sarah Woolner, Ann L. Miller, and William M. Bement

3 Live-Cell Imaging of the Cytoskeleton and Mitochondria–Cytoskeleton Interactions in Budding Yeast 41
Theresa C. Swayne, Thomas G. Lipkin, and Liza A. Pon

PART II DYNAMICS OF ACTIN FILAMENTS AND MICROTUBULES

4 Jasplakinolide: An Actin-Specific Reagent that Promotes Actin Polymerization 71
Andreas Holzinger

5 Analysis of Centrosome Function and Microtubule Dynamics by Time-Lapse Microscopy in Xenopus Egg Extracts. 89
Christiane Wiese, Jonathan R. Mayers, and Alison J. Albee

PART III FLUORESCENCE MICROSCOPY PROTOCOLS FOR INVESTIGATING CYTOSKELETON COMPONENTS

6 Quantitative Fluorescence Microscopy Techniques 117
Alessandro Esposito, Simon Schlachter, Gabriele S. Kaminski Schierle, Alan D. Elder, Alberto Diaspro, Fred S. Wouters, Clemens F. Kaminski, and Asparouh I. Iliev

7 A FRET-Based Approach for Studying Conformational Changes of a Cytoskeleton-Related Tumor Suppressor Molecule. 143
Robert F. Hennigan, Mary F. Chaiken, Lauren A. Foster, and Wallace Ip

8 Sample Preparation for Fluorescence Imaging of the Cytoskeleton in Fixed and Living Plant Roots 157
Julia Dyachok, Cheol-Min Yoo, Karuppaiah Palanichelvam, and Elison B. Blancaflor

9 Imaging of the Cytoskeleton and Mitochondria in Fixed Budding Yeast Cells 171
Theresa C. Swayne, Istvan R. Boldogh, and Liza A. Pon

PART IV ELECTRON MICROSCOPY PROTOCOLS FOR IMAGING THE CYTOSKELETON

10 Imaging Cytoskeleton Components by Electron Microscopy 187
Tatyana Svitkina

11 Purification and Localization of Intraflagellar Transport Particles and Polypeptides 207
Roger D. Sloboda

12 High Pressure Freezing, Electron Microscopy, and Immuno-Electron Microscopy of *Tetrahymena thermophila* Basal Bodies 227
Janet B. Meehl, Thomas H. Giddings, Jr., and Mark Winey

13 Strategies for Imaging Microtubules in Plant Cells 243
Andreas Holzinger, Eiko Kawamura, and Geoffrey O. Wasteneys

PART V ANALYSIS OF CELL AND ORGANELLE MOTILITY

14 A Rapid Tracking Method for the Quantitative Analysis of Organelle Streaming Velocity 265
Carola Luise Holweg

15 Melanosome Motility in Fish Retinal Pigment Epithelial Cells 275
Christina King-Smith

16 Analysis of Properties of Cilia Using *Tetrahymena thermophila* 283
Vidyalakshmi Rajagopalan, Elizabeth O. Corpuz, Mark J. Hubenschmidt, Caroline R. Townsend, David J. Asai, and David E. Wilkes

17 Application of Cell Traction Force Microscopy for Cell Biology Research 301
James H-C. Wang and Bin Li

18 2D and 3D Quantitative Analysis of Cell Motility and Cytoskeletal Dynamics 315
Deborah Wessels, Spencer Kuhl, and David R. Soll

19 Detergent-Extracted Models for the Study of Cilia or Flagella 337
Charles B. Lindemann and Kathleen A. Lesich

PART VI: GENETIC AND PROTEOMICS APPROACHES FOR CYTOSKELETON PROTEIN FUNCTION

20 The Analysis of Intermediate Filament Dynamics Using Transfections and Cell Fusions 357
Jesús M. Paramio

21 Functional Analysis of Actin-Binding Proteins in the Central Nervous System of *Drosophila* 367
Qi He

22 Proteomic Tools for the Analysis of Cytoskeleton Proteins 375
Ewa Wywial, Vishnubhat Nataraj Dongre, and Shaneen M. Singh

Index 389

Contributors

Alison J. Albee • *Department of Biochemistry, University of Wisconsin – Madison, Madison, WI, USA*

David J. Asai • *Grants and Special Programs, Howard Hughes Medical Institute, Chevy Chase, MD, USA*

William M. Bement • *Department of Zoology, University of Wisconsin – Madison, Madison, WI, USA*

Elison B. Blancaflor • *Plant Biology Division, The Samuel Roberts Noble Foundation Inc., Ardmore, OK, USA*

Istvan R. Boldogh • *Department of Pathology and Cell Biology, College of Physicians and Surgeons, Columbia University, New York, NY, USA*

Mary F. Chaiken • *Department of Cancer and Cell Biology, University of Cincinnati, Cincinnati, OH, USA*

Elizabeth O. Corpuz • *Department of Biology, Harvey Mudd College, Claremont, CA, USA*

Alberto Diaspro • *LAMBS-MicroScoBio, Department of Physics, University of Genoa, Genoa, Italy*

Vishnubhat Nataraj Dongre • *Department of Biology, Brooklyn College-CUNY, Brooklyn, NY, USA*

Julia Dyachok • *Plant Biology Division, The Samuel Roberts Noble Foundation Inc., Ardmore, OK, USA*

Alan D. Elder • *Department of Chemical Engineering and Biotechnology, University of Cambridge, Cambridge, UK*

Alessandro Esposito • *Department of Chemical Engineering and Biotechnology, University of Cambridge, Cambridge, UK*

Lauren A. Foster • *Department of Cancer and Cell Biology, University of Cincinnati, Cincinnati, OH, USA*

Thomas H. Giddings, Jr. • *Department of MCD Biology, University of Colorado, Boulder, CO, USA*

Qi He • *Department of Biology, Brooklyn College-CUNY, Brooklyn, NY, USA*

Robert F. Hennigan • *Department of Cancer and Cell Biology, University of Cincinnati, Cincinnati, OH, USA*

Carola Luise Holweg • *Institute of Biology II, Freiburg, Germany*

Andreas Holzinger • *Institute of Botany, Department of Physiology and Cell Physiology, University of Innsbruck, Innsbruck, Austria*

Mark J. Hubenschmidt • *Department of Biology, Harvey Mudd College, Claremont, CA, USA*

Asparouh I. Iliev • *Rudolf Virchow Center & Institute of Pharmacology and Toxicology, University of Würzburg, Würzburg, Germany*

Wallace Ip • *Department of Cancer and Cell Biology, University of Cincinnati, Cincinnati, OH, USA*

Clemens F. Kaminski • *Department of Chemical Engineering and Biotechnology, University of Cambridge, Cambridge, UK*

Gabriele S. Kaminski Schierle • *Department of Chemical Engineering and Biotechnology, University of Cambridge, Cambridge, UK*

Eiko Kawamura • *Department of Biology, University of British Columbia, Vancouver, BC, Canada*

Christina King-Smith • *Department of Biology, Saint Joseph's University, Philadelphia PA, USA*

Spencer Kuhl • *W.M. Keck Dynamic Image Analysis Facility, Department of Biological Sciences, University of Iowa, Iowa City, IA, USA*

George M. Langford • *Department of Biology, Life Sciences Complex, Syracuse University, Syracuse, NY, USA*

Kathleen A. Lesich • *Department of Biological Sciences, Oakland University, Rochester, MI, USA*

Bin Li • *MechanoBiology Laboratory, Departments of Orthopaedic Surgery, Bioengineering, and Mechanical Engineering and Materials Science, University of Pittsburgh, Pittsburgh, PA, USA*

Charles B. Lindemann • *Department of Biological Sciences, Oakland University, Rochester, MI, USA*

Thomas G. Lipkin • *Department of Pathology and Cell Biology, College of Physicians and Surgeons, Columbia University, New York, NY, USA*

Jonathan R. Mayers • *Department of Biochemistry, University of Wisconsin – Madison, Madison, WI, USA*

Janet B. Meehl • *Department of MCD Biology, University of Colorado, Boulder, CO, USA*

Ann L. Miller • *Department of Zoology, University of Wisconsin – Madison, Madison, WI, USA*

Karuppaiah Palanichelvam • *Plant Biology Division, The Samuel Roberts Noble Foundation Inc., Ardmore, OK, USA*

Jesús M. Paramio • *Molecular Oncology Unit, Basic Research Department, Centro de Investigaciones Energéticas, Madrid, Spain*

Liza A. Pon • *Department of Pathology and Cell Biology, College of Physicians and Surgeons, Columbia University, New York, NY, USA*

Vidyalakshmi Rajagopalan • *Department of Biology, Indiana University-South Bend, South Bend, IN, USA*

Simon Schlachter • *Department of Chemical Engineering and Biotechnology, University of Cambridge, Cambridge, UK*

Shaneen M. Singh • *Department of Biology, Brooklyn College-CUNY, Brooklyn, NY, USA*

Roger D. Sloboda • *Department of Biological Sciences, Dartmouth College, Hanover, NH, USA*

David R. Soll • *Keck Dynamic Image Analysis Facility, Department of Biological Sciences, University of Iowa, Iowa City, IA, USA*

Tatyana Svitkina • *Department of Biology, University of Pennsylvania, Philadelphia, PA, USA*

Theresa C. Swayne • *Department of Pathology and Cell Biology, College of Physicians and Surgeons, Columbia University, New York, NY, USA*

Caroline R. Townsend • *Department of Biology, Harvey Mudd College, Claremont, CA, USA*

James H.-C. Wang • *MechanoBiology Laboratory, Departments of Orthopaedic Surgery, Bioengineering, and Mechanical Engineering and Materials Science, University of Pittsburgh, Pittsburgh, PA, USA*

Geoffrey O. Wasteneys • *Department of Biology, University of British Columbia, Vancouver, BC, Canada*

Deborah Wessels • *Keck Dynamic Image Analysis Facility, Department of Biological Sciences, University of Iowa, Iowa City, IA, USA*

Christiane Wiese • *Department of Biochemistry, University of Wisconsin – Madison, Madison, WI, USA*

David E. Wilkes • *Department of Biology, Indiana University-South Bend, South Bend, IN, USA*

Mark Winey • *Department of MCD Biology, University of Colorado, Boulder, CO, USA*

Torsten Wöllert • *Department of Biology, Life Sciences Complex, Syracuse University, Syracuse, NY, USA*

Sarah Woolner • *Faculty of Life Sciences, University of Manchester, Manchester, UK*

Fred S. Wouters • *Laboratory for Molecular and Cellular Systems, Department of Neuro- and Sensory Physiology, University Medicine Göttingen, Göttingen, Germany*

Ewa Wywial • *Department of Biology, Brooklyn College-CUNY, Brooklyn, NY, USA*

Cheol-Min Yoo • *Plant Biology Division, The Samuel Roberts Noble Foundation Inc., Ardmore, OK, USA*

Part I

Live – Cell Imaging of the Cytoskeleton

Chapter 1

High Resolution Multimode Light Microscopy of Cell Migration: Long-Term Imaging and Analysis

Torsten Wöllert and George M. Langford

Summary

Cell migration is a multi-step process that involves sequential changes in the cytoskeleton, cell–substrate adhesion and components of the extracellular matrix. In multicellular organisms, directional cell migration is important for normal development, wound healing and immune responses and contributes to disease states such as tumor formation and metastasis. Many cells such as fibroblasts migrate as individuals while others, such as keratinocytes, move as groups or sheets of cells.

In this chapter, we use human oral keratinocytes (OKF6/TERT-2) to illustrate the complex patterns of cell migration and its regulation. In culture, sheets of keratinocytes migrate and respond to human pathogens such as *Candida albicans*. The dynamic changes of the cytoskeleton, cell-cell and cell-substrate interactions that change during an infection for example require observation over long periods of time in order to identify the spatio-temporal coordinated regulation of the cytoskeleton and its associated components as well as the signaling pathways that control them.

Microscopic techniques for long-term live cell observation and analysis of cell migration require high-resolution imaging systems that maintain perfect focus and optimal growth conditions (temperature, CO_2) for cells. We describe two multimode digital imaging systems (VEC-DIC and BioStation IM), both with wide-field epifluorescence and transmitted light objectives for long-term time-lapse imaging and motion analysis.

Key words: Keratinocytes, Cell migration, Live cell imaging, Time-lapse, DIC, Phase contrast, Motion analysis

1. Introduction

1.1. Cell Migration

Cell migration is a directed and fundamental process that contributes to multiple biological and pathological processes of most organisms. It is essential for the embryogenesis, inflammatory response, tissue repair, and wound healing. If cell migration is

R.H. Gavin (ed.), *Cytoskeleton Methods and Protocols,* Methods in Molecular Biology, vol. 586
DOI 10.1007/978-1-60761-376-3_1
© Humana Press, a part of Springer Science + Business Media, LLC 2009

not properly controlled during these processes, serious congenital defects and diseases, including tumor cell metastasis, multiple sclerosis, and brain defects may result *(1)*.

Cell migration is a four-step cyclical process that spatially and temporally coordinates forces in the cytoskeleton with extracellular adhesion *(2)*. The dynamic reorganization of the actin cytoskeleton provides the driving force that directs the protrusion at the front and retraction at the rear of the cell. The process of cell migration begins with the polarization of the cell and the extension of protrusions in the direction of migration. The second phase of the process involves attachment of the newly formed protrusions to the extracellular matrix by focal adhesions. The third step involves contractile forces between F-actin and myosin2 that generate strong traction on adhesion sites in the front and weaker adhesions that disassemble at the cell rear, and finally the cell body moves forward *(3, 4)*. Many different molecules serve as external signals that polarize the cell and initiate and promote cell migration. These molecules and their receptors must transmit the extracellular signals across the cell membrane and convert those signals into cellular responses *(5, 6)*. The local activation of specific Rho GTPases contributes to the different phases of migration through multiple effector pathways that stimulate actin polymerization and dynamics at the leading edge *(7)*.

Cell migration can be viewed and characterized by different light microscopic techniques including bright-field imaging in either phase contrast or differential interference contrast (DIC), fluorescence spinning disk, and laser scanning confocal microscopy. Bright-field microscopy is commonly used in combination with fluorescence microscopy in the presence of vital dyes or fluorescent fusion proteins to visualize living cells and cellular components, and therefore, dynamic processes can be observed and analyzed quantitatively as they occur. Furthermore, light microscopy allows the observation of fixed cells and tissues using antibodies to stain specific components and provides detailed information about internal structures and organization of cells *(8, 9)*.

When selecting an appropriate microscopy system for live cell imaging, four things should be considered: *(1)* sensitivity of detection, *(2)* speed of image acquisition, *(3)* minimizing cell damage, and *(4)* optimizing viability of the specimen. As the actual movement of cells over a surface tends to be random and very slow – usually a few μm/min – a system for long-term time-lapse imaging must be used to investigate the cell behavior over long periods of time. In this chapter, we describe the use of two multimode digital imaging systems using wide-field epifluorescence and transmitted light optics with video and cooled CCD cameras for live cell imaging of human oral keratinocytes (OKF6/TERT-2) *(10)* and motion analysis during cell migration.

1.2. Microscope Systems for Time-Lapse Imaging

1.2.1. VEC-DIC Imaging System

The basic components of a high-resolution video-enhanced-contrast differential interference contrast (VEC-DIC) and epifluorescence light microscopy system are shown in **Fig. 1a**. The high-resolution video camera is probably the most significant part of the microscope hardware. The C2400 (video tube cameras) or C8000 (video rate CCD cameras) series are special lines of cameras capturing phase contrast or DIC images of highly dynamic processes, like cell migration and intracellular vesicle transport. We use a Hamamatsu C2400–07 Newvicon tube camera to acquire high contrast VEC-DIC images at a framing rate of 30 frames/s at full resolution and low noise. The camera controller provides analog contrast enhancement and shading correction of the captured image. Further image processing such as background subtraction and digital contrast enhancement is performed with the Argus-20 (Hamamatsu) real time image processor that allows real-time observation of high-resolution images without loss of original camera resolution. Finally, the captured images are displayed on a standard black/white monitor and images are stored in real time on S-VHS videotapes or directly on the computer *(11–14)*.

Images of fluorescent specimens observed by conventional epifluorescence microscopy are captured with a charge-coupled device (CCD) camera such as the Hamamatsu C4742–98–24NR (ORCAII) **(Fig. 1)**. This scientific-grade dual scan camera provides a low-light level detection with high signal-to-noise ratio and high resolution (1,280 × 1,024 pixels), and a wide dynamic range. This camera is cooled to –50 °C to reduce heat and hence image noise. Using this cooled CCD camera, multi-color images can be generated from specimens stained with multiple fluorescent dyes. Image processing and analysis software is required to control the microscope peripherals (the digital cooled CCD camera or video camera) and to perform 2D or 3D deconvolution, object tracking and motion analysis (*see* **Subheading 1.4**).

1.2.2. BioStation IM Imaging System

The BioStation IM combines a cell incubation and imaging system into one compact unit. Its software controls temperature, humidity and CO_2 gas concentration of the culture chamber and time-lapse image acquisition using phase contrast and two channel epifluorescence optics **(Fig. 1b)**. The BioStation uses red LED light for phase contrast imaging and is equipped with a 2.0 megapixel monochrome cooled CCD camera for quick image acquisition to reduce specimen photobleaching. All optical and mechanical components for phase contrast and epifluorescence imaging are motorized which allows the user to change magnification and multichannel or multipoint (multiple cell locations) settings during a time-lapse experiment. Finally, the BioStation minimizes focus drift using specific hardware components (e.g., motorized objective lens) and complete environmental control

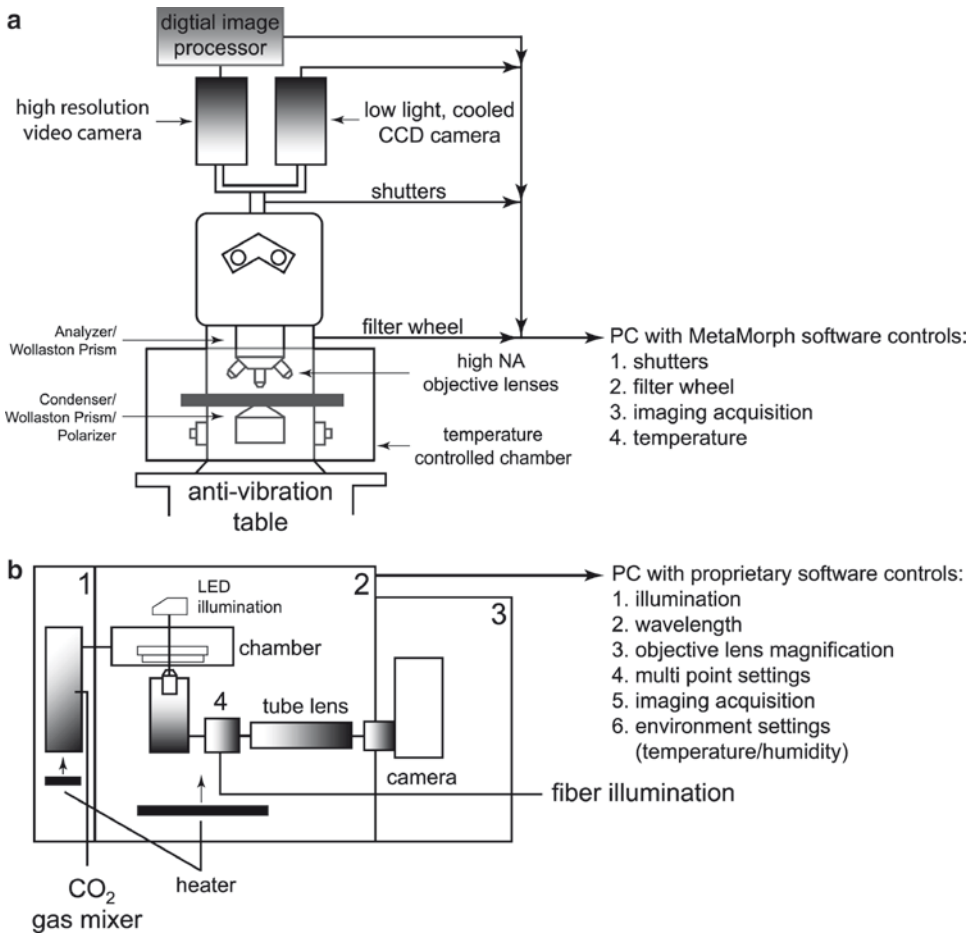

Fig. 1. Schematic diagrams of two multi-mode digital imaging systems for live cell observation. (**a**) Multi-mode high-resolution light microscope system for epifluorescence and video microscopy with differential interference contrast (DIC) optics. A light microscope (e.g., Zeiss Axioplan2) on a vibration isolation table is equipped with a low-light cooled CCD camera (e.g., Hamamatsu ORCAII), a high-resolution video camera with a framing rate of 30 frames/s (e.g., Hamamatsu Newvicon tube camera) and a digital image processor (e.g., Hamamatsu Argus-20 real-time image processor) for contrast enhancement (e.g., image averaging, background subtraction and contrast enhancement). The DIC optics include polarizer, beam splitter (Wollaston prism), condenser (1.4 NA), beam combiner (Wollaston prism) and analyzer that are located above the 1.4 NA objectives. (**b**) Basic design of a long-term time-lapse imaging system from Nikon. The BioStation IM consists of three major compartments, (1) the humidifier for the CO_2 mixer, (2) the microscope compartment, and (3) a camera compartment that contains a high-sensitivity 2.0 megapixel monochrome cooled CCD camera. The microscope compartment contains a red LED illumination light source for phase contrast imaging, the 40× objective, up to two mountable fluorescence filter sets (4), and the tube lens. Phase contrast and fluorescence imaging modes are motorized at the BioStation IM.

including temperature, CO_2 and humidity. Because the BioStation IM has been optimized only to minimize focus drift, the best solution for long-term live cell imaging would be an imaging system that prevents focus drift completely as described below.

1.3. Precise Control of the Focal Plane

Long-term time-lapse observations require that the focal plane of interest remain in focus for the period of observation. Software programs available as part of imaging software packages have been generated to maintain and correct the focus on a point of interest within a specimen. Over the last 2 years, a number of manufacturers (e.g., Nikon, Zeiss, Olympus and Applied Scientific Instrumentation Inc.) have introduced hardware-based solutions to prevent focus drift during long-term live cell imaging. Hardware-based auto-focus continuously readjusts the focus caused by thermal drift during temperature changes around the microscope or mechanical instability due to stage movement. Other causes of focus drift that result in a loss of focus on the target/specimen include changes in the properties of culture medium over time, the addition of reagents or drugs to the medium and vibration due to air handling systems or foot traffic *(15)*.

The *Perfect Focus System* (PFS) was created by Nikon to maintain automatically the focus at the coverslip/culture vessel surface or to the point of interest within a specimen independent of environmental changes **(Fig. 2a)**. LED light in the infrared range (770 nm) that is emitted through the objective lens of a microscope and an internal linear CCD detector are used for real time focus correction. A Telan or tube lens is placed within the body tube between the object and the oculars, which permits the introduction of a beam splitter to the imaging path and allows the introduction of an additional light source. An offset lens, which is part of the "Optical Offset feature" (Nikon), allows one to correct the focus at any focal plane of interest within the specimen. The PFS supports a variety of different microscopy methods including bright-field imaging (fluorescence, DIC, phase contrast) and TIRF multi-fluorescence imaging.

The *Definite Focus* (DF) from Zeiss was specially designed for fluorescence applications and time-lapse experiments **(Fig. 2b)**. The DF also uses infrared light of an LED with a wavelength of 835 nm that is coupled directly to the nosepiece carrier, which directs the light into the beam path of the microscope. The supplied hardware comprises a sensor module on the nosepiece carrier, a beam combiner below the nosepiece, and a DF controller. To measure the distance between the objective lens and the specimen, a grid is projected onto the bottom of the culture vessel, and a slanted camera chip analyzes the reflection of the grid projection until it is well focused. The DF corrects the relative position of the projected grid to the camera chip during focus drift. Furthermore, the DF can be used as "focus finder" when changing the culture vessel and it supports all applications for long-term live cell imaging such as all contrasting techniques, TIRF, laser scanning or multiphoton microscopy.

Olympus has introduced the Zero thermal drift compensation (ZDC) to help prevent focus drift **(Fig. 2c)**. Focus drift

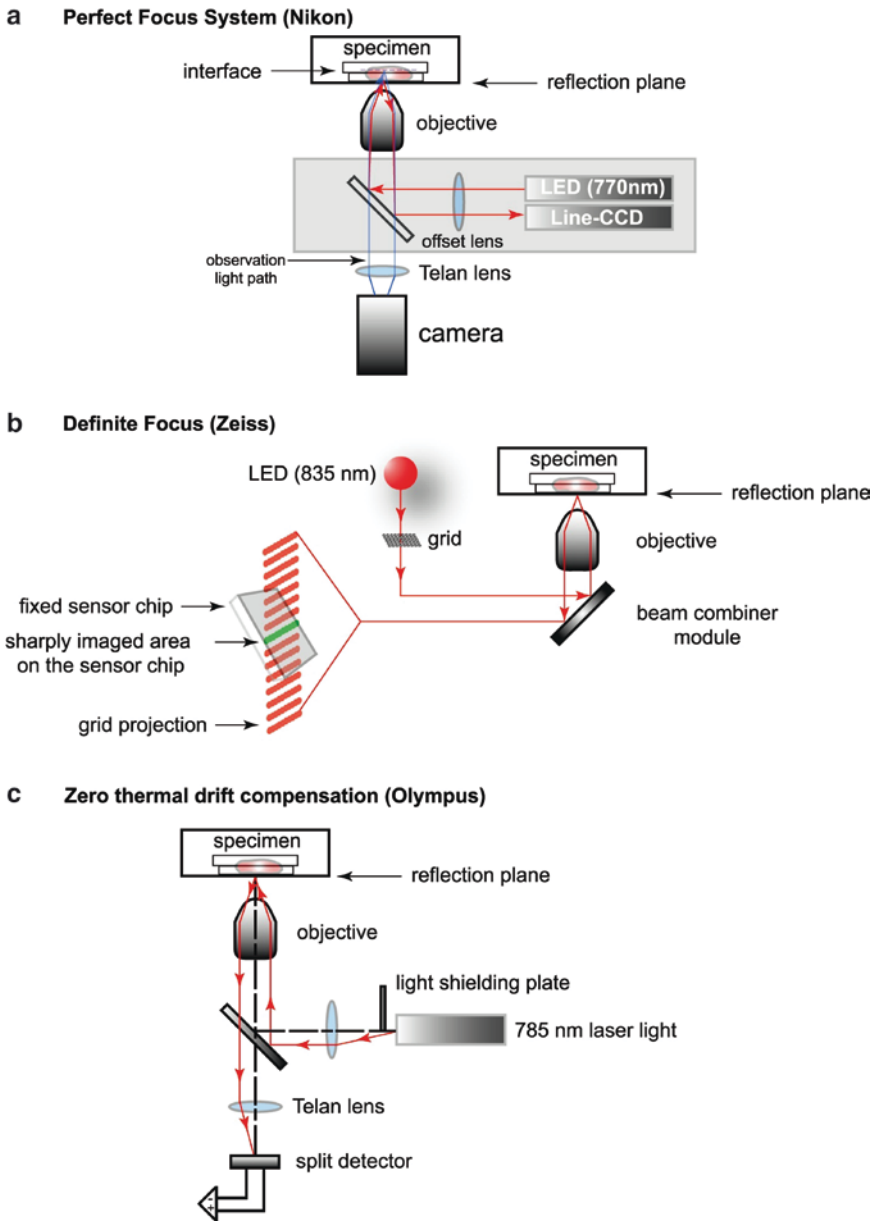

Fig. 2. Details of the light path and configuration of optical components designed to prevent focus drift during long-term time-lapse imaging. Schematic drawings of the perfect focus system (PFS) created by Nikon (**a**), the Definite Focus from Zeiss (**b**), and the Zero Thermal Drift Compensation (ZDC) system developed by Olympus (**c**). LED (Nikon and Zeiss) or laser light (Olympus) in the infrared range is used to perform focus drift compensation and single images are taken in reference to the bottom surface of the cell culture dish or coverslip. The focus is automatically corrected before image acquisition during time-lapse imaging. Note that the laser light for the ZDC (Olympus) uses a light path separate from the light path for imaging.

compensation is also performed automatically in reference to a reflection plane e.g., the bottom surface of a culture vessel or coverslip. Instead of infrared LED light to measure the distance between objective and surface, Olympus uses a near infrared laser line (785 nm) which is introduced into its own light path. This allows the other light paths to be used for imaging the specimen.

A similar set up to measure the focus position is available from Applied Scientific Instrumentation (ASI) Inc. (Eugene, OR). The *Continuous reflective-interface feedback focus* (CRIFF) system that was designed for time-lapse imaging at high magnification is like the Olympus ZDC system but uses infrared laser light of 780 nm. The actual focus position is detected by a sensor that uses the signal from reflected laser light for the Z-axis control of the microscope. This application is very useful for (total internal reflection fluorescence) TIRF microscopy using high NA oil immersion objective lenses (1.45 NA or higher). In addition, ASI provides a video auto-focus system that controls the microscope focus when using an analog video camera. For this, a "focus value" for each frame is detected from an electronic circuit that uses the information from the analog video signals as a reference point to initiate auto-focus.

1.4. Software-Based Motion Analysis

Motion analysis software used to quantify cell migration includes a large number of parameters such as velocity, straightness of path, length of excursion, pauses, etc. Various PC-based software packages are available for motion analysis, e.g., MetaMorph (Molecular Devices, Downingtown, PA), NIS elements (Nikon Instruments Inc., Melville, NY), Volocity (Improvision Inc., Waltham, MA), CellTrak (MotionAnalysis Corp., Santa Rosa, CA), BD IPLab imaging (BD Biosciences, Rockville, MD), and ImageJ (National Institutes of Health). Motion analysis software can produce quantitative data based on time series analysis of any movement including cell organelles, single cells and cell sheets, microorganisms and chemotaxis. To obtain information about the type of motion at given points of a cell, timelines of the regions can be displayed as kymographs *(16)* that represent a time-space plot and provide detailed information about the dynamics within a user-defined region of interest. A short overview of the most common PC-based imaging software is given below.

MetaMorph is probably one of the most established image acquisition and analysis software that is used to analyze the movement of objects such as distance, average and instantaneous velocities over time using the kymograph function. This creates a cross-sectional view of the intensity values of a user-defined line region through the planes in a stack. MetaMorph also provides automated and semi-automated particle tracking of individual tagged particles, such as fluorescently labeled cellular structures,

e.g., surface molecules, microtubules, nuclei, or lipids. One or more selected objects can be tracked through each image in a stack or sequential series of images and measurements of the paths, positions, and velocities of these objects can be obtained. Furthermore, MetaMorph provides modules for intensity measurements of fluorescent samples, for the calculation of cell numbers by counting the nuclei, information about the cell cycle status using a DNA stain, colocalization tools to measure overlapping regions of two fluorescent probes, and a cell viability module to classify the ratio of live/dead cells after staining procedures. Finally, 2D and 3D deconvolution and different binning modes can be applied to reduce background noises and to increase the signal intensities specifically for fluorescent specimen.

IPLab is an image acquisition, processing, measurement, and analysis software for both operating systems, Windows and Macintosh OS. IPLab directly supports the acquisition of images and time-lapse series with the ability to automate imaging routines by using the scripting tool. IPLab supports the measurement of individual objects, regions of interest, and entire images. This imaging software also includes densitometry measurements and generates plots and histograms that can be user defined. The resulting data can exported for further analysis in a spreadsheet program such as Excel (Microsoft Corp.).

NIS elements imaging and analysis software is a platform, which provides control over the microscope, cameras and additional devices, including third-party shutter, illumination sources and controller for Z directional movements. The NIS elements software package facilitates live cell and time-lapse image capturing, 3D deconvolution or 2D real-time deconvolution, object measurements and automatic or manual tracking of moving objects, particle analysis and counting options, archiving and data analysis.

The features of *CellTrak* include a rapid and quantitative tracking of the motion of single cells that were captured using standard microscopy imaging modes. CellTrak uses AVI files as data sources and does the tracking, editing of the paths with a mathematical termination (ASCII files), which can be exported into Excel or other software. Time series calculations and manipulations can be also performed on the path data. CellTrak does extract measurements of single or multiple moving objects, which include velocity, orientations, linear acceleration, and grayscale information.

ImageJ software package is an image processing and analysis application written in Java. This public domain software is free with open software architecture for plugins, which makes it an attractive platform for many users. Image J supports standard image processing functions (e.g., contrast manipulation, sharpening and edge detection), and it can measure distances and

angles. Additional features are area calculations, pixel value statistics, the creation of density histograms, and line profile plots of user-defined selections.

2. Materials

2.1. Cell Culture

1. Human oral keratinocytes (OKF6/TERT-2) (Harvard Skin Disease Research Center & BWH/Partners) (*see* **Note 1**).
2. Keratinocyte serum free medium (K-SFM) (Invitrogen, Carlsbad, CA) supplemented with bovine pituitary extract (BPE) and 0.2 ng/mL epidermal growth factor (EGF). BPE and EGF are supplied with K-SFM.
3. Calcium chloride ($CaCl_2$) is dissolved at 1 M in molecular grade water (cellgro, Mediatech, Inc., Herndon, VA) and filter sterilized before storage at 4 C.
4. Sterile phosphate buffered saline (PBS) (1×) from cellgro.
5. Solution of trypsin (0.05%) and ethylenediamine tetraacetic acid (EDTA) from Gibco (Invitrogen, Carlsbad, CA).

2.2. Transient Cell Transfection

1. Optifect transfection reagent (Invitrogen) (*see* **Note 2**).
2. Opti-MEM reduced serum medium supplemented with Hepes, 2.4 g/L sodium bicarbonate and L-glutamine (Gibco).
3. pAcGFP1-actin vector (Clontech Laboratories Inc., Mountain View, CA).
4. 24-well plate (Beckton Dickinson Labware, Franklin Lakes, NJ).

2.3. Live Cell Imaging using VEC-DIC

1. Microscope slides (75 × 25 mm) from Corning Inc. (Corning, NY), and coverslips (11 × 11 mm) from Fisher Scientific (Pittsburgh, PA).
2. VALAP (a 1:1:1 heated mixture of Vaseline, lanolin, and paraffin), all reagents are obtained from Sigma-Aldrich (St. Louis, MO).
3. Scotch double-stick tape (3 M, St. Paul, MN).
4. Cotton swabs.
5. Zeiss Axioplan2 microscope equipped with differential interference optics (DIC) and a 40×/1.0 NA Plan Apo objective (Carl Zeiss Inc, Thornwood, NY).
6. C2400–07 Newvicon tube camera from Hamamatsu (Hamamatsu Photonics, Bridgewater, NJ) and an Orca-2 C4742–98 dual scan cooled CCD camera (Hamamatsu).
7. 100 W halogen lamp for transmitted light for DIC applications and a X-Cite120 light source for epifluorescence microscopy (EXFO America, Addison, TX).

8. SVO-9500 MD high quality super VHS (S-VHS) VCR cassette recorder (Sony Electronics Inc.).
9. Late model PC computer with the fastest processor and most random access memory (RAM).
10. MetaMorph image acquisition and analysis software (Molecular Devices, Downingtown, PA).

2.4. Long-Term Time-Lapse Live Cell Imaging Using BioStation IM

1. 35 mm glass bottom dishes (MatTek, Ashland, MA).
2. BioStation IM for glass bottom dishes (Nikon Instruments Inc., Melville, NY) equipped with a 2.0-megapixel cooled CCD camera and a 40×/0.8 NA Plan Flour objective.
3. 130 W Mercury precentered fiber illuminator (Nikon Instruments Inc.).
4. CO_2 gas mixer (MIGM) from Tokken Inc. (Kashiwa, Japan).
5. Latest model PC computer with the fast processor and most random access memory (RAM).

2.5. Data Analysis

1. MetaMorph image acquisition and analysis software (Molecular Devices).

3. Methods

3.1. Cell Culture and Transfection of OKF6/TERT-2 Cells with pAcGFP1-actin

1. The oral mucosal cell line, OKF6/TERT-2 keratinocytes are maintained in keratinocyte serum free medium (K-SFM) at 37 °C in a 5% CO_2 in air, atmosphere. Before microscopic observation, cells are grown in 10 cm plastic cell culture dishes and are fed every other day with 10 mL of K-SFM.
2. OKF6/TERT-2 keratinocytes are passaged when they reached ~30% confluence (~7–9 × 10^5 cells) with trypsin/EDTA. The K-SFM is removed from the cell culture dish and cells are washed with 10 mL PBS. 2 mL trypsin/EDTA solution is added to the cells followed by a 2–10 min incubation at 37 °C until the cells are detached from the dish. 8 mL of K-SFM is added to the cells, which are then transferred to a 15 mL centrifugation tube followed by centrifugation at 75 g for 5 min in a clinical centrifuge. A 1:3 split (~1 × 10^5 cells) of the OKF6/TERT-2 cells will provide experimental cell cultures that will reach ~30% confluence after 2 days.
3. For transient transfections using the pAcGFP1-actin vector, cells are plated on either 12 mm sterile glass coverslips that are placed in 10 cm dishes or 35 mm glass bottom dishes 1 day before transfection. Before using, the coverslips are sterilized with an autoclave and then placed in the 10 cm cell culture dish.

4. The following protocol used to transfect human oral keratinocytes was optimized in our laboratory.
5. Coverslips are removed from the 10 cm cell culture dish and placed into single wells of a 24-well plate that contain 500 µL K-SFM. Importantly, the cells should be grown in K-SFM without antibiotics 1 day before transfection to prevent cell death.
6. To prepare the DNA-Optifect complexes, 2 µL (~0.8 mg) of pAcGFP1-actin DNA is added to 48 µL of Opti-MEM and the solution should be mixed gently. 2 µL of Optifect transfection reagent is diluted with 48 mL Opti-MEM gently mixed and incubated for 5 min at room temperature. The diluted pAcGFP1-actin DNA and diluted Optifect solution are combined and incubated for 20 min at room temperature.
7. The DNA–Optifect complexes (100 µL total volume) are added while rocking the plate to the well that contains the cells and 500 µL K-SFM, which is replaced after 4 h of incubation. The cells are incubated for a period of 24 h at 37 C prior to live cell imaging.
8. When using 35 mm glass bottom dishes for live cell imaging with the BioStation IM, a total volume of 2 mL plating medium and 500 mL of DNA–Optifect complexes are used.

3.2. Live Cell Imaging

3.2.1. VEC-DIC and Epifluorescence Microscopy

1. OKF6/TERT-2 cells are passaged and transfected as described above (*see* **Subheading 3.1**).
2. The microscope chamber is prepared by placing two strips of double-stick tape along each of the two long edges of a glass slide. This will create the space where the cells grown and the coverslip will be placed. The length of the tape strips should be equivalent to the length of the coverslips.
3. The coverslip is removed from the 24-well plate, washed with 500 µl K-SFM, and then placed onto the microscope chamber. The microscope chamber is filled with 10–20 µL of K-SFM to maintain the cells. The edges of the microscope chamber are dried with filter paper, and a cotton swab is used to seal the chamber completely with melted VALAP. Do not introduce bubbles during this step.
4. Cells are imaged over periods of 10 min at room temperature (25–30°C). Cell motility and cellular edge activity are determined by VEC-DIC and epifluorescence microscopy (*see* **Note 3**). Microscope control and image acquisition are done with the MetaMorph imaging software.
5. Prior to epifluorescent illumination, DIC microscopy is used to locate the focal plane and to focus the specimen to prevent photobleaching of the fluorescent specimen. First, a droplet of immersion oil is placed on the bottom and the top

of the microscope chamber. When the cells are in focus, Köhler illumination (the field diaphragm is focused by adjusting the height of the condenser) is performed to provide even illumination over the specimen field. The specimen is projected on the monitor by switching the light from the ocular to the video camera with the beam splitter. The light intensity of the microscope is then adjusted with the rheostat to saturate the video camera. To obtain the best image contrast and brightness, the gain and the offset level of the camera are manipulated with the camera controller. Finally the digital image processor Argus-20 is used for contrast enhancement and an out of focus background subtraction to remove electronic noise and background mottle (*see* **Notes 4–7**). Single DIC images are taken with the MetaMorph imaging software **(Fig. 3b, b′)** or recorded in real-time directly on videotape.

6. Epifluorescence microscopy is used to detect positive transfected cells and to monitor actin-dependent dynamics during cell migration. The field diaphragm is adjusted to illuminate the area of interest only, and light is then switched from the ocular to the CCD camera with the beam splitter.
7. Finally the camera conditions are optimized with the MetaMorph imaging software. To achieve accurate image acquisition, the exposure time should be optimized. If the exposure time is too long, the camera will be over saturated, the specimen is photo damaged or bleed through from another wavelength can occur. A too short exposure time will lower the signal-to-noise ratio. The ratio between the brightest specimen pixel value and the least bright background pixel value should be ~3:1. To obtain the pixel values, a single image is acquired in the auto expose mode and the mouse pointer is moved over the brightest specimen area and over the background. The pixel values are displayed on the status bar at the bottom of the screen. The signal intensity and the image acquisition speed of the camera can be increased with binning. This method combines the signal from multiple pixels, which results in shorter exposure times, an increased pixel size and a decreased camera resolution.
8. Single images and time-lapse series are taken with the MetaMorph imaging software. To acquire time-lapse series for actin-dependent movement, single images should be taken every 10–30 s. An example of individual images taken from a time-lapse movie obtained with epifluorescence microscopy are shown in **Fig.3a**.

3.2.2. Long-Term Time-Lapse Phase Contrast Microscopy

1. Cells are grown and transfected in a 35 mm glass bottom dish as described above (*see* **Subheading 3.1**).

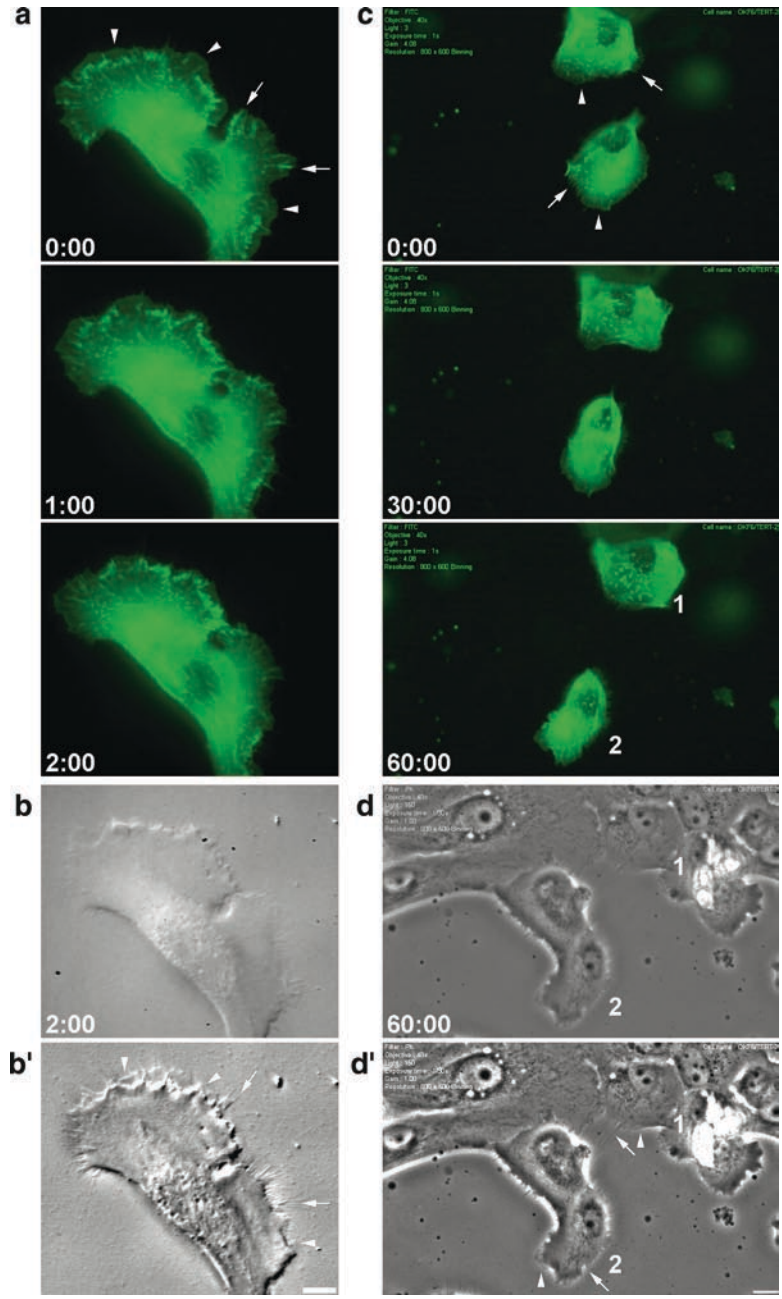

Fig. 3. Micrographs of migrating human oral keratinocytes (OKF6/TERT-2) observed with epifluorescence (**a**) and high-resolution VEC-DIC microscopy (**b,b′**) or epifluorescence (**c**) and phase contrast microscopy (**d,d′**). OKF6/TERT-2 cells were transiently transfected with pAcGFP1–actin, grown for 24 h and processed for live cell imaging. Filopodia (*arrows*) and lamellipodia (*arrow heads*) are the predominant actin-containing structures at the cellular edge at each time interval. (**a**) Single frames from a fluorescence time-lapse movie (0–2 min) and corresponding DIC image before (**b**) and after digital contrast enhancement with the Argus 20 (**b′**). Images were obtained with a Zeiss Axioplan2 microscope using a 40× oil-immersion objective as described in **Subheading 2.3**. (**c**) Single frames from a fluorescence time-lapse movie (0–60 min) and corresponding phase contrast image before (**d**) and after digital contrast enhancement using the MetaMorph imaging software (**d′**). The time-lapse movie was obtained with the BioStation IM from Nikon using a 40× objective lens. Time in min is given at the lower left corner. Bars represent 20 µm.

2. The 35 mm glass bottom dish is placed into the microscope chamber. Wait until the water and chamber temperature have been stabilized at the selected temperature (usually 37°C) to prevent focus drift (*see* **Notes 8–10**).
3. Phase contrast and fluorescence imaging modes are motorized at the BioStation IM, which allows one to change the microscopy settings e.g., the magnification (20×, 40× or 80× via tube lens) during a time-lapse experiment.
4. Two observation modes are available, the live observation mode and the time-lapse observation mode. The Live image screen displays the actual image that is captured with either phase contrast or epifluorescence microscopy. During this mode the region of interest is changeable in the X, Y and Z position using the imaging software or an ergo controller. The Time-lapse image screen provides information about the time-lapse settings e.g., magnification, image acquisition, and regions of interest.
5. The imaging software also possesses a focus and auto-enhancement (AE) mode to optimize imaging acquisition. After the specimen is in focus, the focus mode will recognize this position and keep the specimen in focus during time-lapse imaging. The AE mode allows one to determine the correct exposure time for both phase contrast and epifluorescence illumination before image acquisition.

3.2.3. Motion Analysis

1. Our laboratory uses the MetaMorph imaging and analysis software with outstanding success, and we describe it here as an example of what can be achieved (*see* **Subheading 1.4**).
2. First the pixel-to-distance conversion factor is calibrated using a reference image (e.g., a calibrated stage micrometer) that has been acquired with the objective lens for image acquisition. The Calibrate Distance dialog box from the Measure menu is used to set up and change the calibration settings.
3. The brightness and contrast of the time-lapse image series is adjusted to increase the appearance of structures of interest by changing the grayscale or color level.
4. To analyze the movement (e.g., paths, positions and velocities of points) of migrating cells from time-lapse series, the tracking region of objects is defined by individual particles (e.g., nucleoli inside the nucleus) or fluorescently labeled structures (e.g., microtubules, mitochondria, nuclei acids), and tracking parameters are configured with the dialog box **(Fig. 4a)**. High contrast DIC images that contain "white and black spots" work best because they allow a precise tracking through the images of a time-lapse series. The tracked movements of objects are displayed as separate paths **(Fig. 4c)** and data are exported into Excel for further analysis.

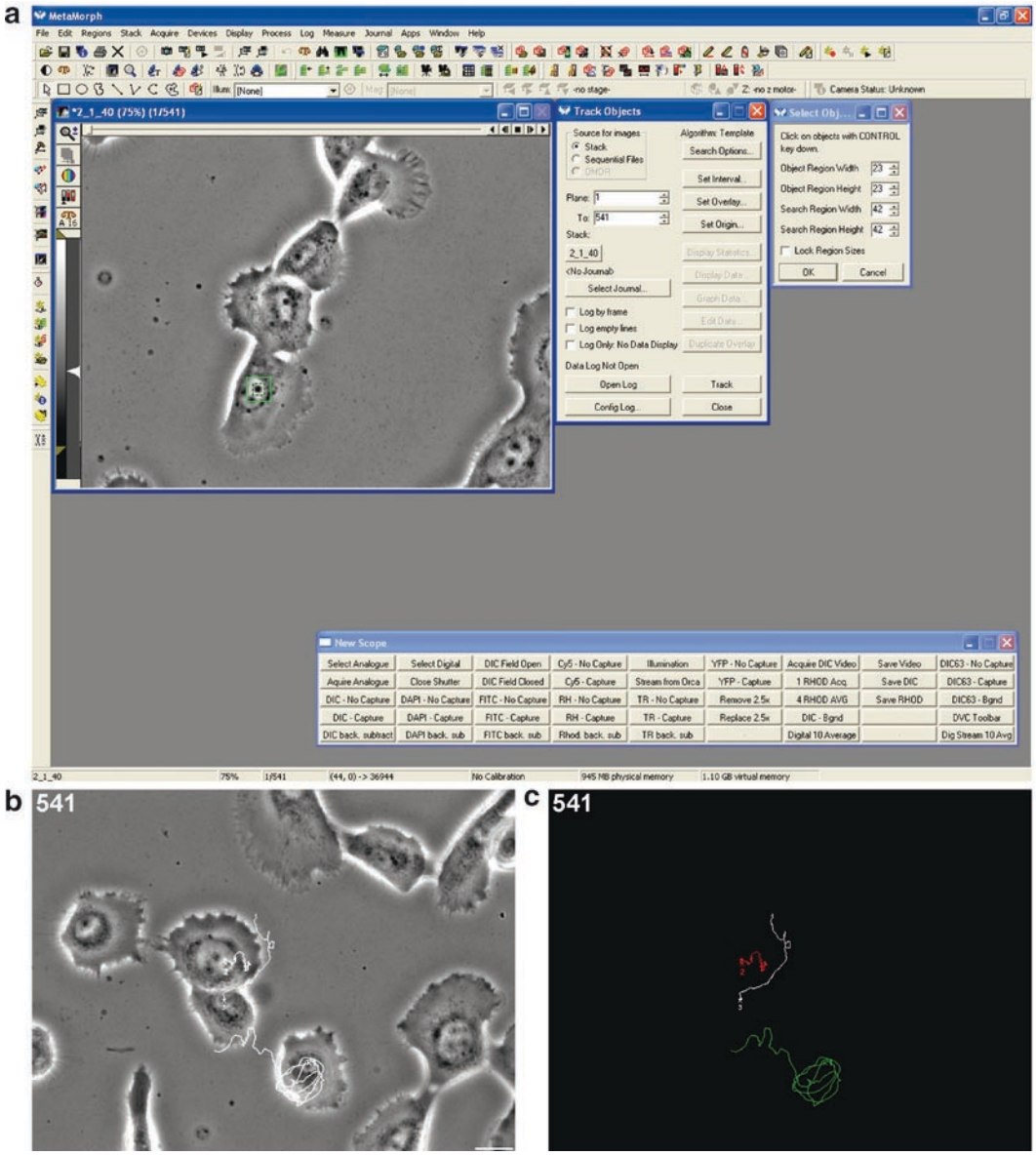

Fig. 4. Motion analysis of cell migration of human oral keratinocytes. Screen shot of the MetaMorph imaging software during an online measurement of migrating OKF6/TERT-2 cells. (**a**) The track object function enables the user to follow the movement of particles within cells and single cells using MetaMorph. An object that has been selected can be tracked through each image in a stack or time series. (**b**) Last frame of time-lapse movie, from a phase contrast time-lapse series (0–180 min) obtained with the BioStation IM (Nikon) using a 40× objective lens. (**c**) Tracks of three individual migrating cells for duration of 3 h as shown in (**b**). The number indicates the end of the track. Bar represents 20 μm.

5. The protrusion velocity of the leading edge is determined by kymographic analysis from time-lapse series of images. To create a kymograph with the MetaMorph software, a line is placed at the margins of individual cells along the direction of movement on the first image of the time-lapse series using the

point-to-point line drawing **(Fig. 5a)**. This will create pixel intensity values along the user-defined line region for each image of a time-lapse series. These values are combined in a single image that displays distances (horizontal direction) versus time (single images in the time series vertical direction) **(Fig. 5a)**.

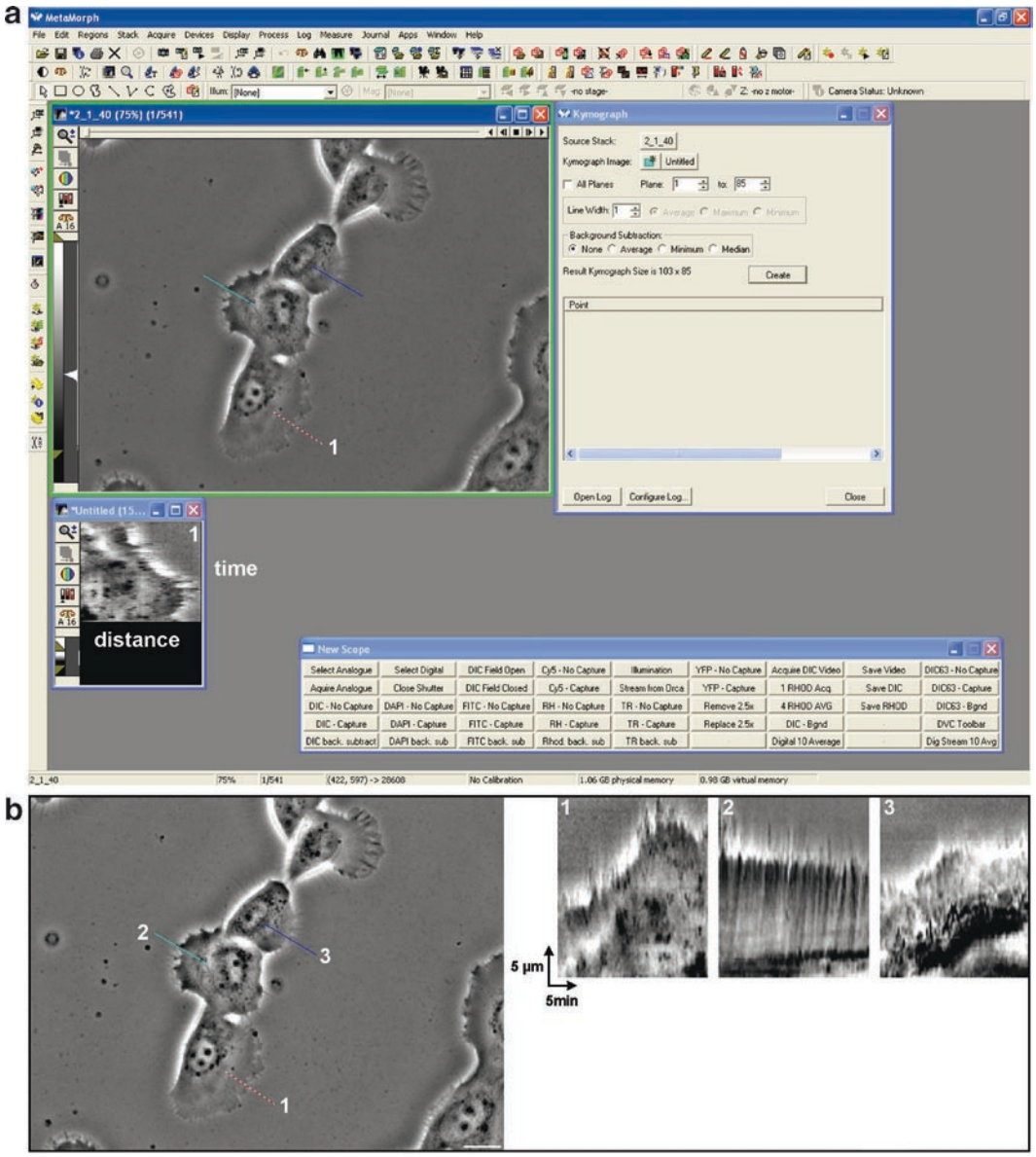

Fig. 5. Motion analysis of migrating human oral keratinocytes. (**a**) Screen shot of the MetaMorph analysis software during an online measurement of migrating OKF6/TERT-2 cells obtained with the BioStation IM (Nikon) using a 40× objective lens. The kymograph (time-distance plot) function enables the user to measure linear movement as a function of time and velocity (insert). (**b**) Single frame (*left*) from the screen shot above of a phase contrast time-lapse series (0–180 min) and corresponding kymographs (*right*) from three single cells shown in (**b**). Lines show location used to create kymographs. Kymographs of leading edges that were created to analyze the cellular edge behavior and cell migration velocity demonstrated that the non-contacted edges of these cells exhibit protrusive and retractive activity. Bar represents 20 µm.

4. Notes

1. Human oral keratinocytes (OKF6/TERT-2) can be obtained only from the Harvard Skin Disease Research Center & BWH/Partners.
2. The Optifect transfection reagent should be used for optimal transfection of cells that are plated at low densities (30–70% confluence).
3. Successful video microscopy requires knowledge and experience in high-resolution VEC-DIC microscopy, whereas the BioStation IM allows users with minimal microscopy experience to conduct live cell imaging.
4. DIC images have a much better resolution compared to phase contrast images, but an analyzer has to be placed in the light path for DIC microscopy which reduces the amount of light transmitted to the camera using sensitive fluorescence methods. Therefore, the analyzer should be removed from the light path.
5. A more detailed protocol can be found in *Methods in Molecular Biology* Volume 161 (Langford, Video-enhanced microscopy for analysis of cytoskeleton structure and function. pp. 31–43).
6. Different types of immersion oil should not be combined and containers should be kept closed when not in use.
7. When using different chemical fluorophores, the addition of Oxyrase EC (Oxyrase Inc.) to the medium can reduce photobleaching by removal of dissolved oxygen. The amount of Oxyrase that is been added has to be determined for each cell type.
8. The microscopy chamber of the BioStation can be easily detached and autoclaved to prevent cell contamination, which makes this system suitable for multiple users imaging different specimen.
9. The BioStation IM is limited to one 35 mm plastic or glass bottom dish and the price does not include the mercury illuminator for epifluorescence observation and a CO_2 gas mixer. Additional software is required (if no other data analysis software is available in the laboratory) for specific analyses, e.g., cell counting, morphological measurements, motion analysis and intensity analysis, has to be purchased separately.
10. The temperature control management ranges from 32°C to 39°C only, which limits the number of users and applications.

11. The BioStation IM facilitates a broad array of long-term time-lapse experiments, including studies of cell growth, morphology, and protein expression. Further applications are studies of cell migration, cell division or cell death, drug screening, and gene knock downs, and cellular processes including cellular signaling. These observations can be easily done with multi color imaging of single or multiple cells.
12. The BioStation CT ("the big brother") from Nikon consists of a standard sized tissue culture incubator that provides a macro and micro observation system for a total of 30 different culture vessel types (e.g., 24-well plate, culture flasks, 60 mm and 10 cm culture dishes). Phase contrast and optional epifluorescence imaging with 3 colors LED illumination are available for image acquisition.
13. A similar observation system for long-term time-lapse imaging is now available from Olympus called the "Incubator fluorescence microscope" LCV110U. This microscopy system allows one to do parallel time-lapse imaging of up to eight cell culture dishes and to produce high-contrast DIC images of multiple regions of interest. Image processing and image analysis software is included to perform intensity measurements, morphology analysis, and image deconvolution.
14. Nikon has modified the PFS and now uses LED light with a wavelength of 870 nm, which allows one to use near-infrared fluorescence dyes such as Cy5.5.

References

1. Webb, D.J., Parsons, T.J., and Horwitz, A.F. (2002) Adhesion assembly, disassembly and turnover in migrating cells – over and over and over again. *Nat Cell Biol* **4**, E-97–100
2. Lauffenburger, D.A. and Horwitz, A.F. (1996) Cell migration: a physically integrated molecular process. *Cell* **84**, 359–369
3. Vicente-Manzanares, M., Webb, D.J., and Horwitz, A.R. (2005) Cell migration at a glance. *J Cell Sci* **118**, 4917–4919
4. Ridley, A.J., Schwartz, M.A., Burridge, K., Firtel, R.A., Ginsberg, M.H., Borisy, G, Parsons, J.T., and Horwitz, A.R. (2003) Cell migration: integrating signals from front to back. *Science* **302**, 1704–1709
5. Etienne-Manneville, S. (2008) Polarity proteins in migration and invasion. *Oncogene* **27**, 6970–6980
6. Jaffe, A.B. and Hall, A. (2004) Rho GTPases: biochemistry and biology. *Annu Rev Cell Dev Biol* **21**, 247–269
7. Nobes, C.D. and Hall, A. (1999) Rho GTPases control polarity, protrusion, and adhesion during cell movement. *J Cell Biol* **144**, 1235–1244
8. Stephens, D.J. and Allan, V.A. (2003) Light microscopy techniques for live cell imaging. *Science* **300**, 82–86
9. Dormann, D. and Weijer, C.J. (2006) Imaging of cell migration. *EMBO J* **25**, 3480–3493
10. Dickson, M.A., Hahn, W.C., Ino, Y., Ronfard, V., Wu, J.Y., Weinberg, R.A., Louis, D.N., Li, F.P., and Rheinwald, J.G. (2000) Human keratinocytes that express hTERT and also bypass a p16 (INK4a)-enforced mechanism that limits life span become immortal yet retain normal growth and differentiation characteristics. *Mol Cell Biol* **20**, 1436–1447
11. Allen, R.D., Allen, N.S., and Travis, J.L. (1981) Video-enhanced contrast differential interference contrast (AVEC-DIC) microscopy: a new method capable of analyzing microtubule-related motility in the reticulopodial network of *Allogromia laticollaris*. *Cell Motil Cytoskeleton* **1**, 291–302

12. Langford, G.M. (2001) Video-enhanced microscopy for analysis of cytoskeleton structure and function. *Methods Mol Biol* **161**, 31–43
13. Weiss, D.G., Maile, W., Wick, R.A., and Steffen, W. (1999) Video microscopy. In: Electronic Light Microscopy in Biology – A Practical Approach (ed. A.J. Lacey), pp. 221–278, *IRL Press*: Oxford
14. Salmon, E.D. and Tran, P.T. (1998) High-resolution video-enhanced differential interference contrast (VE-DIC) light microscopy. *Methods Cell Biol* **56**, 153–184
15. Lachia, E. (2006) Keeping life in focus new systems prevent Z-axis drift in time lapse studies. *Micros Today* **14**, 42–46
16. Hinz, B., Alt, W., Johnen, C., Herzog, V., and Kaiser, H.W. (1999) Quantifying lamella dynamics of cultured cells by SACED, a new computer-assisted motion analysis. *Exp Cell Res* **251**, 234–243

Chapter 2

Imaging the Cytoskeleton in Live *Xenopus laevis* Embryos

Sarah Woolner, Ann L. Miller, and William M. Bement

Summary

Historically, much of our understanding of actin filaments, microtubules and intermediate filaments has come from the study of fixed cells and tissues. But the cytoskeleton is inherently dynamic, and so developing the means to image it in living cells has proved crucial. Advances in confocal microscopy and fluorescent protein technologies have allowed us to dynamically image the cytoskeleton at high resolution and so learn much more about its cellular functions. However, most of this work has been performed in cultured cells, and a critical next step is to understand how the cytoskeleton functions in the context of an intact organism. We, and others, have developed methods to image the cytoskeleton in living vertebrate embryos. Here, we describe an approach to image the cytoskeleton in embryos of the frog, *Xenopus laevis*, using mRNA to express fluorescently tagged cytoskeletal probes and confocal microscopy to visualize their dynamic behavior.

Key words: Live imaging, Embryos, *Xenopus laevis*, Microtubules, Actin

1. Introduction

The eukaryotic cytoskeleton has been intensively studied for over a century and yet much of our knowledge of actin filaments, microtubules, and intermediate filaments and their subcellular distribution has come from the imaging of fixed samples. However, the cytoskeleton is inherently dynamic, and so the ability to image it in living cells is vital to developing a complete understanding of its functions and mechanics. In the last 15 years, advances in live confocal imaging and, in particular, the development of fluorescent protein tags, such as eGFP, mRFP and mCherry *(1–6)*, have permitted major leaps forward in the study of the cytoskeleton. The majority of this work has been performed in cultured cells,

R.H. Gavin (ed.), *Cytoskeleton Methods and Protocols,* Methods in Molecular Biology, vol. 586
DOI 10.1007/978-1-60761-376-3_2,
© Humana Press, a part of Springer Science + Business Media, LLC 2009

which has proved to be a very powerful system for investigating the dynamics of the eukaryotic cytoskeleton. However, to build on these findings, the next step is to understand how a cell's cytoskeleton functions within the context of an intact, living organism. To date, this has been tackled predominantly by using invertebrate rather than vertebrate embryos. However, we, and others, have had larger success imaging cytoskeletal dynamics in living vertebrate embryos *(7–10)* (*see* **Fig. 1**). In this review, we highlight approaches to image the cytoskeleton in living embryos of the frog, *Xenopus laevis*.

Xenopus laevis embryos are an ideal system for these studies as they are large and therefore relatively easy to microinject and manipulate. Furthermore, since these embryos develop externally and at room temperature, they are highly amenable to live imaging. The one disadvantage of *Xenopus laevis* embryos for live imaging is their opacity, which makes imaging of deep

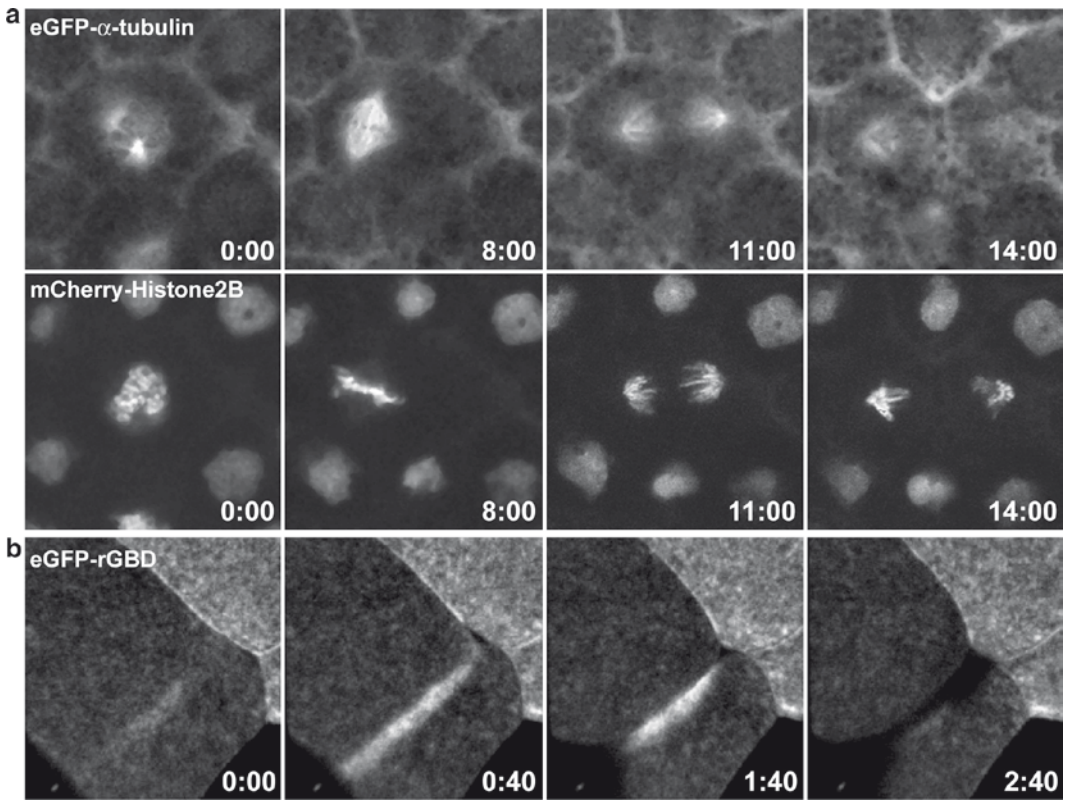

Fig. 1. Live imaging of cytoskeletal probes in *Xenopus laevis* embryos. (**a**). A mitotic spindle imaged in an early *Xenopus laevis* embryo using eGFP-α-tubulin (*top*) to highlight microtubules and mCherry-Histone2B (*bottom*) to show chromosomes. (**b**). The activation of Rho GTPase at the site of the cytokinetic furrow is shown using eGFP-rGBD, a probe that binds specifically to active Rho. In both examples, stills were taken from timelapse movies and timestamps represent time in minutes and seconds. *See* **Note 1** for more a more detailed description of these and other cytoskeletal probes.

tissues more challenging; we, therefore, concentrate on the most superficial cells of the early embryo, where the cytoskeleton can be readily imaged using live confocal microscopy.

Traditionally, imaging of actin filaments or microtubules in cultured cells was accomplished by microinjection of actin or tubulin protein labeled with small fluorescent molecules *(11)*. More recently, the development of fusion constructs comprised of fluorescent proteins (e.g., eGFP or mCherry) fused to actin or tubulin has permitted generation of stable cell lines expressing these proteins by transfection with the relevant DNA *(12)*. However, we have found that injection of fluorescent actin or tubulin protein into embryos can be less than satisfactory, for two reasons. First, the small volumes required (5 nL or less) means that extremely high protein concentrations are required. This, in turn, leads to clogging of the microinjection needle. Second, even if clogging is avoided, it is often difficult to obtain sufficient protein for adequate labeling in these very large cells. Conversely, microinjection of plasmid DNA encoding either fluorescent tubulin or fluorescent actin, which overcomes these problems, has its own attendant difficulties. First, it takes some time before appreciable levels of the probe accumulate, in part because transcription is very limited before the midblastula transition. Second, expression from microinjected plasmids tends to be highly mosaic, with some cells expressing robustly and others not at all. We, therefore, recommend that probes for cytoskeleton proteins be expressed by microinjection of capped RNA into *Xenopus* embryos. The mRNA is less viscous than the protein but, unlike DNA, expresses rapidly and relatively uniformly.

2. Materials

2.1. In Vitro Transcription of Capped RNA for Cytoskeletal Probes

1. Plasmid DNA (containing cytoskeletal probe construct).
2. Restriction enzyme for linearizing plasmid DNA.
3. 20% SDS (RNase-free).
4. 20 mg/mL Proteinase K (Ambion).
5. Phenol-chloroform-isoamyl alcohol mixture (25:24:1; pH 7.9).
6. 5 M Ammonium Acetate (NH_4OAc).
7. Ethanol (100 and 70%).
8. mMESSAGE mMACHINE® capped RNA transcription kit (Ambion).
9. Nuclease-free water (Ambion).
10. RNAse*Zap*® (Ambion).
11. Chloroform.

12. Phenol (pH 6.6).
13. Isopropanol.
14. Pipettors wiped down with RNase Zap and nuclease-free pipette tips.
15. 1.5 mL eppendorf tubes (nuclease-free).
16. Microcentrifuges (at room temperature and 4°C).
17. Gel electrophoresis apparatus.
18. Spectrophotometer.
19. Water bath that can be set to 37°C or 50°C.
20. –80°C freezer.
21. Speed Vac (optional).

2.2. Xenopus laevis Ovulation and In Vitro Fertilization

1. Human chorionic gonadotrophin (HCG, MP Biomedicals), 1unit/μL in dH_2O, filter sterilized and stored at –80°C.
2. Benzocaine (Ethyl 4-aminobenzoate; Sigma-Aldrich), make 10% solution in 95% ethanol and store at 4°C.
3. Marc's Modified Ringer's solution (MMR). For 1×: 100 mM NaCl, 2 mM KCl, 2 mM $CaCl_2$, 1 mM $MgCl_2$, 5 mM HEPES, pH7.4. Make a 10× solution and dilute to make 1× and 0.1× MMR.
4. Testes prep media: for 5 mL: 4 mL 1× MMR, 1 mL Foetal Bovine Serum (heat inactivated), 250 μg Gentamicin, 250 Units Penicillin, 250 μg Streptomycin.
5. L-Cysteine (Sigma-Aldrich): 2% solution in 1× MMR, pH 7.8, made fresh on day of fertilization.
6. Small tank with lid for anesthetizing frog in benzocaine.
7. Forceps and surgical scissors.
8. Small Petri dishes: 35 mm diameter.
9. Deep Petri dishes: 60 mm (diameter) × 20 mm (depth).
10. 50 mL falcon tubes.
11. 3 mL transfer pipettes.
12. 1 mL sterile syringes.
13. 27 G 1/2 sterile needles.
14. Cooled incubator (set at 17°C).

2.3. Microinjection of Xenopus laevis Embryos

1. Capped RNA (*see* **Subheading 3.1**).
2. Nuclease-free water (Ambion).
3. 0.1× MMR (*see* **Subheading 2.2**).
4. Injection buffer: 5% Ficoll in 0.1× MMR, rotate overnight to dissolve.
5. RNase*Zap*® (Ambion).
6. Mineral oil (Sigma-Aldrich).

7. 10 µL Drummond glass capillaries (Fisher Scientific).
8. Micropipette puller.
9. Dissecting microscope.
10. Microinjector, micromanipulator and N_2 gas tank.
11. Micrometer.
12. Sharp forceps.
13. Pipettors wiped down with RNase Zap and nuclease-free pipette tips.
14. Parafilm.
15. Injection dish: 35 mm diameter Petri dish, Spectra Mesh macroporous filter (Spectrum Labs) cut to fit in bottom of Petri dish, use modeling clay to hold the mesh in place on floor of Petri dish.
16. 35 mm diameter Petri dishes. `
17. 3 mL transfer pipettes.

2.4. Mounting *Xenopus laevis* Embryos for Live Imaging

1. Dow Corning® high vacuum grease.
2. Plain glass microscope slides.
3. Glass cover slips: 22 × 22 mm, thickness no. 1.
4. 10 mL syringe.
5. Parafilm.
6. P200 pipette tips.
7. Hair-loop: form a small loop with a single strand of hair and place into the tip of a Pasteur pipette. Melt a small amount of paraffin and use this to hold the hair-loop in place.
8. 3 mL transfer pipettes.
9. Dissecting microscope.

2.5. Live Imaging Embryos Using Confocal Microscopy

1. Confocal microscope.
2. Mounted embryos (*see* **Subheading 3.4**).

3. Methods

3.1. In Vitro Transcription of Capped RNA for Cytoskeletal Probes

While it is possible to microinject fluorescently labeled cytoskeletal proteins into the *Xenopus* embryo, we have had by far the most success with microinjection of capped RNA encoding fluorescently tagged cytoskeletal probes (*see* **Note 1** for a detailed description of these probes). Here, we describe our method for the *in vitro* transcription of probes from a vector containing an SP6 or T7 promoter (we use pCS2+-based vectors).

3.1.1. Linearizing the DNA Plasmid

1. Prepare a mini-prep of plasmid DNA containing the fluorescently tagged cytoskeletal probe (cloned downstream of an SP6 or T7 promoter). Note that the cleaner your template DNA is, the greater the yield of the transcription reaction should be.
2. Linearize the plasmid using a restriction enzyme which cuts downstream of the cytoskeletal probe:
   - 5 µg Plasmid DNA
   - 10 µL appropriate 10× Restriction Enzyme Buffer
   - 1 µL BSA solution
   - 8 µL (80 units) Restriction Enzyme
   - Make up to total volume of 100 µL with ddH_2O
   - Note that it is necessary to linearize the plasmid because RNA polymerases are extremely processive, so circular template DNA will lead to a mess of longer-than-expected transcription products.
3. Incubate reaction at 37°C for 1 h, then add 2 µL (20 units) Restriction Enzyme and incubate for an additional hour at 37°C. From this point on use *RNase-free* reagents (*see* **Note 2**)
4. Add 2.5 µL 20% SDS and 0.5 µL Proteinase K to digest reaction and incubate at 50°C for 30 min.
5. Purify the linearized DNA using a phenol/chloroform extraction as follows:
   a) Dilute DNA digest reaction with 100 µL nuclease-free H_2O.
   b) Add 200 µL Phenol-chloroform-isoamyl alcohol mixture (25:24:1; pH 7.9), vortex vigorously, spin in a room temperature microcentrifuge at full speed for 1 min.
   c) Remove and retain aqueous (top) layer in a fresh tube.
   d) Back extract organic layer by adding 200 µL nuclease-free H_2O, vortex vigorously, spin at full speed for 1 min.
   e) Remove aqueous layer and combine with previous aqueous layer.
6. Ethanol precipitate aqueous layers with 40 µL 5 M NH_4OAc and 800 µL 100% ethanol. Incubate at –20°C for 1 h to overnight.
7. Pellet precipitated linearized DNA by spinning at full speed in a microcentrifuge at room temperature for 15 min. Then remove ethanol, wash with 800 µL 70% ethanol, spin at full speed for 5 min, remove ethanol and dry pellet in a speed vac or leave to air dry.
8. Resuspend the linearized DNA pellet in 10 µL nuclease-free H_2O. Quantify a small volume of the DNA (0.5–1 µL) by gel electrophoresis or spectrophotometer. Note that it is important to confirm that your plasmid has been linearized into a single band by gel electrophoresis before proceeding.

3.1.2. Capped RNA Synthesis

We use the Ambion mMESSAGE mMACHINE® kit (Ambion, Inc; Applied Biosystems) to synthesize capped RNA, as follows:

1. Set up the transcription reaction at room temp, adding the components in the order listed below:
   a) Nuclease-free H_2O (to make total volume of 20 µL).
   b) 1 µg linear DNA.
   c) 2 µL 10× mMESSAGE mMACHINE® Reaction Buffer (vortex before use).
   d) 10 µL 2× mMESSAGE mMACHINE® NTP/CAP (vortex before use).
   e) 2 µL mMESSAGE mMACHINE® Enzyme Mix (SP6 or T7 depending on vector).
2. Incubate at 37°C for 2–3 h.
3. To terminate reaction, add 115 µL nuclease-free H_2O and 15 µL NH_4OAc mMESSAGE mMACHINE® Stop Solution.
4. Phenol/Chloroform extract the capped RNA, as follows:
   a) Add 75 µL chloroform and 75 µL phenol (pH 6.6) to the RNA reaction, vortex vigorously and spin at full speed in a microcentrifuge for 1 min.
   b) Transfer aqueous phase to a fresh tube.
   c) Back extract the organic layer by adding 50 µL nuclease-free H_2O, vortex vigorously, spin at full speed for 1 min and combine this aqueous layer with the previous.
   d) Extract the combined aqueous layers with 200 µL chloroform, vortex vigorously, spin at full speed for 1 min and transfer aqueous layer to a fresh tube.
5. Precipitate RNA by adding 200 µL isopropanol and incubating at –80°C for 1 h to overnight.
6. Pellet RNA by spinning at maximum speed in a microcentrifuge at 4°C for 15 min.
7. Remove isopropanol – take care as the RNA pellet is clean and therefore quite mobile at this point. Wash pellet with 200 µL 70% ethanol and then spin at full speed at 4°C for 5 min.
8. Carefully remove all ethanol and allow pellet to air-dry.
9. Resuspend RNA pellet in 10 µL nuclease-free H_2O (to prevent loss of pellet, add H_2O and leave for about 10 min before mixing by gentle pipetting).
10. Run a small amount of the product on an RNA denaturing gel to confirm that the transcript is of the expected size and intensity.
11. Quantify by spectrophotometry and aliquot into small samples (we routinely make 1 µL aliquots at 1 µg/µL concentration). Store capped RNA at –80°C.

3.2. Xenopus laevis Ovulation and In Vitro Fertilization

Here we briefly describe the methods used to induce ovulation in female frogs, collect eggs and *in vitro* fertilize. More detailed information on frog husbandry can be found in Peng and Kay *(13)* and suggestions on how to increase egg quality can be found in **Note 3**. A further important consideration is whether to use pigmented or albino frogs; this will depend on the type of experiment being carried out, as is described in **Note 4**.

3.2.1. Inducing Ovulation

1. Prime female frogs 4–7 days before use by injection of 50 units of human chorionic gonadotrophin (HCG) into the dorsal lymph sac using a 1 mL syringe with a 27 G 1/2 needle.
2. 18 h before use, inject frogs with an additional 500–800 units of HCG.
3. Following the injection place frogs in individual tanks of water and store at 17°C until use (*see* **Note 3**). About 12–18 h after injection with HCG most female frogs will begin to ovulate independently and eggs will be clearly visible in the tank.

3.2.2. Isolating Testes

For *in vitro* fertilization testes are harvested from male frogs as follows:

1. To anesthetize frog prepare a solution of 0.02% benzocaine (Ethyl 4-aminobenzoate) in water in a small tank with lid.
2. Place frog into benzocaine solution and leave for 10 min.
3. Remove frog from tank and check for unconsciousness by firmly squeezing the leg (the frog should be completely limp and there should be no reaction to this).
4. Make incisions to expose the lower belly of frog by first cutting through the outer skin and then inner muscle layers.
5. The testes are attached to yellow fat bodies and are white in color and kidney shaped. Carefully remove the testes using surgical scissors and forceps.
6. Blot testes on a paper towel and rinse twice in 1× MMR and then place in testes prep media. Store in a 35 mm Petri dish at 4°C and use within 7 days.
7. Wrap the frog carcass in your gloves and freeze at –20°C before disposal.

3.2.3. In Vitro Fertilization

About 18 h following injection with HCG, female frogs should be producing eggs (which will be visible in the tank) and will be ready to "squeeze", whereby frogs are gently massaged to lay fresh eggs. If no eggs have been laid, the frog can be injected with a further 100–200 units of HCG.

1. Fill a 60 × 20 mm^2 Petri dish with 1× MMR.
2. Pick up ovulating frog and hold in hands with head covered by the palm of hand and legs held apart by fingers. A damp

paper towel can be placed over the frog's head, as covering her eyes will help keep the frog calm.

3. Hold frog over the Petri dish of 1× MMR and massage her lower back until she begins to deposit eggs into the dish.
4. Once there are a few hundred eggs in the dish (or the frog stops laying), pipette out most of the MMR until there is just a shallow covering of liquid over the eggs (about 1/10 of the volume of the dish).
5. Cut a small piece of testes using forceps and add to the eggs. Macerate the testes using forceps and mix with the eggs. Try to have the testes come in direct contact with as many of the eggs as possible.
6. Let eggs stand in testes solution for 30 s and then gently fill Petri dish with dH_2O (so that 1× MMR is diluted approximately tenfold). Leave at room temperature for 30 min. Note that fertilized eggs will rotate within 30 min so that the animal hemisphere is facing upwards.
7. To dejelly the fertilized eggs, remove liquid and add 2% cysteine (in 1× MMR, pH 7.8), transfer to a 50 mL falcon tube (using a 3 ml transfer pipette) and gently swirl for 2–5 min until the jelly coat is removed (visualized by the embryos settling against each other with no gaps).
8. Rinse the embryos five times with ~20 mL 1× MMR and five times with ~20 mL 0.1× MMR.
9. Remove any dead or unfertilized eggs and store the embryos in 0.1× MMR at 17°C. The embryos will undergo their first cleavage about 1.5 h after fertilization.

3.3. Microinjection of Xenopus laevis Embryos

We microinject *Xenopus* embryos at the 1-, 2-, 4- or 8-cell stage using a PLI-100 picoinjector (Harvard Apparatus; *see* **Note 5**). Here we describe our most routine microinjection scenario where both cells of the 2-cell stage embryo are microinjected with capped RNA encoding a cytoskeletal probe (*see* **Subheading 3.1**). For information on microinjecting at alternative stages or with alternative reagents (e.g., morpholino) *see* **Note 6**. When injecting RNA, we use measures to limit RNases by cleaning injection areas with RNase*ZAP*® (Ambion), using RNase-free reagents and by wearing gloves at all times.

3.3.1. Needle Calibration

Needle calibration can be performed while waiting for fertilized embryos to begin their first cleavage, which occurs about 1.5 h after fertilization (at 17°C).

1. Pull needles using 10 µL glass capillaries and a micropipette puller.
2. Using dissecting microscope and sharp forceps, cut off the end of the needle to produce a point approximately 5–10 µm in diameter.

3. Connect needle to microinjector and secure in micromanipulator (*see* **Note 5**).
4. Fill needle with approximately 1 µL nuclease-free water (we do this by pipetting a drop of water onto parafilm and front-loading the needle using the "fill" function, but the needle can also be filled by back-loading prior to connecting to the microinjector, *see* **Note 5**).
5. Place a drop of mineral oil onto the micrometer and place under dissecting microscope.
6. Carefully lower the needle into oil so that the point sits just above the micrometer scale.
7. Dispense one injection volume and measure the diameter of the hanging water drop against the micrometer scale.
8. Adjust microinjector controls (pressure/time) to give a drop size that corresponds to 5 nL (e.g., on a micrometer with 0.1 mm graduations, the diameter of a 5 nL drop is 2.5 graduations).
9. Dispense a few more drops to ensure that the 5 nL volume is reproducibly dispensed.

3.3.2. Microinjection of Capped RNA

We inject a variety of concentrations of RNA depending on the probe being used. When using a new probe it is a good idea to inject several concentrations and ultimately use the lowest concentration that gives good expression levels. High concentrations of RNA are toxic to the embryo, and a good upper limit is generally a needle concentration of 1 mg/mL. Occasionally, for weakly expressed probes, we have used concentrations higher than this (up to 2 mg/mL), however this should be avoided if at all possible. In order to help hold the embryos in place during injection we place a plastic mesh (Spectra Mesh, Spectrum Labs) in the bottom of a Petri dish and secure it with modeling clay (*see* **Subheading 2.3**), these "injection dishes" can be reused many times.

1. As the time approaches 1.5 h since fertilization, check embryos to see if they are beginning to undergo their first cleavage. If they are, proceed to (2) if not wait a few more minutes and check again. Once the embryos start to divide, it will take around 30 min for the next division to take place, resulting in a 4-cell embryo.
2. Empty water out of needle and fill with the RNA to be injected (keep RNA on ice until ready to fill needle). It is possible to mix different RNAs together and inject them simultaneously.
3. Pour injection buffer (5% Ficoll in 0.1× MMR) into the injection dish (see above) and use a transfer pipette to transfer 15–20 embryos into dish (embryos should be selected for good health and even cleavage plane).

4. Place dish under dissecting microscope and lower needle into injection buffer.
5. To inject embryos, slowly lower needle so that it touches the cortex of a cell and then further lower needle until it pierces cell membrane and dispense one 5 nl volume into cell. Once the volume has been dispensed gently raise needle until the tip is out of the cell.
6. Repeat with the second cell of embryo and then with all other embryos by keeping the needle centered and moving the dish.
7. When all are injected, pipette the embryos into 0.1× MMR to rinse and then into fresh 0.1× MMR.
8. Return the embryos to 17°C incubator.
9. 1–2 h after injection, check embryos and remove any dead or dying ones and refresh 0.1× MMR.

3.4. Mounting Xenopus laevis Embryos for Live Imaging

Here we describe a simple method for mounting *Xenopus* embryos using a vacuum grease ring, although mounting embryos in specially made metal shims or in glass-bottomed culture dishes also works well. For imaging the cytoskeleton during cell division, we image embryos as early as the 16-cell stage, once RNAs have begun expressing, through to stages 10–11 (approximately 18–22 h after fertilization at 17°C). For imaging the mitotic spindle we use embryos at stages 10–11, when cells are smaller and spindles are easier to see.

1. Fill a 10 mL syringe with vacuum grease by squeezing grease into the back of the syringe.
2. Place a P200 pipette tip into the end of the syringe and secure with parafilm. Cut off the tip of the pipette to make a wider hole (*see* **Fig. 2**).
3. Use the grease-filled syringe to pipe a grease circle onto a plain glass slide. Build up the walls of the circle by piping round 1–2 more times (*see* **Fig. 2**).
4. Pipe four dots of grease around the circle (these will help support the cover-slip).
5. Use a transfer pipette to put 1 or 2 healthy, microinjected embryos into the grease circle.
6. Top up with more 0.1× MMR, so that the meniscus is level with the top of the grease circle.
7. The embryos will automatically sit with their animal hemisphere upright and so need little manipulation. If necessary, a hair-loop (*see* **Subheading 2.4**) can be used to gently push the embryos toward the center of the circle.
8. Place a glass coverslip over the embryos and press gently onto the grease ring. The coverslip should make contact with the

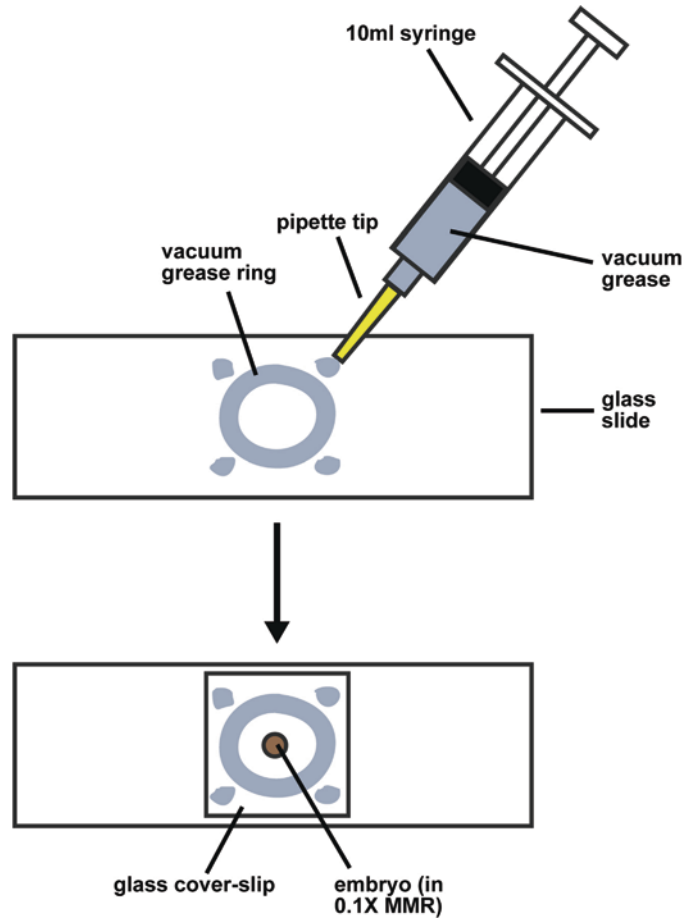

Fig. 2. Mounting *Xenopus laevis* embryos using vacuum grease. We mount embryos for live imaging by making a vacuum grease ring on glass slides. To "pipe" the grease we use a syringe with a pipette tip held at the end with parafilm. A ring of grease is then piped onto a glass slide and four supporting spots of grease are added as shown. The embryo, in 0.1× MMR, is then pipetted into the grease ring and a glass coverslip is placed on top. The coverslip should be gently pushed down so that it is just touching the embryo.

embryos so that they are pressed slightly against the glass and are held securely in place. Remove any excess liquid.

3.5. Live Imaging Embryos Using Confocal Microscopy

Since different confocal microscope systems will vary, here we provide general pointers in order to help the reader get started with live imaging.

1. Place slide containing the embryos onto microscope stage and move appropriate objective into place – we generally use 25× or 63× oil objectives for very early embryos (16-cell stage up to mid-blastula transition) and a 63× oil objective for later stage embryos (stage 10 upwards).
2. Using bright-field or epifluorescent illumination, carefully adjust the focus until you see the most superficial cells of the

embryo. It is important to be gentle when focusing, as it is possible to squash the embryos by pushing the coverslip too close to the slide.

3. Once the embryo is in focus, turn off the bright-field/epifluorescence and switch to confocal scanning. For live imaging it is important to set the laser power as low as possible, to prevent photobleaching and possible phototoxicity. We usually scan using a format of 512 × 512 pixels for live imaging, as this provides a good compromise between scanning speed and image resolution.
4. Once a good area of the embryo has been selected, and zoomed if necessary, set the gain and offset for each channel. The gain and offset should be adjusted to levels high enough to see all that is required but where there are few pixels at their maximum intensity and where a minimum of background noise is seen. These levels can be adjusted by eye or by using a look-up-table (LUT) such as the glow-over/glow-under LUT found on Leica microscopes.
5. For two-color live imaging it is usually best to set the confocal to scan the two channels simultaneously. Simultaneous scanning will save time, allowing faster time points and is especially important if you are imaging a highly dynamic process where changes may occur between sequential scans of the two channels. However, when scanning two channels simultaneously it is important to set the levels of gain, offset and laser power for each channel very carefully to ensure that bleed-through from one channel to another does not occur. If bleed-through still occurs, it may be necessary sacrifice some scan time and collect sequentially.
6. If you wish to collect a z-series over time, you must next set your upper and lower z limits and the number of sections you wish to collect. Note that if you are imaging a highly dynamic process you should limit the number of z-sections taken – when we image mitotic spindles we generally find that imaging a single plane works well and allows us to collect very frequent time points; in contrast imaging the cytokinetic furrow requires multiple z-sections (usually 13 z-sections, approximately 1 μm apart).
7. Next set the appropriate time interval and number of time points to be collected. Again this will vary according to how dynamic the process being imaged is. For mitotic spindles we find a time interval of 6 s collected 200 times works well, while for imaging cytokinesis we use a time interval of 20 s, and collect this 50–100 times.
8. The appearance of images can be greatly improved by using a scan averaging algorithm such as a Kalman accumulation.

This will slow down scanning time, so should be limited to the lowest number of averages needed to improve the image quality.

9. Once all the settings have been finalized, start the time series. It is advisable to stay by the microscope and watch the image during scanning so that manual adjustments to the focus can be made if required.

4. Notes

1. As noted above, most imaging of the actin and microtubule cytoskeletons has been done using fluorescent actin or tubulin protein. This approach has many virtues, but it also has certain drawbacks. It is becoming increasingly clear that fluorescent actin does not label all pools of F-actin equally (for discussion see Burkel et al. *(14)*). Further, when used at high levels, both fluorescent actin and fluorescent tubulin tend to suppress the assembly of their respective polymers. An alternative approach is to use fluorescent proteins fused to isolated domains of proteins that bind to F-actin or microtubules. This typically does not prevent assembly of the polymer in question. In addition, the background is typically lower, because unlike fluorescent tubulin or actin, which represents both the assembled and unassembled forms of their respective polymers, fluorescent polymer-binding proteins accumulate specifically on the assembled form. However, herein lies their major disadvantage: too much of such probes can inhibit disassembly. Nonetheless, we have had considerable success with eGFP, mRFP or mCherry fused to the calponin homology (F-actin binding) domain of utrophin *(9–10)*, which permits very bright labeling of F-actin without obvious stabilization of actin filaments. We have also had success with using 3XGFP (three copies of eGFP fused together) fused to the microtubule-binding domain of ensconsin *(10)*, a probe originally developed by the Bulinski lab *(15)*. mRNA encoding this probe, however, must be carefully titered for microinjection to find a range that labels microtubules well but does not cause microtubule stabilization. Using a similar rationale, we and others have developed fluorescent probes based on effector protein domains that bind to the active forms of the Rho GTPases *(16–18)*. The Rho GTPases are key regulators of the cytoskeleton but one of the major problems with using the simple fluorescent protein fusions with Rho proteins is the failure of these fusions to target properly *(19)*. Instead, by using effector domain based probes, it is possible to visualize Rho or Cdc42 activation in *Xenopus* oocytes,

eggs, and embryos *(10, 18, 20–22)* (*see* **Fig. 1**). While these probes avoid the targeting problems seen with simple Rho GTPase fusions they must still be tittered carefully to avoid inhibiting the proteins they report on.

2. It is vital when working with RNA to keep your samples free of any RNases; there are a number of precautions that must be taken to prevent RNases from contaminating your work. First, always wear gloves when handling samples as our fingers are a rich source of RNases; it is also good practice to change your gloves regularly during the experiment. Second, use pipette tips and eppendorf tubes that are guaranteed RNase-free. We keep all plasticware for use with RNA separate from the rest of the lab to limit contamination and we also have a set of pipettors that are exclusively used for RNA work. Third, keep all work surfaces clean; we use the RNase decontamination solution, RNase*Zap*® (Ambion), to wipe down lab benches and to clean pipettors. Fourth, use RNase-free solutions: these can be made either by treating with diethylpyrocarbonate (DEPC) to inactivate RNases or by purchasing guaranteed RNase-free solutions from companies such as Ambion. We tend to favor the latter, as we've found these reagents to be highly reliable. However, if you wish to DEPC treat solutions, add 0.1% DEPC to the solution in a fume-hood, leave overnight at room temperature and then autoclave for 15 min; Tris solutions will reduce the activity of DEPC, so either more DEPC (e.g., 1%) should be added or solutions should be made up with molecular biology grade powdered reagents in DEPC-treated water.
3. Acquiring high quality eggs is crucial for these live imaging studies, and there are a number of considerations that will help to obtain them. First, we usually prime two female frogs for each experiment to maximize our chances of having an ovulating frog that produces good eggs. Second, frogs should be cycled so that they have at least a 4-month break between ovulations; an even longer recovery period may help improve egg quality. Third, we have found that incubating the frogs at 17°C after their second injection of HCG increases the chances of ovulation and may improve the quality of eggs laid.
4. Wild-type *Xenopus laevis* lay eggs with a pigmented animal hemisphere; while the eggs laid by albino frogs lack this pigment. We have found albino embryos to be far superior for imaging mitotic spindles, as the pigment in wild-type embryos obscures confocal visualization of the fluorescent spindles. However, in other experiments the presence of pigment can be helpful as it is much easier to assess the health of these embryos and they are simpler to microinject.
5. There are many choices of microinjectors available, ranging from the basic through to the sophisticated; however, the major requirement is that they are able to accurately dispense specific

volumes. Some microinjectors possess a "fill" function, which allows the user to frontload the needle; this can be useful as very small volumes can be drawn into the needle – an advantage when using a precious RNA prep. The second major piece of equipment required for microinjection is a micromanipulator, which holds the glass capillary needle and allows the user to accurately move the needle up and down to inject the embryo. The micromanipulator must hold the needle firmly at an angle of approximately 45°; a micromanipulator that is fixed to a microscope and can't be angled is not suitable for *Xenopus* injections *(23)*.

6. As well as being injected at the 2-cell stage with capped RNA, *Xenopus* embryos can also be microinjected at alternative stages and with alternative reagents. 1-cell and 4-cell embryos can be microinjected with an injection volume of 5 nL just as described for 2-cell stage embryos. Individual cells of 8-cell embryos can also be easily microinjected but a slightly finer needle that dispenses an injection volume of 2.5 nL should be used. In order to track injected cells (and their progeny) as the embryo develops, a cell dye such as fluorescently labeled dextran can be included in the injection. It is possible to microinject *Xenopus* embryos with fluorescently labeled proteins using the methods described here, although protein preparations should be centrifuged (we use an air-driven ultracentrifuge for this) prior to injection to remove debris that would clog the microinjection needle. Anti-sense morpholino oligos are an effective means of gene knockdown in *Xenopus* embryos *(24)* and can be microinjected using the methods described here, except that the morpholino should be heated prior to injection for 5 min at 65°C and kept at 37°C until ready to inject. A good starting concentration for morpholino injection is a needle concentration of 1 mM (in nuclease-free water), however we have used concentrations of up to 5 mM and down to 0.25 mM.

References

1. Shaner, N.C., Campbell, R.E., Steinbach, P.A., Giepmans, B.N., Palmer, A.E., and Tsien, R.Y. (2004). Improved monomeric red, orange and yellow fluorescent proteins derived from *Discosoma* sp. red fluorescent protein. Nat Biotechnol *22*, 1567–1572
2. Matz, M.V., Fradkov, A.F., Labas, Y.A., Savitsky, A.P., Zaraisky, A.G., Markelov, M.L., and Lukyanov, S.A. (1999). Fluorescent proteins from nonbioluminescent *Anthozoa* species. Nat Biotechnol *17*, 969–973
3. Prasher, D.C., Eckenrode, V.K., Ward, W.W., Prendergast, F.G., and Cormier, M.J. (1992). Primary structure of the *Aequorea victoria* green-fluorescent protein. Gene *111*, 229–233
4. Campbell, R.E., Tour, O., Palmer, A.E., Steinbach, P.A., Baird, G.S., Zacharias, D.A., and Tsien, R.Y. (2002). A monomeric red fluorescent protein. Proc Natl Acad Sci U S A *99*, 7877–7882
5. Chalfie, M., Tu, Y., Euskirchen, G., Ward, W.W., and Prasher, D.C. (1994). Green fluorescent protein as a marker for gene expression. Science *263*, 802–805
6. Heim, R. and Tsien, R.Y. (1996). Engineering green fluorescent protein for improved brightness, longer wavelengths and fluorescence resonance energy transfer. Curr Biol *6*, 178–182
7. Megason, S.G. and Fraser, S.E. (2003). Digitizing life at the level of the cell: high-performance laser-scanning microscopy and image analysis for in toto imaging of development. Mech Dev *120*, 1407–1420

8. Kieserman, E.K., Glotzer, M., and Wallingford, J.B. (2008). Developmental regulation of central spindle assembly and cytokinesis during vertebrate embryogenesis. Curr Biol *18*, 116–123
9. Woolner, S., O'Brien, L.L., Wiese, C., and Bement, W.M. (2008). Myosin-10 and actin filaments are essential for mitotic spindle function. J Cell Biol *182*, 77–88
10. Miller, A.L., and Bement, W.M. (2009). Regulation of cytokinesis by Rho GTPase flux. Nature Cell Biology *11*, 71–7
11. Mikhailov, A. and Gundersen, G.G. (1998). Relationship between microtubule dynamics and lamellipodium formation revealed by direct imaging of microtubules in cells treated with nocodazole or taxol. Cell Motil Cytoskeleton *41*, 325–340
12. Charras, G.T., Hu, C.K., Coughlin, M., and Mitchison, T.J. (2006). Reassembly of contractile actin cortex in cell blebs. J Cell Biol *175*, 477–490
13. Peng, H.B. and Kay, B.K. (1991). *Xenopus laevis*: practical uses in cell and molecular biology. Methods Cell Biol *36*, 679–681
14. Burkel, B.M., von Dassow, G., and Bement, W.M. (2007). Versatile fluorescent probes for actin filaments based on the actin-binding domain of utrophin. Cell Motil Cytoskeleton *64*, 822–832
15. Faire, K., Waterman-Storer, C.M., Gruber, D., Masson, D., Salmon, E.D., and Bulinski, J.C. (1999). E-MAP-115 (ensconsin) associates dynamically with microtubules in vivo and is not a physiological modulator of microtubule dynamics. J Cell Sci *112(Pt 23)*, 4243–4255
16. Pertz, O. and Hahn, K.M. (2004). Designing biosensors for Rho family proteins – deciphering the dynamics of Rho family GTPase activation in living cells. J Cell Sci *117*, 1313–1318
17. Kim, S.H., Li, Z., and Sacks, D.B. (2000). E-cadherin-mediated cell-cell attachment activates Cdc42. J Biol Chem *275*, 36999–37005
18. Benink, H.A. and Bement, W.M. (2005). Concentric zones of active RhoA and Cdc42 around single cell wounds. J Cell Biol *168*, 429–439
19. Yonemura, S., Hirao-Minakuchi, K., and Nishimura, Y. (2004). Rho localization in cells and tissues. Exp Cell Res *295*, 300–314
20. Sokac, A.M., Co, C., Taunton, J., and Bement, W. (2003). Cdc42-dependent actin polymerization during compensatory endocytosis in Xenopus eggs. Nat Cell Biol *5*, 727–732
21. Ma, C., Benink, H.A., Cheng, D., Montplaisir, V., Wang, L., Xi, Y., Zheng, P.P., Bement, W.M., and Liu, X.J. (2006). Cdc42 activation couples spindle positioning to first polar body formation in oocyte maturation. Curr Biol *16*, 214–220
22. Bement, W.M., Benink, H.A., and von Dassow, G. (2005). A microtubule-dependent zone of active RhoA during cleavage plane specification. J Cell Biol *170*, 91–101
23. Sive, H.L., Grainger, R.M., and Harland, R.M. (1998). *Early Development of Xenopus laevis: A Laboratory Manual*. Cold Spring Harbor Laboratory Press: New York
24. Heasman, J. (2002). Morpholino oligos: making sense of antisense? Dev Biol *243*, 209–214

Chapter 3

Live-Cell Imaging of the Cytoskeleton and Mitochondria–Cytoskeleton Interactions in Budding Yeast

Theresa C. Swayne, Thomas G. Lipkin, and Liza A. Pon

Summary

This chapter describes labeling methods and optical approaches for live-cell imaging of the cytoskeleton and of a specific organelle–cytoskeleton interaction in budding yeast.

Key words: Yeast, Mitochondria, Fluorescent proteins, Immunofluorescence, Vital staining, Microscopy, Live-cell imaging, Deconvolution

1. Introduction

The actin and microtubule cytoskeletons of budding yeast, and their cargos, were first detected by staining fixed cells with dyes or antibodies. These methods continue to be the only methods to detect native proteins or to detect proteins in yeast strains that are not amenable to transformation. However, proper localization by immunofluorescence may be compromised by fixation and/or staining artifacts, and relies on the availability of antibodies that are specific and can bind to antigens in fixed cells.

Over the last 10 years, methods have been developed to visualize the actin and microtubule cytoskeleton, as well as cargos that undergo cytoskeleton-driven transport, in living yeast cells. Live-cell imaging enables visualization of events that cannot be seen in fixed cells, including the dynamics and function of the cytoskeleton and its intracellular cargos. It typically relies on detection using fluorescent protein (FP) tags or vital dyes, and is not subject to fixation artifacts. Some vital dyes offer the additional ability to assess the function of cellular compartments,

R.H. Gavin (ed.), *Cytoskeleton Methods and Protocols,* Methods in Molecular Biology, vol. 586
DOI 10.1007/978-1-60761-376-3_3,
© Humana Press, a part of Springer Science + Business Media, LLC 2009

including membrane potential of mitochondria and other membranous structures.

Here, we describe methods to tag yeast genes at their chromosomal loci, determine whether FP tags are deleterious, visualize tagged gene products expressed ectopically or from their endogenous promoters, and carry out quantitative analysis of cytoskeletal dynamics and motility events. We also describe methods to stain mitochondria and detect mitochondria–cytoskeleton interactions in living yeast cells using targeted FPs and vital dyes.

1.1. Strategies for Detection of Specific Cellular Structures using Targeted Fluorescent Proteins

1.1.1. Visualization of the Actin Cytoskeleton

Actin patches and actin cables are the two F-actin-containing structures that persist throughout the cell cycle in budding yeast. Actin patches are endosomes that are invested with a coat of F-actin and localize to the bud and mother-bud neck. Actin cables are bundles of F-actin that align along the mother-bud axis and are implicated as tracks for the movement of cargos including secretory vesicles, mRNA, spindle alignment elements, mitochondria, Golgi and vacuoles along the mother-bud axis.

Early studies revealed that tagging of the actin-encoding *ACT1* gene of yeast with GFP compromised function. Specifically, plasmid borne-*ACT1-GFP* did not complement loss of the endogenous *ACT1* gene *(1)*. This loss of function presumably occurred because virtually every surface of the actin protein must be available to engage in protein-protein interactions for processes including microfilament nucleation and polymerization; interaction with motor proteins and other force generators; and microfilament assembly, capping, cross-linking, and severing. On the other hand, tagging of actin-binding proteins, including fimbrin (Sac6p) or Abp1p, with GFP resulted in a robust fluorescence signal that localized correctly to actin patches, but did not have any obvious effect on cytoskeleton organization or cell growth. Although Sac6p and the two tropomyosin isoforms of yeast (Tpm1p and Tpm2p) localize to actin cables, expression of Sac6p, Tpm1p or Tpm2p that are tagged at their C-termini does not result in fluorescent labeling of actin cables. However, tagging of another resident actin cable protein, Abp140p, at its chromosomal locus with GFP results in weak, but detectable labeling of actin cables in living cells *(2)*. **Table 1** lists genes that have been tagged with FPs to serve as probes for actin patches and actin cables in budding yeast.

1.1.2. Visualization of the Microtubule Cytoskeleton

The microtubule cytoskeleton of yeast is similar to, but considerably less complex than, that of other eukaryotes. The microtubule organizing center of yeast is called the spindle pole body (SPB) and is embedded in the nuclear envelope, which remains intact throughout the mitotic cell cycle. During interphase, short microtubules radiate from the SPB. During mitosis, the SPB duplicates. The two daughter SPBs migrate to opposite

Table 1
GFP-tagged actin patch proteins in budding yeast

Actin-containing structure	GFP-tagged proteins
Actin patch (early)	Las17p *(12, 13)*,Sla1p *(14, 13)*, Pan1p *(15, 13)*, End3p *(16)*, Sla2p *(13, 17)*, Bzz1p *(18)*, Vrp1 *(19)*
Actin patch (mid)	Myo3p *(20)*, Myo5p *(21)*, Bbc1p *(18)*,
Actin patch (late)	Abp1p *(1, 22, 13, 23)*, Arp2p *(12)*, Arp3p *(12)*, Arc15p *(24, 13)*, Sac6p *(25, 23)*, Cap1p *(26)*, Cap2p *(27)*, Scp1p *(28)*, Cof1p *(29)*
Actin cable (vegetative)	Abp140p *(2)*
Actin cable (G_0)	Lifeact (Abp140 aa 1–17) *(30)*

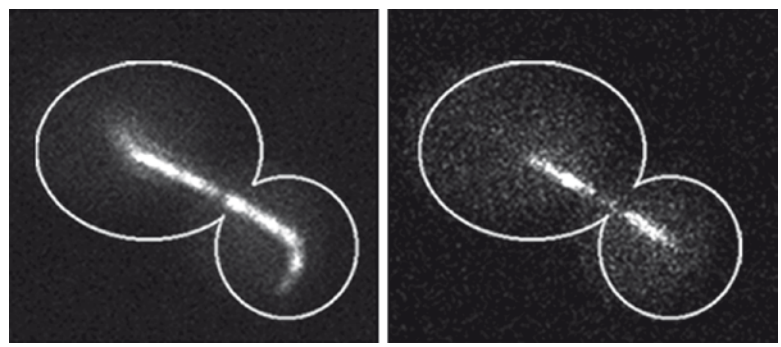

Fig. 1. Visualization of astral and spindle microtubules using Tub1p-Cherry (left) and spindle microtubules using the chromosomal passenger protein Sli15p-GFP (right) in living yeast. Cell boundaries are outlined in white.

sides of the nucleus, where they serve as organizing centers for astral microtubules, which extend into the cytosol, and for polar and kinetochore microtubules, which take part in chromosomal alignment and segregation. **Figure 1** shows the organization of astral and spindle microtubules in dividing yeast cells. **Table 2** lists genes that have been tagged with FPs to serve as probes for astral microtubule, spindle, and SPBs.

1.1.3. Visualization of Mitochondria

Ectopic Expression of Mitochondria-Targeted FPs

Mitochondria contain two membranes (the outer and the inner), and two soluble compartments (the intermembrane space and the matrix). They also contain submitochondrial structures including contact sites (where outer and inner membranes are closely apposed) and mtDNA nucleoids. Over 95% of the proteins that are present in mitochondria are encoded in the nucleus, synthesized in the cytoplasm, and imported into the organelle. The targeting

Table 2
GFP-tagged microtubule associated proteins in budding yeast

MT-containing structure	GFP-tagged proteins
Spindle MTs	Tub1p *(31)*, Tub3p *(32)*, Cin8p *(33)*, Ase1p *(33)*, Bik1p *(34)*, Stu1p *(33)*
Astral MTs	Dyn1p/Dhc1p *(35)*
Spindle pole bodies	Kar3p *(36)*, Stu2p *(37)*, Nuf2p *(38)*, Tub4p *(39)*, Spc42p *(40)*, Spc110p/Nuf1p *(41)*

Table 3
Mitochondria-targeted signal sequence-FP fusion proteins[a]

Site	Targeting	Promoter	Vector	FP	References
Matrix	*OLI1*[b] signal sequence	*ADH1*	2 μ pRS426 derivative	HcRed	*(42)*
	CIT1[c] signal sequence	*CIT1*	CEN-*URA3*	bGFP (F99S, M153T, V163A)	*(43)*
	CIT1 signal sequence	*GAL1*	CEN-*URA3*	bGFP	*(43)*
	OLI1	*GAL1*	CEN-*URA3*	DsRed	*(44)*
OM	*TOM6* signal sequence	*GAL1*	CEN-*URA3*	bGFP	*(43)*
IM	*YTA10*	*GAL1*	CEN-*URA3*	bGFP	*(43)*
mtDNA	*ABF2*	*GAL1*	CEN-*URA3*	bGFP	*(43)*

[a]For other mitochondria-targeted fusion proteins see *(55–56)*
[b]F_0ATP synthase subunit 9
[c]Citrate synthase 1

information for import of proteins into mitochondria resides in signal sequences, which may be in the N-terminus, C-terminus, or within nuclear-encoded mitochondrial proteins *(3)*. Mitochondrial signal sequences or full-length proteins containing mitochondrial signal sequences have been used to target FPs to mitochondria and to specific compartments within mitochondria. We have used several plasmid-borne targeted FPs to label yeast mitochondria (**Table 3**). All of the targeted FPs are used to produce a robust fluorescent signal that is specific for mitochondria, and they have no deleterious effect on cell growth or on mitochondrial morphology, motility, or respiratory activity.

DNA-Binding Dyes

In yeast and other eukaryotes, mitochondrial DNA (mtDNA) assembles into punctate structures, mtDNA nucleoids, that are associated with the inner leaflet of the inner mitochondrial membrane. mtDNA nucleoids contain multiple copies of mtDNA and proteins that contribute to the organization, replication, and expression of mtDNA. As mitochondria are the only extranuclear organelles in animal cells and fungi that contain DNA, cytoplasmic DNA staining can be diagnostic for mitochondria. In yeast, a species in which mtDNA is dispensable, DNA-binding dyes are also used to determine if a strain is *rho*^{0} (lacks mtDNA).

DAPI (4′,6′-diamidino-2-phenylindole) is the most common DNA-binding dye used in yeast **(Table 4)**. Upon binding to nucleic acids, DAPI fluorescence increases greatly, and this increase is more pronounced with DAPI binding to DNA than with RNA. These characteristics make DAPI a strong nuclear and mtDNA marker with little cytoplasmic background staining. Another advantage is that it stains mtDNA independent of the metabolic state of the mitochondria. Consequently, it can be used in cells whose mitochondrial function may be impaired. Finally, DAPI stains DNA in living and fixed cells, and produces a robust, persistent fluorescent signal.

There are two issues to bear in mind when working with DAPI. First, because DAPI also stains nuclear DNA, mtDNA nucleoids in close proximity to the nucleus are not well resolved. Second, because DAPI is visualized with UV illumination, sustained imaging of DAPI in live cells results in phototoxicity. Indeed, mitochondrial fragmentation or rupture can occur in

Table 4
Vital dyes for yeast mitochondria

Dye	IUPAC name	λ_{ex}	λ_{em}
$DiOC_6$ *(4)*	3,3′-dihexyloxacarbocyanine iodide	484	501
DASPMI	4-(4-(dimethylamino)styryl)-*N*-methylpyridinium iodide (4-Di-1-ASP)	475	605[a]
Rhodamine 123	2-(6-Amino-3-imino-3H-xanthen-9-yl)benzoic acid methyl ester	505	534[a]
MitoTracker[b]	Various	Various	Various
DAPI	4′,6′diamidino-2-phenylindole	358	461

[a]Broad emission range; not recommended for green/red double-label studies
[b]Proprietary dyes from Invitrogen, Inc.

DAPI-stained cells after 1–2 min of continuous illumination with conventional fluorescent light sources.

Lipophilic Membrane Potential-Sensing Dyes

Membrane potential-sensing dyes are lipophilic, positively charged fluorophores that accumulate in cellular compartments that have a membrane potential. Because functioning mitochondria have the most negative membrane potential in the cell, these dyes accumulate in the mitochondria more readily than in any other compartment. Moreover, in contrast to the DNA-binding dyes, which stain punctate intramitochondrial structures, membrane potential-sensing dyes stain the entire mitochondrial compartment. As a result, they are excellent tools for investigating mitochondrial distribution and morphology. Finally, these dyes provide information regarding mitochondrial function and integrity.

The membrane potential-sensing dyes that work well in yeast are the carbocyanine $DiOC_6$ *(4)*, the styryl dye DASPMI, the cationic rhodamine derivative rhodamine 123, and the fixable stains of the MitoTracker family **(Table 4)**. Of the dyes described here, rhodamine 123 is least lipophilic and consequently the most sensitive to membrane potential. $DiOC_6$ *(4)* and various MitoTrackers are useful for double-label experiments because they have narrow excitation and emission spectra. Finally, the orange and red MitoTracker dyes persist in mitochondria after aldehyde fixation and permeabilization by acetone or Triton X-100, and thus are the only membrane potential-sensing dyes that can be used together with immunofluorescence staining.

1.2. Strategies for Tagging Endogenous Proteins

1.2.1. Choosing the Best FP for Your Application

The discovery, cloning and heterologous expression of the green fluorescent protein (GFP) from the jellyfish *Aequorea victoria* have revolutionized imaging in cell biology. GFP is now one member of a large family of homologous FPs with different colors from variations in chromophore covalent structure and noncovalent environment. Laboratory mutagenesis has further diversified FPs' spectra, increased their brightness and folding efficiencies, and decreased oligomerization.

The intrinsic brightness of a FP is determined by its extinction coefficient and quantum yield. However, the actual brightness of a FP is determined by its intrinsic brightness, the properties of the imaging system (the efficiency of FP excitation, and the sensitivity of detection of the emission spectrum of the FP), and FP behavior upon ectopic expression (its rate of folding and stability). Other factors that will affect which FP is best for a given application are: FP photostability (particularly for long-term imaging studies), size (which can impact on the function and/or localization of FP-tagged proteins), and oligomerization (which can produce artifactual protein–protein interactions). The physical properties of the brightest FPs within each spectral class of FP are shown in **Table 5**.

Table 5
Physical properties of FPs

Class	Protein	Source laboratory (references)	Λ_{ex} (nm)	Λ_{em} (nm)	Bright-ness
Far-red	mPlum	Tsien	590	649	4.1
Red	mCherry	Tsien	587	610	16
	tdTomato	Tsien	554	581	95
	mStrawberry	Tsien	574	596	26
	J-Red	Evrogen	584	610	8.8
	Ds-Red-monomer	Clontech	556	586	3.5
Orange	mOrange mKO	Tsien MBL Intl.	548 548	565 559	49 31
Yellow–green	mCitrine	Tsien	516	529	59
	Venus	Miyawaki	515	528	53
	Ypet	Daugherty	517	530	80
	EYFP	Invitrogen	14	527	51
Green	Emerald EGFP	Invitrogen Clontech	487 488	509 507	39 34
Cyan	CyPet	Daughtery	435	477	18
	mCFPm	Tsien	433	475	13
	Cerulean	Piston	433	475	27
	T-Sapphire	Griesbeck	399	511	26

Please refer to Shaner et al., 2005 *(45)* for information on the photostability, pKa and oligomerization of these FPs

For chromosomal tagging, an insertion cassette, double-stranded linear DNA that encodes the tag of interest plus a selectable marker, is inserted into a target site in the genome by homologous recombination. Tagging vectors have been developed for insertion of a variety of FPs (e.g., GFP, GFP color variants, and GFPs that have been optimized for expression in yeast), epitopes (e.g., HA or myc), affinity tags (e.g., GST, TAP, or His), and various combinations of FPs, epitopes, and affinity tags (e.g., yECFP+3xMyc). Finally, since FP and epitope tags can be used in antibody-based techniques including affinity purification, immunoprecipitation, Western blot analysis, and immunofluorescence, chromosomal tagging technology has facilitated biochemical characterization of proteins. Some readily available tagging vectors are shown in **Table 6**.

Table 6
Yeast tagging cassette vectors

Plasmid family	Tag position	Promoter	Tags	Markers
pFA6a[a]	C terminal	Endogenous	GFP(S65T) 3xHA 13xMyc GST	*TRP1* *kanMX6* *HIS3MX6*
pFA6a-PGAL1[a]	N terminal or internal	*GAL1*	GFP(S65T) 3xHA GST	*TRP1* *kanMX6* *HIS3MX6*
pUR[b]	C terminal	Endogenous	DsRed	*HIS3* *URA3(K.l.)*
pYM[c]	C terminal	Endogenous	yEGFP EGFP EBFP ECFP EYFP DsRed, DsRedI RedStar, RedStar2 eqFP611 FlAsH 1xHA, 3xHA, 6xHA 3xMyc, 9xMyc 1xMyc+7xHis TAP Protein A	*kanMX4* *hphNT1* *natNT2* *HIS3MX6* *klTRP1*
pKT[d]	C terminal	Endogenous	yEGFP yECFP yEVenus yECitrine yESapphire yEmCFP[e] yEmCitrine tdimer2[f] yECitrine+3xHA yECitrine+13xMyc yECFP+3xHA yECFP+13xMyc	K*anMX* *SpHIS5* *CaURA3*
pOM[g]	N terminal or internal	Endogenous[h]	yEGFP 6xHA 9xMyc Protein A TEV-ProteinA TEV-GST-6xHis TEV-ProteinA-7xHis	K*anMX6* *URA3(K.l.)* *LEU2(K.l.)*

[a] *(46)* [b] *(47)*
[c] *(48)*, available through EUROSCARF)
[d](*(49)*, available through EUROSCARF or Harvard University)
[e]Monomeric version
[f]Tandem dimer of DsRed
[g](*(50)*, available through EUROSCARF)
[h]After Cre-mediated removal of auxotrophic marker

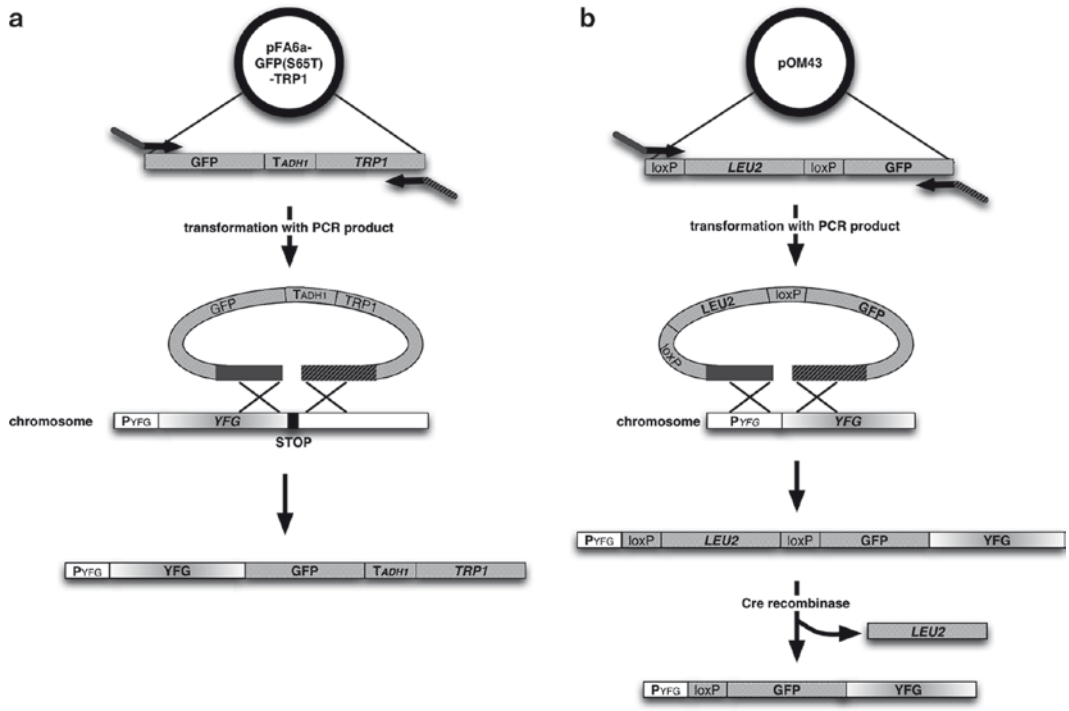

Fig. 2. Approaches for insertion of FPs or epitope tags into target sites in the yeast genome. See text for description.

1.2.2. Vectors for PCR-Mediated Tagging of Chromosomal Genes

Insertion cassettes are produced by PCR using tagging vectors as templates, and primers that hybridize both to the insertion cassette within the tagging vector and the target site within the yeast chromosome. The amplified DNA contains the desired tag and a selectable marker, flanked by DNA that is homologous to the desired insertion site (**Fig. 2**). The amplified DNA is transformed directly into yeast using a standard protocol *(5)*. Recombinants that carry the inserted tag are identified using the selectable marker in the insertion cassette and characterized.

Tagging vectors are versatile, as different tags can be inserted into a target gene using a single set of primers and different cassettes from the same family. In addition, vectors are available for expression of tagged genes from their endogenous promoter or from the *GAL1* inducible promoter. Finally, variations in the tagging cassettes have been developed in which the selectable markers can be excised from the tagged gene (**Fig. 2b**). As a result, tags can be inserted anywhere within the coding region of the gene of interest, and the tagged gene can be expressed at wild-type levels under control of the endogenous promoter. Moreover, the same selectable marker can be used for multiple rounds of insertion.

2. Materials

2.1. Yeast Growth Media

1. Lactate medium: For 1 L combine 3.0 g yeast extract, 0.5 g glucose, 0.5 g $CaCl_2$, 0.5 g NaCl, 0.6 g $MgCl_2$, 1 g KH_2PO_4, 1g NH_4Cl, 1 g 22 mL 90% lactic acid, and 7.5 g NaOH pellets. Dissolve ingredients in 800 mL distilled H_2O. Adjust pH to 5.5 with NaOH. Bring volume to 1 L with distilled H_2O. Optional: For growth of *ade2* cells, add 0.1 mg/mL adenine.
2. Raffinose medium: For 1 L, combine 10 g yeast extract, 20 g bacto-peptone, and 20 g raffinose. Bring volume to 1 L with distilled H_2O. Optional: For growth of *ade2* cells, add 0.1 mg/mL adenine.
3. SE medium: For 1 L, combine 1 g glutamic acid (monosodium salt), 1.7 g yeast nitrogen base (without amino acids or ammonium sulfate), 20 g dextrose and amino acid supplements as needed. Dissolve ingredients in 800 mL distilled H_2O. Adjust pH to 5.5 with $NaHCO_3$. Bring volume to 1 L with distilled H_2O. Optional: Supplement after autoclaving with 200 μg/mL G418.

2.2. Yeast Transformation

1. 50%, w/v Polyethylene glycol 3350 in H_2O, autoclaved.
2. 1 M Lithium acetate stock, filter sterilized.
3. 2 mg/mL single stranded calf-thymus DNA stock in H_2O, store frozen.

2.3. PCR Amplification of Insertion Cassettes

1. 3.3× PCR buffer (buffer II stock, contains no Mg^{2+}).
2. 25 mM $Mg(OAc)_2$ stock.
3. dNTP mix: 2.5 mM ea. dNTP.
4. 2×10^{-5} M primers stock.
5. ~50 ng/μL vector template stock.
6. *rTth* DNA Polymerase (Applied Biosystems).

2.4. Imaging Mitochondria in Living Cells

For Agarose Bed Growth Chamber: 5 mL drop-out media (*see* **Note 1**) and 0.1 g 2% agarose (low melting). Combine ingredients in 50 mL Falcon tube and boil approximately 5 min to ensure contents are fully dissolved. Dispense 200-μL aliquots (*see* **Note 2**) into eppendorf tubes. Store at room temperature, in the dark.

For VALAP combine petrolatum (Vaseline), lanolin and paraffin (hard) in 1:1:1 ratio. Melt by submerging in a 70°C water bath. Aliquot melted Valap into 60 × 15 mm Petri dishes. Store at room temperature.

3. Methods

3.1. Transformation of Yeast with Plasmid-Borne Targeted FPs

The lithium acetate method *(5)* is commonly used for yeast transformation. The following protocol is for one transformation reaction. A mock transformation containing no DNA should always be carried out in parallel as a negative control.

1. Grow yeast to mid-log phase.
2. Remove 10^8 cells from the culture.
3. Wash cells with 100 mM lithium acetate and resuspend in 50 µL of 100 mM lithium acetate (*see* **Note 3**).
4. Add the following reagents *in order, without mixing*: 240 µL polyethylene glycol 3350 (50%, w/v stock), 36 µL 1.0 M lithium acetate, 25 µL of 2 mg/mL single stranded calf-thymus DNA, 50 µL dH_2O and at least 1 µg plasmid DNA.
5. Vortex vigorously and incubate in a water-bath at 30°C for 30 min.
6. Heat shock at 42°C for 15–25 min.
7. Concentrate cells by mild centrifugation (30 s, 7,000 × *g*).
8. Resuspend cell pellet gently in 200 µL of sterile water.
9. On nonselective media (YPD), plate 1 µL of the reaction (*see* **Note 4**). On selective media, plate 10 µL, 50 µL, and the remainder of the reaction.

3.2. Methods for Modification of Genes at Their Chromosomal Locus in Yeast

3.2.1. Primer Design for PCR Amplification of Insertion Cassette

Primers should be 60 or more bases long. The 5′-end of each primer should contain 40–45 bases of perfect homology to the target site. At the 3′-ends of the primers, 18–25 bases are complementary to and enable amplification of sequences encoding the epitope tag and the selectable marker from the plasmid (*see* also **Fig. 2**).

We find that GFP fluorescence can often be optimized by varying the length of the linker region between the target gene and the GFP molecule. For C-terminal tagging, this is accomplished by introducing sequence DNA encoding extra amino acids between the 40 bases of DNA homologous to the target gene and the 20 bases corresponding to the plasmid template in the forward primer. We suggest starting with five alanines.

3.2.2. Amplification of Insertion Cassette from Tagging Vector

1. The cassette is amplified using standard PCR conditions: 30 µL PCR buffer (3.3× stock, contains no Mg^{2+}), 8 µL $Mg(OAc)_2$ (25 mM stock) (*see* **Note 5**), 8 µL dNTP mix (2.5 mM ea. dNTP), 1 µL 2 × 10^{-5} M stock forward primer (*see* **Note 6**), 1 µL 2 × 10^{-5} M stock reverse primer, 1 µL (~50 ng/µL vector template stock, 1 µL r*Tth* DNA Polymerase and 50 µL dH_2O.

2. Thermocycler conditions: 1 cycle of 94°C for 5 min; 30 cycles of: 94°C for 1 min, 55°C for 1 min and 72°C (2–4 min, about 1 min per kb product length); and 1 cycle of 72°C for 10 min.

Eight to ten 100-μL PCR reactions should be pooled to obtain DNA sufficient for a single yeast transformation (1 μg of DNA per 1×10^8 cells). Purify the PCR product by ethanol precipitation and 1% agarose gel electrophoresis to remove contaminants and undesired products. After cutting out the band containing the desired PCR product, isolate and concentrate it using a gel extraction kit.

3.2.3. Transformation of Yeast with Amplified Insertion Cassette

Transform the purified PCR product into the target strain as described in **Subheading 3.1**. For transformations using auxotrophic markers, a single reaction typically yields 10–20 transformed clones for further characterization. For transformations using drug resistance markers (e.g., kanMX6), plate all cells from a single transformation on a nonselective (YPD) plate. Incubate for 2–3 days and replica-plate onto a plate containing the drug (e.g., 200 μg/L G418 for kanMX6; *see* **Note 7**). Incubate 2–3 days, and replica-plate onto a fresh plate containing the drug. Colonies can be picked from this plate for further analysis.

3.2.4. PCR Screening, Protein Expression, and Functional Analysis

PCR is used to validate insertion of the tag into the target locus. This analysis uses genomic DNA isolated from transformants as a template and a pair of primers (20–25 bases) that hybridize on both sides of the insertion. Optional PCR can be carried out using a third primer that anneals to a region within the integration cassette. Cells with correct tag integration at the target locus should be validated using Western blots to analyze protein expression. Finally, tagged constructs should be characterized for functionality given knowledge about the gene of interest. For example, if an inserted tag compromises function of a nonessential gene, then the tagged strain may show a phenotype resembling that of cells mutated in that gene.

3.2.5. Marker Excision by Cre Recombinase

The tagging vectors were first developed for C-terminal tag insertion. Similar vectors for one-step N-terminal tagging insert the selection marker and tag into the 5′ end of genes of interest. However, because the selection marker in these cassettes separates the tagged gene from its promoter, the tagged gene is expressed from a nonendogenous promoter included in the tagging cassette. These tagging vectors are used for regulated expression or overexpression studies. Until recently, tagging vectors were not available that could both (1) insert tags in the N-terminus or internal regions of proteins, and (2) express tagged proteins from their endogenous promoter (i.e., at wild-type levels).

The pOM family of tagging vectors, which were designed for removal of the selection marker after tag insertion, solved this problem (*see* **Fig. 2b**). In this set of vectors, the selection marker is flanked by loxP sites, and can be removed using bacteriophage Cre recombinase *(6)*. Insertion and validation of the tagging cassette is carried out as described above. Yeast bearing integrated tags are then transformed with a plasmid that encodes Cre recombinase under control of the galactose-inducible promoter. To induce Cre expression, cells are grown in liquid media selecting for the plasmid, incubated for 4 h in media containing 1% raffinose + 1% galactose, and plated on nonselective (YPD) media. Colonies are then screened for loss of the tagging cassette marker by replica-plating or patching on selective plates. Further characterization is performed by PCR, Western blot analysis and visualization, as described above. We use pSH47, which expresses Cre from a *GAL* promoter and contains the *URA3* selectable marker. We prefer *URA3* as a marker because it allows curing cells of the plasmid by counter-selection on 5-fluoroorotic acid (5-FOA) plates after marker excision.

3.3. Staining Yeast Mitochondria with Vital Dyes

1. Grow yeast cells to mid-log phase in liquid media.
2. Concentrate cells by centrifugation at ~13,000 × *g* for 5 s (*see* **Note 8**).
3. Wash cell pellet in 1× PBS or growth media. While PBS has lower background fluorescence, it should be used only if cells will be observed for less than 30 min.
4. Resuspend cells to ~2 × 10^8 cells/mL in 1× PBS or growth media (*see* **Note 9**).
5. Add appropriate volume of dye stock solution and mix thoroughly (*see* **Note 10**).
6. Incubate in the dark.
7. Pipette gently to resuspend cells (*see* **Note 11**).
8. Mount cells for short-term or long-term observation as described in **Subheading 3.4**.

3.4. Visualization of FP-Tagged Proteins in Living Cells

3.4.1. Equipment for Wide-Field Deconvolution

Selection of an appropriate microscope and camera to detect fluorescence is essential for imaging living or fixed yeast cells. The small size of yeast cells requires a microscope equipped with a high-magnification objective lens and a high-resolution camera. Phototoxicity and photobleaching can be greatly reduced by using a camera that supports low-intensity illumination and short exposure times. Data processing speed and memory capacity of the computer linked to the digital camera can affect imaging speed and therefore should be tested thoroughly before committing to a particular imaging system.

An imaging system that works well for visualizing structures in yeast is based on an upright epifluorescence microscope equipped with a Plan-Apochromat 100×, 1.4 NA objective lens, and a cooled CCD camera. A shutter driver is synchronized with the camera shutter to control excitation light from the 100 W mercury arc lamp. A software package is used to control the camera and shutter, capture images at defined time intervals, and export them to TIFF format for further analysis. Filter wheels or beam splitters are used for automated two-color imaging. We control sample temperature using a heating collar on the objective lens. Finally, for z-axis control, we use stepper motors coupled to the microscope fine focus drive, or piezoelectric focus motors on the objective lens.

3.4.2. Equipment for Two-Color Time-Lapse Imaging of Cytoskeleton–Membrane Interactions

Monochromatic cameras offer greater dynamic range, resolution, and speed of detection compared to color cameras. Therefore, for imaging multiple fluorophores, each fluorophore should be imaged independently to generate a grayscale image. Color is then applied to grayscale images (e.g., green for EGFP and red for mCherry) and the resulting pseudocolored images are superimposed. Several optical devices have been developed to rapidly alter excitation or emission light, either through the use of filter changers or rapid switching of excitation light from the light source for sequential time lapse imaging of multiple fluorophores. The beam splitter can be used for simultaneous multicolor imaging. Each accessory comes with inherent advantages and disadvantages, which are discussed below.

Filter wheels can be inserted into the incident and emitted light paths and produce rapid switching of excitation and emission filters for multicolor time-lapse imaging. For example, for imaging of actin cables using Abp140p-GFP and actin patches using Abp1p-DsRed, the sample is illuminated using a broad-spectrum light source (e.g., a mercury or xenon arc lamp) and an image is taken first with the green excitation and emission filter sets, and then with the red. Since commercially available filter wheels hold up to five filters and there are at least six different spectral classes of FPs, this approach can be used for imaging two or more fluorophores. However, imaging with filter wheels is sequential, not simultaneous. Moreover, the time interval between acquisition of each fluorophore image may be too long for imaging highly dynamic events. The time for switching between filter sets using filter wheels can be as low as 35 ms. However, rotation of the filter wheel generates vibrations that persist for 100–150 ms and compromise the resolution of acquired images. Therefore, the actual time interval between channels in imaging with filter wheel switching is ~200 ms.

An alternative approach to switching excitation light is through the light source. New technologies for illumination of

samples using narrow spectrum, high intensity light-emitting diodes (LEDs) have been developed. This illuminator contains four LEDs that match the bandwidth of many commonly used FPs, and are individually controlled by electrical current. Light from each LED is channeled into the microscope using fiber optics. Excitation light can be changed rapidly, without any mechanical devices.

For simultaneous imaging of two fluorophores, we use a dual band-pass excitation filter in the excitation light path, and the beamsplitter device in the emitted light path. The beamsplitter utilizes a single beamsplitter to split the light emitted from the sample into two independent beams. After passing through independent emission filters, each of these emission channels is projected onto half of the CCD array at exactly the same point in time. Thus, imaging is simultaneous. Moreover, variants of the original beamsplitter can be used for imaging up to four fluorophores.

Two potential drawbacks of this imaging approach are resolution and throughput. Since only half of the imaging surface of the camera's CCD chip is used for each fluorophore, there may be a reduction in image resolution. However, for budding yeast cells, which occupy a small fraction of the acquired image, this is not an issue. On the other hand, as a result of decreased throughput, the image acquisition times for each individual fluorophore are longer using this imaging approach compared to the filter wheel approach described above. First, the throughput of the excitation light for each fluorophore from the dual-band pass filter is less than that of two single band-pass filters. Moreover, the beamsplitter physically extends the light path, which reduces the strength of emitted light that reaches the camera. That said, since fluorophore imaging is simultaneous, the time interval between image acquisitions can be shorter using this method compared to the filter wheel approach described above.

3.4.3. Short-Term Imaging Conditions for Actin Cables

Short-term visualization is carried out by adding cells directly to a glass microscope slide and imaging immediately for a period of no longer than 10 min. After 10 min, cells experience a significant decrease in viability and the use of a growth chamber becomes necessary. A protocol for the preparation of yeast for short-term visualization is described below, followed by a protocol useful for those visualizations requiring longer imaging periods. All manipulations should be performed rapidly, as the Abp140p-GFP signal fades after 4 min. Since cells are only maintained on microscope slides for 4 min, we do not use agarose pads for live-cell actin cable imaging. **Figure 3** shows still frames of a time-lapse series of actin cable dynamics using Abp140p-GFP.

1. Grow 5 mL cultures of *Abp140p*-GFP-tagged strains overnight in lactate medium at RT (*see* **Note 12**).

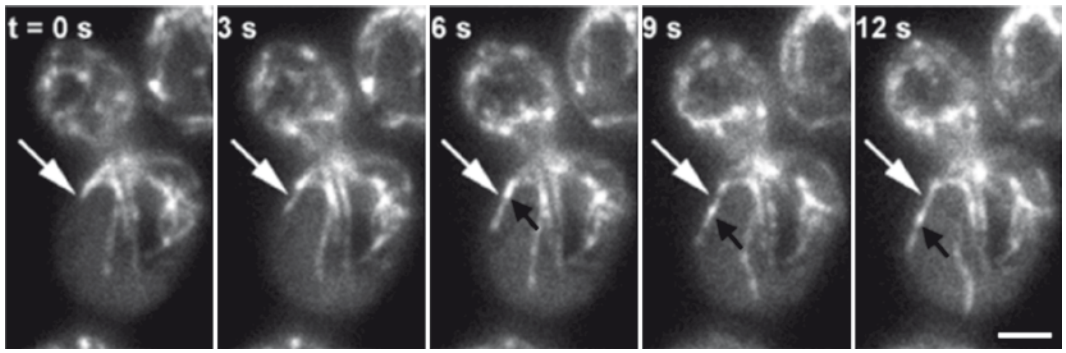

Fig. 3. Visualization of actin cable dynamics in living yeast cells using Abp140p-GFP.

2. In the morning, cultures are diluted to log phase (1:20 dilution) and allowed to recover for 2 h at RT.
3. Once log phase is achieved, remove 200 µL of culture, and concentrate cells by centrifugation in a microfuge for ~4 s (*see* **Note 13**).
4. Remove ~188 µL of medium, making sure not to disturb the pellet. Vary this amount depending on pellet size.
5. Resuspend the pellet in residual medium.
6. Transfer ~2 µL of the cell suspension to a microscope slide, and apply a 1.0 mm thick cover slip (*see* **Note 14**). Avoid creating bubbles between slide and cover slip.
7. Acquire images. For illumination from a high-intensity mercury arc lamp, we typically use 350 ms exposures (*see* **Note 15**) over a total of 20 s and 1 × 1 binning.

3.4.4. Long-Term Imaging

The growth chamber described below supports cell growth at wild-type levels for up to 5 h. The growth chamber also immobilizes cells in low-melting agarose, reducing cellular movement that can decrease image resolution. Finally, the chamber has minimal autofluorescence and remains transparent and thin enough for observation with oil-immersion lenses. For time-sensitive imaging trials, such as those involving the addition and removal of dyes or drugs, note that it takes roughly 5 min to make an agarose bed **(Fig. 4)**.

1. Grow yeast cells to mid-log phase in liquid medium. Concentrate cells to appropriate density for imaging, as needed.
2. Melt an aliquot of agarose bed material in a boiling water bath (ca. 2 min).
3. Pipet 35 µL of agarose bed material onto a glass microscope slide. Cool slightly (5 s).
4. Place a second microscope slide on top of agarose, applying light pressure to distribute the agarose bed until it is the size of a standard cover slip.
5. Let bed harden between microscope slides (ca. 2 min).

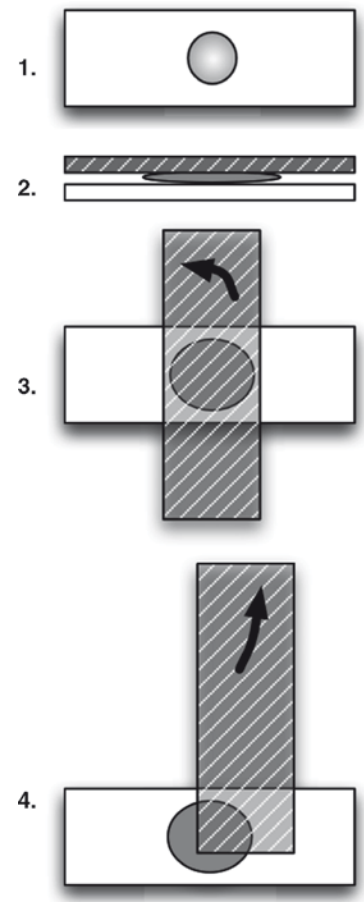

Fig. 4. Preparation of agarose bed for long-term live-cell imaging. (1) 35 μL of agarose bed material on a microscope slide. (2) Side view of agarose sandwiched between two microscope slides. (3–4) Rotation and removal of top slide.

6. Gently remove top slide by rotating the slide 90° and then sliding it past bottom slide.
7. Pipet 1.5 μL of imaging sample onto surface of the agarose bed (*see* **Note 16**).
8. Cover with a 22 × 22 mm cover slip and seal with VALAP. (To seal with VALAP, heat metal spatula in flame, dip into solid VALAP, and drag spatula along edges of cover slip.)

3.5. Functional Characterization of Targeted FPs

3.5.1. Characterization of FP-Tagged Cytoskeletal Proteins

When generating FP-tagged proteins it is imperative to validate each tagged protein to ensure that activity is not compromised. In order to illustrate steps for proper validation, we discuss our analysis of the use of Abp140p-GFP to visualize actin cables in budding yeast.

Transformed cells were fixed and screened for the presence of green actin cables and for colocalization of Abp140p-GFP with

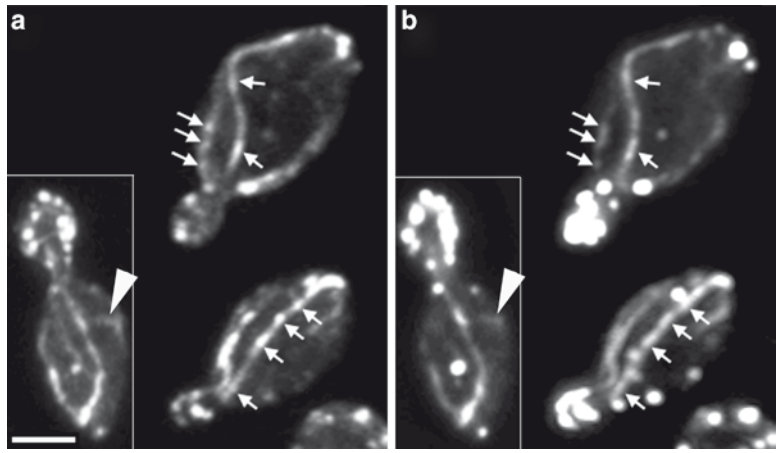

Fig. 5. Co-localization of Abp140p-GFP (*left*) and rhodamine phalloidin-labeled actin cables (*right*).

rhodamine-phalloidin-labeled actin cables (**Fig. 5**). Please refer to the chapter by Swayne et al. in this volume for the method for rhodamine-phalloidin staining. Various colonies from the transformation were screened, as some strains exhibit a brighter signal. Colonies were also tested for any morphological or growth rate changes at elevated temperatures compared to the untagged strain. Finally, effects on the underlying cell machinery were examined. The GFP-tagged Abp140p exhibited no obvious effects on actin cable and patch morphology or dynamics.

3.5.2. Characterization of Mitochondria-Targeted FPs

Targeted FPs must be checked for toxicity, localization, and effect on mitochondrial morphology and function. Mislocalization of FP fusion markers may occur because targeting information is masked or insertion of the fusion protein into membranes is inhibited. For example, fusion proteins consisting of GFP fused to the C terminus of *QRC1* (subunit 6 of the cytochrome bc_1 complex) or to porin localize to the cytosol *(7)*. Localization of FP fusion proteins may be assessed by visual inspection of the FP in cells in which mitochondria are counterstained using vital dyes, or by biochemical methods for subcellular and submitochondrial fractionation. Possible effects of fusion proteins on mitochondrial morphology or respiratory activity can be assessed by visual inspection of mitochondria in fixed or living cells and by analysis of cell growth and growth rates on nonfermentable carbon sources.

3.5.3. Optimizing Imaging Conditions and Preventing Toxicity

During live-cell imaging, photons react with cellular molecules to produce free radicals and reactive oxygen species. Cell health and viability can suffer as a result. We use the following specific criteria to confirm that our imaging conditions are not harmful to organelle and cytoskeletal function:

1. Intact cytoskeletal and mitochondrial structure. Intense or long excitation can cause cleavage or fragmentation.
2. Dynamics. Behavior of photodamaged mitochondria and cytoskeletal components has not been fully investigated; however, photodamage should be suspected if mitochondria or cytoskeletal elements show altered velocity of movement in wild-type cells.
3. If potential-sensitive dyes are used: maintenance of mitochondrial membrane potential (dye retention) throughout the imaging period.

If phototoxicity or photobleaching occurs, the following techniques (in order of preference) should be tried to reduce harmful light exposure:

1. Reduce excitation intensity (e.g., with a neutral density filter). Generally, a longer exposure time at lower intensity gives a comparable quality image with less photodamage.
2. Reduce exposure time.
3. Increase time interval and/or z sectioning interval.

To increase signal-to-noise ratio without increasing light exposure:

1. Apply binning in the camera (if necessary, preserve spatial resolution by adding a projection tube before the camera).
2. Increase gain in the camera.
3. If these techniques fail, consider trying alternative filter sets with higher throughput: either a broader spectral window or more efficient coating processes.

3.6. Analysis of Fluorescence Area and Intensity

Quantitative fluorescence imaging rests on two assumptions: first, that emitted fluorescence is proportional to the number of fluorescent molecules present; second, that recorded pixel intensities in the image are proportional to the amount of light emitted by the sample. Under well-controlled conditions, these assumptions hold true with sufficient precision to measure many biologically interesting parameters.

The methods described here employ ImageJ *(8)*, which is the most widely accessible image analysis program and is the tool of choice in our own laboratory. However, the same functions are available in most commercially available software packages for image analysis and processing.

3.6.1. Controlling Probe and Imaging Conditions

With many variables complicating the linearity of both fluorescence emission and pixel intensities, absolutely quantitative fluorescence imaging is a serious challenge *(9)*. However, with proper controls and validation, relative changes in fluorescence intensity and area can be powerful tools for hypothesis testing.

The minimum variables that must be controlled in any fluorescence imaging experiment where intensities are compared include the following:

1. Probe concentration and age (if an exogenous probe is used).
2. Sample age (unless photobleaching is known to be negligible).
3. Objective lens.
4. Illumination intensity (including filter set, aperture settings, alignment).
5. Camera model, binning, exposure, gain, offset, bit depth (for digital cameras).
6. Pinhole size, detector gain, amplifier gain, averaging, scan zoom, scan resolution, bit depth, scan speed (for confocal imaging).

Wherever possible the experimental design should be validated by positive and negative controls. This will ensure that the sensitivity and consistency of the quantitation are sufficient to test the hypothesis.

3.6.2. Measuring Concentration from Fluorescence Intensity

Local fluorescence intensity, measured as mean intensity of pixel values in a sub-region of an image, is a useful indicator of probe density or concentration. In cytoskeletal research the fluorescence intensity could be used for example to indicate local concentrations of cytoskeletal monomers, filaments or filament-binding proteins.

The following procedure describes how to use ImageJ to measure the mean fluorescence of a sub-region (Region of Interest, ROI) of an image.

1. From the Analyze menu, choose Set Measurements. Check the following boxes: Mean gray value, Display label.
2. Define the ROI you wish to measure. ImageJ allows rectangular, polygonal, circular, oval, or freehand ROIs. Use display zoom (+ to increase, – to decrease magnification) to make it easier to outline the desired area.
3. From the Analyze menu, choose Measure (or press M).
4. Define an ROI in the background (outside the cells) and measure it.
5. Copy or save the measurements that appear in the Results window. The data format is tab-delimited text, which is readable by spreadsheet or graphing software.
6. When comparing mean fluorescence intensity values, first subtract the background from each mean value.

3.6.3. Measuring Total Fluorescence

The mean fluorescence intensity gives an approximation of the concentration of fluorescent probe in a given area. For areas of similar size, the mean fluorescence intensity is also proportional to the total number of fluorescent molecules present. However, when comparing fluorescence within areas of different sizes, one needs a more accurate representation of the total fluorescence (e.g., comparing the amount of phalloidin-labeled F-actin in

yeast buds of different sizes). The same number of molecules that produces bright average intensity in a small bud can spread out in a large bud, leading to a lower mean intensity. In this situation, the best indication of the total amount of fluorescent probe is the integrated density or integrated intensity. This is the sum of all pixel intensities in the area. It can be conveniently calculated by multiplying the area of the region by the mean intensity.

1. From the Analyze menu, choose Set Measurements. Check the following boxes: Area, Mean Gray Value, Integrated Density, Display Label.
2. Define the ROI you wish to measure. ImageJ allows rectangular, polygonal, circular, oval, or freehand ROIs. Use display zoom (+ to increase, – to decrease magnification) to make it easier to outline the desired area.
3. From the Analyze menu, choose Measure (or press M).
4. Define an ROI in the background (outside the cells) and measure it.
5. Copy or save the measurements that appear in the Results window. The data format is tab-delimited text, which is readable by spreadsheet or graphing software.
6. When comparing integrated density values, first subtract the background integrated density from the integrated density of each measured ROI. To find the background integrated intensity for an ROI, multiply the background mean gray value by the area of the measured ROI. Note that this correction value will vary with the area of the measured ROI.

3.6.4. Measuring Labeled Area and Volume

The size of objects can be estimated by fluorescence imaging. To define the area occupied by a labeled structure, a threshold must be defined to differentiate labeled from unlabeled structures. Minimizing nonspecific background during sample preparation, and maximizing signal-to-noise ratio during image acquisition, will help in defining a clear threshold. In cases where structures may be superimposed and cannot be resolved by fluorescence imaging, as in the case of actin cables or aggregated mitochondria, the integrated density can be more accurate than area in indicating the total amount of a labeled structure.

If optical sectioning techniques are available, such as digital deconvolution or confocal microscopy, the volume of structures can be calculated using a Cavalieri-like method. In this approach, the cross-sectional areas of the structure are summed over a z-series of images collected at successive focal planes. To determine absolute volume, the z-series interval must match the z resolution of the technique. However, if only relative values are needed, the intervals need not match, but they must be the same for all analyzed images.

Here we describe the procedure for measuring labeled volume and integrated intensity in a z-series, which is an extension of measuring area and integrated intensity in a single thresholded image.

1. From the Analyze menu, choose Set Measurements. Check the following boxes: Area, Mean Gray Value, Integrated Density, Display Label, Limit To Threshold.
2. From the Image menu, choose Adjust and Threshold. Drag the lower slider to the maximum value. Drag the upper slider so that the pseudocolored red areas encompass all of the labeled structures and none of the background.
3. Define the ROI you wish to measure. ImageJ allows rectangular, polygonal, circular, oval, or freehand ROIs. Use display zoom (+ to increase, – to decrease magnification) to make it easier to outline the desired area.
4. Add the ROI to the ROI Manager: press the "t" key, or from the Analyze menu, choose Tools, ROI Manager, and then click Add.
5. In the ROI Manager window, click the ROI name, then More >>, then MultiMeasure. Check both boxes and click OK.
6. Copy or save the measurements that appear in the Results window. The data format is tab-delimited text, which is readable by spreadsheet (e.g., Microsoft Excel) or graphing software.
7. To estimate volume, sum the measured areas. To estimate total probe amount, sum the integrated densities.

3.7. Analysis of Intracellular Movement

The velocity of a motile structure can be measured by recording the position of the object at successive timepoints in a time-lapse series. For punctate structures, the centroid can be tracked. For structures with elongated, irregular or dynamic shapes, a landmark on the object of interest can be defined as a reference point for velocity measurements. For example, since Abp140p-GFP labeling along the length of actin cables is not uniform, morphologically distinguishable accumulations of Abp140p-GFP on actin cables are used as landmarks, or fiduciary marks. In the case of mitochondria, labeling is uniform, but the leading tip of the mitochondrion constitutes an identifiable point that can be tracked.

Typically, tracking analysis is used to collect motility parameters such as velocity, distance traveled, frequency of movement, persistence of movement, and direction of movement. Tracking is most easily performed in 2D series (a single focal plane), but it can also be performed in three spatial dimensions. Motility histograms are generated which show the distribution of motility parameters (such as velocity and frequency of movement) among the population of mitochondria. These histograms can be used to identify subpopulations of motile structures with different motility behaviors.

The following is a procedure for direct tracking of objects using ImageJ.

1. From the Analyze menu, choose Set Measurements. Check the following boxes: Display Label, Centroid.
2. By viewing the time-lapse series, identify structures that meet criteria for motility: for example, linear movement for a minimum of two successive time-lapse intervals.
3. Reference points for tracking can be identified manually or by calculating the centroid of a complex structure. Use display zoom (+ to increase, – to decrease magnification) to make it easier to outline the desired area.

   For centroid marking: Display the first frame where the motility occurs. Use the freehand ROI tool to outline the motile structure. From the Analyze menu, select Measure (or press "m") to calculate the centroid position.

   For manual marking:
   (a) Select the Point Selection (crosshair) tool from the ImageJ toolbar.
   (b) Double-click the tool icon to set parameters.
   - Mark width: a reference mark of the given width will be drawn on the image at each measured position. Set to 0 if you do not wish to modify the image series. If you prefer to see the marks, save a copy of the raw image series first.
   - Check Auto-Measure and Auto-Next Slice. The position of each marked point will be automatically logged in the Results window, and the window will automatically display the next slice.
   - Leave other boxes unchecked.

   (c) Display the first frame where the motility occurs. Click the structure with the crosshair tool.
4. Continue marking the motile structure for the duration of observable movement. Repeat for each motile object in the series.
5. Copy or save the measurements that appear in the Results window. The data format is tab-delimited text, which is readable by spreadsheet (e.g., Microsoft Excel) or graphing software.
6. Calculate distance traveled between each set of successive timepoints t_1 and t_2 using the Pythagorean Theorem, where d is distance and the positions are (x_1,y_1) and (x_2,y_2) respectively:

$$d_{(t_1,t_2)} = \sqrt{(x_1 - x_2)^2 + (y_1 - y_2)^2}$$

Calculate velocity as distance traveled divided by time elapsed. To find mean velocity, calculate the average of all incremental velocities.

4. Notes

1. SC and lactate media are suggested choices.
2. 200 µL aliquots are recommended to avoid repeated boiling.
3. The lithium acetate wash should be as brief as possible, since this reagent is toxic to cells.
4. When plating <100 µL, add 50–100 µL sterile water to facilitate spreading.
5. For different plasmid templates, we suggest first titrating the $Mg(OAc)_2$ concentration; for example, try four reactions with final $Mg(OAc)_2$ concentrations of 0.5 mM, 1.0 mM, 2.0 mM, and 3.0 mM.
6. To assure PCR specificity, for new primers we suggest three control reactions: (a) no primers in the reaction, (b) forward primer only, and (c) reverse primer only. These can be omitted in future PCR runs if nonspecific reactions do not occur.
7. Synthetic media containing ammonium sulfate interferes with G418 activity. To make drop-out plates containing G418, use SE (synthetic media with glutamate) rather than SC.
8. Extended centrifugation can cause breakage of tubular mitochondria.
9. A culture with OD_{600} = 1.0 contains ~10^7 cells/mL.
10. The dye concentrations suggested in **Table** 7 should be considered only as a starting point. Specificity is highly dependent on concentration and mitochondrial membrane potential. Titration of dye concentration and incubation times should be performed when working with a new strain or mitochondrial mutant. In general, dye concentration should be kept as low as possible because excessive accumulation of dye in mitochondria results in organelle swelling and respiratory defects.
11. Washing cells is generally not necessary, as the fluorescence of most vital dyes is low until the dye binds to cell lipids. If high background is observed, cells can be washed once in media.
12. For this step, it is helpful to set up a microfuge beside the microscope.
13. Growing and imaging cells in lactate media empirically yields brighter fluorescence of actin cables as opposed to imaging in YPD, which exhibits increased background fluorescence. Other groups have reported using three tandem repeats of GFP (3xGFP) to enhance fluorescence output *(10)*. However, adding increasingly larger tags to endogenous proteins requires additional care in characterizing protein function and

Table 7
Conditions for staining yeast mitochondria with vital dyes

		Staining conditions	
Dye	**[Stock][a]**	**[Dye]**	**Incubation**
$DiOC_6$ *(4)*[b]	10 mg/mL in ethanol	10–100 ng/mL	15–30 min RT
DASPMI[c]	1 mg/mL in ethanol	10–100 μg/mL	30 min RT
Rhodamine 123[d]	10 mg/mL in DMSO[e]	5–10 μg/mL	15–30 min RT
MitoTracker[f]	1 mM in DMSO[e]	25–500 nM	15–30 min RT
DAPI	1 mg/mL in H_2O	0.1 μg/mL	15 min RT

[a]All stock solutions should be stored in the dark
[b] *(51)*
[c] *(52)*
[d] *(53)*; Broad emission range; not recommended for green/red double-label studies
[e]DMSO can be toxic and inhibits partitioning of the dye into the aqueous environment of the cells. If DMSO is the solvent, use a stock concentration that is at least 100×
[f] *(54)*

overall cell phenotype. In addition, some media, such as YPD, autofluoresce. Therefore, we recommend growing cultures for visualization in either SC dropout media, or in lactate media.

14. The volume used is important, since excess volume can cause cells to float, and too little volume can affect cell structure and results in uneven spreading.

15. We employ several imaging techniques in order to minimize photobleaching, optimize acquisition time, and increase resolution. It has been previously reported that photobleaching can be reduced if photons are delivered with high intensity for a shorter time, rather than low intensity for a longer time *(11)*. For this reason, we acquire images using a high-intensity mercury arc lamp at 350 ms exposures over a total of 20 s. Furthermore, actin cables are imaged on a single focal plane in order to decrease acquisition time and allow for more accurate tracking of actin cable dynamics. Use of a cooled CCD camera (Hamamatsu) enhances resolution of actin cables, due to its high sensitivity in the visible light region and low noise at high frame rates, as opposed to other commercially available CCD cameras.

16. If cells are not immobilized, decrease the volume of sample added to agarose bed. Additionally, the water content of the agarose bed can be adjusted by letting solidified bed stand, uncovered, for a few seconds before adding sample.

References

1. Doyle, T. and Botstein, D. (1996) Movement of yeast cortical actin cytoskeleton visualized in vivo. *Proc Natl Acad Sci U S A* **93**: 3886–3891
2. Yang, H.C. and Pon, L.A. (2002) Actin cable dynamics in budding yeast. *Proc Natl Acad Sci U S A* **99**: 751–756
3. Koehler, C.M. (2004) New developments in mitochondrial assembly. *Annu Rev Cell Dev Biol* **20**: 309–335
4. Riezman, H., et al. (1983) Import of proteins into mitochondria: a 70 kilodalton outer membrane protein with a large carboxy-terminal deletion is still transported to the outer membrane. *EMBO J* **2**: 2161–2168
5. Gietz, R.D., et al. (1995) Studies on the transformation of intact yeast cells by the LiAc/SS-DNA/PEG procedure. *Yeast* **11**: 355–360
6. Gueldener, U., et al. (2002) A second set of loxP marker cassettes for Cre-mediated multiple gene knockouts in budding yeast. *Nucleic Acids Res* **30**: e23
7. Okamoto, K., Perlman, P.S., and Butow, R.A. (2001) Targeting of green fluorescent protein to mitochondria. *Methods Cell Biol* **65**: 277–283
8. Abramoff, M.D., Magelhaes, P.J., and Ram, S.J. (2004) Image processing with imageJ. *Biophotonics International* **11**: 36–42
9. Pawley, J. (2000) The 39 steps: a cautionary tale of quantitative 3-D fluorescence microscopy. *Biotechniques* **28**: 884–886, 888
10. Buttery, S.M., Yoshida, S., and Pellman, D. (2007) Yeast formins Bni1 and Bnr1 utilize different modes of cortical interaction during the assembly of actin cables. *Mol Biol Cell* **18**: 1826–1838
11. Vigers, G.P., Coue, M., and McIntosh, J.R. (1988) Fluorescent microtubules break up under illumination. *J Cell Biol* **107**: 1011–1024
12. Madania, A., et al. (1999) The *Saccharomyces cerevisiae* homologue of human Wiskott-Aldrich syndrome protein Las17p interacts with the Arp2/3 complex. *Mol Biol Cell* **10**: 3521–3538
13. Kaksonen, M., Sun, Y., and Drubin, D.G. (2003) A pathway for association of receptors, adaptors, and actin during endocytic internalization. *Cell* **115**: 475–487
14. Warren, D.T., et al. (2002) Sla1p couples the yeast endocytic machinery to proteins regulating actin dynamics. *J Cell Sci* **115**: 1703–1715
15. Miliaras, N.B., Park, J.H., and Wendland, B. (2004) The function of the endocytic scaffold protein Pan1p depends on multiple domains. *Traffic.* **5**: 963–978
16. Morishita, M. and Engebrecht, J. (2005) End3p-mediated endocytosis is required for spore wall formation in *Saccharomyces cerevisiae*. *Genetics* **170**: 1561–1574
17. Sun, Y., et al. (2007) PtdIns(4,5)P2 turnover is required for multiple stages during clathrin- and actin-dependent endocytic internalization. *J Cell Biol* **177**: 355–367
18. Sun, Y., Martin, A.C., and Drubin, D.G. (2006) Endocytic internalization in budding yeast requires coordinated actin nucleation and myosin motor activity. *Dev Cell.* **11**: 33–46
19. Vaduva, G., Martin, N.C., and Hopper, A.K. (1997) Actin-binding verprolin is a polarity development protein required for the morphogenesis and function of the yeast actin cytoskeleton. *J Cell Biol* **139**: 1821–1833
20. Evangelista, M., et al. (2000) A role for myosin-I in actin assembly through interactions with Vrp1p, Bee1p, and the Arp2/3 complex. *J Cell Biol* **148**: 353–362
21. Jonsdottir, G.A. and Li, R. (2004) Dynamics of yeast myosin I: evidence for a possible role in scission of endocytic vesicles. *Curr Biol* **14**: 1604–1609
22. Sekiya-Kawasaki, M., et al. (2003) Dynamic phosphoregulation of the cortical actin cytoskeleton and endocytic machinery revealed by real-time chemical genetic analysis. *J Cell Biol* **162**: 765–772
23. Huckaba, T.M., et al. (2004) Live cell imaging of the assembly, disassembly, and actin cable-dependent movement of endosomes and actin patches in the budding yeast, *Saccharomyces cerevisiae*. *J Cell Biol* **167**: 519–530
24. Boldogh, I.R., et al. (2001) Arp2/3 complex and actin dynamics are required for actin-based mitochondrial motility in yeast. *Proc Natl Acad Sci U S A* **98**: 3162–3167

25. Smith, M.G., Swamy, S.R., and Pon, L.A. (2001) The life cycle of actin patches in mating yeast. *J Cell Sci* **114**: 1505–1513
26. Karpova, T.S., et al. (2000) Role of actin and Myo2p in polarized secretion and growth of *Saccharomyces cerevisiae*. *Mol Biol Cell* **11**: 1727–1737
27. Waddle, J.A., et al. (1996) Movement of cortical actin patches in yeast. *J Cell Biol* **132**: 861–870
28. Winder, S.J., Jess, T., and Ayscough, K.R. (2003) SCP1 encodes an actin-bundling protein in yeast. *Biochem J* **375**: 287–295
29. Okreglak, V. and Drubin, D.G. (2007) Cofilin recruitment and function during actin-mediated endocytosis dictated by actin nucleotide state. *J Cell Biol* **178**: 1251–1264
30. Riedl, J., et al. (2008) Lifeact: a versatile marker to visualize F-actin. *Nat Methods* **5**: 605–607
31. Straight, A.F., et al. (1997) Mitosis in living budding yeast: anaphase A but no metaphase plate. *Science* **277**: 574–578
32. Carminati, J.L. and Stearns, T. (1997) Microtubules orient the mitotic spindle in yeast through dynein-dependent interactions with the cell cortex. *J Cell Biol* **138**: 629–641
33. Khmelinskii, A., et al. (2007) Cdc14-regulated midzone assembly controls anaphase B. *J Cell Biol* **177**: 981–993
34. Carvalho, P., et al. (2004) Cell cycle control of kinesin-mediated transport of Bik1 (CLIP-170) regulates microtubule stability and dynein activation. *Dev Cell* **6**: 815–829
35. Shaw, S.L., et al. (1997) Imaging green fluorescent protein fusion proteins in *Saccharomyces cerevisiae*. *Curr Biol* **7**: 701–704
36. Zeng, X., et al. (1999) Slk19p is a centromere protein that functions to stabilize mitotic spindles. *J Cell Biol* **146**: 415–425
37. Wang, P.J. and Huffaker, T.C. (1997) Stu2p: A microtubule-binding protein that is an essential component of the yeast spindle pole body. *J Cell Biol* **139**: 1271–1280
38. Kahana, J.A., Schnapp, B.J., and Silver, P.A. (1995) Kinetics of spindle pole body separation in budding yeast. *Proc Natl Acad Sci U S A* **92**: 9707–9711
39. Marschall, L.G., et al. (1996) Analysis of Tub4p, a yeast gamma-tubulin-like protein: implications for microtubule-organizing center function. *J Cell Biol* **134**: 443–454
40. Jaspersen, S.L., et al. (2004) Cdc28/Cdk1 regulates spindle pole body duplication through phosphorylation of Spc42 and Mps1. *Dev Cell* **7**: 263–274
41. Adams, I.R. and Kilmartin, J.V. (1999) Localization of core spindle pole body (SPB) components during SPB duplication in *Saccharomyces cerevisiae*. *J Cell Biol* **145**: 809–823
42. Fehrenbacher, K.L., et al. (2004) Live cell imaging of mitochondrial movement along actin cables in budding yeast. *Curr Biol* **14**: 1996–2004
43. Okamoto, K., Perlman, P.S., and Butow, R.A. (1998) The sorting of mitochondrial DNA and mitochondrial proteins in zygotes: preferential transmission of mitochondrial DNA to the medial bud. *J Cell Biol* **142**: 613–623
44. Mozdy, A.D., McCaffery, J.M., and Shaw, J.M. (2000) Dnm1p GTPase-mediated mitochondrial fission is a multi-step process requiring the novel integral membrane component Fis1p. *J Cell Biol* **151**: 367–380
45. Shaner, N.C., Steinbach, P.A., and Tsien, R.Y. (2005) A guide to choosing fluorescent proteins. *Nat Methods* **2**: 905–909
46. Longtine, M.S., et al. (1998) Additional modules for versatile and economical PCR-based gene deletion and modification in *Saccharomyces cerevisiae*. *Yeast* **14**: 953–961
47. Rodrigues, F., et al. (2001) Red fluorescent protein (DsRed) as a reporter in *Saccharomyces cerevisiae*. *J Bacteriol* **183**: 3791–3794
48. Janke, C., et al. (2004) A versatile toolbox for PCR-based tagging of yeast genes: new fluorescent proteins, more markers and promoter substitution cassettes. *Yeast* **21**: 947–962
49. Sheff, M.A. and Thorn, K.S. (2004) Optimized cassettes for fluorescent protein tagging in *Saccharomyces cerevisiae*. *Yeast* **21**: 661–670
50. Gauss, R., et al. (2005) New modules for the repeated internal and N-terminal epitope tagging of genes in *Saccharomyces cerevisiae*. *Yeast* **22**: 1–12
51. Simon, V.R., Swayne, T.C., and Pon, L.A. (1995) Actin-dependent mitochondrial motility in mitotic yeast and cell-free systems: identification of a motor activity on the mitochondrial surface. *J Cell Biol* **130**: 345–354
52. McConnell, S.J., et al. (1990) Temperature-sensitive yeast mutants defective in mitochondrial inheritance. *J Cell Biol* **111**: 967–976
53. Skowronek, P., et al. (1990) Flow cytometry as a tool to discriminate respiratory-competent and respiratory-deficient yeast cells. *Curr Genet* **18**: 265–267
54. Nunnari, J., et al. (1997) Mitochondrial transmission during mating in *Saccharomyces cerevisiae* is determined by mitochondrial fusion and fission and the intramitochondrial

segregation of mitochondrial DNA. *Mol Biol Cell* **8**: 1233–1242

55. Nunnari, J., Wong, E.D., Meeusen, S., and Wagner, J.A. (2002) Studying the behavior of mitochondria. *Methods Enzymol* **351**: 381–393

56. Westermann, B. and Neupert, W. (2000) Mitochondria-targeted green fluorescent proteins: convenient tools for the study of organelle biogenesis in *Saccharomyces cerevisiae*. *Yeast* **16**: 1421–1427

Part II

Dynamics of Actin Filaments and Microtubules

Chapter 4

Jasplakinolide: An Actin-Specific Reagent that Promotes Actin Polymerization

Andreas Holzinger

Summary

Jasplakinolide, a cyclo-depsipeptide is a commonly used actin filament polymerizing and stabilizing drug. The substance has originally been isolated from a marine sponge, and can now be synthesized and has become commercially available. This, together with the benefit that jasplakinolide is membrane permeable has made it a commonly used tool in cell biology, when actin filament stabilization or polymerization has to be achieved. This may either be the case in studies on morphogenesis, motility, organelle movement, or when apoptosis has to be induced. Its use as a potent anticancer drug is discussed. The direct action on actin filaments may have further consequences in golgi body and membrane raft protein organization. In this chapter, the visualization of jasplaklinolide effects by different fluorescent and transmission electron microscopic methods is described. As competitive binding capacities of jasplakinolide and phalloidin make the detection of actin filaments by fluorescently labeled phalloidin problematic, alternatives are given here.

Key words: Actin filaments, Chondramides, Cytochalasins, Depsipeptide, Jasplakinolide, Latrunculin, Phalloidin

1. Introduction

Since this chapter *(1)* was published in the first edition of this book, a vast body of literature (nearly 350 citations in *PubMed*) on the use of jasplakinolide in cell biology has been added. This is mostly due to the fact that this substance is the only commercially available actin polymerizing drug. In contrast, substances with similar effects like chondramides *(2)*, remain underrepresented due to their limited availability. Given these facts it is worthwhile to write an update of the initial chapter, including an overview on the new literature and some additional protocols.

R.H. Gavin (ed.), *Cytoskeleton Methods and Protocols,* Methods in Molecular Biology, vol. 586
DOI 10.1007/978-1-60761-376-3_4,
© Humana Press, a part of Springer Science + Business Media, LLC 2009

The actin system is involved in different cellular processes like exo- and endocytosis, organelle motions and maintenance of organelle distribution, motility, cell division, and cytoplasmic streaming. Several substances are known to influence these processes by altering intracellular actin organization and have been used extensively for cell biological research *(3)*. Their mechanisms of action are mostly destructive on actin filaments (F-actin), either by inhibition of F-actin elongation as in the case of cytochalasins *(4)* or by interaction with actin monomers (G-actin) in order to avoid actin polymerization as described for latrunculins *(5)*. Actin stabilization is generated by another group; phalloidin is one of the best known members of it. The common feature of these actin stabilizing substances is a cyclic depsipeptide, which is a polymeric compound containing both, amino acids and hydroxy acids, joined by peptide and ester bounds *(3)*. Jasplakinolide also belongs to this group and in addition to stabilization, F-actin polymerizing capacities were described for this substance *(6–10)*. Moreover jasplakinolide has the valuable advantage of being membrane permeable *(11)*.

Originally jasplakinolide was isolated from the marine sponge *Jaspis* sp. collected at Fiji or the Palau islands *(12, 13)*. The sponge was authenticated as *Jaspis johnstoni (14)*, however, taxonomic difficulties were pointed out *(15)* and the compound can also be isolated form other sponge genera *(15, 16)*. Detailed procedures for jasplakinolide extraction can be found in *(17)*.

Different approaches were made to synthesize this substance *(18, 19)* or generate nonpeptide mimetics *(20)*, finally Jasplakinolide became commercially available from Molecular Probes in the late 1990s. An enantioselective total synthesis of (+)-jasplakinolide has been described recently *(21)*.

Chemically jasplakinolide is a cyclo-depsipeptide containing a tripeptide moiety linked to a polyketide chain *(12, 14)*, **(Fig. 1)**. Jasplakinolide is also called jaspamide *(13, 14, 22, 23)*, however, in the recent literature exploring this substance the name jasplakinolide is preferably used (e.g., *(6, 7, 9, 12, 24–30)*), occasionally abbreviated as JAS *(24, 31)*.

The biological activities of jasplakinolide are described as anthelminthic, antifungal, insecticidal, and selective antimicrobial *(12, 13, 32)*. Moreover, jasplakinolide has been reported to induce apoptosis *(25, 33–35)* or influences virus infection capacities *(36)*. The actin polymerizing and stabilizing capacities of jasplakinolide result in changes in membrane raft proteins *(37)* or the organization of the Golgi apparatus *(38, 39)*. The basis of the general cytotoxic effect of jasplakinolide *(6, 19, 40)* was found in the selective action on the actin cytoskeleton. Especially in vitro investigations have elucidated the actin polymerizing- and stabilizing capacities of jasplakinolide *(6, 10, 41)*.

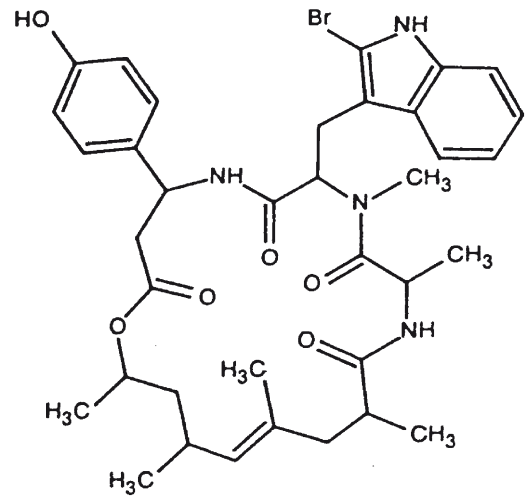

Fig. 1. Molecular structure of jasplakinolide, as reported by Scott et al. *(32)*.

Cell biological experiments were carried out in different carcinoma cell lines *(16, 42–45)*, a human stellate cell line (LX-2, *(46)*), epithelial cells *(34, 47)*, MDCK cells *(24)*, endothelial cells *(48)*, lymphocytes *(25)*, macrophages *(49)*, starfish oocytes *(50)*, fibroblasts *(51, 52)*, crane-fly spermatocytes *(30)*, murine oocytes *(31)*, starfish oocytes *(53)*, HeLa cells *(36)*, neutrophils *(8)*, amoebae *Dictyostelium (9)*, parasites like *Toxoplasma gondii (26, 54)* and yeast *(17)* amongst others.

In plant systems the unicellular green alga *Micrasterias (7)*, green algae *Acetabularia*, *Pseudobryopsis* and *Nitella (55)*, fucoid (brown algal) Zygotes of *Silvetia compressa* and *Pelvetia compressa (28)*, *Allium* bulb scale cells and *Sinapis* root hairs *(55)*, tobacco BY-2 cells *(27)*, *Lilium* pollen tubes *(29)*, *Papaver rhoeas* pollen tubes *(56)* have been tested for jasplakinolide reaction.

Jaspalkinolide causes tremendous effect already visible at the light microscopic level by malformation of cells as in the example of *Micrasteris (7)* (**Fig. 2a**). Inhibition or retardation of cell development occurs, during recovery from drug treatment the cells develop a malformed pattern *(7)*. In pollen tubes the normal bidirectional cytoplasmic streaming is altered, instead a rotary streaming is observed in the swollen apex *(29)*. Moreover altering F-actin levels or dynamics by jasplakinolide plays a functional role in initiating programmed cell death in *Papaver* pollen, triggering a caspase-3-like activity *(56)*. Polarity establishment is severely changed in fucoid zygotes *(28)*. Latrunculin A induced membrane depolymerization is avoided by Jasplakinolide *(53)*. Changes of the cell shapes are reported in different animal cells, where protrusions of the cell surface are formed *(25, 43)*.

Moreover, when applied during mitosis, binucleated cells are generated as a consequence of jasplakinolide treatment *(7, 43)* (**Fig. 2b**).

Visualization of the effect of this drug *in situ* was achieved by the use of fluorescently labeled phalloidin as F-actin targeting agent. After jasplakinolide treatment an altered F-actin distribution was found, characterized by a patchy appearance of cortical actin *(25)*, the formation of actin dots *(48)* or a disruption of the actin cytoskeleton *(43, 55)*.

As competitive binding inhibition of phalloidin to F-actin by jasplakinolide is described *(6)*, and decreased FITC-phalloidin labeling is noted as a consequence of jasplakinolide treatment in MDCK cells *(24)*, the problems visualizing jasplakinolide effects by fluorescently labeled phalloidin are obvious. Moreover, phalloidin and jasplakinolide have the same effect when applied to living *Dictyostelium* cells, namely the formation of actin aggregates *(9)*.

In order to avoid the difficulties mentioned, only electron microscopy appears to be a sufficient technique for detection of jasplakinolide effects on F-actin *(7, 26)*. At electron micrographs tangential sections of F-actin can easily be recognized by the filament diameter of about 4–5 nm. In organisms like *Micrasterias*,

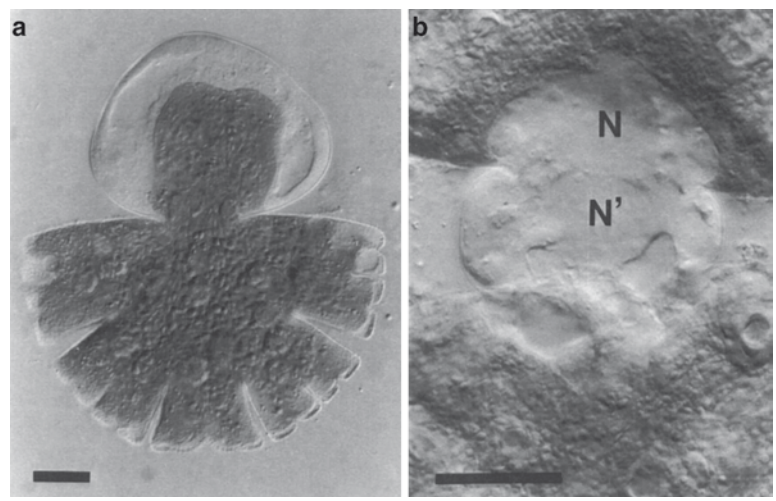

Fig. 2. Effect of jasplakinolide treatment on developing *Micrasterias denticulata* cells according to **Subheading 3.1**. (**a**) very young developmental stage treated with 3 μM jasplakinolide for 0.5 h and allowed to recover for 3 h in nutrient solution, young semi-cell exhibits complete loss of normal cell pattern (*above*) when compared to non-growing semi-cell (*below*). (**b**) treatment before septum formation with 10 μM jasplakinolide for 2 h, two nuclei (*N*, *N'*) are visible in the isthmus region, septum is not formed. Bar = 20 μm. Reprinted from reference *(7)* with permission. "Copyright (1997) Wiley-Liss, Inc., a subsidiary of John Wiley & Sons, Inc".

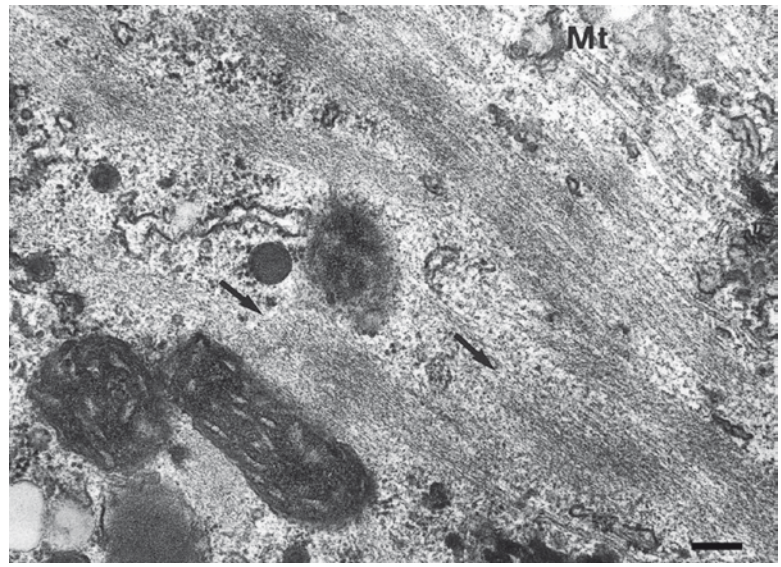

Fig. 3. Detail of the ultrastructure of *Micrasterias denticulata* cell treated with 3 μM jasplakinolide for 2 h and fixed for electron microscopy according to **Subheading 3.2.1**, dense accumulations of F-actin are visible in the cytoplasm. Bar = 0.2 μ`m. Reprinted from ref. *(7)* with permission "Copyright (1997) Wiley-Liss, Inc., a subsidiary of John Wiley & Sons, Inc".

where normally almost no bundling of F-actin occurs, and thus F-actin is hardly found at electron microscopical images, alterations causing extensive bundling of actin are easily detected *(7)* (**Fig. 3**). In *Toxoplasma gondii* tachyzoites jasplakinolide induces the formation of F-actin-containing apical extensions *(26)* (**Fig. 4**). Also immunodetection of the altered F-actin system after jasplakinolide treatment is successful *(25)* and allows a comprehensive picture to be drawn in combination with other techniques.

As jasplakinolide specifically targets F-actin, other cytoskeletal components like desmin or β-tubulin were not influenced by jasplakinolide in carcinoma cells *(43)*, microtubule dependent processes are not affected *(57)* and the distribution of microtubules and microtubule dependent processes were not altered in green algae *(7)*.

Herein different procedures shall be described for the detection of actin filament aggregates generated by application of jasplakinolide. Due to the advantages of electron microscopy and/or immunomethods, these will be mentioned more in detail, however, different protocols for phalloidin stainings will be given as they have been used for some organisms in combination with jasplakinolide treatment *(9, 24, 25)*.

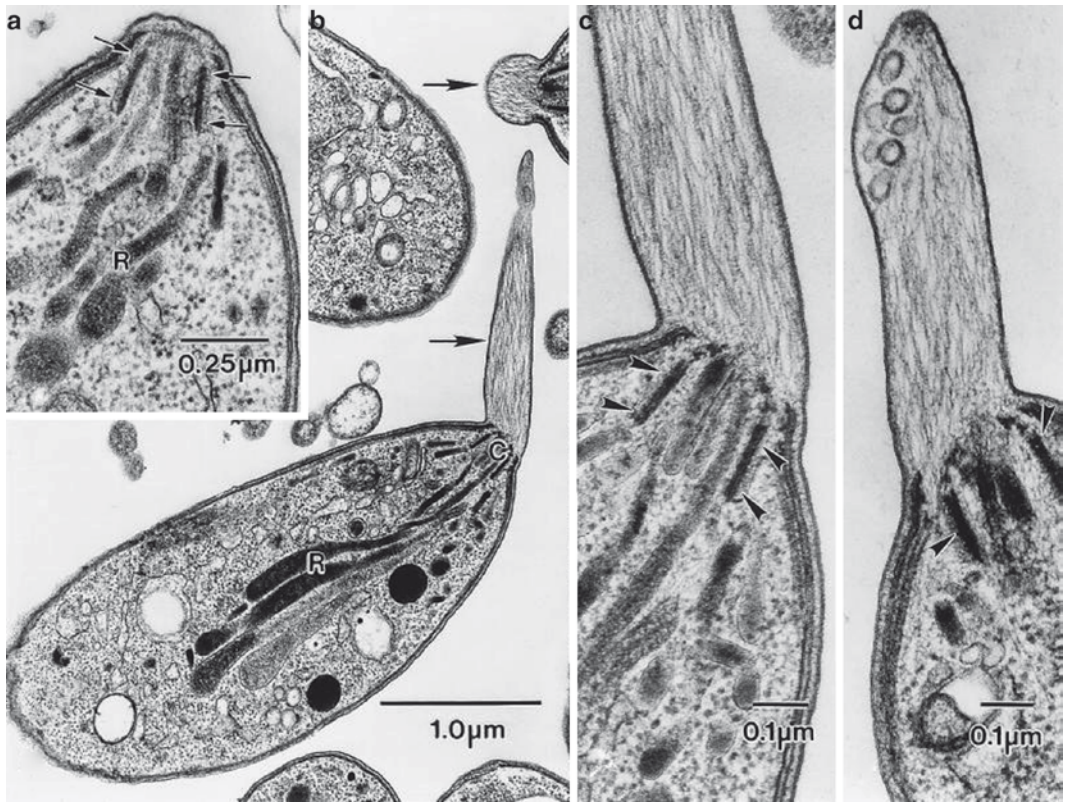

Fig. 4. Jasplakinolide induces the formation of actin-containing apical extensions in isolated *Toxoplasma gondii* tachyzoites fixed according to **Subheading 3.2.2**. (**a**) High magnification of the apical end of a tachyzoite from an untreated control culture showing the walls of the conoid (*arrows*) with the necks of the rhoptries (R) closely associated with it. Apart from some fuzzy material associated with the conoid, there is no filamentous material in any part of the apical region. (**b**) Low-power electron micrograph of isolated tachyzoites treated with 1 mM jasplakinolide for 60 min at 37°C. Filament-containing apical extensions are present in two of the parasites (*arrows*). *C* conoid complex; *R* rhoptries. (**c**, **d**) Higher-magnification micrographs of the apical end of jasplakinolide-treated tachyzoites showing the membrane-bounded apical extensions, each of which contains many filaments extending from the conoid. Note also the presence of membrane-bounded vesicles and membrane-associated dense material at the anterior end of the protrusions (**d**). In (**c**) and (**d**), arrowheads denote the walls of the conoid. Reprinted from reference *(26)* with permission "Copyright (1999) National Academy of Sciences, U.S.A.".

2. Materials

2.1. Cell Cultures

1. *Micrasterias denticulata* Bréb. (unicellular green algae) are used for light microscopy and electron microscopy *(7)* and immuno-electron microscopy since alterations in the cell shape caused by drug treatments are easily detected. The cells are grown in culture medium under semisterile conditions in a light/dark regime of 14/10 h at 20°C.
2. *Toxoplasma gondii* tachyzoites *(26)* for electron microscopic investigations.

3. Murine interleukin 2 dependent T cell line CTLL-20 *(25)* are grown in RPMI 1640 medium and examined by fluorescence microscopy.
4. *Dictyostelium* cells NC4A2, AX4 *(9)* are grown in HL-5 medium and examined by fluorescence microscopy techniques.
5. MDCK cells, strain II *(24)* are examined by fluorescence microscopy.

2.2. Chemicals, Buffers, Solutions

2.2.1. Drug

1. Methanol reagent.
2. DMSO (dimethyl sulfoxide) reagent.
3. Jasplakinolide, Mol. Wt. 709.68, Molecular Probes (Eugene, Oregon, USA; Leiden, The Netherlands, ordering no. J-7473). 100 µg, diluted upon arrival in methanol to achieve 10 mM stock solution and kept refrigerated at –20°C (*see* **Note 1**).

2.2.2. Chemicals, Buffers and Solutions for Electron Microscopy

1. Cacodylic buffer: 50 mM cacodylic acid sodium salt, pH 7.2.
2. Cacodylate-glutaraldehyde: 50 mM cacodylic buffer, 1% glutaraldehyde, pH 7.2.
3. Cacodylate-osmium: 50 mM cacodylic acid buffer, 1% osmiumtetraoxide, 0.8%, potassium hexacyanoferrate III.
4. Phosphate buffer-fixative: 25 mM sodium hydrogen phosphate, 25 mM potassium dihydrogen phosphate, 1% glutaraldehyde, 1% osmiumtetroxide, pH 6.2.
5. Calcium chloride.
6. 2% Aqueous uranyl acetate dihydrate.
7. Ethanol solutions: 15%, 30%, 40%, 50%, 60%, 70%, 80%, 90%, 95%, 100%.
8. 1,2-Propylene oxide reagent.
9. Propylene oxide–ethanol mixture: 1,2- Propylene oxide and ethanol (1:1, v/v).
10. A suitable embedding resin: Embed 812, Araldite 502, Spurr's resin or others.
11. Propylene oxide–embedding resin mixture: Mixture of 1,2 Propylene oxide and embedding resin (1:1, v/v).
12. Formvar 1595 E.
13. Chloroform reagent.
14. Lead citrate.

2.2.3. Chemicals, Buffers and Solutions for Immunoelectron Microscopy

1. Lecithin (10%) dissolved in chloroform.
2. Liquid nitrogen.
3. Acetone–tannic acid: acetone containing 0.1% tannic acid (v/v).

4. Acetone–osmium: acetone containing 2% osmiumtetroxide and 0.05% uranyl acetate.
5. LR white resin (London resin company, medium grade).
6. TBS: Tris buffered saline, 50 mM, pH 7.5.
7. Blocking solution: TBS containing 1% BSA (fraction V), 1% acetylated BSA, 01% Tween-20.
8. 10% bovine calf fetal serum.

   Primary Antisera/Antibodies, e.g., monoclonal anti actin N 350 monoclonal anti actin (Amersham).
9. 10 nm collodial gold conjugated, secondary antibody appropriate for the primary antibody.

2.2.4. Chemicals, Buffers and Solutions for Fluorescence Microscopy

1. Paraformaldehyde fixative: 4% paraformaldehyde and cytospin (Cytospin 3 preparation systems, Shandon Scientific Ltd. Cheshire, UK).
2. 50 μM ammonium chloride.
3. PBS: Phosphate buffered saline: 137 mM sodium chloride, 2.7 mM potassium chloride, 4.3 mM sodium hydrogen phosphate, 1.4 mM potassium dihydrogen phosphate.
4. Triton solution: 0.1% Triton X-100 in PBS.
5. 2% bovine serum albumin (BSA).
6. Anti actin monoclonal antibody N 350 (Amersham) (*see* **Note 2**).
7. Phalloidin: 0.4 mg/mL FITC (or alexa) conjugated phalloidin.
8. MCPB fixative: 10 mM sodium hydrogen phosphate, 10 mM potassium dihydrogen phosphate, 2 mM manganese chloride, 0.2 mM calcium chloride, pH 6.5) containing 2.5% formaldehyde, 0.1% glutaraldehyde, 0.01% Triton X-100 and 1 μM fluorescent phalloidin.
9. Jasplakinolide stock solution (*see* **Subheading 2.2.1**).
10. Glycerol-gallate mounting medium: 50% glycerol, 1% *n*-propyl gallate in PBS.
11. Phenylenediamine.
12. Texas red conjugated anitmouse IgM antibody (Jackson Immuno Research).

3. Methods

3.1. Treatment and Recovery Experiments

1. Incubate *Micrastieras denticulata* cells (or other cell types or tissue) in 1 mL of culture medium containing 1.5, 3, 10 μM jasplakinolide for time periods of 0.5, 1, 2, 3, 4, 24, 48 h (*see* **Note 3**).

2. Incubate cells in 1 mL of culture medium containing 3 μM jasplakinolide for 0.5 h, remove the jasplakinolide solution, wash several times with culture medium, and allow to develop in culture medium for 3 h. This is regarded as "recovery experiment".
3. Investigate the cells treated as in **steps 2**. and **3**. under a regular light microscope or fix for electron microscopy (*see* **Subheadings 3.2.1** and **3.2.2**).

3.2. Visualization of F-Actin Aggregates After Jasplakinolide Treatment

The procedure described herein has first been used for the unicellular green alga *Micrasterias* by *(58)*.

3.2.1. Chemical Fixation/ Electron Microscopy of Algal Cells after Holzinger and Meindl (7)

1. Fix treated cells, cells allowed to recover in nutrient solution and untreated control cells in cacodylate-gultaraldehyde for 15 min (*see* **Note 4**).
2. Wash cells three times 5 min each in cacodylic buffer.
3. Postfix cells in cacodylate-osmium for 2 h.
4. Wash cells, as in **step 2**, three times 5 min each in distilled water.
5. Incubate cells in 2% uranyl acetate for 2 h (*see* **Note 5**).
6. Wash cells, as in **step 2**, three times 5 min each in distilled water.
7. Dehydrate the cells in increasing concentrations of cold ethanol (*see* **Note 6**), 15 min per concentration:

   15%, 30%, 40%, 50%, 70%, 80%, 90%, 95%, 100%. Keep in 100% for 30 min.
8. Transfer the cells to the propylene oxide-ethanol mixture, allow to equilibrate for 10 min, transfer to propylene oxide.
9. Transfer the cells to the propylene oxide-embedding resin mixture (*see* **Note 7**).
10. Rotate the cells in this mixture for 48 h in order to allow the propylene oxide to evaporate and a sufficient penetration of the cells with the resin to be achieved.
11. Transfer the cells to freshly prepared resin in aluminum dishes and orientate them by the use of eyelashes connected to holders.
12. Incubate in an exsikkator for 4 days.
13. Polymerize the resin for 24 h at 60°C.
14. Select cells and section at an ultramicrotome.
15. Collect sections on formvar coated copper grids (*see* **Note 8**).
16. Counterstain the sections with 2% uranyl acetate and Reynold's lead citrate (*see* **Note 9**).
17. Investigate and photograph at a transmission electron microscope at 80 kV.

3.2.2. Fixation Method for Protozoan Parasites after Shaw and Tilney (26)

1. Fix 1 μM jasplakinolide treated, isolated *Toxoplasma gondii* (extracellular tachyzoites) in phosphate buffer-fixative.
2. Add the phosphate buffer-fixative at room temperature and then place samples over ice (4°C) for 45 min.
3. Pellet the samples after fixation.
4. Rinse with distilled water to remove phosphate ions.
5. Stain with 0.5% uranyl acetate for 6–16 h at 4°C.
6. Dehydrate with acetone.
7. Embed in embedding resin mixture (continue as in **Subheading 3.2.1**, **step 11**).

3.2.3. Immunoelectron Microscopy

The following fixation technique has been carried out for *Micrasterias* for the first time by Meindl et al. *(59)*. The recipe for actin detection by means of immunogoldlocalization is based on *(60)*.

1. Prepare gold or aluminum specimen holders with bed depths of 100–300 μm by dipping in lecithin.
2. Collect treated cells to be transferred to specimen holders. Large cells like *Micrasterias* (200 μm in diameter) can be easily collected under a stereo microscope by wrapping with cotton fibers.
3. Fix treated cells by high pressure freeze fixation by the use of a Hyperbaric freeze device (formally Balzers HPM 010, later taken over by BAL-TEC; then produced by ABRA Fluid AG, Widnau, Switzerland; currently available as "High Pressure Freezing Machine HPM 010" by Boeckeler Instruments Inc., Tucson/AZ, USA), for other methods (*see* **Note 10**).
4. Collect and store samples under liquid nitrogen.
5. Transfer samples to a freeze substitution device (Reichert-Jung, cs auto or LEICA EM AFS, Leica Microsysteme GmbH, Vienna, Austria).
6. Substitute samples at −80°C for 24 h in acetone–tannic acid solution.
7. Wash several times with acetone.
8. Substitute samples at −80°C for 24 h in acetone–osmium solution (*see* **Note 11**).
9. Allow samples to reach −30°C within 5 h.
10. Continue substitution at −30°C for 10 h.
11. Allow samples to reach room temperature (20°C) within 5 h.
12. Remove osmium tetroxide/uranyl acetate solution and rinse several times with acetone.
13. Change acetone for ethanol by several rinses.

14. Transfer samples to LR white in aluminum dishes and cover with cellophane foil.
15. Allow samples to infiltrate in an exsikkator for 24 h.
16. Polymerize under UV light at room temperature for 24 h.
17. Prepare sections for electron microscopy (compare **Subheading 3.2.1**) and transfer to formvar coated gold- or gilded copper grids.
18. Incubate in blocking solution for 30 min up to 1 h. A blocking step with 10% bovine calf fetal serum may be applied if blocking is not sufficient.
19. Transfer into primary antibody against actin. Purified antibody may be diluted in blocking solution. Incubation should last for 1.5 h at room temperature or for up to 24 h at 4°C.
20. Wash four times 15 min in TBS by transferring grids to 50 µL droplets of TBS.
21. Incubate in 10 nm-gold (*see* **Note 12**) labeled secondary antibody diluted in blocking solution (*see* **Note 13**).
22. Wash by rinsing with TBS, followed by incubation in droplets of TBS for 2 min, followed by a brief rinse with distilled water.
23. Counterstain with uranyl acetate and lead citrate if necessary (*see* **Subheading 3.2.1**).
24. Investigate at a transmission electron microscope at 80 kV.

3.2.4. Immunofluorescence Microscopy of Jasplakinolide Treated Lymphocytes After Posey and Bierer (25)

1. Grow CTLL-20 cells in RPMI 1640 medium.
2. Wash cells with RPMI 1640 three times and resuspend at a final density of 2×10^5cells/mL.
3. Transfer cells to RPMI 1640 medium containing 100 nM jasplakinolide.
4. Fix cells (1×10^6/sample) in paraformaldehyde fixative on glass slides.
5. Incubate cells in ammonium chloride for 5 min.
6. Permeabilize cells with Triton solution for 2.5 min.
7. Block with BSA.
8. Incubate with 30 µg/mL anti actin monoclonal antibody for 30–45 min at room temperature.
9. Wash three times with PBS.
10. Incubate with 15 µg/mL Texas red conjugated anti-Mouse IgM antibody for 30 min at room temperature.
11. Wash three times and mount samples in glycerol mounting medium.
12. View at a confocal laser scanning microscope.

3.2.5. FITC–Phalloidin Staining of Jasplakinolide Treated Dictyostelium Cells After Lee et al. (9) **(see Note 14)**

1. Grow wild-type (NC4A2, AX4) *Dictyostelium* amoebae in 100 mm petri dishes at 22°C in HL-5 medium.
2. Plate the cells over night in a 35 mm dish and remove the cover slip to a Rose chamber.
3. Replace the medium with fresh HL-5 medium containing 3 μM jasplakinolide for 1–2 h.
4. Fix treated *Dictyostelium* cells in MCPB fixative.
5. Investigate at a confocal laser scanning microscope.

3.2.6. FITC–Phalloidin Staining of Jasplakinolide Treated MDCK Cells After Shurety et al. (24)

1. Grow MDCK cells for 4 days at coverslips or semipermeable filters.
2. Treat cells with 1 μM jasplakinolide for 45 min.
3. Fix cells with paraformaldehyde for 5 min.
4. Permeabilize cells in Triton solution.
5. Incubate in FITC-conjugated phalloidin.
6. Mount cover slips in glycerol–gallate mounting medium.
7. Examine at a confocal microscope or a light microscope fitted for epifluorescence.

4. Notes

1. Jasplakinolide is also dissolvable in DMSO *(32)*.
2. The choice of the anti-actin antibody is very important. The epitope of the N 350 (a mouse monoclonal IgM antibody directed against chicken gizzard actin) binding site is obviously not changed by jasplakinolide *(55)*, whereas binding sites for other actin antibodies (e.g., C4 - a mouse monoclonal IgG antibody directed against chicken gizzard actin, ICN) seem to be altered substantially which prevents visualization of F-actin after jasplakinolide treatment *(55)*.
3. For *Micrasterias denticulata* 1.5 μM of jasplakinolide was found to be the lowest effective concentration. Concentrations above 250 μM of jasplakinolide were lethal. The concentrations of jasplakinolide needed for other cells have to be found empirically. Variations in the literature range from as low as 100 nM to 1 μM, 2.5 μM to 10 μM *(25, 28, 37, 55)*, However, they should be in the same range as described herein, since the effective concentrations correlate with data obtained from the literature *(9, 24, 32)*. Lee et al. *(9)* remark that the effective concentration has varied with different batches and that therefore each lot should be titrated to find an effective concentration before usage.

4. The fixation procedure is performed in a "Balzers Fixomat" – a device not commercially available anymore – consisting of sintered glass suction filters connected via a valve to a pump station, allowing to remove solutions by underpressure while cells remain in the filter. Moreover the temperature can be adjusted via a cooling bath. Alternatively the cells can be fixed in glass dishes, ideally in the shape of a hemisphere. In this case it is best to remove only the solutions with a pipette and not to transfer the cells. For other organisms more specialized methods might be necessary – for example embedding of the specimens in agarose prior to the fixation procedure.
5. During incubation in uranyl acetate solution it is necessary to keep the cells in darkness, by covering the filter or dish with aluminum foil.
6. During the whole procedure of dehydration the temperature should be kept at 6°C. At the steps 50% and 70% ethanol temperature might be lowered to 4°C. In case of fixation in round glass dishes they should be kept over ice. At the step of 100% ethanol the temperature should be increased to room temperature.
7. Very good results are obtained with a 1:1 mixture of glycid ether 100 (a substance equivalent to Epon 812) and MNA. Prior to use DMP must be added (five droplets to 10 mL of resin). However, a mixture of Embed-812/Araldite 502/DDSA (DMP-30 or BDMA must be added prior to use) will also give adequate results. When different hardness has to be achieved, Spurr's resin may be the best choice: As several components of the original mixture are not deliverable any more, we now use the kit "Agar Low Viscosity Resin (LV)" by Agar Scientific Ltd. Essex CM24 8DA, England.
8. Coating of grids with formvar may not be necessary for all objects. We use the following procedure: A light microscopic slide is cleaned with lens tissue, tipped into 0.3% formvar dissolved in chloroform. The resulting formvar film is cut at the edges of the slide and allowed to float on distilled water. Grids are placed on the film which is then removed with parafilm.
9. The time periods needed for counterstaining depend on the staining already achieved during the fixation/staining procedure and are typically 5–30 min for uranyl acetate and 1–5 min for Reynold's lead citrate.
10. For large cells like *Micrasterias* (about 200 μm in diameter) high pressure freezing has been found the only appropriate technique for freeze fixation. Alternatively to the HPM 010, also the Leica EMPACT high pressure freezer (Leica Microsysteme GmbH, Vienna, Austria) gives reasonable

results. However, for small and less vacuolated cells plunge freezing which might be achieved with a relative simple equipment, will also give reasonable results.

11. Osmium tetroxide dissolves well in acetone. Uranylacetat is best to be sonicated to dissolve it. For other organisms it might be appropriate to substitute without osmium tetroxide and uranyl acetate.
12. Gold particles with 10 nm diameter are used commonly. The usage of smaller gold particles might enhance the accuracy of the detected locus.
13. The actual dilution factor has to be found empirically for each system, but it should be in the range of 1:50–1:200.
14. As mentioned in the introduction, the use of fluorescently labeled phalloidin is problematic due to competitive binding with jasplakinolide *(6, 10)*. It has been reported that simultaneous addition of jasplakinolide and FITC–phalloidin (1:1) did not result in F-actin labeling, whereas addition of the inactive analogue jasplakinolide B and FITC–phalloidin resulted in staining as strong as in controls *(55)*. However, some authors were successful in detection of actin aggregates with the methods described in **Subheadings 3.2.5** and **3.2.6**.

References

1. Holzinger, A. (2001) Jasplakinolide: an actin-specific reagent that promotes actin polymerization. In: *Methods in Molecular Biology, Vol. 161, Cytoskeleton Methods and Protocols* (Gavin, R.H., ed.), Humana, Totowa, NJ, pp. 109–120
2. Holzinger, A. and Lütz-Meindl, U. (2001) Chondramides, novel cyclodepsipeptides from myxobacteria, influence cell development and induce actin filament polymerization in the green alga *Micrasterias*. *Cell Motil. Cytoskeleton* **48**, 87–95
3. Allingham, J.S., Klenchin, V.A., and Rayment, I. (2006) Actin-targeting natural products: structures, properties and mechanisms of action. *Cell. Mol. Life Sci.* **63**, 2119–2134
4. Brown, S.S., and Spudich, J.A. (1979) Cytochalasin inhibits the rate of elongation of actin filament fragments. *J. Cell Biol.* **83**, 657–662
5. Coué, M., Brenner, S.L., Spector, I., and Korn, E.D. (1987) Inhibition of actin polymerization by latrunculin A. *FEBS Lett.* **213**, 316–318
6. Bubb, M.R., Senderowicz, A.M.J., Sausville, E.A., Duncan, K.L.K., and Korn, E.D. (1994) Jasplakinolide, a cytotoxic natural product, induces actin polymerization and competitively inhibits the binding of phalloidin to F-actin. *J. Biol. Chem.* **269**, 14869–14871
7. Holzinger, A., and Meindl, U. (1997) Jasplakinolide, a novel actin targeting peptide inhibits cell growth and induces actin filament polymerization in the green alga *Micrasterias*. *Cell Motil. Cytoskeleton* **38**, 367–372
8. Sheikh, S., Gratzer, W.B., Pinder, J.C., and Nash, G.B. (1997) Actin polymerisation regulates integrin-mediated adhesion as well as rigidity of neutrophils. *Biochem. Biophys. Res. Commun.* **238**, 910–915
9. Lee, E., Shelden, E.A., and Knecht, D.A. (1998) Formation of F-actin aggregates in cells treated with actin stabilizing drugs. *Cell Motil. Cytoskeleton* **39**, 122–133
10. Visegády, B., Lörinczy, D., Hild, G., Somogyi, B., and Nyitrai, M. (2005) A simple model for the cooperative stabilization of actin filaments by phalloidin and jasplakinolide. *FEBS Lett.* **579**, 6–10
11. Matthews, J.B., Smith, J.A., and Hrnjez, B.J. (1997) Effects of F-actin stabilization or

disassembly on epithelial Cl- secretion and Na-K-2Cl cotransport. *Am. J. Physiol. Cell Physiol.* **272**, C254–C262

12. Crews, P., Manes, L.V., and Boehler, M. (1986) Jasplakinolide, a cyclodepsipeptide from the marine sponge, *Jaspis* sp. *Tetrahedron Lett.* **27**, 2797–2800
13. Zabriskie, M.T., Klocke, J.A., Ireland, C.M., Marcus, A.H., and Molinski, T.F. (1986) Jaspamide, a modified peptide from a *Jaspis* sponge, with insecticidal and antifungal activity. *J. Am. Chem. Soc.* **108**, 3123–3124
14. Braekman, J.C., Daloze, D., and Moussiaux, B. (1987) Jaspamide from the marine sponge *Jaspis johnstoni*. *J. Nat. Prod.* **50**, 994–995
15. Murray, L.M., Johnson, A., Diaz, M.C., and Crews, P. (1997) Geographic variation in the tropical marine sponge Jaspis cf. Johnstoni: an unexpected source of new terpene-benzoides. *J. Org. Chem.* **62**, 5638–5641
16. Fabian, I., Shur, I., Bleiberg, I., Rudi, A., Kashman, Y., and Lishner, M. (1995) Growth modulation and differentiation of acute myeloid leukemia cells by jaspamide. *Exp. Hematol.* **23**, 583–587
17. Ayscough, K.R., Stryker, J., Pokala, N., Sanders, M., Crews, P., and Drubin, D.G. (1997) High rates of actin turnover in budding yeast and roles for actin in establishment and maintenance of cell polarity revealed using the actin inhibitor latrunculin-A. *J. Cell Biol.* **137**, 399–416
18. Chu, K.S., Negrete, G.R., and Konopelski, J.P. (1991) Asymmetric total synthesis of (+)-jasplakinolide. *J. Org. Chem.* **56**, 5196–5202
19. Inman, W., and Crews, P. (1989) Novel marine sponge derived amino acids. 8. Conformational analysis of jasplakinolide. *J. Am. Chem. Soc.* **111**, 2822–2829
20. Kahn, M., Nakanishi, H., Su, T., Lee, J.Y.H., and Johnson, M. (1991) Design and synthesis of nonpeptide mimetics of jaspamide. *Int. J. Pept. Prot. Res.* **38**, 324–334
21. Ghosh, A.K., and Moon, D.K. (2007) Enantioselective total synthesis of +-jasplakinolide. *Org Lett.* **9**, 2425–2427
22. Fabian, I., Halperin, D., Lefter, S., Mittelman, L., Altstock, R.T., Seaon, O., and Tsarfaty, I. (1999) Alteration of actin organization by jaspamide inhibits ruffling, but not phagocytosis or oxidative burst, in HL-60 cells and human monocytes. *Blood* **93**, 3994–4005
23. Terracciano, S., Bruno, I., D'Amico, E., Bifulco, G., Zampella, A., Sepe, V., Smith, C.D., and Riccio, R. (2008) Synthetic and pharmacological studies on new simplified analogues of the potent actin-targeting jaspamide. *Bioorg. Med. Chem.* **16**, 6580–6588
24. Shurety, W., Steward, N.L., and Stow, J.L. (1998) Fluid-phase markers in the basolateral endocytic pathway accumulate in response to the actin assembly-promoting drug jasplakinolide. *Mol. Biol. Cell* **9**, 957–975
25. Posey, S.C., and Bierer, B.E. (1999) Actin stabilization by jasplakinolide enhances apoptosis induced by cytokine deprivation. *J. Biol. Chem.* **274**, 4259–4265
26. Shaw, M.K., and Tilney, L.G. (1999) Induction of an acrosomal process in *Toxoplasma gondii*: visualization of actin filaments in a protozoan parasite. *Proc. Natl. Acad. Sci. U.S.A.* **96**, 9095–9099
27. Ou, G.S., Chen, Z.L., and Yuan, M. (2002) Jasplakinolide reversibly disrupts actin filaments in suspension-cultured tobacco BY-2 cells. *Protoplasma* **219**, 168–175
28. Hable, W.E., Miller, N.R., and Kropf, D.L. (2003) Polarity establishment requires dynamic actin in fucoid zygotes. *Protoplasma* **221**, 193–204
29. Cárdenas, L., Lovy-Wheeler, A., Wilsen, K.L., and Hepler, P.K. (2005) Actin polymerization promotes the reversal of streaming in the apex of pollen tubes. *Cell Motil. Cytoskeleleton* **61**, 112–127
30. Xie, L., and Forer, A. (2008) Jasplakinolide, an actin stabilizing agent, alters anaphase chromosome movements in crane-fly spermatocytes. *Cell Motil. Cytoskeleton* **65**, 876–889
31. Terada, Y., Simerly, C., and Schatten, G. (2000) Microfilament stabilization by jasplakinolide arrests oocyte maturation, cortical granule exocytosis, sperm incorporation cone resorption, and cell-cycle progression, but not DNA replication, during fertilization in mice. *Mol. Reprod. Dev.* **56**, 89–98
32. Scott, V.R., Boehme, R., and Matthews, T.R. (1988) New class of antifungal agents: jasplakinolide, a cyclodepsipeptide from the marine sponge *Jaspis* species. *Antimicrob. Agents Chemother.* **32**, 1154–1157
33. Odaka, C., Sanders, M.L., and Crews, P. (2000) Jasplakinolide induces apoptosis in various transformed cell lines by a caspase-3-like protease-dependent pathway. *Clin. Diagn. Lab. Immun.* **7**, 947–952
34. White, S.R., Williams, P., Wojcik, K.R., Sun, S., Hiemstra, P.S., Rabe, K.F., and Dorscheid, D.R. (2001) Initiation of apoptosis by actin cytoskeletal derangement in human airway epithelial cells. *Am. J. Resp. Cell Mol.* **24**, 282–294
35. Genescà, M., Sola, A., and Hotter, G. (2006) Actin cytoskeleton derangement induces apoptosis in renal ischemia/reperfusion. *Apoptosis* **11**, 563–571

36. Locker, J.K., Kuehn, A., Schleich, S., Rutter, G., Hohenberg, H., Wepf, R., and Griffiths, G. (2000) Entry of the two infectious forms of vaccinia virus at the plasma membane is signaling-dependent for the IMV but not the EEV. *Mol. Biol. Cell* **11**, 2497–2511
37. Chichili, G.R., and Rodgers, W. (2007) Clustering of membrane raft proteins by the actin cytoskeleton. *J. Biol. Chem.***282**, 36682–36691
38. Lázaro-Diéguez, F., Jiménez, N., Barth, H., Koster, A.J., Renau-Piqueras, J., Llopis, J.L., Burger, K.N., and Egea, G. (2006) Actin filaments are involved in the maintenance of golgi cisternae morphology and intra-Golgi pH. *Cell Motil. Cytoskeleton* **63**, 778–791
39. Lázaro-Diéguez, F., Colonna, C., Cortegano, M., Calvo, M., Martínez, S.E., and Egea, G. (2007) Variable actin dynamics requirement for the exit of different cargo from the trans-Golgi network. *FEBS Lett.***581**, 3875–3881
40. Inman, W., and Crews, P. (1989) Novel marine sponge derived amino acids. 8. Conformational analysis of jasplakinolide. *J. Am. Chem. Soc.***111**, 2822–2829
41. Bubb, M.R., Spector, I., Beyer, B.B., and Fosen, K.M. (2000) Effects of jasplakinolide on the kinetics of actin polymerization – an explanation for certain in vivo observations. *J. Biol. Chem.***275**, 5163–5170
42. Stingl, J., Andreson, R.J., and Emerman, J. (1992) In vitro screening of crude extracts and pure metabolites obtained from marine invertebrates for the treatment of breast cancer. *Cancer Chemother. Pharmacol.* **20**, 401–406
43. Senderowicz, A.M.J., Kaur, G., Sainz, E., Laing, C., Inman, W.D., Rodriguez, J., Crews, P., Malspeis, L., Grever, M.R., Sausville, E.A., and Duncan, K.L.K. (1995) Jasplakinolide's inhibition of the growth of prostate carcinoma cells in vitro with disruption of the actin cytoskeleton. *J. Natl. Canc. Inst.* **87**, 46–51
44. Duncan, M.D., Harmon, J.W., and Duncan, K.L.K. (1996) Actin disruption inhibits bombesin stimulation of focal adhesion kinase ($pp125^{FAK}$) in prostate carcinoma. *J. Surg. Res.* **63**, 359–363
45. Takeuchi, H., Ara, G., Sausville, E.A., and Teicher, B. (1998) Jasplakinolide: interaction with radiation and hypothermia in human prostate carcinoma and Lewis lung carcinoma. *Cancer Chemother. Pharmacol.* **42**, 491–496
46. Momma, K., Masuzawa, Y., Nakai, N., Chujo, M., Murakami, A., Kioka, N., Kiyama, Y., Akita, T., and Nagao, M. (2008) Direct interaction of Cucurbitacin E isolated from *Alsomitra macrocarpa* to actin filament. *Cytotechnology* **56**, 33–39
47. Murthy, K., and Wadsworth, P. (2005) Myosin-II-dependent localization and dynamics of F-actin during cytokinesis. *Curr. Biol.* **15**, 724–731
48. Braet, F., Spector, I., DeZanger, R., and Wisse, E. (1998) A novel structure involved in the formation of liver endothelial cell fenestrae revealed by using the actin inhibitor misakinolide. *Proc. Natl. Acad. Sci. U.S.A.* **95**, 13635–13640
49. Rosestolato, C.T.F., Dutra, J.D.F., De Souza, W., and de Carvalho, T.M.U. (2002) Participation of host cell actin filaments during interaction of trypomastigote forms of *Trypanosoma cruzi* with host cells. *Cell Struct. Funct.* **27**, 91–98
50. Kyozuka, K., Chun, J.T., Puppo, A., Gragnaniello, G., Garante, E., and Santella, L. (2008) Actin cytoskeleton modulates calcium signaling during maturation of starfish oocytes. *Dev. Biol.* **320**, 426–435
51. Raucher, D., Stauffer, T., Chen, W., Shen, K., Guo, S.L., York, J.D., Sheetz, M.P., and Meyer, T. (2000) Phosphatidylinositol 4,5-bisphosphate functions as a second messenger that regulates cytoskeleton-plasma membrane adhesion. *Cell* **100**, 221–228
52. Mseka, T., Bamburg, J.R., and Cramer, L.P. (2007) ADF/cofilin family proteins control formation of oriented actin-filament bundles in the cell body to trigger fibroblast polarization. *J. Cell Sci.* **120**, 4332–4344
53. Moccia, F. (2007) Latrunculin A depolarizes starfish oocytes. *Comp. Biochem. Physiol. A Mol. Integr. Physiol.* **148**, 845–852
54. Poupel, O., and Tardieux, I. (1999) Toxoplasma gondii motility and host cell invasiveness are drastically impaired by jasplakinolide, a cyclic peptide stabilizing F-actin. *Microbes Infect.***1**, 653–662
55. Sawitzky, H., Liebe, S., Willingale-Theune, J., and Menzel, D. (1999) The anti-proliferative agent jasplakinolide rearranges the actin cytoskeleton of plant cells. *Eur. J. Cell Biol.* **78**, 424–433
56. Thomas, S.G., Huang, S., Li, S., Staiger, C.J., and Franklin-Tong, V.E. (2006) Actin depolymerization is sufficient to induce programmed cell death in self-incompatible pollen. *J. Cell Biol.* **174**, 221–229
57. daCosta, S.R., Yarber, F.A., Zhang, L., Sonee, M., and Hamm, A.S.F. (1998) Microtubules facilitate the stimulated secretion of beta-hexosaminidase in lacrimal acinar cells. *J. Cell Sci.* **111**, 1267–1276
58. Meindl, U. (1990) Effects of temperature on cytomomorphogenesis and ultrastructure of

Micrasterias denticulata Bréb. *Protoplasma* **157**, 3–18

59. Meindl, U., Lancelle, S., and Hepler, P.K. (1992) Vesicle production and fusion during lobe formation in *Micrasterias denticulata* visualized by high pressure freeze fixation. *Protoplasma* **170**, 104–114
60. Holzinger, A., De Ruijter, N., Emons, A.M., and Lütz-Meindl, U. (1999) Spectrin-like proteins in green algae. *Cell Biol. Int.* **23**, 335–344

Chapter 5

Analysis of Centrosome Function and Microtubule Dynamics by Time-Lapse Microscopy in Xenopus Egg Extracts

Christiane Wiese, Jonathan R. Mayers, and Alison J. Albee

Summary

Centrosomes are essential organelles that organize the microtubule cytoskeleton during interphase and mitosis. Centrosomes are assembled from tens to hundreds of proteins, but how these proteins are organized into functional microtubule nucleating and organizing centers is not yet clear. An important step in understanding the role of individual proteins in centrosome function is to understand whether they are involved in forming, stabilizing, or anchoring microtubules. It is becoming increasingly clear that the analysis of fixed samples is inadequate for a true understanding of the dynamics that drive cell biological processes. In this chapter we focus on methods to analyze microtubule nucleation, organization, and dynamics using assays based on mitotic *Xenopus* egg extracts and in vitro reactions. These methods can easily be adapted to the study of interphase processes, or to the study of other cytoskeletal proteins and their dynamics.

Key words: *Xenopus* egg extract, Microtubule, Centrosome, Aster, Labeled protein, Time-lapse microscopy, In vitro assay, Dynamic instability, Immunodepletion

1. Introduction

Microtubules have essential roles in cellular organization as they position cellular organelles, facilitate directional transport of proteins and vesicles, and provide the tracks for the segregation of chromosomes during cell division. Microtubule organization within the cell is influenced by a number of proteins that regulate when and where microtubules are formed, how stabile they are, how cross-linked they are, or whether they move with respect to one another. In addition, molecular motors use microtubules as tracks

R.H. Gavin (ed.), *Cytoskeleton Methods and Protocols,* Methods in Molecular Biology, vol. 586
DOI 10.1007/978-1-60761-376-3_5,
© Humana Press, a part of Springer Science + Business Media, LLC 2009

to position protein complexes or RNP particles within the cell. In most cell types, microtubules are nucleated and organized mainly by microtubule organizing centers (MTOCs), named centrosomes in animal cells **(1)**. The centrosome is a small (1 μm^3) nonmembrane bound organelle that replicates once and only once per cell cycle, usually in concert with DNA replication. Recent proteomic approaches **(2)** have contributed valuable information to our knowledge of the components of the centrosome; however, a detailed understanding of how these components interact to allow the centrosome to function is still missing. Centrosomes harbor proteins involved in microtubule initiation as well as those involved in microtubule stability and anchoring **(3, 4)**. They play a major role in the assembly of the mitotic spindle, the elaborate macromolecular structure responsible for moving sister chromatids during cell division. In recent years, it has become clear that spindles are assembled by at least two distinct pathways, with microtubule assembly initiating at centrosomes or near the chromatin, respectively **(5)**. Microtubules originating from different pathways are integrated into the final structure. Information about the relative contributions of these pathways in different cells, and about the proteins that are responsible for regulating each pathway, is beginning to emerge.

Xenopus laevis egg extracts are a powerful model system for studying microtubule-related activities **(6)**. The egg extracts lack centrosomes and DNA, but they are capable of assembling centrosomes that serve to nucleate and organize microtubules from added sperm chromatin **(7)**. Addition of sperm chromatin to egg extracts mimics the process of fertilization. The sperm chromatin is tightly associated with a pair of centrioles (which are structures that also serve as the core of the centrosome, which is made up of centrioles and "pericentriolar material") that nucleate and anchor the axoneme, the central structure inside the sperm flagellum responsible for the movement of the sperm tail. Sperm centrioles serve as a foundation for the assembly of a functioning centrosome in the egg extracts by recruiting pericentriolar material proteins from the extract **(8)**. This allows us to test the function of individual proteins in centrosome and/or microtubule formation by testing the effect of removing these proteins from the egg extract. Traditionally, protein function has been assayed using fixed samples. However, these assays have the major disadvantage that three explanations are possible if one finds that fewer microtubules are associated with centrosomes: (1) the microtubules were never made, i.e., the centrosomes have a nucleation defect, (2) the microtubules were made but were unstable, or (3) the microtubules were made but were released from the centrosome. To distinguish these possibilities, one has to follow individual centrosomes and their associated microtubules for some time.

In this chapter, we describe how to prepare the reagents (extracts, sperm chromatin, and centrosomes) to examine the function of a protein of interest in microtubule formation or dynamics. We also describe the assays we use to test microtubule nucleation and dynamics and centrosome function. We have used these assays to examine microtubule formation around added sperm chromatin, which led to the discovery of a novel, non-centrosomal microtubule nucleation site associated with sperm chromatin **(Fig. 1)**. These assays also showed that the centrosome protein, maskin, is not required for microtubule nucleation or stability but its absence results in greater microtubule release (an example of a microtubule release event is shown in **Fig. 2**). Lastly, we describe a "bead nucleation assay" **(Fig. 3)** that we use to understand how candidate centrosomal proteins interact with microtubules.

2. Materials

2.1. Xenopus Egg Extracts

1. 3–4 oocyte positive female *Xenopus laevis* frogs (Nasco, Inc., Fort Atkinson, WI).
2. Pregnant Mare Serum Gonadotropin (PMSG; EMD Chemicals, Gibbstown, NJ): 200 U/mL in sterile water. Store at –20°C. Use 0.5 mL (100 U) per frog.
3. Human Chorionic Gonadotropin (hCG; Sigma-Aldrich, St. Louis, MO): 1,000 U/mL in sterile water. Stable at 4°C for up to 3 weeks. Use 0.5–1 mL (500–1,000 U) per frog.
4. Needles (25 gauge (BD 25G5/8; #305122) and 18 gauge (BD 18G11/2; # 305196)) and syringes (1 mL (#309602) and 3 mL (309585); Becton Dickinson, Franklin Lakes, NJ).
5. 25× MMR: 2.5 M NaCl, 50 mM KCl, 25 mM $MgCl_2$, 50 mM $CaCl_2$, 2.5 mM EDTA, 125 mM Na–HEPES, pH 7.8. Autoclave and store at room temperature.
6. Dejellying solution: 2% (w/v) cysteine, pH 7.8. Prepare immediately before use (*see* **Note 1**).
7. Extract Buffer (XB): 10 mM K–HEPES, pH 7.7, 100 mM KCl, 1 mM $MgCl_2$, 0.1 mM $CaCl_2$, 50 mM sucrose, pH 8. Store at 4°C but warm to room temperature before use.
8. Mitotic extract Buffer (CSF–XB): 10 mM K–HEPES, pH 7.7, 100 mM KCl, 2 mM $MgCl_2$, 0.1 mM $CaCl_2$, 50 mM sucrose, 5 mM EGTA, pH 8. Store at 4°C but warm to room temperature before use.

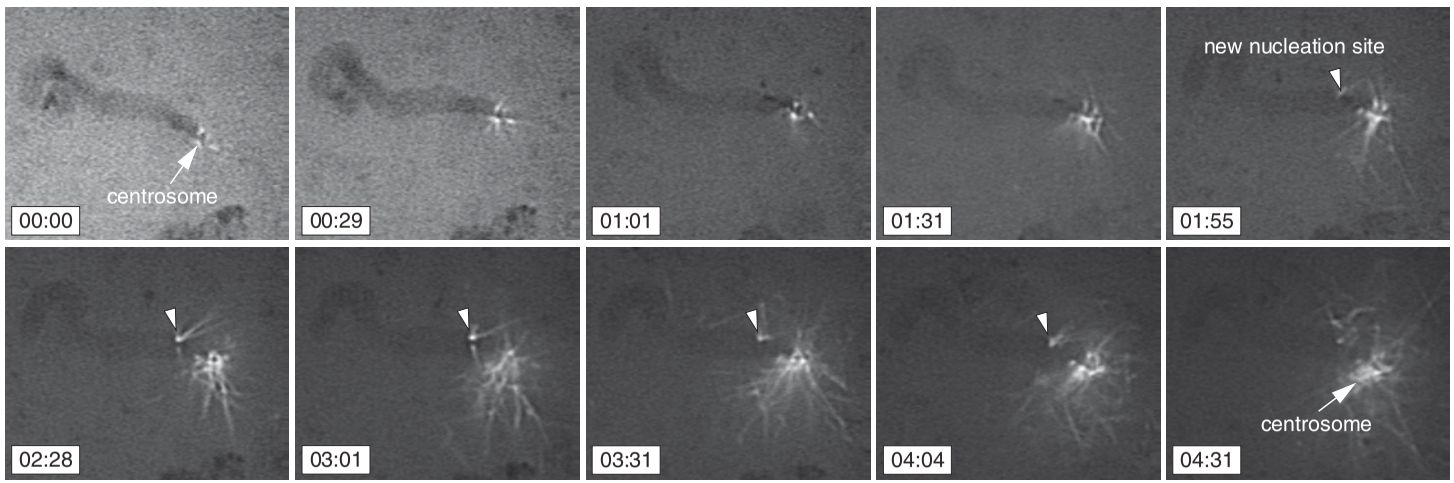

Fig. 1. Sperm-induced microtubule nucleation in *Xenopus* egg extracts examined by time-lapse microscopy show that microtubules are nucleated from the centrosome (indicated in the fist and last panel by the *small white arrow*) and lead to the discovery of a second, as of yet uncharacterized nucleation site (JRM and CW, unpublished observation). The novel nucleation site (indicated in two of the panels by a *white arrowhead*) became obvious only with time-lapse microscopy, but can be seen in "traditional" fixed samples as well (JRM and CW, unpublished observation). Interestingly, this nucleation site occurs at a fixed distance from the centrosome (usually within 2–3 μm). The novel nucleation site lacks centrioles, and its molecular composition is currently unknown. Elapsed time is indicated in the white box in each panel as minutes:seconds

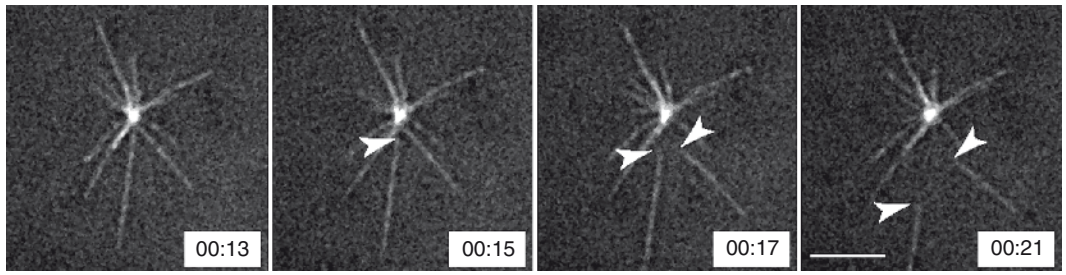

Fig. 2. Timelapse fluorescent microscopy shows microtubule release from centrosomes incubated in mitotic *Xenopus* egg extract. Purified centrosomes were incubated in egg extract supplemented with a small amount of rhodamine-labeled tubulin, which copolymerizes with the egg extract tubulin and allows visualization of microtubules as they form. The dynamic behavior of individual microtubules can be tracked over time, as can be the release of microtubules from the centrosome (two microtubule release events are highlighted by the *arrowheads*). Time is indicated in the white box in each panel as minutes:seconds. Scale bar, 10 μm.

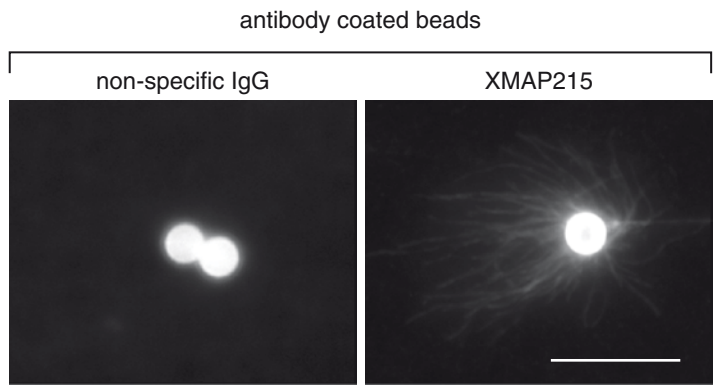

Fig. 3. In vitro microtubule nucleation in the presence of protein-coated beads provides clues about how proteins interact with microtubules. *Left panel*, control beads coated with antibody; *right panel*, beads coated with XMAP215, a *Xenopus* microtubule binding protein. Although XMAP215 influences microtubule stability by changing their plus end dynamics, the microtubules shown here are attached to the XMAP215-coated beads by their minus ends (*see* Albee and Wiese ***(17)*** for a description of the experiments that allowed us to determine the polarity of microtubules in this case). We further showed using this bead assay that maskin, a centrosomal protein involved in microtubule anchoring, regulates the interaction of XMAP215 with microtubules and causes the microtubules to be released from the beads (*see* **ref.** *17)*. Scale bar, 10 μm.

9. Protease Inhibitors (1,000×): 10 mg/mL chymostatin, 10 mg/mL leupeptin, 10 mg/mL pepstatin. Dissolve in DMSO and store aliquots at −20°C. Add 100 μL protease inhibitor stock per 100 mL of XB immediately before use.
10. Cytochalasin D (1,000×): 10 mg/mL cytochalasin D dissolved in DMSO and stored at −20°C. Use 100 μL per 100 mL of XB; add immediately before use.
11. Versilube F-50 mineral oil (*see* **Note 2**).
12. SW55 rotor and thin walled SW55 centrifuge tubes (Beckman, Palo Alto, CA; *see* **Note3**).

2.2. Isolating Xenopus Sperm Chromatin

1. 1–2 male *Xenopus laevis* frogs (Nasco, Inc., Fort Atkinson, WI).
2. Human Chorionic Gonadotropin (hCG; Sigma-Aldrich, St. Louis, MO): 100 U/mL in sterile water. Stable at 4°C for up to 3 weeks. Use 1 mL (100 U) per male frog.
3. Sterile dissecting tools: mouse-tooth tweezers, forceps, and scalpel or sharp pointy scissors.
4. Buffer A salts (10×): 800 mM KCl, 50 mM EDTA, 150 mM Na-PIPES pH 7.4, 150 mM NaCl.
5. Solution X: dilute Buffer A salts to 1×, add 0.2 M sucrose and 7 mM $MgCl_2$. Need about 10 mL per frog.
6. Anesthesia: 2.5 g 3-aminobenzoic acid ethyl ester (Tricaine; Sigma-Aldrich, St. Louis, MO) per liter in distilled water. Handle with extreme care as tricaine is toxic.
7. 25× MMR: 2.5 M NaCl, 50 mM KCl, 25 mM $MgCl_2$, 50 mM $CaCl_2$, 2.5 mM EDTA, 125 mM Na–HEPES, pH 7.8. Autoclave and store at room temperature.
8. Clinical centrifuge (IEC, VWR Scientific).
9. Lysolecithin solution (10×): 0.5% lysolecithin (also named lysophosphatidylcholine; catalog #62962, Sigma Aldrich, St. Louis, MO), 200 mM maltose, 7 mM $MgCl_2$. Store at –20°C.
10. X + lysolecithin: Dilute 100 µL lysolecithin stock into 900 µL solution X. Need 2 mL per frog.
11. Solution X + 3% (w/v) bovine serum albumin (BSA; fraction V; Sigma Aldrich, St. Louis, MO). Need 5 mL per frog.

2.3. Isolating Centrosomes from Tissue Culture Cells

1. F12 medium (Gibco, Invitrogen, Carlsbad, CA) supplemented with 10% FBS (Gibco, Invitrogen, Carlsbad, CA) and 1% penicillin/streptomycin (Gibco, Invitrogen, Carlsbad, CA).
2. 150 mm tissue culture dishes.
3. Cytochalasin D (1,000×): 10 mg/mL cytochalasin D dissolved in DMSO; store at –20°C.
4. Nocodazole (1,000×): 10 mg/mL nocodazole dissolved in DMSO; store at –20°C.
5. PE: 10 mM PIPES, 1 mM EDTA, 8 mM β-mercaptoethanol; make as a 50× stock (without β-mercaptoethanol) and pH to 7.2 with KOH. Add β-mercaptoethanol to 8 mM immediately before use. Store at 4°C.
6. 8% sucrose (w/w) in 1 mM Tris–HCl (pH 8.0).
7. Lysis buffer (LB): 1 mM Tris-HCl, 8 mM β-mercaptoethanol. 1 mM Tris-HCl solution can be made ahead of time, but add the β-mercaptoethanol immediately before use. Store at 4°C.

8. LB + 0.5% NP-40: Add 0.5% NP-40 (also called IGEPAL CA-630, Sigma, St. Louis, MO) to LB (1 mM Tris–HCl) and warm to 37°C for 30 min to ensure that the detergent has dissolved. Store at 4°C. Add β-mercaptoethanol immediately before use.
9. PBS (10×): 1.37 M NaCl, 20 mM KCl, 80 mM Na_2HPO_4, 20 mM KH_2PO_4. Store at room temperature.
10. 0.1× PBS + 8% (w/w) sucrose: Dilute PBS to 0.1× in water and add 8% (w/v) sucrose (*see* **Note 4**). Store at 4°C.
11. 20% and 62.5% (w/w) sucrose solution in 1XPE/0/1% Triton X-100 (*see* **Notes 4** and **5**). Store at 4°C. Add 8 mM β-mercaptoethanol immediately before use.
12. 20% (w/w) Ficoll (MW 400,000) cushion: Weigh out 10 g of Ficoll and add 1× PE + 0.1% NP-40 until the total weight reaches 50 g. Stir at room temperature for several hours to dissolve. Make the day before the prep. Immediately before use, add β-mercaptoethanol to 8 mM.
13. SW28 rotor and centrifuge tubes (344058, Beckman, Palo Alto, CA).
14. BRB80 (5×): 400 mM PIPES–KOH, pH 6.8; 5 mM $MgCl_2$; 5 mM EGTA. Filter-sterilize, and store at 4°C (*see* **Note 6**).
15. Methanol stored at –20°C to keep it cold.
16. TBS + 0.1% Triton X-100: 150 mM NaCl, 20 mM Tris–HCl, pH7.4, 0.1% Triton X-100. Store at room temperature.
17. Microscope slides and coverslips (12 mm circles; Fisher, Pittsburg, PA, catalog #12–545–81).

2.4. Purifying and Labeling Proteins to be Analyzed by Microscopy

We generally express the proteins we wish to study as glutathione S-transferase (GST) fusion proteins (using vectors such as Amersham's pGEX6P2) in bacteria and cleave off the GST portion after purification over glutathione-agarose (according to the manufacturer's instructions). The choice of fusion protein depends on vector availability, personal preference, and the protein to be expressed/purified.

An array of fluorophores (for example, Alexa Fluor® 488; product #A-10235) is available from Molecular Probes (now Invitrogen, Carlsbad, CA). The choice of fluorophore to be used depends on the filter sets on the microscope to be used for imaging, but usually includes fluorophores that emit red (e.g., rhodamine or Texas red) or green (fluorescein). Labeling chemistries can either involve succinimides (*N*-hydroxysuccinimde, NHS), which attach to primary amines, or maleimide, which covalently attaches to the sulfhydryl group in cysteines. The choice of fluorophore and conjugating chemistry will strongly depend on the protein to be analyzed and needs to be determined empirically.

We follow the manufacturer's instructions for covalently labeling proteins and have had good success with this approach. As an alternative, fusion proteins with green fluorescent protein (GFP) or any of its derivatives and/or relatives can be used.

2.5. In Vitro Assays

2.5.1. Measuring Microtubule Dynamics in Egg Extracts

1. Hoechst DNA dye: dissolve 200 µg/mL bisbenzimide H33342 trihydrochloride (EMD Chemicals, Gibbstown, NJ) in water. Light sensitive, store at room temperature in the dark. For a working stock, dilute 1:1,000 in water.
2. Valap: equal parts petroleum jelly (vasline), lanolin, and paraffin (*see* **Note 7**).
3. Saturated hemoglobin solution (*see* **Note 8**). Prepare fresh and store on ice until use.
4. BRB80 (5×): 400 mM PIPES–KOH, pH 6.8; 5 mM $MgCl_2$; 5 mM EGTA. Filter-sterilize, and store at 4°C (*see* **Note 6**).
5. BRB80 (1×): 80 mM PIPES–KOH, pH 6.8; 1 mM $MgCl_2$; 1 mM EGTA. Prepare as a 5× stock (*see* **Note 6**). Filter-sterilize and store at 4°C.
6. Glucose oxidase: 10 mg/mL in 50% (v/v) glycerol/1× BRB80. Store in single use aliquots at –80°C.
7. Catalase: dissolve 10 mg/mL in 50% (v/v) glycerol/1× BRB80. Store in single use aliquots at –80°C.
8. Glucose: prepare a 1 M solution in water. Filter-sterilize and store in 1 mL aliquots at –80°C. The glucose solution can be thawed and re-frozen several times.
9. Antifade solution: mix 5 µL glucose oxidase with 5 µL catalase, then add 5 µL glucose and mix again. Make immediately before use and store in a capped tube on ice (*see* **Note 9**).
10. Egg extract, prepared as described in **Subheading 3.1**.

2.5.2. Time-Lapse Microscopy

Imaging microtubule dynamics requires a high resolution fluorescence microscope with at least a 60× (1.4 NA) objective (but preferably a 100×/1.4 NA), a set of standard filter sets for red (rhodamine) and green (fluorescein) fluorophores, a cooled CCD camera, a shutter to prevent excessive photo-damage, and a computer with enough memory and storage capacity to capture and display large image data sets. Imaging analysis software is also required.

2.5.3. Centrosome Complementation

1. Humidified incubation chamber: waterproof box of suitable size for several coverslips, parafilm, and kimwipes (*see* **Note 10**).
2. Microscope slides and coverslips (12 mm in diameter, 0.13–0.17 mm thick) from Fisher, Pittsburg, PA (*see* **Note 11** for coverslip preparation).
3. Waterbath, set to 30°C.

4. Centrosomes: prepared as described in **Subheading 2.3** and **3.3**.
5. BRB80 (5×): 400 mM PIPES–KOH, pH 6.8; 5 mM $MgCl_2$; 5 mM EGTA. Filter–sterilize and store at 4°C (*see* **Note 6**).
6. BRB80 (1×): 80 mM PIPES–KOH, pH 6.8; 1 mM $MgCl_2$; 1 mM EGTA. Prepare by dilution (1:5) from 5× stock. Filter-sterilize and store at 4°C.
7. 4 M KI in 1× BRB80. This solution should be prepared fresh before each use and should be kept in the dark because it is light sensitive.
8. HEPES Block (HB): 50 mM HEPES, pH 7.6, 100 mM KCl, 1 mM EGTA, 1 mM $MgCl_2$, 10 mg/mL BSA. Filter-sterilize and store at 4°C.
9. Tubulin Dilution Buffer (TDB): 10 mg/mL BSA and 10% glycerol in 1× BRB80. Filter- sterilize and store at 4°C.
10. Bovine brain tubulin, 10–20 mg/mL stock (*see* **Note 12**).
11. Rhodamine-labeled tubulin (*see* **Note 12**).
12. GTP: 0.1 M in 1× BRB80. Store aliquots at −20°C (*see* **Note 13**).
13. Fixing solution: 1% glutaraldehyde in 1× BRB80. This solution should be prepared fresh before use and kept warm at 30°C to prevent microtubule depolymerization (*see* **Note 14**).

2.5.4. Bead Nucleation

1. Protein A Dynabeads (Dynal, Invitrogen, Carlsbad, California).
2. Magnet for collecting beads (Dynal, Invitrogen, Carlsbad, California).
3. Waterbath, set to 30°C.
4. TBS + 0.1% Triton X-100: 150 mM NaCl, 20 mM Tris–HCl, pH7.4, 0.1% Triton X-100. Filter-sterilize TBS before adding the detergent. Store at room temperature.
5. XB: 10 mM K–HEPES, 100 mM KCl, 1 mM $MgCl_2$, 0.1 mM $CaCl_2$, 50 mM sucrose, pH 7.6. Store at 4°C.
6. Bovine brain tubulin, 10–20 mg/mL stock (*see* **Note 12**).
7. Rhodamine-labeled tubulin (*see* **Note 12**).
8. BRB80 (5×): 400 mM PIPES–KOH, pH 6.8; 5 mM $MgCl_2$; 5 mM EGTA. Filter-sterilize and store at 4°C (*see* **Note 6**).
9. BRB80 (1×): 80 mM PIPES–KOH, pH 6.8; 1 mM $MgCl_2$; 1 mM EGTA. Prepare by dilution (1:5) from 5× stock. Filter-sterilize and store at 4°C (*see* **Note 6**).
10. GTP: 0.1 M in 1× BRB80. Store aliquots at −20°C (*see* **Note 13**).

11. Fixing solution: 1% glutaraldehyde in 1× BRB80. This solution should be prepared fresh before use and kept warm at 30°C to prevent microtubule depolymerization (*see* **Note 14**).
12. 80% glycerol in BRB80: dilute glycerol to 80% in 1× BRB80. Store at room temperature.
13. Microscope slides and coverslips (18 × 18 mm) from Fisher (Pittsburg, PA).

3. Methods

3.1. Xenopus Egg Extracts

This section describes the preparation of CSF-arrested *Xenopus* egg extracts ***(9)***, which serve as the basis for the experiments described in **Subheading 3.4**.

1. Several days (3–7) before the extracts are needed, prime the frogs by injecting 100 U (0.5 mL) of PMSG (*see* **Note 15**) into the dorsal lymph sac of each frog using a 1 mL syringe and a 25 gauge needle.
2. The evening before extracts are needed (*see* **Note 16**), induce ovulation by injecting each frog with 500 U (0.5 mL) of hCG and keep frogs overnight in separate containers in 2 L of 1× MMR (*see* **Note 17**).
3. The next morning, *gently* squeeze the frogs (caution: wear non-powdered gloves at all times while handling frogs; *see* **Note 18**) and collect eggs into 1× MMR (*see* **Note 19**). Transfer eggs into a 250 mL glass beaker to estimate the volume of eggs and assess quality. Using a sawed off (diameter slightly larger than the eggs) fire-polished glass Pasteur pipette, remove detritus (frog skin and feces) and as many uneven and bad-looking eggs as possible before pooling eggs from different frogs. Do not use eggs from batches with large numbers of bad eggs.
4. Rinse eggs once briefly with 2% cysteine, decant, replace with fresh 2% cysteine. Dejellying takes 7–10 min at room temperature and is complete when the eggs pack tightly. To speed up dejellying, eggs can be rinsed with fresh cysteine several times during dejellying process (but *see* **Note 20**). Minimize the exposure of the eggs to cysteine and do not expose them for more than 10 min. If the eggs have not lost their jelly coat within 10 min, the cysteine has gone bad on the shelf or the pH is not correct.
5. While the eggs are dejellied, set up the spin tubes (Beckman SW55; *see* **Note 3**). For each 5 mL of dejellied eggs, add

1 mL CSF-XB + 1X protease inhibitors to a clean thin walled SW55 tube. Add cytochalasin D to 100 μg/mL (10 μL of 10 mg/mL stock) to each tube and mix.

6. Carefully pour the cysteine and gently rinse the eggs four times with XB (*see* **Note 21**). All the while, continue to "garden" out bad eggs with a fire-polished Pasteur pipette.
7. Finally, rinse the eggs four times with CSF-XB + protease inhibitors. You should still be gardening, but hopefully by the time you get to the last wash, most if not all of the "bad" eggs have been picked out.
8. Transfer the eggs to the spin tubes in a minimal amount of buffer to keep the cytochalasin D as concentrated as possible. Cut-off, flame-polished glass Pasteur pipettes work best for this. Remove as much liquid as possible from the eggs.
9. Overlay the eggs with a layer (~1 mL) of Versilube.
10. Pack the eggs in a clinical centrifuge for 60 s at setting #3 followed by 30 s at setting #5. Remove as much liquid as possible to minimize extract dilution.
11. Crush the eggs by spinning them for 15 min at ~9,500 g (RCFavg) in an SW55 rotor. Perform this spin at 16°C. (*see* **Note 3**).
12. Following the crushing spin, place the tubes on ice and set the centrifuge temperature to 2°C.
13. At this point, the extracts will be stratified into at least three layers: yellowish lipids float on top, greenish black yolk and pigment granules pellet at the bottom, and the grayish-yellow cytoplasm will be in the middle. Collect the cytoplasm (middle layer) by puncturing the centrifuge tube with an 18 gauge needle attached to a 3 mL syringe. Position the needle just above the pigment layer (and thus, at the bottom of the cytoplasmic layer) with the bevel facing up. Withdraw the cytoplasm with a very slow but steady suction. Slowly expel the cytoplasmic extract into a fresh SW55 tube.
14. Clarify the extract at ~9,500 g (RCFavg) for 15 min at 2°C in an SW55 rotor.
15. Collect the clear cytoplasmic layer, which will make up most of the volume in the tube. The extract should be straw-colored and slightly viscous.
16. Add 1/1,000 volume of protease inhibitors and cytochalasin D. Use the extract immediately (preferred) or quick-freeze 100 μL aliquots in liquid N_2 and store at −80°C (*see* **Note 21**).
17. To immunodeplete the extracts, prebind antibodies to Affi-prep proteinA (BioRad, Hercules, CA) or preferably to Protein A Dynabeads (Dynal Biotech (now Invitrogen), Carlsbad, California; *see* **Note 22**).

3.2. Isolating Xenopus Sperm Chromatin

Production of microtubules in *Xenopus* eggs requires a trigger, which is provided by the entering sperm during fertilization. This process can be mimicked in the test tube by the addition of demembranated sperm chromatin to the egg extract. The protocol described here for the preparation of sperm chromatin suitable for adding to egg extract is based on the methods described by ***(7)*** and ***(10)***.

1. Inject 1–2 male frogs with 100 U hCG the day before the testes are needed. Let the frog rest for 1 h.
2. Anesthetize the frog in tricaine (2.5 g/L) for 20 min or until it no longer fights being turned on its back (handle with extreme care, as tricaine is toxic).
3. Pith the frog and dissect out the testes: lay the frog on its back and cut through the skin and body wall muscles. The testes are the shiny, kidney-shaped white ovals (~1 cm long) attached to the base of the yellow fat body on either side of the midline in the lower half of the body cavity. Remove the testes and trim off as much of the yellow fatty tissue as possible, taking care to avoid cutting the major blood vessels.
4. Place testes in a vial with 10 U/mL hCG in 1× MMR.
5. Incubate testes at 18°C overnight. Rinse in 1× MMR. **Steps 6–24** are preformed at room temperature.
6. Rinse testes in solution X. Remove as much of buffer as possible.
7. Mince testes with mouse-tooth tweezers and/or a scalpel to release sperm. Add 1 mL of X. Mince well but do not cause disintegration of outer tissue.
8. Allow large chunks to sink to the bottom of the tube. Spin 10 s at setting #3 in a clinical centrifuge.
9. Collect supernatant into a new tube. This contains the released sperm.
10. Back-extract the pelleted tissue with an additional 0.5 mL of X and spin as in step 8.
11. Combine the supernatants and spin for 10 min at ~1,500 g (RCFavg) (setting #7 in a clinical centrifuge) to pellet the sperm.
12. Discard the supernatant.
13. Resuspend the white part of the pellet in solution X, using five times 100 μΛ (for a total of ~500 μL). Avoid the red, dirty part of the pellet, which contains red blood cells and somatic nuclei.
14. Pellet the sperm for 10 min at ~1,500 g (RCFavg).
15. Resuspend sperm in 5 × 100 μL aliquots of solution X, as in **step 13**.
16. Pellet the sperm for 10 min at ~1,500 g (RCFavg).

17. Resuspend sperm in 200 µL of X and place 100 µL each into two separate tubes.
18. To each tube, add 1 mL of X + 0.05% lysolecithin and incubate at room temperature for 5 min (*see* **Note 23**).
19. To stop the reaction, add 3 mL of X + BSA to each tube and mix gently.
20. Pellet the chromatin for 10 min at setting #5 in a clinical centrifuge.
21. Resuspend the pellets in 200 µL of X + 3% BSA. Mix gently and add an additional 1 mL of X + 3% BSA.
22. Pellet the chromatin for 10 min at setting #5 in a clinical centrifuge.
23. Resuspend the pellet in 50–150 µL of solution X. From now on, keep the sperm chromatin on ice. Use a hemacytometer to determine sperm concentration. Adjust the sperm concentration of the preparation with Solution X to 40,000 per µL. Recount the adjusted preparation to ensure accuracy.
24. Aliquot sperm chromatin into 2 µL aliquots, freeze in liquid nitrogen and store at −80°C (*see* **Note 24**).

3.3. Isolating Centrosomes from Tissue Culture Cells

This procedure for isolating centrosomes follows the methods developed by Mitchison and colleagues ***(11)***; see also the Mitchison lab web page at Harvard Medical School, http://mitchison.med.harvard.edu/protocols/). We found that it also works to isolate centrosome from *Xenopus* tissue culture cells, but it is described for Chinese hamster ovary (CHO) cells here.

1. Pass CHO-K1 cells and plate onto 20 large (150 mm) tissue culture dishes and allow the cells to grow to confluency. Change the medium the day before the procedure to ensure that the cells have enough nutrients.
2. The day before the prep, prepare 600 mL each of the following solutions and store them in the cold room (*see* **Note 25** about cold-room set up). Make the following buffers without β-mercaptoethanol, but add the β-mercaptoethanol immediately before use:

   (1) 1X PBS, (2) 0.1X PBS + 8% (w/w) sucrose, (3) 8% (w/w) sucrose, (4) LB, (5) LB + 0.5% NP-40.
3. On the day of the centrosome prep, set up sucrose gradients (18 mL; 20%–62.5%) in two SW28 tubes (*see* **Note 26**).
4. Warm 600 mL of CHO medium to 37°C and add 5 µg/mL cytochalasin D (300 µL of 10 mg/mL stock) and 10 µg/mL nocodazole (600 µL of 10 mg/mL).
5. Add 20 mL of drug medium to each of ten dished and return the dishes to the incubator (start the drug treatment for the second set of 20 plates 45 min later).

6. After 90 min in the drug medium, process the first set of 10 plates: bring the plates into the cold room and, processing one plate at a time through all of the wash steps (do this as quickly as possible), wash the cells quickly with the following buffers in the order listed by adding 30 mL of solution onto the plates, swirling briefly, and removing the wash solution by aspiration (*see* **Note 27**):

   (1)) 1× PBS, (2) 0.1× PBS, 8% (w/w) sucrose, (3) 8% (w/w) sucrose, (4) LB. Lastly, add 10 mL of LB + 0.5% NP-40 and transfer plate to a rocker in the cold room. Gently rock the plates for 10 min.

7. Combine the lysates into a 50 mL conical tube. Add 1/50 volume of 50× PE (don't forget to add β-mercaptoethanol) and mix gently.

8. Spin the lysates for 3 min at 1,500 × *g* (3,000 rpm in a JS 13.1 rotor or equivalent) at 4°C to pellet the nuclei.

9. Transfer the supernatants to 30 mL Corex tubes (8–10) and underlay each with 2 mL of 20% Ficoll 400 in PE/0.1% NP-40 (*see* **Note 28**).

10. Spin at 12,700 rpm (22,500 × *g*) for 15 min at 4°C in a JS 13.1 rotor or equivalent. Process the next set of plates during this spin.

11. Gently aspirate the supernatant, leaving approximately 2 mL above the cushion. Collect the clear interface between the Ficoll cushion and the top layer by "grazing" with a Pasteur pipette (~2 mL/tube) and pool the interfaces into a new tube.

12. Combine pooled interfaces from the first and second set of plates. Check the Ficoll concentration by refractometry and dilute to 10% (w/w) or less to make sure the solution layers are onto the sucrose gradient in the next step and does not sink. Load onto two 20–62.5% sucrose gradients in SW28 tubes. Spin for 1 h at ~100,000 g (RCFavg) in a SW28 rotor at 2°C.

13. Fractionate the gradient from the bottom (*see* **Note 29**). Collect 0.3–0.5 mL fractions and read the sucrose concentration by refractometry. Check fractions between 48 and 60% (w/w) sucrose for centrosomes.

14. Assay each fraction in a10 μL in vitro polymerization reaction containing 3 mg/mL tubulin, 0.3 mg/mL rhodamine-labeled tubulin, 1 mM GTP, and 1 μL centrosome fraction in 1× BRB80.

15. Set up the polymerization reactions in 1.5 mL tubes on ice. Move the tubes to 30°C and incubate for 10 min.

16. Stop the reaction by adding 10 volumes (100 μL) of 1% glutaraldehyde in BRB80 and incubate at room temperature for 3 min.

17. Dilute each reaction with 1 mL of 30% glycerol in BRB80.
18. Layer the polymerization reaction over a 2 mL cushion of 40% glycerol in BRB80 in spindown tubes (*see* **Note 30**).
19. Spin in JS13.1 rotor for 10 min at ~10,000 g (RCFavg) at 25°C.
20. Aspirate the top layer and wash the cushion interface once by adding 1 mL of BRB80.
21. Aspirate, leaving a small amount of liquid above the coverslip.
22. Postfix coverslips in −20°C methanol for 3 min.
23. Transfer the coverslips to TBS + 0.5% Triton X-100 for 3 min.
24. Rinse coverslips in water.
25. Mount coverslips by inverting them onto 2 μL of mounting medium; seal the edges with nail polish. Count the number of centrosomes per field of view in 20–50 randomly chosen fields.
26. Combine the peak centrosome-containing fractions, mix well (but gently), and freeze in small (20 μL) aliquots in liquid nitrogen. Store at −80°C.

3.4. Purifying and Labeling Proteins to be Analyzed by Microscopy

In some cases, it is important to localize specific proteins on mitotic spindles or asters and observe their dynamic behavior, for example to determine whether they move on or with microtubules. For these types of experiments, we start with purified recombinant protein, covalently attach a commercially available fluorophore to the purified protein, and add a small amount of the protein into a microtubule assembly reaction (as described in **Subheading 3.5**, **step 1**). We have successfully used both types of labeling chemistries (cysteine-reactive maleimide or primary amine-reactive succinimidyl esters). Proteins can also be expressed as fusions with green fluorescent protein (GFP) or one of its derivatives, circumventing the need for chemical labeling with fluorophores. In either case, it is important to establish that the labeled protein is functional. We do this by immuno-depleting the endogenous protein (*see* **Note 22**) and testing whether the labeled protein can rescue the depletion phenotype by reconstituting the extract to endogenous levels with labeled protein. This test can be done with fixed samples, using methods described in other parts of this chapter.

1. Assemble the 10–15 μL reaction in a 1.5 mL eppendorf tube on ice according to **Subheading 3.5**, **step 1**, omitting antifade, hemoglobin, and Hoechst dye solutions.
2. Start the reaction by moving the Eppendorf tube to room temperature and incubating for the appropriate amount of time (sperm chromatin assembles microtubule asters within ~15 min and spindles in ~60–90 min when incubated in this way).

3. Fix, dilute, and spin the samples onto coverslips as described in **step 17** (addition of 1 mL of 30% glycerol in BRB80) in **Subheading 3.3**.

If the labeled protein is active, it can now be analyzed by time-lapse microscopy in mitotic **(Subheading 3.1)** or interphase (*see* **Note 21**) egg extracts.

3.5. In Vitro Assays

3.5.1. Measuring Microtubule Dynamics in Egg Extracts

1. On ice, assemble the following in a test tube:
   - 10 μL extract (either untreated or immunodepleted as described in *see* **Note 22**; see also *see* **Note 21**).
   - 0.5 μL hemoglobin solution (freshly made).
   - 0.33 μL antifade solution (freshly made).
   - 0.25 μL rhodamine-labeled tubulin (~2 mg/mL).
   - 0.3 μL sperm chromatin (*see* **Note 31**).
   - 0.25 μL Hoechst dye solution (diluted stock).
   - (optional: a small amount of green-labeled protein to be imaged).
2. Gently mix the reaction (*see* **Note 32**).
3. Spot 2 μL of the reaction on a microscope slide at room temperature. The reaction time starts when the drop is placed on the slide. Start the timer (The remaining extract can be stored on ice and used within 2–3 h.).
4. Carefully cover the drop with an ethanol-washed and dried 22 × 22 mm coverslip. If necessary, gently tap the coverslip to ensure even spreading of the reaction (*see* **Note 33**).
5. Seal the edges of the coverslip with Valap.
6. View in the microscope. Find the sample using the DAPI channel (UV). Centrosomes (and microtubule structures) assemble at one end of the comma-shaped sperm nuclei. Once you have located a sperm, switch to the rhodamine channel to visualize the microtubules and determine minimum exposure time. If your sample also contains a green-fluorescing protein (either GFP fusion or chemically labeled, as described in **Subheading 3.4**), switch to the green channel and determine minimum exposure time in this channel as well. Start recording time-lapse images as soon as possible.

The samples degrade if they are incubated on the slide for more than 5 or 10 min. To image later timepoints, it might help to incubate the reactions at room temperature in an eppendorf tube and spot an aliquot of the reaction onto a microscope slide immediately before you want to image the reaction. However, we have found that the microtubule density at the later timepoints makes the sample very difficult to image. It might help to block non-specific binding of protein to the microscope slide and coverslips by pre-treating them for 3–5 min with a solution of 5 mg/mL

casein (*see* **Note 34**), followed by washing with XB. An alternative method is to use a thick sample and image microtubules by spinning disk confocal microscopy.

3.5.2. Time-Lapse Microscopy

1. For time-lapse, acquire images (at a wavelength appropriate for the fluorophore you wish to image) every 1–2 s for 5 min and compile the images into stacks. Use the minimum possible exposure time (generally 500 ms or less). Monitor image quality throughout acquisition and refocus the image if you are working on a microscope that does not monitor and adjust the focal plane automatically.
2. Use appropriate computer software to generate microtubule dynamics data. For example, the "track points" function of MetaMorph works well for this purpose.
3. Generate vector plots for microtubules using least-squares linear regression analysis.
4. Microtubule dynamics are characterized by four parameters: rate of growth, rate of shrinkage, frequency of transition from growth to shrinkage (catastrophe), and frequency of transition from shrinkage to growth (rescue) ***(12)***. Dynamic parameters for growth and shrinkage are determined from the slope of the plot for microtubules that grow or shrink at least 0.5 μm in four consecutive frames (6–8 s). Rates are expressed as μm per minute. Microtubules are also known to pause. Determine separate parameters for pausing during growth and pausing during shrinkage.
5. Frequencies of catastrophe or rescue are calculated by dividing the number of catastrophes or rescue events by the total time microtubules spent growing or shrinking, respectively. Frequencies are expressed as events per second.

3.5.3. Centrosome Complementation

The centrosome complementation assay, refined and adapted for fly centrosomes by Moritz et al. ***(13)*** and for surf clam centrosomes by Schnackenberg et al. ***(14)*** is useful for understanding the contribution a given protein makes to the nucleation capacity of centrosomes. This assay is based on the observation that the nucleating capacity of isolated centrosomes can be destroyed by treating the centrosomes with chaotropic agents (such as high salt, as in this case). The nucleation capacity can be restored to the salt-stripped centrosomes by incubating them in cytoplasmic extracts. We describe the basic assay here. Of course, the centrosomes can be "complemented" with extracts depleted of individual proteins or protein complexes, as well as extracts supplemented or reconstituted with a variety of agents or proteins. This assay, properly adapted, can also reveal differences in requirements for centrosomal proteins in interphase and mitosis.

1. Set up a humidified incubation chamber (*see* **Note 10**) and place the required number of coverslips on the parafilm inside the chamber. Incubate the chamber in a 30°C water bath. Pre-warm HB and TDB in the water bath.
2. Mix equal volumes of 4 M KI (freshly prepared) and centrosomes (final KI concentration is 2 M) and incubate on ice for 10 min. This step serves to salt-strip the centrosomes, leaving them unable to nucleate microtubules.
3. Pipette KI/centrosome mix onto the coverslips and incubate for 10 min to allow the centrosomes to settle and bind to the glass coverslips.
4. Briefly wash the centrosomes three times by pipetting 150 µL of warm HB on the coverslips and aspirating off the liquid. Leave the final wash on the coverslips for 5 min.
5. Add 50 µL of *Xenopus* egg extract (untreated or depleted) and incubate for 10 min.
6. Wash the coverslips three times with 200 µL TDB.
7. Add 25 µL of in vitro microtubule polymerization reaction (2–3 mg/mL tubulin, 0.3 mg/mL rhodamine-tubulin, 1 mM GTP in BRB80) to the coverslip and incubate for 10 min at 30°C.
8. Fix for 3 min with 60 µL 1% glutaraldehyde in BRB80, followed by a 3 min incubation with cold (−20°C) methanol. Wash the coverslips with TBS to rehydrate.
9. Mount coverslips with 2 µL mounting medium on microscope slides.
10. Assess complementation by counting the number of centrosome-nucleated asters in 50 randomly chosen microscope fields.

3.5.4. Bead Nucleation Assay

The bead nucleation assay provides information about the interaction of a given microtubule binding protein with microtubules. For example, the microtubule binding protein, XMAP215 ***(15)***, appears to nucleate and/or anchor microtubule minus ends (**Fig. 3**; *see* also ***(16)*** and ***(17)***). The basic protocol for the bead assay is as follows. This simple assay can easily be modified to test the effect of regulators on the interaction between microtubules and a given microtubule binding protein.

1. Gently resuspend Dynabeads and remove 10 µL of bead slurry. Remove excess buffer. Wash beads with 200 µL of TBS + 0.1% Triton-X100. Incubate 10 µL antibody with beads for 40 min at room temperature or 1 h at 4°C.
2. Remove excess antibody solution from beads using the magnet. Wash the antibody-coated beads three times with XB. Remove as much buffer as possible. Add 50–100 µL egg extract to the beads and incubate for 1 h at 4°C with rotating (*see* **Note 35**).

3. Separate the extract from the beads (*see* **Note 36**). Wash the beads three times with 200 μL XB. Resuspend beads in 10 μL XB.
4. Add 0.5 μL beads to a 10 μL in vitro polymerization reaction (2–3 mg/mL tubulin, 0.2–0.3 mg/mL rhodamine-tubulin, 1 mM GTP in BRB80). Incubate the reaction for 10 min at 30°C.
5. Fix for 3 min with 100 μL of fix solution (1% glutaraldehyde in BRB80).
6. Dilute with 250 μL of 80% glycerol in BRB80.
7. Spot 3 μL of the reaction on a microscope slide and cover with an 18 × 18 coverslip. Seal the edges of the coverslip with nail polish and view samples in the microscope.

4. Notes

1. Dejellying solution: dissolve cysteine (free base; Sigma, catalog #C-7755) in H_2O; titrate to pH 7.8 with 1 N NaOH (this will take ~4.5 mL per 100 mL dejellying solution). Prepare immediately before use. The amount of 2% cysteine needed depends on the volume of eggs laid. Estimate that you need at least 5–10 times more 2% cysteine than volume of eggs. For example, if you have ~50 mL of eggs, make up at least 250 mL of 2% cysteine.
2. Versilube F-50 mineral oil (General Electric).
3. The cytoplasmic fraction of the egg extract is collected by puncturing the side of the centrifuge tube with a needle attached to a syringe; thus, the centrifuge tube has to be soft enough to allow an 18 gauge needle to pass through. Either type of Beckman thin wall centrifuge tube (polyallomer or ultraclear) will work (part number 326819 or 344057, respectively). In a pinch, the extracts can also be fractionated in a 15 mL tube (Falcon 2059) in a Beckman JS13 swinging bucket rotor (centrifuged at 14,500 g (RCFavg) for 15 min at16°C). Make sure centrifuge tubes are at least half full.
4. The quality of sucrose is critical to the success of the centrosome preparation. Use only ultra-pure sucrose (S7903, Sigma, St. Louis, MO) or equivalent.
5. To make the sucrose solutions, weigh out 20 g (20%) or 62.5 g (62.5%) of sucrose in a beaker on a balance and then add 1× PE + 0.1% Triton X-100 until the weight is 100 g.
6. PIPES will not dissolve in water unless the pH is near neutral. Place powdered PIPES in a beaker with a stir bar, add 0.9 vol water and start adding **potassium** hydroxide solution (not NaOH) while stirring. Adjust the pH to 6.8 once all

the powder has dissolved and the solution has reached room temperature.

7. Valap: weigh out equal parts of petroleum jelly (vasline), lanolin, and paraffin and place in a glass bottle.Cap the bottle loosely and place it inside a glass beaker containing a small amount of water (enough to mostly cover the Valap inside the bottle, but not so much that the bottle floats) to make a waterbath. Heat the waterbath on a hotplate to melt the Valap. Mix gently and carefully by swirling the bottle (caution: bottle will be hot, and hot steam will escape). Allow the Valap to cool (it will solidify) and store at room temperature. Melt the Valap before use by heating it in a waterbath on a hot plate.
8. To make saturated hemoglobin solution, place a few micrograms of horse hemoglobin (Sigma Aldrich, St. Louis, MO; catalog #H4632) in a 1.5 mL microfuge tube. Add 50 μL of water to dissolve the hemoglobin and spin the solution in a microfuge for 3 min at top speed to pellet undissolved hemoglobin. Use the supernatant as an oxygen scavenger in live imaging reactions.
9. The antifade solution has a limited lifespan; it is stable on ice for 30–45 min. Make fresh as needed from the individual components (glucose oxidase, catalase, and glucose), which are stable on ice for several hours.
10. Humidified incubation chamber is assembled by placing a piece of parafilm inside a plastic box. The lid of a pipette tip box works well. The box should be water-tight and float in a water bath. Place several kimwipes around the inside perimeter of the box and wet them with water. Cover the humidified chamber with a lid during incubation. Incubation of the samples in the humidified incubation chamber reduces evaporation of the small sample volumes used in this type of experiment.
11. Coverslips should be acid washed to ensure that they are free from dust. Place coverslips in a glass beaker, add 1 M HCl to cover them, and heat to 55–65°C for 4–16 h. Rinse coverslips five times in water and five times in 70% ethanol. Dry coverslips by individually placing them on fluted Whatman paper. If coverslips overlap during the drying process they will stick together.
12. Bovine brain tubulin (both fluorescently labeled and unlabeled) can be purchased from Cytoskeleton, Inc. (Denver, CO; for example, catalog # T238). Alternatively, tubulin can also be purified from cow brains by the method described on the Mitchison lab web page at Harvard Medical School, http://mitchison.med.harvard.edu/protocols/tubprep.

html, or on the Walczak lab web page at Indiana University, http://mypage.iu.edu/~walczak/). For making labeled tubulin, see ***(18)***.

13. Dissolving powdered GTP in water results in a very acidic solution. Therefore, GTP needs to be made up in buffer. To determine the exact concentration of the final solution, measure the absorption at 260 nm and use extinction coefficient & 13.7 × 10^3 M^{-1} × cm^{-1} (pH 7.0) to calculate the concentration of GTP. If necessary, adjust the volume of the stock solution. Aliquot and store at –20°.
14. The quality of glutaraldehyde is important for efficient fixing. We purchase 25% EM-grade glutaraldehyde from Ted Pella Inc. (Redding, CA; product # 18426). Aliquot the contents of one 10 mL ampule at a time into 100 µL aliquots and store air-tight at –20°C.
15. All injections should be performed into the dorsal lymph sac using a 25 gauge needle (BD 25G5/8; order #305122). We inject 0.5 mL of 200 U of PMSG. Frogs can be used for egg laying between 3 and 7 days after PMSG injection. They should not be fed during this time as they will regurgitate their food.
16. The time for the beginning of egg-laying is dependent on temperature (7 h at room temp to 14 h at 16°C). Ovulation will continue for at least 6 h at both temperatures. Keep the frogs in separate containers for egg laying. This will make it much easier to separate out batches of eggs that should not be used for the extracts - i.e., batches with >10% "puffballs" (which are larger than healthy eggs and are white) or "stringy" eggs.
17. Frogs should be kept in containers with tight-fitting lids (with air-holes, of course). The lids should be weighed down with books or bottles or other suitable weights to prevent the frogs from escaping. They tend to be more jumpy after the injections, and they can escape surprisingly well. If a frog does escape and is found before it dries out, it needs to be kept in a small (escape-proof) container separate from the other frogs, treated with antibiotics for a few days, and carefully watched.
18. Aquatic species like *Xenopus* can carry parasites (including nematodes and mycoplasmas) that *can* cause infections in humans. Wear gloves at all times while handling frogs (to protect the frogs make sure they are nonpowdered) and wash your hands with soapy water after handling them.
19. Both the eggs laid spontaneously and the freshly squeezed eggs can be used for making extracts, although the freshly squeezed eggs tend to make higher-quality (albeit smaller

volume) extracts. If you collect eggs by squeezing, keep the back end of the frog under water while squeezing to prevent egg activation. Squeeze gently and front-to-back to prevent injuring the frog.

20. The eggs become much more fragile once the jelly coat has been removed - they should be handled very gently from now on to avoid breakage.
21. If you wish to make interphase extracts, make the following changes to the protocol: keep the frogs in salted water (2 g NaCl/L) overnight. Do not use CSF-XB. Instead, wash and crush the eggs in S-lysis buffer (250 mM sucrose (ultrapure), 50 mM KCl, 2.5 mM $MgCl_2$, 1 mM DTT, 50 μg/mL cycloheximide (from 10 mg/mL stock in water – toxic), 5 μg/mL cytochalasin B (from 10 mg/mL stock in DMSO – toxic) and perform the crushing spin at 4°C. Place the extracts on ice after the crushing spin and collect the cytoplasmic layer as for mitotic extracts. Use extracts immediately as interphase extracts prepared in this way do not freeze well. See ***(10)*** for a protocol describing the steps to prepare the extract for freezing. Fresh extracts do not require an ATP regenerating system (they contain mitochondria), but you need to add an ATP regenerating system (a 20× stock is 150 mM creatine phosphate, 20 mM ATP, and 20 mM $MgCl_2$; store in 100 μL aliquots at –20°C) to previously frozen extracts.
22. The amount of antibody required to deplete the protein of interest has to be determined empirically. It is important to minimize additions to the extract to minimize dilution (the general rule is to keep additions to less than 20%), and it is therefore a good idea to prebind the antibodies to the beads. In general, we use no more than 15–30 μL of beads per 100 μL extract. The antibody binding capacity of the beads is quite high and in most cases we use substantially less than 30 μL. Deplete 100 μL of extract at a time in a 0.5 mL microfuge tube. To allow good mixing of the beads with the extract, introduce a small air-bubble into the extract and rotate the extract at 4°C for 1–1.5 h. Pellet the beads by a 10 s spin in a nanofuge (if using Protein A beads) or by collecting them for 10 min on a magnet held on ice (if using Dynabeads). Avoid the beads when withdrawing depleted extract for experimentation.
23. Lysolecithin strips away the sperm plasma membrane and nuclear membranes. We have anecdotal evidence that the same can be achieved by treating the sperm with Triton X-100, but we have not tried this ourselves. Centrosomes can also be used instead of sperm to initiate microtubule assembly. Do not include Hoechst dye with centrosomes.
24. Sperm settles quickly, so keep mixing thoroughly by pipetting while aliquotting.

25. In the coldroom, set out the buffers in the order listed. Also set up in the coldroom a vacuum line with a large trap (at least 4 L) and a rocker.
26. Pour a 16 mL linear sucrose gradient (20–62.5%) on top of a 2 mL pad of 62.5% sucrose in each of two SW28 tubes. The centrosomes will concentrate near the bottom of the gradient. The pad prevents the centrosomes from entering the curve of the tube and gives a little bit of wiggle room when setting up the fractionation. The sucrose gradients can be poured during the drug treatment.
27. These washes should be done as quickly as possible. All washes should be under 1 min per plate. Pour the wash buffer from a beaker or graduated cylinder (~30 mL), aiming for the side of the tissue culture dish. If the buffer is added directly to the bottom of the plate, the cells may detach and wash away. After addition of buffer, carefully rock the plate back and forth without dislodging the cells and aspirate quickly before pouring on the next wash. It is critical to do this rapidly to get good lysis or most of the centrosomes will be lost in the nuclear pellet.
28. Underlay by using a 10 cc syringe filled with the Ficoll solution with a thin piece of tygon tubing attached to the end of the syringe.
29. Perform this step in the coldroom. Pierce the bottom of the SW28 tube with an 18 gauge needle (BD 18G11/2; order # 305196) and allow the sucrose to drip through the needle into labeled 1.5 mL tubes. At higher sucrose concentrations (the bottom of the gradient), the solution will flow slowly. As the sucrose concentration decreases, fraction collection will speed up.
30. Spin tubes are homemade devices set up in 15 mL corex glass tubes. A 1 cm flat-top round-bottom adapter is fixed in place at the bottom of the tube. A 1 cm flat-bottom/flat-top chuck with a notch on one side (running down the length of the chuck) is placed on top of the fixed adapter and will be used to hold and remove the 12 mm coverslip, which is placed on top of the chuck. The chuck can be removed with a piece of wire with a small hook at the end. The adapter and chuck should be small enough to allow the glycerol cushion to cover the coverslip.
31. Centrosomes can also be used instead of sperm to initiate microtubule assembly. When using centrosomes omit Hoechst dye.
32. Introduce an air bubble with a pipette and turn the tube over several times using the hemoglobin as a guide for efficiency of mixing. The hemoglobin is much darker than the extract and when the reaction is a homogenous color, the reaction is sufficiently mixed.

33. To prevent blurriness of the images, it is important that the reaction spreads out evenly and thinly. We therefore use coverslips that are free of dust and dirt.
34. Prepare casein solution in the following way: dissolve powdered casein (Sigma # C-5890) to 15 mg/mL in 20 mM Tris, pH 8.0. Allow to rotate on a rotator at 4°C for several hours. Clarify the solution by spinning at ~205,000 g (RCFavg) in a TLA100.4 rotor and collect the clear middle layer. Measure protein concentration using the Bradford assay and adjust the concentration to 5 mg/mL. Filter and store aliquots at –20°C.
35. Depending on the circumstances, protein-coated beads can also be generated by incubating the antibody-covered beads with recombinant protein rather than extract. Alternatively, protein can be coupled directly to activated (not Protein A-coated) Dynabeads without the use of antibody as an adaptor.
36. The extract can be viscous and difficult to separate from the beads. To make this easier, place the magnet on ice and incubate the extract and beads for at least 10 min on ice.

Acknowledgments

Work in the Wiese Lab is supported by NSF CAREER award MCB-0643878 (to CW).

References

1. Wiese, C., and Zheng, Y. (2006) Microtubule nucleation: γ-tubulin and beyond. *J. Cell Sci* **119**, 4143–4153
2. Andersen, J. S., Wilkinson, C. J., Mayor, T., Mortensen, P., Nigg, E. A., and Mann, M. (2003) Proteomic characterization of the human centrosome by protein correlation profiling. *Nature* **426**, 570–574
3. Azimzadeh, J., and Bornens, M. (2007) Structure and duplication of the centrosome. *J Cell Sci* **120**, 2139–2142
4. Bettencourt-Dias, M., and Glover, D. M. (2007) Centrosome biogenesis and function: centrosomics brings new understanding. *Nat Rev Mol Cell Biol* **8**, 451–463
5. Gadde, S., and Heald, R. (2004) Mechanisms and molecules of the mitotic spindle. *Curr Biol* **14**, R797–R805
6. Belmont, L. D., Hyman, A. A., Sawin, K. E., and Mitchison, T. J. (1990) Real-time visualization of cell cycle-dependent changes in microtubule dynamics in cytoplasmic extracts. *Cell* **62**, 579–589
7. Lohka, M. J. and Masui, Y. (1983) Formation in vitro of sperm pronuclei and mitotic chromosomes induced by amphibian ooplasmic components. *Science* **220**, 719–721
8. Felix, M.A., Antony, C., Wright, M. and Maro B. (1994) Centrosome assembly in vitro: role of γ-tubulin recruitment in *Xenopus* sperm aster formation. *J Cell Biol* **124**, 19–31
9. Murray, A. W. (1991). Cell cycle extracts. *Methods Cell Biol* **36**, 581–605
10. Newmeyer, D.D., and Wilson, K. L. (1991) Egg extracts for nuclear import and nuclear assembly reactions. *Methods Cell Biol* **36**, 607–634

11. Mitchison, T. J., and Kirschner, M. W. (1986) Isolation of mammalian centrosomes. *Methods Enzymol* **134**, 261–268
12. Mitchison, T. J., and Kirschner, M. W. (1984). Dynamic instability of microtubule growth. *Nature* **312**, 237–242
13. Moritz, M., Zheng, Y., Alberts, B. M., and Oegema, K. (1998) Recruitment of the g-tubulin ring complex to Drosophila salt-stripped centrosome scaffolds. *J Cell Biol* **142**, 775–786
14. Schnackenberg, B. J., Khodjakov, A., Rieder, C. L., and Palazzo, R. E. (1998) The disassembly and reassembly of functional centrosomes in vitro. *Proc Natl Acad Sci USA* **95**, 9295–9300
15. Gard, D. L., and Kirschner, M. W. (1987) A microtubule-associated protein from *Xenopus* eggs that specifically promotes assembly at the plus-end. *J Cell Biol* **105**, 2203–2215
16. Popov, A. V., Severin, F., and Karsenti, E. (2002) XMAP215 regulates microtubule-nucleating activity of centrosomes. *Curr Biol* **12**, 1326–1330
17. Albee, A. J., and Wiese, C. (2008) *Xenopus* TACC3/maskin is not required for microtubule stability but is required for anchoring microtubules at the centrosome. *Mol Biol Cell* **19**, 3347–3356
18. Hyman, A., Drechsel, D., Kellogg, D., Salser, S., Sawin, K., Steffen, P., Wordeman, L., and Mitchison, T. J. (1991) Preparation of modified tubulins. *Methods Enzymol* **196**, 478–485

Part III

Fluorescence Microscopy Protocols for Investigating Cytoskeleton Components

Chapter 6

Quantitative Fluorescence Microscopy Techniques

Alessandro Esposito, Simon Schlachter, Gabriele S. Kaminski Schierle, Alan D. Elder, Alberto Diaspro, Fred S. Wouters, Clemens F. Kaminski, and Asparouh I. Iliev

Summary

Fluorescence microscopy is a non-invasive technique that allows high resolution imaging of cytoskeletal structures. Advances in the field of fluorescent labelling (e.g., fluorescent proteins, quantum dots, tetracystein domains) and optics (e.g., super-resolution techniques and quantitative methods) not only provide better images of the cytoskeleton, but also offer an opportunity to quantify the complex of molecular events that populate this highly organised, yet dynamic, structure.

For instance, fluorescence lifetime imaging microscopy and Förster resonance energy transfer imaging allow mapping of protein–protein interactions; furthermore, techniques based on the measurement of photobleaching kinetics (e.g., fluorescence recovery after photobleaching, fluorescence loss in photobleaching, and fluorescence localisation after photobleaching) permit the characterisation of axonal transport and, more generally, diffusion of relevant biomolecules.

Quantitative fluorescence microscopy techniques offer powerful tools for understanding the physiological and pathological roles of molecular machineries in the living cell.

Key words: FRET, FLIM, FRAP, FLAP, FLIP, Bioimaging

1. Introduction

Fluorescence microscopy is a fundamental modern biology technique that allows a non-invasive, multiscale (from molecules to entire organisms) imaging of biological samples with high resolution and high contrast *(1)*. Innovations in imaging and labelling techniques provide opportunities to expand our knowledge of biological systems and molecular machineries in physiological and pathological conditions.

R.H. Gavin (ed.), *Cytoskeleton Methods and Protocols,* Methods in Molecular Biology, vol. 586
DOI 10.1007/978-1-60761-376-3_6,
© Humana Press, a part of Springer Science + Business Media, LLC 2009

The cytoskeleton, consisting of various types of intracellular polymeric fibrillar structures, dynamically maintains the three-dimensional shape of the otherwise amorphous cell. It contributes to the cellular mechanical properties as it is involved in the generation of – and resilience against – adhesion, push-pull and torsional forces. The cytoskeleton is also essential for the intracellular-active motor-driven molecular transport. This chapter reviews established techniques that can be used for the characterisation of molecular interactions and transports occurring at or relevant for the cytoskeleton: Förster resonance energy transfer (FRET) imaging **(Subheading 3.1**), fluorescence lifetime imaging (FLIM – **Subheading 3.2**), fluorescence recovery after photobleaching (FRAP), fluorescence loss in photobleaching (FLIP), and fluorescence localisation after photobleaching (FLAP) **(Subheading 3.3**).

FRET imaging is being widely used in biology because it allows the quantitative mapping of molecular interactions *(2,3)* and the read-out of a wide variety of FRET-based biosensors. When a (donor) fluorophore is in close proximity with an (acceptor) chromophore, the energy of the donor excited state can be transferred non-radiatively to the acceptor via FRET. FRET can occur when the absorption spectrum of the acceptor overlaps with the emission spectrum of the donor *(2, 4, 5)*. Typically, a donor-acceptor pair undergoes FRET at an intermolecular distance of less than 10 nm: a range relevant to detect molecular proximity. FRET can thus be used for the detection of protein–protein interactions *(3,6)*. FRET alters the emission spectra, fluorescence anisotropy, and fluorescence lifetime of the coupled fluorophores *(2)*; any quantitative measurement of these spectroscopic features can, therefore, visualise molecular interactions in the cell. FRET is usually quantified by the estimation of the FRET efficiency (E), i.e., the quantum yield of the energy transfer transition.

Intensity-based techniques for the detection of FRET (sensitised emission FRET, seFRET, and acceptor photobleaching FRET, apbFRET) can be implemented using standard wide-field or confocal microscopes that are available in many biomedical laboratories *(3, 7, 8)*. Therefore, apbFRET and seFRET have been widely used in the past decade. For instance, apbFRET and seFRET have recently been used for the characterisation of the interaction of the epidermal growth factor receptor with actin *(9)* and for the detection of focal adhesion kinase activity, respectively *(10)*.

One of the most robust techniques for the detection of FRET is fluorescence lifetime imaging microscopy *(11–13)*. The fluorescence lifetime is the average time that a fluorophore spends in an excited state; this is a molecular property that can be altered by the biochemical environment within a cell. Therefore, the fluorescence lifetime can act as a reporter on properties of the

molecular environment, e.g., pH *(14,15)*, ion concentration *(16)*, and viscosity *(17)* in a quantitative manner. FLIM is often used for the measurement of FRET in biological samples in as much as FRET shortens the fluorescence lifetime of a donor fluorophore (τ) in proportion to the FRET efficiency (E) *(2)*:

$$\tau = \tau_0(1 - E) \tag{1}$$

where τ_0 is the fluorescence lifetime of a donor in the absence of FRET. FLIM has been restricted to specialised laboratories until recently as the increasing availability of commercial systems provides turn-key FLIM systems to the biological community *(12, 18, 19)*. For instance, FLIM allowed mapping of the interaction of the Parkinson's disease-related protein α-synuclein with the cytoskeletal protein tau *(20)* and the protein kinase C-regulated association of CD44 with the cytoskeletal protein linker ezrin *(21)*.

Also, techniques for the characterisation of the molecular transports occurring at the cytoskeleton are necessary to expand our knowledge on the cystoskeletal functions. For instance, synaptic proteins synthesised in the cytoplasm of a neuron are actively anterogradely transported by kinesins on microtubules along axons and reach their correct localisation at the axon terminals. Dynein motor proteins are involved in the retrograde transport of cargo to the cell body. It is believed that some axonally/synaptically generated signals have to be physically transported to the cell body in the form of activated or modified proteins in order to exert their, often long-term transcriptional, effect in neurons. Therefore, techniques that are capable of mapping the transport of cargos in space and time are important for the characterisation of axonal transport. Time-lapse imaging of molecular diffusion and binding in living cells is possible, thanks to the techniques based on the measurement of photobleaching kinetics: FRAP, FLIP, and FLAP. Upon localised photobleaching of a fluorescent tag fused to a molecule of interest, a "dark" fraction of labelled protein is created. Diffusion or active transport of this "photoswitched" pool of spectrally altered molecules generates time-dependent variations in fluorescence distributions that FRAP, FLIP, and FLAP can exploit for the quantification of protein mobility/immobility *(22)*. For instance, measurement of photobleaching kinetics allows the characterisation of axonal transport of cargo vesicles by synaptophysin-EGFP construct *(23)* and the oligomerisation/aggregation of the cytoskeletal protein tau *(24)*.

Cytoskeleton is one of the most fascinating biological structures (**Fig. 1**): it forms the "muscles", the "bones", and the "blood vessels" of the cell. It is a highly organised, yet highly

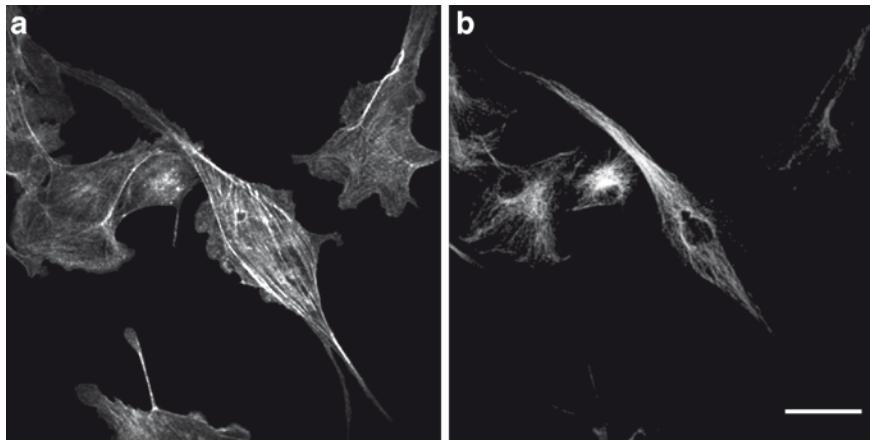

Fig. 1. The actin (**a**) and tubulin (**b**) cytoskeletons immunostained with BODIPY and Texas Red-X phalloidin, respectively. Scalebar: 25 μm.

dynamic, structure that offers mechanical stability and movement to the cell, and active transport of molecules inside the cytoplasm. FRET, FLIM, and FRAP allow the investigation of a plethora of molecular interactions and dynamic transport phenomena that populate this living network of proteins.

2. Materials

2.1. Cell Culture

1. Cell types:
   (a) SH-SY5Y human neuroblastoma cells.
   (b) CHO fibroblast cells.
   (c) C57Bl/6 mice for primary neurons.
2. Media:
   (a) SH-SY5Y: RPMI1640, 1% penicillin–streptomycin, 10% fetal calf serum (FCS).
   (b) CHO cells: BME, 1% penicillin–streptomycin, 1% L-Glutamin, 10% FCS.
   (c) Neuronal medium: BME (alternatively, Neurobasal medium can also be used), B-27 supplement, 1% penicillin/streptomycin, 1% FCS. Medium is not changed throughout the culturing period.
3. Neuronal culture dish was coated with 0.1 mg/mL poly-L-ornithin for several hours at 37°C.

2.2. Live Cell Imaging

1. Cells were seeded on LabTek 4-well chamber slide with 0.17 mm-thick coverslip bottom (Nunc GmbH & Co. KG, Thermo Fisher Scientific, Langenselbold, Germany).
2. Transfection can be performed with the following methods (*see* **Notes 1** and **2**): Effectene transfection reagent (Qiagen GmbH, Hilden, Germany), MATra (Magnetic Transfection-assisted) reagent (IBA GmbH, Goettingen, Germany) or electroporation. Neurones were transfected in suspension (with Effectene) or within 5 days after seeding (with magnetofection).
3. Cells were imaged in RPMI1640, BME or DMEM medium depending on the cell line, without phenol red and with 25 mM HEPES buffer, pH = 7.2, 1 mL/well, 24 h after transfection.
4. When needed, the stage and objective were heated at 37°C.

2.3. Fixed Samples

1. Cells were seeded on LabTek 4-well glass chamber slides (Nunc GmbH & Co. KG, Thermo Fisher Scientific, Langenselbold, Germany).
2. Wells were washed once with PBS and fixed with 4% formaldehyde in PBS, pH 7.4 for 10 min (*see* **Note 3**).
3. The chamber gasket was then removed and cells were mounted on Mowiol with a 0.17 mm-thick coverslip.

3. Methods

3.1. FRET and Intensity-Based Methods

The quantification of energy transfer, by the detection of the fluorescence intensity emitted by donor and acceptor fluorophores, is hindered by the dependence of the detected signals on the local concentration of the fluorescent labels. For this reason, various methods have been described for the detection of reference measurements that enable the ratiometric detection of FRET on comparatively simple microscopy systems (*see* **Notes 4** and **5**) *(3,25)*.

3.1.1. Acceptor Photobleaching FRET

The fluorescence emission of a donor is decreased by FRET. Methods that allow the measurement of donor emission in the absence of energy transfer permit the estimation of the FRET efficiency. An acceptor fluorophore can be rendered "FRET incompetent" either by depletion of its ground state *(26)* or by altering its spectral characteristics *(27)*. The most common and straightforward method relies on the photobleaching of the acceptor (apbFRET), which results in either the photo-destruction of the chromophore

or the trapping of the molecule in a metastable "dark state" with energy levels not suitable for FRET *(3,28)*. Photobleaching is achieved by exposing the sample to high excitation intensities or prolonged illumination of the acceptor. Therefore, apbFRET is more suitable for the imaging of fixed samples, where diffusion does not diminish the ability to photobleach the fluorophore in a controlled manner and where phototoxicity is not a problem. The following method describes a typical protocol to obtain FRET efficiency estimates by apbFRET.

1. Choose the spectral characteristics of the excitation light sources and the emission filters (*see* **Notes 6** and **7**):
   (a) Selectively photobleach the acceptor without photodamaging the donor.
   (b) Detect the fluorescence emission of the donor without bleed-through of fluorescence emitted by the acceptor.
   (c) Minimise the donor photobleaching during the pre- and post-bleaching imaging.
2. Acquire a fluorescence image of both the donor and acceptor. Although not strictly necessary, the acceptor image can be useful as a control to identify the bleached region and to quantify the amount of photobleaching obtained (*see* **Note 8**) *(29)*.
3. Photobleach the acceptor. Typically, only a region of interest is photobleached (or one cell in a field of view that contains other cells). The non-bleached regions will serve for control purposes (*see* **Note 9**). In a standard wide-field microscope, selective photobleaching can be achieved by partially closing the field iris of the microscope; confocal laser scanning systems and specialised wide-field setups offer an opportunity to select regions of interest for photobleaching or to zoom in and out within the same field of view.
4. Assess the quality of measurement:
   (a) Donor intensity in the photobleached regions should not have decreased (*see* **step 1**).
   (b) Donor intensity in the non-bleached regions should not have altered significantly (*see* **Note 10**).
   (c) Acceptor intensity should be significantly lower relative to the pre-bleaching values.
5. Calculate FRET efficiencies (E_{APB} – *see* **Note 9**) by computing the relative difference of the donor intensity from the pre- (I^D) and post-beaching (I^D_{APB}) conditions *(3)*:

$$E_{APB} = 1 - \frac{I^D}{I^D_{APB}} \tag{2}$$

Figure 2 shows an image of a CHO cell expressing an ECFP:EYFP fusion construct. The acceptor EYFP **(Fig. 2b–d)** was photobleached in the areas that spell he word "FRET". Acceptor photobleaching cause the de-quenching of the donor, and using **Eq. 2**, the images of ECFP acquired before **(Fig. 2a)** and after **(Fig. 2c)** photobleaching provide an estimate for the FRET efficiency (~15%, **Fig. 2e**). This FRET-dependent recovery of donor fluorescence is also apparent from the histogram **(Fig. 2f)** of the FRET image.

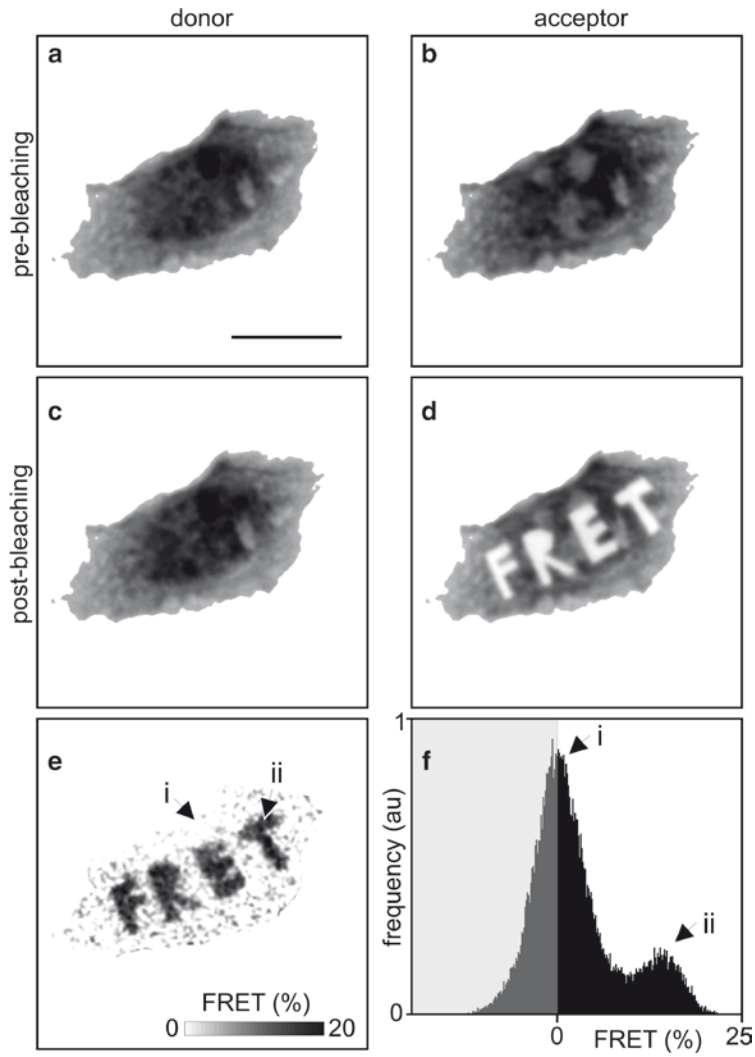

Fig. 2. Acceptor photobleaching FRET. (**a**, **b**) Donor and acceptor images of CHO cells expressing an ECFP:EYFP fusion construct, respectively. The donor (**c**) is de-quenched in regions where the acceptor is photobleached (**d**). **Equation 2** allows quantification of FRET efficiencies (**e**). The histogram of FRET efficiencies (**f**) shows that no FRET is detected in the non-bleached areas (i) whereas an average FRET value of about 15% is measured in the photobleached area (ii). Scale bar: 20 μm.

Control experiments using cells tagged with only the acceptor are not necessary on a regular basis, although their use may be advisable to exclude the presence of photoconversion of the acceptor to a photoproduct with donor-like properties *(30)*. If a fluorescence signal appears in the donor channel upon photobleaching, the use of a different fluorophore may be necessary. Additionally, a sample exhibiting a known amount of FRET could be used to assess the effects of incomplete photobleaching of the acceptor *(29,31)*.

3.1.2. Sensitised Emission FRET

The transfer of energy from a donor to an acceptor fluorophore causes the acceptor fluorophore to emit fluorescence. The so-called "sensitised emission" of the acceptor is a FRET signal that can be used to estimate energy transfer. For instance, when a FRET-based biosensor is used and the stoichiometry for donor–acceptor molecules is fixed (typically 1:1), the ratio between the donor intensity and the acceptor intensity upon excitation of the donor can be directly used as a FRET indicator. More generally, however, the stoichiometry of donor–acceptor fluorophores is unknown (even in single polypeptide fusion constructs that carry the donor and acceptor moieties due to differences in folding efficiency or pH/halide dependence of the fluorescent proteins). Furthermore, spectral cross-talk between the donor and acceptor channels requires calibration of the signals. For instance, the excitation source used for the illumination of the donor often also directly excites the acceptor molecules. Sensitised emission of the acceptor would then add to the fluorescence induced by direct excitation. Additionally, with typical FRET pairs, the fluorescence emitted by the donor fluorophore bleeds-through the emission filters used for the detection of acceptor fluorescence. Both direct excitation of the acceptor and donor bleed-through render the estimation of FRET by sensitised emission prone to artefacts.

Many protocols *(7, 25, 32)* and some software routines *(7,33)* have been proposed for the calibration of seFRET. In spite of the need for a careful calibration, seFRET provides several advantages over apbFRET: (a) it is a non-invasive tool that can be used for time-lapse quantitative imaging of dynamic protein–protein interactions and (b) it can provide fast, reliable read-out of FRET-based biosensors. Also, seFRET can be implemented with any wide-field or confocal microscopes equipped with suitable excitation sources and emission filters.

The following method describes a typical protocol for the estimation of FRET by the detection of sensitised emission with a confocal microscope *(7)*. The implementation using wide-field systems is similar *(25)*.

1. Using a control sample labelled "acceptor-only" (e.g., an EYFP fusion, if ECFP and EYFP are used as a FRET pair), compute the acceptor excitation ratio (AER), i.e., the ratio of the fluorescence intensity measured in the acceptor channel with donor excitation wavelength (I^{DA}) relative to the fluorescence signal measured with acceptor excitation wavelength (I^{AA}): $\mathrm{AER} = I^{DA} / I^{AA}$. AER is used to correct the direct excitation of the acceptor (*see* **Eq. 3**).
2. Using a control sample labelled "donor-only" (e.g., an ECFP fusion), compute the donor emission ratio (DER), i.e., the ratio of the fluorescence intensity measured in the acceptor channel upon excitation at a donor wavelength (I^{DA}) relative to the signal measured in the donor channel (I^{DD}): $\mathrm{DER} = I^{DA}/I^{DD}$. DER is required to correct the donor bleed-through (*see* **Eq. 3**).
3. Once the AER and DER parameters are measured, imaging parameters (e.g., laser intensities, detector gains, and filters) should not be changed for the rest of the experiment (*see* **Notes 6** and **7**).
4. Acquire images I^{DA}, I^{DD}, and I^{AA} on the sample of interest (*see* **Note 8**).
5. Determine the corrected FRET signal (cFRET) on a pixel-by-pixel basis with the following equation *(7,25)*:

$$\mathrm{cFRET} = I^{DA} - \mathrm{DER}\, I^{DD} - \mathrm{AER}\, I^{AA} \tag{3}$$

   cFRET does not depend on cross-talk contributions and is a useful FRET index that can be applied to compare samples acquired using an identical imaging setting on a specific imaging system. For more general applications, cFRET can also be normalised to provide an estimate for FRET efficiency (*see* **Note 11**).
6. Quality assurance: check that AER and DER are constant over the measured range of intensities, otherwise corrections for the non-linearity of the detectors are necessary *(33)*.

Figure 3 shows I^{DA}, I^{DD}, I^{AA} **(Fig. 3a–c)** for cells expressing a ECFP:EYFP fusion construct. Donor and acceptor normalisations (**Fig. 3d–f**, *see* also **Note 11**) of cFRET provide a quantitative estimation of the FRET efficiency (~25%).

3.2. Fluorescence Lifetime Imaging Microscopy and FRET

Many instruments and techniques can be applied to the fluorescence lifetime imaging microscopy (*see* **Note 5**) *(18)*. The fluorescence lifetime can be measured by the time-resolving fluorescence decay of a fluorophore upon excitation by a short pulse of light (time domain techniques) *(12,34)*. The fluorescence lifetime can also be measured by the analysis of the harmonic response (i.e., the phase delay and demodulation of the fluorescence emission relative to the excitation) of the sample illuminated by some

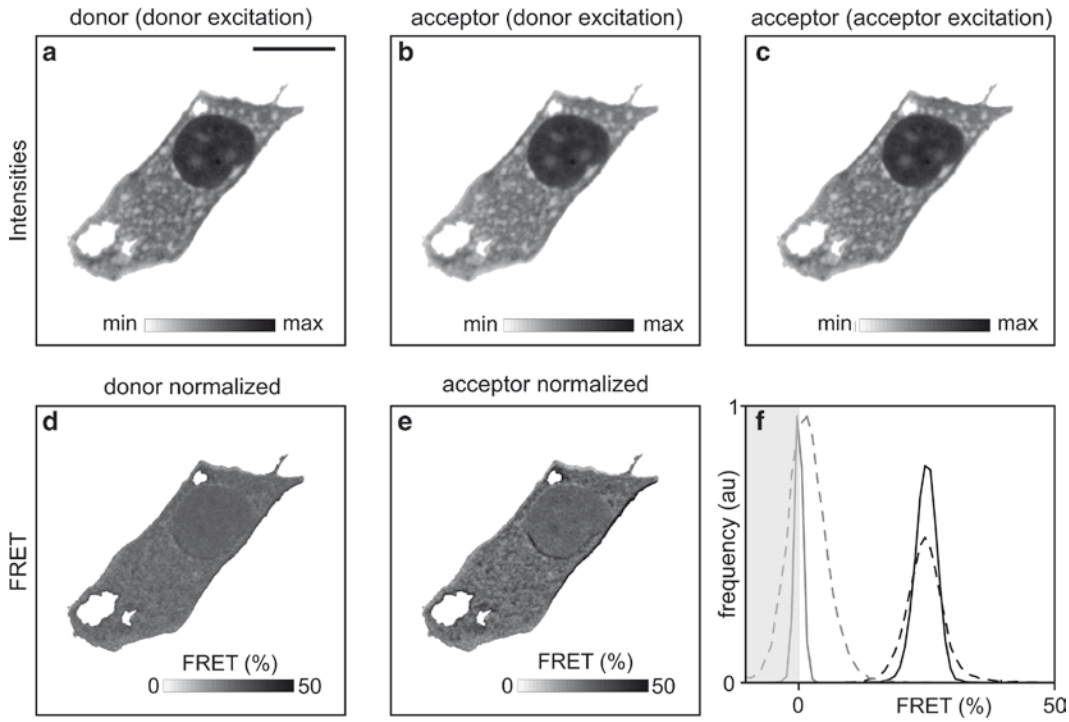

Fig. 3. Sensitised emission FRET. (**a**, **b**) Donor and acceptor images of SH-SY5Y cells, respectively, that were transfected with an ECFP:EYFP fusion construct (17 amino acids long, linked *(74)*) with excitation at the donor wavelength. (**c**) Acceptor fluorescence when the acceptor is directly excited. From these images, mapping of energy transfer efficiencies was possible, the images and histograms are shown in (**d**) (dFRET), (**e**) (aFRET) and (**f**)(dFRET: *solid curves*; aFRET: *dashed curves* – *see* **Note 11**); *grey curves* show histograms of control cells co-transfected with non-linked EYFP and ECFP. Scale bar: 20 μm.

periodic pattern encoded in the excitation light intensity (frequency domain techniques) *(35,36)*. Time domain techniques are often used in laser scanning microscopes (confocal and two-photon systems) *(37,38)* and frequency domain methods are commonly adopted by wide-field systems *(39,40)*; although these typical applications will be described in the following sections, time-domain wide-field systems *(16)* and frequency-domain scanning microscopes are also available *(41)*.

3.2.1. Time Domain FLIM

The fluorescence lifetime can be estimated by exciting a fluorophore with a short pulse of light (fs–ps) and subsequently detecting the fluorescence emission decay. The fluorescence decay of typical fluorophores is no longer than 1–50 ns and thus, requires specialised instrumentation to be resolved. Two techniques are widely used: time-correlated single photon counting (TCSPC) *(12,42)* and time-gating *(34,38)*. Both the techniques are based on the collection of histograms of arrival times for detected photons which are fitted with exponential models to infer fluorescence lifetimes.

Time-gated systems usually provide faster imaging than TCSPC; on the other hand, TCSCP provides an inherently self-referenced and precise detection scheme. Although instrumentation for time domain detection may differ substantially, system operation and data analysis techniques are quite similar *(13,43)*.

The following method describes the operation of a time domain FLIM system based on a confocal laser scanning system.

1. (Only for time-gated systems) Start the first time gate with a finite time delay $\Delta t \geq 0$ after the excitation pulse. A fluorophore like Rose Bengal ($\tau \sim 80$ ps in phosphate buffer saline *(44)*) can be used as a zero-lifetime reference. Δt should be as short as possible to allow collection of photons in the fluorescence decay **Fig. 4b**, *arrow*). Background signals with very fast decays (e.g., stray excitation light and, often, also background fluorescence) may be minimised by introducing an additional delay *(43)*.
2. Select filters to detect only fluorescence emitted by the donor (*see* **Note 6**).
3. Start acquisition of a sample containing only molecules tagged with a donor fluorophore (*see* **Note 7**).
4. Stop acquisition after an appropriate integration time (typically 30s or longer for time-gating, 1–2 min or longer for TCSPC). At least ~400 (TCSPC) or ~700 (time-gating with four gates) photons per pixel are necessary to characterise a single exponential decay with sufficient accuracy (~5%); several thousand photons are necessary for a two-exponential decay *(34)* (*see* **Note 8**).
5. Repeat **steps 2–4** on a sample containing both donor and acceptor labels.
6. Fit the data with the most appropriate (exponential) model (*see* **Notes 12** and **13**). The average fluorescence lifetime of a donor in the absence of an acceptor (τ_0) can be estimated.
7. FRET images can be computed by rationing the measured fluorescence lifetime (τ) at each pixel location with the fluorescence lifetime of the donor only:

$$E_{\mathrm{FLIM}} = 1 - \tau / \tau_0 \tag{4}$$

Figure 4 shows a fluorescence image (**Fig. 4a**) of a CHO cell expressing α-synuclein tagged with ECFP and EYFP-tau *(20)* acquired by TCSPC. The fluorescence lifetime map (**Fig. 4b**) shows lower fluorescence lifetime values in the cytoplasm compared to the nucleus where tau does not localise. A representative fit of the data and the lifetime histograms (**Fig. 4c–d**) also show the net reduction of fluorescence lifetime relative to a

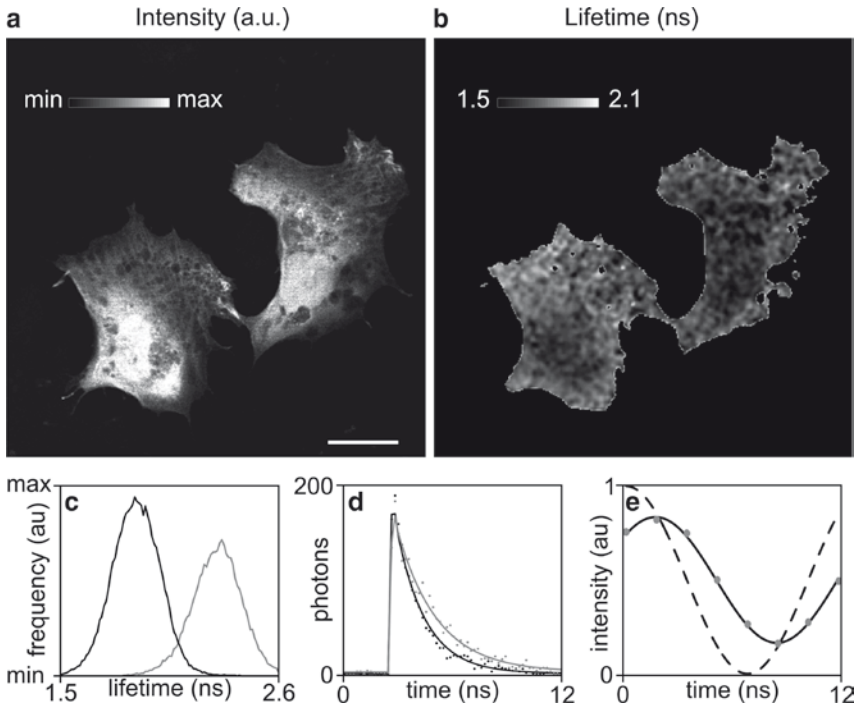

Fig. 4. Time domain FLIM by TCSPC: (**a**) Fluorescence intensity of CHO cells expressing ECFP:α-synuclein; (**b**) the fluorescence lifetime of ECFP is reduced by the presence of EYFP:tau localised in the cytoplasm. (**c**) Comparison between the fluorescence lifetime distribution of cells expressing only ECFP:α-synuclein (*grey*) and cells shown in (**a**, **b**) co-expressing both donor and acceptor fluorophores (black). (**d**) Representative fluorescence decays of a donor molecule (fit: *solid curves*; experimental data: *circles*) in the presence (*grey*) or absence (*black*) of an acceptor. (**e**) Representative fit of modulated excitation light (*dashed curve*) and fluorescence emission (*solid curve*; *circles*: experimental data for a sample expressing ECFP:α-synuclein in the presence of EYFP:tau) handled in frequency-domain FLIM. Scale bar: 5 μm.

control (acceptor fluorophore omitted) that demonstrate the interaction between the α-synuclein and the cytoskeletal protein tau.

3.2.2. Frequency Domain FLIM

The fluorescence lifetime can also be estimated by the analysis of the harmonic response of the fluorophore. The intensity of the excitation light should be periodically modulated at a circular frequency (ω) within the same order of magnitude as the inverse of τ. The fluorophore will thus alter the phase (φ) and the modulation (m) of the fluorescence emission relative to the excitation signal (**Fig. 4e**) from which two estimates of the fluorescence lifetime can be inferred *(35,45)*:

$$\begin{aligned} \tau_\phi &= \omega^{-1} \tan\phi \\ \tau_m &= \omega^{-1}\sqrt{m^{-2}-1} \end{aligned} \qquad (5)$$

Typical modulation frequencies are in the 30–100 MHz range and therefore, specialised fast detectors are required for imaging *(11,46)*. Non-imaging frequency domain techniques rely on the measurement of modulation and phase delay at multiple modulation frequencies *(2)*; however, lifetime imaging at multiple frequencies is not always possible with imaging systems *(47)*. Therefore, lifetime imaging in the frequency domain is typically performed at a single frequency. The following method describes the operation of a typical wide-field frequency domain FLIM.

1. Use a well-characterised sample to calibrate the microscope (*see* **Notes 6** and **14**). Scattered excitation light *(48)* can be used as zero-lifetime reference. In order to calibrate the sample with settings similar to those used under experimental conditions, it is advisable to calibrate a system with a fluorescence reference, for instance, Rose Bengal (*see* **Subheading 3.2.1**, **step 1**) or Rhodamine 6 G ($\tau \sim 4.1$ ns in water *(49)*), exhibiting a single-exponential decay or similar standards emitting on spectral regions of interest *(13)*. Wide-field systems may require a pixel-by-pixel calibration because of spatial heterogeneity of the detector response.
2. Set imaging parameters (e.g., excitation light intensity and exposure time) for the optimal use of the dynamic range of the detector: for each phase image, no pixel should be saturated (*see* **Note 7**).
3. Acquire a set of images at different phases with a sample tagged with only the donor fluorophore (*see* **Note 8**). Ideally, the phase values should follow a pseudo-random sequence *(50)* allowing for robust photobleaching compensation. Acquire more than five phase images to avoid aliasing *(51)*. Less images may be required for fast applications *(46,52)*; in principle, two-phase acquisition is possible for fast lifetime imaging *(53)* at the cost of lower acquisition system and estimator efficiencies.
4. Compute the fluorescence lifetime images (*see* **Notes 12** and **13**). Fast and efficient algorithms make use of Fourier coefficients *(54)*, allowing the estimation of fluorescence lifetime and heterogeneity of decay in each pixel *(35)*. Data fitting can be used as an alternative; although slower in computation, it will generate a pixel-by-pixel error estimate *(45)*.
5. Typical FD-FLIM requires frequent calibrations. If the microscope does not provide automated calibration *(48,52)*, repeat **step 1**.
6. Repeat imaging for the sample stained with both donor and acceptor fluorophores, possibly alternating among them to compensate for non-random instrumental drifts *(13)*. FRET efficiency can be computed using **Eq.4** on a pixel-by-pixel basis.

3.3. Photobleaching Kinetic Techniques

In this section, photobleaching is strictly defined as the light-induced, irreversible inactivation of a fluorophore. Although the fluorescent tag loses its capability to fluoresce, the labelled molecule is still linked to the "dark" tag and, typically, exhibits mechanical and biological properties similar to the non-bleached moieties. Almost all fluorophores undergo photobleaching and, more recently, novel photoactivatable fluorophores *(55,56)* have been demonstrated. Both photobleachable and photoactivatable fluorophores can be exploited to characterise the (three-dimensional) diffusion of labelled proteins upon inactivation *(22)* or activation *(57)* of fluorescence.

In the case of completely diffusible molecules, diffusion of fluorescent molecules causes the fluorescence intensity within a bleached area of the sample to regain its initial levels after photobleaching, with a time constant proportional to the molecular weight of the labelled molecule and temperature. FRAP exploits this principle for the estimation of diffusional coefficients *(58)*.

Conversely, diffusion dilutes the fluorescent molecules with non-fluorescent moieties outside the photo bleached region, causing a decrease of fluorescence. FLIP exploits this variation of fluorescence intensity to determine the diffusion of molecules.

For completely mobile and diffusible molecules in a living cell, the fluorescence intensity will stabilise with a characteristic half-time ($t_{1/2}$) after photobleaching (**Fig. 5a**). Recovery half-times will be shorter for small molecules and larger for bigger molecules and molecular complexes (**Fig. 5b**). On the other hand, no diffusion is observed when the labelled molecules are completely immobile resulting in no loss of fluorescence outside the bleached region and no recovery within this area (**Fig. 5c**).

In general, both diffusion and binding occur (**Fig. 5d**). The difference of steady-state fluorescence intensities before and after photobleaching relates to the molecular immobile fraction.

3.3.1. Frap

Figure 6 shows the FRAP analysis of an aggregation of the microtubule-binding protein tau (wild-type; WT). Tau binds to the microtubules reversibly and diffuses freely in the cytosol. Human SH-SY5Y neuroblastoma cells, expressing a GFP fusion construct of tau (WT-GFP) exhibited a nearly complete recovery of fluorescence after photobleaching, i.e., no immobile fraction was present (**Fig. 6a**). Cells expressing a GFP fusion construct of an aggregating-prone mutant of tau (3PO-GFP) exhibited a slow and incomplete recovery caused by the aggregation of the 3PO-GFP tau mutant (**Fig. 6b**) *(24)*.

The fluorescence intensity measured on a reference area (out-of-bleaching area) is used to normalise the values measured in the bleaching region (**Fig. 6**, "RAW DATA"), to obtain corrected FRAP curves (**Fig. 6**, "NORMALISED DATA" – *see* **Note 10**). The fluorescence intensities measured in the reference area also

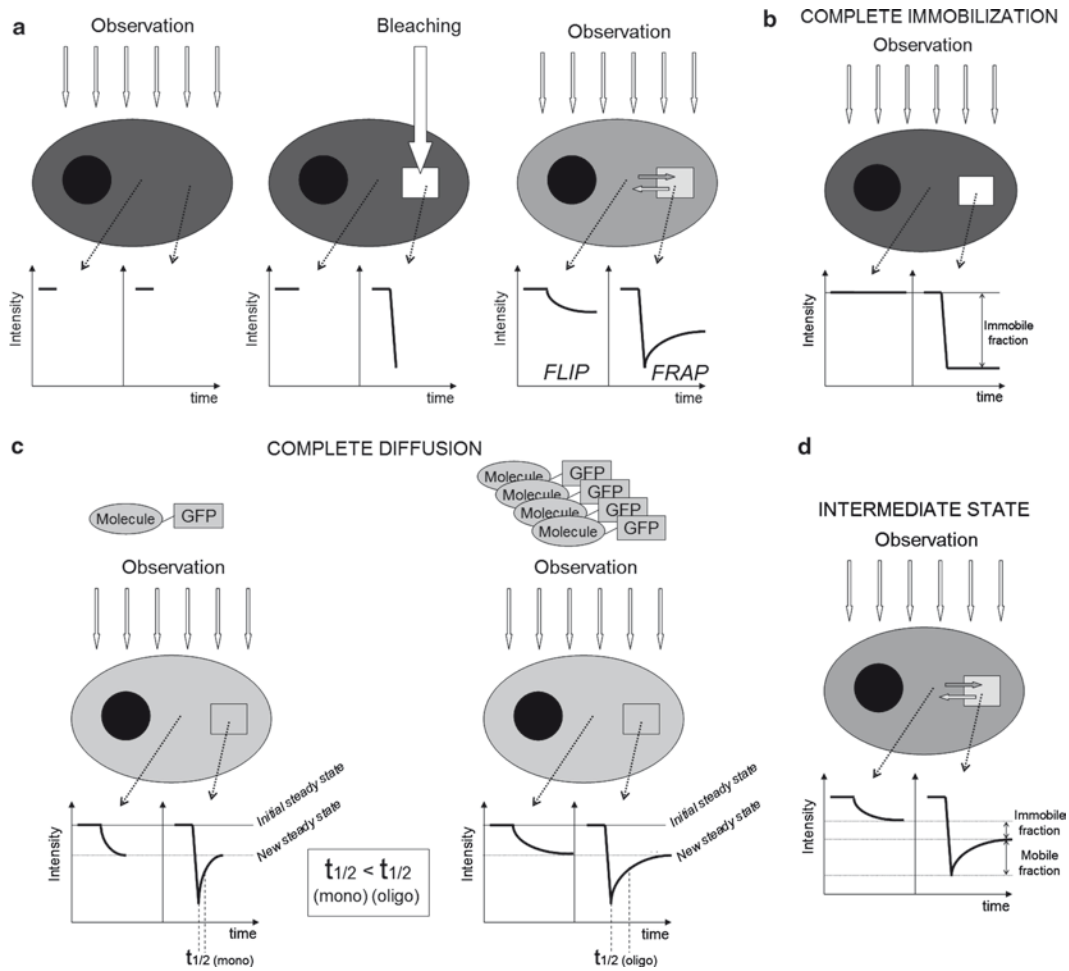

Fig. 5. Principles of FRAP and FLAP: (**a**) Upon inactivation of a fluorophore by photobleaching within a small area of the cell, intact fluorophore–protein complexes diffuse from the surrounding areas towards the bleached area (FRAP) causing partial recovery of fluorescence. At the same time, the photobleached fluorophores dilute the intact fluorophore pool outside the area of bleaching (FLAP). (**b**) When the proteins of interest are completely immobilised, no FRAP and FLAP effects should occur. (**c**) FRAP and FLAP half-times are otherwise proportional to the size of the diffusible complexes. Because of the net reduction of fluorescent tags, a new steady state at lower intensities can be observed. (**d**) When both diffusion and binding occur, an intermediate behaviour of the fluorescence intensities will be present (*mono* monomers; *oligo* oligomers; example of diffusion modulation caused by oligomerisation/aggregation).

provide information on molecular interactions: the amount of fluorescence loss is significant for WT tau and negligible for the 3PO mutant because of the high aggregation propensity of the latter.

3.3.2. FLIP and FLAP

Figure 7a shows the primary mouse neurons expressing a fusion construct of synaptophysin and GFP under the control of human synapsin promoter. This construct localises to the presynapse and

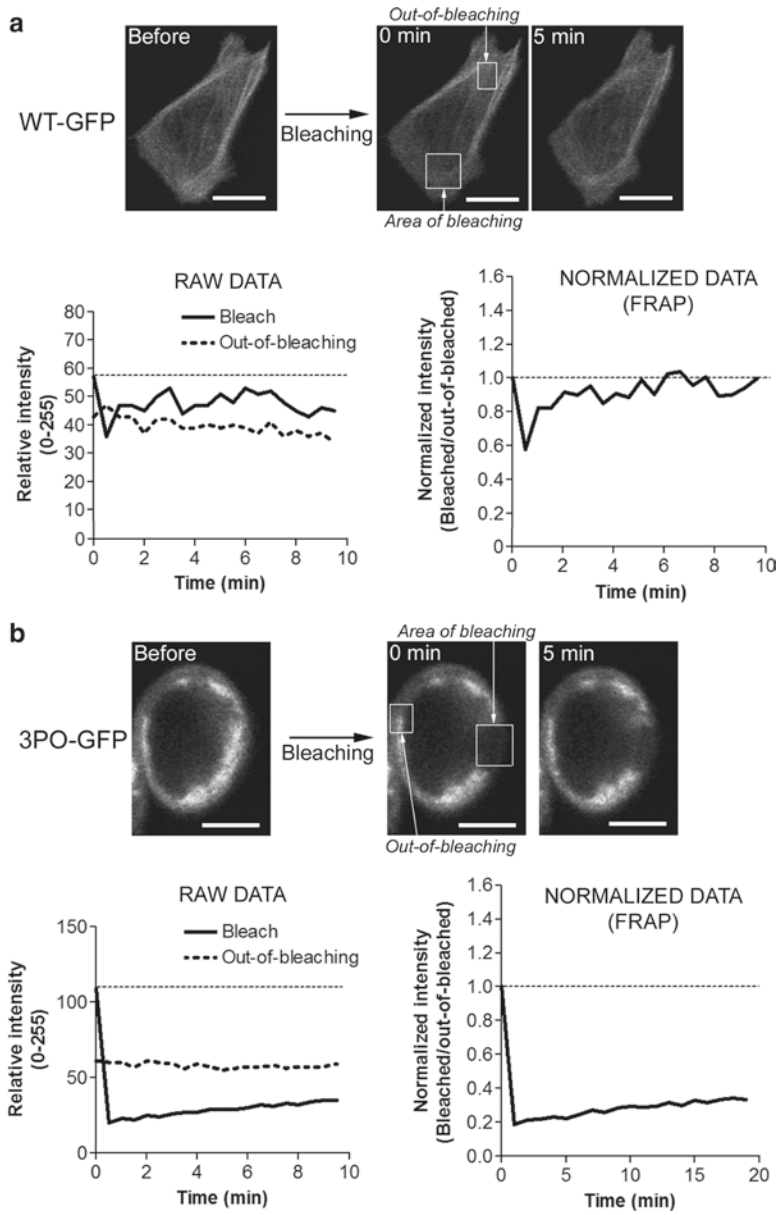

Fig. 6. FRAP of mobile and immobile tau protein: (**a**) Photobleaching of wild-type tau-GFP is followed by a rapid recovery of fluorescence within the area of bleaching with no immobile fraction detectable. In the case of strong FLIP, normalisation of the recovery curve to the intensity of the probe outside the bleaching area is needed. (**b**) 3PO-mutant tau protein-GFP bleaching shows minimal recovery and high level of immobility. Because no FLIP is detectable, normalisation of the FRAP curve is not needed. All scale bars: 10 μm.

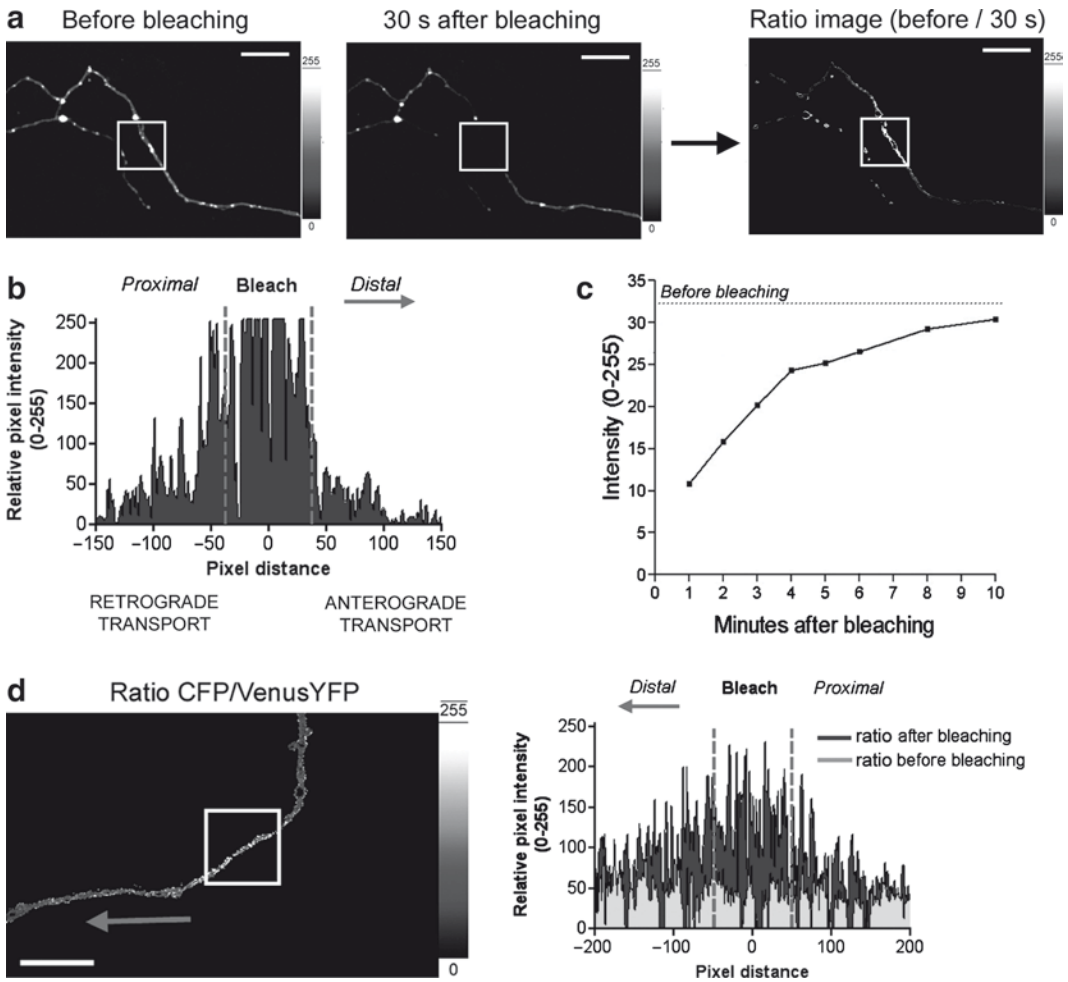

Fig. 7. Axonal transport evaluation by FRAP, FLIP and FLAP: (**a**) Photobleaching of synaptophysin tagged with a GFP allows following fluorescence loss outside the area of bleaching and the directionality of the axonal transport. (**b**) Profile of the ratio (pre-bleaching/30 s after bleaching) along the axon (**c**) FRAP within the area of bleaching allows the evaluation of the rate axonal transport. (**d**) Ratiometric imaging (FLAP) of the synaptophysin-CFP/VenusYFP chimeric probe (*left*: image; *right*: profile of the ratio along the axon) after photobleaching of YFP. All scale bars: 10 μm.

is also incorporated into synaptic vesicles transported on microtubules. Synaptophysin-GFP allows the investigation of axonal transport *(23,59)*. Axonal transport resulted in FRAP within the bleached area of the axon (**Fig.** 7b) and a fluorescence loss in the neighbouring areas along the axon (FLIP). The ratio between the image, before and after bleaching, allows the visualisation of directionality and magnitude of the axonal transport (**Fig.** 7c).

Sample movement and reduction of signal-to-noise ratio, caused by photobleaching, can be significant problems that hinder the possibility to obtain images by FLIP. The use of a reference fluorophore, FRET-based tags and photochromic fluorophores

can be used to circumvent this limitation *(59)*. **Fig. 7d** shows the primary neurons expressing a fusion construct of synaptophysin and CFP linked to YFP. CFP was partially quenched by YFP due to intramolecular FRET within the construct. Upon photobleaching of the acceptor (YFP), the donor is de-quenched. Therefore, the CFP/YFP ratio image allowed pixel-by-pixel referencing and permitted mapping of FLAP with high spatial resolution to display the retrograde transport of synaptophysin.

The following protocol describes a method showing the time-lapse imaging of fluorescence variation upon photobleaching that can be used for FRAP, FLIP, and FLAP techniques (*see* **Note 15**).

1. Keep the stage and objective at a constant temperature and allow the equilibration of cells to the desired temperature and imaging conditions (e.g., CO_2-independent medium – *see* **Note 6**).
2. Select the imaging parameters (e.g., pinhole size, laser intensity, detector gain, and pixel resolution) by preliminary image acquisitions (*see* **Note 16**). Avoid saturation of the detector and operate the system in its linear working range (*see* **Note 7**).
3. Imaging parameters should not be altered during the experiment.
4. Select the cell to be imaged.
5. Pre-select the region of interest to be photobleached (it is often convenient to set this area at the center of the field of view).
6. Photobleach the region of interest using high laser intensities. Photobleaching may be more effective on small areas because of the high zoom factor and faster scan rates (*see* **Notes 8** and **9**).
7. As soon as photobleaching is achieved, start the time-lapse sequence by selecting the frame rate and the acquisition times sufficient to allow the time course of the diffusional process (by FRAP, FLIP or FLAP) to be captured (*see* **Note 17**).
8. Rationing and analysis of images (e.g., before/after photobleaching or FRET-based FLIP analysis) can be performed using ImageJ Image Calculator (http://rsbweb.nih.gov/ij/). Mask cells by intensity thresholding in order to remove the background, otherwise noise artefacts present in the background will limit the dynamic range of the resulting images significantly.
9. Fit the data with the appropriate model (*see* **Notes 10** and **18**). FRAP fitting function can be complex to model *(60)*, but often the following fitting function can be used *(22,61)*:

$$F(t < t_{PB}) = F_i$$
$$F(t > t_{PB}) = F_0 + (F_\infty - F_0)\left(1 - e^{-\frac{t}{t_{1/2}}}\right)s \quad (6)$$

where t_{PB} is the time of photobleaching, F_i is the initial pre-bleaching fluorescence baseline, F_0 is the fluorescence intensity measured immediately after photobleaching and F_∞ the post-bleaching steady-state; the mobile fraction can be estimated as $M_f = (F_\infty\text{-}F_0)/(F_i\text{-}F_0)$, $t_{1/2}$ and M_f are used to compare diffusion and mobile fraction of different samples.

4. Notes

1. Sample preparation: many fluorescent labelled molecules tend to incorporate less efficiently into the cellular structures, relative to wild-type (non-labelled) molecules. This is especially true for cytoskeleton markers, e.g., actin and tubulin. Effort should be made to limit their level of expression so that it does not interfere with cellular function.
2. Sample preparation: over-expression systems are commonly used in fluorescence imaging because they provide good signal-to-noise ratios. It should always be kept in mind that the localisation and function of proteins may be altered at high expression level. Often, over-expression systems based on transient transfection exhibit extensive heterogeneity in fluorescence intensity. As a practical rule, cells exhibiting the highest fluorescence intensity should not be imaged because protein concentrations may be at such levels that physics and photophysics of the proteins and fluorophores may lead to artefacts *(62)*.
3. Sample preparation: immunocytochemistry of tubulin preparations requires different fixation procedures. Most of the commercial antibodies against α-tubulin require fixation with ice-cold methanol (–20°C; all procedures should be carried out at –20°C) for about 5–10 min. Exceptions exist, e.g., the monoclonal 236–10,501 (Molecular Probes) which requires 4% formalin fixation and does not work with methanol-fixed samples. Currently, some companies (e.g., Cytoskeleton Inc.) offer novel buffer formulations in an attempt to overcome these limitations. Note that most of the cytoskeletal labelling antibodies require membrane permeabilisation (e.g., with 0.1% Triton X-100 in PBS).

4. New fluorophores: new fluorescent proteins, organic tag and inorganic fluorophores are in constant development *(63)*. In particular, development of photo-switchable and photochromic molecules are likely to have a major impact on quantitative imaging *(55,64)*. For example, there is potential to obviate the need for controlled samples as controls could be performed directly through switching the spectroscopic properties of fluorescent tags in a controlled manner.
5. When deciding the technique to be used for FRET imaging, the following advantages (+) and disadvantages (–) may be considered *(3, 5, 31, 65)*:
   (a) apbFRET: + easy to implement, + few control experiments needed, – more suitable for fixed sample, – invasive technique, - may be prone to artefacts in the presence of incomplete acceptor photobleaching or acceptor photoconversion.
   (b) seFRET: + non-invasive technique, + fast imaging of living cells possible, – requires many control experiments.
   (c) FLIM: + robust self-reference technique, – requires specialised instrumentation, – only a few custom-built systems provide fast lifetime imaging.
6. System start-up: microscope instruments need to be switched on for a certain period of time before they reach a stable operation. This is mostly the case when a thermal equilibration has been reached (20 min should be sufficient).
7. Saturation, detector linearity and pulse pile up: avoid operating the system in non-linear operating regimes. Saturation of the detector will generate artefactual results. Hence, it is always convenient to use lookup tables that permit the direct visualisation of saturated pixels within an image. In the case of photobleaching-based techniques or time-lapse imaging, select a detector gain that permits detection far enough from saturation to allow for an increase of intensity (e.g., time-dependent variations and post-bleaching de-quenching); however, detector gain should also be selected to use the most of the dynamic range available. Although a large majority of detection system exhibits a linear response, with the light intensity arriving on the photosensitive area, some microscopes do not provide a linear response. In this case, characterise the response or contact the supplier. FLIM systems can also suffer from non-linear effects caused by the dead time of detector and electronics *(2,43)*. When two photons are incident on the detector in a shorter time than the detector dead time, the second photon will not be detected (pulse pile up). Pulse pile up distorts measured fluorescence decays and thus may cause artefacts.

8. Imaging in living cells: living cells are vulnerable to phototoxicity induced by prolonged illumination or high illumination intensities. There is always a trade-off between the signal-to-noise ratio and the phototoxicity, and the optimum balance should be determined from control experiments. Particular care should be taken for techniques that require photobleaching (FRAP, FLIP, and apbFRET), long-exposure times (TCSPC) or when time-lapse acquisition is performed (i.e., with seFRET).
9. Photobleaching in apbFRET and FRAP: complete photobleaching of fluorescent signals is often not possible in apbFRET and FRAP. In apbFRET, the presence of autofluorescence or of donor spectral bleed-through into the acceptor channel may cause an apparent incomplete photobleaching of the acceptor fluorophore. The FRET efficiency estimator for apbFRET can be corrected (E^{c}_{APB}) for incomplete photobleaching *(7)*:

$$E^{c}_{APB} = \frac{1 - \frac{I^{D}}{I^{D}_{APB}}}{1 - \frac{I^{D}}{I^{D}_{APB}}(1 - P_{B})} \tag{7}$$

where P_B is the fraction of photobleached acceptor.

In FRAP, fast diffusion of the fluorophore may contribute to this effect in addition to autofluorescence; in the latter case, imaging at faster frame rates and faster switching between bleaching/imaging operation may be necessary.

10. Accidental photobleaching (apbFRET and FLIP): the fluorescent intensity (of the donor for apbFRET) in the non-bleached regions should not be altered significantly; scaling of the post-bleaching (donor) image can be performed to render the intensity in the non-bleached regions equal to the pre-bleaching intensity only if drifts are moderate (typical causes: excitations, source power fluctuations, and donor photobleaching) *(29)*.
11. Normalisation of seFRET: cFRET can be normalised relative to the donor (dFRET) or the acceptor intensity (aFRET) using the following equations:

$$\text{dFRET} = \text{cFRET}(\alpha / \text{DER}) / (I^{DD} + \text{cFRET}(\alpha / \text{DER})) \tag{8a}$$

$$\text{aFRET} = \text{cFRET} / (\text{AER}\, I^{AA} \beta) \tag{8b}$$

where α is the relative molecular brightness of the donor to acceptor with the selected imaging settings and β the relative excitation

cross-section of the donor excited with the donor excitation wavelength to the donor excited with the acceptor wavelength. The parameters α and β can be estimated by the transmission curves of the filters and the spectroscopic properties of the fluorophores *(7)*; however, their estimation by measuring aFRET and dFRET with a control sample which exhibits a known FRET efficiency and stoichiometry (adjusting α and β to obtain aFRET = dFRET = E) is recommended. The same fluorophores used in the experiment should be used in the control, for instance, linked ECFP and EYFP, if these fluorescent proteins are used as FRET pair. Normalisation of cFRET by a combination of donor and acceptor intensities *(7,25)* and photobleaching corrections *(66)* are also reported; here, only the estimators dFRET and aFRET, quantities more directly related to the product of the FRET efficiency with the fraction of donor molecules or acceptor molecules are involved in the interaction.

12. FLIM data analysis: in spite of the robustness provided by fluorescence lifetime detection, data analysis may appear cumbersome to the non-specialist user. This mostly depends on the expertise required to judge when the signal-to-noise and the signal-to-background ratios are sufficient to fit a particular model to the experimental data *(34)*. Care should be taken to inspect indicators of goodness-of-fit (e.g., χ^2, randomness of the residuals) *(2, 13, 18)*. The F-statistics can be used to decide between adopting the different fits with more or less fit parameters *(2)*. Recently, new methods for data analysis based on AB-plots (or phasors) have been described that allow the graphical interpretation of the data *(67,68)* and lifetime based segmentation of the images *(69)*. These techniques can help in the interpretation of the data.
13. FLIM data analysis: global analysis algorithms may provide the highest and most homogeneous signal-to-noise ratios across the entire image, allowing also for discrimination of multiple fluorescence lifetime components *(70,71)*.
14. Calibration of frequency domain systems: a multi-point calibration for frequency domain FLIM systems has been described where various solutions of known fluorescence lifetime can be used to carefully calibrate the system *(13,49)*.
15. FRET and FRAP can be combined for the characterisation of the stability of interacting complexes *(72)*.
16. Scan rate and signal-to-noise ratio: FRAP and FLIP requires time-lapse imaging which should be optimised for each experiment. Molecules that exhibit half-time of recovery of a few seconds or shorter (e.g., tau) require fast imaging which

may result in low signal-to-noise ratios. In contrast, molecules that diffuse slowly allow for lower frame rates.

17. Typically, FLIP is performed by photobleaching an area of the cell in a continuous way and imaging the coincidental loss of photobleaching across the image *(73)*. Regions exhibiting loss of fluorescence allow diffusion of the protein of interest from the area of bleaching.
18. Sample preparation and data interpretation: the experimental results should be interpreted considering the fact that the comparatively high molecular weight of fluorophores such as fluorescent proteins affects the diffusional (and binding) properties of the protein of interest.

Acknowledgements

AE is funded by the Engineering and Physical Sciences Research Council (EPSRC, EP/F044011/1), UK. AII is financed by the Emmy Noether Programme of the German Science Foundation (Deutsche Forschungsgemeinschaft (DFG)) and the DFG-funded Rudolf Virchow Zentrum for Experimental Medicine at the University of Würzburg, Germany. CFK is funded by the Leverhulme Trust (UK), the Biotechnology and Biological Sciences Research Council (BBSRC, UK) and the EPSRC. FSW is financed by the Excellence Cluster 171 "Microscopy on the Nanometer Scale" of the DFG-funded Center for Molecular Physiology of the Brain (CMPB) and by the German Federal Ministry for Education and Research (BMBF). AD is funded by the University of Genoa and the Ministry of Education, University and Research (MIUR).

References

1. Diaspro, A. (2001) *Confocal and Two-Photon Microscopy: Foundations, Applications, and Advances*. Wiley-Liss, New York, p. 576
2. Lakowicz, J. R. (1999) *Principles of Fluorescence Spectroscopy*. Kluwer Academic/Plenum Publishers, New York
3. Wouters, F. S., Verveer, P. J., and Bastiaens, P. I. (2001) Imaging biochemistry inside cells. *Trends in Cell Biology* 11, 203–211
4. Clegg, R. M. (1995) Fluorescence resonance energy transfer. *Current Opinion in Biotechnology* 6, 103–110
5. Jares-Erijman, E. A., and Jovin, T. M. (2003) FRET imaging. *Nature Biotechnology* 21, 1387–1395
6. Jares-Erijman, E. A., and Jovin, T. M. (2006) Imaging molecular interactions in living cells by FRET microscopy. *Current Opinion in Chemical Biology* 10, 409–416
7. Elder, A. D., Domin, A., Kaminski-Schierle, G. S., Lindon, C., Pines, A., Esposito, A., and Kaminski, C. F. (2009) A quantitative protocol for dynamic measurements of protein interactions by FRET-sensitized fluorescence

emission. *Journal of the Royal Society Interface* 6(S1), S59–S81

8. Hoppe, A., Christensen, K., and Swanson, J. A. (2002) Fluorescence resonance energy transfer-based stoichiometry in living cells. *Biophysical Journal* 83, 3652–3664
9. Song, W., Wu, J., Ge, G., and Lin, Q. (2008) Two domains of the epidermal growth factor receptor are involved in cytoskeletal interactions. *Biochemical and Biophysical Research Communications* 370, 589–593
10. Cai, X. M., Lietha, D., Ceccarelli, D. F., Karginov, A. V., Rajfur, Z., Jacobson, K., Hahn, K. M., Eck, M. J., and Schaller, M. D. (2008) Spatial and temporal regulation of focal adhesion kinase activity in living cells. *Molecular and Cellular Biology* 28, 201–214
11. Gadella, T. W. Jr., Jovin, T. M., and Clegg, R. M. (1993) Fluorescence lifetime imaging microscopy (FLIM) – spatial-resolution of microstructures on the nanosecond timescale. *Biophysical Chemistry* 48, 221–239
12. Becker, W., Bergmann, A., Hink, M. A., Konig, K., Benndorf, K., and Biskup, C. (2004) Fluorescence lifetime imaging by time-correlated single-photon counting. *Microscopy Research and Technique* 63, 58–66
13. Esposito, A., Gerritsen, H. C., Wouters, F. S., and Resch-Genger, U. (2007) In: Wolfbeis, O. S. (Ed.) *Standardization in Fluorometry: State of the Art and Future Challenges*, Springer, Berlin Heidelberg New York
14. Sanders, R., Draaijer, A., Gerritsen, H. C., Houpt, P. M., and Levine, Y. K. (1995) Quantitative pH imaging in cells using confocal fluorescence lifetime imaging microscopy. *Analytical Biochemistry* 227, 302–308
15. Esposito, A., Gralle, M., Dani, M. A. C., Lange, D., and Wouters, F. S. (2008) pHlameleons: a family of FRET-based protein sensors for quantitative pH imaging. *Biochemistry* 47, 13115–13126
16. Agronskaia, A. V., Tertoolen, L., and Gerritsen, H. C. (2004) Fast fluorescence lifetime imaging of calcium in living cells. *Journal of Biomedical Optics* 9, 1230–1237
17. Webb, S. E. D., Gu, Y., Leveque-Fort, S., Siegel, J., Cole, M. J., Dowling, K., Jones, R., French, P. M. W., Neil, M. A. A., Juskaitis, R., Sucharov, L. O. D., Wilson, T., and Lever, M. J. (2002) A wide-field time-domain fluorescence lifetime imaging microscope with optical sectioning. *Review of Scientific Instruments* 73, 1898–1907
18. Esposito, A., Wouters, F. S., Bonifacino, J. S., Dasso, M., Harford, J. B., Lippincott-Schwartz, J., and Yamada, K. M. (2004) Fluorescence lifetime imaging microscopy. In: Bonifacino, J. S., Dasso, M., Harford, J. B., Lippincott-Schwartz, J., and Yamada, K. M. (Eds.) *Current Protocols in Cell Biology*. Wiley, New York, NY
19. Elder, A. D., Frank, J. H., Swartling, J., Dai, X., and Kaminski, C. F. (2006) Calibration of a wide-field frequency–domain fluorescence lifetime microscopy system using light emitting diodes as light sources. *Journal of Microscopy* 224, 166–180
20. Esposito, A., Dohm, C. P., Kermer, P., Bahr, M., and Wouters, F. S. (2007) α-synuclein and its disease-related mutants interact differentially with the microtubule protein tau and associate with the actin cytoskeleton. *Neurobiology of Disease* 26, 521–531
21. Legg, J. W., Lewis, C. A., Parsons, M., Ng, T., and Isacke, C. M. (2002) A novel PKC-regulated mechanism controls CD44-ezrin association and directional cell motility. *Nature Cell Biology* 4, 399–407
22. Reits, E. A. J., and Neefjes, J. J. (2001) From fixed to FRAP: measuring protein mobility and activity in living cells. *Nature Cell Biology* 3, E145–EE47
23. Stagi, M., Dittrich, P. S., Frank, N., Iliev, A. I., Schwille, P., and Neumann, H. (2005) Breakdown of axonal synaptic vesicle precursor transport by microglial nitric oxide. *Journal of Neuroscience* 25, 352–362
24. Iliev, A. I., Ganesan, S., Bunt, G., and Wouters, F. S. (2006) Removal of pattern-breaking sequences in microtubule binding repeats produces instantaneous tau aggregation and toxicity. *Journal of Biological Chemistry* 281, 37195–37204
25. Gordon, G. W., Berry, G., Liang, X. H., Levine, B., and Herman, B. (1998) Quantitative fluorescence resonance energy transfer measurements using fluorescence microscopy. *Biophysical Journal* 74, 2702–2713
26. Esposito, A. (2006) *Molecular and Cellular Quantitative Microscopy: Theoretical Investigations, Technological Developments and Applications to the Neurosciences*. Utrecht University, The Netherlands
27. Mao, S., Benninger, R. K. P., Yan, Y. L., Petchprayoon, C., Jackson, D., Easley, C. J., Piston, D. W., and Marriott, G. (2008) Optical lock-in detection of FRET using synthetic and genetically encoded optical switches. *Biophysical Journal* 94, 4515–4524
28. Wouters, F. S., Bastiaens, P. I., Wirtz, K. W., and Jovin, T. M. (1998) FRET microscopy demonstrates molecular association of non-specific

lipid transfer protein (nsL-TP) with fatty acid oxidation enzymes in peroxisomes. *EMBO J* 17, 7179–7189

29. Berney, C., and Danuser, G. (2003) FRET or no FRET: a quantitative comparison. *Biophysical Journal* 84, 3992–4010
30. Valentin, G., Verheggen, C., Piolot, T., Neel, H., Coppey-Moisan, M., and Bertrand, E. (2005) Photoconversion of YFP into a CFP-like species during acceptor photobleaching FRET experiments. *Nature Methods* 2, 801
31. Piston, D. W., and Kremers, G. J. (2007) Fluorescent protein FRET: the good, the bad and the ugly. *Trends in Biochemical Sciences* 32, 407–414
32. Elangovan, M., Wallrabe, H., Chen, Y., Day, R. N., Barroso, M., and Periasamy, A. (2003) Characterization of one- and two-photon excitation fluorescence resonance energy transfer microscopy. *Methods* 29, 58–73
33. Feige, J. N., Sage, D., Wahli, W., Desvergne, B., and Gelman, L. (2005) PixFRET, an ImageJ plug-in for FRET calculation that can accommodate variations in spectral bleed-throughs. *Microscopy Research and Technique* 68, 51–58
34. Gerritsen, H. C., Asselbergs, M. A., Agronskaia, A. V., and Van Sark, W. G. (2002) Fluorescence lifetime imaging in scanning microscopes: acquisition speed, photon economy and lifetime resolution. *Journal of Microscopy* 206, 218–224
35. Esposito, A., Gerritsen, H. C., and Wouters, F. S. (2005) Fluorescence lifetime heterogeneity resolution in the frequency-domain by Lifetime Moments Analysis (LiMA). *Biophysical Journal* 89, 4286–4299
36. Colyer, R. A., Lee, C., and Gratton, E. (2007) A novel fluorescence lifetime imaging system that optimizes photon efficiency. *Microscopy Research and Technique* 71, 201–213
37. Ghiggino, K. P., Harris, M. R., and Spizzirri, P. G. (1992) Fluorescence lifetime measurements using a novel fiberoptic laser scanning confocal microscope. *Review of Scientific Instruments* 63, 2999–3002
38. Buurman, E. P., Sanders, R., Draaijer, A., Gerritsen, H. C., Vanveen, J. J. F., Houpt, P. M., and Levine, Y. K. (1992) Fluorescence lifetime imaging using a confocal laser scanning microscope. *Scanning* 14, 155–159
39. Wang, X. F., Uchida, T., and Minami, S. (1989) A fluorescence lifetime distribution measurement system based on phase-resolved detection using an image dissector tube. *Applied Spectroscopy* 43, 840–845
40. Morgan, C. G., Mitchell, A. C., and Murray, J. G. (1990) Nanosecond time-resolved fluorescence microscopy: principles and practice. *Transactions of the Royal Microscopical Society* 1, 463–466
41. Gratton, E., Breusegem, S., Sutin, J., Ruan, Q., and Barry, N. (2003) Fluorescence lifetime imaging for the two-photon microscope: time-domain and frequency-domain methods. *Journal of Biomedical Optics* 8, 381–390
42. O'Connor, D. V., and Phillips, D. (1984) *Time Correlated Single Photon Counting*. Academic Press, London
43. Gerritsen, H. C., Agronskaia, S., Bader, A., and Esposito, A. Time Domain FLIM: theory and Instrumentation in FRET & FLIM Imaging Techniques, Gadella, T. W. G ed. Series Laboratory techniques in biochemistry & molecular biology, van der Vliet PC and Pillai S eds., 33, 95–132
44. Stiel, H., Teuchner, K., Paul, A., Leupold, D., and Kochevar, I. E. (1996) Quantitative comparison of excited state properties and intensity-dependent photosensitization by rose bengal. *Journal of Photochemistry and Photobiology B* 33, 245–254
45. Gadella, T. W., Jr., Clegg, R. M., and Jovin, T. M. (1994) Fluorescence lifetime imaging microscopy: pixel-by-pixel analysis of phase-modulation data. *Bioimaging* 2, 139–159
46. Esposito, A., Gerritsen, H. C., Lustenberger, F., Oggier, T., and Wouters, F. S. (2006) Innovating lifetime microscopy: a compact and simple tool for the life sciences, screening and diagnostics. *Journal of Biomedical Optics* 11, 34016
47. Squire, A., Verveer, P. J., and Bastiaens, P. I. (2000) Multiple frequency fluorescence lifetime imaging microscopy. *Journal of Microscopy* 197(Pt 2), 136–149
48. Hanley, Q. S., and Ramkumar, V. (2005) An internal standardization procedure for spectrally resolved fluorescence lifetime imaging. *Applied Spectroscopy* 59, 261–266
49. Hanley, Q. S., Subramaniam, V., Arndt-Jovin, D. J., and Jovin, T. M. (2001) Fluorescence lifetime imaging: multi-point calibration, minimum resolvable differences, and artifact suppression. *Cytometry* 43, 248–260
50. van Munster, E. B., and Gadella, T. W., Jr. (2004) Suppression of photobleaching-induced artifacts in frequency-domain FLIM by permutation of the recording order. *Cytometry* 58A, 185–194
51. van Munster, E. B., and Gadella, T. W., Jr. (2004) phiFLIM: a new method to avoid alias-

ing in frequency-domain fluorescence lifetime imaging microscopy. *Journal of Microscopy* 213, 29–38

52. Esposito, A., Dohm, C. P., Bahr, M., and Wouters, F. S. (2007) Unsupervised fluorescence lifetime imaging microscopy for high-content and high-throughput screening. *Molecular and Cellular Proteomics* 68, 1446–1454
53. Schneider, P. C., and Clegg, R. M. (1997) Rapid acquisition, analysis, and display of fluorescence lifetime-resolved images for real-time applications. *Review of Scientific Instruments* 68, 4107–4119
54. Clegg, R. M., Schneider, P. C., and Slavik, J. (1996) Fluorescence lifetime-resolved imaging microscopy: a general description of lifetime-resolved imaging measurements. In: Slavik, J. (Ed.) *Fluorescence Microscopy and Fluorescence Probes*, Plenum Press, New York, pp. 15–33
55. Testa, I., Parazzoli, D., Barozzi, S., Garre, M., Faretta, M., and Diaspro, A. (2008) Spatial control of pa-GFP photoactivation in living cells. *Journal of Microscopy-Oxford* 230, 48–60
56. Lippincott-Schwartz, J., Altan-Bonnet, N., and Patterson, G. H. (2002) Photobleaching and photoactivation: following protein dynamics in living cells. *Nature Biotechnology* 20, 87–90
57. Mazza, D., Braeckmans, K., Cella, F., Testa, I., Vercauteren, D., Demeester, J., De Smedt, S. S., and Diaspro, A. (2008) A new FRAP/FRAPa method for three-dimensional diffusion measurements based on multiphoton excitation microscopy. *Biophysical Journal* 95, 13
58. Teissie, J., Tocanne, J. F., and Baudras, A. (1978) A fluorescence approach of the determination of translational diffusion coefficients of lipids in phospholipid monolayer at the air–water interface. *European Journal of Biochemistry* 83, 77–85
59. Iliev, A. I., and Wouters, F. S. (2007) Application of simple photobleaching microscopy techniques for the determination of the balance between anterograde and retrograde axonal transport. *Journal of Neuroscience Methods* 161, 39–46
60. Sprague, B. L., Pego, R. L., Stavreva, D. A., and McNally, J. G. (2004) Analysis of binding reactions by fluorescence recovery after photobleaching. *Biophysical Journal* 86, 3473–3495
61. Lippincott-Schwartz, J., Snapp, E., and Kenworthy, A. (2001) Studying protein dynamics in living cells. *Nature Reviews. Molecular cell biology* 2, 444–456
62. Grailhe, R., Merola, F., Ridard, J., Couvignou, S., Le Poupon, C., Changeux, J. P., and Laguitton-Pasquier, H. (2006) Monitoring protein interactions in the living cell through the fluorescence decays of the cyan fluorescent protein. *Chemphyschem* 7, 1442–1454
63. Bunt, G., and Wouters, F. S. (2004) Visualization of molecular activities inside living cells with fluorescent labels. *International Review of Cytology* 237, 205–277
64. Palamidessi, A., Frittoli, E., Garre, M., Faretta, M., Mione, M., Testa, I., Diaspro, A., Lanzetti, L., Scita, G., and Di Fiore, P. P. (2008) Endocytic trafficking of Rac is required for the spatial restriction of signaling in cell migration. *Cell* 134, 135–147
65. Takanishi, C. L., Bykova, E. A., Cheng, W., and Zheng, J. (2006) GFP-based FRET analysis in live cells. *Brain Research* 1091, 132–139
66. Zal, T., and Gascoigne, N. R. J. (2004) Photobleaching-corrected FRET efficiency imaging of live cells. *Biophysical Journal* 86, 3923–3939
67. Digman, M., Caiolfa, V. R., Zamai, M., and Gratton, E. (2007) The Phasor approach to fluorescence lifetime imaging analysis. *Biophysical Journal* 94, L14–L16
68. Hanley, Q. S., and Clayton, A. H. (2005) AB-plot assisted determination of fluorophore mixtures in a fluorescence lifetime microscope using spectra or quenchers. *Journal of Microscopy* 218, 62–67
69. Wouters, F. S., and Esposito, A. (2008) Quantitative analysis of fluorescence lifetime imaging made easy. *HFSP Journal* 2, 7
70. Verveer, P. J., and Bastiaens, P. I. (2003) Evaluation of global analysis algorithms for single frequency fluorescence lifetime imaging microscopy data. *Journal of Microscopy* 209, 1–7
71. Verveer, P. J., Squire, A., and Bastiaens, P. I. (2000) Global analysis of fluorescence lifetime imaging microscopy data. *Biophysical Journal* 78, 2127–2137
72. Vermeer, J. E. M., Van Munster, E. B., Vischer, N. O., and Gadella, T. W. J. (2004) Probing plasma membrane microdomains in cowpea protoplasts using lipidated GFP-fusion proteins and multimode FRET microscopy. *Journal of Microscopy-Oxford* 214, 190–200
73. Cole, N. B., Smith, C. L., Sciaky, N., Terasaki, M., Edidin, M., and Lippincott-Schwartz, J. (1996) Diffusional mobility of golgi proteins in membranes of living cells. *Science* 273, 797
74. Domin, A., Hooper, R., Rauch, U., Lindon, A. C., and Kaminski, C. F. (2003) Linked-fluorophore FRET calibration and FRET studies of the cyclin-CDK switch in mammalian cells. *Proceedings of SPIE* 5139, 7

Chapter 7

A FRET-Based Approach for Studying Conformational Changes of a Cytoskeleton-Related Tumor Suppressor Molecule

Robert F. Hennigan, Mary F. Chaiken, Lauren A. Foster, and Wallace Ip

Summary

Changes in conformation are an important regulatory mechanism for a wide variety of proteins. Proteins whose activity must change in response to external stimuli often undergo dramatic changes in their tertiary structure in a temporally and spatially coordinated manner, resulting in a change in enzymatic activity or in the profile of binding partners. To understand how these proteins function, it is critically important to be able to monitor the timing and subcellular localization of these conformational changes, preferably in a quantitative manner and in the context of a living cell. Unfortunately, there is a dearth of experimental techniques that can detect changes in conformation directly. In this chapter, we describe an approach that takes advantage of fluorescence resonance energy transfer (FRET), a well-known physical phenomenon between a spectrally compatible pair of fluorescent molecules, which is exquisitely sensitive to the distance between them. Combined with the use of proteins of the green fluorescent protein (GFP) family, this approach can be used to detect changes in protein conformation in vitro and in vivo effectively.

Key words: Fluorescent resonance energy transfer, Green fluorescent protein, Protein conformation, Neurofibromatosis type 2, Merlin

1. Introduction

Changes in conformation are an important regulatory mechanism for a wide variety of proteins. A classic example is the conformational changes in myosin upon hydrolysis of its bound ATP, which allows it to undergo a ratcheting motion while bound to actin at high affinity, thus driving muscle contraction *(1)*. The activity of a wide range of signaling molecules are also characterized by changes

R.H. Gavin (ed.), *Cytoskeleton Methods and Protocols,* Methods in Molecular Biology, vol. 586
DOI 10.1007/978-1-60761-376-3_7,
© Humana Press, a part of Springer Science + Business Media, LLC 2009

in conformation in response to a stimulus, resulting in a measurable change in activity *(2)*. These include the action of tyrosine kinases, G-proteins, integrins and adaptor proteins *(3–5)*. These molecules undergo a dramatic change in their tertiary structure in a temporally and spatially regulated manner, resulting either in a change in enzymatic activity or in the profile of binding partners. Therefore, it is critically important to understand the timing and subcellular localization of these conformational changes, preferably in a quantitative manner and in the context of a living cell.

Unfortunately, there is a dearth of experimental techniques for this purpose. A number of biochemical methods, such as analytical ultracentrifugation and NMR spectroscopy, are capable of detecting changes in conformation. However, with these methods it is often necessary to work with highly purified material under nonphysiological conditions and at unrealistically high concentrations. Experimental techniques exist to detect protein modifications that are associated with conformational change, such as phosphorylation, glycosylation or acetylation, but these are indirect measures of protein conformation. In this chapter, we highlight an approach that takes advantage of fluorescent protein technology and molecular cloning techniques to construct genetically encoded biomolecular probes to measure protein conformational changes directly. This approach uses fluorescence resonance energy transfer (FRET) and can be used to detect changes in protein conformation in vitro and in vivo *(6)*.

We will use our studies on merlin, the product of the neurofibromatosis Type II (NF2) tumor suppressor gene, to illustrate the method. This disease is caused by biallelic inactivation of the *NF2* gene and is characterized by bilateral schwannomas of the eighth cranial nerve and a range of other neurological tumors *(7)*. Merlin is a 595 amino acid long, ~70-kDa protein that shares significant homology with the Ezrin–Radixin–Moesin (ERM) branch of the band 4.1 superfamily *(8)*. ERM proteins are adaptor molecules that integrate signals between the actin cytoskeleton, cell surface receptors, and internal signal transduction machinery *(9)*. ERM, and merlin, are characterized by a domain structure consisting of a conserved N-terminal FERM domain followed by an α-helical region and a C-terminal domain (CTD). Interestingly, ERM proteins contain a conserved actin-binding motif in the CTD but merlin does not. An intramolecular interaction between the N-terminal FERM domain and the CTD regulates the activity of merlin and the ERM proteins *(10)*. For the ERM proteins, this interaction masks the F-actin binding domain and possibly other protein binding sites, thereby inactivating the molecule. For merlin, the FERM-CTD interaction is believed to activate it as a growth suppressor, in a mechanism that is still poorly understood *(11)*. Clearly, understanding the

conformational regulation of ERM proteins and merlin is crucial for learning how they function.

2. Materials

2.1. DNA Constructs

For bacterial expression we use the pET-30b (Novagen) plasmid to express the FRET probes 6xHis-Cerulean, 6XHis-C6Vst, and 6xHis-C-Mer-Vst **(Fig. 1a)**. The Strep-Tag epitope, WSHPQFEK *(12)* was fused to the C terminus of Venus using an oligonucleotide adaptor molecule. For mammalian expression we constructed a variant of the adenoviral shuttle vector pShuttle-CMV (Stratagene), which allows experiments based on transient transfection and subsequent construction of recombinant adenovirus.

2.2. Bacterial Expression and Purification of Proteins

1. LB Kan50,CAM30: LB broth supplemented with kanamycin at 50 μg/ml and chloramphenical at 30 μg/ml.
2. Competent Rosetta 2 BL21 (Novagen).
3. Tris buffered saline (TBS): 50 mM Tris–Cl pH 7.5, 150 mM NaCl.

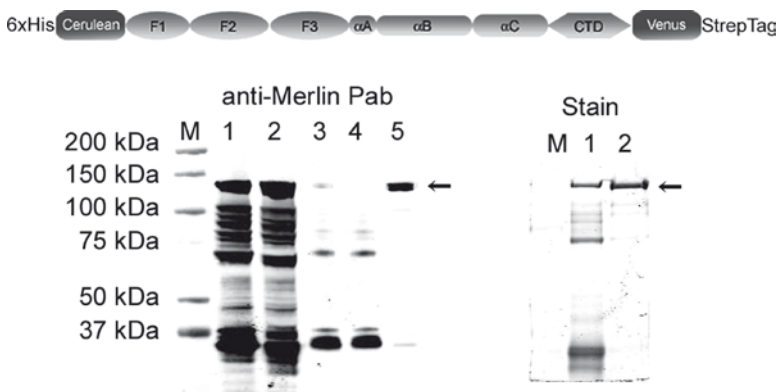

Fig. 1. Intramolecular FRET probe for merlin conformation. *Top*: Schematic diagram of C-Mer-V depicting the donor, Cerulean fused in-frame to the N-terminal FERM domain and the acceptor, Venus, fused to the C terminus of merlin. The affinity tags 6xHis and Strep-Tag are fused to the N terminus of Cerulean and the C terminus of Venus respectively. *Bottom left*: Immunoblots of C-Mer-V purified from IPTG induced bacteria by dual-tag affinity chromatography probed with anti merlin antibodies. *M* molecular weight markers; *1* bacterial lysate; *2* nickel column flowthrough; *3* nickel column eluate; *4* Streptactin column flowthrough; *5* Streptactin column eluate. The *arrow* indicates the position of full length C-Mer-V. *Bottom right*: Infared protein stain (krypton) of purified C-Mer-V. *1* nickel column eluate; *2* Streptactin column eluate.

4. TBS lysis Buffer: 50 mM Tris–Cl pH 7.5, 150 mM NaCl, 10 mM $MgCl_2$, 0.1% Triton X-100, 1:100 6x-His Protease Inhibitor cocktail (Sigma), 10 μg/ml DNase I (Sigma), 100 μg/ml RNase I (Sigma), 1 mg/ml lysozyme (Sigma).
5. Nickel chromatography wash buffer: TBS + 20 mM imidazole.
6. Nickel chromatography elution buffer: TBS + 250 mM imidazole.
7. Nickel agarose resin (Qiagen): 1 ml 50% Ni-agarose slurry per 5 ml lysate (1 g *E. coli*) in a disposable column.
8. Streptactin chromatography wash buffer: TBS pH 7.5.
9. Streptactin chromatography elution buffer: TBS pH 7.5 + 2.5 mM Desthiobiotin.
10. 50% slurry of Streptactin-Sepharose (IBA Biotagnology) in TBS.

2.3. Mammalian Cell Lysates

1. TBS.
2. Lysis buffer: TBS + 1% Triton X-100, plus protease inhibitors.
3. Disposable centrifuge columns (Pierce cat# 89868).
4. Nickel chromatography wash buffer: TBS + 20 mM imidazole.
5. Nickel chromatography elution buffer: TBS + 250 mM imidazole.
6. Nickel agarose resin (Qiagen): 1 ml 50% Ni-agarose slurry per 5 ml lysate (1 g *E. coli*) in a disposable column.
7. Streptactin chromatography wash buffer: TBS pH 7.5.
8. Streptactin chromatography elution buffer: TBS pH 7.5 + 2.5 mM Desthiobiotin.
9. 50% slurry of Streptactin-Sepharose (IBA Biotagnology) in TBS.

3. Methods

The techniques we describe are based on the chameleon series of intramolecular FRET probes *(13)*. These constructs were designed as reporter proteins to measure physiological signals such as calcium flux or GTPase activation, utilizing chimeric molecules that change conformation in response to specific stimuli *(14, 15)*. In this chapter, we will describe the adaptations we developed to study the conformational regulation of merlin.

3.1. Fluorescence Resonance Energy Transfer

FRET is a well-established spectroscopic and microscopic technique that measures molecular interactions in the 100 Å range *(6)*. It is based on the nonradiative transfer of energy between compatible donor and acceptor fluorophores that are in the correct orientation and in close proximity to each other *(16)*. In practice, the donor fluorophore is specifically excited and the emission is measured at the acceptor wavelength. If the donor and acceptor are within 100 Å of each other, then the donor transfers energy to the acceptor and acceptor emission occurs. The efficiency of energy transfer is described by the equation, $E^{\mathrm{FRET}} = R_0^6 \div (R_0^6 + r^6)$, where r is the distance between the donor and acceptor and R_0 the Förster distance, a constant based on the photo-physical properties and orientation of the particular donor and acceptor pair that equals the distance at which E^{FRET} is 50% *(6)*. Since FRET efficiency is inversely proportional to the sixth power of the distance between the donor and acceptor, small changes in distance or orientation lead to large changes in FRET efficiency, making it uniquely suited for measuring small changes in protein conformation at the molecular level.

The objective of our studies is to detect conformational transitions in merlin using a genetically encoded FRET based probe. We employ two variants of GFP, Cerulean and Venus, fused in frame to the N- and C termini of merlin. Cerulean is a GFP mutant with a blue-shifted emission spectrum that will act as a donor to Venus, a GFP mutant with a yellow-shifted emission spectrum *(17, 18)*. The Cerulean and Venus FRET pair has a Förster distance, R_0, of 54 Å *(19)*. It is therefore essential that Cerulean and Venus are fused into the protein of interest such that they are within 40–60 Å of each other. Practically, this means that detailed structural information of the target molecule, such as X-ray crystallography, is critical to the success of these methods.

FRET may be measured in a number of experimental contexts. Proteins may be purified from bacterial expression systems to study them in isolation by spectrofluorimetry. Alternatively the FRET probes may be expressed in mammalian cells to measure changes in FRET efficiency in different subcellular locations over time by microscopy *(20)*.

3.2. Experimental Design

We use an intramolecular FRET probe consisting of a fusion between a protein of interest and both Cerulean and Venus. This produces a molecule with a 1:1 ratio of donor to acceptor, thus obviating experimental error introduced by difference in expression levels of the donor and acceptor. As mentioned above, the probe can be constructed in either bacterial or mammalian expression vector, making it possible to measure FRET in purified protein preparations or in lysates of mammalian cells expressing the probe. Here we describe the bacterial expression of FRET

probes in detail, as the purity and integrity of the purified probe critically influence the efficacy and success of the method. The preparation of cell lysates is straightforward, and lysis conditions depend greatly on the solubility of the protein being studied. A brief description of our own protocol is provided and may be used as a starting point.

Certain proteins, merlin among them, are difficult to purify as full length molecules because of mammalian codon bias, proteolytic cleavage and insolubility in bacteria. To facilitate the rapid purification of full length FRET probes we created a bacterial expression plasmid, based on pET-30b, that fuses a 6xHis tag to the N-terminal of the Cerulean open reading frame and an eight amino acid epitope, Strep-Tag, in frame, C-terminal to Venus. Merlin is fused, in frame between Cerulean and Venus to create a fusion protein with affinity tags at both the N- and C-termini. As a positive control for FRET we fused 6xHis-Cerulean in frame to Venus-strep-tag separated by six amino acids. To express fusion proteins, we use the Novagen Rosetta-2 *E. coli* strain that expresses seven mammalian tRNAs corresponding to codons that are rarely used in bacteria. In our experience, this strain enhances the expression of full-length merlin in bacteria by reducing premature termination caused by tRNA depletion. Also, since a high proportion of bacterially expressed merlin is in insoluble inclusion bodies, we grow the bacteria at 22°C and use the ethanol based "cold drunk" protocol that, in our hands, yields a greater amount of soluble recombinant merlin. Recombinant proteins are then purified by sequential nickel and streptactin affinity chromatography (*see* **Note 1**).

3.3. Induction of pC-mer-V (See Note 2)

1. Inoculate a 30 ml culture in LB Kan50, CAM30 with an isolated colony of pET-CmerVst.
2. Grow overnight at 37°C with shaking.
3. Transfer 25 ml of the overnight culture into 500 ml (20 vols.) LB Kan in a 2-l flask.
4. Incubate at 37°C with shaking until the OD600 = 0.8–1.2, remove 1-ml aliquot.
5. Cool the flask on ice for 30 min.
6. Add 500 ml ice cold (4°C) LB + 0.2 mM IPTG + 20 ml EtOH.
7. Incubate overnight at 20°C (room temp.) with shaking, remove 1-ml aliquot.
8. Harvest the bacteria in 500-ml bottles, spin 4,000 × *g*, 4°C for 10 min in the SLA-3000 rotor.
9. Weigh the pellet and label the tube, including the date.
10. Snap freeze in liquid N_2 for 5 min.
11. Store at –70°C.

3.4. Bacterial Lysis

1. Prepare 5 ml TBS lysis buffer per gram.
2. Thaw the cells in a room temp. water bath, 5 min.
3. Resuspend to 5 ml lysis buffer per gram of bacteria.
4. Rotate at 4°C protected from light for 30 min (cold room). The material should become viscous, indicating lysis.
5. Sonicate on ice. 6 cycles, 10 s on, 10 s off. Lysate should lose viscosity.
6. Pellet cell debris, 14,000 × *g* on the benchtop centrifuge for 30 min at 4°C.
7. Save supernatant on ice. Remove aliquot for analysis.

3.5. Nickel Chromatography

1. Pack 1 ml 50% Ni-agarose slurry per 5 ml lysate (1 g *E. coli*) in a disposable column and wash with 10 volumes wash buffer. (Assume 1 ml packed bed volume = 2 ml 50% slurry and bind to 10–20 mg 6xHis protein.)
2. Resuspend to 1 ml in wash buffer.
3. Add lysate to beads and incubate at 4°C with rotation in the dark for 60 min.
4. Pour into the column and collect the flowthrough.
5. Wash with 10 bed volumes of wash buffer; save the first and last drops of the wash to compare fluorescence (*see* **Note 1**).
6. Elute stepwise with 5 × 0.5 ml elution buffer.
7. Pool fluorescent fractions.
8. Proceed to Streptactin column.
9. Wash column with 5 vol. elution buffer and 10 volumes wash buffer, store at 4°C (*see* **Note 3**).

3.6. Streptactin Chromatography

1. Add 1 ml 50% slurry of the Streptactin agarose to a disposable column (0.5 ml bed volume).
2. Equilibrate with 2 bed volumes of wash buffer.
3. Add pooled nickel eluates to column beads and collect the flowthrough.
4. Wash with 10 bed volumes of wash buffer; save the first and last drops of the wash to compare fluorescence (*see* **Note 1**).
5. Elute stepwise with 5 × 0.5 bed volumes elution buffer.
6. Pool fluorescent fractions.
7. Dialyze 3× against 1 l TBS at 4°C.

3.7. Preparing Mammalian Cell Lysates for FRET Measurement

1. Plate cells in 10-cm plates and incubate overnight.
2. Change to PenStrep free media.

3. Set up lipofectamine 2,000 transfections as per manufacturer's instructions: 12 μg DNA per plate, incubate overnight, and then change into fresh DMEM + 10% FBS + PenStrep.
4. Rinse with cold PBS.
5. Add 0.5 ml cold lysis buffer.
6. Scrape into 1.5-ml tube.
7. Incubate for 20 min at 4°C with rotation.
8. Spin down at 14,000 rpm benchtop centrifuge at 4°C. Save supernatant.

3.8. Dual Affinity Purification of FRET Probes from Mammalian Cell Lysates

1. Add 50 μl of a 50% slurry of nickel agarose resin, equilibrated in TBS to 0.5 ml cell lysate in a disposable centrifuge column (Pierce cat# 89868). Screw on the cap.
2. Incubate at 4°C with rotation in the dark for at least 60 min.
3. Twist off the bottom tip of the column and place in a 1.5-ml centrifuge tube.
4. Spin in a benchtop centrifuge for 30 s at 1,500 × *g* (5,000 rpm); save the supernatant as unbound flowthrough.
5. Wash the column 3× with 0.5 ml TBS.
6. Elute the column three times with 100 μl 0.5 ml TBS + 250 mM imidazole.
7. Pool the fluorescent fractions.
8. Add 50 μl of a 50% slurry of Streptactin resin, equilibrated in TBS.
9. Transfer to a disposable centrifuge column (Pierce cat# 89868). Screw on the cap.
10. Incubate at 4°C with rotation in the dark for at least 60 min.
11. Twist off the bottom tip of the column and place in a 1.5-ml centrifuge tube.
12. Spin in a benchtop centrifuge for 30 s at 1,500 × *g* (5,000 rpm), save the supernatant as unbound flowthrough.
13. Wash the column 3× with 0.5 ml TBS.
14. Elute the column three times with 100 μl 0.5 ml TBS + 2.5 mM Desthiobiotin.
15. Pool the fluorescent fractions for spectrofluorimetry.

3.9. Spectrofluorimetry

We use a Horiba Jobin Yvon Fluorolog-3 spectrofluorimeter, but any instrument capable of collecting a spectrum is usable. For purified proteins, samples are diluted to a concentration of 1 μM in TBS. Desthiobiotin has no effect on protein conformation so

dialysis is unnecessary. Samples are excited at 435 nm with a 2-nm slit width and emission spectra are acquired from 450 to 600 nm at 1-nm intervals, also with 2-nm slit width. Transfected cell lysates are analyzed the same way except using 5-nm slit widths at emission and excitation for enhanced sensitivity.

The simplest way to present the data is a graph depicting the emission spectrum. In this case we normalize the relative fluorescence intensity at each wavelength to the peak value of the range. In the example provided **(Fig. 2)**, the emission from the Cerulean peaks at 477 nm, displays a characteristic "hump" in the 490–510 nm range, then decays precipitously. In contrast, the positive control, C6V, has a strong peak at 525 nm and a reduced emission at 477 nm. This is evidence of efficient energy transfer from Cerulean to Venus in this molecule. FRET is easily detectable in C-Mer-V as a bulge in the emission spectrum from 515 nm to more than 550 nm, relative to the negative control.

These data are then used to calculate the average distance between Cerulean and Venus. The FRET signal, *F*, is expressed as a ratio of the acceptor emission (515–550 nm) to the donor emission (460–490 nm), when excited at the donor's peak excitation wavelength, 435 nm:

$$F = \mathrm{Ex}^{435\mathrm{nm}}\mathrm{Em}^{515-550\mathrm{nm}} \div \mathrm{Ex}^{435}\mathrm{Em}^{460-490}$$

The FRET efficiency, E^{FRET}, is expressed as normalized to a negative control consisting of the donor without acceptor:

$$E^{\mathrm{FRET}} = 1 - (F^{\mathrm{Control}} \div F^{\mathrm{FRET}})$$

Recalling that the relationship between the FRET efficiency and the distance between the donor and acceptor is described by the equation *(6)*:

$$E^{\mathrm{FRET}} = R_0^6 \div (R_0^6 + r^6)$$

The distance between Cerulean and Venus, can therefore be calculated by solving the above equation for *r*:

$$r = R_0 \times ((1 / E^{\mathrm{FRET}}) - 1)^{1/6}.$$

As mentioned previously, R_0 is a constant for each donor and acceptor pair, and is the distance at which the E^{FRET} is 50%. For Cerulean and Venus, R_0 is 54 Angstroms (*see* **Note 4**).

Purified Cerulean alone is used as a negative control. Alternatively, since GFP is insensitive to trypsin, trypsinized FRET probes, in which Cerulean and Venus are separated by cleavage of the intervening protein, may be used as an internal negative control for FRET *(21)* (*see* **Note 5**).

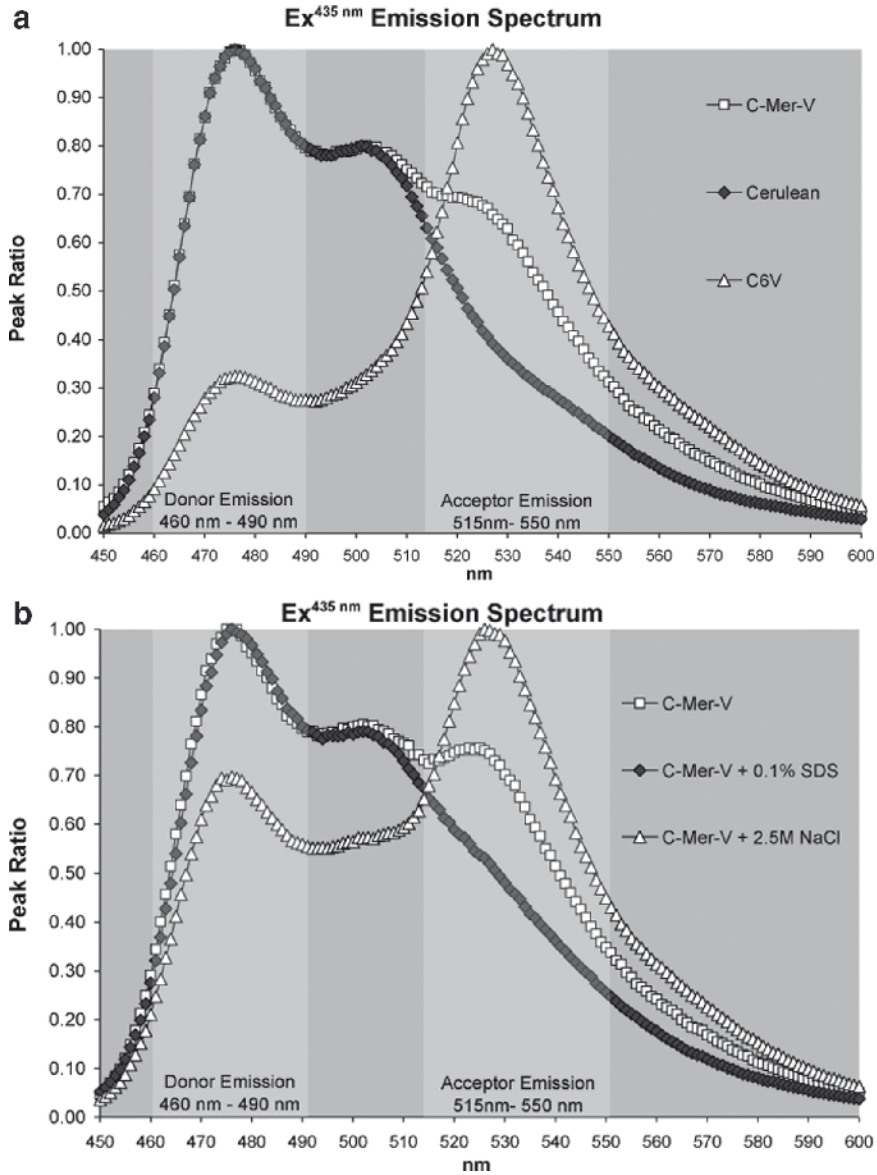

	Cerulean	C6V	C-Mer-V	C-Mer-V + 0.1% SDS	C-Mer-V + 2.5M NaCl
FRET Ratio	0.259	1.336	0.413	0.334	0.820
E^{FRET}	0.000	0.806	0.373	0.225	0.685
Distance (Å)	>100	42.57	58.88	66.37	47.46

Fig. 2. Emission spectrum from 450 to 600 nm, excited at 435 nm, of purified proteins at 1 μM in TBS at 20°C. The donor emission peaks, from 460 to 490 nm, and the acceptor emission peaks from 515 to 550 nm are depicted in *light grey*. The FRET ratio, FRET efficiency, and donor to acceptor distances are calculated as described in **Subheading 3.9** and are shown in the table. (**a**) FRET from the intramolecular FRET probe C-Mer-V (*white squares*). Purified Cerulean is a negative control for FRET (*dark diamonds*). C6V is the positive control for FRET (*white triangle*). (**b**) Conformational changes of C-Mer-V caused by detergent and salt. C-Mer-V in TBS (*white squares*), treated with 0.1% SDS (*dark diamonds*) or 2.5 M NaCl (*white triangles*).

Figure 2b is an example of the utility of this method for measuring changes in protein conformation. The FRET efficiency of C-Mer-V increases dramatically in a hypotonic solution. This indicates that high salt conditions compress this molecule further. Most likely this is a result of strengthening of the hydrophobic interaction within the merlin structure that increases the strength of the coiled coil that the central α-helical region assumes. In contrast, treatment of C-Mer-V with 0.1% SDS completely abolished the FRET, without affecting the fluorescence of either Cerulean or Venus *(22)*. These are two extreme examples of the FRET signal responding to enforced changes in tertiary structure and highlight the range of conformations that may be detected with these methods.

3.10. FRET Imaging in Live Cells

The FRET probes may also be expressed in mammalian cells to correlate subcellular localization or physiological state with changes in protein conformation. In our studies of merlin, SC4 cells are plated in 35-mm Matek dishes, which have a coverslip at the bottom for optimal optics, and transfected as described above. After 24 h cells are rinsed and the media is changed into phenol red-free DMEM containing 25 mM HEPES pH 7.5. Cells are imaged live on a Zeiss Axioplan microscope using a 63× 1.4 NA PlanApo water immersion objective, a Hamamatsu Orca ER camera and a Uniblitz shutter controlled by Metamorph imaging software. The filter sets used for FRET are from Chroma. The excitation filter, dichroic mirror, and emission filter sets for Cerulean are D436/20x, 455DCLP and D480/40m, for Venus: HQ515/20, Q515LP and HQ535/30m, and for FRET: D436/20x, 455DCLP and HQ535/30m. The exposure times for donor, acceptor, and FRET channels are always kept the same. Each field yielded three 1,280 × 1,024 pixel 12-bit images, representing the donor, acceptor and FRET channels. Typically ten fields are acquired for each transfection.

The most informative way to visualize intramoleular FRET probes - those with a 1:1 donor to acceptor ratio by design - is to display the images as the ratio of the FRET channel to the donor channel **(Fig. 3)**. Images are analyzed using the Image J package (http://rsbweb.nih.gov/ij/). For the FRET: donor ratio images the background is subtracted using a rolling ball algorithm with a 50 pixel radius. A mask is then created by thresholding the donor image, setting the background pixels to a value of zero and the cell body pixels to a value of one. The ratio image is generated by dividing the background subtracted FRET channel image by the background subtracted donor channel image and multiplying the result by the mask. The resulting 32-bit floating point image is used to measure the average pixel intensity in order to calculate FRET efficiencies. For display, 32-bit floating point images are converted to 8-bit images, and then pseudocolored for intensity

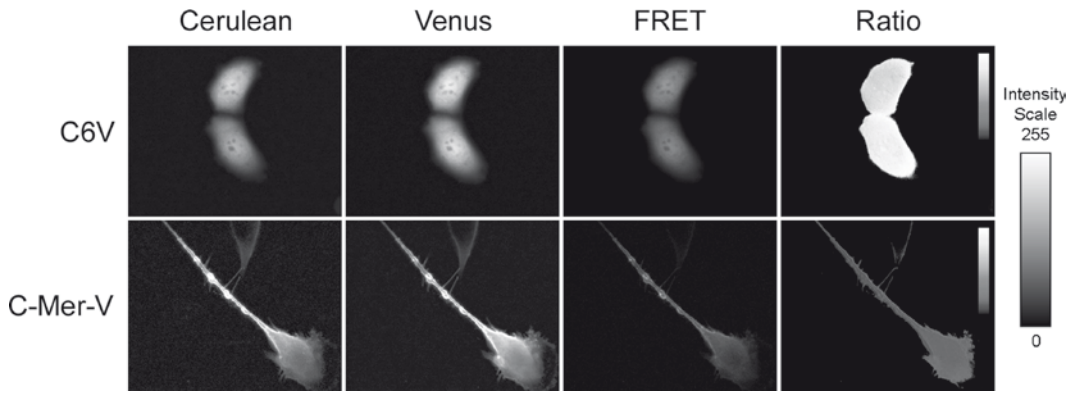

Fig. 3. C-Mer-V FRET in live cells. Confluent SC4 schwannoma cells were transfected with the indicated plasmids. Images were acquired using filter sets specific for the donor, acceptor, and FRET signals. The FRET efficiency is represented in the images at the far right depicting the ratio of the FRET channel to the donor channel as a *greyscale* intensity with the maxima normalized to the C6V positive control.

using the Image J lookup table called Fire. For display, the donor, acceptor, and FRET channel images are background subtracted as described above, converted into 8-bit images, then pseudocolored using the cyan, yellow, and red lookup tables in Image J.

4. Notes

1. The purification is easily monitored by measuring the fluorescence of aliquots during induction, lysis, binding, wash, and elution. We use a plate fluorimeter to monitor fluorescence during purification but placing tubes on a UV transilluminator works just as well.
2. This induction protocol is used for our merlin probe, C-mer-V, which is largely, but not entirely insoluble when expressed in bacteria. To induce well expressed, soluble proteins such as the C6V control we grow smaller culture volumes and a more conventional induction protocol.
   (a) Inoculate an isolated colony of pET-C6V in 20 ml LB Kan.
   (b) Grow overnight at 37°C with shaking.
   (c) Inoculate 5 ml of the overnight culture into 100 ml LB Kan. (1:20).
   (d) Incubate at 37°C with shaking until the OD^{600} = 0.8–1.2, remove 1-ml aliquot.

(e) Add IPTG to 1 mM, incubate at 37°C with shaking for 4–5 h, remove 1-ml aliquot.

(f) Confirm induction by pelleting the bacteria in a microfuge then placing the tubes on a UV transilluminator, induction will cause the pellet to glow green.

(g) Harvest the bacteria at 4,000 × *g*, 4°C for 10 min. Discard the supernatant.

(h) Weigh the pellet, then snap freeze in liquid N_2 for 5 min. The pellet may be stored for several months at –70°C.

3. The nickel and streptactin resin may be regenerate and reused.

(a) Wash the nickel agarose column with 5 volumes of elution buffer and then 10 bed volumes of TBS.

(b) Wash the Streptactin column with 3× with 5 vol. regeneration buffer, then 2 × 4 bed volumes of TBS wash buffer. Store at 4°C as a 50% slurry with TBS.

4. R_0 is calculated for each FRET pair from their photo-physical properties such as extinction coefficient and quantum yield of the donor, spectral overlap between donor and acceptor, and the refractive index of the medium and it is dependent upon the relative orientation of the flurophores *(6)*. The value of R_0 cited for Cerulean and Venus 54 Å assumes that the orientation is random.

5. This control is a little more accurate than that using Cerulean alone because it compensates for the small amount of direct excitation of Venus at 435 nm, which is typically less than 1% when Cerulean and Venus are equimolar. Cerulean and Venus may also be separately purified and mixed in a 1:1 molar ratio.

Acknowledgments

The authors gratefully acknowledge the grant support from the National Cancer Institute (R01-CA78524 to WI) and the Department of Defense CDMRP NFRP (NF043043 to WI). We also wish to thank Drs. Peixuan Guo and Chia-chi Ho (University of Cincinnati) for the use of their spectrofluorimeters. Resources at the Center for Biological Microscopy (http://microscopy.uc.edu), University of Cincinnati, were utilized for the FRET imaging studies.

References

1. Ikebe, M. (2008). Regulation of the function of mammalian myosin and its conformational change. Biochem Biophys Res Commun *369*(1), 157–164
2. Changeux, J.P., and Edelstein, S.J. (2005). Allosteric mechanisms of signal transduction. Science *308*, 1424–1428
3. Carman, C.V., and Springer, T.A. (2003). Integrin avidity regulation: are changes in affinity and conformation underemphasized? Curr Opin Cell Biol *15*, 547–556
4. Ouyang, M., Sun, J., Chien, S., and Wang, Y. (2008). Determination of hierarchical relationship of Src and Rac at subcellular locations with FRET biosensors. Proc Natl Acad Sci USA *105*, 14353–14358
5. Yeagle, P.L., and Albert, A.D. (2003). A conformational trigger for activation of a G protein by a G protein-coupled receptor. Biochemistry *42*, 1365–1368
6. Piston, D.W., and Kremers, G.J. (2007). Fluorescent protein FRET: the good, the bad and the ugly. Trends Biochem Sci *32*, 407–414
7. McClatchey, A.I. (2003). Merlin and ERM proteins: unappreciated roles in cancer development? Nat Rev Cancer *3*, 877–883
8. Gautreau, A., Louvard, D., and Arpin, M. (2002). ERM proteins and NF2 tumor suppressor: the Yin and Yang of cortical actin organization and cell growth signaling. Curr Opin Cell Biol *14*, 104–109
9. Tsukita, S., and Yonemura, S. (1997). ERM (ezrin/radixin/moesin) family: from cytoskeleton to signal transduction. Curr Opin Cell Biol *9*, 70–75
10. Bretscher, A., Edwards, K., and Fehon, R.G. (2002). ERM proteins and merlin: integrators at the cell cortex. Nat Rev Mol Cell Biol *3*, 586–599
11. Sherman, L., Xu, H.M., Geist, R.T., Saporito-Irwin, S., Howells, N., Ponta, H., Herrlich, P., and Gutmann, D.H. (1997). Interdomain binding mediates tumor growth suppression by the NF2 gene product. Oncogene *15*, 2505–2509
12. Zwicker, N., Adelhelm, K., Thiericke, R., Grabley, S., and Hanel, F. (1999). Strep-tag II for one-step affinity purification of active bHLHzip domain of human c-Myc. Biotechniques *27*, 368–375
13. Shimozono, S., and Miyawaki, A. (2008). Engineering FRET constructs using CFP and YFP. Methods Cell Biol *85*, 381–393
14. Miyawaki, A., Llopis, J., Heim, R., McCaffery, J.M., Adams, J.A., Ikura, M., and Tsien, R.Y. (1997). Fluorescent indicators for Ca^{2+} based on green fluorescent proteins and calmodulin. Nature *388*, 882–887
15. Mochizuki, N., Yamashita, S., Kurokawa, K., Ohba, Y., Nagai, T., Miyawaki, A., and Matsuda, M. (2001). Spatio-temporal images of growth-factor-induced activation of Ras and Rap1. Nature *411*, 1065–1068
16. Vogel, S.S., Thaler, C., and Koushik, S.V. (2006). Fanciful FRET. Sci STKE 2006(331), re2
17. Nagai, T., Ibata, K., Park, E.S., Kubota, M., Mikoshiba, K., and Miyawaki, A. (2002). A variant of yellow fluorescent protein with fast and efficient maturation for cell-biological applications. Nat Biotechnol *20*, 87–90
18. Rizzo, M.A., Springer, G.H., Granada, B., and Piston, D.W. (2004). An improved cyan fluorescent protein variant useful for FRET. Nat Biotechnol *22*, 445–449
19. Koushik, S.V., Chen, H., Thaler, C., Puhl, H.L., III, and Vogel, S.S. (2006). Cerulean, Venus, and VenusY67C FRET reference standards. Biophys J *91*, L99–L101
20. Chen, Y., Mills, J.D., and Periasamy, A. (2003). Protein localization in living cells and tissues using FRET and FLIM. Differentiation *71*, 528–541
21. Ohashi, T., Galiacy, S.D., Briscoe, G., and Erickson, H.P. (2007). An experimental study of GFP-based FRET, with application to intrinsically unstructured proteins. Protein Sci *16*, 1429–1438
22. Alkaabi, K.M., Yafea, A., and Ashraf, S.S. (2005). Effect of pH on thermal- and chemical-induced denaturation of GFP. Appl Biochem Biotechnol *126*, 149–156

Chapter 8

Sample Preparation for Fluorescence Imaging of the Cytoskeleton in Fixed and Living Plant Roots

Julia Dyachok, Cheol-Min Yoo, Karuppaiah Palanichelvam, and Elison B. Blancaflor

Summary

During the past decade the use of live cytoskeletal probes has increased dramatically due to the introduction of the green fluorescent protein. However, to make full use of these live cell reporters it is necessary to implement simple methods to maintain plant specimens in optimal growing conditions during imaging. To image the cytoskeleton in living Arabidopsis root cells, we rely on a system involving coverslips coated with nutrient supplemented agar where the seeds are directly germinated. This coverslip system can be conveniently transferred to the stage of a confocal microscope with minimal disturbance to the growth of the seedling. Parallel to our live cell imaging approaches, we routinely process fixed plant material via indirect immunofluorescence. For these methods we typically use nonembedded vibratome-sectioned and whole mount permeabilized root tissue. The clearly defined developmental regions of the root provide us with an elegant system to further understand the cytoskeletal basis of plant development.

Key words: Actin, Arabidopsis, Microtubules, Green fluorescent protein, Living cells, Roots, Immunofluorescence, Fixed plant material, Sectioning

1. Introduction

An important requirement for research on plant cytoskeleton is the ability to routinely and reliably image its organization in the cell. This goal has been facilitated in large part by advances in fluorescence microscopy not only with regard to the development of advanced microscope systems such as confocal microscopes but also through the introduction of reagents that allow for in vivo labeling of cytoskeletal elements *(1, 2)*. Microtubules and actin filaments (F-actin), the two major components of the

R.H. Gavin (ed.), *Cytoskeleton Methods and Protocols,* Methods in Molecular Biology, vol. 586
DOI 10.1007/978-1-60761-376-3_8,
© Humana Press, a part of Springer Science + Business Media, LLC 2009

cytoskeleton, can now be visualized readily in living plant cells using an array of green fluorescent protein (GFP) constructs (e.g. *(3–8)*). Despite the rapid implementation of live cell imaging tools, methods for optimal fixation of plant tissues for cytoskeletal studies will remain an essential tool for plant biologists. This is because these fixation approaches not only verify results from live cell probes, they also have led to the discovery of novel cytoskeletal structures not always revealed by in vivo cellular reporters (e.g. *(9–11)*). Furthermore, most of the work on live imaging of the cytoskeleton has been conducted on cells located on the plant surface such as epidermal cells, trichomes, and root hairs. In cells located within the plant interior especially those from plant species with thicker organ systems, it is necessary to utilize conventional methods of sectioning and permeabilization to allow access of the cytoskeletal label (e.g. *(10, 12, 13)*). In this chapter, we describe procedures for fluorescent labeling of the cytoskeleton in plant roots for observation with confocal microscopy. Our primary focus is on the root because it provides an elegant system for studying the cytoskeletal basis of plant development *(14)*. We first describe procedures for fluorescent antibody labeling of non-embedded root sections and permeabilized whole roots. We then outline a simple method for preparing Arabidopsis roots for live cell imaging of fluorescently labeled cytoskeletal structures.

2. Materials

2.1. Vibratome Sectioning and Whole Mount Immunolabeling of Fixed Roots

1. 37% formaldehyde (Sigma-Aldrich, St. Louis, MO).
2. Paraformaldehyde (16% solution; Electron Microscopy Sciences, Hatfield, PA).
3. Dimethyl sulfoxide (DMSO; Sigma-Aldrich, St. Louis, MO).
4. PME buffer: 50 mM PIPES (piperazine-*N*,*N*′ bis [2-ethansesulfonic acid]), 2 mM $MgCl_2$ and 10 mM EGTA. Adjust pH of PME to 7.0 using 10 *N* NaOH.
5. Phosphate buffered saline (PBS), pH 7.2 for diluting antibodies and pH 8.5 for preparing the mounting medium. PBS buffer: 135 mM NaCl, 25 mM KCl, 5 mM Na_2HPO_4 and 2 mM KH_2PO_4. To prepare PBS with a pH of 8.5, omit the KH_2PO_4 and adjust the pH with 10 *N* NaOH.
6. Cellulase YC and Pectolyase Y23 (Karlan Research Products, Cottonwood, AZ).
7. 1% (v/v) Triton X-100 (Fischer Scientific, Pittsburgh, PA) in PME buffer.
8. Mowoil 4-88 (Calbiochem, La Jolla, CA).

9. Vibratome 1000 Plus (Ted Pella Inc., Redding, CA).
10. Superglue.
11. Double edged razor blades and fine forceps (Electron Microscopy Sciences, Hatfield, PA).
12. Bovine serum albumin and normal goat serum (Sigma-Aldrich, St. Louis, MO).
13. Maleimidobenzoyl-*N*-hydroxysuccinimide ester (MBS, Pierce Biotechnology, Chicago, IL). To prepare 0.16 M MBS stock solution, dissolve 50 mg MBS in 1 mL DMSO. MBS stock solution can be stored at −20°C for several months.
14. Methanol prechilled to −20°C.
15. PEMT: 0.05% (v/v) Triton X-100 in PME buffer.
16. PBST: 0.05% (v/v) Triton X-100 in PBS buffer, pH 7.0.
17. Tissue culture inserts (TCIs, Corning Netwell Plate, 12-Well Cluster, 500 μm pore size).
18. Vectashield (Vector Laboratories, Burlingame, CA).
19. Rotating shaker table.

2.2. Preparing Arabidopsis Seedlings for Live Cell Imaging of Roots

1. Agar (Sigma-Aldrich, St Louis, MO or Caisson Laboratories , Inc., North Logan, UT (*see* **Note 1**).
2. Murashige and Skoog (MS) basal salt mixture (*Phyto*Technology Laboratories, Lenexa, KS).
3. 48 × 64 × 0.13 ~ 0.17 mm coverslips (Fisher Scientific, Pittsburgh, PA or VWR International, West Chester, PA).
4. Sterilized pointed end toothpicks.
5. Polystyrene sterile Petri dishes (VWR International, West Chester, PA).
6. Sterilized filter paper.

3. Methods

3.1. Immunolabeling of Fixed Roots

In both sectioning and whole mount permeabilization of roots, the general methods for fixation to preserve cytoskeletal structures are roughly similar. The only major difference is that the latter requires specialized sectioning equipment while the former relies on extensive digestion of the root with cell wall degrading enzymes.

3.1.1. Immunolabeling the Cytoskeleton in Vibratome Sectioned Roots

1. For plant species with large roots (ca. 300 μm to 1 mm in diameter) such as *Zea mays* or *Medicago truncatula*, excise the terminal 5 mm of the primary root with a razor blade

and immerse root segments in 3.7% formaldehyde and 5% DMSO in PME buffer (v/v) (*see* **Note 2**). We typically use clear 20-mL scintillation glass vials with rubber-lined caps (Wheaton, Millville, NJ) to hold the fixative containing the root segments. Place uncapped vials containing fixative and the collected root tissues in a small vacuum dessicator jar equipped with a T connector. Apply a light vacuum for 10–20 min. After releasing the vacuum most of the root samples should sink to the bottom of the vial.

2. After incubating samples in fixative for 2 h, slowly aspirate the fixative with a pipette and dispose excess fixative in clearly marked waste bottles in a fume hood. Wash the samples by immersing them in PME buffer for 3–5 min. Repeat this process three times to fully remove residual fixative.
3. For larger roots (i.e., >300 μm in diameter), longitudinal or cross sections can be easily obtained using a vibratome 1000 (**Fig. 1a**). To prepare root segments for vibratome sectioning, gently lift the excised root segment with a fine pair of forceps and blot excess liquid using filter paper or kimwipes (**Fig. 1b**). Spread a thin layer of superglue onto the surface of the vibratome mounting block and carefully position the root segment onto the block (**Fig. 1c**). To obtain good longitudinal sections, the long axis of the root must be perpendicular to the cutting surface of the blade (**Fig. 1a**). When the root contacts the thin layer of superglue, it takes about 60 s or less for the glue to polymerize allowing the root segment to firmly attach to the block (**Fig. 1c**; *see* **Note 3**).
4. Break a double edged razor blade in half and fasten half of the broken blade to the vibratome. Fill the vibratome specimen bath with deionized water and secure the block with the

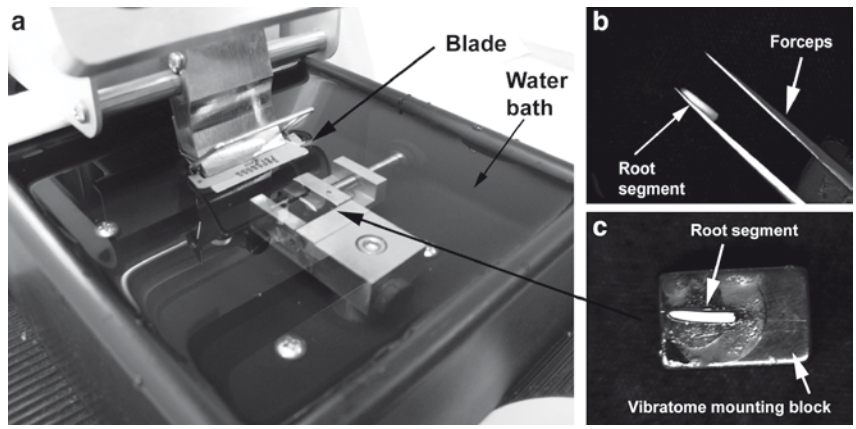

Fig. 1. Handling root tissues for vibratome sectioning. (**a**) The specimen holder of a vibratome 1000 showing the blade and block holder. (**b**) A segment of a fixed maize primary root on the tip of a pair of fine forceps. (**c**) Handling fixed root tissue as shown in (**b**) facilitates mounting the root on superglue coated vibratome block.

adhered root segment onto the block holder making sure that the root sample is fully immersed in water **(Fig. 1a)**. Set the vibratome to section at 50–100 μm thickness following the manufacturers' instructions (*see* **Note 4**). Depending on the size of the root, one can obtain about 3–8 good quality longitudinal sections for cytoskeletal labeling.

5. Collect sections from the vibratome water bath using the wide end of a Pasteur pipette or a pair of fine forceps and transfer sections to polystyrene Petri dishes containing PME buffer. Alternatively, sections can be directly placed onto 22 × 22 coverslips or glass slides. Use a small piece of filter paper to remove excess PME buffer by touching the liquid adjacent to the root sections. Allow sections to partially dry onto the surface of the slide or coverslip (*see* **Note 5**).
6. When sections are secured onto the coverslip, apply a cocktail of 1% cellulose YC in PME buffer for 10 min. The cellulose solution should cover the root sections during incubation. Slowly decant the cellulose solution and wash sections three times with PME buffer. During the washing steps, PME buffer can simply be added onto the surface of the coverslips containing the root sections and decanted (*see* **Note 6**). After cell wall treatment, incubate samples in 1.0% Triton X-100 in PME for 15–20 min and wash three times with PME buffer.
7. Apply primary antibody diluted in PBS, pH 7.2 onto the surface of the coverslips containing the root sections and place in a humid chamber for 2–3 h. Wash three times with PME buffer and apply secondary antibody conjugated to a fluorescent dye that specifically recognizes the primary antibody. Incubate sections in a humid chamber for another 2 h (*see* **Notes 7** and **8**).
8. Prepare the mounting medium while samples are incubating in the secondary antibody. This is accomplished by preparing 20% Mo wiol 4-88 in PBS, pH 8.5 (v/v). A 2 mL volume of mounting media is sufficient for mounting about 10–20 samples. The Mowiol-PBS solution can be prepared in 20-mL scintillation vials similar to those used for tissue fixation (*see* **step 1** above). To dissolve the Mowiol crystals, stir the solution for 2 h using a small magnetic stir bar (*see* **Note 9**).
9. After secondary antibody treatment, wash samples with PME buffer three times and allow the sections to partially dry. Blot any excess liquid with filter paper and use the wide end of a Pasteur pipette to collect the mounting medium (*see* **Note 10**). Carefully drop Mowiol onto the surface of the coverslip and mount sections on clean glass slides. After allowing the

Mowiol to polymerize overnight, root sections can then be observed with a confocal microscope. Examples of the quality of cytoskeletal labeling from vibratome-sectioned roots is shown in **Fig. 2** (*see* **Note 11**).

3.1.2. Immunolabeling of the Cytoskeleton in Whole Mount Arabidopsis Roots

1. Gently pick 3–4-day-old *Arabidopsis* seedlings growing on nutrient supplemented gel media (*see* **Subheading 3.2** below for tips on growing Arabidopsis seedlings) with a fine pair of forceps and directly immerse seedlings into the fixative. For preserving F-actin in Arabidopsis roots we use 2% (v/v) paraformaldehyde, 0.1% (v/v) Triton X-100, 400 μM MBS in PME buffer while for microtubules we use 3.7% (v/v) paraformaldehyde. We routinely perform fixation in 20-mL glass scintillation vials, adding 1–5 mL fixative per vial. Incubate samples in fixative for 1 h, applying a light vacuum for the initial 30 min. Place uncapped vials containing fixative and collected seedlings in a small vacuum dessicator jar equipped with a T connector. Open the vacuum vent slowly and keep it open until the hissing sound subsides. Close the vent and continue incubation. Release the vacuum slowly after 30 min and continue incubation so that the total time of fixation is about 1 h.
2. Subsequent steps, including washes, permeabilization, and immunolabeling, are carried out in tissue culture inserts (TCIs), on a rotating shaker table. Upon fixation carefully transfer seedlings with fine forceps into a TCI inserted in a well of a 12-well plate containing 2 mL PEMT (*see* **Note 12**). Rinse seedlings in PEMT 3–4 times for 10 min each.
3. Permeabilize samples for 1 h in 1% Triton X-100 in PME, followed by rinsing three times in PEMT, 5 min each.
4. For cell wall digestion, incubate samples for 20 min in 0.05% (w/v) Pectolyase Y-23, 0.1% (v/v) Triton, 1% Bovine serum

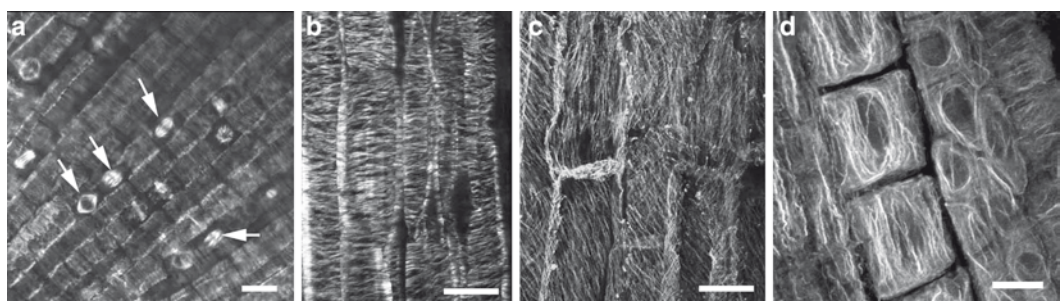

Fig. 2. Confocal microscopy of the cytoskeleton in root vibratome sections. (**a**) Microtubules in the meristematic region of a *Medicago truncatula* root. *Arrows* indicate mitotic figures. Transverse and oblique cortical microtubules in the elongation (**b**) and maturation zone (**c**) of a maize primary root. (**d**) F-actin organization in the vascular region of maize roots. Bars = 20 μM (**a**, **d**); 10 μM (**b**, **c**).

albumin, 0.4 M mannitol in PME. Wash by incubating three times in PEMT for 10 min each.

5. Permeabilize samples for 10 min in cold (−20°C) methanol (*see* **Note 13**). When labeling microtubules, the cold methanol treatment should be omitted. Wash three times in PBS, 5 min each.
6. Incubate samples in blocking solution (5% normal goat serum in PBS) for 1 h.
7. Primary and secondary antibodies are diluted in blocking solution (*see* **Note 14**). Primary antibody, mouse monoclonal anti-chicken gizzard actin ("C4," Chemicon, Temecula, CA) is used at a dilution of 1:1,000. For microtubules, we use the monoclonal rat antiyeast tubulin antibody (YOL1/34, Accurate Chemicals, Westbury, NY; *see* **Subheading 3.1.1**). Incubate samples with the primary antibodies for 16 h (usually overnight) at room temperature on a rotating shaker table.
8. Wash samples with PBST 3–4 times for a total duration of 1 h.
9. Add secondary antibodies (fluorescently labeled monoclonal anti-mouse for actin or antirat for microtubules) to the samples. We use AlexaFluor 488 goat antimouse or goat antirat (InVitrogen, Eugene, OR) as the secondary antibody, diluted 1:200 in blocking solution (*see* **Note 15**). Incubate samples with the secondary antibodies for 5–6 h at room temperature on a rotating shaker table.
10. Wash samples with PBST 3–4 times for the total duration of 1 h and once with PBS for at least 10 min. Seedlings can be mounted for immediate observation or stored in PBS at 4°C for up to 1 week (*see* **Note 16**).
11. For observation, mount seedlings in Vectashield and image with a confocal microscope. Examples of the quality of cytoskeletal labeling from whole mount Arabidopsis roots is shown in **Fig. 3**.

3.2. Preparing Arabidopsis Roots for Live Cell Imaging

Most of the live cell imaging work on the plant cytoskeleton has been conducted using the model plant Arabidopsis. This is because Arabidopsis is readily transformed with various GFP cytoskeletal reporters and the smaller roots of Arabidopsis make sample preparation for live cell imaging very convenient. However, a number of precautions have to be taken to ensure that growth of the root is not compromised by excessive physical handling of the seedling. If at all possible, imaging of live Arabidopsis roots should be done directly on the media where the seeds are germinated.

1. Surface sterilize the seeds by immersing them for 3 min each in 95% ethanol, 20% bleach, and sterilized deionized water. Rinse the seeds in deionized water at least three times after bleach treatment. Transfer seeds to sterilized 90-mm filter paper in 100 × 15 mm polystyrene Petri dishes, and spread the seeds evenly on the filter paper using a 1-mL pipette **(Fig. 4a)**. Let the seeds dry in a laminar flow bench overnight. The seeds can be planted immediately after spreading onto the filter paper-lined polystyrene Petri dishes but for long term storage they must be dried thoroughly prior to sealing with parafilm.
2. Prior to seed sterilization a coverslip–agar medium for germinating seeds must be prepared in advance. This system consists of sterilized coverslips with about a 1 mm layer of nutrient

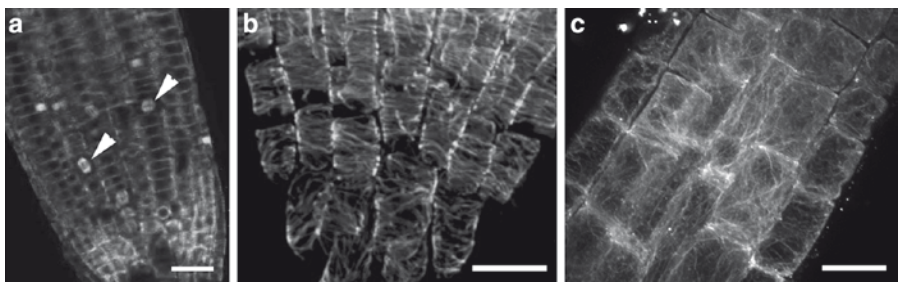

Fig. 3. Confocal microscopy of the cytoskeleton in whole mount Arabidopsis roots. (**a**) Low magnification image of microtubule labeling in the root meristem. *Arrowheads* indicate mitotic figures. (**b**) Transverse cortical microtubules in the root cap. (**c**) F-actin organization in the root distal elongation zone. Bars = 20 μM.

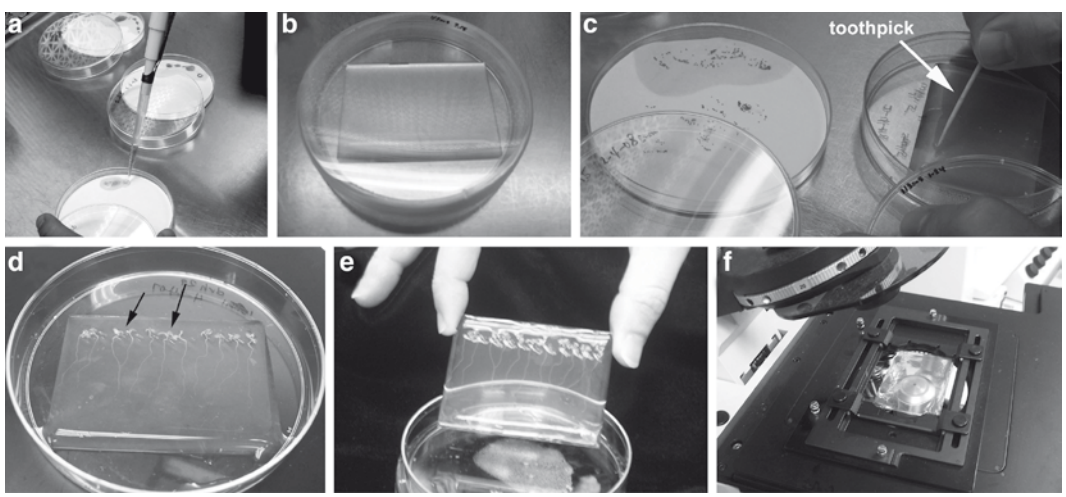

Fig. 4. Arabidopsis seed sterilization and planting for live cell confocal imaging of the cytoskeleton. (**a**) Spreading sterilized seeds on filter paper. (**b**) Agar-coverslip set-up for planting Arabidopsis seeds. (**c**) Sterilized seeds can be picked individually using pointed toothpicks and planted directly on the agar-coverslip system. (**d**) Seven-day-old Arabidopsis seedlings (*arrows*) growing on the agar-coverslip system. The agar-coverslip system with the growing seedlings can be easily picked up by gently pressing the bottom of the polystyrene Petri dish (**e**) and directly transferred to the stage of the confocal microscope for imaging (**f**).

supplemented polymerized 0.5–1% agar. The coverslip–agar system is placed inside 100 × 15 mm polystyrene Petri dishes, wrapped with parafilm, and kept at 4°C for future use **(Fig. 4b)**.

3. To prepare the coverslip–agar system, autoclave 0.5× MS salts in 0.5–1% agar (v/v) supplemented with 0.5 mg/mL pyridoxine–HCL, 0.5 mg/mL nicotinic acid and 1 mg/mL thiamine. The vitamins can be dissolved in water as 1,000× stock, filter sterilized and stored at 4°C prior to use. Add 0.10 g/L myo-inositol, 0.5 g/L MES, and 1% sucrose to the MS vitamin solution. Adjust pH to 5.7 with 10 M KOH, add agar and autoclave. After autoclaving, carefully add the agar-MS solution on top of the coverslip using a pipette until the entire surface of the coverslip is covered with agar (**Fig. 4b**; *see* **Note 17**).
4. When the agar has fully polymerized and cooled, pick Arabidopsis seeds individually with a sterile toothpick and gently push the seed into the agar media so that the seed touches the bottom of the coverslip **(Fig. 4c)**. This helps the roots grow straight inside the medium facilitating microscopic observation. Dried seeds can be easily picked up with a moist toothpick. This is done by immersing the tip of the toothpick into the agar and gently touching the seed.
5. After planting, seal the Petri dish with parafilm and transfer it to a growth chamber. The Petri dish should be positioned at a 60° angle horizontally to allow the roots to direct their growth toward the surface of the coverslip. It takes about 3–4 days for the roots to be ready for imaging **(Fig. 4d)**.
6. When the roots have reached the desired age for imaging, remove the coverslip containing the seedlings by gently pressing the bottom of the polystyrene Petri dish and lifting the coverslip making sure that the polymerized agar does not slide off **(Fig. 4e)**.
7. Mount the coverslip directly on the stage of a confocal microscope for observation **(Fig. 4f)**. Examples of cytoskeletal structures in living Arabidopsis roots prepared in this manner is shown in **Fig. 5**.

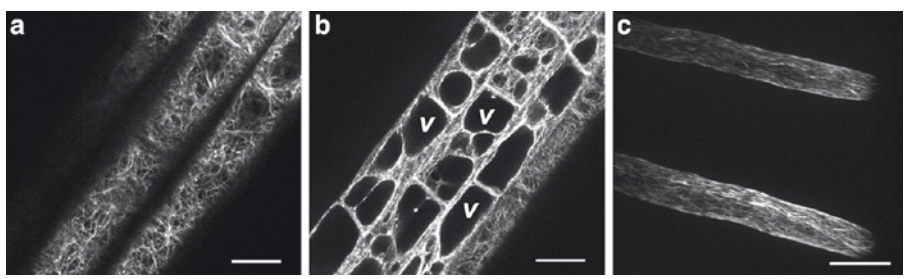

Fig. 5. Live cell imaging of Arabidopsis roots expressing F-actin and microtubule GFP reporters. Cortical (**a**) and cytoplasmic (**b**) F-actin networks in epidermal cells from the root elongation zone. Images in (**a**) and (**b**) were taken at two different focal planes. Vacuoles (***v***). (**c**) Longitudinal cortical microtubules in growing Arabidopsis root hairs imaged with a spinning disk confocal microscope. Bars = 20 μM.

4. Notes

1. There are several companies that sell agar, which can be used for preparing the agar–coverslip system. For imaging live Arabidopsis roots, however, we found that agar from Sigma-Aldrich (A1296) gives the clearest gel when mixed with the MS solution.
2. In our experience, root microtubules have been preserved adequately with fixative solution containing 3–4% (v/v) formaldehyde or paraformaldehyde *(15–17)*. On the other hand, we have resorted to lower concentrations of paraformaldehyde (1.5–2%) to optimally preserve the delicate F-actin structures in roots *(13, 18–20)*.
3. Make sure that superglue is spread evenly and thinly on the vibratome block surface so that only the outer cells of the root are in contact with the superglue. Typically a touch of superglue is sufficient for the root tissue to adhere to the block surface. If too much glue is used, sectioning and subsequent labeling steps can be compromised.
4. Without any embedding support, vibratome sections of plant tissues typically break apart at a thickness of less than 40 μm.
5. The sections can be left on the lab bench to allow the remaining PME buffer to evaporate. However, make sure that sections remain moist. Do not allow sections to dry completely as this could lead to distortion of cells during imaging. One way to secure the sections onto coverslips for subsequent antibody labeling is to use a thin film of bactoagar as originally proposed in Brown and Lemmon *(12)*. Dissolve 0.75 g bactoagar (BD and Co., Frankin Lakes, NJ) in 100 mL deionized water in a 250-mL beaker. Microwave the solution until it comes to a boil. When the contents of the beaker start to rise, turn off the microwave and briefly swirl the contents of the beaker. Microwave the solution for a second time to completely dissolve the bactoagar granules. A loop can be constructed using copper or chromium-nickel wire. Material for making such loops can easily be found in the lab. For example, we have successfully used wire from the base of test tube brushes to make agar casting loops. To secure the sections, allow the agar film to solidify on the loop and slowly cover the sections with the agar film. Placing the coverslip on the caps of vials facilitates layering of the agar film onto the sections **(Fig. 6)**. This procedure requires patience since the thin agar film can rupture easily. All solutions for labeling the sections can easily penetrate the agar film.
6. During subsequent treatments and washing steps one has to be careful that sections do not detach from the coverslip. Although the thin agar film described in **Note 5** typically

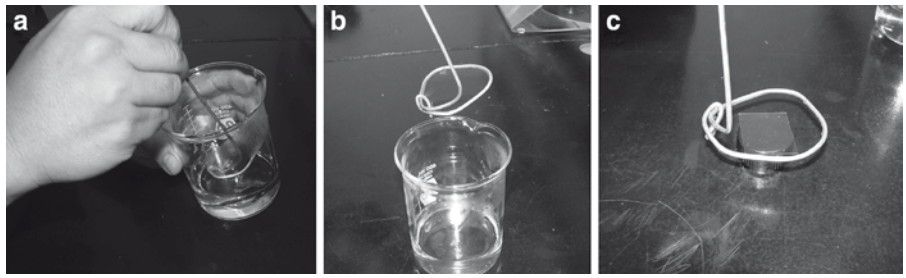

Fig. 6. Procedure for securing root vibratome sections on coverslips for indirect immunofluorescence labeling of the cytoskeleton. A thin film of agar is collected on a loop from molten 0.75% agar solution (**a**, **b**). The coverslip containing the root section is placed on top of a cap of a scintillation vial and the loop with the thin agar film is passed over the coverslip to hold the root section in place (**c**).

prevents sections from floating away during sample treatment, there are cases when the bactoagar film will slide off because of constant exposure to the liquid solutions. When this happens, one has to take extra care so that samples are not lost during the various washing steps.

7. Overnight incubation in primary antibody has sometimes led to improvements in the quality of cytoskeletal labeling and also allows flexibility with the labeling schedule if time becomes an issue. When overnight incubation in the primary antibody becomes necessary, the samples can be kept at 4°C. A humid chamber can be constructed using 9-mm round polystyrene Petri dishes lined with moist filter paper. Coverslips or glass slides containing the root sections can be laid on top of rubber lined caps of scintillation vials to prevent moisture from spreading onto the sample **(Fig. 6c)**. Laying coverslips on top of vial caps also facilitates casting of the thin bactoagar film used for securing sections (*see* **Note 5**).
8. The choice of primary antibodies is critical for the success of labeling. There are a number of commercially available anti-tubulin and actin antibodies. For microtubules, we have been successful with the Rat anti-yeast tubulin (monoclonal rat and yeast tubulin antibody YOL1/34, Accurate Chemicals, Westbury, NY) and mouse monoclonal anti-chicken gizzard actin antibody (C4, Chemicon, Temecula, CA). As an alternative to antibodies, fluorescently conjugated phalloidin (Molecular Probes, Eugene, OR) can be used to label F-actin in roots *(13, 15, 18)*. Commercial primary and secondary antibodies and fluorescently conjugated phalloidin typically come with recommendations for dilutions. However, it is advisable to test the dilution that is most effective for the plant tissue being studied. Antibodies and fluorescently conjugated phalloidin should be aliquoted into small volumes and stored at −20°C prior to use to avoid repeated freezing and thawing.

9. Do not worry if residual Mowiol crystals remain after 2 h of stirring. Just be sure that you do not include any of the crystals when mounting your samples.
10. The Mowiol mounting medium will be viscous after 2 h of stirring and will occasionally contain air bubbles. Only a small drop (ca. 100–200 μL) of the Mowiol solution is needed to mount one coverslip. Be sure to avoid air bubbles when mounting your samples as this could affect the quality of imaging.
11. Because vibratome sections are thick the best images are obtained using a confocal microscope.
12. Solutions (2 mL per well) are added and removed directly to and from the well using a pipette. TCIs with sample seedlings are transferred from one solution to another by moving between wells. Tapping the TCI gently on a paper towel before inserting it into the well facilitates solution exchange. This arrangement allows for better preservation of fragile seedlings during the procedure.
13. Place a 12-well plate with methanol (2 mL per well) at –20°C 1 h in advance.
14. To minimize the volume of antibody solution, TCI bottoms can be sealed with parafilm before inserting into the well. Antibody solution (350–400 μL) is then added directly to the TCI with the sample. Seedlings should be fully submerged into the antibody solution. After the incubation with the antibodies, remove parafilm from the bottoms of TCIs with samples and tap TCIs gently on a paper towel to remove the antibody solution. Proceed with washes.
15. Sealing TCI bottoms with parafilm can also be used at this stage to minimize the volume of antibody solution required to cover samples fully.
16. During storage, keep plates with samples covered in aluminum foil to prevent loss of fluorescent signal.
17. Surface tension of the molten agar will form a dome on the surface of the coverslip. Avoid pouring excess agar on the coverslip as this will break the dome and cause the agar to flow out of the coverslip.

Acknowledgements

Work on the plant cytoskeleton in the authors' laboratory is supported by the Noble Foundation and grants from the National Science Foundation (DBI-0722635) and the Oklahoma Center for the Advancement of Science and Technology (OCAST PSB-003).

References

1. Blancaflor, E. B. and Gilroy, S. (2000) Plant cell biology in the new millennium: new tools and new insights. *Am. J. Bot.* **87**, 1547–1560.
2. Dixit, R., Cyr, R. and Gilroy, S. (2006) Using intrinsically fluorescent proteins for plant cell imaging. *Plant J.* **45**, 599–615.
3. Marc, J., Granger, C. L., Brincat, J., Fisher, D. D., Kao, T.-h., McCubbin, A. G. and Cyr, R. J. (1998) A GFP-MAP4 reporter gene for visualizing cortical microtubule rearrangements in living epidermal cells. *Plant Cell* **10**, 1927–1940.
4. Kost, B., Spielhofer, P. and Chua N. H. (1998) A GFP-mouse talin fusion protein labels plant actin filaments in vivo and visualizes the actin cytoskeleton in growing pollen tubes. *Plant J.* **16**, 393–401.
5. Wang, Y.-S., Motes, C. M., Mohamalawari, D. R. and Blancaflor, E. B. (2004) Green fluorescent protein fusions to Arabidopsis fimbrin 1 for spatio-temporal imaging of F-actin dynamics in roots. *Cell Motil. Cytoskeleton* **59**, 79–93.
6. Sheahan, M. B., Staiger, C. J., Rose, R. J. and McCurdy, D. W. (2004) A green fluorescent protein fusion to actin-binding domain 2 of Arabidopsis fimbrin highlights new features of a dynamic actin cytoskeleton in live plant cells. *Plant Physiol.* **136**, 3968–3978.
7. Voigt, B., Timmers, A. C. J., Samaj, J., Muller, J., Baluška, F. and Menzel, D. (2005) GFP-ABD2 fusion construct allows *in vivo* visualization of the dynamic actin cytoskeleton in all cells of Arabidopsis seedlings. *Eur. J. Cell Biol.* **84**, 595–608.
8. Wang, Y.-S., Yoo, C.-M. and Blancaflor, E. B. (2008) Improved imaging of actin filaments in transgenic *Arabidopsis* plants expressing a green fluorescent protein fusion to the C and N termini of the fimbrin actin binding domain 2. *New Phytol.* **177**, 525–536.
9. Lovy-Wheeler, A., Wilsen, K. L., Baskin, T. I. and Hepler, P. K. (2005) Enhanced fixation reveals the apical cortical fringe of actin filaments as a consistent feature of the pollen tube. *Planta* **221**, 95–104.
10. Collings, D. A. and Wasteneys, G. O. (2005) Actin microfilament and microtubule distribution patterns in the expanding root of *Arabidopsis thaliana*. *Can. J. Bot.* **83**, 579–590.
11. Wilsen, K. L., Lovy-Wheeler, A., Voigt, B., Menzel, D., Kunkel, J. G. and Hepler, P. K. (2006) Imaging the actin cytoskeleton in growing pollen tubes. *Sex. Plant Reprod.* **19**, 51–62.
12. Brown, R. C. and Lemmon, B. E. (1995) Methods in plant immunolight microscopy. In: *Methods in Cell Biology* (Galbraith, D. W., Bohnert, H. J., Bourque, D. P., eds). Academic, San Diego, CA, pp 85–107.
13. Blancaflor, E. B. and Hasenstein, K. H. (2000) Methods for detection and identification of F-actin organization in plant tissues. In: *Actin: A Dynamic Framework for Multiple Plant Cell Functions* (Staiger, C., Baluška, F., Volkmann, D., Barlow P. W., eds). Kluwer, Dordrecht, the Netherlands, pp 601–618.
14. Blancaflor, E. B., Wang, Y.-S. and Motes, C. M. (2006) Organization and function of the actin cytoskeleton in developing root cells. *Int. Rev. Cytol.* **252**, 153–198.
15. Blancaflor, E. B. (2000) Cortical actin filaments potentially interact with cortical microtubules in regulating polarity of cell expansion in primary roots of maize (*Zea mays* L.). *J. Plant Growth Regul.* **19**, 406–414.
16. Blancaflor, E. B., Zhao, L. and Harrison, M. J. (2001) Microtubule organization in root cells of *Medicago truncatula* during development of an arbuscular mycorrhizal symbiosis with *Glomus versiforme*. *Protoplasma* **217**, 154–165.
17. Blancaflor, E. B., Hou, G. and Chapman, K. D. (2003) Elevated levels of *N*-Lauroylethanolamine, an endogenous constituent of desiccated seeds, disrupt normal root development in *Arabidopsis thaliana* seedlings. *Planta* **217**, 206–217.
18. Blancaflor, E. B. and Hasenstein, K. H. (1997) The organization of the actin cytoskeleton in vertical and graviresponding primary roots of maize. *Plant Physiol.* **113**, 1447–1455.
19. Hou, G., Mohamalawari, D. R. and Blancaflor, E. B. (2003) Enhanced gravitropism of roots with a disrupted cap actin cytoskeleton. *Plant Physiol.* **131**, 1360–1373.
20. Hou, G., Kramer, V. L., Wang, Y.-S., Chen, R., Perbal, G., Gilroy, S. and Blancaflor, E. B. (2004) The promotion of gravitropism in Arabidopsis roots upon actin disruption is coupled with the extended alkalinization of the columella cytoplasm and a persistent lateral auxin gradient. *Plant J.* **31**, 113–125.

Chapter 9

Imaging of the Cytoskeleton and Mitochondria in Fixed Budding Yeast Cells

Theresa C. Swayne, Istvan R. Boldogh, and Liza A. Pon

Summary

The budding yeast ***Saccharomyces cerevisiae*** has many advantages as a model system, but until recently, high-resolution microscopy was not often attempted in this organism. Its small size, rounded shape, and rigid cell wall were obstacles to exploring the cell biology of this model eukaryote. However, it is now feasible for laboratories to acquire and analyze high-resolution multidimensional images of yeast cell biology. As a result, imaging of yeast has emerged as an important tool in eukaryotic cell biology. This chapter describes labeling methods and optical approaches for visualizing the cytoskeleton and interactions of the actin cytoskeleton with mitochondria in fixed yeast cells using fluorescence microscopy.

Key words: Yeast, Actin, Microtubules, Mitochondria, Immunofluorescence, Microscopy, Deconvolution

1. Introduction

Cytoskeletal proteins, organization and function in budding yeast are similar to those found in other eukaryotes. However, the cytoskeleton of yeast is genetically and structurally less complex compared to that of other eukaryotes. As a result, the budding yeast has emerged as a model system to study cytoskeletal assembly, organization and function in processes including cell division, establishment and maintenance of cell polarity, and intracellular movement of organelles and other cellular cargos.

In this chapter, we describe methods for visualization of actin and microtubule cytoskeletons in fixed yeast cells. There is only one actin gene in budding yeast. Moreover, there are only two

R.H. Gavin (ed.), *Cytoskeleton Methods and Protocols,* Methods in Molecular Biology, vol. 586
DOI 10.1007/978-1-60761-376-3_9,
© Humana Press, a part of Springer Science + Business Media, LLC 2009

F-actin containing structures that persist throughout the yeast cell division cycle: actin patches and actin cables (**Fig. 1**). Actin patches are endosomes that are invested with a coat of F-actin and localize to the bud and mother-bud neck. Actin cables are bundles of F-actin that align along the mother-bud axis and are implicated as tracks for the movement of secretory vesicles, mRNA, spindle alignment elements, mitochondria, Golgi and vacuoles along the mother-bud axis (for review ***see*** **ref.** *1)*.

The microtubule cytoskeleton of yeast is also similar, but considerably less complex compared to that of other eukaryotes. During interphase, short microtubules radiate from the spindle pole body (SPB), the MTOC of yeast, which is embedded in the nuclear envelope. During mitosis, the SPB duplicates, migrates to opposite sides of the nucleus, and serves as organizing centers for astral microtubules, which extend into the cytosol, and for polar and kinetochore microtubules (**Fig. 1**).

As one important function of the cytoskeleton is to control intracellular movement, we also describe methods to visualize one of the cargos for cytoskeleton-driven movement, the mitochondrion. In the mother cell of budding yeast, mitochondria are long tubular structures that align along the mother-bud access and co-localize with actin cables. Yeast mitochondria also accumulate at the tips of budding yeast, which are the bud tip and tip of the mother cell distal to the bud (**Fig. 1**). Here, we describe methods for visualizing mitochondria–cytoskeleton interactions and for determining and quantitating the co-localization of a cargo (mitochondria) with its cytoskeletal tracks (actin cables) in fixed yeast cells.

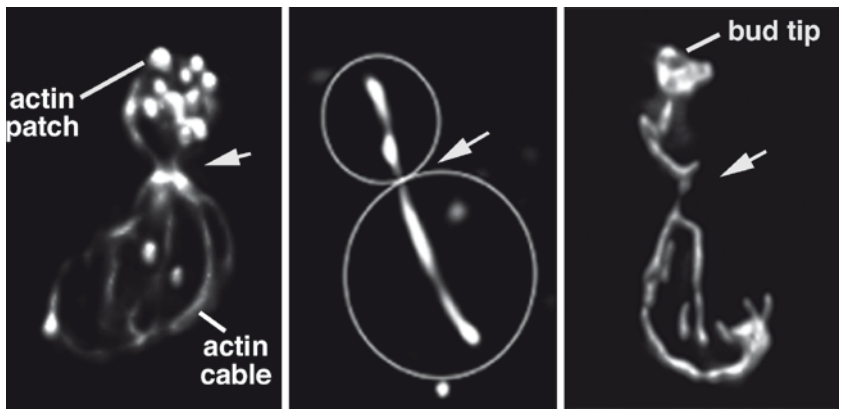

Fig. 1. Organization of the actin and microtubule cytoskeleton and mitochondria in budding yeast cells. (**a**) The actin cytoskeleton was visualized using rhodamine phalloidin. Actin patches localize to the bud, and actin cables align along the mother-bud axis. (**b**) Microtubules in the spindle of budding yeast visualized by indirect immunofluorescence. Cell boundaries are outlined in **white**. (**c**) Mitochondria in budding yeast cells. In all images, **arrows** point to the mother-bud neck. All images are 2D projections of deconvolved 3D images.

1.1. Visualization of the Cytoskeleton and Mitochondria by Immunostaining

For indirect immunofluorescence staining, yeast cells are typically grown to mid-log phase and fixed with paraformaldehyde. As antibodies will not penetrate the yeast cell wall, the cell wall is removed from fixed cells enzymatically (e.g. with zymolyase or lyticase). Spheroplasts are then permeabilized using a non-ionic detergent, and immobilized on a microscope cover slip. The sample-coated cover slip is then incubated with the primary antibody, which binds to the antigen of interest, and the secondary antibody, which binds to the invariant (Fc) region of the primary antibody and is tagged with a fluorophore. Finally, the stained cover slip is applied to a microscope slide using mounting solution.

There is generally more background fluorescence in samples stained by indirect immunofluorescence than in samples that are visualized using targeted fluorescent proteins. This is due, in part, to non-specific binding of primary and/or secondary antibodies. In addition, because the yeast cell wall is highly antigenic, most polyclonal antibodies contain contaminating antibodies that recognize the yeast cell wall. The methods described here can deplete but not completely eliminate these contaminants from antibody preparations. In addition, although the cell wall is digested prior to incubation of cells with primary antibody, its removal is not complete.

That said, there are several cases where immunofluorescence is the method of choice for visualization of cellular structures. First, the tagging of proteins with any adduct, including fluorescent proteins, may alter the protein structure, stability, or localization. In contrast, indirect immunofluorescence visualizes native proteins expressed at wild-type levels. Second, indirect immunofluorescence can be used with yeast strains that are not amenable to transformation (e.g. strains with limited or no genetic markers for transformation).

2. Materials

2.1. Yeast Growth Media

1. Synthetic Complete medium (SC): 6.7 g yeast nitrogen base without amino acids, 20 g dextrose. Dissolve ingredients in 800 ml distilled H_2O. Supplement with the following bases and amino acids as needed: 10 ml adenine (2 mg/ml stock in 0.05 M HCl), 10 ml uracil (2 mg/ml stock in 0.5% $NaHCO_3$), 10 ml arginine 10 ml (1 mg/ml stock in H_2O), 10 ml histidine (1 mg/ml stock in H_2O), 10 ml leucine (10 mg/ml stock in H_2O), 10 ml lysine (3 mg/ml stock in H_2O), 10 ml methionine (2 mg/ml stock in H_2O), 10 ml phenylalanine (5 mg/ml stock in H_2O), 10 ml tryptophan (2 mg/ml stock in

H_2O), 10 ml tyrosine (3 mg/ml stock in 0.05 M HCl). Adjust pH to 5.5 with $NaHCO_3$. Bring volume to 1 l with distilled H_2O. Sterilize by autoclaving.

2. Lactate medium: 3.0 g yeast extract, 0.5 g glucose, 0.5 g $CaCl_2$, 0.5 g NaCl, 0.6 g $MgCl_2$, 1 g KH_2PO_4, 1 g NH_4Cl, 22 ml 90% lactic acid, 7.5 g NaOH. Dissolve ingredients in 800 ml distilled H_2O. Adjust pH to 5.5 with NaOH. Bring volume to 1 l with distilled H_2O. Sterilize by autoclaving. Optional: For growth of *ade2* cells, add 0.1 mg/ml adenine.
3. Raffinose medium: 10 g yeast extract, 20 g bacto-peptone, 20 g raffinose. Dissolve ingredients to 1 l with distilled H_2O. Sterilize by autoclaving. Optional: For growth of *ade2* cells, add 0.1 mg/ml adenine.

2.2. Staining the Cytoskeleton and Mitochondria in Fixed Yeast Cells

1. Wash solution: 12.5 ml 1 M potassium phosphate, pH 7.5, 400 ml 1 M KCl. Bring volume to 500 ml with distilled water. Sterilize by autoclaving.
2. Tris/DTT: 10 ml 1 M Tris–SO_4, pH 9.4, 1 ml 1 M DTT. Bring volume to 100 ml with distilled H_2O. Make the preparation on the day of use.
3. Zymolyase (Seikagaku Inc., Tokyo, Japan): Dissolve Zymolyase 20T in wash solution to a concentration of 0.125 mg/ml. Make the preparation on the day of use.
4. NS: 10 ml 1 M Tris-HCl, pH 7.5, 21.4 g sucrose, 1 ml 0.5 M EDTA, pH 8.0, 0.5 ml 1 M $MgCl_2$, 0.05 ml 1 M $ZnCl_2$, 0.05 ml 0.5 M $CaCl_2$. Adjust volume to 500 ml with distilled H_2O. Filter sterilize and store in 40 ml aliquots at –20°C.
5. NS^+: On the day of use, supplement 10 ml NS with 50 µl of 200 mM phenylmethylsulfonylfluoride (PMSF) dissolved in ethanol, and 500 µl 10% (w/v) NaN_3.
6. 10× PBS stock: 80 g NaCl, 2 g KCl, 14.4 g Na_2HPO_4, 2.4 g KH_2PO_4. Dissolve ingredients in 800 ml distilled H_2O. Adjust pH to 7.4 with HCl. Bring volume to 1 l with distilled H_2O.
7. PBS^+: 5 ml 10× PBS, 0.5 g bovine serum albumin, 0.5 ml 10% (w/v) NaN_3. Bring volume to 50 ml with distilled H_2O. Sterilize by passing through a 0.2-µm filter. Make the preparation on the day of use.
8. PBT^+: Include 0.1% Triton X-100 in PBS^+ solution. Sterilize by passing through a 0.2-µm filter.
9. Polylysine (a polycation that adheres spheroplasts to cover slips): Dissolve polylysine in distilled H_2O to 0.5 mg/ml. Sterilize by passing through a 0.2-µm filter. Store in aliquots at –20°C.

10. Rhodamine phalloidin (Invitrogen, Carlsbad, CA): Dissolve in 100% methanol to 200 units/ml. Break into 50-µl aliquots. Store at –20°C.
11. Mounting solution (*see* **Note 1**): 10 ml 10× PBS, 100 mg *p*-phenylenediamine. Stir vigorously until dissolved. Adjust pH to 9 with NaOH. Add 90 ml glycerol and mix thoroughly. Optional: For DAPI counterstaining of nuclear and mitochondrial DNA, add 100 µl of a stock solution of 1 mg/ml DAPI (4′,6-diamidino-2-phenylindole) in distilled H_2O (*see* **Note 2**). Store at –20°C in aliquots.
12. Paraformaldehyde (*see* **Note 3**): (16% solution, EM grade. Electron Microscopy Sciences, Hatfield, PA).

2.3. Antibodies for Indirect Immunofluorescence

Two commercially available monoclonal antibodies have been used for visualization of microtubules and actin in a variety of cell types, including budding yeast: YL 1/2 and C4. YL 1/2 is a rat monoclonal antibody that recognizes tubulin in yeast, birds and mammals and gives clear immunofluorescent staining of yeast mitotic spindles *(2)*. C4 is a mouse monoclonal antibody obtained using chicken gizzard actin as the immunogen *(3)*. It recognizes a region that is conserved in the actins, recognizes actin in yeast and other cell types, and is widely used for immunofluorescence staining.

Several proteins can serve as markers for immunofluorescence visualization of mitochondria in S. cerevisiae. These include proteins targeted to each of the submitochondrial compartments (**Table 1**). In addition to these antibodies to specific proteins, a polyclonal antibody raised against outer mitochondrial membranes has been used successfully for immunofluorescence *(9, 12)*. Finally, with the advent of chromosomal tagging, proteins can be epitope-tagged and visualized by immunofluorescence using commercially available, well-characterized antibodies.

Table 1
Useful marker antigens for yeast mitochondria

Protein	Location	References
Porin	OM	*(4, 5)*
Cytochrome oxidase	IM	*(6, 7)*
Citrate synthase I	MAT	*(8)*
OM14	OM	*(9, 10)*
Abf2p	mtDNA	*(11)*

Abbreviations: ***OM*** mitochondrial outer membrane; ***IM*** mitochondrial inner membrane; ***MAT*** mitochondrial matrix; ***mtDNA*** mitochondrial DNA

3. Methods

3.1. Immunofluorescence Methods

3.1.1. Pretreatment of Antibodies with Yeast Cell Walls

Rabbit antisera, even after affinity purification, often contain antibodies that recognize the yeast cell wall, bind to residual cell wall on spheroplasts, and generate background staining which may be punctate or uniformly distributed over the surface of the spheroplast. Here, we describe a simple method for removing these contaminating antibodies by preadsorbing them to intact yeast cells. A batch of antibody may be pretreated in this way and stored for later use.

1. Grow yeast to late log phase (24–30 h).
2. Dilute antiserum to 1/25 in PBS^+.
3. Remove an aliquot of cells from the late log phase culture: 250 µl of cell culture/ml diluted antibody.
4. Concentrate cells by centrifugation (5 s at ~12,500 × *g*). Resuspend cell pellet in 1 ml of PBS^+. Repeat this wash procedure three times.
5. Resuspend washed cell pellet in diluted antibody and incubate with gentle mixing at 4°C for 2 h.
6. Concentrate cells by centrifugation, and transfer pre-treated antibody to a fresh tube.
7. Carry out a second round of pre-treatment. Repeat **steps 3–4** and resuspend cell pellet in pre-treated antibody recovered from **step 6**. Incubate with gentle mixing at 4°C for 2 h.
8. Concentrate cells by centrifugation, and transfer pre-treated antibody to a fresh tube. Store pre-adsorbed antibody in aliquots at –20°C.

3.1.2. Protocol for Fixation (*See* **Note 4**) and Spheroplast Formation

1. Grow a 5 ml culture to mid-log phase (10^6–10^7 cells/ml) (*see* **Note 5**).
2. Add paraformaldehyde to the culture medium to a final concentration of 3.7%.
3. Incubate cells with fixative under normal culture conditions for 1 h.
4. Concentrate cells by centrifugation (5 s at ~12,500 × *g*) and resuspend cell pellet in 1 ml Tris/DTT and incubate for 20 min at 30°C.
5. Concentrate cells by centrifugation. Resuspend cell pellet in 1 ml of zymolyase solution and incubate for 1.5 h at 30°C (*see* **Note 6**).
6. Concentrate cells by centrifugation and resuspend cell pellet in 1 ml of NS^+. Repeat this wash two times and resuspend the final cell pellet in 2 volumes NS^+.
7. Store fixed spheroplasts at 4°C for up to 1 week.

3.1.3. Preparation of a Staining Chamber for Immunofluorescence

For all incubations, the sample-coated cover slip is placed on 20–40 µl of incubation solution on a platform of Parafilm sheets in a dark, humid chamber **(Fig. 2)**. The staining chamber protects fluorescent dyes from unnecessary exposure to light, and the sample from desiccation. To make the staining chamber, a platform consisting of ten 10 × 15 cm sheets of Parafilm is placed on a stack (ca. 2 cm) of damp paper towels, and both are covered by an inverted opaque tray or pan. The Parafilm platform can be washed and reused.

3.1.4. Protocol for Indirect Immunofluorescence Staining: The Cover Slip Method

1. Place a 20–40 µl of polylysine solution on the Parafilm platform.
2. Using forceps, lay a 22 mm^2 cover slip on the polylysine drop, taking care to avoid creating bubbles at the cover slip-slide interface (*see* **Note** 7).
3. After at least 10 s, remove the cover slip from the polylysine. To do so, apply 200–300 µl distilled water under one edge of the cover slip. This will float the cover slip off the Parafilm so it can be lifted off the drop with forceps.
4. Rinse by dipping the cover slip in a beaker containing distilled water 5–10 times, draining excess liquid with filter paper. Allow cover slip to air dry.
5. Mix 10 µl of the fixed spheroplast suspension with 100 µl 1× PBS.
6. Place coated cover slip on Parafilm platform, coated side facing up. Apply the spheroplast mixture to the coated side of the cover slip and incubate for 30 min at RT in the staining chamber.
7. Remove unbound spheroplasts by dipping cover slip 5–10 times in beaker containing PBT. Drain excess liquid with filter paper.

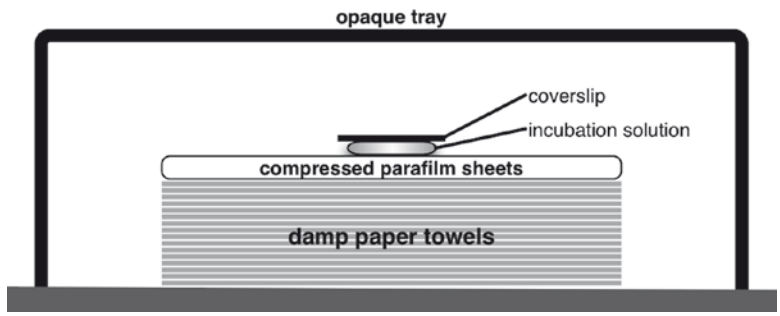

Fig. 2. Chamber for immunofluorescence. See text for description

8. Place the 20–40 µl of diluted primary antibody in a drop on the Parafilm platform. Lay the spheroplast-coated side of the cover slip on the drop of antibody and incubate for 2 h at RT in the staining chamber (*see* **Note 8**).
9. Lift the cover slip by introducing 200–300 µl PBT under the edge of the cover slip with a micropipette. Rinse cover slip in PBT as in **step 7**. Drain excess liquid with filter paper.
10. Place the cover slip on a 20–40 µl drop of secondary antibody and incubate for 1 h at RT in the staining chamber.
11. Remove cover slip from secondary antibody, rinse and drain, as in **step 9**.
12. Place 1–2 µl mounting solution on a microscope slide. Lower the cover slip, sample side down, onto the mounting solution. Dry any residual liquid from the edges of the cover slip. Seal the edges with clear nail polish and let dry.
13. Rinse the cover slip surface with distilled H_2O to remove residual salt deposits from staining and dry gently with a Kimwipe or Q-tip. View samples as soon as possible, definitely within a week after preparation.

3.1.5. Fixation Methods for Labeling of the Actin Cytoskeleton Using Anti-actin Antibodies

For optimal preservation of the actin cytoskeleton, an additional methanol/acetone fixation is advised for immobilized spheroplasts on cover slips. However, care should be taken when localizing non-cytoskeletal antigens in methanol–acetone-fixed cells. The precipitation induced by this fixation may alter the distribution of membrane-localized antigens. While methanol–acetone gives a cleaner cytoskeletal preparation, paraformaldehyde fixation should be considered the standard for localization.

Methanol/Acetone fixation:

1. Immobilize spheroplasts on poly-lysine coated cover slips **(Subheading 3.1.4).**
2. Incubate cover slips in 100% methanol at –20°C for 6 min.
3. Incubate cover slips in 100% acetone at –20°C for 30 s.
4. Allow coverslips to air dry.
5. Wash coverslips five times with 1× PBS, then ten times with PBT. Incubate with primary and secondary antibodies as described in **Subheading 3.1.4.**

3.2. Visualization of the Actin Cytoskeleton in Fixed Cells Using Rhodamine Phalloidin

The following protocol describes the staining procedure for cells in suspension (*see* **Note 9**).

1. Grow a 5 ml culture to mid-log phase (10^6–5×10^6 cells/ml).
2. Add 16% paraformaldehyde solution to the culture medium to a final concentration of 3.7% and incubate for 45 min (*see* **Note 10**).

3. Concentrate cells by centrifugation (1 min, 12,000 × g) and wash cell pellet three times with 500 µl wash solution.
4. Wash cells with 200 µl PBT and resuspend cell pellet in 100 µl PBT.
5. Add 25 µl 200 units/ml rhodamine phalloidin solution and incubate for 20–40 min, at RT, in the dark.
6. Concentrate cells by centrifugation and wash them twice with 50 µl 1× PBS.
7. Resuspend cells in 5–10 µl 1× PBS.
8. To make slides, transfer 0.6 µl of the cell suspension and 1.5 µl mounting solution to the microscope slide, and mix using a yellow pipette tip. Place a cover slip on sample and seal the edges of the cover slip with nail polish.

3.3. Visualization of Stained Samples by Wide Field Deconvolution

The selection of an appropriate microscope and camera to detect fluorescence is essential for imaging stained yeast cells. The small size of yeast cells requires a microscope equipped with a high-magnification objective lens and a high-resolution camera. Phototoxicity and photobleaching can be greatly reduced by using a camera that supports low-intensity illumination and short exposure times. Data processing speed and memory capacity of the computer linked to the digital camera can affect imaging speed and therefore, before a particular imaging system is committed to, it should be tested thoroughly.

An imaging system that works well for visualizing the cytoskeleton and mitochondria in yeast is based on an upright epifluorescence microscope (e.g. Zeiss Axioskop 2 or Nikon 80i) equipped with a Plan-Apochromat 100×, 1.4 NA objective lens, and a cooled CCD camera (e.g. Orca ER, Hamamatsu or HQ Monochrome, Roper). A shutter driver (Uniblitz D122, Vincent Associates) is synchronized with the camera shutter to control excitation light from the 100 W mercury arc lamp. A software package (e.g. OpenLab, Improvision Inc. or Metamorph, Universal Imaging) is used to control the camera and shutter, capture images, and export them to TIFF format for further analysis. Filter wheels (e.g. Sutter or Ludl) or beam splitters (Dual-View, Optical Insights) are used for automated two-color imaging. We control sample temperature using a heating collar on the objective lens (Bioptechs). Finally, for *z*-axis control, we use stepper motors coupled to the microscope fine focus drive (Ludl), or piezoelectric focus motors on the objective lens (Physik Instrumente).

3.4. Quantitative Analysis of Colocalization in Stained Cells

The *xy* resolution of optical images is normally around 0.2 µm at best. Thus, where membranes or proteins are bound to cytoskeletal elements, these structures will appear partly or completely

superimposed at light-microscope resolution. This superimposition can be quantified in order to test for conditions that alter these interactions. The following mask-based procedure measures colocalization in a manner that is unbiased with regard to the intensity of the labeled structures. The results are expressed as the percentage of one labeled structure that is coincident with the second label. This can be computed in terms of either labeled area (reflecting the size of the structures) or integrated density (reflecting both the size of the structures and the concentration of the fluorescent probe).

The method described here employs the free, open-source, public-domain program ImageJ (Rasband, W.S., ImageJ, U. S. National Institutes of Health, Bethesda, Maryland, USA, http://rsb.info.nih.gov/ij/, 1997–2008). ImageJ is the most widely accessible image analysis program and is the tool of choice in our own laboratory. However, the same functions are available in most commercially available software packages for image analysis and processing. Please refer to Chapter 3 by Swayne et al. for methods to measure fluorescence area and intensity.

1. If channels are merged in an RGB image, split the channels into individual grayscale images: from the Image menu, choose Color, then Split Channels. In the following steps the two channels to be analyzed will be called Channel 1 and Channel 2.
2. Convert both channel images to 32-bit format: from the Image menu, choose Type, then 32-bit. Save these converted images as "32-bit Channel 1" and "32-bit Channel 2."
3. From the Analyze menu, choose Set Measurements. Check the following boxes: Area, Mean gray value, Display label, Limit To Threshold.
4. Determine threshold for Channel 1: From the Image menu, choose Adjust, then Threshold. Drag the lower slider to the maximum value. Drag the upper slider so that the pseudo-colored red areas encompass all of the labeled structures and none of the background. Record the threshold value indicated by the upper slider.
5. Measure Channel 1: From the Analyze menu, choose Measure (or press M).
6. On the Threshold window, click Apply. Uncheck "Set background pixels to NaN." The result should be a black-and-white 8-bit image with all labeled pixels set to a gray value of 255 and all other pixels set to 0. Save the resulting thresholded Channel 1 image as "Thresholded Channel 1."
7. Repeat **steps 4–6** for Channel 2. The threshold value may be different for each channel.

8. With the thresholded images still open, open the 32-bit channel images. From the Process menu, choose Image Calculator and select the following options:
   - Image1: Thresholded Channel 2
   - Operation: AND
   - Image2: 32-bit Channel 1
   - Check "Open New Window" and "32-bit Result"
9. Click OK. The resulting image represents the subset of Channel 1 that is also positive for Channel 2. Save this image as "Masked Channel 1."
10. Repeat **steps 8–9** using Thresholded Channel 1 and the 32-bit Channel 2. Save the result as "Masked Channel 2."
11. Open the 32-bit and masked Channel 1. On the Threshold window, click Set and enter the value previously used to threshold Channel 1.
12. Measure the 32-bit Channel 1: From the Analyze menu, choose Measure (or press M).
13. Measure Masked Channel 1, making sure the threshold is the same as for the original Channel 1.
14. Repeat **steps 11–13** with the Channel 2 images and the threshold determined for Channel 2.
15. The Results window should now contain four measurements in the following order:
    - C1: Channel 1 without mask
    - C1M: Masked Channel 1
    - C2: Channel 2 without mask
    - C2M: Masked Channel 2

Using either area or integrated density values as desired, calculate the % colocalization as follows:

– % of Channel 1 that is colocalized with Channel 2 = C1M/C1
– % of Channel 2 that is colocalized with Channel 1 = C2M/C2

4. Notes

1. The mounting solution used here consists of glycerol, which reduces spheroplast movement during imaging and prevents freezing of the samples during storage at –20°C. It also contains *p*-phenylenediamine, an anti-photobleaching agent, which helps to prevent destruction of fluorophores by oxygen radicals generated during illumination.

2. DAPI is a possible carcinogen. It is harmful if inhaled, swallowed or absorbed through the skin. Wear gloves, face mask, and safety glasses when working with the dry compound.
3. Paraformaldehyde is toxic and carcinogenic. It is absorbed through the skin and is irritating to the eyes, skin, and the respiratory tract. Always wear gloves and safety glasses when working with this fixative. When possible, work in a chemical hood.
4. There are two main classes of fixatives: crosslinkers and precipitants. The protocol described here uses paraformaldehyde, a crosslinking fixative which forms hydroxymethylene bridges between spatially adjacent amino acid residues. Methanol and acetone, a commonly used precipitating fixative mixture, is suitable for some immunofluorescence staining, including staining of the actin cytoskeleton. However, we find it to be a poor choice for mitochondria. It solubilizes many membranes and can cause extraction of antigens from mitochondria *(13)*. The fixation conditions can affect the quality of the immunofluorescence results. Common manipulations, including centrifugation and increasing or decreasing temperature, can alter internal structures in *S. cerevisiae (14)*. Therefore, we add the fixative directly to a liquid culture under growth conditions, to minimize such disruptions. The other important variables in paraformaldehyde fixation are the concentration of fixative, duration of fixation, and pH of the fixative solution. High paraformaldehyde concentrations, low pH and a long fixation period increase the number of crosslinks formed and thereby improve structural preservation. Excessive crosslinking, however, can decrease antibody binding to antigens of interest and result in crosslinking of fluorescent substances in the media to cells, which increases background fluorescence surface. The optimal protocol strikes a balance between structural preservation and antigen accessibility.
5. While it is sometimes possible to perform immunofluorescent staining on cells picked from colonies on solid media, internal structures, including mitochondria, of mid-log phase cells from liquid culture are better preserved and more reproducible. The choice of carbon source for growth affects the abundance and morphology of mitochondria *(15–17)*. Glucose represses mitochondrial biogenesis, which decreases the abundance of mitochondria and facilitates resolution of individual mitochondrial tubules. Lactate selects cells with mtDNA and mitochondrial metabolic potential. For strains that cannot grow on non-fermentable carbon sources, replace glucose with raffinose.

6. The optimum time for cell wall removal varies among strains and can be determined by visual inspection using phase-contrast or bright-field microscopy. Intact cells have prominently refractile edges, while spheroplasts, which do not have cell walls, are less refractile. Excessive zymolyase treatment can damage cellular structures.
7. If desired, the cover slip may be labeled with a fine-point marker in one corner of the uncoated side.
8. Detection of two antigens simultaneously can be achieved by combining the two primary antibodies in the first step and the two secondary antibodies in the second step. For such an experiment, the primary antibodies must be raised in different species, and the fluorophores used for detection must have sufficiently separated excitation and emission spectra.
9. Rhodamine phalloidin-labeling of fixed cells can be carried out on immobilized, spheroplasted cells on cover slips. In this case, add ¼ volume of 200 units/ml rhodamine phalloidin solution to the secondary antibody solution (**step 10** in **Subheading 3.1.4**) and proceed as described in **Subheading 3.1.4**.
10. As actin cytoskeleton can undergo temporary depolarization upon temperature changes, make sure that the paraformaldehyde solution has the same temperature as the culture medium.

Acknowledgements

The work in our laboratory was supported by National Institutes of Health grant GM45735.

References

1. Moseley, J.B. and B.L. Goode (2006) The yeast actin cytoskeleton: from cellular function to biochemical mechanism. *Microbiol. Mol. Biol. Rev.* **70**, 605–645.
2. Kilmartin, J.V., B. Wright, and C. Milstein (1982) Rat monoclonal antitubulin antibodies derived by using a new nonsecreting rat cell line. *J. Cell Biol.* **93**, 576–582.
3. Lessard, J.L. (1988) Two monoclonal antibodies to actin: one muscle selective and one generally reactive. *Cell Motil. Cytoskeleton* **10**, 349–362.
4. Mihara, K. and R. Sato (1985) Molecular cloning and sequencing of cDNA for yeast porin, an outer mitochondrial membrane protein: a search for targeting signal in the primary structure. *EMBO J.* **4**, 769–774.
5. Roeder, A.D., G.J. Hermann, B.R. Keegan, S.A. Thatcher, and J.M. Shaw (1998) Mitochondrial inheritance is delayed in *Saccharomyces cerevisiae* cells lacking the serine/threonine phosphatase PTC1. *Mol. Biol. Cell* **9**, 917–930.
6. Poot, M., Y.Z. Zhang, J.A. Kramer, K.S. Wells, L.J. Jones, D.K. Hanzel, A.G. Lugade, V.L. Singer, and R.P. Haugland (1996) Analysis of mitochondrial morphology and function with novel fixable fluorescent stains. *J. Histochem. Cytochem.* **44**, 1363–1372.

7. Taanman, J.W. and R.A. Capaldi (1993) Subunit VIa of yeast cytochrome c oxidase is not necessary for assembly of the enzyme complex but modulates the enzyme activity. Isolation and characterization of the nuclear-coded gene. *J. Biol. Chem.* **268**, 18754–18761.
8. Ruprich-Robert, G., D. Zickler, V. Berteaux-Lecellier, C. Velot, and M. Picard (2002) Lack of mitochondrial citrate synthase discloses a new meiotic checkpoint in a strict aerobe. *EMBO J.* **21**, 6440–6451.
9. Riezman, H., R. Hay, S. Gasser, G. Daum, G. Schneider, C. Witte, and G. Schatz (1983) The outer membrane of yeast mitochondria: isolation of outside-out sealed vesicles. *EMBO J.* **2**, 1105–1111.
10. McConnell, S.J., L.C. Stewart, A. Talin, and M.P. Yaffe (1990) Temperature-sensitive yeast mutants defective in mitochondrial inheritance. *J. Cell Biol.* **111**, 967–976.
11. Diffley, J.F. and B. Stillman (1991) A close relative of the nuclear, chromosomal high-mobility group protein HMG1 in yeast mitochondria. *Proc. Natl Acad. Sci. U. S. A.* **88**, 7864–7868.
12. Smith, M.G., V.R. Simon, H. O'Sullivan, and L.A. Pon (1995) Organelle-cytoskeletal interactions: actin mutations inhibit meiosis-dependent mitochondrial rearrangement in the budding yeast *Saccharomyces cerevisiae*. *Mol. Biol. Cell* **6**, 1381–1396.
13. Boldogh, I.R., H.-C. Yang, W.D. Nowakowski, S.L. Karmon, L.G. Hays, J.R. Yates, III, and L.A. Pon (2001) Arp2/3 complex and actin dynamics are required for actin-based mitochondrial motility in yeast. *Proc. Natl Acad. Sci. U. S. A.* **98**, 3162–3167.
14. Lillie, S.H. and S.S. Brown (1994) Immunofluorescence localization of the unconventional myosin, Myo2p, and the putative kinesin-related protein, Smy1p, to the same regions of polarized growth in *Saccharomyces cerevisiae*. *J. Cell Biol.* **125**, 825–842.
15. Damsky, C.H. (1976) Environmentally induced changes in mitochondria and endoplasmic reticulum of *Saccharomyces carlsbergensis* yeast. *J. Cell Biol.* **71**, 123–135.
16. Stevens, B.J. (1977) Variation in number and volume of the mitochondria in yeast according to growth conditions. A study based on serial sectioning and computer graphics reconstitution. *Biologie Cellulaire* **28**, 37–56.
17. Visser, W., E.A. van Spronsen, N. Nanninga, J.T. Pronk, J.G. Kuenen, and J.P. van Dijken (1995) Effects of growth conditions on mitochondrial morphology in *Saccharomyces cerevisiae*. *Antonie Van Leeuwenhoek* **67**, 243–253.

Part IV

Electron Microscopy Protocols for Imaging the Cytoskeleton

Chapter 10

Imaging Cytoskeleton Components by Electron Microscopy

Tatyana Svitkina

Summary

The cytoskeleton is a complex of detergent-insoluble components of the cytoplasm playing critical roles in cell motility, shape generation, and mechanical properties of a cell. Fibrillar polymers–actin filaments, microtubules, and intermediate filaments– are major constituents of the cytoskeleton, which constantly change their organization during cellular activities. The actin cytoskeleton is especially polymorphic, as actin filaments can form multiple higher order assemblies performing different functions. Structural information about cytoskeleton organization is critical for understanding its functions and mechanisms underlying various forms of cellular activity. Because of the nanometer-scale thickness of cytoskeletal fibers, electron microscopy (EM) is a key tool to determine the structure of the cytoskeleton.

This article describes application of rotary shadowing (or metal replica) EM for visualization of the cytoskeleton. The procedure is applicable to thin cultured cells growing on glass coverslips and consists of detergent extraction of cells to expose their cytoskeleton, chemical fixation to provide stability, ethanol dehydration and critical point drying to preserve three-dimensionality, rotary shadowing with platinum to create contrast, and carbon coating to stabilize replicas. This technique provides easily interpretable three-dimensional images, in which individual cytoskeletal fibers are clearly resolved, and individual proteins can be identified by immunogold labeling. More importantly, replica EM is easily compatible with live cell imaging, so that one can correlate the dynamics of a cell or its components, e.g., expressed fluorescent proteins, with high resolution structural organization of the cytoskeleton in the same cell.

Key words: Electron microscopy, Cytoskeleton, Critical point drying, Rotary shadowing, Actin, Microtubules, Immunogold, Correlative microscopy

1. Introduction

Electron microscopy (EM) has been instrumental in discovering the cytoskeleton in the first place, and also in investigating its structural organization in different cells and conditions. The initial progress in the cytoskeletal studies closely paralleled the development of EM techniques. Thus, the introduction of heavy

R.H. Gavin (ed.), *Cytoskeleton Methods and Protocols,* Methods in Molecular Biology, vol. 586
DOI 10.1007/978-1-60761-376-3_10,
© Humana Press, a part of Springer Science + Business Media, LLC 2009

metal fixation led to the discovery of actin filaments in non-muscle cells *(1)*, while the discovery of microtubules *(2)* was made possible after the introduction of aldehyde fixation *(3)*.

A great value of EM is its ability to obtain structural information at a high resolution level, which for biological samples is limited by a sample preparation procedure rather than by the power of a transmission electron microscope (TEM). However, vacuum in the TEM column and electron beam irradiation impose strict restrictions on how samples should be prepared, which in turn greatly affect the quality of images and the rate of success. A large number of different EM protocols have been developed over the years to improve the quality of samples and the amount of collected information, and to avoid artifacts. Each technique has its pluses and minuses, making it more suitable for some applications than for others.

The thin sectioning technique was initially a dominant way to visualize the cytoskeleton *(4, 5)*. It involves the embedding of chemically fixed specimens into a resin, followed by thin sectioning to allow for beam penetration. Contrast is generated by positive staining of the sections with heavy metal salts, and the limited ability of stains to bind bioorganic material reduces the resolution of this technique. Thin sections provide a 2D view of the sample at a single plane, and a series of sections is required to retrieve the 3D information. Such reconstruction works well with relatively large and simple objects, but is not efficient in revealing the details of complex and delicately organized cytoskeletal structures, such as, for example, the actin filament networks in lamellipodia of locomoting cells.

Different versions of whole mount EM have been used to investigate the structural organization of the cytoskeleton in its entirety. Thus, the structural arrangement of actin filaments in lamellipodia was first visualized by the negative staining EM of cultured cells *(6)*. In this technique, partially permeabilized cells growing on EM grids are immersed into a heavy metal stain solution, which is blotted off shortly after, and the samples are dried in open air. The dried stain generates a dark amorphous background on which the structures appear as translucent shapes. Negative staining EM provides high resolution and allows one to see the thin regions of a cell all the way through. Weaknesses of the procedure include sample flattening during air drying, relatively low contrast, and low stability of the samples.

In cryo EM technique, the samples are quickly frozen (to prevent ice crystal formation) and viewed while still embedded in amorphous ice, either as whole mounts or after cryosectioning, so that they remain hydrated and the proteins retain their natural conformation *(7, 8)*. To view frozen samples, a TEM should be equipped with a chilled sample holder and electron beam power and the observation time should be minimized to

keep the specimen frozen. No contrasting procedures are used in this technique except for the specimen's own contrast, which is quite low. Therefore, significant image processing is required for the presentation and analysis of images. The major limitation of the technique is the significant difficulty in obtaining successful samples.

In metal replica EM, heavy metals are evaporated onto a 3D sample at an angle, which reveals its surface topography *(9)*. The quality of the samples is greatly enhanced if rotary, and not unilateral, coating is used, as it helps to avoid deep featureless shadows. As metal coating is not cohesive, it is subsequently stabilized by a layer of carbon, which keeps the metal grains together, and it is fairly transparent for the electron beam. The coated sample, or just a metal-carbon replica, is subsequently removed from its original support and placed onto EM grids. The resolution of replica EM is quite high, but it depends on the metal grain size, the thickness of the coating, and the angle of shadowing. Platinum is the most popular metal, as it provides a good compromise between the grain size and ease of evaporation. The replica technique was initially introduced to study freeze-fractured samples *(10)*, but it is applicable for a large range of samples, such as single molecules *(11, 12)*, cells *(13–15)*, and tissues *(16, 17)*. This approach can reveal the 3D structure in great detail, but it is limited by the depth of shadowing penetration.

For our studies of the cytoskeleton organization in cultured cells, we chose platinum replica EM, in which detergent extraction is used to expose the cytoskeleton; chemical fixation helps to preserve the sample structure; ethanol dehydration followed by critical point drying (CPD) preserves the cell's 3D organization; and rotary shadowing with platinum creates contrast. Over the years, we have found a good combination of individual steps to develop a reliable and relatively simple protocol that consistently produces highly informative images with excellent yield that can be combined with immunochemistry *(18–20)*. However, this approach is not universal, but is limited to relatively thin samples attached to glass surfaces. Also, because of extensive fixation and dehydration, it cannot achieve the molecular level of resolution, but is optimal for analyses of the fine architecture of macromolecular assemblies.

As EM, in general, cannot work with live samples, investigators can only guess the kind of activity the cell was involved in at the moment of fixation, and what it would do next. A partial solution for this problem is provided by correlative light and EM, in which the dynamics of a living cell is followed by time-lapse optical imaging, and the same sample is subsequently analyzed by EM. Our EM protocol made it possible to perform correlative light and EM routinely, as it allowed us to obtain high quality structural information for a cell of interest with high probability

(15, 18–20). Several other EM techniques have also been used in a correlative approach, including thin sections of resin-embedded samples *(21–24)*, cryosections *(25, 26)*, and negatively contrasted cells *(27)*, although for correlative cryo EM, light microscopy served only to survey the sample rather than to study its dynamics.

2. Materials

2.1. Cell Culture and Extraction

1. Small (6–12 mm) coverslips that can be made by cutting regular coverslips with a diamond pencil. Trapezoidal (square with one oblique side) coverslips lacking mirror symmetry are helpful to easily determine the cell-containing side. Commercially available 12 mm round coverslips are also acceptable (*see* **Note 1**).
2. Phosphate-buffered saline (PBS) with Ca^{2+} and Mg^{2+}.
3. PEM buffer: 100 mM PIPES (free acid), pH 6.9 (adjust with KOH), 1 mM $MgCl_2$, and 1 mM EGTA. Working buffer is prepared from 2× stock solution, which can be stored up to 1 month at 4°C (*see* **Note 2**).
4. Extraction solution: 1% Triton X-100 in PEM buffer supplemented (optionally) with 1–4% polyetheleneglycol (PEG) (MW 20,000–35,000), 2 μM phalloidin, and/or 2 μM taxol (paclitaxel) (*see* **Note 3**). Use a stirrer and allow 15–20 min to dissolve PEG. Extraction solutions can be stored for up to 3 days at 4°C, but phalloidin and taxol should be added before use. Stock solutions (1,000×) of phalloidin and taxol are made in dimethylsulfoxide (DMSO) and stored at –20°C in aliquots.

2.2. Fixation

1. Glutaraldehyde solution: 2% glutaraldehyde (EM grade, Sigma) in 0.1 M sodium cacodylate, pH 7.3. The working solution can be stored at 4°C for up to 1 week, 2× stock solution of sodium cacodylate is stable at 4°C. *Caution*: Glutaraldehyde is toxic and volatile, so a fume hood should be used when working; sodium cacodylate is toxic.
2. Tannic acid solution: 0.1% tannic acid (Fisher) in distilled water. Use within a day.
3. Aqueous uranyl acetate solution: 0.2% uranyl acetate in distilled water. Use a stirrer to dissolve. Store at room temperature. *Caution*: Uranyl acetate is toxic.

2.3. Dehydration and Critical Point Drying

1. Graded ethanol solutions: 10%, 20%, 40%, 60%, 80% and 100% ethanol in distilled water.

2. Alcohol uranyl acetate solution: 0.2% uranyl acetate in 100% ethanol. Use a stirrer to dissolve. Use within a day. *Caution*: Uranyl acetate is toxic.
3. Dehydrated ethanol: Wash molecular sieves (4 Å, 8–12 mesh) (Fisher) with several changes of water to remove dust. Dry in the air, bake at 160°C overnight, cool down, and add to a bottle of 100% ethanol (~50 g per 500 mL). Seal with Parafilm and store at room temperature. Do not shake, as the beads are fragile and easily generate dust.
4. CPD sample holder and scaffolds: A holder with a lid and two scaffolds are homemade with a stainless-steel wire mesh. The holder should fit into the chamber of the CPD apparatus. A scaffold is required to maintain the holder above the stirring bar during stirring. It should fit a beaker in which dehydration will be processed, e.g., a 50 mL glass beaker.
5. CPD device: We use Samdri PVT-3D (Tousimis) CPD with manual operation, but other devices are also appropriate.
6. Carbon dioxide: Use liquid dehydrated CO_2 (bone dry grade) in a tank with a siphon (deep tube) and a water and oil-absorbing filter (Tousimis). Siphonized tanks make it possible to take the liquid phase of CO_2 from the bottom of the tank.

2.4. Platinum and Carbon Coating

1. Vacuum evaporator: We use Auto 306 coater (Boc Edwards) equipped with a water-cooled diffusion pumping system, carbon and metal evaporation sources, a rotary stage, and a thickness monitor.
2. Metals for evaporation (Ted Pella): Tungsten wire (0.76 mm), platinum wire (0.2 mm), carbon rods (3 mm).

2.5. Preparation of Replicas

1. Hydrofluoric acid (HF): 5–10% HF in distilled water is prepared from the concentrated acid (49%). Do not use glassware to handle acid containing solutions. *Caution*: Extremely volatile and toxic, it causes severe skin burns. Use a fume hood and gloves.
2. Platinum loop: The optimal loop diameters are 3–5 mm.
3. EM Grids: Formvar-coated EM grids with low mesh size (e.g., 50) to provide a large viewing area. Other options are acceptable.

2.6. Immunogold EM

1. Immunogold buffer: 20 mM Tris–HCl, pH 8.0, 0.5 M NaCl, and 0.05% Tween 20. For dilution of antibodies, the buffer is supplemented with 1% bovine serum albumin (BSA); for washing, 0.1% BSA is added. Stock solutions (5×) are stable at 4°C for several months. Sodium azide can be added to the stock solution to prevent microbial contamination. *Caution*: Sodium azide is toxic.

2. Quenching solution: 2 mg/mL sodium borohydrate ($NaBH_4$) in PBS. Use immediately.
3. Blocking solution: 1 mg/mL glycine (or lysine) in PBS. Stable at 4°C.

2.7. Correlative EM

1. Marked coverslips: Homemade coverslips with reference marks are prepared by evaporating gold through a finder grid placed in the middle of a 22 × 22 square or 25 mm round coverslip. A variety of finder grids are available commercially. Baking (160°C overnight) of gold-coated coverslips is necessary for the firm adhesion of gold to glass (*see* **Note 4**). For light microscopy, choose cells on the clear footprint of the finder grid.
2. Light microscopy: The light microscopic system should be equipped with an environmental chamber to maintain normal cell behavior; it should allow for fast exchange of culture medium to extraction solution to quickly stop cellular activity during imaging. A simple option is to use open dishes on a heated stage with the cells growing in a bicarbonate-free medium.

3. Methods

In a basic form, replica EM can be used to study the cytoskeleton architecture in a cell population. In an advanced form, it can be combined with immunogold staining to detect specific proteins in the cytoskeleton **(Fig. 1)**, and with light microscopy to correlate the cytoskeleton organization with cell behavior or with the distribution and dynamics of fluorescent probes **(Figs. 1 and 2)**. The basic procedure consisting of extraction, fixation, dehydration, CPD, metal shadowing, and preparation of replicas is described first, and it is followed by the description of the advanced applications.

A major source of artifacts in this technique is the failure to perform a genuine CPD, which may occur if wet samples are transiently exposed to air, or water is not fully exchanged to ethanol or ethanol to CO_2, or if the dried samples absorb ambient humidity. In order to get a high quality preparation, it is critical not to allow a liquid-gas interface to touch the samples at any point during the procedure. Practically, it means keeping the cells away from air while they are wet, and away from water, while they are dry. Changes of solutions need to be done quickly, with a layer of liquid always being retained above the cells. After drying, the cells should be kept at low humidity until they are coated with carbon.

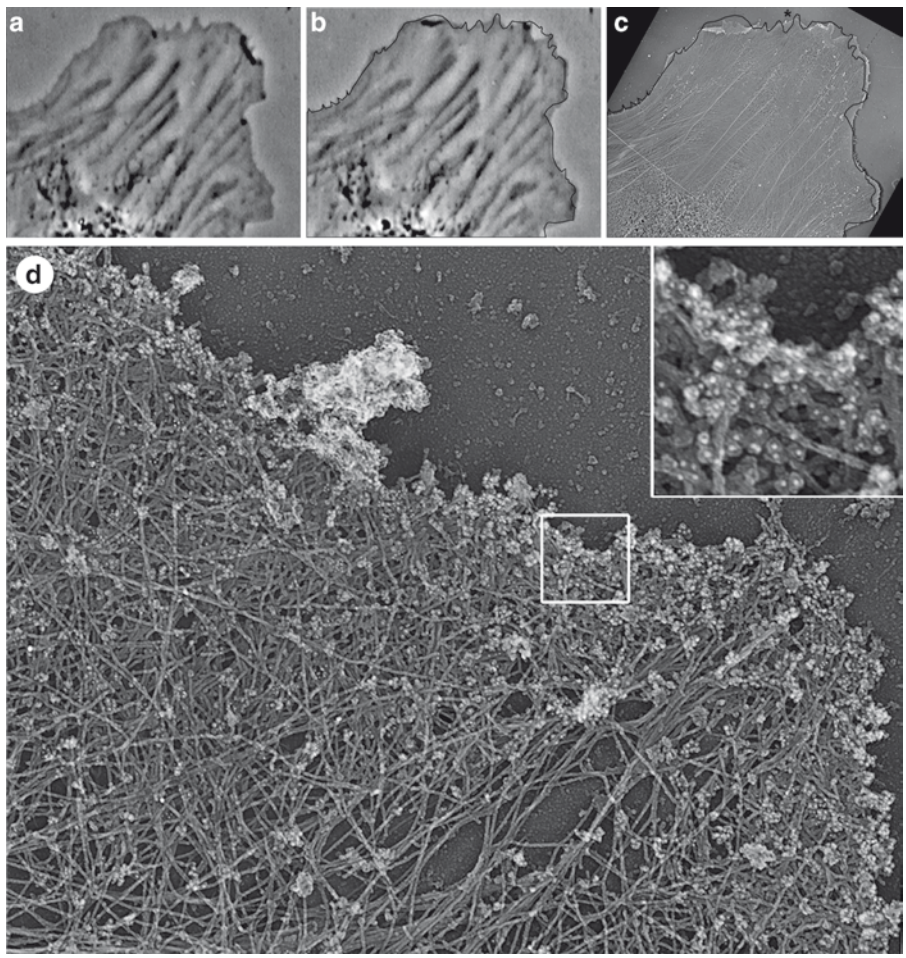

Fig. 1. Correlative phase-contrast and EM of cultured Rat-2 fibroblast combined with immunogold staining of ADF/cofilin. (**a**, **b**) Frames from time-lapse sequence showing the last live cell image (**b**) and an image 12 s earlier (**a**). *Black line* in (**b**) shows the cell edge outline from (**a**). (**c**) Low magnification EM image of the cell overlaid with the cell outline, as in (**b**). (**d**) EM of the protruding edge (*asterisk* in (**c**)) comprising a lamellipodium filled with dense actin network. Before the EM processing, the sample was immunogold labeled by cofilin antibody; inset in (**d**) shows gold particles as white dots.

3.1. Cell Culture and Extraction

Detergent extraction is used to expose the internal cytoskeletal structures, while the carrier buffer is designed to maximally preserve them until fixation. Additional preservation may be achieved using specific and non-specific stabilizers.

1. Put small glass coverslips into a culture dish and plate the cells. Cell culture conditions are specific for each system and are not discussed here. If several coverslips are placed into the same dish, make sure that they do not overlap and that there are no bubbles underneath.

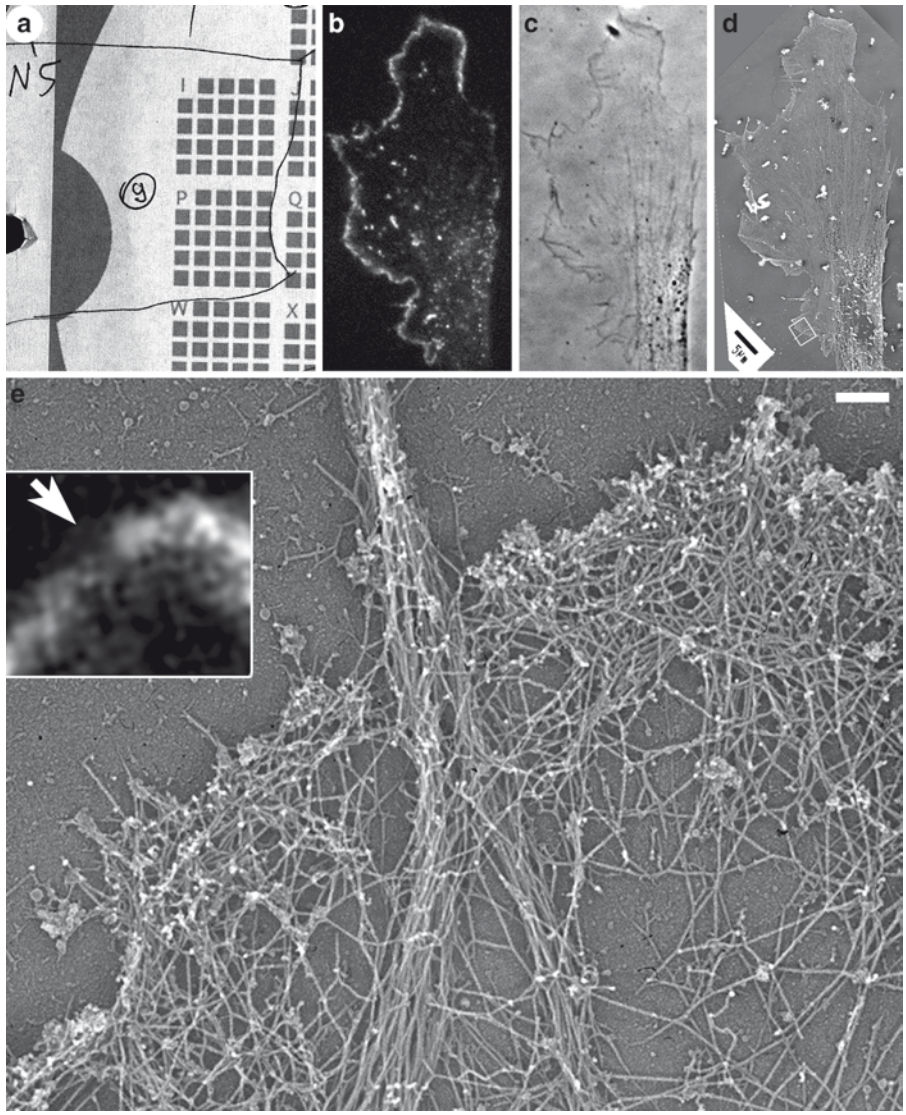

Fig. 2. Correlative fluorescence and EM of cultured B16F1 mouse melanoma cell expressing EGFP-capping protein. (**a**) Map showing position of the cell (number 9 in a circle) relative to the reference marks on the coverslip. (**b**) Fluorescence image the cell showing localization of EGFP-capping protein to the edge of lamellipodia and puncta in lamella. (**c**) Phase contrast image of the same cell. (**d**) Low magnification EM image of the same cell. Box indicate a region enlarged in (**e**). (**e**) High magnification EM of the boxed region from (**d**) showing actin filament bundle in a filopodium in the center and dense branched network of actin filaments in lamellipodia. Inset shows the same region by fluorescence microscopy. Bright fluorescence corresponds to lamellipodia, while the dim region (*arrow*) corresponds to the filopodium.

2. When the cells are ready, remove the culture medium from the dish using a pipette or by pouring out; quickly rinse with the pre-warmed to 37oC PBS? (*see* **Note 5**).
3. Immediately, but gently, add extraction solution equilibrated to room temperature; gently stir the dish to ensure that the

extraction solution instantly reaches all the cells (*see* **Note 6**). Incubate for 3–5 min at room temperature.

4. Rinse cells with PEM buffer 2–3 times, for a few seconds each time, at room temperature (*see* **Note 7**).

3.2. Fixation

Chemical fixation provides cytoskeletal structures with physical resistance against subsequent procedures, especially dehydration and CPD. It is a three-step procedure using different fixatives: glutaraldehyde, tannic acid and uranyl acetate.

1. After the last PEM rinse, add glutaraldehyde solution and incubate for at least 20 min at room temperature. If necessary, the samples can be stored at this stage at 4°C for up to 3 weeks. Take care to prevent evaporation during storage.
2. Transfer coverslips to another container with tannic acid solution, or change solutions in the same dish (*see* **Note 8**). Make sure that the cells remain covered with liquid during transfer. No washing is necessary before this step. Incubate for 20 min at room temperature.
3. Take the coverslips out of the tannic acid solution one by one, rinse by dipping sequentially into two water-filled beakers, and place in a new plate with distilled water. Do not keep the coverslips out of the solution longer than necessary. Incubate for 5 min (*see* **Note 9**).
4. Take the coverslips out of the water one by one, rinse twice again by dipping into water, and place in a new plate with aqueous uranyl acetate solution. Avoid drying during transfer. Incubate for 20 min at room temperature.
5. Wash off uranyl acetate solution with distilled water by transferring the samples or exchanging the solutions.

3.3. Dehydration and CPD

Drying of the samples is necessary to expose the surfaces for metal coating in a vacuum. However, plain drying in the open air generates major structural distortions. When the liquid-gas interface passes through the samples, the forces of the surface tension that are enormous at the cellular scale flatten the samples. During CPD, the temperature and pressure of a liquid are raised above its critical point, at which the phase boundary and surface tension do not exist. In this state, the liquid can well be considered as compressed gas. When the pressure is released, the samples remain dry with the 3D organization intact, because they never experienced the surface tension. Carbon dioxide has reasonably low values of critical point pressure and temperature that can be tolerated by biological samples. However, a direct transfer of the samples from water to CO_2 is not possible and ethanol, which is freely miscible with both water and CO_2, is used as an intermediate. For dehydration and CPD, the coverslips are stacked in the sample holder with pieces of lens tissue as spacers, and processed simultaneously.

1. Cut lens tissue with loosely arranged fibers into pieces fitting the size of the CPD sample holder or a little larger (*see* **Note 10**).
2. Place the CPD sample holder into a wide container with distilled water. Put a piece of lens tissue at the bottom of the holder, place a coverslip with the cell side up on the lens tissue, and cover with another piece of lens tissue. Continue loading the coverslips into the holder, alternating them with pieces of lens tissue. All loading should be done under water. Make sure that the coverslips are minimally exposed to air during loading. Do not overload the holder, as it will interfere with the exchange of solutions (*see* **Note 11**). Keep track of sample identity based on its position in the holder.
3. Put a stirrer bar into a 50 mL glass beaker, place a scaffold over it, and add 10% ethanol in the amount sufficient to cover the CPD holder. Quickly transfer the CPD holder with samples from the water-filled container into the beaker. Place the beaker on a magnetic stirrer, and stir for 5 min.
4. Prepare another beaker with a stirrer bar and a scaffold and add 20% ethanol. Transfer the CPD holder from the first beaker into the second, and stir for 5 min.
5. Continue dehydration by transferring the CPD holder sequentially through the remaining graded ethanols, 5 min in each: 40%, 60%, 80%, and 100% (twice). Alternate the two beakers with their scaffolds and stirrer bars (*see* **Note 12**).
6. Place the CPD holder into a beaker with 0.2% uranyl acetate in ethanol to fully cover it. Incubate for 20 min. Stirring is not necessary.
7. Transfer the CPD holder through beakers with 100% ethanol (twice) and dehydrated 100% ethanol dried over a molecular sieve (twice), as in **steps 3–5**. Stir for 5 min in each.
8. Fill the chamber of the CPD apparatus with dehydrated ethanol, just sufficient to cover the CPD holder. Place the holder in the ethanol and close the lid. Operate the CPD according to the manufacturer's instructions or following the procedure below (*see* **Note 13**).
9. Open the CO_2 tank. Cool down the CPD chamber to 10–15°C to keep the CO_2 in a liquid state. Maintain this temperature until the heating step (*see* **Note 14**).
10. Open the inlet valve on the CPD to allow the CO_2 to fill the chamber. If the device is equipped with a magnetic stirrer, turn it on and keep it running till the heating step. Wait for 5 min. This is a mixing step, during which the ethanol in the chamber, the sample holder, and the samples, are equilibrated with the liquid CO_2 from the tank.

11. With the inlet valve still open, open the outlet valve slightly until you clearly see that the liquid exchange is happening in the chamber, but do not allow the level of the liquid to go below the top of the sample holder. Wait for 30 s. This is a washing step, when the ethanol–CO_2 mixture is released from the chamber and replaced with pure CO_2 from the tank. If the CPD is not equipped with a magnetic stirrer, shake the CPD manually during the washing to mix the chamber contents better (*see* **Note 15**).
12. Close the outlet valve. Wait for 5 min.
13. Repeat **steps 11** and **12** nine more times (total ten washes). After the last wash, wait only until the chamber is completely filled with CO_2; that may take less than 5 min.
14. Close both the inlet and outlet valves and turn on the heat. As the chamber is isolated, heating will raise both the temperature and the pressure. Wait until both parameters exceed the critical values for CO_2 (critical pressure = 1,072 psi or 73 atm, critical temperature = 31°C) and reach values of ~1,250 psi (85 atm) and ~40°C. If one value is reached sooner than the other, maintain the former at a steady-state level by turning the heater or the outlet valve on and off until both the values are reached.
15. Open the outlet valve slightly to slowly release the pressure until it reaches the atmospheric pressure. It should take about 10 min (*see* **Note 16**).
16. Open the CPD chamber, remove the sample holder and immediately put it into a desiccator.

3.4. Platinum and Carbon Coating

Platinum shadowing generates the contrast of the samples. The angle and the thickness of the coating are critical parameters influencing the quality of the image. Lower angles provide higher contrast, but do not penetrate deep into the sample. Thinner coats provide higher resolution, but lower contrast. For cellular studies, we shadow platinum at a ~45° angle with rotation to achieve a ~2 nm thickness of the coat, which is controlled by the thickness monitor. Carbon is applied from the top of the samples with a thickness of 3.5–5 nm. The basic steps of coating are listed below. Use the equipment manual for detailed operation.

1. Open the coating chamber of the vacuum evaporator. Load the evaporation materials, platinum and carbon. Adjust the angles of coating.
2. Mount the samples onto the rotary stage of the vacuum evaporator using a double-sided tape. This will prevent the dislodging of the samples during rotation (*see* **Note 17**). To prevent damage of the samples by ambient humidity, perform mounting as quickly as possible (*see* **Note 18**).

3. Pump down the coating chamber till ~5 × 10^{-6} atm.
4. Turn on the stage rotation, shadow with platinum (2 nm) and then with carbon (3.5–5 nm) (*see* **Note 19**).
5. Vent the coating chamber. Remove the samples together with the mounting tape and place in a Petri dish. The samples can be safely stored in a room at this stage.

3.5. Preparation of Replicas

The release of the replicas from the coverslips is achieved by floating the coverslips onto the surface of hydrofluoric acid solution, which dissolves glass. After that, the replicas are washed and mounted on EM grids.

1. While the coverslips are still attached to the sticky tape, scratch the coated surface of each coverslip with a needle or a razor blade to make regions fitting the size of an EM grid.
2. Fill the wells of a 12-well plate with ~10% HF almost to the top, which makes replica handling easier.
3. Detach a coverslip from the sticky tape and place it on the surface of the HF solution, so that the coverslip remains floating. Wait until the glass sinks, leaving the platinum replica floating. The replica will fall apart along the scratches made in **step 1** (*see* **Note 20**).
4. Fill the wells of another 12-well plate with distilled water, and add a trace amount of a detergent to decrease the surface tension of water. Stock solution of the detergent is prepared by dissolving ~1 drop of detergent in ~20 mL of water. To make a working solution, dip a platinum loop into the stock solution, take it out (this will create a film on the loop), and dip the loop into a water-filled well. The final concentration of detergent is ~10^{-6}% (*see* **Note 21**).
5. Using a platinum loop, transfer the replica pieces onto the surface of the detergent-containing water. Wait for 1 min or more.
6. Fill the wells of another 12-well plate with distilled water without detergent. Transfer the replica pieces onto the surface of the water. Wait for 1 min or more.
7. Pick up the replica pieces onto Formvar-coated EM grids with the lower side of the replica attached to the Formar film. The technique of replica mounting is similar to the way thin sections are picked up onto grids. Fasten a grid in a pair of forceps, partially submerge the grid into water at a ~45° angle, bring the grid close to a piece of replica and allow them to make contact; then, gently pull the grid out of the water making sure that the replica piece remains attached to, and spreads over the grid (*see* **Note 22**).

8. Examine the samples in TEM. Present the images in inverse contrast (as negatives) because it gives a more natural view of the structure, as if illuminated with scattered light.

3.6. Immunogold EM

Structural information has much greater value if the identity of the structures is known. Immunostaining is a conventional way to identify cellular components. For EM purposes, the antibodies are labeled with electron-dense markers. A popular marker, colloidal gold, has a higher electron density than platinum and thus is appropriate for platinum replica EM. For successful immunogold replica EM, a primary antibody should work after glutaraldehyde fixation, which optimally preserves the structure (*see* **Note 23**).

1. After glutaraldehyde fixation **(Subheading 3.2, step 1)**, wash the samples with three changes of PBS. Incubate for at least 5 min in the last change.
2. Quench samples with $NaBH_4$ for 10 min at room temperature. Shake off the bubbles occasionally. Rinse with PBS as in **step 1**.
3. Incubate with blocking solution for 20 min at room temperature.
4. Apply primary antibody at concentration giving bright staining by light microscopy. Incubate for 30–45 min at room temperature. Wash with PBS as in **step 1**.
5. Rinse once in immunogold buffer with 0.1% BSA. Apply gold-conjugated secondary antibody diluted ~1:10 in immunogold buffer with 1% BSA. Incubate overnight at room temperature in a sealed container in moist conditions (*see* **Note 24**).
6. Rinse in immunogold buffer with 0.1% BSA as in **step 1**, and perform the remaining steps starting from **Subheading 3.2, step 1**.

3.7. Correlative EM

The correlative light and EM combines the advantages of both the microscopic techniques, namely, the high spatial resolution of EM and the high temporal resolution of live imaging. In this procedure, the cell dynamics is recorded by light microscopy, and then the same cell is analyzed by EM. The correlative analysis is extremely important from at least two points of view: to control for potential artifacts and to establish functional connections between the cytoskeletal organization and the cell's motile behavior or the dynamics of cytoskeletal components *(28, 29)*. Modifications of the basic procedure as required for correlative EM are described below.

1. *Cell culture and light microscopy*:
   (a) Grow cells in dishes with marked coverslips mounted over a hole in the bottom of the dish. To make a dish, drill a 18-mm hole in the bottom of a 35-mm dish; polish the edges to remove any burrs; apply a thin layer of vacuum

grease just outside the edges of the hole; place a marked coverslip symmetrically over the hole with the coated side facing up; press firmly to spread the grease until it forms a clear circle and all the air bubbles are gone (*see* **Note 25**).

(b) While imaging a region of interest, mark its position on a map with a pattern of reference marks.

(c) Because of the large difference in the resolution of light and EM, perform light microscopy at the highest possible resolution.

(d) EM is able to reveal even minor photodamage, not recognizable at the light microscopic level; therefore, keep the illumination of the samples to a minimum.

2. *Extraction*: Change the culture medium to extraction solution as soon as possible after the acquisition of the last live image, and take another image after extraction. It will serve as a reference to correlate the light and EM images.

3. *Fixation*: Perform all the fixation and washing steps with the marked coverslips still attached to the dishes, by exchanging solutions.

4. *Dehydration*: Before loading the coverslips into the CPD sample holder, excise the central marked area of the coverslip as following:

(a) Wipe away the immersion oil from the bottom of the dish using dry cotton swabs first, followed by ethanol-soaked swabs.

(b) Detach the marked coverslip from the bottom of the dish and immediately place it into a water-filled 100 mm Petri dish.

(c) Lightly press down the coverslip to allow the vacuum grease on the underside to secure the coverslip in the dish. Make sure that grease does not contaminate the region of interest.

(d) Use a diamond pencil as a cutter and a razor blade as a ruler to cut off the greasy margins of the coverslip. Do not press the pencil hard, but instead make several light cuts along the same line, guided by the razor blade, until the margin detaches. Move it out of the way and cut off another margin. This procedure should be done with the coverslip completely submerged in the water (*see* **Note 26**). When done, transfer the excised central region to another water-filled container. Use a new dish for the next coverslip, as the remaining glass crumbs may cause shattering of the coverslip.

All subsequent processing, including coating, is performed as in the basic procedure.

5. *Preparation of replicas*: After the samples are coated, the region of interest needs to be specifically recovered for EM analysis as follows:
   (a) Immobilize a coated coverslip in the middle of a 100 mm Petri dish, with two pieces double-sided tape positioned under opposite corners of the coverslip, so that the region of interest is not obstructed and the coverslip is not attached too strongly.
   (b) Under a dissection microscope, localize the cells of interest using locator marks. Dried and shadowed cells have sufficient contrast for their shape to be seen even at low magnification. If necessary, use a regular light microscope with a low power lens.
   (c) Using a razor blade (or a needle), make cuts in the platinum–carbon layer around the region of interest (*see* **Note 27**). To facilitate the separation of this region from the rest of the replica after HF treatment, make additional cuts connecting the region of interest with the edges of the coverslip.
   (d) Make a drawing on the map to depict the exact shape of the outlined region of interest, which will help to identify it from among the other replica pieces during replica preparation.
   (e) Perform the washing and mounting on grids, as described in the basic protocol, handling only the replica piece with the region of interest. While mounting on a grid, use a dissection microscope to make sure that the cell of interest does not go to a grid bar; or use single-hole grids.

4. Notes

1. Small coverslips allow for better exchange of solutions during dehydration and CPD, and thus for better quality of samples at the end.
2. Stock solutions with a concentration of more than 2× change pH significantly after dilution to the working concentration. Free acid PIPES is not soluble in water and forms a milky suspension, but becomes soluble upon neutralization. KOH granules can be used for neutralization initially, until the solution almost clears. However, remember to allow enough time for the granules to dissolve before adding more. Finish the pH adjustment with 1 N KOH. KOH is preferable over NaOH, because K^+-containing buffer, more faithfully imitates the cytoplasm composition.

3. PEG is a non-specific stabilizer of the cytoskeleton; phalloidin and taxol are specific stabilizers of actin filaments and microtubules, respectively.
4. Commercially available etched coverslips are not suitable for replica EM, as the marks are not visible in TEM.
5. Rinsing with PBS is optional, but if omitted, the extraction solution at the next step should be added in sufficient quantity to overcome the potentially harmful effects from the remaining medium and serum.
6. The choice of the extraction solution depends on a cell type and a goal. For a new experimental system, try different options in the preliminary experiments. Basic extraction solution (Triton X-100 in PEM) gives a better clarity of the cytoskeleton, but it is easier to damage the cells during extraction. If using this protocol, handle the samples extremely gently, and use phalloidin and taxol to better preserve the actin filaments and microtubules, respectively. The addition of PEG to the extraction solution provides for better preservation of the cells, but it also retains many cytoskeleton-associated components, which may partially obscure the filament arrangement. Such an effect is increased with PEG concentration and molecular weight, but PEGs in the range of 20,000–40,000 act similarly. We typically use 2% PEG (35,000). Phalloidin and taxol are not as necessary in this case. For extremely fragile and poorly attached cells, low concentrations of glutaraldehyde can be used as stabilizing supplements for the extraction solution. In this case, the detergent and fixative compete with each other, and the results depend on their ratio. The extraction solution containing 0.5% Triton X-100 and 0.25% glutaraldehyde in PEM buffer worked well in our experiments.
7. For PEG-containing extraction solutions, use a longer washing time, at least 1 min in each change. If drugs are used during extraction, add them also to the rinsing buffer in a four fold to five fold lower concentration.
8. It is convenient to use a multiwell plate with numbered wells (24-well for 6–8 mm coverslips or 12-well for 9–12 mm coverslips) to transfer the samples. This makes it possible to combine samples from different experiments for EM processing while keeping parallel samples in the original container as a backup.
9. Uranyl acetate and tannic acid react with each other and form a precipitate. Extensive washing is important to avoid the formation of debris on the samples.
10. Pieces of lens tissue slightly larger, than the holder's bottom area, will make minor wrinkles which promote a

looser packing of the coverslips in the holder and facilitate the liquid exchange.

11. The acceptable number of samples for a load depends on the sizes of the holder and the coverslips. For an 18 × 12 mm holder and ~7 × 7 mm coverslips, the maximum load is 12. For larger coverslips, the load should be decreased. Larger holders may accept more samples, especially if the coverslips are staggered.
12. It is not necessary to dry the beakers before the next incubation, as the ethanol concentration may not be exact, except for 100% ethanol, when it is better to dry the beakers and scaffolds with tissue. Incubation for 5 min is minimal. For larger coverslips or greater loads, increase the incubation time.
13. The process of CPD is most commonly used for scanning EM and production of microelectronics. Consequently, the protocols suggested by the manufacturers or incorporated into automated procedures of CPDs are designed for those applications. Replica TEM, however, is more demanding in terms of sample quality. We adjusted the CPD processing to fully remove all traces of ethanol from the samples before bringing the CO_2 to the critical point; this helps to eliminate minor artifacts that appear as a fusion of closely positioned filaments in the cytoskeleton. The CPD operation described here is applicable to manual CPDs, such as Samdri PVD-3D (Tousimis), which we use in the lab, or to semi-automatic CPDs switched to a manual mode of operation, e.g., Samdri-795 (Tousimis).
14. Lower temperatures are acceptable, but the diffusion of ethanol from the samples will be slower, so that longer washing time is needed. Warming up the chamber till the ambient temperature is allowed if the outlet valve of the CPD is closed, and the CO_2 remains pressurized and in liquid form. However, it is important to cool down the chamber back to 15°C before opening the outlet valve for purging out the ethanol–CO_2 mixture.
15. Letting the liquid level go below the samples will irreversibly damage them. On the other hand, too low a rate of liquid exchange is also a mistake. Adjust the outlet valve to get a steady-state liquid level, about halfway from the top of the holder to the top of the chamber. This will also make the liquid mixing more efficient. Although the shaking step sounds a bit amusing, it does make a difference by helping to remove the ethanol from the samples.
16. Fast release of pressure may cause condensation of CO_2 back to liquid state and ruin the dried samples.

17. Conventional Scotch double-sided tape becomes too sticky in a vacuum, preventing the safe detachment of the samples after coating. To avoid this problem, sandwich the double-sided tape between the glued parts of two Post-It notes, with the sticky sides exposed.
18. Humidity in the room should be below 35%; the 35–50% humidity level may be acceptable, but much caution and the speedy mounting of the samples is required; humidity >50% is not acceptable. Try to run a powerful dehumidifier in the latter case.
19. If the evaporator is not equipped with a thickness monitor, the thickness of the coating may be adjusted in the preliminary experiments based on the amount of coating material loaded (for platinum) or used (carbon) for evaporation.
20. To safely float a coverslip, grab it with the forceps from the top for parallel edges, lift the coverslip, and carefully place it onto the liquid surface, keeping it in a horizontal position. Practice first by placing a coverslip onto a clean solid surface. If the replica does not fall apart along the scratches, use the platinum loop to reach the replica from below, lightly touch it and pull or shake it to detach it from other pieces. Extreme care should be used not to ruin the replicas with these manipulations.
21. Water has much greater surface tension than HF, which may cause severe replica breakage, if detergent is not added. Test the detergent concentration before applying it to the samples. An overdose of detergent causes shrinkage and drowning of the replicas. Stock solutions should be changed at least every 2 weeks. Old detergents leave contamination on the samples, looking like semi-transparent films between filaments. Household non-colored detergent, such as Ivory, works fine. Triton X-100 can also be used, but it should be changed more frequently.
22. Sometimes, replicas appear to be repelled by the grid, making it difficult to establish the initial contact between a replica piece and a grid. Try to gently guide a piece of replica to the wall of the well to restrict its motility, and then pick it up. However, there is a danger of smashing the replica against the wall with this approach. In severe cases, use glow discharge to treat grids.
23. The efficiency of staining may be improved if the cells are fixed with a lower (e.g., 0.2%) glutaraldehyde concentration before staining. For some antibodies that do not work after glutaraldehyde fixation, it may be possible to stain unfixed samples by incubating them with primary antibodies diluted in PEM for 10–15 min, then fixing with glutaraldehyde, and quenching and staining with a secondary antibody.

24. Gold size of 10–20 nm is optimal for this technique, as smaller particles are poorly visible, and larger particles are too disruptive for an image.
25. The coverslips can be mounted either inside or outside the dish, but inside mounting is more convenient at later stages, when the centerpiece of the coverslip needs to be cut out. For mounting, use a minimal amount of grease, just sufficient to seal the dish; excessive grease causes complications at later stages. Commercially available glass-bottom dishes have coverslips permanently glued to the bottom, which makes it difficult to remove them for EM processing.
26. Cutting under water is more difficult than in the air; therefore, use a sharp diamond pencil and avoid glass crumbs.
27. To reduce the effect of shaky hands, hold a razor blade with one hand with the sharp blade corner pointing down; stabilize the blade by putting the index finger of the other hand onto the blunt blade corner pointing up; rest the forearms on the table and the other fingers of both hands on the microscope stage and/or dish edges; keep the blade above the sample and find its unfocused image in the microscope; slowly bring down the sharp corner of the blade until it almost comes to focus; bring the blade corner to a region where a cut is to be made; under microscope control, bring it down to the sample and make a scratch.

Acknowledgments

The author acknowledges the current support from NIH grant R01 GM 70898.

References

1. Wohlfarth-Bottermann, K. E. (1962) Weitreichende fibrillare Protoplasmadifferenzierungen und ihre Bedeutung fur die Protoplasmastromung. I. Elektronenmikroskopischer Nachweis und Feinstruktur. *Protoplasma* **54**, 514–539
2. Ledbetter, M. C., and Porter, K. R. (1963) A "microtubule" in plant cell fine structure. *J Cell Biol* **19**, 239–250
3. Sabatini, D. D., Bensch, K., and Barrnett, R. J. (1963) Cytochemistry and electron microscopy. The preservation of cellular ultrastructure and enzymatic activity by aldehyde fixation. *J Cell Biol* **17**, 19–58
4. Wohlfarth-Bottermann, K. E. (1964) Differentiations of the ground cytoplasm and their significance for the generation of the motive force of ameboid movement. *In* "Primitive Motile Systems in Cell Biology" (Allen, R. D., and Kamiya, N., Eds.), pp. 79–109, Academic Press, New York-London
5. Abercrombie, M., Heaysman, J. E., and Pegrum, S. M. (1971) The locomotion of fibroblasts in culture. IV. Electron microscopy of the leading lamella. *Exp Cell Res* **67**, 359–367
6. Small, J. V., Isenberg, G., and Celis, J. E. (1978) Polarity of actin at the leading edge of cultured cells. *Nature* **272**, 638–639

7. Costello, M. J. (2006) Cryo-electron microscopy of biological samples. *Ultrastruct Pathol* **30**, 361–371
8. Murphy, G. E., and Jensen, G. J. (2007) Electron cryotomography. *Biotechniques* **43**, 413, 15, 17 passim
9. Heuser, J. (1981) Preparing biological samples for stereomicroscopy by the quick-freeze, deep-etch, rotary-replication technique. *Methods Cell Biol* **22**, 97–122
10. Steere, R. L. (1957) Electron microscopy of structural detail in frozen biological specimens. *J. Cell Biol.* **3**, 45–60
11. Heuser, J. (1989) Protocol for 3-D visualization of molecules on mica via the quick-freeze, deep-etch technique. *J Electron Microsc Tech* **13**, 244–263
12. Loesser, K. E., and Franzini-Armstrong, C. (1990) A simple method for freeze-drying of macromolecules and macromolecular complexes. *J Struct Biol* **103**, 48–56
13. Heuser, J. E., and Kirschner, M. W. (1980) Filament organization revealed in platinum replicas of freeze-dried cytoskeletons. *J Cell Biol* **86**, 212–234
14. Svitkina, T. M., Shevelev, A. A., Bershadsky, A. D., and Gelfand, V. I. (1984) Cytoskeleton of mouse embryo fibroblasts. Electron microscopy of platinum replicas. *Eur J Cell Biol* **34**, 64–74
15. Svitkina, T. M., Verkhovsky, A. B., and Borisy, G. G. (1995) Improved procedures for electron microscopic visualization of the cytoskeleton of cultured cells. *J Struct Biol* **115**, 290–303
16. Meyer, H. W., and Richter, W. (2001) Freeze-fracture studies on lipids and membranes. *Micron* **32**, 615–644
17. Hirokawa, N. (1989) Quick-freeze, deep-etch electron microscopy. *J Electron Microsc (Tokyo)* **38 Suppl**, S123–S128
18. Svitkina, T. (2007) Electron microscopic analysis of the leading edge in migrating cells. *Methods Cell Biol* **79**, 295–319
19. Svitkina, T. M., and Borisy, G. G. (2006) Correlative light and electron microscopy studies of cytoskeletal dynamics. *In* "Cell Biology: A Laboratory Handbook; 3rd Edition" (Celis, J., Ed.), Vol. 3, pp. 277–285, Elsevier, Amsterdam
20. Svitkina, T. M., and Borisy, G. G. (1998) Correlative light and electron microscopy of the cytoskeleton of cultured cells. *Methods Enzymol* **298**, 570–592
21. Kapoor, T. M., Lampson, M. A., Hergert, P., Cameron, L., Cimini, D., Salmon, E. D., McEwen, B. F., and Khodjakov, A. (2006) Chromosomes can congress to the metaphase plate before biorientation. *Science* **311**, 388–391
22. Ostap, E. M., Maupin, P., Doberstein, S. K., Baines, I. C., Korn, E. D., and Pollard, T. D. (2003) Dynamic localization of myosin-I to endocytic structures in Acanthamoeba. *Cell Motil Cytoskeleton* **54**, 29–40
23. Sosinsky, G. E., Giepmans, B. N., Deerinck, T. J., Gaietta, G. M., and Ellisman, M. H. (2007) Markers for correlated light and electron microscopy. *Methods Cell Biol* **79**, 575–591
24. Verkade, P. (2008) Moving EM: the Rapid Transfer System as a new tool for correlative light and electron microscopy and high throughput for high-pressure freezing. *J Microsc* **230**, 317–328
25. Kandela, I. K., Bleher, R., and Albrecht, R. M. (2008) Immunolabeling for correlative light and electron microscopy on ultrathin cryosections. *Microsc Microanal* **14**, 159–165
26. Sartori, A., Gatz, R., Beck, F., Rigort, A., Baumeister, W., and Plitzko, J. M. (2007) Correlative microscopy: bridging the gap between fluorescence light microscopy and cryo-electron tomography. *J Struct Biol* **160**, 135–145
27. Nemethova, M., Auinger, S., and Small, J. V. (2008) Building the actin cytoskeleton: filopodia contribute to the construction of contractile bundles in the lamella. *J Cell Biol* **180**, 1233–1244
28. Svitkina, T. M., Bulanova, E. A., Chaga, O. Y., Vignjevic, D. M., Kojima, S., Vasiliev, J. M., and Borisy, G. G. (2003) Mechanism of filopodia initiation by reorganization of a dendritic network. *J Cell Biol* **160**, 409–421
29. Yang, C., Czech, L., Gerboth, S., Kojima, S., Scita, G., and Svitkina, T. (2007) Novel roles of formin mDia2 in lamellipodia and filopodia formation in motile cells. *PLoS Biol* **5**, e317

Chapter 11

Purification and Localization of Intraflagellar Transport Particles and Polypeptides

Roger D. Sloboda

Summary

The growth and maintenance of almost all cilia and flagella are dependent on the proper functioning of the process of intraflagellar transport (IFT). This includes the primary cilia of most cells in humans that are in interphase or the G_o phase of the cell cycle. The model system for the study of IFT is the flagella of the bi-flagellate green alga *Chlamydomonas*. It is in this organism that IFT was first discovered, and genetic data from a *Chlamydomonas* mutant first linked the process of IFT to polycystic kidney disease in humans. The information given in this chapter addresses procedures to purify IFT particles from flagella and localize these particles, and their associated motor proteins, in flagella using light and electron microscopic approaches.

Key words: Flagella, Cilia, Intraflagellar transport, Motility, Immunofluorescence, Immunogold EM

1. Introduction

The term intraflagellar transport (IFT) refers to the bi-directional movement of protein complexes from the base to the tip and back again in flagella[1]. This process was initially discovered by Kozminski et al. *(2)* in the flagella of the green alga *Chlamydomonas*, but IFT is now known to exist in almost all cilia and flagella that

[1]The term 'flagella' will be used throughout this manuscript, but readers should realize that the process of IFT occurs—and is just as important—in cilia as well. Indeed, many developmental problems and diseases of humans are related to defects in primary cilia, some of which derive from defects in IFT (see reference *(1)* R.D. Sloboda, and J.L. Rosenbaum, Making sense of cilia and flagella. J Cell Biol 179 (2007) 575–82. for a recent overview of this field).

R.H. Gavin (ed.), *Cytoskeleton Methods and Protocols,* Methods in Molecular Biology, vol. 586
DOI 10.1007/978-1-60761-376-3_11,
© Humana Press, a part of Springer Science + Business Media, LLC 2009

studied to date. IFT is required for the assembly and maintenance of flagella, and this was demonstrated using cells defective in one of the motor proteins that power the process of IFT *(3)*. IFT can be visualized using high resolution differential interference contrast (DIC) microscopy *(4)*, and related methods are detailed elsewhere in this volume (*see* Chap. 10 and 12). A cell line is also available in which the non-motor subunit (KAP) of kinesin-2, the anterograde IFT motor, is fused to GFP *(5)*. IFT in these cells can be visualized with fluorescence microscopy.

The flagella of *Chlamydomonas* represent the only microtubule-based motility system in which *all* of the following have been established: (a) the microtubule-based motors powering the movements of IFT particles in both directions along flagella are known *(3,6–8)*; (b) individual strains carrying mutations in one or the other motors are available *(3, 6, 9)*; (c) IFT particles can be isolated, their constituent polypeptides have been cloned and sequenced, and mutations have been identified in a number of these polypeptides *(10,11)*; (d) IFT particle motility occurs in clearly defined directions, i.e., out and back along the flagellum, essentially in only one dimension, between the outer doublet microtubules and the membrane *(3)*; (e) motility occurs in a biochemically defined, easily isolated, membrane-bound compartment; (f) microtubule assembly and disassembly – indeed, assembly and disassembly of the entire organelle – occurs only at the flagellar tip *(12)*; (g) because IFT particles move from the base to the tip without pauses *(2)*, the enzyme(s) regulating the IFT motors must also be restricted to the flagellar tip; and (h) structures unique to the flagellar tip complex (FTC) have been identified *(13–15)*. Thus, it is clear that *Chlamydomonas* offers many advantages for the study of the mechanism of IFT, organelle assembly, control of motor enzyme activity, cargo unloading and loading, etc. One can readily observe IFT in *Chlamydomonas* flagella with video enhanced DIC microscopy or fluorescence microscopy (the latter with GFP-labeled cells), isolate IFT particles in quantities sufficient for biochemical characterization, and localize their constituent proteins by light and electron microscopic immunocytochemistry.

2. Materials

All solutions are prepared with deionized (18 MΩ) water.

2.1. Cells and Culture Conditions

1. *Chlamydomonas* cells are available from the stock center <http://www.chlamy.org/>. Unless a specific genotype or mutation is required for a specific analysis, the standard wild type strain is

CC125 (wild type, mt+ 137C), which was originally isolated in 1945 near Amherst, MA, by G. M. Smith.

2. TAP medium: Stock solutions for TAP (Tris–Acetate-Phosphate, see Gorman and Levine *(16)*) are the following: 100× Tris–acetate: 242 g Tris base dissolved in 750 mL of water; pH to 7.0 with glacial acetic acid and bring to 1 L with water. TAP salts: 40 g NH_4Cl, 10 g $MgSO_4{\cdot}7H_2O$, 5 g $CaCl_2{\cdot}2H_2O$, water to 1 L.1 M Phosphate solution: 28.8 g K_2HPO_4, 14.4 g KH_2PO_4, water to 100 mL. A working solution of TAP medium is then made by combining 10 mL of 100× Tris–acetate, 10 mL TAP salts, 1 mL phosphate, 1 mL Hutner trace metals (*see* **Subheading 2.1**, **item 3** below), and 1 mL glacial acetic acid. Bring to 1 L with water.
3. Hutner's trace metals: This solution is based on the work of Hutner et al. *(17)*, and the procedure given below is adapted from Surzycki *(18)*. Preparation of this stock solution is complex and time consuming (*see* **Note 1**). This begins by dissolving the number of grams indicated in **Table 1** for each trace metal salt in the volume of water listed. Combine these seven solutions and boil. Boil a separate volume of 250 mL of water and add 50 g of the disodium salt of EDTA to the boiling water. Then, combine this with the seven other ingredients. When the solution is clear and greenish in tint, indicating all components have dissolved, cool the solution to 70°C. Adjust the pH to 6.7, *while the solution is at 70°C*, using hot 20% KOH (*see* **Note 2**). Bring to a final volume of 1 L with water. Place the 1 L solution in a 2 L flask, stopper with a cotton plug to allow gas exchange, and let the solution rest at RT for 1 week or more. Swirl the solution briefly each day. Eventually, the solution will turn purple, and a brown precipitate will form (*see* **Note 3**). Filter with Whatman #1 paper and repeat

Table 1 Trace Metal Solution Components

Trace metal salt	Grams	Ml
$ZnSO_4{\cdot}7H_2O$	22.0	100
H_3BO3	11.4	200
$MnCl_2{\cdot}4H_2O$	5.1	50
$CoCl_2{\cdot}6H_2O$	1.6	50
$CuSO_4{\cdot}5H_2O$	1.6	50
$(NH_4)_6MO_7O_{24}{\cdot}4H_2O$	1.1	50
$FeSO_4{\cdot}7H_2O$	5.0	50

the filtration, if necessary, until the solution is clear; two or three sheets of #1 filter paper can be used at the same time, if needed. Store the trace metals stock at 4°C.

4. TAP culture plates/slants: sterile 1% agarose in TAP, poured into Petri dishes or slants in screw cap tubes.

2.2. Flagellar Isolation and Extraction

1. HMDS buffer *(19)*: 10 mM HEPES, pH 7.5, 5 mM $MgSO_4$, 1 mM DTT, and 5% sucrose.
2. Sucrose cushion: HMDS in which the sucrose concentration is increased to 20%.
3. Extraction solution: HMDS containing 10 mM Mg-ATP and 0.1% NP-40.
4. Pefabloc stock: 200 mM Pefabloc (Roche) in water (*see* **Note 4**).
5. HMDEK buffer: 10 mM HEPES, pH 7.5, 5 mM $MgSO_4$, 1 mM DTT, 0.5 mM EDTA, 25 mM KCl, and 2 mM Pefabloc.
6. 100 mM Mg-ATP.
7. 10% NP-40.
8. Sucrose gradient solutions: 10% sucrose in HMDEK; 30% sucrose in HMDEK.

2.3. Gel Electrophoresis

The gel solutions in this section are based on the buffer formulations of Laemmli *(20)*.

1. Acrylamide: bis (30:0.8). This can be made from powdered acrylamide and bis-acrylamide; however, acrylamide in the unpolymerized state is a neurotoxin and, thus, should be handled with appropriate precautions (fume hood and mask for weighing, protective gloves always). Alternatively, pre-made solutions can be purchased at reasonable cost from Sigma-Aldrich and other vendors.
2. 3 M Tris base, brought to pH 8.8 with HCl.
3. 0.5 M Tris base, brought to pH 6.8 with HCl.
4. 20% SDS. The powder is a bronchial irritant, and so care (fume hood and mask) should be taken in weighing and handling this reagent. Very pure (expensive) SDS is not recommended, as the tubulin subunits (α- and β-) will not separate well in the presence of purified SDS *(21,22)*.
5. TEMED (*N*,*N*,*N*′,*N*′-Tetramethylethylenediamine).
6. Ammonium persulfate, 10% in water, made fresh and stored at RT for up to 1 week.
7. 2× sample buffer: 0.0625 M Tris–HCl, pH 6.8 (i.e., an eightfold dilution of the 0.5 M Tris stock from **Subheading 2.3**, **item 3** above, 4% SDS (fivefold dilution from the 20% stock of **Subheading 2.3**, **item 4** above), 20% glycerol, 10%

β-mercaptoethanol, and 10 μg/mL Pyronin-Y, the latter to serve as a tracking dye. In cases where sample protein concentrations are dilute, it is often preferable to use a more concentrated sample buffer. To prepare, for example, 10 mL of 5× sample buffer: In a fume hood mix 1.25 mL of 0.5 M Tris–HCl, pH 6.8, 2.5 mL β-mercaptoethanol, 1 g SDS, 5 mL glycerol, and 10 μg/mL Pyronin-Y. Stir slowly to dissolve the SDS, and bring to 10 mL with water.

8. 10× stock electrode buffer: 0.25 M Tris and 1.92 M glycine, weighed very carefully, and combined. These amounts will generate the appropriate pH of 8.3. For a working solution, the stock is diluted tenfold and adjusted to a final concentration of 0.1% SDS using 5 mL of the 20% SDS stock **(Subheading 2.3, item 4** above**)** per liter of solution.
9. Staining and destaining solutions *(23)*: Fix and stain the gel in 25% isopropanol, 10% acetic acid, and 0.05% Coomassie blue; destain in 10% isopropanol, and 10% acetic acid.

2.4. Immunoblotting

1. Electrode buffer: tenfold dilution of the 10× electrode buffer stock noted in **Subheading 2.3**, **item 8**, with no further additions (*see* **Note 5**).
2. Nitrocellulose (NC) membrane (nylon supported NC is easier to handle than plain NC).
3. Sheets of Whatman 3MM filter paper, cut to the size of the blotting apparatus/gel.
4. Tris buffered saline (TBS), 10× stock: 250 mM Tris base, 1.5 M NaCl, adjusted to pH 7.4 with HCl.
5. TBS-T: TBS adjusted to 0.05% Tween-20 (500 μL TWEEN-20 per liter of TBS).
6. Blocking buffer: TBS plus 5% nonfat dry milk and 0.02% NaN_3.
7. Primary and secondary antibodies suitably diluted in blocking buffer. Secondary antibodies conjugated with peroxidase (*see* **Note 6**). For this purpose, we use horse radish peroxidase (HRP)-conjugated goat anti-rabbit or anti-mouse antibodies from Promega.
8. ECL reagents from GE Healthcare; X-ray film.

2.5. Immunofluorescence Microscopy

1. For processing several antibodies on a single slide, we use precleaned, PTFE printed ten well slides (Electron Microscopy Sciences catalog number 63424–06). These have wettable surfaces and minimize the use of expensive antibodies.
2. 0.1% polyethyleneimine (PEI) in water.
3. 10 mM HEPES, pH 7.4.

4. 10× PBS: To make 1 L of 10× phosphate buffered saline (PBS), dissolve 80 g NaCl, 2 g KCl, 14.4 g $Na_2HPO_4{\cdot}2H_2O$, and 2.4 g KH_2PO_4 in 800 mL water and bring to 1 L final volume (*see* **Note** 7).
5. Blocking buffer: 1× PBS containing 5% nonfat dry milk, 1 mg/mL BSA, and 10% goat serum.
6. 100% methanol, pre-chilled to –20°C.

2.6. Scanning Electron Microscopy

1. HMDEK, described above in **Subheading 2.2**, **item 5**.
2. Round glass coverslips (#1 thickness, 12 mm diameter; e.g., Bellco Glass catalog number 1943–10012).
3. Secondary antibodies labeled with colloidal gold (e.g., 12 nm gold from Jackson ImmunoResearch or 25 nm gold from Electron Microscopy Sciences).
4. Electron microscopy grade glutaraldehyde, purchased as an 8% stock in ampoules sealed under nitrogen, diluted to 1% with HMDEK just before use.

3. Methods

3.1. Growth and Maintenance of Cell Cultures

1. The main cell line stocks are maintained on agar slants (1% agarose in TAP) in screw cap tubes in an incubator at 18°C, provided with 14 h of light and ten of dark. Working plates are made from the stocks in Petri dishes containing 1% agarose in TAP and are maintained in a walk in incubator at 23°C. The incubator is also rigged to provide a light:dark cycle of 14:10. The fluorescent lamps for illumination are fixed beneath the shelf **(Fig. 1a)**. The working plates are made fresh every few weeks, whereas the stocks on slants are made fresh every 4–6 weeks (*see* **Note 8**).
2. Cells are grown in a liquid culture for a given experiment. To do this, starter flasks of 150 mL sterile TAP in 250 mL flasks are prepared. The flasks are closed with a foam plug through which is inserted a cotton plugged 5.75 in. Pasteur pipette (e.g., Fisher catalog # 13–678–8A), and the entire assembly (pipette, foam plug, and neck of the flask) is wrapped in aluminum foil and autoclaved. Using sterile technique, a loop of cells from a single colony growing on a TAP plate is suspended in the TAP of a starter flask, and then the flask is placed in the culture room and aerated with 0.5 μm filtered air **(Fig. 1b)**. The cells will begin growing and are ready for the use in a few days, at late log phase, when they are at a density of 10^6–10^7 cells/mL. Before proceeding further, it is a good idea

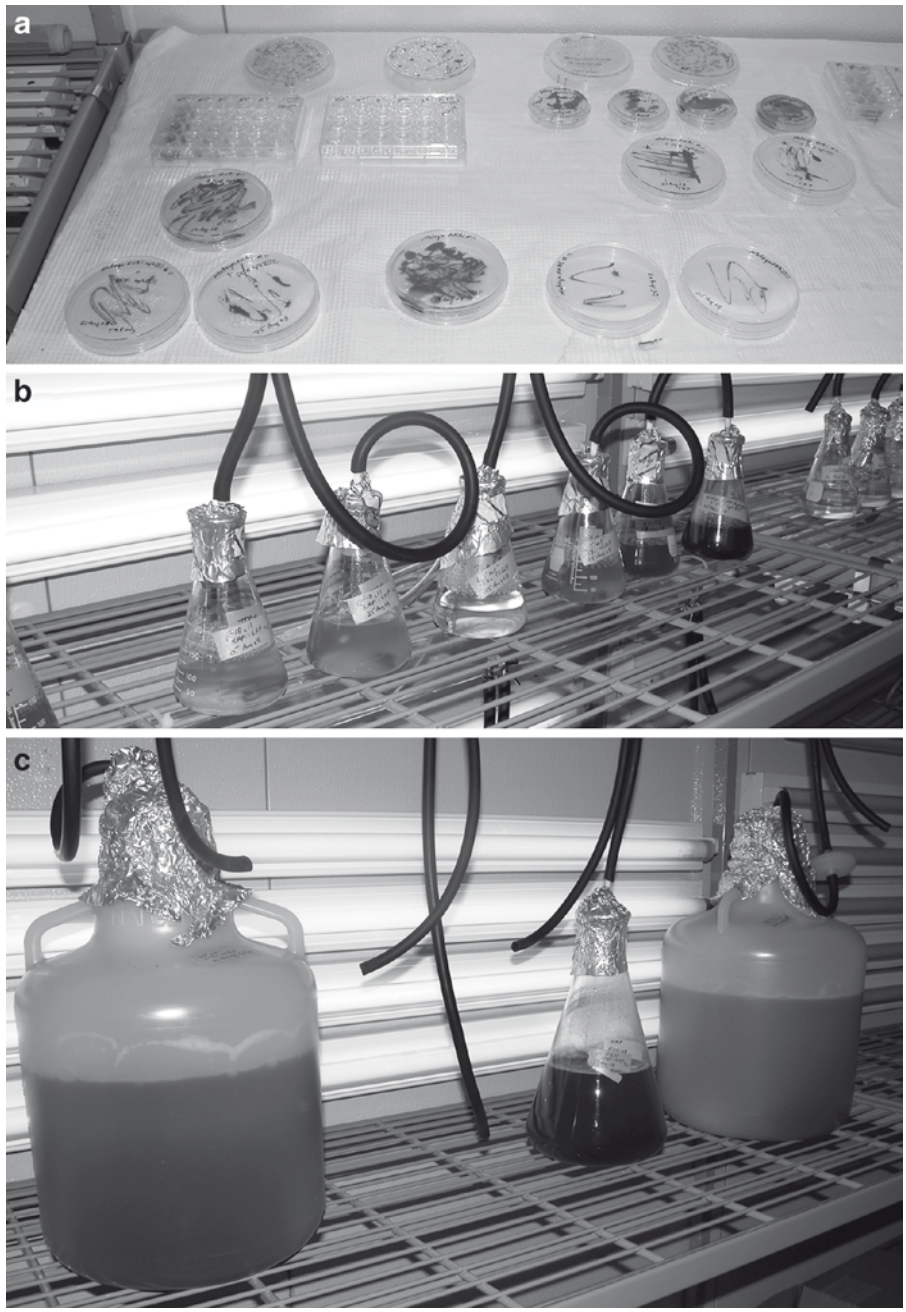

Fig. 1. Growing cultures of *Chlamydomonas*. (**a**) Cells growing on 1% agarose in TAP in large and small Petri dishes and in liquid TAP in 24 well microtiter plates (the latter used for analyzing RNAi strains). (**b**) Cells growing in starter flasks (125 mL). (**c**) Cells growing in two large carboys and a 3 L flask. The samples are illuminated from above in (**a**) and from the side in (**b**) and (**c**).

to check an aliquot of cells to ensure they are flagellated (the flagella – two per cell – should be 10–12 μm in length), and that the culture is free of microbial contamination.

3. For immunofluorescence, a single starter flask of cells is sufficient. However, for biochemical experiments, more flagella, and hence a greater volume of cells, are often required. In such cases, the starter flask is decanted into either (a) a 3 L flask containing 1.5 L of sterile TAP and a 9″″ cotton plugged Pasteur pipette, or (b) a 10 L Nalgene jug (e.g., United States Plastic Corporation, item # Item No.: 72021) containing 8 L of sterile TAP **(Fig. 1c)**. For the latter, aeration is provided by a sintered glass *(24)* dispersion tube (Ace Glass cat. # 7202–18). The fluorescent lights for the illumination of the liquid cultures (starter flasks and larger volumes) are fixed to the wall of the incubator **(Fig. 1b,c)**.

3.2. Flagellar Isolation and Fractionation

1. Collect cells from the culture vessel by centrifugation at 1,500 × *g* for 5 min and resuspend in 1/5 the original volume of HMDS and aerate in the incubator or on the bench top in a water bath at 23°C for an hour, with illumination provided by a low watt halogen desk lamp. Make one last check of the cells by phase microscopy to see that they are healthy: two full length flagella, actively swimming, and no contamination with microorganisms. Deflagellate the cells by pH shock *(25)*. To do this, stir the cells while monitoring pH, and rapidly drop the pH to 4.8 using 0.5 N acetic acid. Hold the cells at pH 4.8 for 60 s, and then rapidly return the pH to 7.5 using 0.5 N KOH. Be careful not to overshoot the pH in either direction. Check that the cells are deflagellated using a phase microscope.
2. Separate the cell bodies from the released flagella by centrifugation at 1,500 × *g* for 5 min, and remove the supernatant being careful to minimize contamination of it by the cell bodies in the relatively soft pellet. Centrifuge the supernatant at 12,000 × *g* for 10 min at 4°C, decant the supernatant, and resuspend the flagellar pellet in HMDS. Underlay the solution of flagella with HMDS in which the sucrose concentration is increased to 20%, and centrifuge in a swinging bucket rotor (Sorvall HB-4 or equivalent) at 1,500 × *g* for 5 min at 4°C. This will sediment any contaminating cell bodies into the sucrose cushion. Remove the supernatant containing the flagella, and collect the flagella again as mentioned above. Resuspend in HMDS. Check the flagella for cell body and/or debris contamination by phase or DIC microscopy and repeat the sucrose cushion centrifugation as needed to remove contaminating cell bodies and cell fragments. Two such steps are usually sufficient for small quantities of flagella (i.e., from 1 to

2 starter flasks), but more will be needed for larger volumes (i.e., from a 10 L jug). Adjust the final flagellar sample to 2 mM Pefabloc to block protease activity during subsequent steps.

3. For immunofluorescence of intact, isolated flagella, proceed from this point to **Subheading 3.5**. To continue with fractionation of the flagella into membrane–matrix (MM) and axoneme (Axo) fractions, and to purify IFT particle polypeptides, collect the isolated flagella as above and resuspend in a small volume (~1 mL) of HMDEK. Adjust the sample to 10 mM Mg-ATP and 0.1% NP40, and incubate at RT for 20–30 min with occasional gentle agitation. Centrifuge the sample at 12,000 × *g* for 15 min. The supernatant is the MM fraction and contains solubilized membrane proteins, soluble components of the flagellar matrix, IFT particles, and IFT motor proteins. The pellet contains the axoneme (9 + 2 structure) comprised of outer doublet microtubules, dynein arms, radial spokes, nexin links, and the central pair apparatus.

4. The paradigm for IFT particle isolation is the procedure developed by Cole et al. *(10)* and on which the following method is based. To purify IFT particle polypeptides, prepare a 10–30% sucrose gradient in HMDEK. We use tubes that fit a Beckman SW41Ti rotor for this purpose. The centrifuge tube has a volume of 12 mL; we prepare an 11 mL gradient and load ~1 mL of the MM fraction, described in **step 3** above, isolated from 16 to 32 L of cells. Centrifuge the gradient at 150,000 × *g* (ave) for 18 h at 4°C. We then use an Isco Model 185 density gradient fractionator (Teledyne Isco) to fractionate the gradient into 0.6–0.7 mL fractions. The IFT particle polypeptides will be found in the heavy end of the gradient, sedimenting at about 16 S (*see* **Note 9**). Two complexes of IFT particles have been identified *(10)* when the gradient is run at low ionic strength (10 mM HEPES, pH 7.4). These are IFT Complex A composed of five polypeptides sedimenting at 16.1–16.4 S and IFT Complex B, sedimenting at 15–16 S and composed of ~11–12 polypeptides *(11)*. As the ionic strength increases, Complex A and B will fractionate more closely together on the gradient *(10)*. Note that flagella with an elevated level of IFT particle polypeptides can be obtained from *fla2* cells, which, as reported initially by Cole et al. *(10)*, contain 2–3× as much Complex A and B as wild type flagella.

3.3. SDS Polyacrylamide Gel Electrophoresis (SDS-PAGE)

1. These instructions are designed for pouring and running two mini-gels in a Bio-Rad Mini Protean 3 gel apparatus. Component ratios can be easily adapted for gels of slightly different dimensions. To begin, scrub the glass plates (two per gel) with a good laboratory detergent, and then rinse well with tap

water, distilled water, and finally 70% ethanol. Our gel plates have affixed, 1.5 mm spacers; mount the plates in the pouring stand of the apparatus.

2. Prepare the separating gel (8%) by combining the following components in the order listed: 2.2 mL acrylamide stock, 1.0 mL 3 M Tris–HCl, pH 8.8, 5.0 mL water, 5 μL TEMED, and 50 μL 10% ammonium persulfate (*see* **Note 10**). Swirl to mix after each addition, and immediately pour the solution between the gel plates to a height roughly 1 cm below the top surface of the plates. The separating gel solution must fill the plates to a level that leaves room to cast a stacking gel of adequate length. For example, when the comb is inserted to make the wells in the stacking gel (*see* **Subheading 3.3**, **step 3**) the height of the stacking gel (i.e., the space between the bottom of the sample wells and the top of the separating gel) is at least equal to the depth of the sample well. This is required to provide the samples enough time in the stacking gel so that they stack effectively before entering the separating gel. Carefully overlay the separating gel solution with 0.1% SDS (*see* **Note 11**). The interface between gel and overlay solution will gradually 'disappear' and then reappear as a sharply defined interface when polymerization is complete (~45 min at RT).
3. Prepare the stacking gel solution as follows: 0.5 mL acrylamide stock, 1.25 mL 0.5 M Tris–HCl, pH 6.8, 3.2 mL water, 5 μL TEMED, and 25 μL 10% ammonium persulfate. When the separating gel has polymerized, pour off the overlay solution, and wick out the remainder by touching the edge of the gel plate sandwich with a paper towel. Rinse the top of the gel with a small amount of stacking gel solution, pour and wick this off, and then fill the space with fresh stacking gel solution. Insert a comb with the desired number of wells (10 or 15 for the Bio-Rad apparatus) into the stacking gel solution, and allow it to polymerize (~45 min at RT).
4. Meanwhile, prepare the samples as follows: Dilute each sample 1:1 if using 2× reducing solution, and 1:4 if using 5× reducing solution. The latter is preferable, especially for sucrose gradient samples, as these tend to be dilute. Mix well, and immediately boil the sample for 3 min in a boiling water bath (*see* **Note 12**).
5. To run the gel, prepare an adequate volume of 1× electrode buffer containing 0.1% SDS. Gently remove the combs from the gels, fill the spaces with electrode buffer, and shake out the buffer. Mount the gels in the apparatus, and add electrode buffer to the bottom and top compartments. Load the samples into the wells (*see* **Note 13**). Run the gels at a constant current; this is important to produce an effective and reproducible stack, and hence migration, using the Laemmli

buffer system (*see* **Note 14**). We run two gels at 20 ma for about 2.5–3 h or until the tracking dye is near the bottom of the gel. The ion front runs behind (i.e., more slowly) than the Pyronin Y tracking dye (not true of other dyes, such as bromophenol blue); the ion front will appear as a faint refractile line. Thus, the gel can be run until the dye has just run off the bottom of the gel to maximize the separation distance of the polypeptides in the sample. However, if the gel is to be immunoblotted, note that the Pyronin Y, if left in the gel, will transfer to the blot and mark the individual lanes of the gel, which can be helpful when analyzing the results of an immunoblot experiment (*see* **Subheading 3.4**).

6. If the gel is to be stained, remove the gel plates from the apparatus and carefully pry them apart with the plastic instrument provided. The gel will stick to one glass plate or the other. It can be carefully picked up by the bottom corners to remove it from the plate. Alternatively, place the plate with the gel in a clean container (we use plastic storage boxes from K-Mart) and cover with stain. Slight rocking will dislodge the gel from the plate, and the latter can be removed. Stain the gel overnight with gentle rocking at RT, and in the morning replace the gel stain with destain solution (several changes). The destained gel is then photographed for documentation; it can also be stored almost indefinitely in destain or distilled water.

3.4. Immunoblotting and Immunodetection

1. The Bio-Rad Mini Protean 3 apparatus used above for SDS-PAGE can also be rigged for immunoblotting, and this is the apparatus described here. Near the end of the gel run, set up the blotting sandwich. Use a clean Pyrex baking dish in which the plastic sandwich can be opened and lay flat. Prepare 1 L of 1× electrode buffer (*no* SDS). Cut a piece of nitrocellulose (NC) paper slightly larger than the gel area to be blotted. Wet this in water with shaking for 10 min, and then in electrode buffer for 10 min. Place one of the ScotchBrite pads (provided with the apparatus) on one side of the plastic sandwich, followed by three sheets of Whatman 3MM paper. Pour enough electrode buffer into the dish to cover the pads and paper.
2. Remove the gel and separate the plates as described above. The easiest way to place the gel against the nitrocellulose is as follows: As mentioned above (*see* **Subheading 3.3**, **step 6**) the gel will adhere to one or the other of the glass plates. Lay this down on the bench, gel side up. Using a razor blade, carefully scrape away the stacking gel. Then lay one of the wetted pieces of 3MM paper on the gel, turn the plate upside down, and carefully, using the tip of a weighing spatula, tease a corner of the gel away from plate. Gravity will eventually

take hold and the gel with the 3MM paper adhering to it will peel off into your hand. Place the 3MM paper, gel side up, on top of the other two pieces of 3MM paper in the Pyrex dish. Cover the gel with the wetted NC paper, and use a gloved finger or a 5.75 in." Pasteur pipette to roll out any bubbles that are between the NC and the gel. It is essential that there are no bubbles between the NC and the gel otherwise the transfer will not occur in the region contaminated by bubbles. Cover the NC with three pieces of 3MM paper previously soaked in electrode buffer, followed by the second piece of Scotch-Brite pad. Close the gel sandwich and, if one is provided, slide the plastic lock closed to hold it together. Fill the reservoir of the apparatus with electrode buffer, and insert the sandwich, being careful to place it in the apparatus with the NC side facing the positive electrode (red, anode).

3. It is important to mark the NC relative to the gel so that the position of the lanes, and hence the samples, can be determined. One way to do this is to cut off a small piece of the bottom corner of the gel where lane #1 is, and then make a corresponding cut in the corner of the NC. If prestained gel standards are used and always loaded on the gel asymmetrically (i.e., to one side or another), their position on the NC will server as a reference point for the identification of the relative positions of the other sample lanes of the gel.
4. Run the blot either in the cold room or, if available, insert into the buffer chamber a block of ice cast in the plastic holder that comes with the apparatus. Run the blot at 340 ma (or at 12 V/cm, measuring the distance between the electrodes of the apparatus) for 60 min. After 60 min, disassemble the sandwich, peel off the NC, and place it, protein side up, in blocking buffer and rock for an hour at RT or overnight at 4°C.
5. Prepare a suitable dilution of primary antibody in blocking buffer. Remove the blocking buffer from the gel and add the primary antibody. Incubate with rocking at RT, 1–4 h, depending on the relative affinity of the antibody being used. Remove the antibody solution and save it at 4°C. Depending on the initial dilution, it can be used many times over the next few months.
6. Wash the blot by immersion in TBS-T, with rapid agitation, three times, 5 min each. Discard the last wash and add secondary antibody diluted in blocking buffer (usually 1:15,000 or 1:20,000, depending on the vendor). Incubate with rocking 30–60 min.

7. Wash the blot by immersion in TBS-T, with rapid agitation, four times, 10–15 min each. Discard the last wash and drain the bulk of the wash buffer off of the blot. Add ECL reagent according to the manufacturer's instructions; the surface area of the blot being treated determines the amount. Rock this solution by hand over the blot for 5 min to ensure that the blot is equally covered and saturated with ECL solution.
8. Remove the blot and press it by hand between two paper towels to remove excess ECL reagent. Mount the blot either between the leaves of an acetate sheet protector, or wrap it in one layer of clear plastic food wrap, avoiding wrinkles in the plastic wrap on the side of the NC to which the proteins were blotted and to which the film will be exposed.
9. Working in the darkroom with 8 × 10 X-Ray film and an X-ray film cassette to hold the blot and film, expose different regions of a single sheet of the film to the blot for varying times (e.g., 5 s, 10 s 30 s, 1 min). This allows one film to contain multiple exposures and decreases film and processing costs. Based on these initial test exposures, re-expose the blot a second time, if necessary, to generate a blot of adequate exposure and background.
10. Finally, be sure to place the exposed film over the blot and, using a Sharpie pen, mark the positions of the corners of the gel, the standards, gel lanes, etc.

3.5. Immunofluorescence

1. The following procedure (based on the work of Pedersen et al. *(26)*) can be used with whole cells, isolated flagella, or axonemes. Prepare a ten well slide fresh for each experiment as follows. Fill each well with 50 μL of 0.1% polyethyleneimine and allow to sit for 5 min at RT. Using an aspirator or other suitable device (e.g., a Pasteur pipette) withdraw the PEI solution, and wash the wells three times with water by alternately adding water to the wells and removing it with the aspirator. Air dry the slide in a covered Petri dish to prevent dust and other such particles settling on the slide.
2. Place the sample of cells, flagella, or axonemes in a microfuge tube and sediment at top speed for 3 min. Using an autopipettor whose plastic tip has been cut off with a razor to widen the bore, gently resuspend the sample in 100 μL 10 mM HEPES, pH 7.4. Add 1.1 mL of 100% methanol pre-chilled to −20°C, and incubate the sample at −20°C for 20 min.
3. Collect the sample as above, and gently resuspend in PBS. Place the resuspended sample(s) in the wells of the PEI coated slide and allow to adhere for ten min at RT.

4. Without removing the samples, immerse the slide in a Coplin jar filled with methanol at –20°C. Incubate at –20°C for 10 min.
5. Remove the slide from the methanol and air dry. Rehydrate the wells with PBS, 10 min, and repeat once with fresh PBS.
6. Block the wells with immunofluorescence blocking buffer for 1 h at RT.
7. Add 20–40 μL of primary antibody at an appropriate dilution, in blocking buffer, to each sample well and incubate the slide overnight at 4°C in a covered Petri dish. Line the inside of the dish with moist filter paper or paper towel to maintain a humid environment to prevent the sample from drying out.
8. Wash the wells 3× with PBS, allowing a few minutes between each change of PBS.
9. Add second antibody diluted in blocking buffer, and incubate 1–2 h at RT.
10. Wash the wells 3× with PBS, allowing a few minutes between each change. Remove the last wash solution and add a drop of antifade reagent to each well to stabilize the fluorescent signal to photobleaching during observation. We use Prolong (Molecular Probes) as an antifade reagent, supplied premixed in 2 mL aliquots in dropper bottles. Cover the slide with a coverslip.
11. Allow the slide to sit in the dark overnight, and then seal the edges to prevent drying prior to observation with fluorescence microscopy optics. We seal the edges with clear nail polish. For observation, a high numerical aperture low magnification objective is required. This is because the fluorescence intensity projected to the image plane of the detector varies directly with numerical aperture and inversely with total magnification. Suitable objectives are 63×/1.4 NA (Zeiss, Leica) or 60×/1.4NA (Nikon, Olympus). IFT particles will appear punctate when detected via immunofluorescence in this manner (*see* **Figs. 2a,b**), while tubulin antibodies will stain the flagellar along their entire length **(Fig. 2c)**.

3.6. Immunogold Scanning Electron Microscopy

1. These procedures describe immunolocalization performed on isolated axonemes at the limit of resolution afforded by the scanning electron microscope (SEM) *(19)*. The instrument we use is an FEI XL-30 field emission gun scanning electron microscope. It is operated at 15 kV with the spot size set at three; this generates a scan probe having a beam diameter of 1.7 nm *(19)*. For biological specimens of the type described here, the resolution is ~5 nm.
2. Collect the flagellar axonemes at 12,000 × *g* for 15 min and resuspend in a small volume of HMDEK. Divide into 50–100 μL

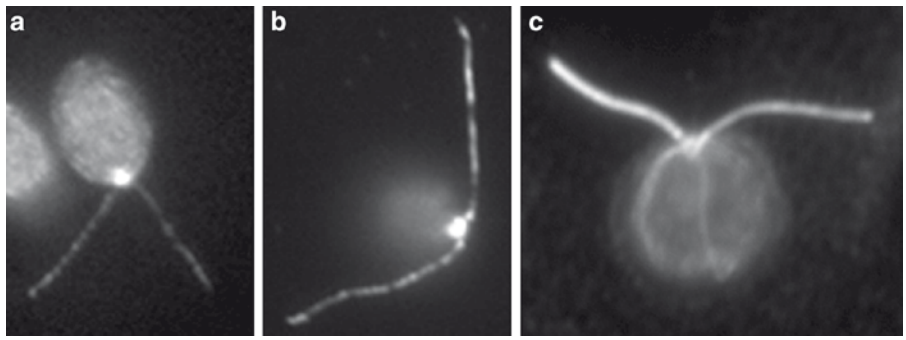

Fig. 2. Immunofluorescence localization of IFT particle polypeptides in *Chlamydomonas* flagella. (**a**) IFT 139, an IFT complex A polypeptide. (**b**) IFT172, a complex B polypeptide. The staining along the flagella is punctate, indicating the particles were present dispersed along the flagella in discrete units at the time of fixation. Staining with tubulin antibody, by contrast, labels the flagella continuously (**c**).

aliquots in microfuge tubes, one aliquot for each primary antibody being assayed.

3. Add primary antibody to the aliquots of sample to achieve an appropriate final dilution of antibody and incubate at RT for 2 h.
4. Collect the axonemes in a swinging bucket rotor (e.g., Sorvall HB-4) at 12,000 × *g* for 15 min, resuspend in HMDEK. Repeat this step once to remove any antibodies non-specifically trapped in the pellet.
5. Add diluted secondary antibodies labeled with colloidal gold (10 and/or 25 nm) and incubate at RT for 2 h.
6. Collect the axonemes in a swinging bucket rotor (e.g., Sorvall HB-4) at 12,000 × *g* for 15 min, resuspend in HMDEK, and repeat twice for a total of three washes.
7. Place the samples on round, 12 mm diameter glass coverslips previously coated with 0.1% PEI as described above in **Subheading 3.5**, **step 1**. Allow the samples to adhere for 10 min at RT.
8. Fix the samples by immersing the coverslips in 1% glutaraldehyde in HMDEK in a small Petri dish. Incubate at 4°C overnight.
9. Critical point dry the samples (we use a Samdri 795 for this purpose) and coat them with 2–3 nm of osmium using an SPI plasma coater. During the coating process, the osmium molecules form a plasma resulting in a metal coat that is almost perfectly amorphous. The grain size of the osmium coating is about the same as the osmium atoms, and thus is well below the 5 nm resolution limit noted above. The result is a stabilizing coat of metal that does not preclude the detection of the gold label on the antibodies.
10. For clear detection of the gold particles, and hence the distribution of the antigen(s) in the sample, operate the SEM to

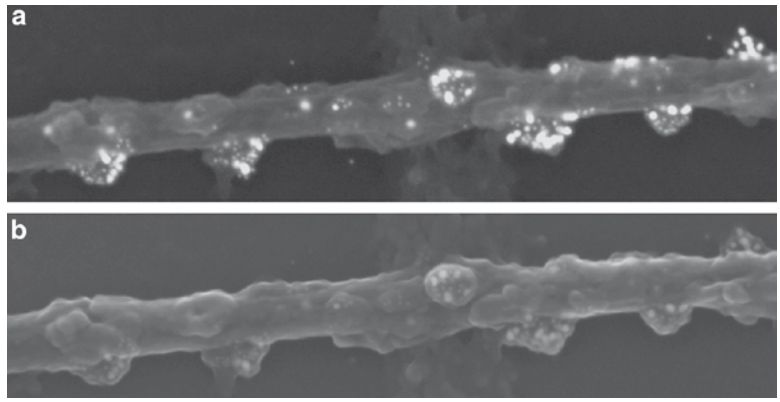

Fig. 3. Localization of IFT particle polypeptides by double label immunogold scanning electron microscopy. 12 nm gold identifies the IFT particle protein IFT139, and 25 nm gold identifies the motor enzyme kinesin-2 which powers anterograde (i.e., base to tip) IFT. A. Image generated by backscattered electrons clearly showing the two sizes of gold particles (white, 12 nm and 25 nm average diameter) on a relatively dark background. The gold particles are localized to the spherical structures (IFT particles) while the underlying microtubule containing axoneme is free of label. B. Conventional scanning electron microscope image (generated by secondary electrons) of the same field shown in (**a**). These images are reproduced, with permission, from **Fig. 4** in **ref.*(19)***, published by Wiley-Liss, Inc.

detect backscattered electrons (**Fig. 3a**). For a conventional three dimensional view of the sample, operate the scanning electron microscope to detect secondary electrons (i.e., conventional SEM, **Fig. 3b**).

4. Notes

1. Readers should estimate how much TAP they might expect to use over the course of a few months, and prepare the trace metal solution accordingly (1 L of stock trace metal solution will yield 1,000 L of TAP). One web site <http://149.152.32.229/~mikeadams/ growthmedium.html> suggests simply borrowing some trace elements solution from a colleague!
2. Do *not* use NaOH to adjust the pH of the trace metals stock solution, and be sure to standardize the pH meter at 70°C as well.
3. It has been reported that the time it takes for the solution to turn purple can be shortened by bubbling with filtered air, but I have never done this.
4. Pefabloc is 4-(2-Aminoethyl) benzenesulfonyl fluoride hydrochloride.

5. We use neither SDS nor methanol in the electrode buffer for immunoblotting with no negative consequences. A positive consequence of the lack of methanol is that special disposal procedures and the associated costs are avoided.
6. NaN_3 (sodium azide) is used to inhibit bacterial growth in the protein laden blocking buffer. NaN_3 may be present in many commercial antibody preparations for the same reason. Note that NaN_3 will also inhibit the action of peroxidase, and this enzyme is often linked to the secondary antibody whose activity is required for detection by ECL. Normally, the TBS-T washes of the blot prior to ECL detection remove the residual NaN_3 from the blocking buffer and antibody solutions. Thus, the TBS and TBS-T solutions should never contain NaN_3.
7. The pH of 10x PBS will be ~6.8–6.9, but will adjust to the working pH of 7.4 upon tenfold dilution.
8. The reason to keep the working cultures of cells separate from the cell stocks on slants is that only lab folks *highly* experienced with sterile technique are allowed to handle the slant cultures, thus protecting them from contamination by inexperienced lab personnel.
9. In a gradient producing 17 fractions (~0.6–0.7 mL each), IFT particles will be found in fractions 14–16 *(27)*.
10. SDS is not required in either the separating gel or stacking gel solutions *(22)*, but SDS is required in the electrode buffer **(Subheading 3.3, step 5)** for electrophoresis (but not in the buffer used for immunoblotting, *see* **Note 5**). Adding SDS to the gel solutions merely increases the chances that bubbles will form when the solutions are poured between the glass plates.
11. Other procedures recommend overlaying the separating gel with water-saturated isobutanol. Isobutanol, however, etches the plastic components of many gel apparatuses. We have found 0.1% SDS works just as well and easily and does not react with the plastic of the gel apparatus.
12. Never leave a gel sample on the top of the bench without boiling. SDS denatures most proteins to the random coil configuration exposing the peptide bonds to contaminating protease activity (some proteases are active in SDS concentrations even higher than those in the sample buffer). Boiling, however, in the presence of SDS and reducing agent denatures all protein in the sample.
13. Depending on your preference, samples can also be loaded into the wells before the electrode buffer is added to the upper chamber. In either case, the glycerol in the sample buffer increases sample density sufficiently to prevent the

mixing of the sample and the electrode buffer during either sample application approach.

14. The opposite is true of those pre-cast gels that do not contain a separate stacking gel and thus do not have a discontinuous pH. Run these gels at constant voltage according to the manufacturer's instructions.

Acknowledgments

Work in the author's lab is supported by the NSF (MCB 0418877) and the NIH (DK 071720). This support is greatly appreciated.

References

1. R.D. Sloboda, and J.L. Rosenbaum (2007). Making sense of cilia and flagella. J Cell Biol 179 575–582
2. K.G. Kozminski, K.A. Johnson, P. Forscher, and J.L. Rosenbaum (1993). A motility in the eukaryotic flagellum unrelated to flagellar beating. Proc Natl Acad Sci U S A 90 5519–5523
3. K.G. Kozminski, P.L. Beech, and J.L. Rosenbaum (1995). The *Chlamydomonas* kinesin-like protein FLA10 is involved in motility associated with flagellar membrane. J Cell Biol 131 1517–1527
4. K.G. Kozminski (1995). High-resolution imaging of flagella. Methods Cell Biol 47 263–271
5. J. Mueller, C.A. Perrone, R. Bower, D.G. Cole, and M.E. Porter (2005). The FLA3 KAP subunit is required for localization of kinesin-2 to the site of flagellar assembly and processive anterograde intraflagellar transport. Mol Biol Cell 16 1341–1354
6. G.J. Pazour, B.L. Dickert, and G.B. Witman (1999). The DHC1b (DHC2) isoform of cytoplasmic dynein is required for flagellar assembly. J Cell Biol 144 473–481
7. M.E. Porter, R. Bower, J.A. Knott, P. Byrd, and W. Dentler (1999). Cytoplasmic dynein heavy chain 1b is required for flagellar assembly in *Chlamydomonas*. Mol Biol Cell 10 693–712
8. D. Signor, K.P. Wedaman, J.T. Orozco, N.D. Dwyer, C.I. Bargmann, L.S. Rose, and J.M. Scholey (1999). Role of a class DHC1b dynein in retrograde transport of IFT motors and IFT raft particles along cilia, but not dendrites, in chemosensory neurons of living *Caenorhabditis elegans*. J Cell Biol 147 519–530
9. Z. Walther, M. Vashishtha, and J.L. Hall (1994). The *Chlamydomonas* FLA10 gene encodes a novel kinesin-homologous protein. J Cell Biol 126 175–188
10. D.G. Cole, D.R. Diener, A.L. Himelblau, P.L. Beech, J.C. Fuster, and J.L. Rosenbaum (1998). *Chlamydomonas* kinesin-II-dependent intraflagellar transport (IFT): IFT particles contain proteins required for ciliary assembly in *Caenorhabditis elegans* sensory neurons. J Cell Biol 141 993–1008
11. D.G. Cole (2003). The intraflagellar transport machinery of *Chlamydomonas reinhardtii*. Traffic 4 435–442
12. K.A. Johnson, and J.L. Rosenbaum (1992). Polarity of flagellar assembly in *Chlamydomonas*. J Cell Biol 119 1605–1611
13. W.L. Dentler, and J.L. Rosenbaum (1977). Flagellar elongation and shortening in *Chlamydomonas*. III. Structures attached to the tips of flagellar microtubules and their relationship to the directionality of flagellar microtubule assembly. J Cell Biol 74 747–759
14. W.L. Dentler (1980). Structures linking the tips of ciliary and flagellar microtubules to the membrane. J Cell Sci 42 207–220

15. W.S. Sale, and P. Satir (1977). The termination of the central microtubules from the cilia of *Tetrahymena pyriformis*. Cell Biol Int Rep 1 56–63
16. D.S. Gorman, and R.P. Levine (1965). Cytochrome f and plastocyanin: their sequence in the photosynthetic electron transport chain of *Chlamydomonas reinhardi*. Proc Natl Acad Sci U S A 54 1665–1669
17. S.H. Hutner, L. Provasoli, Albert Schatz, and C. P. Haskins (1950). Some approaches to the study of the role of metals in the metabolism of microorganisms. Proc Am Philos Soc 94 152–170
18. S. Surzycki (1971). Synchronously Grown Cultures of *Chlamydomonas reinhardi*. Meth Enzymol 23 67–84
19. R.D. Sloboda, and L. Howard (2007). Localization of EB1, IFT polypeptides, and kinesin-2 in *Chlamydomonas* flagellar axonemes via immunogold scanning electron microscopy. Cell Motil Cytoskeleton 64 446–460
20. U.K. Laemmli (1970). Cleavage of structural proteins during the assembly of the head of bacteriophage T4. Nature 227 680–685
21. D. Best, P.J. Warr, and K. Gull (1981). Influence of the composition of commercial sodium dodecyl sulfate preparations on the separation of alpha- and beta-tubulin during polyacrylamide gel electrophoresis. Anal Biochem 114 281–284
22. R.E. Stephens (1998). Electrophoretic resolution of tubulin and tektin subunits by differential interaction with long-chain alkyl sulfates. Anal Biochem 265 356–360
23. G. Fairbanks, T.L. Steck, and D.F. Wallach (1971). Electrophoretic analysis of the major polypeptides of the human erythrocyte membrane. Biochemistry 10 2606–2617
24. G.E. Hunt (1947). A technique for aeration of sterile liquid culture medium. Science 105 184
25. G.B. Witman, K. Carlson, J. Berliner, and J.L. Rosenbaum (1972). *Chlamydomonas* flagella. I. Isolation and electrophoretic analysis of microtubules, matrix, membranes, and mastigonemes. J Cell Biol 54 507–539
26. L.B. Pedersen, S. Geimer, R.D. Sloboda, and J.L. Rosenbaum (2003). The Microtubule plus end-tracking protein EB1 is localized to the flagellar tip and basal bodies in *Chlamydomonas reinhardtii*. Curr Biol 13 1969–1974
27. M.J. Schneider, M. Ulland, and R.D. Sloboda (2008). A protein methylation pathway in *Chlamydomonas* flagella is active during flagellar resorption. Mol Biol Cell 10 4319–4327

Chapter 12

High Pressure Freezing, Electron Microscopy, and Immuno-Electron Microscopy of *Tetrahymena thermophila* Basal Bodies

Janet B. Meehl, Thomas H. Giddings, Jr., and Mark Winey

Summary

Preservation of *Tetrahymena thermophila* basal body ultrastructure for visualization by transmission electron microscopy is improved by a combination of high pressure freezing (HPF) and freeze substitution (FS). These methods also reliably retain the antigenicity of cellular proteins for immuno-electron microscopy, which enables the precise localization of green fluorescent protein (GFP)-tagged and native basal body proteins. The plastic-embedded samples generated by these methods take full advantage of higher resolution visualization techniques such as electron tomography. We describe protocols for cryofixation, FS, immunolabeling, and staining. Suggestions for trouble shooting and evaluation of specimen quality are discussed. In combination with identification and manipulation of a rapidly expanding list of basal body-associated gene products, these methods are being used to increase our understanding of basal body composition, assembly, and function.

Key words: *Tetrahymena thermophila*, High pressure freezing, Freeze substitution, Electron microscopy, Immuno-electron microscopy, Electron tomography

1. Introduction

Over the years, many ultrastructural studies have been carried out to describe the fine structure of basal bodies and cilia of *Tetrahymena* and other ciliates. The best chemical fixation protocols have established a high standard for preserving ultrastructure in *Tetrahymena*, and the architecture of the basal bodies and other organelles of the cell cortex has been resolved in fine detail *(1, 2)*. More recently, renewed attention has been focused on these and other highly reiterated organelles in *Tetrahymena* due to the development of sophisticated molecular analytical techniques

R.H. Gavin (ed.), *Cytoskeleton Methods and Protocols,* Methods in Molecular Biology, vol. 586
DOI 10.1007/978-1-60761-376-3_12,
© Humana Press, a part of Springer Science + Business Media, LLC 2009

(3–5) and the complete sequencing of the genome *(6)*. These advances have improved our ability to investigate basal body structure and assembly at the molecular level *(7, 8)*. In this study, we explore the use of cryofixation by high pressure freezing (HPF) followed by freeze substitution (FS) to improve general basal body ultrastructure for immuno-electron microscopy and electron tomography. By manipulating the many variables in this process, we have developed a combination of conditions capable of producing excellent preservation of ultrastructure and antigenicity **(Figs. 1, 2)**.

HPF has the advantage of arresting cellular processes in milliseconds. The combination of high pressure with rapid freezing prevents the formation of large, damaging ice crystals and instead favors the formation of vitreous ice *(9)*. The cooling rates required to achieve vitrification at high pressures are not as great as those required for ambient pressure methods such as plunge freezing *(10)*; thus, biological samples that are relatively poor thermal conductors, such as large cells or small pieces of plant or animal tissue, can be cryofixed without the formation of damaging ice crystals. Subsequent freeze substitution allows the water to be dissolved out of the cells and be replaced by a solvent/fixative mixture. The fixatives included in the substitution medium serve to stabilize macromolecular structures within the cell; some also act as stains to improve contrast *(11)*. Chemical fixation preserves biological material by infiltrating chemical fixatives into cells via diffusion. This process can take seconds to several minutes, and possibly longer if the cells contain nonpermeable walls, to immobilize cellular contents. During this time, artifacts may be introduced to the cells due to asynchronous fixation of the cytoplasm, repositioning and shape changes, and the failure to stabilize some constituents of the cytoplasm.

One of the challenges with using conventional chemical fixation for immuno-electron microscopy is preserving cell morphology while maintaining antigenicity. HPF, gentle freeze substitution fixation, and embedding in Lowicryl HM20 resin make it possible to achieve superb ultrastructure while retaining antigenicity. In combination with a green fluorescent protein (GFP) tagging system, freeze-substituted samples can be used to localize basal body proteins to very specific areas within the basal body *(5)*. Alternatively, antibodies can be raised to selected peptide sequences to localize native proteins of interest *(7*, **Fig. 2)**. These high resolution localization data are useful in elucidating the functional roles of these proteins in assembly and maintenance of basal bodies.

Tetrahymena basal bodies are excellent candidates for electron tomography. Resolutions of 5–8 nm in three dimensions can be obtained using a properly configured transmission electron microscope and a software package developed by the Boulder

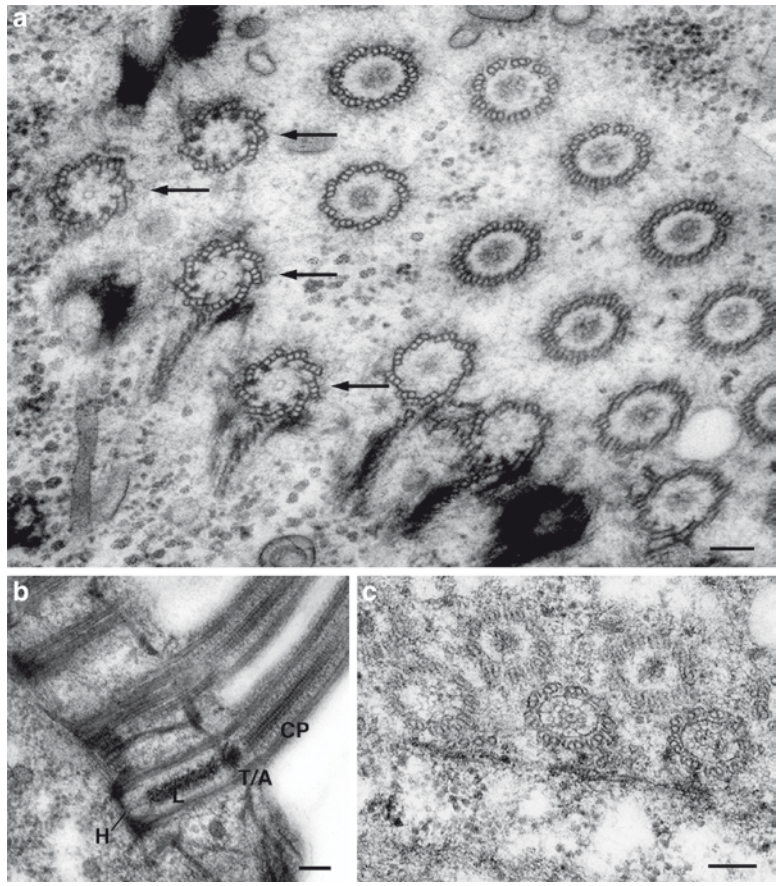

Fig. 1. Electron micrographs of well-preserved basal bodies in *Tetrahymena* oral apparatus. (**a**) The cartwheel and hub structures of the proximal region of the basal body are visible in several of the basal bodies (*arrows*). Cells were frozen in 15% dextran (9–11 kDa)/5% BSA in 10 mM Tris/HCl, freeze-substituted in 2%OsO_4/0.1%UA, and embedded in Epon resin. Bar = 0.1 μm. (**b**) A longitudinal section through basal bodies with attached cilia. The hub (H) is visible at the proximal end of the basal body. Distal to the hub is the electron dense lumen (L), the transition zone/axosome (T/A), and central pair (CP) of microtubules that extend into the cilium. Note the subunit periodicity in the central pairs. Bar = 0.1 μm. (**c**) The delicate structure of the transition zone is preserved in this cross section. Cells from (b) and (c) were frozen in 18% dextran (9–11 kDa) in 10 mM Tris/HCl, freeze-substituted in 0.25%GA/0.1%UA, and embedded in Lowicryl HM20 resin. Bar = 0.1 μm.

Laboratory for 3D-Electron Microscopy of Cells, located at the University of Colorado, Boulder *(12, 13)*. At this level of resolution, it is critical that the specimens be as well preserved as possible. Databases of wild type basal bodies can be collected and used for structural analysis as well as for comparisons with basal body mutants. Tomography is beyond the scope of this chapter, but more information is available at the following website (http://bio3d.colorado.edu/) *(14)*.

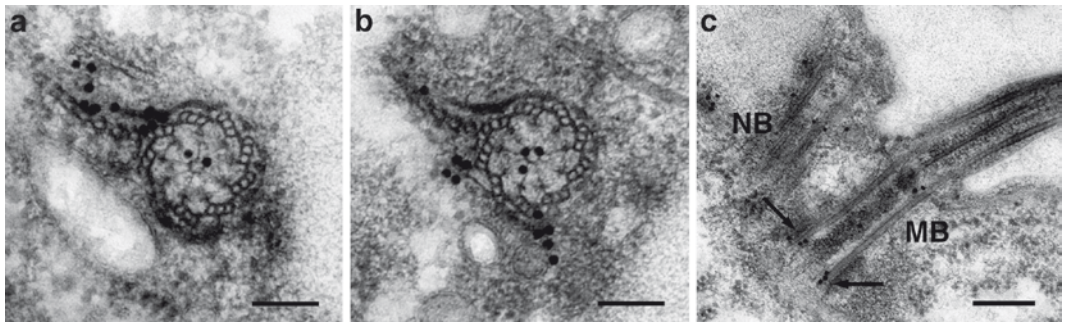

Fig. 2. Immuno-electron microscopy of *Tetrahymena* labeled with an antibody that recognizes SAS6a, a known cartwheel component in *Chlamydomonas* and other organisms *(21)*. (**a**) and (**b**) Cross sections through the cartwheel region of two basal bodies. Bar = 0.1 μm. (**c**) A longitudinal section through a mature basal body (MB) and a newly formed basal body (NB) migrating away from the mother. *Arrows* indicate gold particles localized at the proximal end of the basal body. Cells were frozen in 15% dextran (9–11 kDa)/5% BSA in 10 mM Tris/HCl, freeze-substituted in 0.25%GA/0.1%UA, and embedded in Lowicryl HM20 resin. Bar = 0.2 μm.

Here, we describe a HPF/freeze substitution protocol that we have developed for electron microscopy studies of the basal bodies and other organelles of *Tetrahymena*. We will discuss how to evaluate the quality of specimen preservation and solve some of the problems that may arise with HPF/freeze substitution. Our protocol for immunolabeling GFP-tagged basal body proteins in *Tetrahymena* is also presented.

2. Materials

2.1. Cell Culture

1. Culture medium:
   2% proteose peptone, 0.1% yeast extract, 0.2% glucose, 0.003% ferric EDTA. Supplement with Antibiotic/Antimycotic mix (concentrations are final concentrations in the media): 100 U/ml penicillin, 100 μg/ml streptomycin, 0.25 μg/ml amphotericin B (fungizone).
2. B2086 *Tetrahymena* wild type cells grown overnight at 30°C to a cell density of 2×10^5 cells/ml.
3. Cells expressing GFP-tagged proteins:
   Cells are generated by biolistic transformation of B2086 *(15)* using linearized plasmid pBSMTTGFP-SAS6a (or other plasmid containing a GFP-tagged protein). Selected cells are induced using 500 ng/ml $CdCl_2$ in 2%SPP media supplemented with 15 μg/ml cyclohexamide.

2.2. High Pressure Freezing

1. BAL-TEC HPM-010 (Technotrade International, Manchester, NH).
2. Hexadecene (Sigma), use undiluted.
3. High pressure freezer hats (Technotrade International).
4. Liquid nitrogen (LN_2).

2.3. Cryoprotectant

1×: 15% dextran (9–11 kDa, Sigma)/5% bovine serum albumin (BSA) in 10 mM Tris/HCl pH 7.5, 2×: 30% dextran (9–11 kDa, Sigma)/10% BSA in 2% SPP (or other appropriate *Tetrahymena* growth media).

2.4. Freeze Substitution

1. 100% anhydrous acetone (EM grade, EM Sciences).
2. 5% uranyl acetate (UA) in methanol (MeOH) stock, store at –20°C, UA must be handled and disposed of as a radioactive chemical.
3. 10% glutaraldehyde (GA) in acetone (EM Sciences), GA is toxic, work in hood, requires proper disposal as hazardous waste.
4. Crystalline osmium tetroxide (OsO_4) (EM Sciences), harmful, highly oxidizing and highly toxic, use extreme caution and always work in hood, requires proper disposal as hazardous waste.
5. FS media for Lowicryl HM20 embedding: 0.25% GA/0.1% UA in 100% acetone, aliquot 1 ml/cryovial, store in LN_2.
6. FS media for Epon embedding: 2% OsO_4/0.1% UA in 100% acetone, aliquot 1 ml/cryovial, store in LN_2.
7. Metal block with drilled holes to accommodate cryovials, or lead shot to surround cryovials.
8. 1.5 ml cryovials, internally threaded.
9. Styrofoam box.
10. Dry ice.
11. Glass slide with concave well.
12. Forceps, both fine and blunt tips.
13. Dissecting needle.
14. Dissecting microscope.
15. Plastic one piece pipettes (EM Sciences).

2.5. Embedding

1. Lowicryl HM20 resin (EM Sciences) – make according to kit directions, can be stored at –20°C for a month. If not using a LN_2-based AFS (automatic freeze substitution) system, mixing the components by bubbling with nitrogen is recommended.

2. Epon Araldite (EM Sciences) – make according to kit directions, using medium hardness recipe. Epon without accelerator can be used for a few weeks but after accelerator is added, use immediately.
3. 100% anhydrous acetone.
4. BEEM capsules and holder (EM Sciences).
5. UV polymerization chamber.
6. Polymerization oven.

Use caution and a hood when working with all resins; the components are toxic. The resins as well as anything that has come in contact with them are considered hazardous waste.

2.6. Sectioning

1. Ultramicrotome.
2. Diamond knife.
3. Formvar-coated slot grids – copper, nickel.
4. Contact cement (DAP Weldwood Cement), diluted with toluene to a medium yellow color, approximately 1:10.
5. No. 5 forceps.

2.7. Immunolabeling

1. PBST (phosphate-buffered saline with Tween 20): 10 mM sodium phosphate pH 7.2, 150 mM sodium chloride, 0.1% Tween 20.
2. Blocking solution: 1% nonfat dry milk in PBST.
3. Primary antibody: rabbit polyclonal anti-GFP diluted in blocking solution (*see* **Note 1**). Secondary: goat-anti-rabbit conjugated to 10 or 15 nm gold (Ted Pella, Inc.) diluted 1:20 in blocking solution.

2.8. Poststaining

1. 2% UA in water or 2% UA in 70% MeOH, limit exposure to light by storing in a dark container in a drawer, stain is stable for 3–6 months at room temperature. As mentioned above, UA is handled and disposed of as a radioactive chemical.
2. Reynold's lead citrate:
   a) Boil 100 ml distilled water (use for the lead solution and the NaOH).
   b) Add and mix the following components in a 50 ml volumetric flask: 1.33 g lead nitrate, 1.76 g sodium citrate, 30 ml boiled distilled water.
   c) Shake vigorously for 1 min. Place in a sonicator with occasional swirling for 20 min. The mixture should form a chalky white precipitate.
   d) In a graduated cylinder, make 1N NaOH (if the boiled water is still warm, it can come to a boil as the NaOH dissolves, use caution): 1 g sodium hydroxide (NaOH), add boiled distilled water to 25 ml final volume.

e) Add 8 ml of the 1N NaOH to the volumetric flask containing the lead nitrate and sodium citrate, swirl in sonicator bath until all precipitate is dissolved and the solution is clear.

f) Add boiled distilled water to 50 ml line of volumetric flask.

g) Store at room temperature in an airtight plastic bottle to limit exposure to air. The stain is normally stable for a few months. Lead components are toxic, handle with caution, and dispose of as a hazardous waste.

3. Methods

3.1. High Pressure Freezing

1. Prepare the cryoprotectant solution (*see* **Note 2**).

2a. Centrifuge 10 ml culture at 400 × g for 2 min, decant as much supernatant as possible. Resuspend cells gently and add a volume of cells to an equal volume of 2× cryoprotectant (*see* **Note 3**).

2b. Alternatively, with Pasteur pipette, add 0.5 ml 1× cryoprotectant to the bottom of a conical tube containing 10 ml of cells and centrifuge cells into the cryoprotectant. Remove as much liquid as possible before collecting cells for freezing.

3. Load less than 5 µl of the concentrated cells into a freezing hat previously coated with a droplet of hexadecene. Cover with a second hat, flat side facing sample, to make a "sandwich." Load into freezing holder, and freeze (*see* **Note 4**).

4. Transfer immediately to LN_2 bath. Always chill tweezers before handling frozen samples. Unload sample, separate the two metal holders and put the holder containing the sample into a cryovial containing FS media. Write with pencil on cryovial to identify samples. Samples may be stored under LN_2.

3.2. Freeze Substitution Schedule for GA/UA HM20 Samples

1. Place the vials at –90C° or –80°C to initiate freeze substitution. *see* **Note 5** about options for freeze substitution devices.

2. Keep vials at –90 to –80°C for three full days (days 1–3). On the morning of the 4th day, begin warming the samples slowly to –20°C (*see* **Note 6**). At this time, put a bottle of anhydrous acetone in a –20°C freezer. The GA becomes effective as a fixative at around –50°C.

3. Day 5 – Remove freeze substitution media, being careful not to discard any loose pieces of freeze-substituted sample (*see* **Note 7**). Rinse the samples 1–2× with the chilled acetone.

4. Separate the sample planchettes (hats) from the freeze-substituted sample; work quickly with one vial at a time at room temperature, while the rest stay at –20°C. Add fresh, chilled acetone to the well of a thick glass well slide. Use a forceps to transfer freezer hats from the vial to the well. Make sure the hats are completely submerged in the acetone. The samples should be surrounded by liquid at all times to avoid drying. Use a dissecting microscope for ease of spotting and manipulating samples. To remove biological material from the freezer hats, hold the hat with a blunt forceps and use a dissecting needle to gently nudge the sample out. The samples should look clear and slightly yellow. Break intact discs of sample into a few pieces. Draw up the pieces with a plastic pipette and put back into the vial. Throw away acetone left in the glass slide well and wipe clean before starting the next sample. Do one more acetone change before letting samples sit for 2–3 h at –20°C (*see* **Note 7**).
5. At the end of Day 5, make 25% HM20 in acetone and keep it at –20°C (*see* **Note 8**). Allow ~0.5 ml/vial for all steps of resin infiltration. Pull off as much acetone as possible without pulling up sample, and add the resin. Let samples sit overnight at –20°C.
6. Day 6 – In the morning, remove resin and add 50% HM20 in acetone for 6–8 h. Exchange the 50% HM20 for 75% HM20 in acetone overnight.
7. Day 7 – Three changes of 100% HM20 over the course of the day (approximately every 2.5–3 h).
8. Day 8 – One more change in 100% HM20 (*see* **Note 9**). Before transferring samples to BEEM capsules, put a drop of fresh resin in the bottom of the capsule. Pull off most of the resin from the sample vial, distribute sample between at least two capsules and then fill the BEEM capsules with fresh resin.
9. Load samples into precooled UV polymerization chamber (*see* **Note 10**).

3.3. Freeze Substitution Schedule for OsO_4/UA Epon Samples

1. Keep vials at –90 to –80°C for three full days (days 1–3). On the morning of the fourth day, begin warming the samples very slowly to –20°C (*see* **Note 6**). The OsO_4 begins working as a fixative at around –30°C.
2. Day 5 – Put samples at 4°C for at least 4 h, then move samples to room temperature for 1–2 h before proceeding. All following steps take place at room temperature. Remove FS media and rinse well with acetone (3×). Remove samples from hats as described above. Rinse with fresh acetone and let samples sit for a few hours. Remove acetone and add 25% Epon without accelerator in acetone overnight.

3. Day 6 – In the morning, remove 25% Epon dilution and add 50% Epon without accelerator in acetone. At the end of the day, change to 75% Epon without accelerator in acetone overnight.
4. Day 7 – Remove 75% Epon and add 100% Epon without accelerator. Change one more time during the day and then add Epon with accelerator overnight. The next morning, do one more change with Epon with accelerator. Put samples into BEEM capsules and make sure that the samples rest in the tip of the BEEM capsule (*see* **Note 9**). Polymerize at 60°C for 24–72 h.

3.4. Sectioning

Cut 60–80 nm sections and pick them up on formvar-coated copper slot grids (*see* **Note 11**). If sections will be used for immunolabeling, cut 50–70 nm sections from HM20 blocks and pick them up on formvar-coated nickel slot grids.

3.5. Immunolabeling

1. Float nickel grids, section side down, on 15 µl drops of blocking solution (*see* **Note 12**) for 30 min. Wick most of droplets away, but not to dryness.
2. Place grids onto primary antibody diluted in blocking solution for 2 h, with stirring (*see* **Note 13**).
3. Rinse grids with PBST, 20 s.
4. Place grids onto secondary antibody: goat-anti-rabbit conjugated to 15 nm gold (if the primary antibody is a polyclonal) diluted 1:20 in blocking solution, 1 h with stirring.
5. Rinse grids with PBST, 20 s.
6. Rinse with distilled water and wick grid dry with a wedge of Whatman filter paper.
7. Staining (*see* **Note 14**, **Subheading 3.6** for more detail):

2% aqueous UA, 3 min.

Rinse 20 s with water, wick away excess liquid.

Reynold's lead citrate, 1 min.

Rinse 20 s with water, wick dry.

3.6. Poststaining

1. Place grids section side down, onto 15 µl droplets of aqueous 2%UA, 5 min.
2. Rinse with a stream of water from a squirt bottle, 20 s, wick away extra water with a wedge of Whatman filter paper.
3. Place grids onto 15 µl droplets of lead citrate (*see* **Note 15**), 3 min.
4. Wash grids 20 s with water, wick grids dry with a Whatman wedge.

3.7. Imaging

Sections on grids are examined in a standard transmission electron microscope, typically operating at 80 kV. Images may be captured with digital cameras or on EM film. Each specimen should be critically evaluated for potential artifacts (*see* **Notes 16** and **17**).

4. Notes

1. The rabbit polyclonal primary antibodies to GFP used in these studies were received as generous gifts from colleagues. Commercial sources are available.
2. Cryoprotectants bind water and thereby retard ice crystal formation. This in turn reduces the amount of heat generated by crystallization and increases the cooling rate within aqueous samples *(10, 16)*. Each biological system has its own unique optimal freezing parameters *(17)*. In most cases, some form of chemical cryoprotectant is needed to supplement the suppression of ice crystal growth that is obtained by HPF. A given cryoprotectant may work very well for some organisms and not others. Mannitol, a penetrating cryoprotectant, worked well with *Chlamydomonas (18)*, but when used with *Tetrahymena*, the structural integrity of many basal bodies was compromised and it appeared to be toxic to some strains. In an attempt to find an effective but nonpenetrating cryoprotectant for *Tetrahymena*, we experimented with dextran in the range of 9–40 kDa. The smaller size (9–11 kDa) at concentrations of 15% (with 5% BSA) or 18% (w/v) alone had the advantage of being less viscous and gave the best preservation. Adding BSA, another nonpenetrant cryoprotectant, made it possible to lower the percentage of dextran. Higher concentrations of dextran as well as the larger dextran molecules seem to interfere with freeze substitution and infiltration of the embedding resin, causing the blocks to be brittle and difficult to section.
3. Gentle handling is required to avoid compressing the *Tetrahymena* cells and shearing off cilia. We have had success with both methods of concentrating cells: resuspension in small volumes of cryoprotectant and spinning cells into a cushion of cryoprotectant. Some strains and culture conditions produce cells that cannot be sedimented through the dextran/BSA mixture or higher concentrations of dextran. Low speed centrifugation out of culture media and resuspension in cryoprotectant is a simple and reliable method, but care must be taken to achieve the optimal concentration of cells. With either method, it should be possible to see cells swimming

around in the cryoprotectant, which is an indication that the cells are not overcrowded and most of their cilia are intact.

4. The process of high pressure freezing, a sample with the HPM 010 entails placing the specimen sandwich (cell sample enclosed between two metal planchettes) into a hinged specimen holder tip, inserting the specimen holder into the freezing chamber of the HPM and pressing a button to initiate the HPF process. This process is described in more detail in Dahl and Staehelin *(16)* and McDonald *(19)* for the HPM 010. HPF with a Leica EM-PACT has been detailed in McDonald et al. *(20)*.
5. Freeze substitution is typically conducted at temperatures between –90°C and –80°C. Devices for maintaining these temperatures include a commercially available freeze substitution device (Leica EM AFS, Leica Microsystems), commercial deep freezers, and insulated boxes (such as styrofoam chests) of dry ice. Dedicated freeze substitution devices such as the Leica AFS include metal racks for holding cryovials. If the styrofoam box and dry ice are used, lead shot or a metal block with holes drilled to accommodate cryovials is helpful for keeping samples cold and upright. Place the metal block into a styrofoam box, half filled with dry ice. Do not load the samples until the block reaches –80°C. To check the temperature of the block, put an acetone-filled vial in the holder and insert a thermocouple. After the samples are put into the styrofoam box, fill box completely with dry ice. Keeping the box at –20°C or 4°C slows the sublimation of the dry ice. Placing these fixatives in proximity to sensitive biological reagents is not recommended.
6. A gradual temperature rise after completion of the initial freeze substitution at –80°C allows the fixatives included in the FS medium time to act at the lowest possible temperature. Commercial AFS units can be programmed with predetermined, reproducible temperature protocols. Use of high mass metal blocks approximates these temperature programs to some extent. If the styrofoam box with dry ice technique is being used, the following steps will approximate a slow warm-up to –20°C. On the morning of the 4th day, remove the lid and put the box back into a –20°C freezer. After 7–8 h, remove all but a few small chunks of dry ice and place back into the freezer overnight.
7. To help maintain a cold temperature, place the block and the acetone into a small styrofoam box whenever work is being done on samples. Disposable one-piece plastic pipettes with bulbs work well for sample transfer and resin changes. To avoid the formation of precipitates, be sure to remove all fixatives during FS by rinsing the samples thoroughly with acetone.

8. Resin changes should be carried out in the hood, as HM20 is very noxious. Sample vials are returned to the metal block in a –20°C freezer as soon as possible after a resin change. A pipetman can be used to make the resin dilutions.
9. UV light must be able to access the whole BEEM capsule to completely polymerize the HM20 resin. Do not use paper labels to identify samples. Instead, numbers can be scratched into the plastic of the BEEM capsule with the tip of a dissecting needle. Pencil markings on paper strips may be used with Epon resin.
10. The device we use for UV polymerization is a homemade insulated box with two 7 W UV lights mounted onto the lid. The BEEM capsules are placed in a wire rack immersed in a temperature-controlled bowl of isopropyl or methyl alcohol. Dry ice is placed under the bowl and the temperature is maintained at –45°C by means of a thermocouple and a temperature-controlled holder for the blocks. Alternatively, UV cryo chambers are commercially available (Ted Pella, Inc.).
11. To create stable ribbons of serial sections, we place a droplet of contact cement along one edge of the resin block and let it dry completely prior to sectioning (10–30 min).
12. The labeling steps can be done in a large Petri dish with some water-soaked filter paper (for humidity) covered by parafilm. Nickel grids can be gently agitated during immunolabeling by placing the staining dish over a magnetic stirrer set at the lowest speed.
13. This protocol is suitable for use with both polyclonal and monoclonal primary antibodies. It works best for antigens that are present in reasonable number at discrete locations. A GFP-tagged protein that gives a punctate fluorescence signal without electronic amplification is usually convincingly labeled by this method. The optimal dilution of the antibody should be determined each time a new source is obtained and ideally, for each new protein being localized. If the background is too high, try increasing the concentration of nonfat dry milk from 1% to 2%, increasing the dilution of the primary antibody, or increasing the concentration of Tween 20. Other blocking agents have been described *(19)*. If the signal is too weak, the adjustments should be reversed.
14. Using thinner sections is probably the best way to improve visualization of gold particles over dark structures. Staining times can also be adjusted.
15. Lead citrate stain absorbs carbon dioxide from the air, forming lead carbonate precipitates. To mitigate the formation of precipitates, place the droplets of stain down just before use and rinse the surface of the grids thoroughly after staining.

Consistently low contrast or electron dense particles ("pepper") on the sections probably indicate that the stain solution should be replaced. 2%UA in 70% MeOH/30% water can be used to provide more intense contrast. In that case, rinse grid for 20 s with 70% MeOH and let the grid dry completely (about 10 min) before staining with lead. The choice of FS media and the effectiveness of the penetration and reaction of the fixatives with the sample can affect the contrast as well. As a rule, the clumps of cells that look the darkest in the embedding resin show the best preservation and staining in the TEM.

16. A potential problem of any cryofixation of a hydrated sample is the formation of ice crystals that can destroy the fine structure of organelles and leave the cytoplasm disrupted and extracted in appearance. In our experience, *Tetrahymena* cells have proven to be one of the more difficult samples to freeze well, and many samples exhibit considerable variation in the quality of freezing. One indicator of poor freezing is the presence of small voids or a reticulate texture in the macro and micronuclei **(Fig. 3)**. The cryoprotectant solution described here, containing 15% dextran and 5%BSA, typically yields preparations in which there is no visible ice damage in the majority of cells. If many cells in a section are poorly frozen, we recommend sectioning other blocks or groups of cells from the same sample because the quality of freezing can vary significantly even among cells frozen at the same time. If poor freezing is widespread and reproducible, then it may be necessary to change the cryoprotectant, perhaps by increasing the concentration of dextran, or use a greater ratio of cryoprotectant to cell pellet prior to freezing.

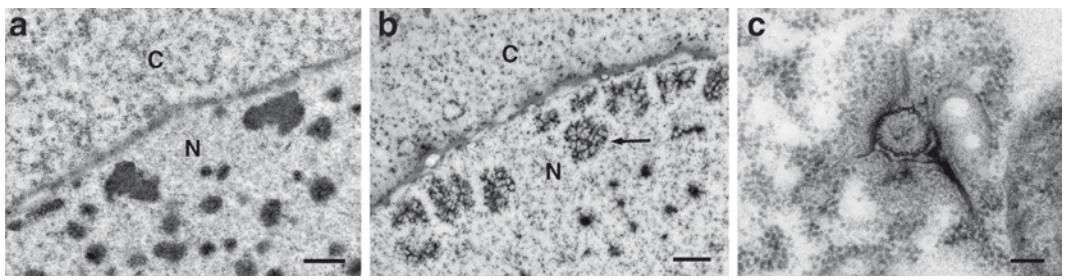

Fig. 3. Examples of good and poor freezing. (**a**) A well-frozen cell in which both the cytoplasm (C) and the nucleus (N) display uniform densities. Cells were frozen in 18% dextran in 10 mM Tris/HCl, freeze-substituted in 0.25% GA/0.1% UA, and embedded in HM20 resin. Bar = 0.5 μm. (**b**) Freezing damage is evident in both the cytoplasm (C) and nucleus (N) of this cell. Note small white voids in the dense chromatin within the nucleus that are not evident in A (*arrow*). Cells were frozen in 10% dextran (9–11 kDa)/10% BSA, freeze-substituted in 2% GA/0.1%UA, and embedded in HM20 resin. Bar = 0.5 μm. (**c**) Collapsed basal body microtubules in an otherwise well-frozen cell pellet. The cells in (a) and (c) are from the same resin block. Bar = 0.1 μm.

The latter strategy apparently works because the cryoprotectant solution freezes better than the *Tetrahymena* cells do. Ice crystal damage can also occur after initial HPF, during the early stages of freeze substitution. It is important to keep samples cold (at least –80°C) to prevent rapid warming at the start of the FS process.

Another frequently encountered problem is the breakage and loss of cilia. Use the gentlest possible centrifugation and handling techniques prior to freezing. Cells should still be swimming vigorously after loading into the specimen hats. While many cilia are well preserved by this technique (**Fig. 1b**), we have found it difficult to completely eliminate this artifact. Loss of cilia and other artifacts can also occur during freeze substitution and embedding. In this case, take extra care when separating the freeze-substituted cell pellet from the metal hats after FS because neither the cytoplasm nor the external cryoprotectant is rigidly fixed and both are prone to shearing forces.

The cell membrane may separate from the pellicle or from the cytoplasm, and the cytoplasm can exhibit rips or tears. Frequently, the pellicle pulls away from the surrounding resin. We found that coating the freezer hats with hexadecene prior to loading the concentrated *Tetrahymena* cells made it much easier to separate the fixed cell pellets from the hats after FS.

Torn or lightly staining cytoplasm, particularly when Lowicryl HM20 is used for embedding, may also reflect extraction of poorly fixed cytoplasmic constituents during freeze substitution or embedding. Shortening the time allotted for these steps or lowering the temperature during infiltration may decrease this artifact. Conversely, inadequate infiltration can lead to embedding problems that manifest themselves during sectioning. Cells may fall out of the resin and sections may rehydrate and disintegrate. In this case, a slower infiltration schedule and smaller stepwise increases in resin concentration may have to be employed.

17. In spite of all precautions, some artifacts can be present in apparently well frozen cells. The C-tubule of basal bodies is sometimes collapsed onto the B-tubule (**Fig. 3c**). Certain structures including components of the basal body (cartwheel and transition zone) and some membranes (ER) do not always stain intensely after FS fixation.

Acknowledgments

Our work on *Tetrahymena* is supported by the NIH (RO1 GM074746) and the March of Dimes Birth Defects Foundation (#1-FY07–520).

References

1. Allen, R.D. (1969) The morphogenesis of basal bodies and accessory structures of the cortex of the ciliated protozoan *Tetrahymena Pyriformis*. *J. Cell Biol.* **40**:716–733.
2. Frankel, J. and Williams, N.E. (1973) Cortical development in *Tetrahymena*. In (Elliot, A.M., ed.) *The Biology of Tetrahymena* Wiley, pp. 375–409.
3. Collins, K. and Gorovsky, M.A. (2005) *Tetrahymena thermophila*. *Curr. Biol.* **9**:R317–R318.
4. Washburn, M.P., Wolters, D., Yates, J.R. 3rd (2001). Large-scale analysis of the yeast proteome by multidimensional protein identification technology. *Nat. Biotechnol.* **19**:242–247.
5. Kilburn, C.L., Pearson, C.G., Romijn, E.P., Meehl, J.B., Giddings, Jr., T.H., Culver, B.P., Yates, J.R. 3rd, Winey, M. (2007) New *Tetrahymena* basal body protein components identify basal body domain structure. *J. Cell Biol.* **178**:905–912.
6. Eisen, J.A., Coyne, R.S., Wu, M., Wu, D., Thiagarajan, M., Wortman, J.R., Badger, J.H., Ren, Q., Amedeo, P., Jones, K.M., et al. (2006) Macronuclear genome sequence of the ciliate *Tetrahymena thermophila*, a model eukaryote. *PLoS Biol.* **4**:e286.
7. Stemm-Wolf, A.J., Morgan, G., Giddings, Jr., T.H., White, E.A., Marchione, R., McDonald, H. and Winey, M. (2005) Basal body duplication and maintenance require one member of the *Tetrahymena thermophila* centrin gene family. *Mol. Biol. Cell* **16**:3606–3619.
8. Shang, Y., Tsao, C.C., and Gorovsky, M.A. (2005) Mutational analyses reveal a novel function of the nucleotide-binding domain of gamma-tubulin in the regulation of basal body biogenesis. *J. Cell Biol.* **171**:1034–1044.
9. Moor, H. (1987) Theory and practice of high pressure freezing. In (Steinbrecht, R.A. and Zierold, K., eds.) *Cryotechniques in Biological Electron Microscopy* Springer, Berlin, pp. 175–191.
10. Gilkey, J.C and Staehelin, L.A. (1986) Advances in ultrarapid freezing for the preservation of cellular ultrastructure. *J. Electron Microsc. Tech.* **3**:177–210.
11. Giddings, Jr., T.H., O'Toole, E.T., Morphew, M., Mastronarde, D.N., McIntosh, J.R., and Winey, M. (2001) Using rapid freeze and freeze-substitution for the preparation of yeast cells for electron microscopy and three-dimensional analysis. *Meth. Cell Biol.* **67**:27–42.
12. Kremer, J.R., Mastronarde, D.N., and McIntosh, J.R. (1996) Computer visualization of three-dimensional image data using IMOD. *J. Struct. Biol.* **116**:71–76.
13. Mastronarde, D.N. (1997) Dual-axis tomography: An approach with alignment methods that preserve resolution. *J. Struct. Biol.* **120**:343–352.
14. O'Toole, E.T., Giddings, Jr., T.H., and Dutcher, S.K. (2007) Understanding microtubule organizing centers by comparing mutant and wild-type structures with electron tomography. *Meth. Cell Biol.* **79**:125–143.
15. Bruns, P.J. and Cassidy-Hanley, D. (2000) Biolistic transformation of macro- and micronuclei. *Meth. Cell Biol.* **62**:501–512.
16. Dahl, R. and Staehelin, L.A. (1989) High-pressure freezing for the preservation of biological structure: Theory and practice. *J. Elect. Microsc.* **13**:165–174.
17. McDonald, K. (2007) Cryopreparation methods for electron microscopy of selected model systems. *Meth. Cell Biol.* **79**:24–52.
18. O'Toole, E.T., Giddings, Jr., T.H., McIntosh, J.R., and Dutcher, S.K. (2003) Three-dimensional organization of basal bodies from wild-type and tubulin deletion strains of *Chlamydomonas reinhardtii*. *Mol. Biol. Cell* **14**:2999–3012.
19. McDonald, K.L. (1999) High-pressure freezing for preservation of high resolution fine structure and antigenicity for immunolabeling. *Meth. Mol. Biol.* **117**:77–97.
20. McDonald, K.L., Morphew, M., Verkade, P., and Mueller-Reichert, T. (2007) Recent advances in high-pressure freezing: Equipment and specimen loading methods. *Meth. Mol. Biol.* **369**:143–173.
21. Nakazawa, Y., Hiraki, M., Kamiya, R., and Hirono, M. (2007) SAS-6 is a cartwheel protein that establishes the 9-fold symmetry of the centriole. *Curr. Biol.* **17**: 2169–2174.

Chapter 13

Strategies for Imaging Microtubules in Plant Cells

Andreas Holzinger, Eiko Kawamura, and Geoffrey O. Wasteneys

Summary

Microtubules are required throughout plant development for a wide variety of processes, and different strategies have been evolved to visualize them. This chapter summarizes the most effective of these methods and points out potential problems and pitfalls. We outline the freeze-shattering method for immunolabeling microtubules in aerial organs such as leaves that require mechanical permeabilization, discuss current options for live cell imaging of MTs with fluorescently tagged proteins (FPs), and provide different fixation protocols for preserving MTs for transmission electron microscopy including chemical fixation, high pressure freezing/freeze substitution, and post-fixation staining procedures for transmission electron microscopy.

Key words: Alexa, Microtubules, Dynein, EB1, GFP, Kinesin, MAP4, MBD, mor1-1

1. Introduction

Microtubules (MTs) are a unifying feature of eukaryotic cells. Studying them in plants is not only important for understanding mechanisms of plant growth and development but also of broader interest for understanding the mechanisms that generate microtubule spatial organization, including the role of accessory proteins in microtubule dynamics. The current literature describes the role of MTs in division plane organization *(1–3)*, cell wall formation and morphogenesis in diffusely expanding organs *(1, 4–8)*, tip growing root hairs *(9, 10)*, stomatal movement *(11)*, nuclear movements *(12, 13)*, chloroplast organization and positioning *(14–16)* or in association with amyloplasts *(17)*.

R.H. Gavin (ed.), *Cytoskeleton Methods and Protocols,* Methods in Molecular Biology, vol. 586
DOI 10.1007/978-1-60761-376-3_13,
© Humana Press, a part of Springer Science + Business Media, LLC 2009

This intensive international effort requires a variety of experimental strategies, ranging from basic description of orientation patterns and associations with other structures to pharmacological and genetic perturbations. With cytoskeleton research in plants on the increase, it is especially important for researchers to be provided with a variety of standard techniques and tools for imaging microtubules in plant cells. In this chapter, we outline preparation methods for imaging microtubules in plant cells by light- and electron microscopy. For analysis in the visible spectrum, we describe here a freeze-shatter method that is suitable for cuticle-laden aerial tissues such as hypocotyls and leaves. Suitable methods for imaging root microtubule and actin filament arrays are provided in Chapter 8.

Immunofluorescence microscopy is now a routine approach for MT imaging at the light level of resolution *(18)*. With the advent of live cell imaging with transgene-introduced fluorescent reporter proteins (e.g. *(19, 20)*), immunofluorescence may now appear to be somewhat old-fashioned. Nevertheless, this technique remains essential under many circumstances and should continue to be widely used, especially in non-model systems where it is not yet feasible to transform plants with live cell reporters or when wild material is collected in its natural habitat. We demonstrate this first point with images of MTs in leaf cells of the high alpine plant *Oxyria digyna* **(Fig. 1a–c)**. Previous work had demonstrated that MTs were a critical factor in the establishment of chloroplast stromules *(21)* and we therefore adopted the

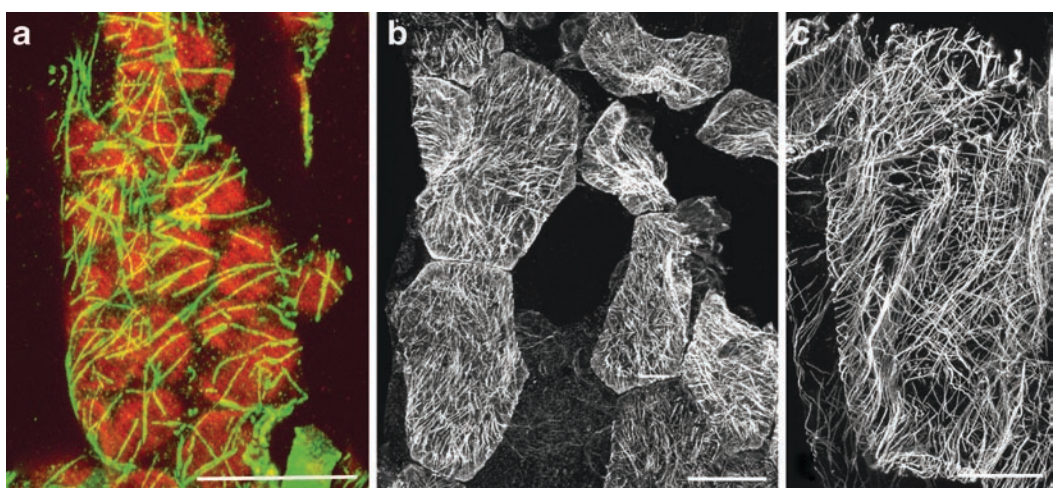

Fig. 1. Immuno localization of MTs in the alpine vascular plant *Oxyria digyna*: (**a**) Merge of MT staining (which would appear green) and chloroplast auto fluorescence showing the close vicinity of MTs with chloroplasts. (**b**) MTs in epidermal cells, (**c**) MTs in parenchyma cells, note the very dense network in z-stack projections, image is composed of approx 100 images, comprising a depth of about 20 μm; Bars 20 μm. Figures (**b–c**) reprinted from reference (Holzinger et al. *(15)*) with permission of Thieme Verlag KG.

"freeze shattering" method *(22)* to permeabilize *Oxyria* leaves for immunolabeling *(15)*.

Immunofluorescence microscopy remains a useful adjunct technology for corroborating evidence from live cell strategies where, as discussed below, artefact needs to be ruled out **(Fig. 2)**. It is also the best option when high intensity light needs to be used, or long exposures are required for the collection of large series of optical sections, which can be toxic to living cells. It also enables microtubules in inner tissue layers to be resolved. Immunofluorescence procedures of course kill the samples but after fixation

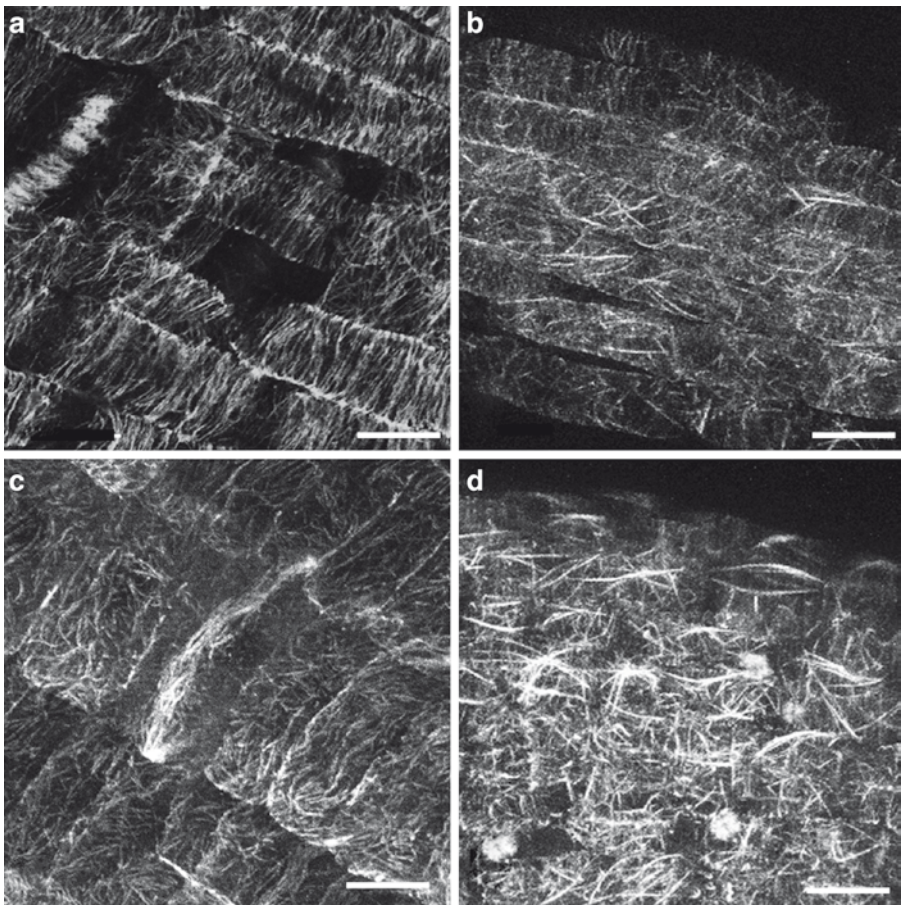

Fig. 2. Comparison of wt (**a**, **b**) and *mor1–1* (**c**, **d**) microtubule bundles via immuno localization (**a**, **c**) and GFP-MBD visualization (**b**, **d**) in *Arabidopsis thaliana* at 31°C. Plants were grown at 21° for 5 days and then transferred to 31°C. (**a**) wt immuno labeled (fixed in a fixative that was preheated to 31°C and labeled with anti-tubulin) and (**b**) wt GFP-MBD expressing root, image taken on a temperature control stage that kept the specimens at 31°C, 2–3.5 h after temperature shifts; (**c**) immuno labeled *mor1–1*, (**d**) *mor1–1* at 31°C showing apparent microtubule bundles in the GFP-MBD fusion protein-expressing line. GFP-MBD labeling identifies bright, bundle-like structures at 31°C. Although some evidence for this is observed in wild-type cells, microtubule remodeling is much more extensive in *mor1–1*. These thickened microtubule structures are not observed with immuno labeling, suggesting this putative bundling of microtubules is dependent on the GFP-MBD fusion protein. Bars 10 μm.

and appropriate fade protection, immunolabeled material can be scanned repeatedly and stored for months with little loss of image quality. Immunofluorescence is also an excellent method for describing the distribution along MTs of proteins known as microtubule-associated proteins (MAPs) using double labeling strategies (**Fig. 3**). And, because it does not require the introduction of transgenes or laborious and time-consuming selection procedures, immunofluorescence can be utilized immediately on any interesting genotype.

Since the successful exploitation of green fluorescent protein (GFP) in the early 1990s, a vast body of literature has been generated on the use of this and other intrinsically fluorescent proteins as reporters of structural proteins *(19, 20)*. Many constructs, cell and plant lines are now available for observing MTs in living plant cells including MBD (**Fig. 2**), TUB (**Fig. 4**), EB1 (**Fig. 5**). There are clear advantages to being able to follow MTs in living cells.

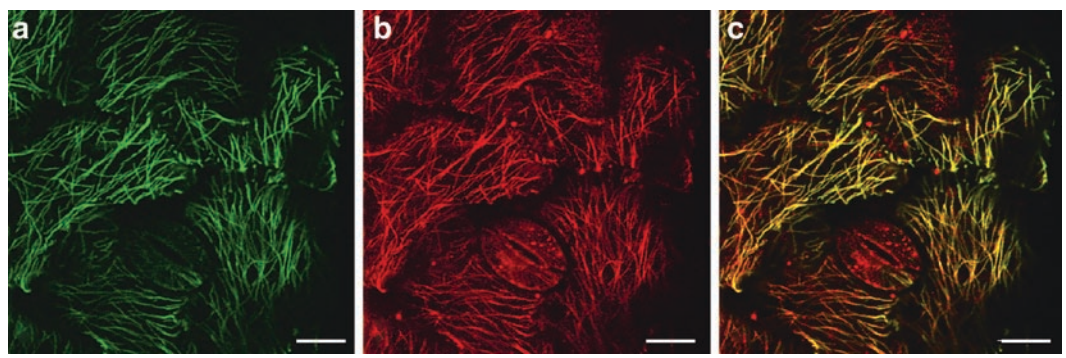

Fig. 3. Immuno labeling of tubulin (**a**) and MOR1 (**b**) in wild-type background at 31°C. For immuno labeling, 11-day-old wild-type plants grown at 21°C were cultured at 31°C for 1 day and fixed in fixative that were preheated to 31°C and double immunolabeled. (**a**) Tubulin, (**b**) MOR1, (**c**) merge of (**a**) and (**b**). The abaxial sides of first leaves are shown in all images. Bars 10 μm.

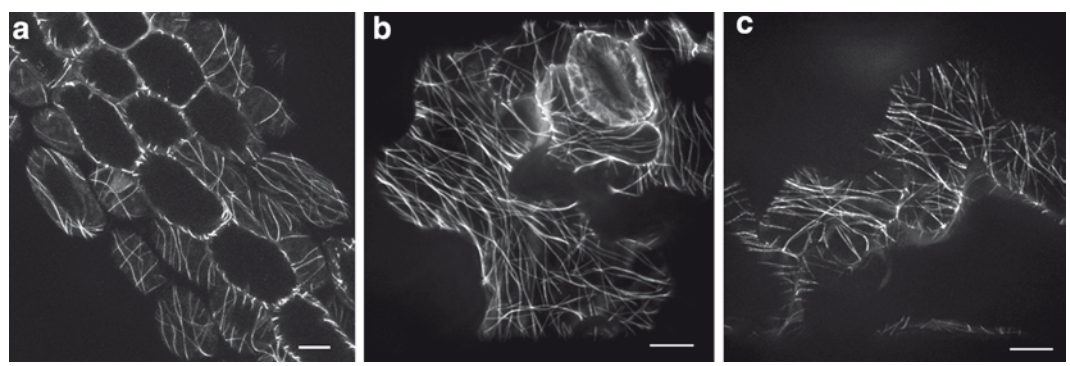

Fig. 4. Comparison of different GFP-transgenic lines in wild-type background of *Arabidopsis thaliana*. (**a**) GFP-MBD in hypocotyl of a 10-day-old plant grown at 21°C, (**b**) GFP-TUA in a 11-day old first leaf, (**c**) GFP-TUB in a 12 day-old first leaf grown at 21°C and imaged within few hours after the temperature was increased to 31°C. Bars 10 μm.

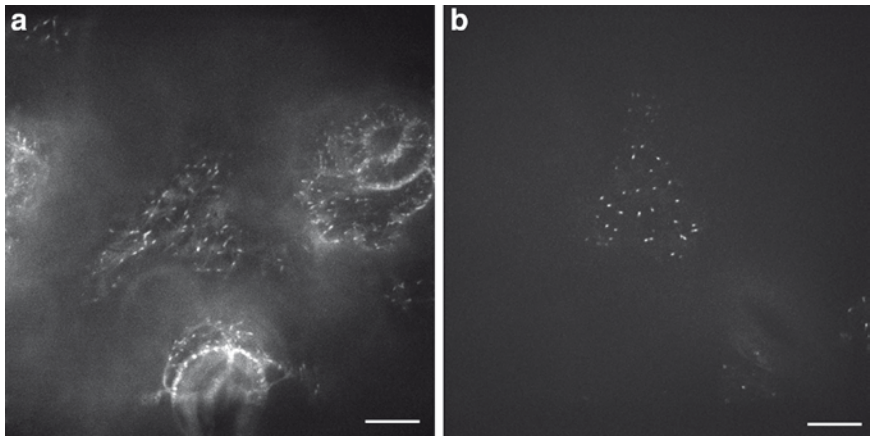

Fig. 5. Images of *p35S::GFP-EB1* (**a**) and *pEB1::EB1-GFP* (**b**) expressing *Arabidopsis thaliana* cells at 21°C. (**a**) *p35S::GFP-EB1*, GFP-EB1 forms comet-like shape and weakly associates with side walls of microtubules, and the background fluorescence is high. (**b**) *pEB1::EB1-GFP*, plus end labeling by EB1-GFP is more concentrated, showing dot-like forms and the background signal is very low. Abaxial surfaces of first leaves from 12-day-old plants were used. Plants were grown at 21°C and imaged with a Quorum Wave FX Spinning Disc Confocal System (Quorum, Guelph, Ontario, Canada) with a 63× NA 1.3 glycerol-immersion lens. A Bionomic Controller BC-110 stage together with a Heat Exchanger HEC-400 kept the specimens at 21°C. Bars 10 μm.

Time lapse imaging enables the growth and shrinkage of microtubules to be followed in near real-time *(23–25)*, processes such as mitosis can be documented and compared in different genotypes *(7, 26)*, and co-localization of associated proteins with microtubules **(Fig.** 3) can be analyzed quantitatively *(27)*. There are several limitations to live cell imaging of microtubules and great care needs to be exercised to avoid acquisition of erroneous information. Some of these problems are outlined in detail by Shaw *(28)*. In Notes 6 to 9 we outline several important issues to consider such as phototoxicity, choice of promoter, fusion protein reporter construction and the culture temperature, when embarking on live cell imaging of microtubules.

Despite the convenience of live cell MT imaging and the opportunity it provides for obtaining data on microtubule dynamics, TEM remains a valuable tool when high resolution analysis is required. The fluorescence intensity of labeled MTs is generally interpreted as showing the degree of MT bundling, but this may be hard to confirm or refute without TEM. Since the 1960s when MTs were first observed in plants on electron micrographs *(29)*, there has been a debate over the best fixation protocol. Chemical fixation does a reasonable job. After glutaraldehyde-osmium fixation **(Fig.** 6a) or potassium hexacyanoferrate fixation MTs appear slightly wrinkled but well-preserved. Presently, high pressure freezing followed by freeze substitution is considered the best method for preserving cellular ultrastructure

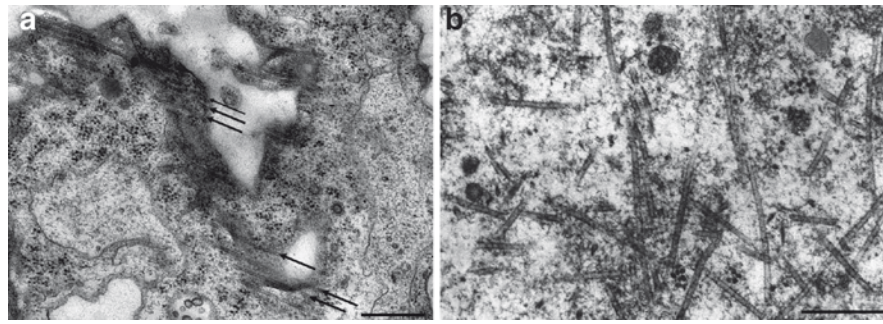

Fig. 6. TEM visualization of microtubules in different algal cells: (**a**) chemical fixation protocol in *Klebsormidium crenulatum* visualizing cortical microtubules in adult cell. The *arrows* indicate the parallel orientation of the MTs. (**b**) Plunge-frozen and freeze-substituted MTs in *Micrasterias muricata*. MTs in association with a migrating nucleus show various orientations in a microtubule organizing centre. Note the clear and sharp outer surfaces of the MTs. Bars 0.2 μm.

(e.g. *(30–33)*) but involves specialized apparatuses and cannot be performed in many research facilities. We therefore also describe plunge freezing as a simple alternative that preserves cortical regions of cells up to ~20 μm very well. This method is acceptable for examining the ultrastructure of cortical MTs in single cells **(Fig. 6b)**. Despite the static picture of MT organization provided, TEM remains essential when resolution beyond the limit of fluorescence microscopy is required, such as when examining the higher order structure of microtubule bundles, the presence of crosslinking proteins and the interaction of microtubules with endomembranous components and other structures. It is also possible to analyze how proteins colocalize *(34)*, or motor proteins of the kinesin family *(12)* and the crosslinking MAP65s interact with MTs *(35)*. Immunolocalization by TEM requires specialized preparation to preserve antigenicity of the protein epitopes. Best results are obtained after high pressure freeze fixation, freeze substitution and embedding in LR white resin *(12)*. We have devoted the last section of this chapter to TEM preparations.

2. Materials

2.1. Plant Material

1. *Arabidopsis thaliana* seeds, constructs: Seed stocks, including transgenic and mutant lines, as well as some DNA stocks, can generally be obtained from the Arabidopsis Biological Resource Centre. See TAIR website for details and ordering information (http://www.arabidopsis.org/abrc/index.jsp).

2. Plant leaf material (this can vary according to the researchers' demands) Immunofluorescence and TEM protocols generally work with every type of plant leaf.
3. Plant cell cultures (e.g. Suspension cell cultures, unicellular green algae).
4. Specific transgenic reporter lines for observing MTs in live cells of *Arabidopsis thaliana* listed under **steps 5–7** in this section (*see* **Note 1**).
5. Pro35S::GFP-TUB: This construct from the Hashimoto lab (NAIST, Japan; contact Dr. T. Hashimoto: hasimoto@bs.naist.jp) fuses GFP to the N terminus of the β tubulin 6 (At5g12550) isoform from *Arabidopsis thaliana (36)* **(Fig. 4b, c)** (*see* **Note 2**).
6. Pro35S::MBD-GFP:This construct was developed in Dr. Richard Cyr's lab (Penn State University; rjc8@psu.edu) and is a heterologous MT reporter that works in plants, constructed from the MT binding domain (amino acid residues 935–1,084) of the mammalian MAP4 *(37)* (**Figs. 2b, d**, and **4a**). (*see* **Note 3**).
7. ProEB1b::EB1-GFP: This reporter generates comet-like fluorescent patterns at the growing plus ends of MTs so can be used to measure MT growth and to analyze MT polarity within an array **(Fig. 5)**. (*see* **Note 4**).

2.2. Technical Equipment

1. Temperature-controlled stage: Bionomic Controller BC-110 together with a Heat Exchanger HEC-400, a Bionomic Controller BC-100 (20–20 Technology Inc., Wilmington, NC, USA).
2. Objective lens heater (BIOPTECHS, Butler, PS, USA).
3. Culture chambers for live cell imaging. (obtained from Electron Microscopy Sciences, Hatfield, USA).
4. Thermocouple device (FLUKE52 (John Fluke MFG. Co., Inc., Everett, Washington, USA).
5. High pressure freezer (formally Balzers HPM 010, later taken over by BAL-TEC; then produced by ABRA Fluid AG, Widnau, Switzerland; currently available as Leica HPM 100
6. Freeze substitution device (LEICA EM AFS, Leica Microsysteme GmbH, Vienna, Austria).

2.3. Chemicals and Reagents

2.3.1. Chemicals and Reagents for Fluorescence Microscopy

1. 50 mM PIPES buffer, pH 7.2.
2. EGTA.
3. Manganese sulphate.
4. Sodium borate.

5. Formaldehyde or paraformaldehyde (best to use EM grade).
6. Glutaraldehyde (EM grade, stored continuously at –20°C).
7. Triton X-100.
8. PBS: Phosphate buffered saline: 137 mM sodium chloride, 2.7 mM potassium chloride, 4.3 mM sodium hydrogen phosphate, 1.4 mM potassium dihydrogen phosphate, pH 7.5.
9. Primary Antibody (e.g. B 512 anti alpha tubulin; Sigma).
10. Corresponding secondary Antibody (Alexa488-conjugated goat anti-mouse IgG, Amersham).
11. Citifluor AF1 antifade agent (Agar Scientific Ltd., Stansted, Essex, England).

2.3.2. Chemicals and Reagents for Live Cell Imaging

1. Agar (Plant Cell Culture tested, Sigma).
2. Sucrose.
3. Hoagland's growth medium.
4. Agarose (low gelling temperature).

2.3.3. Chemicals and Reagents for Electron Microscopy

1. Glutaraldehyde (EM-grade).
2. Osmium tetroxide.
3. Potassium hexacyanoferrate III.
4. 10–50 mM Cacodylic buffer, pH 6.8.
5. Calcium chloride.
6. Uranyl acetate dihydrate.
7. Ethanol.
8. 1,2-Propylene oxide.
9. A suitable embedding resin: Embed 812, Araldite 502, Spurr's resin, Agar Low Viscosity Resin (LV) (Agar Scientific Ltd. Essex CM24 8DA, England).
10. Formvar 1595 E.
11. Chloroform.
12. Reynold's lead citrate.

2.3.4. Chemicals for Immuno-Electron Microscopy

1. LR white resin (London resin company, medium grade).
2. 50 mM Tris buffered saline (TBS), Trizma pre-set crystals, T-8524, Sigma; pH 7.5.
3. BSA (fraction V), acetylated BSA (BSAac).
4. Primary antisera/antibodies (e.g. monoclonal antibody against bovine brain kinesin K-1005; anti alpha tubulin B 512; both Sigma).

5. 10 nm – collodial gold conjugated corresponding secondary antibody.
6. Tween-20.

3. Methods

3.1. Microtubule Staining of Fixed Material

Microtubule staining according to the freeze shattering method *(22)* with useful modifications according to Holzinger et al. *(15)*.

1. Fix samples for 40 min in 0.5% glutaraldehyde and 1.5% formaldehyde in PIPES buffer containing 2 mM EGTA, 2 mM manganese sulphate.
2. Wash in the same buffer containing 0.05% Triton X-100.
3. Blot samples to remove excess buffer, place between two glass slides and dip into liquid nitrogen. Remove and quickly apply pressure by compressing the slides with a pair of pliers before the tissues thaw (*see* **Note 5**).
4. Transfer sample to permeabilization buffer containing PBS and 1% Triton X-100 for 1 h.
5. Transfer samples to PBS (pH 7.4) for 10 min, followed by a 20 min incubation in PBS containing 1 mg/ml Sodium borate.
6. Incubate in primary antibody (Sigma B 512 anti alpha tubulin, 1:1,000) over night at 4°C.
7. Wash extensively in buffer (e.g. three times 10 min).
8. Incubate in secondary antibody (Alexa488-conjugated goat anti-mouse IgG, 1:200) for 1 h at 37°C.
9. Mount samples in Citifluor AF1 antifade agent.
10. Examine with a Confocal Laser scanning Microscope (CLSM), useing a high Numerical Aperture (NA) objective lens (e.g. at a Zeiss Axiovert, 63× 1.4 NA).
11. Generate excitation with an Argon laser at 488 nm.
12. Collect long pass (LP) 560 nm filtered emission and band pass (BP) 505–530 nm filtered emission simultaneously in two channels; if possible collect a DIC image with another channel.
13. Capture Z-stacks.
14. Generate projections, e.g. with ImageJ software (freeware; http://www.imageJ).

3.2. Fluorescent Proteins to Visualize the MT Cytoskeleton

This section describes a standard method of preparing aerial organs such as leaves or cotyledons for live imaging on an inverted microscope.

1. Plant surface sterilized seeds on Petri plates containing nutrient medium in 1.5% agar. Wrap plates with porous surgical tape.
2. Store plates at 4°C for 3–5 days to synchronize germination, then transfer to a growth cabinet, keeping the plants growing under constant light (80 μmol/m^2/s) or in an 18 h light, 8 h dark cycle at 21°C for 11–12 days (*see* **Note 6**).
3. Excise whole leaves or pieces of them and place them on the coverslip that forms the bottom of microscope culture dishes. We obtain dishes suitable for this purpose from Electron Microscopy Sciences, Hatfield, USA. If you are using an upright microscope, the leaves can be placed directly onto a glass slide and covered with cover slips held in place at corners with small amounts of vacuum grease (*see* **Note 7**).
4. Mount leaf cuttings in water, taking care to ensure that the surface of interest is facing the coverslip. With an inverted microscope setup, a small square of 2% agar can be placed on top of the leaf to stabilize it from drifting during imaging (*see* **Note 8**).
5. Allow samples to equilibrate under standard conditions for at least 1 h prior to observation.
6. Place culture chambers on microscope stage and ensure that images are recorded according to the spectral properties of the fluorescent protein. Images can be taken every 8 s over 3–5 min for GFP-TUB and every 5 or 8 s over 40–60 s for Pro_{EB1}::EB1b-GFP (*see* **Note 9**).
7. To keep the temperature stable around the mounted samples, use a temperature-controlled stage: Bionomic controller BC-110 equipped with Heat exchanger HEC-400 (20/20 Technology Inc.). Sometimes, an objective lens heater (Bioptechs) is also required, especially when using immersion lenses. Monitor the temperature of the sample immediately after imaging by measuring the temperature of glycerol on the coverslip using a thermocouple device.
8. Avoid recording images over periods longer than 4 h.

3.3. TEM Preparations to Visualize MTs in Plant Cells

3.3.1. Chemical Fixation Protocol

(Glutaraldehyde-Osmium tetroxide fixation with modifications after Holzinger et al. *(15, 38)*). Potassium Ferricyanide fixation protocol (after Holzinger et al. *(39)*).

1. Fix tissue or cells in 10–50 mM cacodylate buffer (*see* **Note 10**) (**Fig. 6a** *Klebsormidium crenulatum*) containing 1% glutaraldehyde for 30–90 min (*see* **Note 11**).
2. Wash cells 3× 5 min in 50 mM cacodylate buffer.
3. Postfix cells in 50 mM cacodylate buffer containing 1% OsO_4, for 2 h at room temperature or 12 h at 4°C.
4. Wash cells three times 5 min with distilled water.
5. Wash 3× 5 min with distilled water.

6. Dehydrate the cells in increasing concentrations of cold ethanol, 15 min per concentration: 15, 30, 40, 50, 70, 80, 90, 95, 100%. Keep in 100% ethanol for 30 min.
7. Transfer the cells to a 1:1 mixture of propylene oxide: ethanol, allow to equilibrate for 10 min.
8. Transfer to propylene oxide.
9. Transfer the cells to a 1:1 mixture of propylene oxide and embedding resin (*see* **Note 12**).
10. Rotate the cells in this mixture for 24 h in order to allow the propylene oxide to evaporate and for sufficient penetration of the cells with the resin.
11. Transfer the cells to freshly prepared resin in polymerization chambers or aluminum dishes.
12. Incubate in an desiccator for 4 days.
13. Polymerize the resin for 16 h at 60°C.
14. Select samples and section using an ultramicrotome.
15. Collect sections on formvar-coated copper grids (*see* **Note 13**).
16. Counter stain the sections with 2% aqueous uranyl acetate for 30 min (*see* **Note 14**).
17. Wash 2 min with distilled water and allow to dry fully.
18. Counterastain with Reynold's lead citrate (*see* **Note 15**).
19. Wash 2 min with distilled water and allow to dry fully.
20. Investigate and photograph with a transmission electron microscope.

3.3.2. High Pressure Freeze Fixation Protocols to Preserve Microtubules

The protocol described here uses a commercially available hyperbaric freezing device. The methods are basically following the methods of *(30)* **(Fig. 7)**, with addition of own experience and information gained from several other works as stated in **Notes 16 to 22**.

1. Dip specimen cups in lecithin (l-a-phosphatidyl-cholin; 100 mg/ml dissolved in chloroform) and allow to dry until specimen holders are covered with lecithin.
2. Prepare samples in nutrient solutions; for several plant tissues it may be useful to transfer samples in 100 mM sucrose (*see* **Note 16**).
3. Transfer samples into gold or aluminum specimen cups.
4. Ensure that no air bubbles are in the preparation as they will damage the samples with the high pressures involved in this process.
5. Close up two cups face to face or, depending on the sample, orient the face toward the bottom.

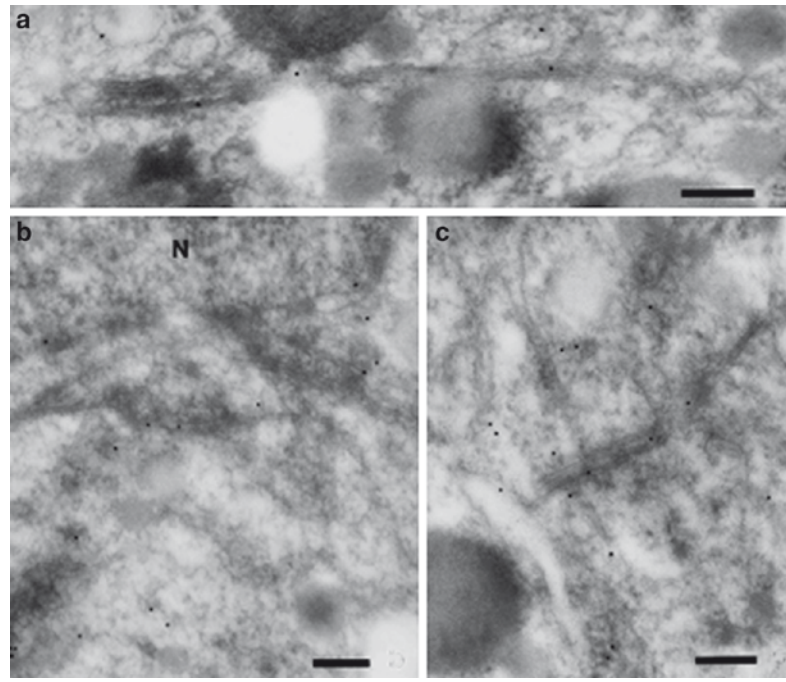

Fig. 7. High pressure-frozen MTs in the vicinity of a migrating nucleus in the green alga *Micrasteris denticulata* immuno-gold (10 nm) stained with an antibody to brain kinesin. Bars 0.2 μm. (Reprinted from *(12)*, Elsevier with permission.).

6. Mount in specimen holder and transfer to the High Pressure Freezing Machine HPM 100 (*see* **Note 17**).
7. Freeze samples in liquid nitrogen according to the manufacturer's instructions.
8. Remove samples immediately after the freezing procedure and transfer them to liquid nitrogen, where they can be stored until the freeze substitution process.
9. Freeze substitute samples in 2% OsO_4 in acetone or 0.1% tannic acid in acetone at –80°C for 24 h and a mixture of 2% OsO_4 and 0.05% uranyl acetate in acetone at –80°C for 28 h (*see* **Note 18**).
10. Allow the temperature to reach –30°C in the same medium within 10 h.
11. Bring to room temperature and rinse in acetone.
12. Embed and further process samples as described in **Subheading 3.3.1, step 8**.

3.3.3. Plunge Freezing for Thin Samples (According to Holzinger (31))

1. Mount thin samples with forceps (*see* **Note 19**).
2. Dip quickly into liquid propane that is cooled by liquid nitrogen.
3. After this freezing step transfer samples into liquid nitrogen.
4. continue as in **Subheading 3.3.2, step 8**.

3.3.4. Post-fixation Immuno-Staining Protocol

The procedures described are modified from *(34)*; and can be adjusted for basically any new MT associated protein or for other cytoskeletal components **(Fig. 7)**.

1. Pre-incubate sections in 50 mM TBS, 1% BSA (Sigma, A2153), 1% acetylated BSA (BSAac, Sigma, B2518), 0.2% Tween-20 for 1 h. (*see* **Note 20**).
2. Incubate sections in primary antibodies (e.g. monoclonal antibody directed against bovine brain kinesin; Sigma K-1005) diluted 1:50, 1:100 in TBS, 1% BSA, 0.1% BSAac, 0.01% Tween-20 for 20–24 h at 4°C.
3. Wash in 50 mM TBS, 1% BSA, four times 15 min provided in droplets.
4. Transfer into secondary antibody (e.g. 10 nm gold-conjugated goat anti-rabbit IgG (Sigma G-7402) or a goat anti-mouse IgM (Sigma G-5652) in TBS, 1% BSA, 0.1% BSAac, 0.01% Tween-20 in a dilution of 1:200 or 1:400 and incubate for 1.5 or 2 h at room temperature.
5. For control purposes omit the first antibody on some sections or incubate in protein-saturated primary antibody.
6. After the staining procedure, rinse the sections extensively (*see* **Note 21**).
7. Continue as in **Subheading 3.3.1**, **step 16** (*see* **Note 22**).

4. Notes

1. *Fusion protein reporter construction*: Not surprisingly, fusing a fluorescent reporter to a protein can alter its function. The GFP-TUA6 construct (GFP is fused to the N terminus of alpha tubulin 6) was the first successful tubulin-based fluorescent reporter to work in plant cells *(40)*. It generates bright labeling of microtubules in aerial tissue (it is expressed, but apparently does not incorporate into microtubules in root tissues) but causes right-handed organ twisting, a phenomenon attributed to inhibition of the tagging of alpha tubulin at its N terminus, which may interfere with its GTP hydrolysis-promoting activity *(41)*. After testing several different fluorescent reporters for imaging microtubules, we recommend the following constructs as listed. These constructs are available upon request from the laboratory of origin or from the *Arabidopsis* stock centres. Most constructs are also available with other fluorescent tags such as yellow fluorescent protein (YFP) and red fluorescent protein (RFP).

2. Its expression in stably transformed lines of the Columbia ecotype is regulated by the cauliflower mosaic virus 35S promoter *(36)*. In comparison to some other MT reporters, this one generates relatively low fluorescence but there are no detectable developmental or morphological phenotypes *(8, 41)*. This line cannot be used reliably to examine microtubules in root cells though some labeling of microtubules can be observed in dividing root cells.
3. This is currently the most reliable probe for examining MTs in root tissues, where it has been used to document MTs in the division *(7, 26)*, elongation zones (*42*) as well as during root hair development *(43, 44)*. Caution needs to be exercised with this reporter. Plants stably expressing MBD-GFP under the CMV35S promoter frequently, have severe developmental defects and low seed yield, and MT bundle formation has been observed under certain conditions (for more details *see* **Notes 9**). We suggest confining the use of MBD-GFP to roots, and then to select specimens that have low level of expression. This can be achieved by selecting heterozygotes from an F2 segregating population *(43)*.
4. There are many different fluorescent EB1 reporters available but this one from the Cyr lab (Penn State University, USA) uses the promoter element from the *Arabidopsis thaliana* EB1b isoform to drive moderate expression levels *(45)*, which confines comets to the growing plus ends. Even so, we have found that MT growth rates are slightly higher when measured with this reporter compared to GFP-TUB –*(25)*, a finding that underscores the importance of carefully regulating the expression of some reporters (for further details *see* **Notes 9**). EB1 reporters seem to work equally well with the fluorescent tag at either the C- or N-terminus.
5. Some delicate samples can be effectively permeabilized by simply repeated freeze–thaw cycles and do not require compression in the frozen state.
6. *Culture temperature*: We recently reported that temperature shifts of only a few degrees significantly alters microtubule dynamics in *Arabidopsis* epidermal cells *(25)*. If the intention is to measure microtubule dynamics (growth and shrinkage velocity, time spent in growth, shrinkage and pause) then a temperature-controlled stage is a good option. The large proportion of metal components in microscopes makes it difficult to manipulate temperatures. Lenses are good temperature sinks and special lens heaters may be required if the desired culture temperature is above ambient.
7. Other physically induced responses include wound and touch responses, gravitropisms and photoinduction. Excising organs

from plants will generate a wound response that may alter microtubule behavior at a site distal to the wound. Forcing cells close to the coverslip for optimal viewing may generate a touch response that manifests itself in aberrant microtubule behavior. Some plant organs such as hypocotyls and roots are strongly gravity or light responsive and when placed on a conventional horizontal microscope stage will undergo differential flank growth in an attempt to resume vertical growth. Horizontally placed roots, for example, will be stimulated to grow more rapidly on the upper flank and growth will be inhibited on the lower flank. With an inverted stage microscope, this will mean that the growth of cells closest the lens will be reduced or prematurely arrested. Upon placement in the horizontal position, cell division in *Arabidopsis* roots has been shown to be temporarily suspended *(7)*. Hypocotyls are exquisitely light responsive and rapid switches in microtubule orientation, involving altered dynamics, have been noted when etiolated hypocotyls are exposed to blue light.

8. *Phototoxicity:* The risk of phototoxicity from the high intensity light used to excite fluorophores is the first consideration when embarking on live cell imaging *(46)*. Scan times need to be limited to avoid bleaching the fluorescence or impairing the function of the tagged protein. This makes it far more challenging to collect the same level of 3-D information that is possible on fixed, immunolabeled material. Choosing fluorescent proteins that can be excited by low energy, longer wavelength light such as RFP is one strategy but special attention to autofluorescence is required. Probably the most important way to limit phototoxicity is to choose the most light-sensitive camera possible, and minimize the intensity of the excitation light source. Spinning disc scan heads can also reduce dwell times, reducing both phototoxicity and photobleaching.
9. *Choice of promoter:* To overcome the need for high intensity excitation, transgenic lines are typically chosen that have high expression levels, usually achieved by using the 35S cauliflower mosaic virus (CMV) promoter element, which drives constitutive and generally high expression, in most tissues of higher plants. Depending on where the transgene is inserted, and whether multiple insertions take place, the level of expression of 35S-driven microtubule reporter proteins can vary considerably. The 35S CMV promoter has been used effectively for most microtubule reporters, but in some cases the high level of expression generates artefacts by changing the dynamics of microtubules or promoting bundle formation. For example, 35S-driven EB1-GFP can decorate both the plus and

minus ends of growing microtubules, is even found along the microtubule lattice and endomembranes *(47, 48)*, whereas it is distributed to the growing plus end when an endogenous promoter is used to drive its expression *(45)*. The MBD-GFP reporter fusion was constructed from the MT binding domain (amino acid residues 935–1,084) of the mammalian MAP4 *(37)*. Under control of the 35S promoter, MBD-GFP expression decorates microtubules in plant cells very effectively **(Fig. 1d)** but can cause significant developmental defects, suggesting that this heterologous protein (there is no MAP4 homologue known in plant cells) interferes with normal function of microtubules. In different genetic backgrounds, the 35S::MBD-GFP has been shown to cause unusual bundle formation that is not observed in the same genotypes with other reporters or by immunofluorescence *(7, 49, 50)*. Interestingly, a recent study in which the IRX7 promoter element was used to control MBD-GFP expression, expression was restricted to vascular and epidermal cells, and no developmental defects were reported *(51)*.

10. The buffer concentration has to be selected carefully according to the physiological demand of the cells; when buffer concentration is too high, osmotic phenomena may occur that leads to a detachment of the plasma membrane from the cell wall.
11. Cells can be alternatively fixed in 50 mM cacodylate buffer, 1% glutar aldehyde, washed, postfixed for 2 h in a mixture of buffered 1% osmium tetroxide, 0.8% potassium hexacyanoferrate and then post-stained in aqueous 2% uranyl acetate according to *(39)*.
12. Spurr's resin may be the best choice when different degrees of hardness have to be achieved according to the needs of different plant tissues. As several components of the original mixture are not available any more, we now use the kit "Agar Low Viscosity Resin (LV)".
13. Prepare formvar coated grids as follows: dip clean coverslip in 0.3% formvar dissolved in chloroform, remove gently and allow to dry, cut the edges on top of the cover slip with a sharp pin, allow the thin film to float on water surface by gently dipping the coverslip in water, put grid on this film and collect from the water surface with Parafilm™.
14. During incubation in uranyl acetate solution it is necessary to keep the sections in darkness by covering the dish with aluminum foil.

15. The following procedure has been found useful for the preparation of Reynolds lead citrate: Allow distilled water to boil for 10 min to remove air and carbon dioxide, let cool and use only this water for the following procedure:; dissolve 1.33 g lead nitrate and 1.76 g sodium citrate in 30 ml boiled distilled water, shake hard for 1 min (the salts will not dissolve right away, but it will remain a white solution); leave for 30 min, add 8 ml of 1 *N* sodium hydroxide until the solution clears if necessary add a little more sodium hydroxide until the solution clears, then fill to 50 ml with boiled distilled water.
16. Samples may be adjusted to increasing sucrose concentrations by cultivating them in a medium containing gradually elevating sucrose *(32)*.
17. Alternatively, samples can be frozen in a Leica EMPACT high pressure freezer (Leica Microsysteme GmbH, Vienna, Austria).
18. Some researchers recommend adding a certain proportion of water to the samples to improve the quality of the final preservation (e.g. *(52, 53)*); this is basically against the theory, so have to look at their explanations. Moreover, it may be useful to prolong the substitution process for several days or up to a week according to the size of the plant samples (A. Staehelin, personal communication).
19. This method is only suitable, when the samples are extremely thin, and it is expected that only the first ~20 μm are preserved well, whereas with high pressure freezing, up to several mm thick samples are preserved well.
20. Depending on the desired blocking, the following "blocking buffers" can be used alternatively: (a) TBS, 1% BSA, 0.1% Tween-20 for 20 min followed by incubation in TBS, 1% acetylated BSA; or (b) TBS containing 1% BSA, 20% bovine fetal serum followed by incubation in TBS, 1% BSA, 1% BSAac, 0.5% Tween-20; or (c) TBS, 5% non-fat milk, 0.1% Tween-20 followed by TBS, 1% BSA, 0.2% gelatine; or (d) 10 mm phosphate-buffered saline (PBS), pH 7.4, 50 mm glycine (Merck), followed by PBS containing 1% BSA, 2% gelatine (Merck).
21. Despite the fact that it is time consuming, follow this procedure: Rinse grids containing the sections with a mild spray of TBS from a Pasteur pipette, transfer onto small droplets of TBS for 2 min, rinse a second time with TBS; complete the washing step with a mild spray of double-distilled water from a plastic spray bottle.
22. Counterstaining may either be omitted or the times reduced drastically according to the desired density of staining.

Acknowledgment

This chapter has been supported in part by a grant from the Universitätszentrum Obergurgl, University of Innsbruck, Austria to AH and funding from the Natural Sciences and Engineering Research Council and the Canadian Institutes of Health Research to GOW. The Thieme Verlag KG is acknowledged for their kind permission to reproduce **Fig.1b**, **c** and Elsevier for reproduction of **Fig. 7**.

References

1. Wasteneys, G. O. (2002) Microtubule organization in the green kingdom: chaos or selforder? *J. Cell Sci.* **115**, 1345–1354.
2. Otegui, M. S. and Austin, J. R. II. (2007) Visualization of membrane-cytoskeletal interactions during plant cytokinesis. *Methods Cell Biol.* **79**, 221–240.
3. Ambrose, J. C., Shoji, T., Kotzer, A. M., Pighin, J. A. and Wasteneys G. O. (2007) The *Arabidopsis* CLASP gene encodes a microtubule-associated protein involved in cell expansion and division. *Plant Cell* **19**, 2763–2775.
4. Green, P. B. (1962) Mechanisms for plant cellular morphogenesis. *Science* **138**, 1404–1405.
5. Kost, B., Bao, Y.-Q. and Chua, N.-H. (2002) Cytoskeleton and plant organogenesis. *Philos. Trans. R. Soc. Lond. B* **357**, 777–789.
6. Smith, L. G. (2003) Cytoskeletal control of plant cell shape: getting the fine points. *Curr. Opin. Plant Biol.* **6**, 63–73.
7. Kawamura, E., Himmelspach, R., Rashbrooke, M. C., Whittington, A. T., Gale, K. R., Collings, D. A. and Wasteneys, G. O. (2006) MICROTUBULE ORGANIZATION 1 regulates structure and function of microtubule arrays during mitosis and cytokinesis in the *Arabidopsis* root. *Plant Physiol.* **140**, 102–114.
8. Ambrose, J. C. and Wasteneys, G. O. (2008) CLASP modulates microtubule-cortex interaction during self-organization of acentrosomal microtubules. *Mol. Biol. Cell* **19**, 4730–4737.
9. Bibikova, T. N., Blancaflor, E. B. and Gilroy, S. (1999) Microtubules regulate tip growth and orientation in root hairs of *Arabidopsis thaliana*. *Plant J.* **17**, 657–665.
10. Ketelaar, T. and Emons, A. M. C. (2001) The cytoskeleton in plant cell growth: lessons from root hairs. *New Phytol.* **152**, 409–418.
11. Yu, R., Huang, R.-F., Wang, X.-C. and Yuan, M. (2001) Microtubule dynamics are involved in stomatal movement of *Vicia faba* L. *Protoplasma* **216**, 113–118.
12. Holzinger, A. and Lütz-Meindl, U. (2002) Kinesin-like proteins are involved in postmitotic nuclear migration of the unicellular green alga *Micrasterias denticulata*. *Cell Biol. Int.* **26**, 689–697.
13. Holzinger, A. and Lütz-Meindl, U. (2003) Evidence for kinesin- and dynein-like protein function in circular nuclear migration in the green alga *Pleurenterium tumidum*: digital time lapse analysis of inhibitor effects. *J. Phycol.* **39**, 106–114.
14. Kandasamy, M. K. and Meagher, R. B. (1999) Actin-organelle interaction: association with chloroplast in Arabidopsis leaf mesophyll cells. *Cell Motil. Cytoskeleton* **44**, 110–118.
15. Holzinger, A., Wasteneys, G. and Lütz, C. (2007) Investigating cytoskeletal function in chloroplast protrusion formation in the arctic- alpine plant *Oxyria digyna*. *Plant Biol.* **9**, 400–410.
16. Holzinger, A., Kwok, E. Y. and Hanson, M. R. (2008) Effects of *arc3*, *arc5* and *arc6* mutations on plastid morphology and stromule formation in green and non-green tissues of *Arabidopsis thaliana*. *Photochem. Photobiol.* **84**, 1324-1335.
17. Zaffryar, S., Zimerman, B., Abu-Abied, M., Belausov, E., Lurya, G., Vainstein, A., Kamenetsky, R. and Sadot, E. (2007) Development-specific association of amyloplasts with microtubules in scale cells of *Narcissus tazetta*. *Protoplasma* **230**, 153–163.
18. Gilroy, S. (1997) Fluorescence microscopy of living plant cells. *Annu. Rev. Plant Mol. Biol.* **48**, 165–190.
19. Cyr, R., Dixit, R. and Gilroy, S. (2006) Live cell imaging using GFPs. *Plant J.* **45**, 599–615.
20. Mathur, J. (2006) The illuminated plant cell. *Trends Plant Sci.* **12**, 506–513.

21. Kwok, E. Y. and Hanson, M. R. (2003) Microfilaments and microtubules control the morphology and movement of non-green plastids and stromules in *Nicotiana tabacum*. *Plant J.* **35**, 16–26.
22. Wasteneys, G. O., Willingale-Theune, J. and Menzel, D. (1997) Freeze shattering: a simple and effective method for permeabilizing higher plant cell walls. *J. Microsc.* **188**, 51–61.
23. Shaw, S. L., Kamyar, R. and Ehrhardt, D. W. (2003) Sustained microtubule treadmilling in Arabidopsis cortical arrays. Science 300, 1715–1718.
24. Chan, J., Calder, G., Fox, S. and Lloyd, C. (2007) Cortical microtubule arrays undergo rotary movements in *Arabidopsis* hypocotyl epidermal cells. *Nat. Cell Biol.* **9**, 171–175.
25. Kawamura, E. and Wasteneys, G. O. (2008) MOR1, the Arabidopsis thaliana homologue of Xenopus MAP215, promotes rapid growth and shrinkage, and suppresses the pausing of microtubules in vivo. *J. Cell Sci.* 121, 4114–4123.
26. Pastuglia, M., Azimzadeh, J., Goussot, M., Camilleri, C., Belcram, K., Evrard, J. L., Schmit, A. C., Guerche, P. and Bouchez, D. (2006) Gamma-tubulin is essential for microtubule organization and development in Arabidopsis. *Plant Cell* **18**, 1412–1425.
27. Chang, H. Y., Smertenko, A. P., Igarashi, H., Dixon, D. P. and Hussey, P. J. (2005) Dynamic interaction of NtMAP65-1a with microtubules in vivo. *J. Cell Sci.* **118**, 3195–3201.
28. Shaw, S. L. (2006) Imaging the live plant cell. *Plant J.* **45**, 573–598.
29. Ledbetter, M. C. and Porter, K. R. (1963) A "microtubule" in plant fine structure. *J. Cell Biol.* **19**, 239–250.
30. Meindl, U., Lancelle, S. and Hepler, P. K. (1992) Vesicle production and fusion during lobe formation in *Micrasterias denticulata* visualized by high-pressure freeze fixation. *Protoplasma* **170**, 104–114.
31. Holzinger, A. (2000) Aspects of cell development in *Micrasterias muricata* (Desmidiaceae) revealed by cryofixation and freeze substitution. *Nova Hedwigia* **70**, 275–288.
32. Seguí-Simarro, J. M., Austin, J. R. II, White, E. A. and Staehelin L. A. (2004) Electron tomographic analysis of somatic cell plate formation in meristematic cells of *Arabidopsis* preserved by high-pressure freezing. *Plant Cell* **16**, 836–856.
33. Eder, M. and Lütz-Meindl, U. (2008) Pectin-like carbohydrates in the green alga *Micrasterias* characterized by cytochemical analysis and energy filtering TEM. *J. Microsc.* **231**, 201–214.
34. Holzinger, A., Valenta, R. and Lütz-Meindl, U. (2000) Profilin is localized in the nucleus-associated microtubule and actin system and is evenly distributed in the cytoplasm of the green alga *Micrasterias denticulata*. *Protoplasma* **212**, 197–205.
35. Gaillard, J., Neumann, E., Van Damme, D., Stoppin-Mellet, V., Ebel, C., Barbier, E., Geelen, D. and Vantard, M. (2008) Two microtubule-associated proteins of *Arabidopsis* MAP65s promote anti-parallel microtubule bundling. *Mol. Biol. Cell*, 19, 4534-4544.
36. Nakamura, M., Naoi, K., Shoji, T. and Hashimoto, T. (2004) Low concentrations of propyzamide and oryzalin alter microtubule dynamics in Arabidopsis epidermal cells. *Plant Cell Physiol.* **45**, 1330–1334.
37. Marc J., Granger, C. L., Brincat, J., Fisher, D. D., Kao, T.-H., McCubbin, A.-G. and Cyr, R. J. (1998) A GFP-MAP4 reporter gene for visualizing cortical microtubule rearrangements in living epidermal cells. *Plant Cell* **10**, 1927–1939.
38. Holzinger, A., Karsten, U., Lütz, C. and Wiencke, C. (2006) Ultrastructure and photosynthesis in the supralittoral green macroalga *Prasiola crispa* (Lightfoot) Kützing from Spitsbergen (Norway) under UV exposure. *Phycologia* **45**, 168–177.
39. Holzinger, A. and Meindl, U. (1997) Jasplakinolide, a novel actin targeting peptide, inhibits cell growth and induces actin filament polymerization in the green alga *Micrasterias*. *Cell Motil. Cytoskeleton* **38**, 365–372.
40. Ueda, K., Matsuyama, T. and Hashimoto, T. (1999) Visualization of microtubules in living cells of transgenic *Arabidopsis thaliana*. *Protoplasma* **206**, 201–206.
41. Abe, T. and Hashimoto, T. (2005) Altered microtubule dynamics by expression of modified alpha-tubulin protein causes right-handed helical growth in transgenic Arabidopsis plants. *Plant J.* **43**, 191–204.
42. Granger CL, Cyr RJ (2001) Spatiotemporal relationships between growth and microtubule orientation as revealed in living root cells of Arabidopsis thaliana transformed with green-fluorescent-protein gene construct GFP-MBD. Protoplasma 216, 201-214
43. Sakai, T., van der Honing, H., Nishioka, M., Uehara, Y., Takahashi, M., Fujisawa, N., Saji, K., Seki, M., Shinozaki, K., Jones, M. A., Smirnoff, N., Okada, K. and Wasteneys, G. O. (2007) Armadillo repeat-containing kinesins and a NIMA-related kinase are required for epidermal cell morphogenesis in *Arabidopsis*. *Plant J.* **53**, 157–171.

44. Van Bruaene, N., Joss, G. and Van Oostveldt, P. (2004) Reorganization and in vivo dynamics of microtubules during *Arabidopsis* root hair development. *Plant Physiol.* **136**, 3905–3919.

45. Dixit, R., Chang, E. and Cyr, R. (2006). Establishment of polarity during organization of the acentrosomal plant cortical microtubule array. *Mol. Biol. Cell.* **17**, 1298–1305.

46. Dixit, R. and Cyr, R. (2003) Cell damage and reactive oxygen species production induced by fluorescence microscopy: effect on mitosis and guidelines for non-invasive fluorescence microscopy. *Plant J.* **36**, 280–290.

47. Chan J., Calder, G. M., Doonan, J. H. and Lloyd, C. W. (2003) EB1 reveals mobile microtubule nucleation sites in Arabidopsis. *Nat. Cell Biol.* **5**, 967–971.

48. Mathur, J., Mathur, N., Kernebeck, B., Srinivas, B. P. and Hulskamp, M. (2003) A novel localization pattern for an EB1-like protein links microtubule dynamics to endomembrane organization. *Curr. Biol.* **13**, 1991–1997.

49. DeBolt, S., Gutierrez, R., Ehrhardt, D. W., Melo, C. V., Ross, L., Cutler, S. R., Somerville, C. and Bonetta, D. (2007) Morlin, an inhibitor of cortical microtubule dynamics and cellulose synthase movement. *Proc. Natl Acad. Sci. U. S. A.* **104**, 5854–5849.

50. Stoppin-Mellet, V., Gaillard, J. and Vantard, M. (2006) Katanin's severing activity favors bundling of cortical microtubules in plants. *Plant J.* **46**, 1009–1017.

51. Wightman, R. and Turner, S. R. (2007) Severing at sites of microtubule crossover contributes to microtubule alignment in cortical arrays. *Plant J.* **52**, 742–751.

52. Buser, C. and Walther, P. (2008) Freeze substitution: the addition of water to polar solvents enhances the retention of structure and acts at temperatures around –60°C. *J. Microsc.* **230**, 268–277.

53. Walther, P. and Ziegler, A. (2002) Freeze substitution of high-pressure frozen samples: the visibility of biological membranes is improved when the substitution medium contains water *J. Microsc.* **208**, 3–10.

Part V

Analysis of cell and Organelle Motility

Chapter 14

A Rapid Tracking Method for the Quantitative Analysis of Organelle Streaming Velocity

Carola Luise Holweg

Summary

A key to understanding cytoskeletal mechanisms of eukaryotic cells is found in their internal motility. In many plant cell types, these motile events, termed "cytoplasmic streaming", are very impressive with rapid movement of organelles over long distances. Like many other features of cytoplasmic streaming, organelle velocity is determined by acto-myosin-related mechanisms. Therefore, the quantification of streaming velocity aids the characterization of important factors contributing to cytoskeleton function. Usually, the movement velocity varies greatly between particles and exhibits rapid changes. This complexity makes measurements very cumbersome and requires large cell numbers and a lot of imaging data for statistical evaluation. Focusing on a triplet of rapidly moving organelles in a single cell proved to be an efficient method for determining organelle displacement in a direct, standardized manner. This approach requires only a few cells and allows the evaluation of potential factors involved in cytoplasmic streaming with a relatively low temporal and technical effort. This chapter evaluates two examples that show the high sensitivity of the method in the detection of differences in organelle streaming velocities. These include the retardation of streaming upon myosin inhibition and a similar, but much less expected, response following the overexpression of actin-binding proteins.

Key words: Actin-binding proteins, Actin-cytoskeleton, Cytoplasmic streaming, Myosin, Organelle transport

1. Introduction

Intracellular motility is a ubiquitous phenomenon of eukaryotic cells. Because of the extremely elongated shape of many plant cells, rapid movement of streaming particles may be observed over long distances. The foundation of these motility events, known as "cytoplasmic streaming", is on the basis of a complex mechanism powered by the actin cytoskeleton *(1)* and its

R.H. Gavin (ed.), *Cytoskeleton Methods and Protocols,* Methods in Molecular Biology, vol. 586
DOI 10.1007/978-1-60761-376-3_14,
© Humana Press, a part of Springer Science + Business Media, LLC 2009

associated motor protein myosin *(2)*. Myosin from Characean algae became famous for its extremely fast *in vitro* motility *(3, 4)*, which coincides well with the rapid movements observed in living algae *(2)*. Myosins from land plants also seem to produce much higher velocities than those of other eukaryotes *(5)*. Plants have evolved actin- and myosin-based mechanisms for the transport of organelles that are microtubule-dependent in animal cells *(6)*.

Myosins move unidirectionally along microfilaments via flexible binding between their heads and actin monomers, while their tails are associated with the surface of organelles. Thereby, myosins are able to tether and direct various kinds of cargos through cytoplasmic strands. Cytoplasmic streaming is believed to regulate the distribution of organelles and the supply of nutrients, including the components of new cell walls. Various signals control these processes in plant cells and they are closely linked with the actin cytoskeleton *(7)*. They include cellular responses such as F-actin reorientation upon exposure to light or auxin *(8)* and the rapid velocity changes of organelle streaming because of Ca^{2+} *(9, 10)*. Thus, the analysis of cellular motility allows the characterization of important factors involved in cytoskeleton function.

A promising approach in this context is the study of changes in cellular motility following the overexpression of cytoskeletal proteins. Normally, because of the high variability of slow and fast movements of organelles in one cell, hundreds of cells have to be examined in order to achieve significant results. Therefore, statistical evaluation is often carried out using leaf epidermis of *Nicotiana benthamiana* after *Agrobacterium*-mediated transformation *(11, 12)*. Automated imaging programs can then be employed to evaluate the large amount of data. However, researchers might prefer leaves of other plant phyla that are not susceptible to *Agrobacterium*, or they may work with vectors that only allow transient protein expression after particle bombardment or microinjection, which result in low numbers of expressing cells. Others simply require a quick method to determine streaming velocity of diverse cellular particles. For these and other purposes, individual-cell assays that are statistically robust but require very limited numbers of cells are useful *(13, 14)*.

The present protocol describes the determination of potential negative effects on organelle displacement by the calculation of the maximal streaming velocity. This is done in a direct and standardized way and is on the basis of time-lapse imaging and simple tracking software. The method is fast and the results are easily obtained without expensive equipment. In the first example, streaming velocity is determined in epidermal cells of *Arabidopsis* hypocotyls

during myosin inhibition with the chemical BDM (2,3-butanedione monoxime). Secondly, retardation of streaming is shown to occur in response to the overexpression of actin-binding proteins in the same cell type. On the basis of these observations, we previously discussed how live markers for actin visualization may affect cellular motility (for GFP-mTn and GFP-FABD2 *see* **ref.** *13*; for a GFP-fused head of myosin XI-2 *see* **ref.** *14*). The results highlight the general need for critical investigation of actin-related processes.

2. Materials

2.1. Plant Preparation and Treatment

1. *Arabidopsis* seeds: wild types from Lehle Seeds, Tucson, AZ; for GFP-FABD2 line see *(15);* for GFP-mTn line see *(16, 17)* (*see* **Fig. 1** and **Note 1**).
2. Whatman filter paper (0.4 mm).
3. Plastic or glass boxes of about 9 × 9 × 9 cm supplied with a cover.
4. Sealing film to make sure that the paper does not dry out.
5. Incubators at 4°C and 21–25°C.
6. Drug treatment: prepare stock solution of 250 mM BDM (Sigma-Aldrich; *see* **Note 2**) in dH_2O. Stock solutions may be stored in the refrigerator for 2 weeks. Working solutions (10, 30, and 50 mM BDM) should be prepared fresh.

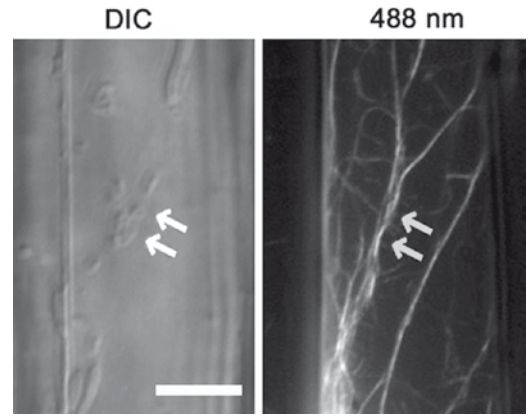

Fig. 1. Cytoplasmic and F-actin arrangements in an epidermal cell from the hypocotyl of a 3-day-old dark-grown *Arabidopsis* seedling transgenic for GFP-FABD2. The image on the left was taken with DIC optics. It shows organelles of various sizes (and speed). The corresponding fluorescent image was taken with a 488 nm excitation wavelength. Bar = 10 μm.

2.2. Material for Microscopic Observation and Programs

1. AxioImager Z.1. epi-fluorescence microscope (Zeiss, Jena, Germany) supplied with the optics for differential interference contrast (DIC) microscopy and equipped with a Zeiss digital camera AxioCam MRm (*see* **Note 3**) and AxioVision Rel. 4.5 software.
2. 20× objective and a 63× plan apochromat oil immersion system N.A 1.4.
3. Glass slides and microscope cover slips (22 × 40 × 0.15 mm) from Roth, Germany, and razor blades (e.g. Wilkinson, USA).
4. Stopwatch, room thermometer.
5. Free IMAGE J software (National Institutes of Health, Bethesda, USA), 1.7 MB download (*see* **Note 4**).
6. Excel software for calculations and diagrams.

3. Method

3.1. Preparation of Plant Material

1. Sow wild-type and transgenic seeds on moist filter paper in boxes.
2. For optimized germination, put them at 4°C overnight and then expose to light for 2–6 h at RT.
3. Germinate seeds for 72 h at 21–25°C in the dark.

3.2. Mounting of Seedlings

1. For microscopy, place etiolated seedlings on a glass slide. In order to obtain flat hypocotyl surfaces and the best contact with the cover slide, immediately and carefully cut off cotyledons and roots with a razor blade.
2. After adding a drop of water, place a cover slide over the hypocotyls (*see* **Notes 5** and **6**).
3. Parameters such as temperature and light, and hypocotyl preparation methods have to be kept as constant as possible for all observations. As cytoplasmic streaming is a temperature-sensitive process, a thermometer placed directly on the slide table of the microscope is useful to monitor and keep the temperature between 22 and 24°C.
4. To further ensure equal experimental conditions for comparisons, always place transgenic seedlings directly beside wild-type seedlings within a distance of 3 mm. Switch between them for each image series.
5. Find the appropriate position on the hypocotyls (*see* **Notes 7** and **8**) and adjust the plane of focus with the 20× objective. Then switch to the 63× objective.

6. Before taking images of cytoplasmic streaming, allow hypocotyls to adapt to the conditions at the microscope including DIC light for 5 min.
7. When observing cells that express GFP-fused proteins (*see* **Notes 9–11**), it is possible to switch from DIC optics to the 488 nm wavelength in order to select cells that exhibit appropriate protein expression.
8. For drug treatment, the solutions have to be temperature-equilibrated and added drop-wise under one edge of the cover slide. Remove excess solution with a paper tissue held onto the opposite edge.

3.3. Processing and Evaluation of Image Data

1. Take several images (frames) from at least three hypocotyls observed on different days. For each frame, take 30 time-series images at 1 s intervals at a resolution of 1,388 × 1,040 pixels. Determine the maximal average velocity from a total of 5–15 cells (= n).
2. Save images as JPEG files.
3. Import images into IMAGE J as an image sequence (activate the conversion to 8-bit grayscale for a faster import). The sequence will appear in a new window.
4. Scroll through the window with the help of the scroll bar, quickly selecting three of the fastest particles by eye (=rapid triplet) (*see* **Note 12**).
5. Observe the translocation of each particle for as long as the fast velocity proceeds.
6. The distance covered by a particle between the first and last images is marked with the "straight line selection" and determined by the "analyze-measure" function. Under "set measurements" (see "analyze"), activate only the number of decimal places.
7. Copy the resulting track lengths (in pixels) into the Excel software.
8. Further processing may require the conversion of dots into commas at the decimal place (depending on the Excel version). This can be done with the "search and replace" function under "file" in Excel.
9. Calculate track lengths in μm with the help of the pixel/μm ratio. This ratio is either obtained directly with the AxioVision software or determined with a micrometer slide.
10. In order to determine the velocity (μm/s), divide the track lengths by the respective number of scrolled images (usually 3–5), i.e. seconds.

11. For comparison, analyze the velocities from treatments or different transgenic lines using a Student's *t*-test at a 97.5% significance level. Error bars are indicated by the SE calculated from n triplets (*see* **Fig. 2**).

4. Notes

1. For comparison of organelle streaming between transgenic plant lines, the corresponding wild types have to be included. Thus, natural differences between different wild types can be excluded. The wild types of the GFP-FABD2 and the GFP-mTn lines are Col and L*er*, respectively. Although certain features of the plant growth of these wild types vary to some extent (e.g. thicker stems and siliques in the case of L*er*), their streaming velocities are very similar *(13)*.
2. BDM inhibits myosins by the formation of a complex between their heads and the nucleotide. **Fig. 2a** shows that rapid retardation of streaming velocity already occurs at low concentrations of BDM, quite similar to the action of the actin-disrupting drug Cytochalasin D (CD) *(13)*. Here, maximal average speeds decreased from 5.2 to 3.5 μm/s during the first 5 min after application of a low concentration of 10 μM CD.
3. A fast digital camera such as the AxioCam MRm (Zeiss) is comfortable but not necessary. Cameras with lower capacity

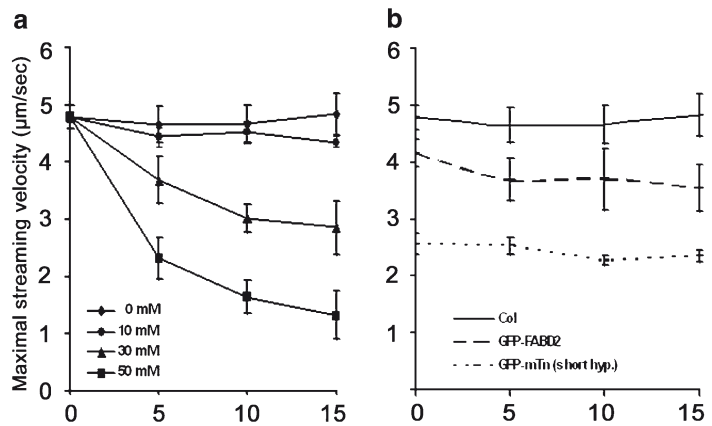

Fig. 2. Response of the maximal streaming velocity in cytoplasmic main tracks to factors interfering with cytoskeleton function. (*a*) Concentration-dependent response to BDM, which blocks myosin function. (*b*) Response to overexpressed actin-binding proteins in FABD2 and short mTn seedlings (hypocotyls). Error bars shown in (a), SE ($n = 4$), in (b), SE ($n = 8$) (Figure reproduced from *ref. 13* with the permission of Wiley and Sons).

also fulfill the requirements of the procedure. As long as the image acquisition time ranges below 2 s, images may be taken manually.

4. The computer-based programs used in our approach are directly applicable and require only low storage capacity. The free version of IMAGE J of only 1.7 MB is quite sufficient and easy to use. In contrast to the video files that are usually required for the more complex image calculation software, this and other minimal programs work with JPEG formats, allowing a more flexible evaluation at any personal computer.
5. Air bubbles are undesirable and careful application of the cover slide during the mounting of hypocotyls minimizes their appearance.
6. During prolonged observation (>10 min), care must be taken to prevent hypocotyls becoming dry because of water evaporation.
7. As cells from different parts of the hypocotyls may behave differently, it is useful to take images from similar heights (e.g. always the central part).
8. As the motility behavior may change in different cellular regions, different responses to cytoskeletal factors might be expected. For example, retarded streaming velocity has been observed near cell plates in epidermal cells of *Arabidopsis* hypocotyls *(13)*. Therefore, additional information might be obtained if the maximal streaming velocity is measured separately in some restricted areas. These may include the peripheries of nuclei or cell plates.
9. The reduced motility in transgenic plants shown in **Fig. 2b** may be explained by a disturbed acto-myosin interplay, if overexpressed actin-binding proteins block the processive movement of myosin along actin filaments *(13, 14)*.
10. **Fig. 2b** shows that organelle motility is severely disturbed in small GFP-mTn seedlings. The small size and other developmental defects that occur in the GFP-mTn line are known to be caused by the talin protein that causes F-actin bundling *(18, 19)*. Indeed, we observed that microfilaments in smaller seedlings were generally labeled more strongly and were thicker than those found in normally elongated GFP-mTn seedlings *(13)*.
11. We have observed that the overexpression of GFP alone may reduce organelle streaming velocity to a low extent. Maximal average speeds in onion cells transiently expressing GFP alone were reduced by about 10% *(14)*. However, this difference was only obtained if the significance level was set at 90% for the *t*-test. Higher significance levels did not reveal a difference. Nevertheless, this information may be useful

when streaming speeds are determined in transgenic cells overexpressing fusion proteins that produce a high cytoplasmic background of GFP. If the amount of diffusive GFP molecules is high, one should also determine organelle speeds in cells expressing GFP alone. In the case of GFP-FABD2, the background of GFP is negligible.

12. The main key to the present approach is the selection of fast moving particles by eye scrolling through the images produced by IMAGE J. It needs some training, but is very useful for comparison between treatments or different lines. It must be kept in mind that the pre-selection of particles via the velocity parameter excludes slow organelles that are slow. Mitochondria, for instance, have been observed to exhibit at least twofold the maximal velocity of peroxisomes (Walter and Holweg, unpublished data). This observation was consistent for different plant phyla, including epidermal cells of the monocot *Allium cepa* (onion bulb) and the dicot *Sinapis alba* (hypocotyls) that transiently expressed organelle markers (organelle markers were a kind donation of A. Nebenführ, see **ref.** *20)*. In general, mitochondria appear to be smaller than peroxisomes in both plant species. In cases where the potential preference of specific organelle types should be avoided, it may be useful to measure fast moving particles of various sizes and shapes. For this purpose, the triplet selection in *Arabidopsis* (compare DIC image of **Fig. 1**) ideally consists of a spindle-like organelle at lengths above 3 μm *(21)*, a smaller particle below 2 μm, and one below 0.5 μm.

Acknowledgments

The author would like to thank Nadine Walter for the measurements of peroxisomal and mitochondrial streaming velocities, A. Nebenführ for the organelle markers, J. Mathur for GFP-mTn, and B. Voigt and D. Menzel for the GFP-FABD2 construct. This work was supported by the DFG (Deutsche Forschungsgemeinschaft), research grant Ho 3327.

References

1. Williamson, R.E. (1993) Organelle movements. *Ann. Rev. Plant Physiol. Plant Mol. Biol.* **44**, 181–202.
2. Shimmen, T. and Yokota, E. (2004) Cytoplasmic streaming in plants. *Curr. Opin. Cell Biol.* **16**, 68–72.
3. Higashi-Fujime, S., Ishikawa, R., Iwasawa, H., Kagami, O., Kurimoto, E., Kohama, K., and Hozumi, T. (1995) The fastest actin-based motor protein from the green algae, Chara, and its distinct mode of interaction with actin. *FEBS Lett.* **375**, 151–154.

4. Morimatsu, M., Nakamura, A., Sumiyoshi, H., Sakaba, N., Taniguchi, H., Kohama, K., and Higashi-Fujime, S. (2000) The molecular structure of the fastest myosin from green algae. *Chara Biochem. Biophys. Res. Comm.* **270**, 147–152.
5. Tominaga, M., Kojima, H., Yokota, E., Orii, H., Nakamori, R., Katayama, E., Anson, M., Shimmen, T., and Oiwa, K. (2003) Higher plant myosin XI moves processively on actin with 35 nm steps at high velocity. *EMBO J.* **22**, 1263–1272.
6. Mathur, J., Mathur, N., and Hülskamp, M. (2002) Simultaneous visualization of peroxisome and cytoskeletal elements reveals actin and not microtubule-based peroxisome motility in plants. *Plant Physiol.* **128**, 1031–1045.
7. Staiger, C. (2000) Signaling to the actin cytoskeleton in plants. *Annu. Rev. Plant Physiol. Plant Mol. Biol.* **51**, 257–288
8. Holweg, C., Süsslin, C., and Nick, P. (2004) Capturing in vivo dynamics of the actin cytoskeleton stimulated by auxin or light. *Plant Cell Physiol.* **45**, 855–863.
9. Yokota, E., Muto, S., and Shimmen, T. (1999) Inhibitory regulation of higher-Plant myosin by Ca^{2}+ ions. *Plant Physiol.* **119**, 231–239.
10. Awata, J., Saitoh, K., Shimada, K., Kashiyama, T., and Yamamoto, K. (2001) Effects of Ca2+ and calmodulin on the motile activity of characean myosin in vitro. *Plant Cell Physiol.* **42**, 828–834.
11. Reisen, D. and Hanson, M.R. (2007) Association of six YFP-myosin XI-tail fusions with mobile plant cell organelles. *BMC Plant Biol.* **7**, 6.
12. Avisar, D., Prokhnevsky, A.I., Makarova, K.S., Koonin, E.V., and Dolja, V.V. (2008) Myosin XI-K is required for rapid trafficking of golgi stacks, peroxisomes and mitochondria in leaf cells of *Nicotiana benthamiana*. *Plant Phys.* **146**, 1098–1108.
13. Holweg, C.L. (2006) Living markers for actin block myosin-dependent motility of plant organelles and auxin in *Arabidopsis thaliana*. *Cell Motil. Cytoskeleton* **64**, 69–81.
14. Walter, N. and Holweg, C. (2008) Head-neck domain of *Arabidopsis* myosin XI, MYA2, fused with GFP produces F-actin patterns that coincide with fast organelle streaming in different plant cells. *BMC Plant Biology* **8**, 74.
15. Voigt, B., Timmers, A.C.J., Šamaj, J., Müller, J., BaluŠka, F., and Menzel, D. (2005) GFP-FABD2 fusion construct allows in vivo visualization of the dynamic actin cytoskeleton in all cells of *Arabidopsis* seedlings. *Eur. J. Cell Biol.* **84**, 595–608.
16. Kost, B., Spielhofer, P., and Chua, N.-H. (1998) A GFP-mouse talin fusion protein labels plant actin filaments in vivo and visualizes the actin cytoskeleton in growing pollen tubes. *Plant J.* **16**, 393–401.
17. Mathur, J., Spielhofer, P., Kost, B., and Chua, N.-H. (1999) The actin cytoskeleton is required to elaborate and maintain spatial patterning during trichome cell morphogenesis in *Arabidopsis thaliana*. *Development* **126**, 5559–5568.
18. Sheahan, M.B., Staiger, C.J., Rose, R.J., and McCurdy, D.W. (2004) A green fluorescent protein fusion to actin-binding domain 2 of *Arabidopsis* fimbrin highlights new features of a dynamic actin cytoskeleton in live plant cells. *Plant Physiol.* **136**, 3968–3978.
19. Ketelaar, T., Anthony, R.G., and Hussey, P.J. (2004) Green fluorescent protein-mTalin causes defects in actin organization and cell expansion in *Arabidopsis* and inhibits actin depolymerizing factor's actin depolymerizing activity in vitro. *Plant Physiol.* **136**, 3990–3998.
20. Nelson, B.K., Cai, X., and Nebenführ, A. (2007) A multicolored set of in vivo organelle markers for co-localization studies in *Arabidopsis* and other plants. *Plant J.* **51**, 1126–1136.
21. Hawes, C., Saint-Jore, C., Martin, B., and Zheng, H.Q. (2001) ER confirmed as the location of mystery organelles in *Arabidopsis* plants expressing GFP! *Trends in Plant Sci.* **6**, 245–246.

Chapter 15

Melanosome Motility in Fish Retinal Pigment Epithelial Cells

Christina King-Smith

Summary

Several model systems have been developed to investigate intracellular organelle motility. A relatively novel system that is simple but useful for studying mechanisms of organelle motility is the fish retinal pigment epithelial (RPE) cell. Primary cultures of dissociated RPE cells are easily prepared and amenable to organelle motility studies. In vivo, melanin-containing pigment granules (melanosomes) within the RPE migrate long distances in response to light flux. When cultured in vitro, RPE cells attach to the substrate with the apical projections extending radially from the central cell body. Melanosomes can be chemically triggered to aggregate or disperse throughout the projections, and can be easily observed using phase contrast microscopy. Melanosome migration in RPE apical projections is dependent on actin filaments, and thus renders this model system useful for investigations of actin-dependent organelle motility.

Key words: RPE, Actin, Microtubules, Organelle transport, Motor proteins, Melanosomes

1. Introduction

Retinal pigment epithelial (RPE) cells are located at the back of the vertebrate eye. In the eyes of fish and other lower vertebrates, RPE melanosomes undergo light-dependent migrations, dispersing out into the cells' long apical projections in the light, and aggregating back into the cell body in darkness. Fish do not have dilatable pupils to control light that enters the retina. Rather, the movable curtain of RPE melanosomes, together with the elongation and contraction of rod and cone photoreceptors serve to modulate light flux. The motility of melanosomes and photoreceptors are collectively called retinomotor movements (*1*).

R.H. Gavin (ed.), *Cytoskeleton Methods and Protocols,* Methods in Molecular Biology, vol. 586
DOI 10.1007/978-1-60761-376-3_15,
© Humana Press, a part of Springer Science + Business Media, LLC 2009

RPE cells can be isolated from the eye, dissociated into single cells, and cultured for up to 24 h. In vitro, RPE cells lose their apical-basal polarity, become radially symmetrical, and attach to the substrate, with the formerly apical projections extending outward from the central, pigment-filled cell body **(Fig. 1)**. Melanosome aggregation can be triggered by application of underivatived cAMP (*2*). Dispersion is stimulated by washout of cAMP in a medium containing dopamine **(Fig. 2)**.

Time-lapse videomicrography of melanosome motility within apical projections of dissociated RPE cells is easily carried out using a simple perfusion chamber on an upright compound microscope. Time-lapse videos reveal that patterns of melanosome motility differ during aggregation (retrograde motility) and dispersion (anterograde motility). During dispersion, melanosome motility is bidirectional and saltatory, at rates of 2–3 μm/min in the anterograde direction. In contrast, aggregation is continuous and unidirectional, also at 2–3 μm/min (*3*). Studies using cytoskeletal inhibitors, time-lapse and fluorescent microscopy, and quantification of pigment position in fixed cells have demonstrated that while microtubules are plentiful in apical projections, they are not required for melanosome motility. Rather, actin filaments are necessary and sufficient to support melanosome motility in

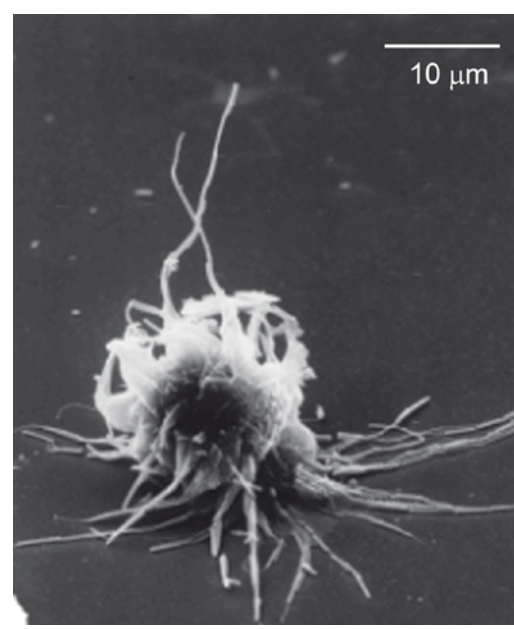

Fig. 1. Scanning electron micrograph of an isolated RPE cell. Formerly apical projections extend from the central cell body of dissociated cells.

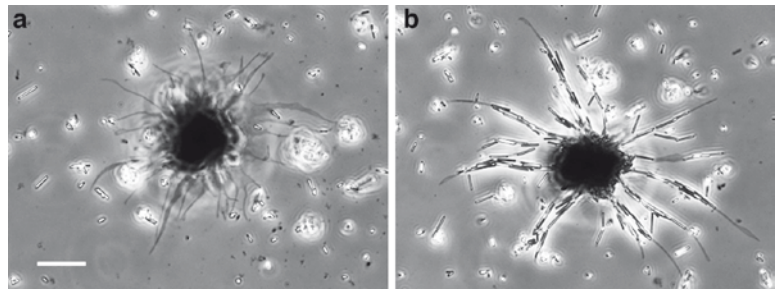

Fig. 2. Isolated RPE cells with aggregated and dispersed melanosomes. The cell on the left was treated with cAMP stimulating migration of melanosomes into the central cell body. Apical projections devoid of melanosomes appear phase-grey. The cell on the right has dispersed melanosomes; these appear phase-bright within the projections. Tips of projections are free of melanosomes because of the bidirectional shuttling of the melanosomes once full dispersion is achieved. Debris surrounding cells are melanosomes from lysed cells. Note that melanosomes are mostly cylindrical, not round. *Bar*: 10 μm.

isolated cells, with microtubules supplying structural support (*3*, *4*). Isolated RPE cells, therefore, represent a useful model system for study of intracellular organelle transport, especially actin-dependent motility.

2. Materials

2.1. Poly-l-Lysine-Coated Coverslips

1. 22 mm × 22 mm No. 1 coverslips.
2. Nitric acid.
3. poly-l-Lysine, (Sigma P-1524; >200 kD); 1 mg/ml in glass distilled, deionised water (ddH_2O). Store dry poly-l-Lysine at –20°C desiccated; store solution at –20°C; it can be reused four times.

2.2. Dissection and Isolation of RPE Sheets

1. Green sunfish *(Lepomis cyanellus)* or bluegill *(Lepomis macrochirus)* 2–4 in. in length, commonly available at fish hatcheries. Maintain on 14 h:10 h light: dark cycle.
2. MS-222 (3-aminobenzoic acid ethyl ester, methane sulfonate salt, Sigma A-5040) anesthetic. Prepare 10 g/l solution in ddH_2O. Aliquot in volumes sufficient for dilution to 75 mg/l in fish tank water, and freeze at –20°C.
3. Dark adaptation box with aeration.
4. Iris spring scissors (14 mm with curved blades; Fine Science Tools #15011–12) and forceps (Dumont #3).
5. HEPES-buffered Earles' Ringer (HER): 116.3 mM NaCl; 5.4 mM KCl; 1.8 mM $CaCl_2$; 0.8 mM $MgSO_4$; 1.0 mM Na_2HPO_4;

25.5 mM glucose; 4.0 mM $NaHCO_3$; 21 mM HEPES; pH 7.2). Made from 10× EBSS with phenol red in ddH_2O with additional 0.36 g/100 ml glucose; 0.034 g/100 ml $NaHCO_3$, and 0.50 g/100 ml HEPES. Make fresh or less than 24 h before use.

6. 35 mm Petri dish lined with soft dental plastic or parafilm.
7. 90 mm Petri dish lined with white silicon rubber or parafilm.

2.3. Preparation of Dissociated RPE Cells

1. Calcium- and magnesium-free HER (CMFHER) containing 1 mM EGTA: Made fresh from 10× CMFEBSS without phenol red, additional glucose, $NaHCO_3$, and HEPES is added as described above for HER. pH 7.4 (*see* **Note 1**).
2. Papain digest solution: 10 U/ml papain (Worthington Biochemical, # LS003126) in 5 ml CMFHER activated with 0.14 mg/ml DNase and 3 μM l-cysteine. Papain suspension is aliquoted and stored at 4°C. DNase and cysteine solutions are prepared fresh using 16.6 mg l-cysteine (Sigma C-8277) in 500 μl ddH_2O, and 10 mg DNase (Sigma DN25) in 500 μl ddH_2O, and kept on ice. Five millilitre papain digest solution is prepared per fish; added to that is enough papain for 10 U/ml, plus 64 μl l-cysteine solution and 36 μl DNase solution (*see* **Note 2**).
3. 35 mm Petri dish lined with parafilm.
4. 12–15 ml glass conical centrifuge tube.
5. HER supplemented with 0.4% BSA (HERB).
6. HERB supplemented with 0.1 mg/ml DNase.
7. Poly-l-Lysine coated coverslips in 35 mm Petri dishes.
8. 100 cm glass Petri dish with moistened filter paper (Whatman #1) in the cover.

2.4. Stimulation and Observation of Melanosome Motility

1. 1 mM cAMP (Sigma A-9501) in HERB made fresh from 10 mM cAMP/HERB stock, stored at –20°C.
2. 10 μM dopamine (3- hydroxytyramine, Sigma H-8502) in HERB made fresh. Dopamine oxidises easily; solutions should be remade after 1 h.
3. For perfusion chamber: standard microscope slides, double stick tape, wedges of filter paper (Whatman #3).

3. Methods

3.1. Preparation of Poly-l-Lysine Coated Coverslips

1. Soak coverslips in nitric acid for a few hours to overnight. (*see* **Note 3**).
2. Wash coverslips in running tap water for 1 h, rinse 5× in deionised water.

3. Remove coverslips from racks and place in 10 cm Petri dish with 1 mg/ml poly-l-Lysine solution (PLL).
4. Rock or rotate for at least 1 h at room temperature.
5. Remove PLL and wash coverslips in ddH_20 at least 10× (*see* **Note 4**).
6. Rinse coverslips in 100% ethanol and allow to air dry on filter paper (Whatman # 1).
7. Store on filter paper; can keep for several months.

3.2. Dissection and Isolation of RPE Sheets

1. Thaw MS-222 and add to fish tank water in dark adaptation box. (*see* **Note 5**).
2. Add fish and dark adapt 30 min to 2 h.
3. In dim light (0.002 J/s/m^2; *see* **Note 6**) enucleate eyes by blunt dissection using closed scissors; cut optic nerve. Place eyes on a paper towel lens side down.
4. Hemisect first eye; remove lens.
5. Holding edge of posterior eyecup with forceps (12 o'clock position) invert the eye cup retinal side down onto a paper towel. Gently press the back of the eyecup (sclera side) downwards onto the paper towel with the closed scissor blades so that the retina adheres to the paper towel; snip optic nerve to detach retina from the eyecup.
6. Transfer eyecup to dissection dish; hold edge of eyecup with forceps.
7. Gently irrigate the RPE/choroid with buffer (HER) using a Pasteur pipette to remove sheets of RPE (1–2 mm in diameter). RPE sheets look like black flecks in the medium.
8. Transfer RPE sheets to ca. 5 ml HER in a wax-lined, 35 mm culture dish using a wide bore pipette or a glass 5 or 10 ml pipette (*see* **Note 7**).
9. Place 35 mm dish with sheets on a rotator at 30 rpm.
10. Repeat **steps 4–9** with the other eye; pool sheets into one dish.

3.3. Preparation of Dissociated RPE Cells

1. Transfer RPE sheets into papain solution in minimal volume of medium using a wide-bore or 10 ml serological pipette. Incubate for 30 min on rotator at 30 rpm.
2. After the digest period, transfer sheets to 3 ml HERB + DNase in a 12–15 ml glass conical centrifuge tube.
3. Allow sheets to settle to the bottom of the tube, then gently resuspend tissue using a Pasteur pipette. Remove debris as tissue is resuspended. Remove solution and repeat in two more changes of 3 ml HERB + DNase (*see* **Note 8**).
4. Add 1 ml of HERB-DNase. Using a 10 ml serological pipette, triturate the solution to dissociate cells by pipetting up and down 35 times, careful not to introduce air bubbles (*see* **Note 9**).

5. After dissociation, add 200–400 ml HERB-DNase to dilute the cell suspension. Optimal cell density is about 7.5×10^4 cells/ml (*see* **Note 10**).
6. Plate cells immediately after dissociation by adding 75–100 µl of the cell suspension to completely dry, poly-l-Lysine coated coverslips in 35 mm dishes. Dishes should be placed in 100 cm glass Petri plates with moistened filter paper in the cover before adding cells, and left undisturbed for 30 min to 1 h, or until cells adhere (*see* **Note 11**).
7. After cells have adhered, change the medium to fresh HERB containing 10 µM dopamine to achieve full melanosome dispersion. Aspirate the old medium from the coverslip using a Pasteur pipette and immediately replace with 100 µl fresh medium. Repeat twice more for a total of three medium changes.

3.4. Stimulation and Observation of Melanosome Motility

1. To stimulate melanosome aggregation, change medium on coverslips to 1 mM cAMP in HERB using three changes of 100 µl. Full melanosome aggregation is achieved after 10–25 min. Melanosomes can be redispersed by washout of cAMP using 10 µM dopamine in HERB.
2. For time-lapse video observation, prepare a perfusion chamber using two strips of double-stick tape aligned along either side of the long edge of a microscope slide. Add a drop of medium to the slide, and invert a coverslip with adherent cells onto the tape. View cells using a 40× to 100× phase contrast objective on an upright microscope. Perfuse by pipetting medium on one side of the coverslip and absorbing it on the other side using a wedge of filter paper.

4. Notes

1. pH of CMFHER is adjusted to 7.4 initially; after addition of the cysteine solution pH will drop to 7.2.
2. Add papain to digest solution 10–15 min prior to dissection to allow 20–30 min activation of the enzyme before adding to RPE sheets. If multiple fish are to be dissected, add papain to separate aliquots of digest solution in parafilm lined, 35 mm plates. Papain should be kept on ice until use.
3. Ceramic coverslip holders are available from Thomas Scientific (#8542E40); coverslips may be stored in nitric acid indefinitely until use.
4. Complete water rinse is critical as free PLL is toxic to cells.

5. We use plastic boxes (former rodent shoe-box style containers) that hold 3 l of water for up to six fish in each box. Boxes are placed in a custom made, light- tight wooden box with an aeration hose and bubbler connected to an aquarium pump outside the box. MS-222 will lower the pH of the water; measure pH before and after addition with pH paper and adjust pH up using a few drops of 10N NaOH. MS-222 is a carcinogen; gloves should be worn.
6. We use a desk lamp with a 25 W incandescent bulb turned against the wall to let a small amount of light through.
7. Wet the inside of the pipette before use so tissue does not adhere to the glass. Do not let the sheets encounter the air–water interface. A wide-bore, fire polished pipette with a slight bend at the end also works well.
8. The washing step can be carried out in room light. Be sure not to introduce air bubbles into the solution during the washing step; likewise do not remove all medium between washes such that the tissue is exposed to air. Each aliquot of wash solution should be added gently by slanting the tube and slowly trickling the wash solution down the side, so as not to dissociate cells during washing. By holding the tube up to a black background, melanosomes from lysed RPE cells are visible in solution as the tissue is resuspended. Tissue should be washed in three changes of medium or until melanosomes from lysed cells are no longer visible.
9. Recently, we have tried dissociation of sheets using a 1 ml syringe and a 26 5/8 gauge needle. The syringe should be thoroughly wetted first. Eight slow passes through the needle (four times in and out) is sufficient to dissociate cells.
10. Cells may be counted on a hemocytometer to gauge correct cell density, however cells must be plated immediately after dissociation or they will not adhere to the coverslips.
11. Be sure not to move cells after plating or they will not be distributed evenly on the coverslip. The moistened filter paper in the glass Petri dish is important to maintain a humidified environment to discourage evaporation of the medium.

Acknowledgements

Thanks to Stephanie Santioleri for providing the scanning electron micrograph. This work was supported by an NIH AREA grant # R15 GM066961.

References

1. Burnside, B. and King-Smith, C. 2009. Retinomotor Movements. In (Squire, L.R., Ed.) *Encyclopedia of Neuroscience*. Elsevier.
2. Garcia, D. and Burnside, B. (1994). Suppression of cAMP-induced pigment granule aggregation in RPE by organic anion transport inhibitors. *Invest Ophthalmol Vis Sci* **35**:178–188.
3. King-Smith, C., Paz, P., Lee, C., Lam, W., Burnside, B. (1997). Bi-directional pigment granule migration in isolated retinal pigment epithelial cells requires actin but not microtubules. *Cell MotilCytoskeleton* **38**:229–249.
4. King-Smith, C., Basciano, P., Pham, N. (2001). Effect of the actin stabilizing drug, jasplakinolide, on pigment granule motility in the retinal pigment epithelium (RPE) of green sunfish, *Lepomis cyanellus. Pigment Cell Research* **14**:14–22.

Chapter 16

Analysis of Properties of Cilia Using *Tetrahymena thermophila*

Vidyalakshmi Rajagopalan, Elizabeth O. Corpuz, Mark J. Hubenschmidt, Caroline R. Townsend, David J. Asai, and David E. Wilkes

Summary

Cilia and eukaryotic flagella are important structures required for the motility of cells, the movement of medium across the surfaces of cells, and the connections between the receptor and synthetic portions of sensory cells. The axoneme forms the cytoskeleton of the cilium comprising several hundreds of proteins that assemble into the 9 + 2 arrangement of outer doublet and central pair microtubules, the inner and outer rows of dynein arms, and many other structures. *Tetrahymena thermophila* is an excellent model organism for the study of cilia and ciliogenesis. The cell is covered by about 1,000 cilia which are essential for survival. Additionally, the *Tetrahymena* genome is available and targeted genetic manipulations are straightforward. In this chapter, we describe five protocols that examine properties of cilia: (a) measuring mRNA levels to see the effect of deciliation on gene expression; (b) swimming velocity and linearity; (c) ciliary length and density; (d) phagocytosis that occurs through the ciliated oral apparatus; and (e) depolarization-induced ciliary reversal.

Key words: Cilia, Ciliary reversal, Deciliation, Dynein, Phagocytosis, *Tetrahymena thermophila*

1. Introduction

In this chapter, we describe several simple methods we use to characterize the properties of cilia on the protozoan *Tetrahymena thermophila*. Cilia and eukaryotic flagella (same structure) are essential organelles. Cilia are required for the motility of cells, the movement of medium across the surfaces of cells, and the connections between the receptor and synthetic portions of sensory cells. The cytoskeleton of the cilium is the axoneme com-

R.H. Gavin (ed.), *Cytoskeleton Methods and Protocols,* Methods in Molecular Biology, vol. 586
DOI 10.1007/978-1-60761-376-3_16,
© Humana Press, a part of Springer Science + Business Media, LLC 2009

prising several hundreds of proteins that assemble into the 9 + 2 arrangement of outer doublet and central pair microtubules, the nexin links that connect outer doublets, the sheath around the central pair, the radial spokes and spokeheads, the inner and outer rows of dynein arms, and other structures (e.g. *(1–4)*). The dyneins transduce the free energy obtained from ATP hydrolysis into mechanical work, producing shear between adjacent outer doublet microtubules *(5–6)*. The active sliding of outer doublets is converted to propagated bending *(7–8)*. Structures interior to the axoneme – e.g., central pair microtubules and radial spokes – control the microtubule sliding and axonemal bending (e.g. *(9)*). The increase in expression of a gene in response to deciliation is strong evidence that the gene product is either a component of the cilium or is involved in ciliogenesis *(10–12)*.

The ciliated protozoan *Tetrahymena thermophila* offers a number of experimental advantages *(13)*. It is easy and inexpensive to culture in the laboratory. Wild-type cells divide every 3 h at 30°C and to densities exceeding 10^6 cells/mL. The cells are relatively large (60 μm × 30 μm), and photogenic. Any gene in the germline micronucleus or the somatic macronucleus can be modified by homologous recombination so that the targeted gene can be disrupted, epitope-tagged, or over-expressed. The 104 MB macronuclear genome has been sequenced and its annotation is well underway (http://www.ciliate.org) *(14)*.

Tetrahymena is an excellent model organism for the study of cilia and ciliogenesis. The cell is covered by approximately 1,000 somatic cilia, which help the cell swim and divide *(15–16)*. Minor abnormalities of individual somatic cilia can cause significant swimming defects. The anterior end is marked by the presence of an oral apparatus that uses cilia organized along four membranelles to engulf food particles. An important advantage to having so many cilia on an easy-to-manipulate organism is that it presents an excellent opportunity with which to study ciliogenesis (e.g. *(17–19)*). At the same time, however, the challenge to having so many cilia is that their density obscures the quantification of ciliogenesis – to count the cilia, to measure their lengths, and to evaluate their motility.

Our laboratory uses *Tetrahymena* – especially exploiting the straightforward "reverse genetics" approaches available in this organism – to explore dynein function. The multi-dynein hypothesis states that every isoform of dynein is built to perform a specific function in the cell *(20)*. *Tetrahymena* expresses 25 different dynein heavy chain genes *(21)*, and thus presents an important opportunity to test the multi-dynein hypothesis. Most of the dyneins affect cilia structure or function, and so it is important to be able to measure changes in ciliary properties.

We describe five protocols: (a) measuring mRNA levels to see the effect of deciliation on gene expression; (b) swimming velocity and linearity; (c) ciliary length and density; (d) phagocytosis that occurs through the ciliated oral apparatus; and (e) depolarization-induced ciliary reversal.

2. Materials (See Note 1)

2.1. Effect of Deciliation on Gene Expression

2.1.1. Deciliation and Regeneration of Cilia.

1. Modified Neffs: 0.5% proteose peptone, 0.5% yeast extract, 1.1% glucose, 100 μM $FeCl_3$.
2. 100× antibiotic/antimycotic mix: 100 U/mL penicillin G, 100 μg/mL streptomycin sulfate, 0.25 μg/mL amphotericin B.
3. 10 mM Tris base, pH 7.5.
4. Deciliation solution: 10% Ficoll, 10 mM $CaCl_2$, 10 mM Na acetate, 10 mM EDTA, pH 4.2.
5. Regeneration solution: 2 mM $CaCl_2$, 15 mM Tris base, pH 7.95.
6. 30°C shaker incubator.
7. 100-mL oil tubes (Fisher Scientific, Pittsburgh, PA).
8. Damon IEC HN-SII Clinical centrifuge (GMI Inc., Ramsey, MN).
9. Sterile flasks for growing cells and cilia regeneration and sterile Fernbach flasks for starving cells.

2.1.2. Isolation of Total RNA

1. 0.1% diethyl pyrocarbonate (DEPC) in water. Autoclave solution before use. Handle DEPC in the fume hood.
2. 4 M guanidinium thiocyanate solution: 4 M guanidinium thiocyanate, 0.5% Na *N*-lauroylsarcosine, 25 mM Na citrate, pH 7.0. 0.1 M β-mercaptoethanol added after adjusting the pH.
3. 7.5 M guanidine HCl solution: 7.5 M guanidine HCl, 25 mM Na citrate, 5 mM DTT, pH 7.0.
4. 1 M glacial acetic acid in 0.1% DEPC water.
5. 2 M K acetate in 0.1% DEPC water, pH 5.0.
6. 30-mL Corex tubes treated with 0.1% DEPC water overnight at 37°C and autoclaved.
7. Beckman model J2–21 centrifuge or equivalent.
8. Spectrophotometer.
9. 100% EtOH set aside just for use with RNA samples.

2.1.3. Deoxyribonuclease I (DNase I) Treatment of RNA

1. DNase I, amplification grade (Invitrogen, Carlsbad, CA).
2. 10× DNase I reaction buffer (Invitrogen).
3. 25 mM EDTA, pH 8.0.
4. 0.1% DEPC water.
5. 100% EtOH.

2.1.4. Reverse Transcription of DNase I-Treated RNA

1. Superscript III RNaseH$^-$ reverse transcriptase (Invitrogen).
2. 50 ng/μL random hexamers (Invitrogen).
3. 10 mM dNTPs (Invitrogen).
4. 5× first-strand buffer (Invitrogen).
5. 0.1 M DTT (Invitrogen).
6. 0.1% DEPC water.
7. 100% EtOH.

2.1.5. Quantitative Real-Time PCR

1. Platinum SYBR Green qPCR SuperMix UDG (Invitrogen).
2. 20 mM gene-specific forward and reverse primers.
3. MicroAmp optical 8-tube strips and optical caps (Applied Biosystems, Foster City, CA).
4. GeneAmp 5700 Sequence Detector (Applied Biosystems).

2.2. Swimming Velocity and Linearity

1. Modified Neffs: 0.5% proteose peptone, 0.5% yeast extract, 1.1% glucose, 100 μM $FeCl_3$.
2. 100× antibiotic/antimycotic mix: 100 U/mL penicillin G, 100 μg/mL streptomycin sulfate, 0.25 μg/mL amphotericin B.
3. Micrometer slide.
4. Microscope with darkfield condenser, 2.5× objective.
5. Digital camera.
6. ImageJ Analysis Software (http://rsbweb.nih.gov/ij/download.html).

2.3. Cilia Length and Density

1. 1× PHEM: 60 mM Pipes, 25 mM HEPES, 10 mM EGTA, 2 mM $MgCl_2$, pH 6.9.
2. Fixative: 2% paraformaldehyde, 0.4% Triton-X 100 diluted in 1× PHEM.
3. Blocking solution: 0.1% BSA in PBS.
4. Primary antibody: anti-tubulin antibody. We use mouse monoclonal antibodies produced against acetylated tubulin, mAb 1–6.1 *(22)*.
5. Secondary antibody: Goat anti-mouse IgG (Kirkegaard and Perry Laboratories, Gaithersburg, MD).
6. Mounting medium: 50% glycerol, 50% PBS, 0.5% *n*-propyl gallate, pH 8.0.
7. Fluorescence microscope.

2.4. Phagocytosis

1. Modified Neffs: 0.5% proteose peptone, 0.5% yeast extract, 1.1% glucose, 100 μM $FeCl_3$.
2. 100× antibiotic/antimycotic mix: 100 U/mL penicillin G, 100 μg/mL streptomycin sulfate, 0.25 μg/mL amphotericin B.
3. 1× PHEM: 60 mM Pipes, 25 mM HEPES, 10 mM EGTA, 2 mM $MgCl_2$, pH 6.9.
4. Fixative: 2% paraformaldehyde in 1× PHEM.
5. 10 mM Tris base, pH 7.5.
6. 2 μm diameter fluorescent latex beads (Sigma-Aldrich, St. Louis, MO).
7. 30°C shaker incubator.
8. Fluorescence microscope.

2.5. Depolarization-Induced Ciliary Reversal

1. 0.67 M KCl.
2. Control solution: 10 mM Tris base, 0.5 mM MOPS, 50 μM $CaCl_2$, pH 7.2.
3. Computer: Pentium 4 @ 3.6 GHz with 2 GB RAM and Microsoft Windows XP Professional (32 bit).
4. Microscope: Nikon DIC microscope with CCD camera.
5. Microscope software: MetaMorph 7.0 r2 (Molecular Devices).

3. Methods

3.1. Effect of Deciliation on Ciliary Gene Expression

3.1.1. Deciliation and Regeneration of Cilia

1. We follow the method of Calzone and Gorovsky *(17)*.
2. Grow desired cell line to 3–4 × 10^5 cells/mL in modified Neffs supplemented with 1× antibiotic/antimycotic mix. We usually grow 100 mL cultures.
3. Wash cells at a density of 3 × 10^5 cells/mL with 10 mM Tris base (pH 7.5) and starve in 10 mM Tris base (pH 7.5) for approximately 18 h.
4. Spin down starved cells in a sterile oil tube at 1,500 rpm for 2 min in a Damon IEC HN-SII clinical centrifuge. Remove the supernatant. Note the volume of the cell pellet. Add 10 volumes of deciliation solution. Quickly resuspend with a sterile Pasteur pipet. Immediately transfer the resuspended cells into a sterile 50-mL Corning centrifuge tube.
5. Cap and repeatedly invert the tube for 45 s. Check a drop of the cells by brightfield microscopy to make sure the deciliated cells are immotile. Add 5 volumes (based on the volume of deciliation solution used) of regeneration solution. The cells will die if left too long in the deciliation solution.

6. Transfer the regenerating cells into a sterile flask. Place the flask in a 30°C incubator shaker at 50 rpm and allow the cells to regenerate their cilia.
7. During the course of the experiment check the cells every 30–60 min to make sure that cells start swimming. Typically cells regenerating their cilia start slow twitching movements after about 30–45 min and they start swimming well about 120 min after resuspension in regeneration solution.
8. At 2 h after the first deciliation, deciliate the cells for a second time. The second deciliation serves two purposes: it ensures that most of the cilia are removed; and it further depletes the ciliary proteins, thus inducing the upregulation of their gene expression.
9. RNA is isolated at specific time points after the second deciliation in order to study the pattern of expression of the gene(s) of interest.

3.1.2. Isolation of Total RNA (See Note 2)

1. We follow the method of Chirgwin et al. *(23)*. RNA is isolated before deciliation and at specific times after the second deciliation. Good induction should be seen at 30–45 min after the second deciliation.
2. Spin down the cells in a sterile oil tube. Discard the supernatant.
3. Resuspend cells in 4 M guanidinium thiocyanate (16 mL per 1 mL pellet).
4. Transfer to a sterile 30-mL Corex tube.
5. Spin 10 min at 9,000 × *g* at 4°C and save the supernatant.
6. Precipitate supernatant with 1/40 volume of 1 M acetic acid, ¾ volume of 100% EtOH. Place tube at –20°C overnight. Volumes are relative to the volume in **step 3**.
7. Spin RNA precipitate 10 min at 7,000 × *g* at –10°C. Discard the supernatant.
8. Resuspend the pellet in 7.5 M guanidine HCl (½ of the volume of guanidinium thiocyanate used in **step 3**).
9. Precipitate the resuspended sample with 1/40 volume of 1 M acetic acid, ½ volume of 100% EtOH at –20°C overnight.
10. Spin RNA precipitate for 10 min at 7,000 × *g* at –10°C. Discard the supernatant.
11. Resuspend in 7.5 M guanidine HCl (½ volume of guanidine HCl used in **step 8**).
12. Precipitate with 1/40 volume of 1 M acetic acid, and ½ volume of 100% EtOH at –20°C overnight.
13. Spin RNA precipitate for 10 min at 7,000 × *g* at –10°C. Discard the supernatant.
14. Wash pellet with 5 mL 100% EtOH. Spin 10 min at 7,000 × *g* at –10°C. Discard the supernatant.

15. Wash pellet again with 5 mL 100% EtOH. Spin 10 min at 7,000 × *g* at −10°C. Discard the supernatant. Invert the tube and air dry the pellet.
16. Resuspend pellet in 1 mL 0.1% DEPC water. Spin 10 min at 12,000 × *g* at 4°C. Save the supernatant in a fresh sterile Corex tube on ice.
17. Re-extract the remaining pellet with 1 mL 0.1% DEPC water. Spin 10 min at 12,000 × *g* at 4°C. Combine supernatant from this step with the supernatant from **step 16**, on ice.
18. Precipitate the RNA from the combined supernatants with 200 μL of 2 M K acetate, 4 mL 100% EtOH. After this step RNA can be stored at −20°C.
19. To estimate the concentration of RNA sample, gently swirl RNA tube, take 100 μL and spin aliquot for 10 min at 16,000 × *g* at 4°C. Remove supernatant. Wash pellet with freshly made 70% EtOH (in 0.1% DEPC water) and repeat the above spin. Remove supernatant. Air dry the pellet for 10–15 min at room temperature. Note that the pellet may be transparent and hard to see.
20. Resuspend the air-dried pellet with 100 μL of 0.1% DEPC water. Take an aliquot of this sample and dilute it 10-fold with 0.1% DEPC water. Using 0.1% DEPC water as the blank, determine the concentration of the RNA using a spectrophotometer. Absorbance of 1.0 at 260 nm indicates that the sample contains 40 μg/mL of RNA *(24)*.

3.1.3. DNase I Treatment of RNA

1. Spin down 10 μg of RNA in a sterile 1.5-mL microfuge tube. Follow **Subheading 3.1.2**, **step 19**, above, to collect and wash RNA. Resuspend the air-dried pellet in 86 μL of 0.1% DEPC water.
2. Add 10 μL of 10× DNase buffer and 4 μL of DNase I enzyme. Incubate at room temperature overnight.
3. Stop the DNase I treatment by adding 10 μL of 25 mM EDTA and heat at 60–65°C for 15 min.
4. Precipitate RNA by adding 200 μL 100% EtOH and incubating overnight at −20°C.

3.1.4. Reverse Transcription of DNaseI-Treated RNA

1. Spin down a desired amount of DNaseI-treated RNA (e.g., 5 μg) in a sterile 1.5-mL microfuge tube for 10 min at 16,000 × *g* at 4°C. Remove the supernatant.
2. Wash pellet with freshly made 70% EtOH (in 0.1% DEPC water) and centrifuge as in **step 1**. Remove the supernatant.
3. Air-dry pellet for 10 min at room temperature.
4. Resuspend pellet in 8 μL of 0.1% DEPC water (RT+) or 9 μL of 0.1% DEPC water for the mock reaction (RT−). Place on ice.

5. To each tube, add 5 µL of 50 ng/µL random hexamers and 1 µL of 10 mM dNTPs.
6. Incubate tube at 70°C for 10 min.
7. Remove tube and incubate on ice for 2 min.
8. With tube on ice, add 4 µL of 5× first-strand buffer, 1 µL of 0.1 M DTT, and 1 µL of Superscript III reverse transcriptase. Do not add enzyme to the mock reaction tube.
9. After 5 min at room temperature, incubate tubes at 42°C overnight.
10. After reverse transcription incubate tubes at 70°C for 15 min to inactivate the enzyme.
11. Make three 10-fold dilutions of the cDNA in sterile water. The three dilutions we typically use are 1/10, 1/100, and 1/1,000.

3.1.5. Quantitative Real-Time PCR

1. The specific volumes, settings, etc. given are optimized for the GeneAmp 5700 Sequence Detector. Details will vary depending on instrument used.
2. Design primer pairs for each gene of interest and a control gene whose expression is not affected by deciliation. We use cytoplasmic dynein heavy chain DYH1 as the uninduced control *(25)*. PCR products should be ≤150 bp. When possible, the primers should span at least one intron so that the differently-sized products from genomic DNA and cDNA can be distinguished by dissociation curves after the reactions are run.
3. Prepare a cocktail containing the SYBR Green qPCR Supermix UDG, forward and reverse primers in sterile water as shown in **Table 1**. Prepare separate cocktails for each gene. For genes with introns, 8 reactions are run. For genes without introns, 14 reactions are run (*see* **Note 3**).
4. Into each tube of the MicroAmp Optical 8-tube strip, aliquot 20 µL of the cocktail. Add 5 µL of the appropriate cDNA dilution to each tube. For genes with introns set up tubes 1–8; for genes without introns set up tubes 1–14. NDC, non-deciliated cDNA; DC, deciliated cDNA;+, reverse-transcribed; –, mock reverse-transcribed.

   – Tube 1 – 1/10 NDC+
   – Tube 2 – 1/100 NDC+
   – Tube 3 – 1/100 NDC+
   – Tube 4 – 1/1,000 NDC+
   – Tube 5 – 1/10 DC+
   – Tube 6 – 1/100 DC+
   – Tube 7 – 1/100 DC+
   – Tube 8 – 1/1,000 DC+
   – Tube 9 – 1/10 NDC-

Table 1
Examples of real-time PCR cocktails for genes with and without introns

	8 rxns (μL)[a]	14 rxns (μL)[b]
SYBR Green qPCR SuperMix UDG	110.0	192.5
Forward primer (20 μM stock)	4.4	7.7
Reverse primer (20 μM stock)	4.4	7.7
H_2O	57.2	100.1
Total	176.0	308.0

[a]Reaction cocktail for genes with intron(s)
[b]Reaction cocktail for genes without intron(s)

– Tube 10 – 1/100 NDC–
– Tube 11 – 1/1,000 NDC–
– Tube 12 – 1/10 DC–
– Tube 13 – 1/100 DC–
– Tube 14 – 1/1,000 DC-

5. Make sure there are no drops on the side of the tube or any air bubbles in the mixture. Pop the air bubbles if possible and drag any drops into the rest of the solution with a pipet tip. Cap the tubes gently avoiding splashing drops onto the side or on the cap.
6. To set up the program in the computer, input the sample names in the appropriate columns, choose *primer* (e.g., PR1) and *type* (unknown). Set the PCR temperature cycles as follows: (1) 1 cycle: 50°C, 2 min; (2) 1 cycle: 95°C, 2 min; (3) 45 cycles: 95°C, 15 s; 55°C, 30 s; 72°C, 30 s.
7. Set the sample volume to 25 μL, and the starting dissociation temperature to 60°C, including dissociation curve. Save the program before starting the cycles.

3.1.6. Analyzing Real Time Data (See Note 4)

1. After the run select the *results* tab, and choose *analyze data*. The computer will request a threshold to be set. Examine each amplification curve and determine the appropriate threshold (e.g., 0.1), then click *analyze* again. The threshold value should be chosen such that it is in the linear portion of the upwardly sloping amplification curve (when the products are being actively amplified and not after the reaction has leveled off).

2. Examine the dissociation curves, making sure each reaction gives only one peak. A flat line means failure of the PCR. Multiple peaks usually indicate either primer-dimers or products from contaminating genomic DNA.
3. Record the number of cycles to reach the threshold (C_t value) for each reaction.
4. Graph the C_t values vs. log of the dilution for each reaction on an XY scatter plot. Two graphs should be made for each gene (i.e., non-deciliated and deciliated).
5. Record the slope and R^2 value (correlation coefficient) for each cDNA sample. Calculate the efficiency for each primer pair by using the formula: efficiency = $10^{(-1/\text{slope})}$. Make sure that the R^2 values are ≥0.95 for each sample. Average all efficiencies for each gene (efficiency mean).
6. Calculate the average of C_t values obtained for duplicate reactions run with the 1/100 dilutions for each cDNA sample. Subtract the NDC average from that of DC sample for each gene to obtain ΔC_t for each time point.
7. Change in expression = efficiency mean$^{(\Delta C_t)}$ for each sample. This refers to the value that has not been normalized to corresponding control value.
8. Divide the change in expression value of gene of interest by change in expression value of control gene. The number thus obtained is the relative expression of the gene of interest compared to its nondeciliated level. The control gene compensates for any difference in total cDNA between nondeciliated and deciliated samples. *See* **Table 2** for example of real-time data calculation.

3.2. Swimming Velocity and Linearity

1. Grow a 1 mL culture of the desired cell line in modified Neffs medium with 1× antibiotic/antimycotic to a final concentration of 0.5–1.0 × 10^5 cells/mL.
2. Set up microscope with darkfield condenser and 2.5× objective.
3. Place a 50 μL drop of cells on a microscope slide without coverslip. You want approximately 10–20 cells per drop. If too dense discard the drop. Use modified Neffs to dilute cells to appropriate density.
4. Capture image with a known exposure time (usually 3–6 s). Move stage to focus on different areas of the slide for obtaining more images. In darkfield, the swimming path of the cells will appear as white lines against the dark background. Save images in suitable format (e.g., JPEG) to analyze with Image J software. If necessary, adjust the brightness and contrast for pictures.

Table 2
Example to show the calculation of gene expression upregulation

Gene-cDNA[a]	1:100 C_t mean[b]	ΔC_t[c]	Slope[d]	R^2[e]	Efficiency of PCR[f]	Efficiency mean[g]	Change in expression[h]	Relative gene expression[i]
DYH1-NDC	23.455		−3.275	0.9964	2.02		–	–
DYH1-DC30	25.31	−1.855	−3.165	0.9899	1.89	1.96	0.29	1
DYH4-NDC	21.52		−3.025	0.9986	2.14		–	–
DYH4-DC30	19.425	2.095	−3.76	0.9836	1.84	1.99	4.24	14.71

[a] DYH1, cytoplasmic dynein 1 heavy chain gene; DYH4, axonemal outer arm dynein (β) heavy chain gene
[b] Mean of C_t values (number of PCR cycles to reach the threshold amount of product) using 1:100 dilution of template
[c] C_t = 1:100 NDC C_t value - 1:100 DC30 C_t value
[d] Slope of the line when plotting C_t vs. log dilution of cDNA
[e] R^2 = correlation coefficient (i.e., line fit obtained from plotting the C_t vs. log cDNA dilutions)
[f] Efficiency of PCR = $10^{(-1/\text{slope})}$
[g] Efficiency mean = average of efficiency of all PCRs for each gene
[h] Change in expression = efficiency mean(ΔC^t)
[i] Relative gene expression = change in expression of gene of interest/raw upregulation of control gene

5. Using the same magnification but with brightfield setting obtain an image of the micrometer slide.
6. Open the micrometer picture using ImageJ. Select desired zoom setting. Measure the length of the micrometer scale in pixels and *set scale* (i.e., 1,000 μm = *x* number of pixels) and select *global* in order for this setting to be applied to all images to be analyzed.
7. Measure the lengths of swimming paths of each cell by tracing along the paths (using the same zoom level and scale settings). Use the *segmented lines* setting to trace paths. Measure only those paths that are full length and nonoverlapping.
8. Divide each path length by exposure time to obtain swimming velocity in μm/s.
9. Measure the shortest distance from start to end of the swim path. Divide this value by the actual pathlength. The resulting value will be the swimming path linearity coefficient (perfect linearity = 1.00).

3.3. Cilia Length and Density

3.3.1. Cell Staining (See Note 5)

1. Grow the desired cell line to l–2 × 10^5 cells/mL density in modified Neffs medium with 1× antibiotic/antimycotic.
2. Spin 1.5 mL cells for 2 min at low speed in a microfuge. Quickly remove supernatant and resuspend cells in 1 mL 1× PHEM buffer. Repeat spin and remove supernatant, leaving a small volume of buffer (e.g., 20 μL) to resuspend the cell pellet.
3. Add 1 mL fixative (including Triton-X 100) and incubate for 30 min at room temperature or overnight at 4°C. Spin and remove supernatant as above.
4. Resuspend cells in 1 mL blocking solution. Spin and remove supernatant. Add 1 mL fresh blocking solution and incubate for 30 min at room temperature. Spin and remove supernatant.
5. Resuspend cells in 100 μL primary antibody (diluted in blocking solution) and incubate at room temperature for 1 h. We use mAb 1–6.1, specific for acetylated α-tubulin *(22)*, diluted 1/50 in blocking solution.
6. Spin and remove supernatant. Wash three times with 1 mL blocking solution.
7. Resuspend cells in 100 μL secondary antibody and incubate at room temperature in the dark for 1 h. Spin and remove supernatant. Wash three times with 1 mL blocking solution.
8. Allow the cells to settle for 15 min. Pipet 5 μL of cells from the pellet and gently mix with 15 μL mounting medium.
9. Place the cells on a cleaned microscope slide and gently place a coverslip over the cells, making sure to minimize air bubbles.

Dry the fluid that oozes around the edges with filter paper. Seal the slide with nail polish and store at 4°C or –20°C.

3.3.2. Measurement of Ciliary Length and Density

1. We use confocal fluorescence microscopy to optically section the cells in order to measure the cilia at the widest "equator" of the cell.
2. We use a Zeiss LSM 510 laser scanning confocal microscope for measuring cilia lengths. Choose the highest magnification (oil immersion if available). For a 63× oil immersion lens we typically set the pinhole at 240 and the thickness of the optical slice is <1.8 μm. Crop the field such that there is only one cell per image. Many images can be obtained from one slide.
3. Using the focus control, find the widest optical section of the cell. Save image (example shown in **Fig. 1a**). Focus step is 1.0 μm.
4. Using the analysis software, measure the length of each cilium from its base to tip. Measure lengths of only those cilia whose base and tip are in focus **(Fig. 1b)**.
5. Using the analysis software, measure the circumference of the cell **(Fig. 1c)**.
6. Count the number of distinct, measurable cilia along the circumference.
7. Obtain cilia density by dividing the number of cilia by the cell's circumference (cilia per μm).

3.4. Phagocytosis

1. Grow a 1 mL culture of the desired cell line in modified Neffs medium with 1× antibiotic/antimycotic to a final concentration of 1.0×10^5 cells/mL.
2. Add 1 μL of undiluted fluorescent beads to the cell culture.

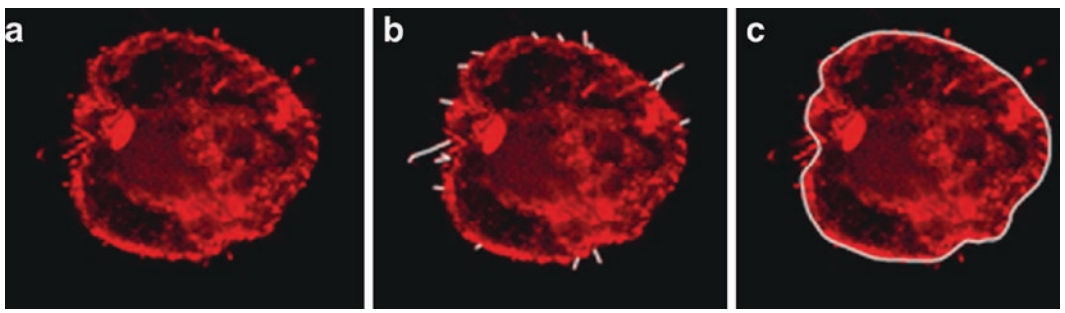

Fig. 1. Confocal imaging to determine cilia length and density. **(a)** Optical section at the "equator" of a single KO-D2LIC cell stained with anti-tubulin. **(b)** Traces of several cilia (*white*). **(c)** Trace of the circumference of the cell (*white*). The cilia in this section are perpendicular to the cell's perimeter and are therefore easy to measure.

3. Incubate culture with beads at 30°C with shaking at 50–100 rpm for a minimum of 1 h. Wild type cells usually will have ingested beads within 1 h.
4. At the desired time point, spin down the cultures; wash the cells with 1 mL of 10 mM Tris base (pH 7.5) three times. The wash steps are recommended to remove uningested fluorescent beads.
5. Resuspend cells in 1 mL fixative and place a small drop of cells on a slide with a coverslip.
6. Observe cells for presence of beads with fluorescence microscope.
7. Calculate percentage of cells that clearly contain at least five or more beads. Frequently, a few beads will adhere to the outside of the cells. To avoid counting these cells, we only score cells with at least five beads.

3.5. Depolarization-Induced Ciliary Reversal

We record live cells using brightfield microscopy with a 4× objective and we capture images with a CCD camera controlled by Metamorph. All of the settings described below are in Metamorph.

3.5.1. Software Settings

1. Click on *Acquire* → *Acquire* to get to the acquisition settings.
2. Set *Binning* and *Live Bin* to 2.
3. Set *Camera Area* to center quad.
4. Click the *Show Live* button.
5. Make a note of the FPS (frames per second) shown in this dialogue box. It will be used later when producing videos.
6. Click the *Close* button.

3.5.2. Set Up the Video Recording

1. Click on the *Acquire* menu.
2. Click *Stream Acquisition*.
3. Choose a location to save this stream (stream to hard disk used) and set the number of frames to the desired length of time (max tested is 9,600 frames).
4. The amount of time the video capture will acquire can be determined by dividing the number of frames by the FPS as noted above.

3.5.3. Record Swimming

1. Grow cells to 4–6 × 10^5 cells/mL in modified Neffs and 1× antibiotic/antimycotic.
2. Place a 17 μL drop of control solution on a slide.
3. Place 3 μL of cells into this drop and wait approximately 30 s for the cells to spread throughout the drop.
4. Place this slide on the microscope stage and ensure focus and location within the field of view. It is recommended that the microscope is focused on the bottom of the drop as this

procedure will cause the majority of the cells to drop towards the bottom of the drop.

5. Click *Acquire* to start the video recording.
6. Immediately add 0.95 μL of the 0.67 M KCl solution to the 20 μL drop on the slide, and mix with the pipette tip.
7. Make sure the camera is focused on the bottom of the drop and let the microscope capture the video.

3.5.4. Video Compression

1. Go to *File* → *Open* → and pick the video that you have recorded (a .stk file).
2. Go to *Stack* → *Make Movie*, check save unselected, make sure that the Video Format selected is appropriate (we use AVI), click save, choose a file name, and then click OK.
3. When prompted to choose a video codec click whichever one is best suited for the computer on which the videos will be viewed.
4. Recommended codecs are either Intel Indeo 5.1 (with maximum quality set in options of that codec) or Xvid MPEG-4 codec.
5. Under *Config* the particular settings for Xvid used for our experiments: *Profile* is Home Use; Single Pass; *Target quantizer* Quality Slider is set to 3; *Quality Preset* is set to General Purpose.
6. Click OK and the software will make the .avi video file. This can take a variable amount of time depending on the codec and content of the video.
7. File sizes using the settings outlined above are about 200 MB for 9,600 frames.

3.5.5. Analyzing the Videos

1. At 30-s intervals, cells (20–30 total in a field) are scored as swimming forward, immotile, or swimming backward.
2. Calculate the percentage of cells that are swimming forward, reversed or stopped at each time point. An example of such data is shown in **Fig. 2**.

4. Notes

1. All solutions should be sterile.
2. All solutions should be sterile, and all glassware should be treated with DEPC-water and autoclaved.
3. The extra samples for intronless genes include reactions from the mock reverse transcription reaction **(Subheading 3.1.4**,

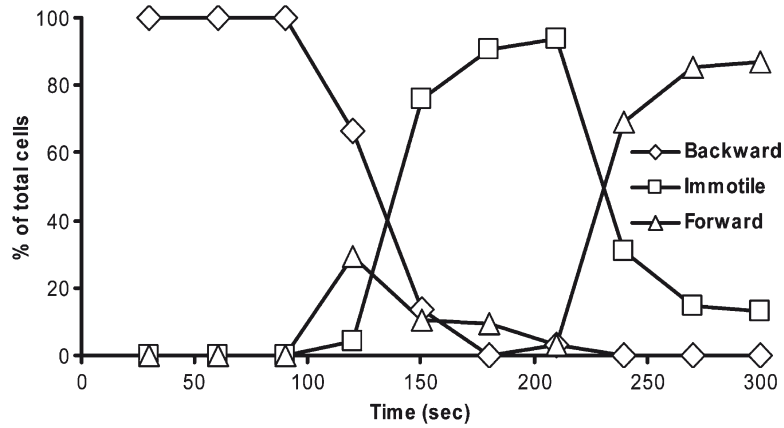

Fig. 2. Graph showing the swimming reversal behavior of wild-type cells. At 30-s intervals all cells in the field were scored as either swimming backwards, immotile, or swimming forward. After stimulation all cells swim backwards then become immotile for a short time. Cells recover and resume forward swimming. *Diamonds* backward; *squares* immotile; *triangles* forward.

step 8) because cDNA and genomic DNA products cannot be distinguished by dissociation temperature.

4. Calculations based on the method of Pfaffl *(26)*.
5. Method described in Asai *(27)*.

Acknowledgments

We thank the past and present undergraduate members of the Asailum who helped develop and test these protocols, including: Nicole Bennardo, Clarence Chan, Jennifer DuMond, Jordan Eboreime, Jonathan Hetzel, Erin Heyer, Hallie Kuhn, Andrea Sand, Oksana Sergeeva, and Hadley Watson. Our laboratory is supported by grants from the National Science Foundation. Several students were provided summer research stipends from grants awarded to Harvey Mudd College from the Howard Hughes Medical Institute and the AAAS-Merck.

References

1. Dutcher SK (1995) Flagellar assembly in two hundred and fifty easy-to-follow steps. Trends Genet 11:398–404.
2. Pazour GJ, Agrin N, Leszyk J, and Witman GB (2005) Proteomic analysis of a eukaryotic cilium. J Cell Biol 170:103–113.
3. Smith JC, Northey JG, Garg J, Pearlman RE, and Siu KW (2005) Robust method for proteome analysis by MS/MS using an entire translated genome: demonstration on the ciliome of *Tetrahymena thermophila*. J Proteome Res 4:909–919.

4. Inglis PN, Boroevich KA, and Leroux MR (2006) Piecing together a ciliome. Trends Genet 22:491–500.
5. Gibbons IR and Rowe AJ (1965) Dynein: a protein with adenosine triphosphatase activity from cilia. Science 149:424–426.
6. Summers KE and Gibbons IR (1971) Adenosine-triphosphate induced sliding of tubules in trypsin-treated flagella of sea-urchin sperm. Proc Natl Acad Sci U S A 68:3092–3096.
7. Satir P (1965) Studies on cilia: II. Examination of the distal region of the ciliary shaft and the role of the filaments in motility. J Cell Biol 26:805–834.
8. Brokaw CJ (1971) Bend propagation by a sliding filament model for flagella. J Exp Biol 55:289–304.
9. Gaillard AR, Fox LA, Rhea JM, Craige B, and Sale WS (2006) Disruption of the A-kinase anchoring domain in flagellar radial spoke protein 3 results in unregulated axonemal cAMP-dependent protein kinase activity and abnormal flagellar motility. Mol Biol Cell 17:2626–2635.
10. Lefebvre PA, Silflow CD, Wieben ED, and Rosenbaum J (1980) Increased levels of mRNAs for tubulin and other flagellar proteins after amputation or shortening of *Chlamydomonas* flagella. Cell 20:469–477.
11. Schloss JA, Silflow CD, and Rosenbaum JL (1984) mRNA abundance changes during flagellar regeneration in *Chlamydomonas reinhardtii*. Mol Biol Cell 4:424–434.
12. Soares H, Galego L, Cóias R, and Rodrigues-Pousada C (1993) The mechanisms of tubulin messenger regulation during *Tetrahymena pyriformis* reciliation. J Biol Chem 268:16623–16630.
13. Asai DJ and Forney JD (2000) *Tetrahymena thermophila*. Methods in cell biology, Vol. 62. Academic, San Diego, CA.
14. Eisen JA and Coyne RS et al. (2006) Macronuclear genome sequence of the ciliate *Tetrahymena thermophila*, a model eukaryote. PLoS Biol 4:1620–1642.
15. Frankel J (2000) Cell Biology of *Tetrahymena thermophila*. Methods Cell Biol 62:27–125.
16. Brown JM, Fin NA, Pandiyan G, Thazhath R, and Gaertig J (2003) Hypoxia regulates assembly of cilia in suppressors of *Tetrahymena* lacking an intraflagellar transport subunit gene. Mol Biol Cell 14:3192–3207.
17. Calzone FJ and Gorovsky MA (1982) Cilia regeneration in *Tetrahymena*. A simple reproducible method for producing large numbers of regenerating cells. Exp Cell Res 140:471–476.
18. Brown JM, Marsala C, Kosoy R, and Gaertig J (1999) Kinesin-II is preferentially targeted to assemblying cilia and is required for ciliogenesis and normal cytokinesis in *Tetrahymena*. Mol Biol Cell 10:3081–3096.
19. Rajagopalan V, Subramanian A, Wilkes DE, Pennock DG, and Asai DJ (2008) Dynein-2 affects the regulation of ciliary length but is not required for ciliogenesis in *Tetrahymena thermophila*. Mol Biol Cell 20:708–720.
20. Asai DJ (1995) Multi-dynein hypothesis. Cell Motil Cytoskeleton 32:129–132.
21. Wilkes DE, Watson H, Mitchell DR, and Asai DJ (2008) 25 dyneins in *Tetrahymena*: a re-examination of the multidynein hypothesis. Cell Motil Cytoskeleton 65: 342–351.
22. Asai DJ, Brokaw CJ, Harmon RC, and Wilson L (1982) Monoclonal antibodies to tubulin and their effects on the movement of reactivated sea urchin spermatozoa. Cell Motil 1:175–180.
23. Chirgwin JM, Przybyla AE, MacDonald RJ, and Rutter WJ (1979) Isolation of biologically active ribonucleic acid from sources enriched in ribonuclease. Biochemistry 18:5294–5299.
24. Sambrook J, Fritsch EF, and Maniatis T (1989) Molecular cloning: a laboratory manual, second edition, Cold Spring Harbor Laboratory Press, Cold Spring Harbor, NY.
25. Gibbons BH, Asai DJ, Tang W-JY, Hays TS, and Gibbons IR (1994) Phylogeny and expression of axonemal and cytoplasmic dynein genes in sea urchins. Mol Biol Cell 5:57–70.
26. Pfaffl MW (2001) A new mathematical model for relative quantification in real-time RT-PCR. Nucleic Acids Res 29:e45.
27. Asai DJ (2008) Immunofluorescence microscopy. In: Gallagher SR and Wiley EA (eds) Current Protocols in Essential Laboratory Techniques, Wiley, New York.

Chapter 17

Application of Cell Traction Force Microscopy for Cell Biology Research

James H-C. Wang and Bin Li

Summary

When a cell migrates, it generates traction forces on the underlying substrate. The cell traction force (CTF) is not only essential for cell migration, but it is also used by cells to control their shape and maintain cellular homeostasis. As such, quantification of CTFs aids in better understanding of many fundamental biological processes such as morphogenesis, angiogenesis, and wound healing of tissues and organs. A new technology called cell traction force microscopy (CTFM) has been developed to determine CTFs in a quantitative fashion. The advantage of this technology is that it directly measures the "cause" (i.e., CTFs) of cell movement instead of the "effect" (i.e., cell movement itself), which is measured by various conventional methods. This chapter provides detailed information of materials and methods that are needed in order to perform typical CTFM experiments. Several examples are also given to illustrate various applications of CTFM in cell biology research.

Key words: Migration, Traction force, Polyacrylamide gel, Fluorescent beads, Cell traction force microscopy, Fibroblast, Myofibroblast, Micropatterning

1. Introduction

Cell migration plays a fundamental role in the normal development and homeostasis of tissues and organs. It is also an essential cellular process for both physiological and pathological processes, including wound healing, tissue morphogenesis, angiogenesis, and metastasis. Several methods have been developed to study cell migration in vitro. These methods usually involve plating cells on a bare glass or plastic surface coated with matrix protein, such as fibronectin or poly-L-lysine *(1)*. On these smooth culture surfaces, cells move around in a random fashion, or undergo so-called

R.H. Gavin (ed.), *Cytoskeleton Methods and Protocols,* Methods in Molecular Biology, vol. 586
DOI 10.1007/978-1-60761-376-3_17,
© Humana Press, a part of Springer Science + Business Media, LLC 2009

"random walk." Using time-lapse microscopy, the cell movement with time is recorded and then analyzed. Because cells move on a two-dimensional (2-D) surface and do "random walk," the analysis, as well as interpretation of cell movement, is complicated. To improve this situation, a microgrooved substrate was recently used *(2)*, allowing individual cells on the substrate to move in only one dimension (1-D). With this 1-D approach, observation of cell movement is easier, and analysis of cell migration, as well as its interpretation, is simpler than those 2-D surface-based methods. Nevertheless, all these approaches are limited in that they provide cell movement information only, not the cause of the cell movement itself – cell traction force (CTF).

CTF is the force that an adherent cell exerts to its underlying substrate, and it is essential for cell migration *(3–5)* (**Fig. 1**). The CTFs are generated through the interaction of actin filaments with myosin-II (a cellular motor protein) and also through the actin polymerization *(6)*. CTFs are transmitted to the extracellular matrix (ECM) or substrate via focal adhesions (FAs), which, composed of structural and signaling proteins (e.g., integrins and kinases), form physical links between actin cytoskeleton and ECM *(7)*. Therefore, determination of CTFs will not only help characterize cell migration but may also aid in defining changes in cell phenotype because of biochemical and biomechanical treatments.

Several methods have been developed to measure CTFs qualitatively or quantitatively. These include thin silicone membranes *(5, 8, 9)*, microfabricated cantilevers *(10)*, micropost force sensor arrays *(11–13)*, and cell traction force microscopy (CTFM) *(14–16)*. Among these methods, CTFM can determine traction forces of individual cells and a group of cells in a quantitative, efficient, and reliable fashion *(6)*. For example, the substrate used in CTFM, polyacrylamide gel (PAG), is linearly elastic in response to a wide range of forces, and the deformation is completely recovered upon removal of the force *(17)*. In addition,

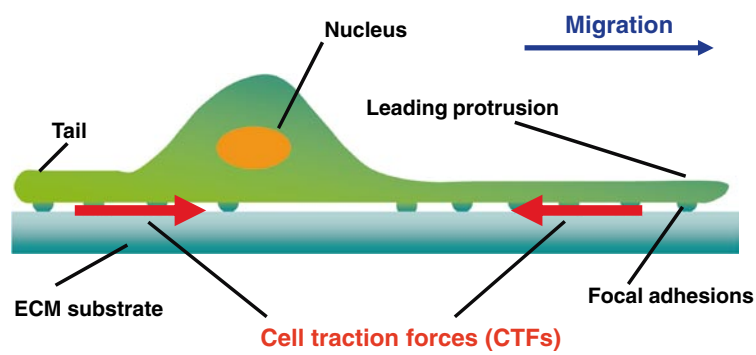

Fig. 1. An illustration of cell migration and cell traction forces (CTFs).

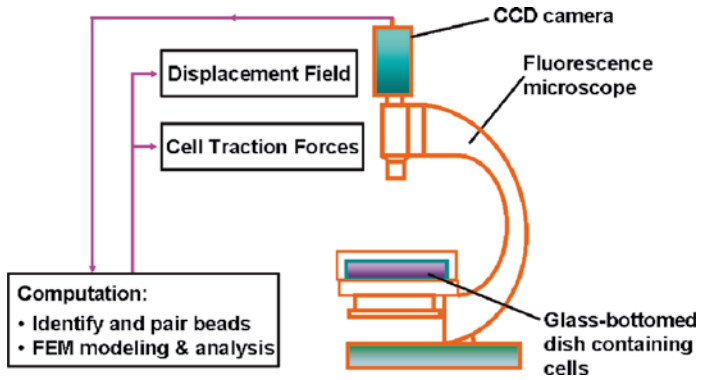

Fig. 2. General scheme of cell traction force microscopy (CTFM).

the stiffness of PAG can be easily adjusted in a broad range and the surface of PAG can be conveniently coated with ECM proteins of interest to cater to specific requirements for measuring traction forces of certain cell types *(18)*. We will demonstrate the application of CTFM through a few examples.

1.1. General Procedures of CTFM

The general scheme of CTFM is illustrated in **Fig. 2**. There are four steps involved in application of CTFM: (1) fabricating elastic PAG embedded with fine fluorescent beads (0.2 ~ 0.5 μm). The PAG is used as a substrate for growing cells after it is coated with ECM protein such as collagen type I; (2) obtaining a pair of fluorescent bead images. The paired images are denoted as "force-loaded" and "null-force" images, which correspond to the times when cells are attached to and then after the cells are removed from the PAG, respectively; (3) using the paired images to determine the PAG substrate displacement field; and (4) "converting" the substrate displacements to CTFs. In this chapter, only the fabrication of ECM protein-coated PAG and CTFM imaging (i.e., **steps 1** and **2**) will be described in detail. Readers who are interested in the **steps 3** and **4**, or the determination of the substrate displacement field and corresponding CTFs, are encouraged to refer to the theoretic background information of the CTFM technology *(6, 14–16)*.

2. Materials

1. Glass-bottomed Petri dish (MatTek, Ashland, MA), Φ35 mm.
2. Cover glass (Fisher Scientific, Pittsburgh, PA), Φ12 mm.
3. Steel ball (Microball Company, Peterborough, NH), Φ0.64 mm, 7.2 g/cm^3.

4. Sodium hydroxide, 0.1N.
5. 3-aminopropyltrimethoxysilane.
6. Glutaraldehyde solution, 0.5%.
7. Acrylamide solution, 10%.
8. N, N'-methylenebisacrylamide (bis-acrylamide) solution, 1%.
9. Fluorescent bead (Molecular Probes, Eugene, OR) solution, Φ0.2 or 0.5 μm.
10. Ammonium persulfate (APS) solution, 10%.
11. N,N,N',N'-Tetramethylethylenediamine (TEMED, Molecular Probes, Eugene, OR).
12. N-sulfosuccinimidyl-6-[4'-azido-2'-nitrophenylamino] hexanoate (Sulfo-SANPAH, Pierce, Rockland, IL), 5 mM.
13. HEPES buffer, 200 mM.
14. Collagen type I (Angiotech Biomaterials, Palo Alto, CA), 100 μg/ml.
15. PBS buffer.
16. Trypsin-EDTA (Invitrogen, Carlsbad, CA), 0.5% (10×).
17. Deionized water (DI water).

Note that those materials whose vendors are not indicated can be obtained from Sigma (St. Louis, MO).

3. Methods

3.1 Activating Glass Surface

The glass surface of a 35-mm glass-bottomed Petri dish is treated with sodium hydroxide solution (0.1 M) for 1 day and allowed to be air-dried. Then, a few drops of 3-aminopropyltrimethoxysilane are placed onto the dried cover glass for 5 min. The dish is then washed with DI water, followed by incubation with 0.5% glutaraldehyde in PBS for 30 min. Next, the dish is thoroughly washed with copious amount of DI water for 30 min and then air-dried.

3.2. Fabricating PAG Substrate

The fabrication process of PAG is described in the flow chart **(Fig. 3)**. Briefly, a mixture of acrylamide/bis-acrylamide (acrylamide, 5%; bis-acrylamide, 0.1%) is prepared and vacuumed for 20 min. It is then thoroughly mixed with a certain amount of fluorescent microbeads (typical volume ratio: 80/1 for 0.2 μm beads and 200/1 for 0.5 μm beads), 40 μl APS, and 4 μl TEMED (*see* **Note 1**). Eleven microliters of the mixture is then added to the center of a pretreated glass-bottomed Petri dish and quickly covered with a piece of circular cover glass (Φ12 mm). The dish is turned upside down and kept at 4°C for 2 h, allowing

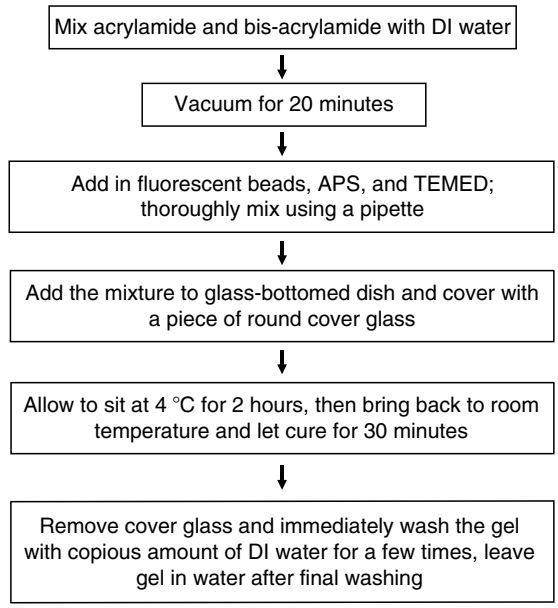
Mix acrylamide and bis-acrylamide with DI water
Vacuum for 20 minutes
Add in fluorescent beads, APS, and TEMED; thoroughly mix using a pipette
Add the mixture to glass-bottomed dish and cover with a piece of round cover glass
Allow to sit at 4 °C for 2 hours, then bring back to room temperature and let cure for 30 minutes
Remove cover glass and immediately wash the gel with copious amount of DI water for a few times, leave gel in water after final washing

Fig. 3. The procedures involved in fabricating polyacrylamide gels (PAGs) embedded with fluorescent beads for CTFM.

the microbeads to settle down to the surface of the cover glass by gravity (*see* **Note 2**). After that, the dish is brought back to room temperature to allow the mixture to cure for 30 min, which results in the formation of a PAG on the glass (*see* **Note 3**). The circular cover glass is then carefully removed with a tweezer, and the gel disk is extensively washed with DI water.

3.3. Conjugating Type I Collagen to PAG

Before conjugating type I collagen to the PAG substrate, its surface is first activated using a photo-linker, Sulfo-SANPAH, with the aid of ultraviolet (UV) light. Briefly, 100 μl Sulfo-SANPAH (5 mM) in 200 mM HEPES solution is added to the surface of the PAG in a 35-mm dish. The dish is exposed to UV light for 5 min, and then the sulfo-SANPAH solution is removed. This process is repeated once, and then the PAG is washed with PBS twice (*see* **Note 4**). Next, 130 μl collagen type I solution (100 μg/ml) is added to PAG surface, followed by incubation overnight at 4°C. The PAG is then thoroughly washed with PBS three times, prior to cell seeding.

3.4. Measuring PAG Thickness

The thickness of the PAG is estimated using a microscopy-based method, which involves sequentially focusing on the embedded fluorescent microbeads at the bottom and top surfaces of the gel. The vertical positions of the microscope stage are recorded. The thickness of the PAG is determined by the difference between these two positions. Alternatively, the gel thickness can be estimated using the formula: the gel volume/the gel area. Typically, a gel thickness of 70–120 μm is used in CTFM experiments *(19)*.

3.5. Determining the Young's Modulus and Poisson Ratio of PAG Substrate

The Young's modulus of PAG is determined according to the published method *(20)*. Briefly, a steel ball (Φ0.64 mm) is placed on the surface of the gel. The indentation caused by the steel ball because of its weight is measured under a microscope by following the vertical position of the fluorescent microbeads under the center of the ball as described above. The Young's modulus is calculated as $\Upsilon = 3(1 - \nu^2)f/4d^{3/2}r^{1/2}$, where ν is the Poisson ratio of the steel ball (0.3), f is the weight of the ball (neglecting the upward buoyancy force produced by the liquid surrounding the ball), d is the amount of indentation, and r is the radius of the steel ball.

Also, a similar method *(21)* is used to determine the Poisson ratio of the PAG substrate. Typically, for a PAG substrate made of a mixture containing 5% acrylamide and 0.1% bis-acrylamide, the Young's modulus is ~3 kPa, and the Poisson ratio is ~0.48.

3.6. Plating Cells on PAG Substrate

For CTFM experiments, 2,000–5,000 cells are used on each PAG substrate (*see* **Note 5**). A cell suspension is added to a collagen-coated PAG substrate in a dish, and the cells are allowed to attach to and spread on the gel for 6 h before cell images are taken (*see* **Note 6**).

3.7. Acquisition of Cell and Fluorescent Bead Images

First, a region where a few individual cells reside on the PAG is selected (*see* **Note 7**). Then, a phase contrast image of the cells is taken through a CCD camera attached to a fluorescence microscope. This is followed by taking a fluorescent image of the microbeads, which is referred to as the "force-loaded" image (*see* **Note 8**). Next, after the medium in the dish is carefully extracted and the cells are removed by application of 2 ml 0.5% trypsin, an image of the fluorescent microbeads of the same view is taken (*see* **Note 9**). This image is termed "null-force" image (*see* **Note 10**).

3.8. Computation for Determining CTFs

A general purpose FEM code (ANSYS 8.0, or AMPS) is used to determine CTFs (*see* **Note 11**).

4. Examples of CTFM Application

4.1. Determining Traction Forces of Individual Cells

To illustrate that CTFM is an effective technology for determining traction forces of various types of cells, we applied CTFM to determine traction forces of individual human patellar tendon fibroblasts (HPTFs). Briefly, a PAG substrate was fabricated and conjugated with collagen type I according to the methods described here. The HPTFs were plated to the PAG substrate and allowed to spread for 6 h. Cells with an elongated shape on each gel were chosen for imaging. The "force-loaded" and "null-force" images were used to determine the substrate displacement field and CTFs on the basis of the published methods *(16)*. The cell image, substrate displacement field, and cell traction

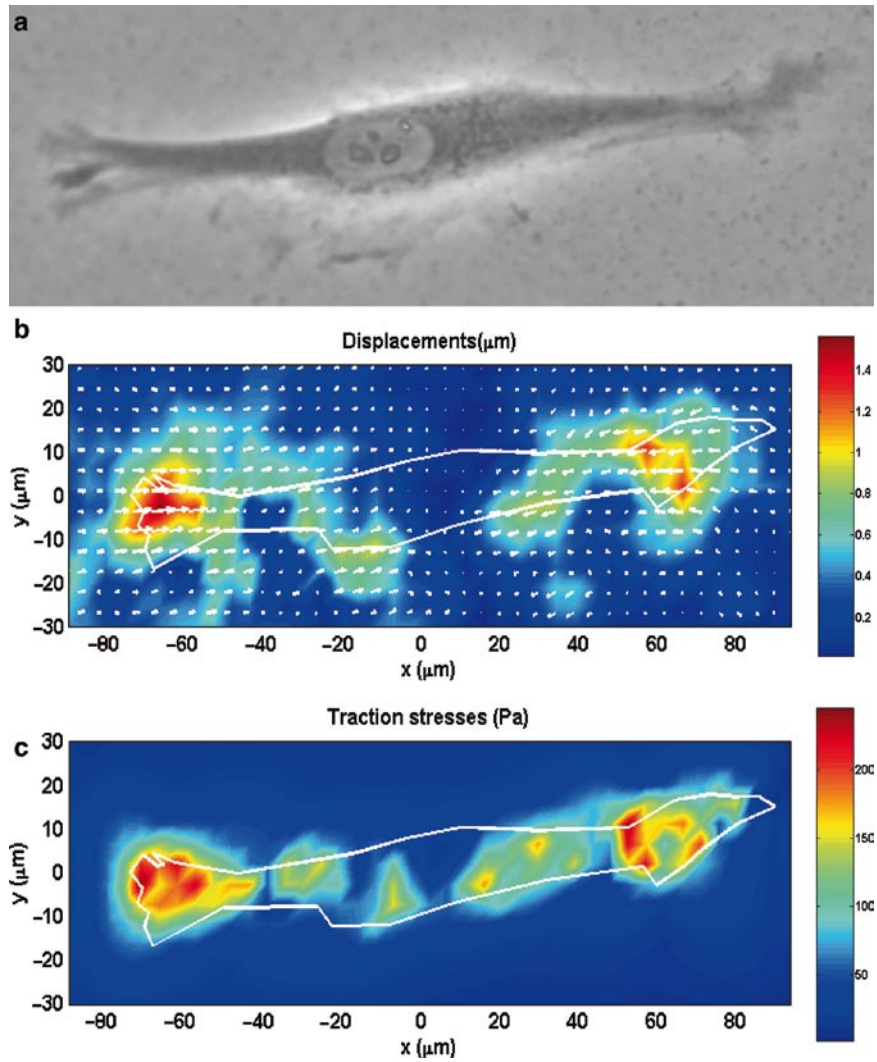

Fig. 4. Application of CTFM to determine traction forces of individual human patellar tendon fibroblasts (HPTFs). (**a**). HPTF on a polyacrylamide gel with embedded fluorescent beads (not shown); (**b**). substrate displacement field; and (**c**). cell traction field.

stress distribution are given in **Fig. 4**. The maximum displacement obtained was ~1.2 μm, and the maximum traction stress was ~250 Pa. The CTFs were concentrated at the front and rear of the cell and sparse around the nucleus, which is consistent with general cell migration mechanism.

4.2. Detecting Cell Differentiation by CTFM

We used rabbit corneal stroma cells as an example to show that CTFM can be used to detect differentiated cells. According to the published protocols *(22)*, rabbit corneal stroma cells were obtained and differentiated into fibroblasts in DMEM (GIBCO-BRL, Grand Inland, NY) containing 10% fetal bovine serum (FBS), 20 ng/ml bFGF, 5 μg/ml heparin, 100 U/ml penicillin, and 100

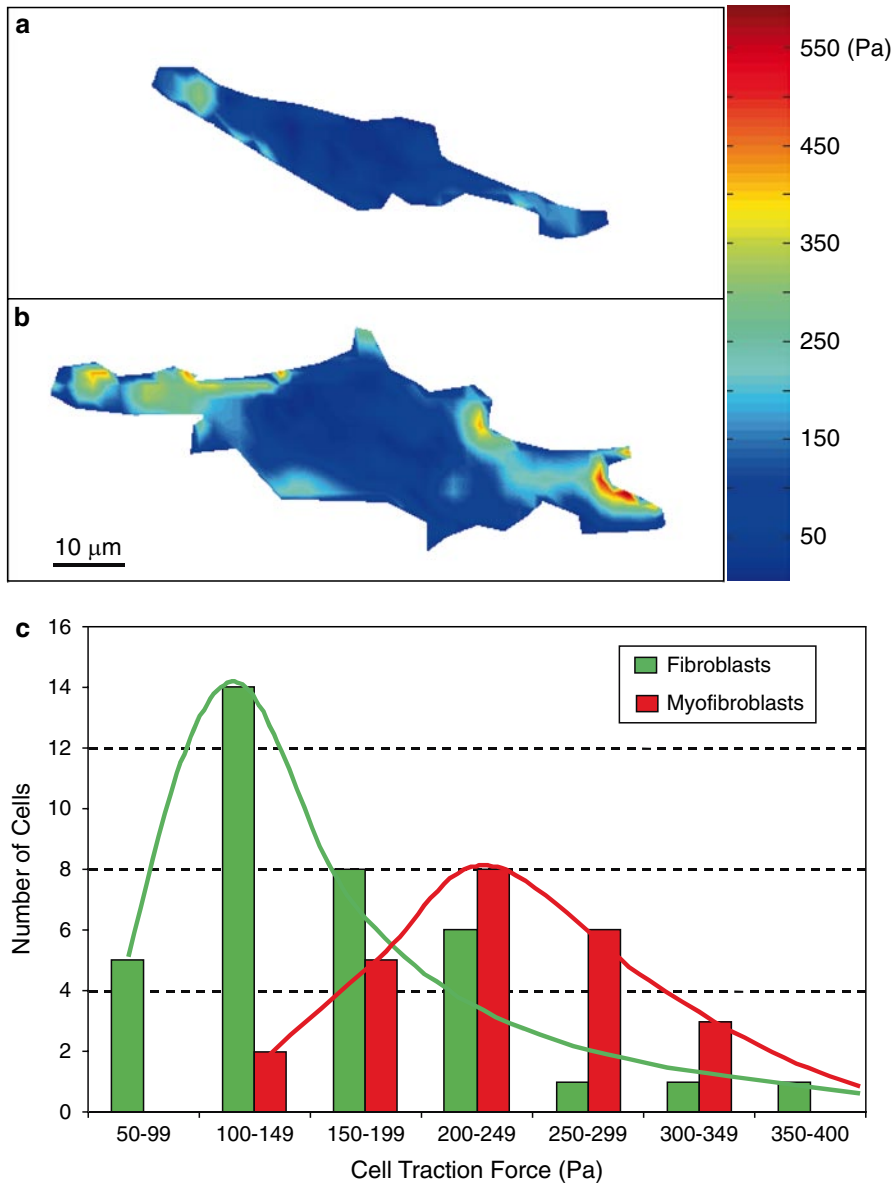

Fig. 5. Cell traction force fields of fibroblasts and myofibroblasts. (**a**) a typical fibroblast. (**b**) a typical myofibroblast. The color within the cells represents the traction force magnitude. The myofibroblast is larger and generates a higher traction force than the fibroblast. (**c**) detecting myofibroblast differentiation by CTFM. After fibroblasts were differentiated into myofibroblasts, their CTF distribution shifted to the right because of their overall larger CTFs compared to fibroblasts. (a and b are adapted with permission from Fig.1 in ref. *19)*.

μg/ml streptomycin. These differentiated fibroblasts expressed minimum α-smooth muscle actin (α-SMA), which is a specific marker of myofibroblasts *(19, 23)*.

To obtain myofibroblasts, the fibroblasts were treated with 2 ng/ml transforming growth factor-β1 (TGF-β1, R&D Systems, Minneapolis, MN) for 24 h. These cells expressed a high level of

α-SMA *(19)*. Then, CTFM was used to determine the CTFs of individual fibroblasts and differentiated myofibroblasts (**Fig. 5a** and **b**). It was found that the fibroblasts generated a mean CTF of about 100 Pa. In contrast, the mean CTF of the differentiated myofibroblasts was three times that of the fibroblasts. On the CTF histogram (**Fig. 5c**), the two cell populations, myofibroblasts and fibroblasts, clearly differ from each other – the myofibroblast population shifted toward the right, which means the overall CTF of the myofibroblast population was larger than that of the fibroblast population. Therefore, this example shows that CTFM may be used to detect differentiation of cells, such as adult and embryonic stem cells, because of biochemical and biophysical stimuli *(24)*.

4.3. Determining Traction Forces of Cells with Controlled Shapes

Understanding the relationship between cell shape and cellular function is important for the study of cell biology and specifically for regulation of cell phenotype. Here, HPTFs of different shapes were obtained using microcontact printing technique. The rectangular cells had an aspect ratio of 4.9, whereas the circular ones had a diameter of 50 μm; however, these cells had the same area of 1,960 μm^2. These HPTFs with different shapes exhibited variations in actin cytoskeletal structure, spatial arrangement of focal adhesions, and spatial distribution and magnitude of CTFs (**Fig. 6**). Long and parallel actin filament bundles were formed in rectangular cells along

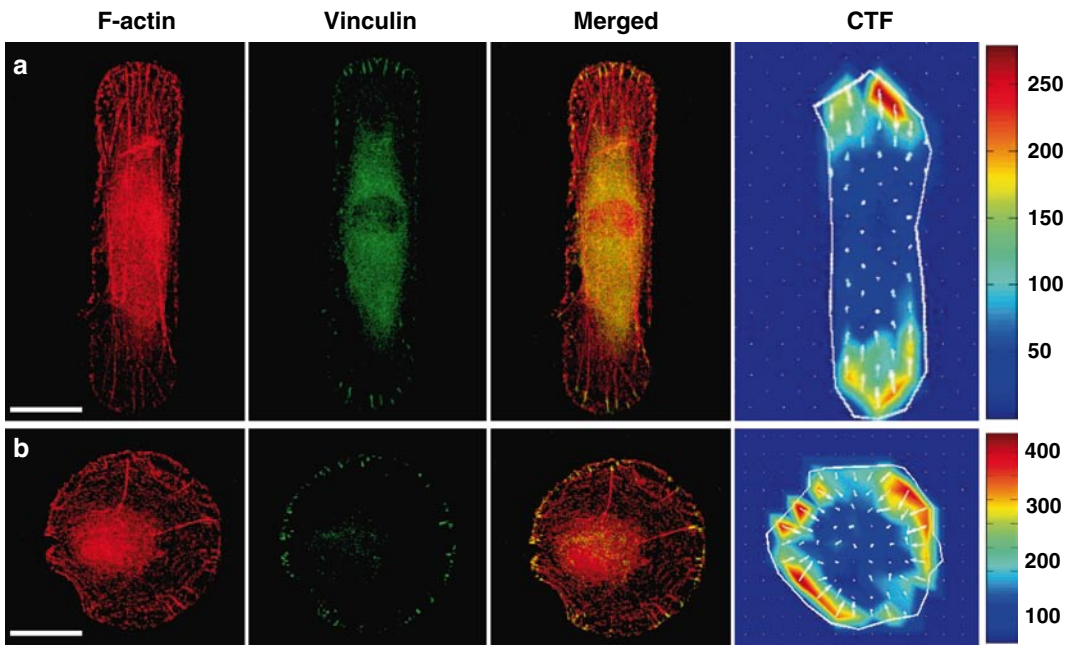

Fig. 6. Application of CTFM to determine traction forces of micropatterned cells. Immunofluorescence microscopy images of F-actin, vinculin, and the overlay of them, as well as CTFs in micropatterned HPTFs. (**a**) rectangular HPTF. (**b**) circular HTF. Development of focal adhesions and stress fibers is seen to be closely related to cell traction force distribution. *scale bars*: 20 μm (adapted with permission from **Fig. 6** in Li et al., 2008, *Cell Motil Cytoskeleton* 65(4):332–41).

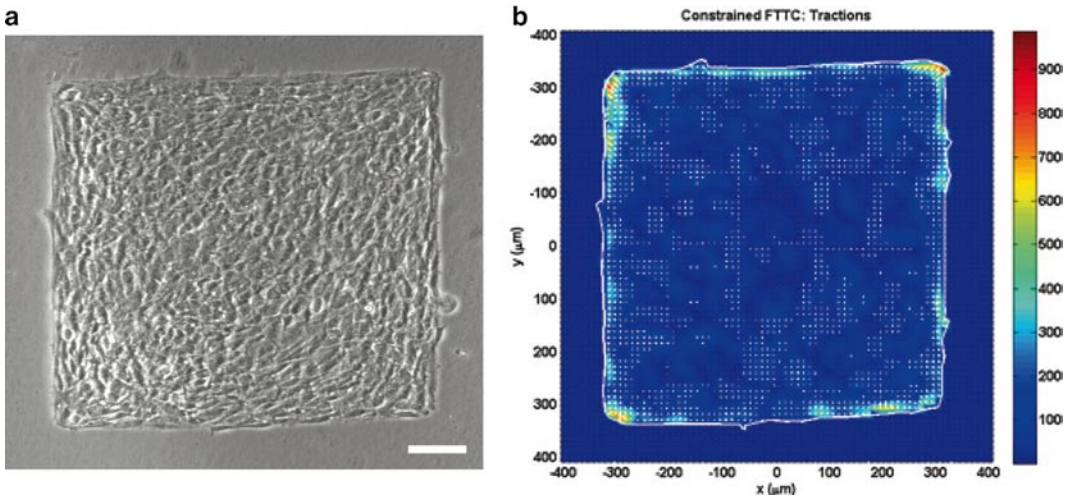

Fig. 7. Application of CTFM to determine traction forces of a micropatterned cell island. **(a)** phase contrast micrograph of a NIH 3T3 cell island; and **(b)** CTF field (*scale bar*: 100 μm).

the longitudinal direction. In circular cells, however, they were along the circumference of the cells, and several bundles were formed from the nuclear area to the edge of the cells. Focal adhesions, revealed by staining vinculin, were concentrated at the two ends of the rectangular cells but uniformly distributed along the edge of the circular cells. These regions were also the locations of the largest CTFs in both rectangular and circular shaped cells. Hence, the same cells with various shapes may differ in their phenotype.

4.4. Determining Traction Forces of a Group of Cells

CTFM can also be used to determine the traction forces of a cell group. To demonstrate this, first microcontact printing technology *(25)* was used to fabricate square fibronectin-coated micro-islands on PAG substrates. NIH 3T3 cells were then plated on the micro-island, and a square-shaped monolayer of cells (herein referred as "cell island") was formed on it after 1 day in culture **(Fig. 7a)**. Similar to the application of CTFM with single cells, CTFM was performed to determine the CTF distribution of the square cell island. It was found that larger CTFs were located at the corners and around the edges of the cell island than at the inner region **(Fig. 7b)**.

5. Notes

1. Depending on the purpose and resolution requirement, imaging at different magnifications can be used for CTFM. Different bead sizes, however, should be used for different magnification. For example, use 10× objective for 0.5 μm

whereas 20× for 0.2 μm. Also, different bead concentrations need to be used. The density of beads for 10× imaging is about half that for 20×.

2. It typically takes a few hours for the fluorescent microbeads to settle down near the surface during PAG fabrication. Keeping the curing mixture at a low temperature (4°C) facilitates this process by preventing the beads from being "frozen" in the gel too quickly.
3. Although the fabrication process for PAG substrates is straightforward, care must be taken to obtain PAG with consistent stiffness and a uniform coating of the collagen layer. Failure to fabricate uniform PAG substrates and achieve an even coating of collagen type I on the PAG surface will affect cell morphology and alter cell behavior, resulting in inconsistent CTF results with large variations from one experiment to another.
4. Washing the PAG after Sulfo-SANPAH treatment should be completed as quickly as possible to avoid hydrolysis of the NHS groups of Sulfo-SANPAH, which are responsible for conjugating protein to the PAG.
5. The seeding density of cells should be low so that isolated individual cells are grown on the PAG for CTF measurement.
6. Depending on the type of cells, the exact spreading time of cells on collagen-conjugated PAG may need to be adjusted.
7. The same criteria should be applied when sampling individual cells for CTFM. Specifically, individual cells with similar spreading areas and shape should be selected to reduce variations in CTF values and thus increase statistical power for detecting differences in CTF between treatment and control groups. In addition, the distance between cells should be at least twice that of cell size so that the influence from adjacent cells is minimized.
8. While an effort is made to let fluorescent beads settle near the surface of the PAG, it is normal that beads exist within a certain depth underneath the surface. When imaging the fluorescent beads, focus on the layer of beads that are most close to the PAG surface.
9. It is very important to not touch the dish when extracting medium; otherwise, any displacement of the dish may result in a non-reversible shift or rigid body motion of the fluorescent bead image, making pairing beads impossible during image analysis. If cells do not readily detach, extract the medium and apply fresh trypsin again.
10. The "null-force" image must be taken at the same location and with the same focus as that when the "force-loaded" image is taken. Where necessary, manually adjust the

microscope stage and focusing knob to assure location and focus consistency.

11. In cases where single cells are concerned with small substrate deformations, Fourier transform traction cytometry, or FTTC *(15)*, can also be used.

Acknowledgement

We gratefully acknowledge the funding support of NIH AR049921 and AR049921S1 (JHW).

References

1. Rodriguez, L.G., Wu, X. and Guan, J.L. (2005) Wound-healing assay. *Methods Mol Biol* **294**, 23–29.
2. Thampatty, B.P. and Wang, J.H. (2007) A new approach to study fibroblast migration. *Cell Motil Cytoskeleton* **64**, 1–5.
3. Ananthakrishnan, R. and Ehrlicher, A. (2007) The forces behind cell movement. *Int J Biol Sci* **3**, 303–317.
4. Lauffenburger, D.A. and Horwitz, A.F. (1996) Cell migration: a physically integrated molecular process. *Cell* **84**, 359–369.
5. Oliver, T., Dembo, M. and Jacobson, K. (1995) Traction forces in locomoting cells. *Cell Motil Cytoskeleton* **31**, 225–240.
6. Wang, J.H. and Lin, J.S. (2007) Cell traction force and measurement methods. *Biomech Model Mechanobiol* **6**, 361–371.
7. Burton, K., Park, J.H. and Taylor, D.L. (1999) Keratocytes generate traction forces in two phases. *Mol Biol Cell* **10**, 3745–3769.
8. Harris, A.K., Wild, P. and Stopak, D. (1980) Silicone rubber substrata: a new wrinkle in the study of cell locomotion. *Science* **208**, 177–179.
9. Balaban, N.Q., Schwarz, U.S., Riveline, D., et al. (2001) Force and focal adhesion assembly: a close relationship studied using elastic micropatterned substrates. *Nat Cell Biol* **3**, 466–472.
10. Galbraith, C.G. and Sheetz, M.P. (1997) A micromachined device provides a new bend on fibroblast traction forces. *Proc Natl Acad Sci U S A* **94**, 9114–9118.
11. du Roure, O., Saez, A., Buguin, A., et al. (2005) Force mapping in epithelial cell migration. *Proc Natl Acad Sci U S A* **102**, 2390–2395.
12. Tan, J.L., Tien, J., Pirone, D.M., et al. (2003) Cells lying on a bed of microneedles: an approach to isolate mechanical force. *Proc Natl Acad Sci U S A* **100**, 1484–1489.
13. Li, B., Xie, L., Starr, Z.C., et al. (2007) Development of micropost force sensor array with culture experiments for determination of cell traction forces. *Cell Motil Cytoskeleton* **64**, 509–518
14. Dembo, M. and Wang, Y.L. (1999) Stresses at the cell-to-substrate interface during locomotion of fibroblasts. *Biophys J* **76**, 2307–2316.
15. Butler, J.P., Tolic-Norrelykke, I.M., Fabry, B., et al. (2002) Traction fields, moments, and strain energy that cells exert on their surroundings. *Am J Physiol Cell Physiol* **282**, C595–C605.
16. Yang, Z., Lin, J.S., Chen, J., et al. (2006) Determining substrate displacement and cell traction fields – a new approach. *J Theor Biol* **242**, 607–616.
17. Pelham, R.J., Jr. and Wang, Y. (1997) Cell locomotion and focal adhesions are regulated by substrate flexibility. *Proc Natl Acad Sci U S A* **94**, 13661–13665.
18. Kandow, C.E., Georges, P.C., Janmey, P.A., et al. (2007) Polyacrylamide hydrogels for cell mechanics: steps toward optimization and alternative uses. *Methods Cell Biol* **83**, 29–46.
19. Chen, J., Li, H., Sundarraj, N., et al. (2007) Alpha-smooth muscle actin expression enhances cell traction force. *Cell Motil Cytoskeleton* **64**, 248–257.
20. Lo, C.M., Wang, H.B., Dembo, M., et al. (2000) Cell movement is guided by the rigidity of the substrate. *Biophys J* **79**, 144–152.

21. Li, Y., Hu, Z. and Li, C. (1993) New method for measuring Poisson's ratio in polymer gels. *J Appl Polym Sci* **50**, 1107–1111.
22. Anderson, S., DiCesare, L., Tan, I., et al. (2004) Rho-mediated assembly of stress fibers is differentially regulated in corneal fibroblasts and myofibroblasts. *Exp Cell Res* **298**, 574–583.
23. Hinz, B., Celetta, G., Tomasek, J.J., et al. (2001) Alpha-smooth muscle actin expression upregulates fibroblast contractile activity. *Mol Biol Cell* **12**, 2730–2741.
24. Wang, J.-C. and Thampatty, P. (2008) Mechanobiology of adult and stem cells. Int Rev Cytol 271, 297-332..
25. Whitesides, G.M., Ostuni, E., Takayama, S., et al. (2001) Soft lithography in biology and biochemistry. *Annu Rev Biomed Eng* **3**, 335–373.

Chapter 18

2D and 3D Quantitative Analysis of Cell Motility and Cytoskeletal Dynamics

Deborah Wessels, Spencer Kuhl, and David R. Soll

Summary

2D- and 3D-Dynamic Image Analysis Systems (2D- and 3D-DIAS) for quantitative analysis of cell motility and chemotaxis are described. Particular attention is given to protocols that have proven useful in the quantitation of cell shape changes and pseudopod dynamics during basic cell motility (i.e. crawling in the absence of a chemotactic or other type of extracellular signal) and directed motion. In addition, methods provided, highlight the applicability of this approach to the accurate phenotypic characterizations of cytoskeletal mutations in *Dictyostelium discoideum*, cytoskeletal alterations in metastatic cells, and cytoskeletal defects in chemotactically defective polymorphonuclear neutrophils.

Keywords: Cell motility, Basic motile behavior, Chemotaxis, DIAS, Confocal microscopy, 2D Motion analysis, 3D Motion analysis

1. Introduction

Structural, motor and regulatory proteins are recruited and organized into dynamic cytoskeletal complexes in a crawling cell *(1–3)*. That these complexes can be fully functional in the absence of an extracellular signal is often overlooked *(4)*. *Dictyostelium discoideum* amoebae and human polymorphonuclear neutrophils (PMNs) *(5)* are two prime examples of amoeboid cells that translocate in the absence of an extracellular signal in a process that has been referred to as basic motile behavior *(4, 6)*. In the presence of a chemotactic, haptotactic or other extracellular cue, signal transduction networks are evoked that manipulate basic motile behavior and orchestrate directed motion during chemotaxis

R.H. Gavin (ed.), *Cytoskeleton Methods and Protocols,* Methods in Molecular Biology, vol. 586
DOI 10.1007/978-1-60761-376-3_18,
© Humana Press, a part of Springer Science + Business Media, LLC 2009

of *Dictyostelium* amoebae *(4)*, chemotaxis of human PMNs *(5)*, metastasis of cancer cells *(7)*, and embryonic development *(8)*, just to cite a few noteworthy examples.

Because the behavioral phenotype of motile cells is so complex, a qualitative analysis is inadequate, and in some cases inaccurate or misleading. A quantitative approach to the analysis of cell motility with attention given to shape changes is, in other words, essential to understanding the contribution of a particular cytoskeletal element to basic motile behavior and/or chemotaxis *(9)*. This is especially true when the behavior of normal cells and abnormal cells (e.g., metastasizing cells, cytoskeletal mutants, regulatory mutants, defective human PMNs from patients with diseases such as SBDS *(10, 11)* or HIES *(12)* are compared.

The chemotactic signal in *Dictyostelium* is a cAMP wave that is relayed over considerable distances relative to the size of a single cell. As a wave, the chemotactic signal has temporal, spatial and concentration components, each of which elicits unique morphological changes and specific cell behaviors *(4)*. Because the behavior and morphology of the cell varies dramatically with its position in the wave *(4)*, it stands to reason, and has been shown *(4, 9)*, that the underlying cytoskeletal elements likewise undergo significant rearrangements in the different phases of the wave. Moreover, PMNs, like *Dictyostelium* cells, respond to temporal waves of chemoattractant *(5)*. For these and other reasons, it is highly improbable that *in vivo* PMNs or metastatic cancer cells *(7)* see or chemotax in response to static spatial gradients. Therefore, in order to fully appreciate the role of a putative signaling molecule or cytoskeletal protein in chemotaxis, we must not only quantitatively examine basic motile behavior in both normal and mutant cells, but we must also quantify phenotypic responses to a dynamic signal.

In this chapter, we will describe the advanced 2D- and 3D-Dynamic Image Analysis Systems, 2D- and 3D-DIAS, for motion analysis *(13–18)*. The 2D system is in place in many university facilities while the 3D system can be accessed by a visit to the W.M. Keck Dynamic Image Analysis Facility at the University of Iowa. Our emphasis here will be on quantitative methods to analyze cell crawling and shape changes during basic motile behavior and chemotaxis. The goal of this approach is to generate accurate phenotypes of cytoskeletal mutants *(8, 18–20)* so that the function of a given cytoskeletal element can be precisely defined. The software is specifically designed to perform sophisticated shape analyses and a few of the most widely used 2D features including perimeter analysis, differencing, windowing and unwrapping will be discussed. We next review protocols for analysis of basic motile behavior and chemotaxis using 3D-DIAS. With the introduction of the advanced gray scale threshold auto-outlining algorithm, trace slots and the OpenGL

processor into the latest generation of 3D-DIAS, a much more accurate phenotype of cell motility and chemotaxis is now possible. The application of 2D- and 3D-DIAS to the quantitative analysis of cytoskeletal proteins tagged with GFP in gradient and non-gradient conditions using confocal microscopy is also included. Finally, we describe methods for a 3D-DIAS analysis of microspheres attached to the surface of a crawling cell as a means to quantify motor activity of cytoskeletal compartments beneath the plasma membrane.

2. Materials

2.1. Culturing Dictyostelium discoideum

1. Nutrient growth media such as HL-5 (http://dictybase.org; *(21)*).
2. Amoebae maintained at the low-log phase of growth (2×10^6 cells/mL HL-5).

2.2. Development of Dictyostelium discoideum

1. BSS: 20 mM KCl, 2.5 mM $MgCl_2$, 20 mM KH_2PO_4, 5 mM Na_2HPO_4 (pH 6.4), 0.34 mM streptomycin sulfate, filter sterilize *(22–23)*. For analysis of chemotactic behavior: 1 mM stock solution of adenosine $3^1,5^1$-cyclic monophosphate (cAMP; Sigma-Aldrich, http://www.sigmaaldrich.com) in BSS is frozen until use.
2. Black filter paper (http://www.thomassci.com/catalog/product/2067).
3. Millipore support filters (catalog AP1004700; http://www.millipore.com).
4. Humidified incubation chamber at 22°C.

2.3. Isolation of Primary Human PMNs

1. Hank's balanced salt solution with $CaCl_2$ and $MgCl_2$ (Gibco BRL, Gaithersburg, MD), pH 7.4 and 0.01 M HEPES buffer. For analysis of chemotactic behavior: *N*-formyl peptide (fMLP): 500 μM stock solution of *N*-formyl-met-leu-phe (Sigma-Aldrich, Inc.) in DMSO is frozen until use.
2. Heparinized vacutainer tubes for collecting whole blood (http://www.bdbiosciences.com).
3. Polymorphprep (Axis-Shield, Oslo, Norway) for separation of viable neutrophils from whole blood.

2.4. Tissue Culture Cells

Tissue culture cell lines can be maintained in DMEM, RPMI or other media supplemented with fetal bovine serum, l-glutamine and antibiotics/antimycotic according to standard culture procedures.

2.5. 2D-DIAS Experiment (See Fig. 1a, b)

1. For quantifying basic motile behavior in the absence of chemoattractant: Perfusion chamber for buffer or media exchange such as the Sykes–Moore chamber *(22, 23)* (Bellco Glass, Inc., Vineland, NJ) or a custom designed microfluidic device (http://www.translume.com).
2. NE-1000 Multiphase Programmable Pumps (New Era Pump Systems, Farmingdale, NY; *(5)* or other pump *see* **Fig. 1a**, **items 1** and **2**) capable of continuously flushing the chamber without introducing oscillations (*see* **Note 1**).
3. For quantifying the response of single cells to chemoattractant: Dunn chamber (http://www.hawksley.co.uk/) *(24)*, Zigmond chamber *(25–26)* (http://www.neuroprobe.com/products/zigmond.html), or modified Zigmond chamber *(27)*. The Sykes–Moore chamber can be coupled to programmable pumps for global exposure to chemoattractant or generating a dynamic gradient of temporal waves *(5, 23)*. Single cells can also be imaged in gradients of chemoattractant generated in a microfluidic device (*see* **Subheading 2.1**, **step 2**).
4. Inverted or upright microscope with 10× or 25× magnification.
5. Heating and/or CO_2 infusion can be introduced into the perfusion system as illustrated in **Fig. 1b**, **items 1–3**.
6. CCD camera such as the grey-scale Hitachi KP-M3 (Hitachi Kokusai Electric, Inc., Japan; (*see* **Fig. 1a**, **item 2**)) connected to an analog to digital converter (Canopus, Co., LTD,

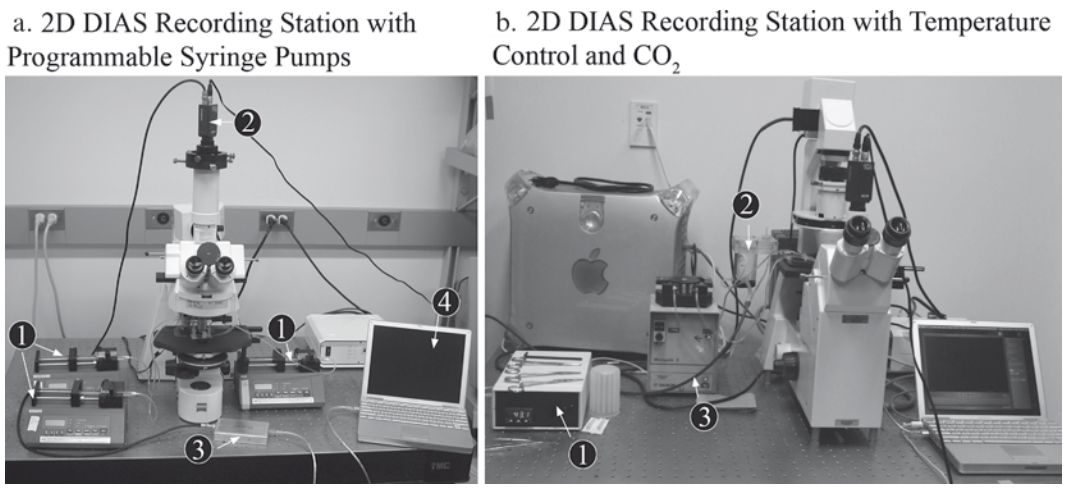

Fig. 1. Typical 2D-DIAS workstations. (**a**) NE-1000 programmable pumps (**items 1** and **3**) are connected to a perfusion chamber and can be used to continuously perfuse buffer or media, globally stimulate cells with a chemical, or generate temporal waves of chemoattractant. Images can be acquired with a low cost analog CCD camera **(2)**, connected to an analog to digital converter **(3)** and then written onto the computer **(4)**. (**b**) Perfusion media can be warmed **(1)** and pumped through a custom-built low cost receptacle **(2)** where CO_2 **(3)** can be introduced.

http://www.canopus.com; (*see* **Fig. 1a**, **item 3**)). One can use a FireWire or other digital camera for direct read-in, if available at requisite acquisition speed.

7. IEEE 1394 (e.g. FireWire) compatible image acquisition software such as Adobe Premiere® and QuickTime Pro®, version 7 or later with Windows XP or Vista operating systems, or iStopMotion, iMovie or QuickTime Pro®, version 7 or later for Macintosh (*see* **Note 2**).
8. Macintosh computer (G3, G4, G5 or Intel based) with OS X version 10.3, 10.4, or 10.5, 128 MB Ram or more and 20 MB hard disk space (*see* **Fig. 1a**, **item 4**).
9. 2D-DIAS software (Soll Technologies, Inc., Iowa City, IA) (*see* **Note 3**).

2.6. 3D-DIAS (DIC) Experiment

1. For 3D-DIAS analysis of basic motile behavior: A perfusion chamber (http://www.bioptechs.com) suitable for high N.A., narrow depth of field DIC microscopy and imaging for 5–10 min is connected to a perfusion apparatus (*see* **(Subheading 2.5**, **step 2**).
2. For quantifying in 3D the response of single cells to chemoattractant: modified Zigmond chamber *(27)* as described in **(Subheading 2.5**, **step 3)**.
3. Microscope with differential interference contrast (DIC) optics and high N.A. objective such as the 63× Planapo (Carl Zeiss Inc.) (*see* **Note4**).
4. Microstepper motor or piezo-electric focus device integrated with the camera and acquisition software so that only scans acquired in the up direction are saved. (*see* **Notes 5** and **6**). Alternatively, a character generator (CG) can connect the camera and computer. The CG must be synchronized with the motor so that frames acquired during the upward sweep of the motor are stamped with a mark that can be recognized by 3D-DIAS software. This provides a means for 3D-DIAS to distinguish upward from downward scans in a z-series and eliminate frames from one of those directions in post-processing (*see* **Note 7**).
5. Camera and video acquisition software (*see* **Subheading 2.5**, **steps 5** and **6**).
6. Computer capable of grabbing and storing images at 29.97 frames per second (*see* **Subheading 2.5**, **step 7**).
7. 3D-DIAS software *(13–17)*.

2.7. 2D and 3D-DIAS Confocal Experiment

1. Cells transfected with a fluorescently tagged cytoskeletal protein.
2. For quantifying basic motile behavior: A perfusion chamber (*see* **(Subheading 2.5**, **item 1**) such as the Sykes-Moore chamber assembled with 25-mM quartz coverslips (SPI Supplies

Division of Structure Probe Inc., West Chester, PA; http://www.2spi.com) to minimize oscillations introduced during perfusion. The chamber is connected to the pump system (*see* **(Subheading 2.5, item 2**).

3. For quantifying the response of single cells to chemoattractant: Dunn chamber (http://www.hawksley.co.uk/) *(24)* or modified Zigmond chamber *(27)* as described in **(Subheading 2.5, item 3** will work with laser illumination.
4. Confocal microscope with a 60× water immersion or 40× high N.A. objective.
5. Native acquisition software capable of collecting a z-series of scans that can be batch converted to standard TIF or QuickTime format and QuickTime Pro software, preferably for Macintosh.
6. 2D- and/or 3D-DIAS.

2.8. Quantitation of Microsphere Movements on the Cell Surface

1. Concanavalin A, type VI.
2. Polystyrene microspheres 0.465 μm diameter ±0.011 μm (Polysciences Inc.).
3. BSS (*see* **Subheading 2.2, step 1**).
4. Sonicator (Sonics and Materials Inc., Newton, CT, http://www.sonics.biz).
5. Dvorak-Stotler (http://www.nevtek.com) or other live cell imaging chamber suitable for high resolution, narrow depth of field, DIC optics.
6. 3D-DIAS software *(13–17)*.

3. Methods

3.1. 2D-DIAS Experiment

3.1.1. Preparation of Dictyostelium discoideum for 2D Analysis of Basic Motile Behavior and Chemotaxis

1. Development on filter pads: Pellet 5.5 × 10^7 growth phase cells, wash in BSS and disperse on a 47-mM diameter black filter paper supported by two Millipore pre-filters saturated with BSS. Incubate in a humidified chamber at 22°C until the onset of aggregation (approximately 6–7 h for wild-type strains); *(28)*. Wash cells from the filter pads and dilute to 3 × 10^4 cells/mL for inoculation into a perfusion or chemotaxis chamber.
2. Certain mutant *Dictyostelium* strains are defective in cAMP signaling and therefore require exogenously applied pulses of the chemoattractant in order to become motile *(29)*. Harvest these cells at the low log phase of growth, wash in BSS and resuspend 10^8 cells in 20 mL BSS. The flask containing the cell suspension is maintained on a rotary shaker at 200

rpm. Cells are pulsed by programming the NE-1000 Pumps (New Era Pump to deliver 100 µL of 10 µM cAMP from a 10-cc syringe every 6 min for six subsequent hours *(29)*. At the completion of pulsing, cells are pelleted, washed in BSS, and diltued to 3×10^4 cells/mL for inoculation into a perfusion or chemotaxis chamber.

3.1.2. Preparation of Primary Human Neutrophils and Cell Lines for 2D Analysis of Basic Motile Behavior and Chemotaxis

1. Whole venous blood is drawn into a heparinized vacutainer tube. The tube is gently inverted several times and 5 mL of blood is layered onto the top of 5 mL of Polymorphoprep (Axis-Shield, Oslo, Norway) in a 15-mL Falcon centrifuge tube according to the manufacturer's instructions *(5, 30)*. A distinct PMN layer can be withdrawn after centrifugation for 30–35 min at 450 × *g*. The PMN suspension is washed three times in H-HBSS and resuspended to a concentration of 1.5×10^6 cells/mL in H-HBSS.
2. Tissue culture cells are plated at the appropriate density on glass bottom culture plates (http://www.glass-bottom-dishes.com/) coated with poly-d-lysine, collagen or the user's coating of choice *(31)*. Cells may also be cultured on coverslips *(32, 33)*.

3.1.3. Chambers for Analysis of Basic Motile Behavior and Chemotaxis with 2D-DIAS

1. For the 2D analysis of cell behavior in the absence of chemoattractant, inoculate 1.1 mL of the dilute cell suspension into the Sykes-Moore perfusion chamber. Allow cells to adhere to the coverslip for 5 min at room temperature. During that time, cells should elongate and resume translocation. Fill tubing with perfusion solution, taking care to remove air bubbles from the tubing and ports, and connect the chamber.
2. The chamber is perfused with buffer or media in order to continuously refresh the environment *(23, 28)* (*see* **Note 8**).
3. For analyzing cells in a spatial gradient of test attractant, cells are deposited on the bridge of a chemotaxis chamber *(26, 27)*. In the Zigmond chamber, a 2 mm wide bridge separates the source and sink troughs. Solution containing the appropriate concentration of chemoattractant (for example, 1 µM cAMP for *Dictyostelium discoideum (27)*, 0.1 µM fMLP for human PMNs *(5, 34)*, and 500 µM fMLP for murine neutrophils *(34)*) is placed in the source trough and solution without the test attractant in the sink trough. Cells are dispersed on the bridge, incubated for 10 min, and then recorded. If using the Dunn chamber, cells are deposited on a coverslip, buffer is added to the inner trough and the appropriate concentration of attractant is added to the outer concentric trough. This chamber may be incubated at 37°C in 5% CO_2 for up to 30 min without evaporation of solutions.

4. At least one frame of a stage micrometer should be recorded at the identical settings used for the experiment in order to determine the scale factor in DIAS software.
5. Cells in glass-bottom or plastic dishes are placed on the stage with the appropriate objective.

3.1.4. Image Capture and Outlining with 2D-DIAS

1. For automatic outlining of individual cells using the threshold method of edge detection in 2D-DIAS (*see* **Fig. 2a**), the image is slightly defocused and processed by adjusting the light level, gain and offset on the camera controls, if possible, to achieve a uniformly dark cell against a lighter background (*see* **Fig. 2b**). 2D-DIAS has image processing capabilities for increasing contrast prior to outlining as well as several manual tracing and editing options for low contrast images.
2. Images are digitized onto the computer. The frame rate may be increased or decreased for faster or slower moving cells.

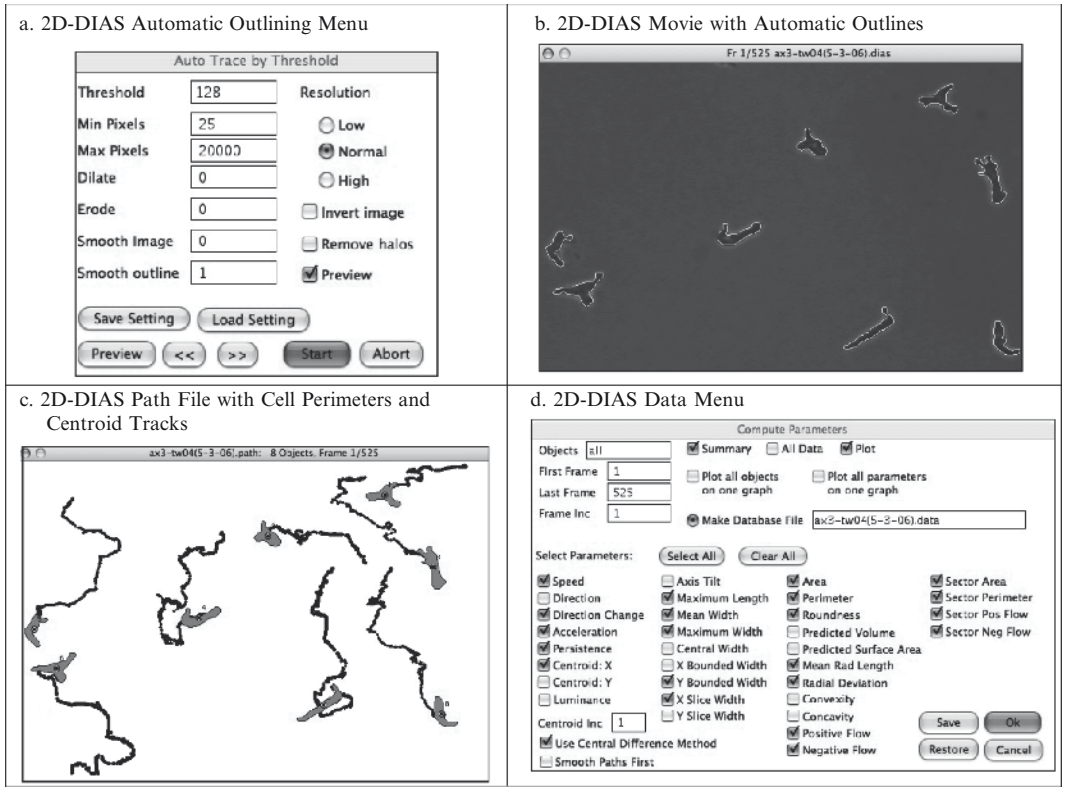

Fig. 2. 2D-DIAS. (**a**) Automatic outlining menu showing adjustable edge detection parameters; (**b**) example of automatically outlined cells in a QuickTime movie; (**c**) path file showing the cell perimeter in frame one and centroid tracks computed for a range of frames for the eight automatically outlined cells from the movie in (**b**) and (**d**) Compute Data menu1.

3. 2D-DIAS automatically detects the edge of the cell image in each frame employing a gray scale threshold algorithm (*see* **Fig. 2a**, **b**), converts the detected perimeter to a mathematically precise beta-spline replacement image, and from this final shape computes the centroid, or geometric center, at each time point (*see* **Fig. 2c**).

3.1.5. Cell Movement Parameters Computed by 2D-DIAS

The user may select up to 40 parameters from the standard 2D-DIAS menu (*see* **Fig. 2d**), or enter user-designed functions using the built in advanced RPN calculator. The position of the cell centroid over time is used to compute parameters such as instantaneous velocity, direction of travel, and direction change *(13–17)*. These data are stored in a DIAS database file (*see* **Fig. 3a**) that can be displayed in tabular or graphic form. The "chemotactic index" is computed as the net distance moved towards the source of chemoattractant divided by the total distance moved in a set period of time *(13–17)* and is stored in the summary (text) file (*see* **Fig. 3b**).

3.1.6. Cell Shape Parameters Computed by 2D-DIAS (See Fig. 4)

2D-DIAS has several methods that are very useful in visualizing and quantifying cell shape changes over time, all of which are based on beta-spline replacement images.

1. Stacked perimeter plots (*see* **Fig. 4a**) provide a visual history of cell movement from which lateral extensions and turning can readily be measured.
2. Difference pictures (*see* **Fig. 4b**) are constructed by overlaying the outline of the cell at frame n with the outline at frame $n - x$ where x is the user-specified increment. Expansion zones are regions in the later image that do not overlap the earlier image (filled areas in **Fig. 4b**) and retraction zones are regions in the earlier image that do not overlap the later image (hatched areas in **Fig.4b**). Gray areas are common zones.
3. Quantitation of expansion and retraction zones (relative flow) can be achieved by windowing the localized area of interest in a difference picture (*see* **Fig. 4c**). The area of expansion and/or retraction within the window is computed as a percent of the total area. This measurement has been effective in identifying aberrant pseudopod dynamics that would otherwise not have been noted in numerous cytoskeletal mutants *(34–39)*.
4. Cell morphology can also be viewed by "unwrapping" and stacking. (*see* **Fig. 4d**).

To generate an "unwrapped perimeter," 2D-DIAS converts polar coordinates to rectangular coordinates and stacks each plot with an offset lower than the previous one. This display accentuates the position and frequency of protrusions and can vividly demonstrate dynamic contributions of cytoskeletal elements to

a. 2D-DIAS Database Parameters

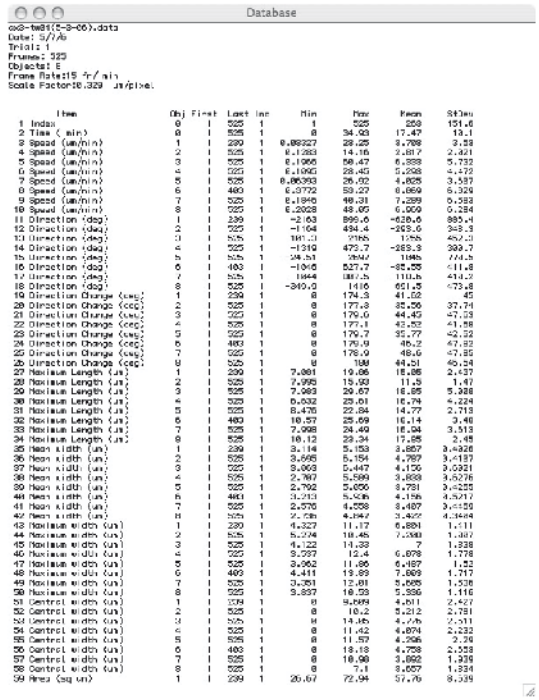

b. 2D-DIAS Database Parameters and Summary Text Imported into Excel®

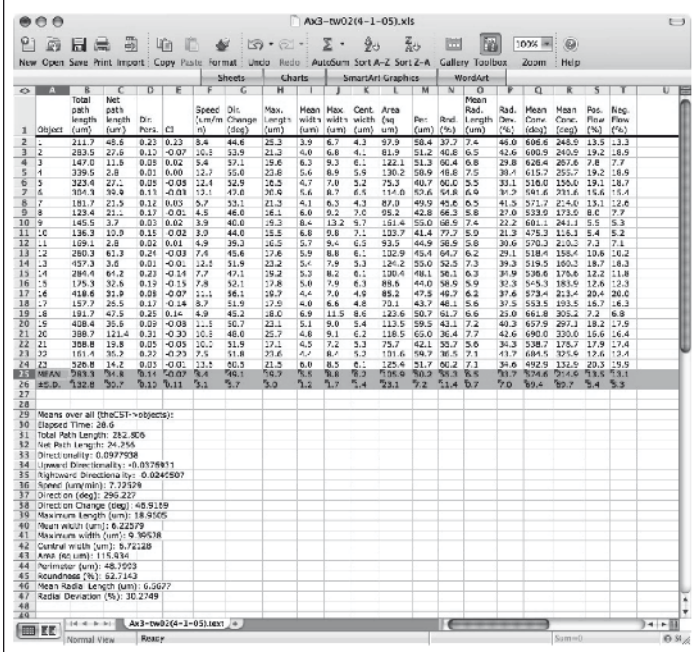

Fig. 3. (**a**) Example of 2D-DIAS data file. The DIAS database file can be viewed in tabular form as shown here and in graphic form. All parameters can be plotted and additional functions can be applied to the plots; (**b**) 2D-DIAS database and summary files can be exported into spreadsheet software for additional statistical analyses or graphic representations.

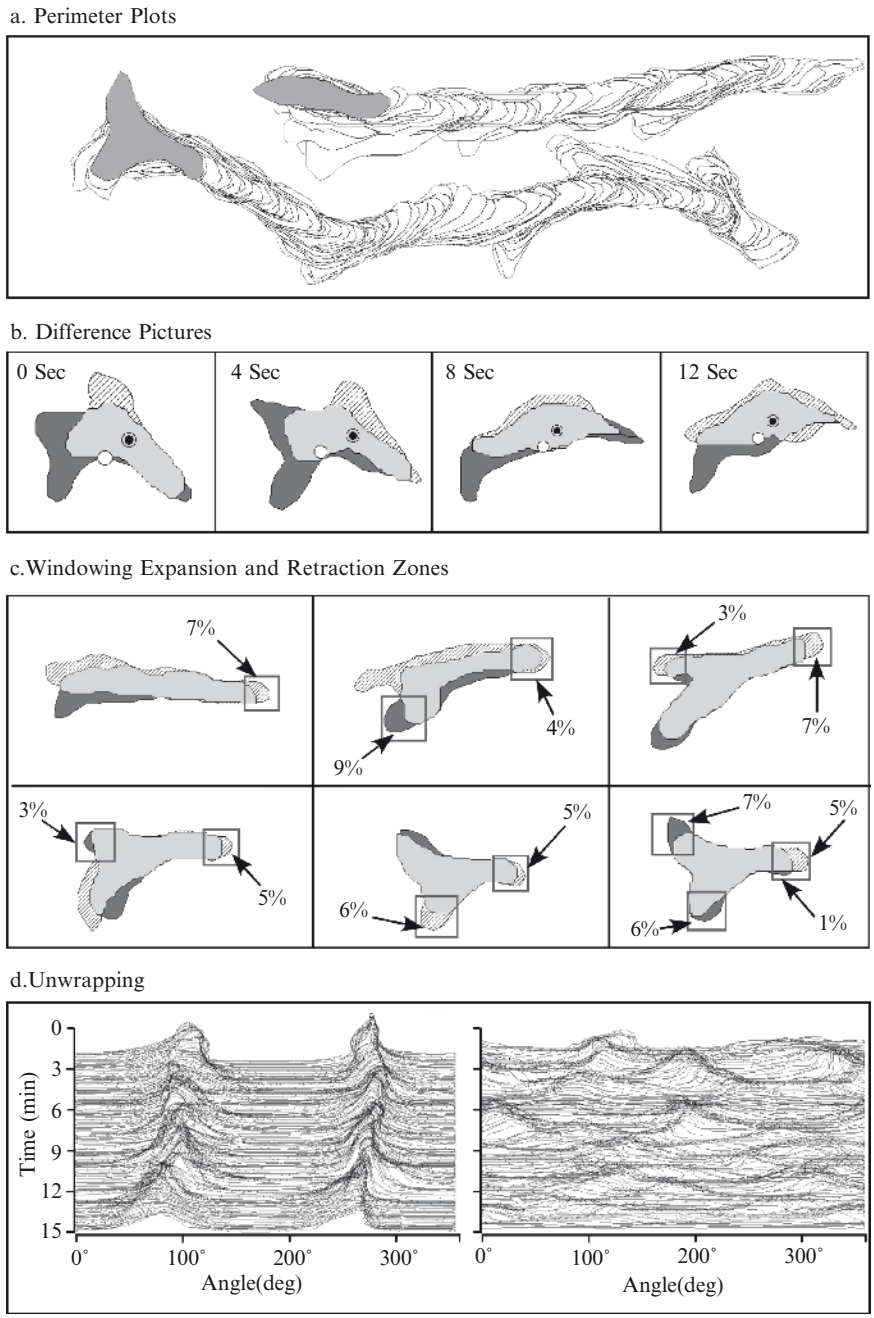

Fig. 4. 2D-DIAS has advanced shape analysis functions. (**a**) Stacked perimeter plots show a history of cell movement, lateral pseudopod extension and turning. In this case, outlines of two *Dictyostelium* amoebae are stacked at 4-s intervals and the last outline in the series is filled in *gray*; (**b**) difference in pictures are generated by overlaying the outline of the cell in frame *n* with the outline from a previous frame (*n* – *x*) where *x* is a user selected interval. In this example, differencing is at 4-s intervals, expansion zones over that interval are filled, retraction zones are hatched, and common zones are *light gray*. The *open circle* is the centroid position of the cell at frame *n* and the *dark circle* is the centroid position at frame *n* – *1*; (**c**) expansion and/or retraction zones can be quantified using the window feature. The area within the user defined window is calculated as a percent of the total area. Expansion and retraction rates can be derived from these data; (**d**) shapes can also be analyzed by "unwrapping," a function in the shape analysis program that converts the coordinates from polar to rectangular using the centroid as the polar coordinate origin. The "unwrapped" shapes are then plotted, each plot offset lower than the previous one.

cell shape, particularly lamellipodial behavior *(31)*. In **Fig. 4d**, an unwrapped normal, polarized PMN is presented on the left and a PMN from a patient with chemotactically defective PMNs is on the right.

3.2. 3D-DIAS (DIC) Experiment

3.2.1. Sample Preparation and Optical Sectioning

1. For 3D-DIAS analysis of basic motile behavior, samples are prepared as described in **(Subheading 3.1.1**. Cells are inoculated into a Dvorak-Stotler chamber and allowed to adhere to the coverslip for 5 min. The Dvorak-Stotler chamber can be sterilized by autoclaving and coverslips can be coated with matrix proteins for tissue culture lines. Cells may also be grown directly on the coverslips.
2. The chamber is connected to a perfusion pump and positioned on the stage of an inverted microscope equipped with DIC optics and a high numerical aperture objective such as the Zeiss 63× Planapochromat.
3. For the 3D reconstruction of single cells responding to a spatial gradient of chemoattractant, a chamber with a quartz bridge developed for the analysis of T cell chemotaxis *(26)* is employed. The glass coverslip onto which cells are deposited can be pre-conditioned if necessary. Once the cells have adhered to the coverslip (5 min in most cases), the coverslip is flipped, sealed with Vaseline and clamped over the bridge and troughs of the chamber. The chamber itself is inverted, one trough is filled with chemoattractant and the other with buffer. The second glass wall of the chamber is then lowered over the troughs and the bridge, sealed with Vaseline and the apparatus is placed on the stage of an inverted microscope for optical sectioning. The assembled chamber can be maintained at 37°C without significant evaporation.
4. To obtain optical sections, the motor is programmed to move the focus from the substratum through the user-determined *z*-axis height, generally 10–20 μm, in 2–3 s for *Dictyostelium discoideum* and human PMNs. As a rule, this yields, about sixty optical sections. The process is repeated every 4–5 s for 10 min or longer.
5. Images are written directly onto a computer hard drive. High-speed acquisition (30 frames per second) is required.

3.2.2. Outlining and Reconstructing Live Cells, Nuclei and Pseudopods Using 3D-DIAS

1. The in-focus perimeter of the cell body in each optical section is automatically outlined by the 3D-DIAS program using a pixel complexity algorithm *(13–17)*, illustrated by the black line in **Fig. 5**.
2. Edge points along each perimeter corresponding to a 2D *x*,*y*-coordinate grid are connected to generate transparent faceted reconstructions of the cell surface (*see* **Fig. 6a**-**Fig. 6c**). Alternatively, the faceted image can be smoothed and presented

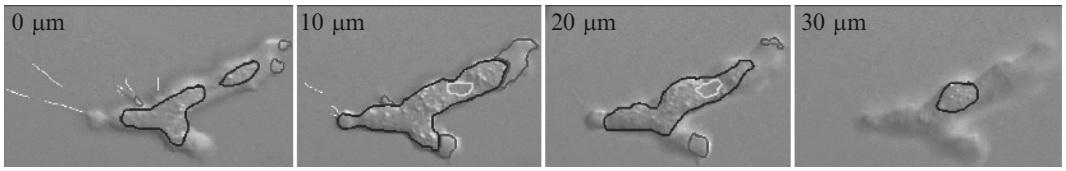

Fig. 5. 3D-DIAS generated outlines of optical sections from a z-series of DIC images. The cell body (*black line*) can be outlined automatically using the pixel complexity algorithm. The nucleus (*white line*), pseudopods (*gray line*), filopodia (*white line*) or any other internal structure identifiable in the DIC image can be outlined in a separate trace slot using the automatic outlining feature in combination with one of several manual outlining options. Optical sections are shown at 10 μm increments beginning at the substrate (0 μm) level.

as a shadowed, nontransparent "wrapped" image (*see* **Fig. 6d**). The 3D reconstructions can then be viewed at any angle and converted to a time series for dynamic 3D display in standard formats such as QuickTime or AVI.

3. Nuclei, pseudopods, filopodia or any other structures that can be discerned in the DIC image can be manually outlined in separate trace slots (*see white and gray outlines in* **Fig. 5**; *(40, 41)*. The trace slot permits independently derived data computation, visualization, and shape analyses of the structure it contains (*see* **Note 9**; *(40)*). A 3D-DIAS faceted reconstruction of a *Dictyostelium discoideum* amoebae with the nucleus (color-coded black), pseudopods (color-coded gray) and filopodia (color-coded dark gray) is presented at 60° and 15° in **Fig. 6a**. The image at 15° has been magnified to accentuate the filopodia.

3.2.3. Motility and Dynamic Morphology Parameters Computed by 3D-DIAS

3D-DIAS computes more than 100 parameters based upon the 3D position of the cell centroid and the 3D contours of the cell body. 3D-DIAS also generates 2D parameters on any planar slice of the cell *(13–17)*.

3.3. Analysis of Confocal Images Using 2D- and 3D-DIAS

3.3.1. Sample Preparation

1. For analysis of basic motile behavior, fluorescently labeled live cells are inoculated into the Sykes–Moore perfusion chamber assembled with quartz coverslips, connected to the perfusion system and placed on the stage of an inverted microscope.
2. For 2D and 3D confocal imaging of cells responding to a spatial gradient of gradient of chemoattractant, the modified Zigmond chamber is preferred *(26)*. (*see* **(Subheading 3.2.1, step 3**).

3.3.2. Image Acquisition and Pixel Intensity Measurements

1. Transmitted and fluorescent images of crawling cells are collected using the appropriate laser line with a high magnification objective such as the Nikon water immersion 60× Planapochromat.
2. A relatively fast scan rate of 166–500 lps is usually necessary for imaging fluorescently tagged cytoskeletal proteins in rapidly crawling cells such as wild-type *Dictyostelium* amoebae and PMNs. For best results in 3D-DIAS reconstructions, a

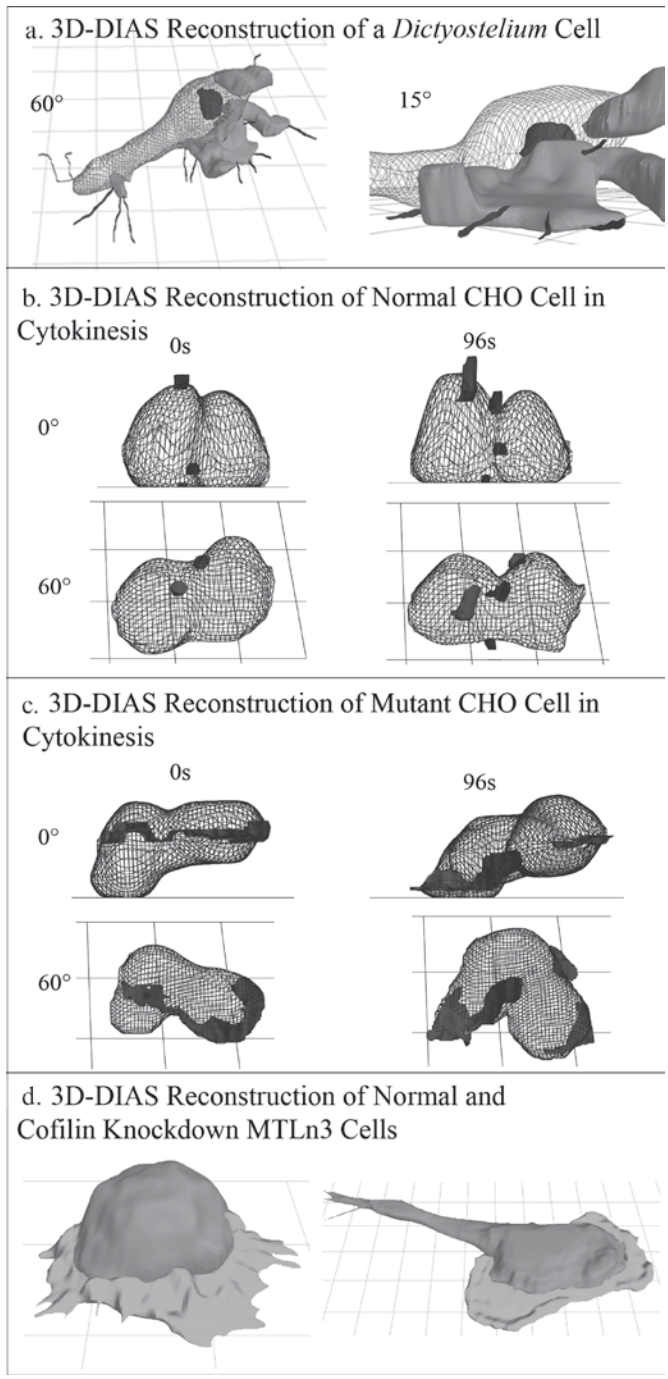

Fig. 6. Examples of 3D-DIAS reconstructions from optical sections of DIC images. (**a**) Faceted reconstruction of a *Dictyostelium discoideum* amoebae showing the nucleus (*black*), pseudopods (*gray*), and filopods (*dark gray*) presented at 60 and 15°; (**b**) faceted 3D-DIAS reconstruction of a normal CHO cell undergoing cytokinesis **(32)**. Surface blebs are filled and color-coded *gray*. Images are present at 0 and 60° at two time points during cytokinesis; (**c**) faceted 3D-DIAS reconstructions of CHO cells expressing a dominant-negative chimeric tropomyosin **(32)** presented at 0 and 60° at two time points during cytokinesis. Note that in contrast to the normal CHO cell in (b), one daughter cell in the mutant is off the substrate and that contiguous surface blebs circumnavigate the cell body. Identification of these aberrant phenotypes required 3D-DIAS; (**d**) 3D-DIAS smoothed reconstructions of a representative MTLn3 cell (*left*) and a representative MTLn3 cell in which cofilin expression was knocked down by siRNA **(31)**.

minimum of ten slices of a 512 × 512 image should be collected in a 5-s interval.

3. Using the native acquisition software, the 2D image or z-series is batch converted to a TIFF sequence and imported into the DIAS compatible QuickTime® Pro 7.
4. The localization of fluorescently tagged cytoskeletal elements, in response to temporal waves or global stimulation of chemoattractant can be analyzed with the pixel intensity parameter in 2D-DIAS. using In these experiments, cells are imaged in the Sykes–Moore chamber and the NE-1000 Multiphase Programmable Pumps. The actin in the *Dictyostelium* cell in **Fig.** 7 is labeled with ABD-GFP *(42)*. The localization and intensity of the GFP-tagged actin is shown during the front

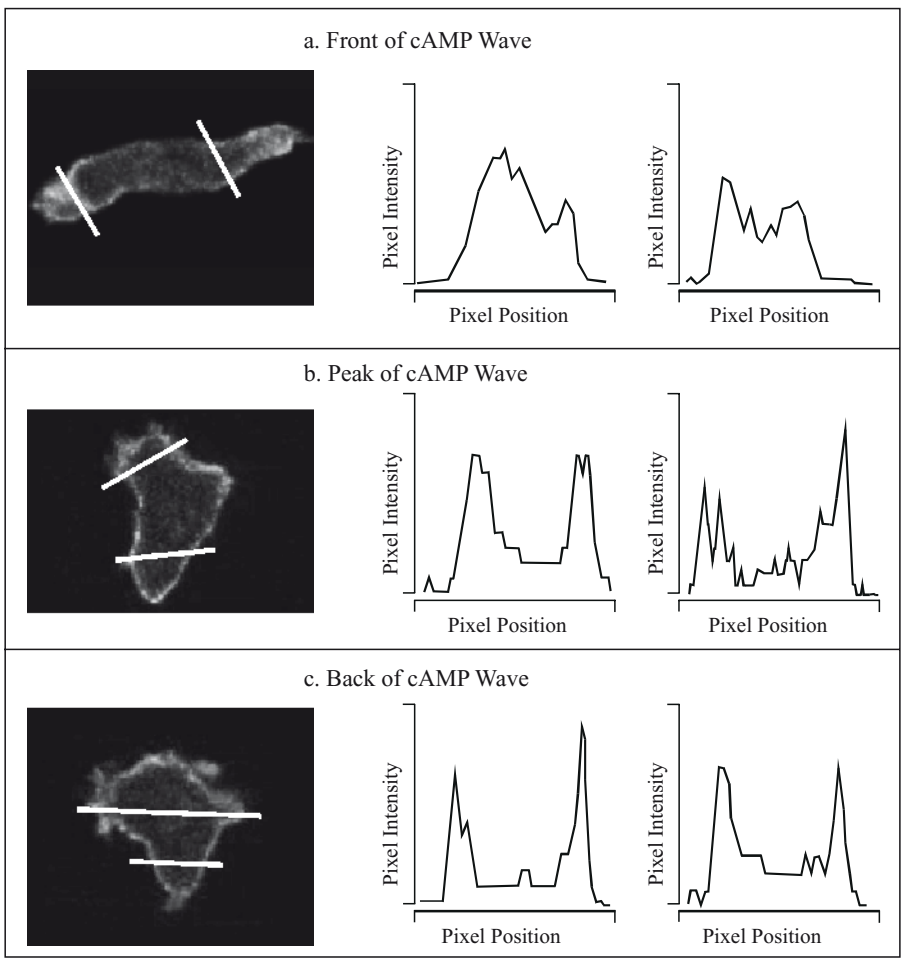

Fig. 7. Localization and quantitation of GFP-tagged actin during (**a**) the increasing or front, (**b**) peak, and (**c**) decreasing (back) of a cAMP wave generated using the NE-1000 programmable pump system connected to the Sykes–Moore perfusion chamber assembled with quartz coverslips. Images were acquired on a confocal microscope and pixel intensity measurements performed in DIAS.

(*see* **Fig. 7a**), peak (*see* **Fig. 7b**), and back (*see* **Fig. 7c**) of a temporal cAMP wave *(23)*.

3.3.3. 3D-DIAS Reconstruction

1. A z-series of a cell with a fluorescently tagged cytoskeletal protein is acquired as described in **(Subheading 3.3.2)**.
2. Trace slots (*see* **Subheading 3.2.2**, **step 3**; *(41)*) can be used to outline and quantify different intensity levels of a fluorescently tagged protein. For example, the cell reconstructed in **Fig. 8**, is expressing the ABD-GFP fusion protein probe that interacts with actin *(42)*. In this figure, the cell body, represented as a transparent faceted reconstruction, is outlined in trace slot 1 while intensely labeled actin, seen in the anterior pseudopod (a), is in a separate trace slot. A lower intensity of labeled actin, automatically outlined in trace slot 3, can be seen to localize primarily to the uropod (u). Actin in the retracting lateral pseudopod (lp) that is not in contact with the surface is dissipating.

3.4. 3D-DIAS Analysis of Microspheres on the Surface of Crawling Dictyostelium discoideum Amoebae

3.4.1. Preparation of Microspheres

1. Dilute 2 mg/mL of Concanavalin A in BSS.
2. Incubate 40 μL/mL of polystyrene microspheres in the Concanavalin A and BSS solution for 30 min at 4°C.
3. Centrifuge at 3,600 rpm for 30 min, pour off supernatant and resuspend the pellet in 10 mL of BSS. Repeat (*see* **Notes 10** and **11**).
4. Sonicate with Vibracell sonicator (Sonics and Materials Inc.) at 15% amplitude for 20 s.
5. Harvest cells as described in **(Subheading 3.1.1**, **steps 1** and **2)**.
6. Mix 80 μL of polystyrene microspheres/Concanavalin A solution with 4 mL of cells at 1×10^5 cells/mL in BSS. Immediately inoculate the mixture into the Dvorak-Stotler chamber.

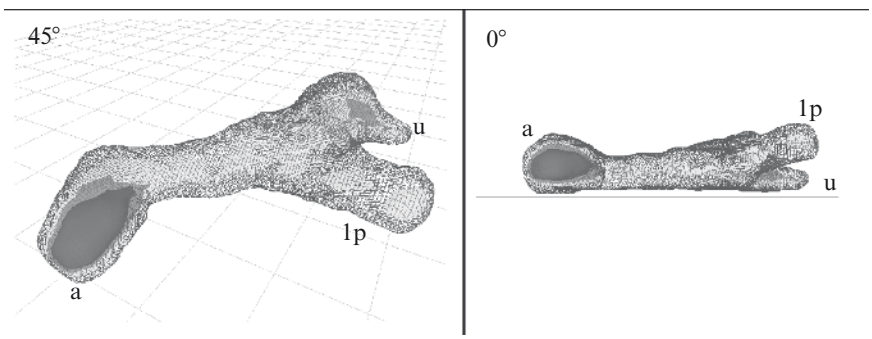

Fig. 8. 3D-DIAS reconstruction of a *Dictyostelium* cell showing intracellular localization of GFP-tagged actin *(42)*. The cell body was outlined in trace slot 1, high pixel intensity fluorescence in trace slot 2 and mid-range pixel intensity in trace slot 3. Data can be calculated for each individual trace slot. The trace slots are combined to generate a 3D image that can be viewed at any angle. The 3D reconstructions presented here at 45 and 0° reveal high levels of actin localized in the anterior pseudopod (**a**), mid-range actin in the uropod (u) and dissipation of actin as the lateral pseudopod (lp) retracts.

3.4.2. 3D-DIAS Reconstruction of Surface Microspheres

To measure the trajectories and compute 3D parameters of microspheres attached to the surface of *Dictyostelium* amoebae, optical sectioning, image acquisition, and outlining using trace slots are performed as described above (*see* **Subheading 3.2.2**) A substrate level DIC image of a cell is presented in **Fig.9a**. Note that the microspheres are not visible at the substrate level and come into focus 20 μm above the substrate (*see* **Fig. 9b**). In this example, the microspheres (arrow) are attached at the cell body/pseudopod interface. A 3D reconstruction of the cell body (gray), anterior pseudopod (dark gray) and the microsphere (white) are presented in **Fig. 9c**. A 3D cross plot of the microsphere centroid track is presented in **Fig. 9d**.

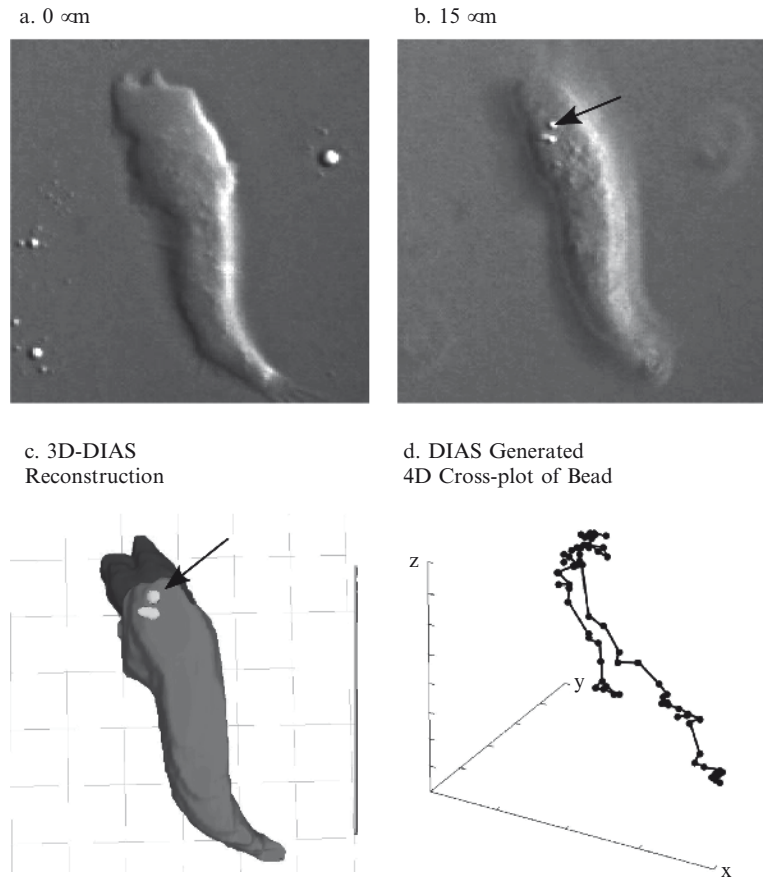

Fig. 9. 3D-DIAS reconstruction of a crawling *Dictyostelium* cell and trajectory plot of a microsphere attached to its surface. (**a**) DIC substrate level image; (**b**) DIC image at 15 μm above the substrate revealed microspheres attached to the cell surface (*arrow*) at the interface between the pseudopod and cell body; (**c**) 3D-DIAS reconstruction of the cell body (*light gray*), pseudopod (*dark gray*), and microspheres (*arrow*) viewed from the top (90°); (**d**) DIAS computed and plotted the microsphere trajectory in 4D.

4. Notes

1. Peristaltic and diastolic pumps are quite smooth for large volumes but oscillate at low flow rates causing variations in the focal plane. Syringe pumps can oscillate as the feed screw turns. Having a rapidly updating perfusion pump, as well as decreasing the diameter of the syringe to obtain the desired flow rate with a relatively fast perfusion rate, can mitigate this problem.
2. Recording experiments directly onto a computer hard drive requires a balance between quality and size of the acquired file. QuickTime® Pro supports dozens of compressions and video codecs. MPEG standard H264 offers the best quality to file size ratio, but it also requires the most processing power to decode. 2D- and 3D-DIAS are compatible with any of the codec's that QuickTime® Pro provides.
3. The equipment for 2D-DIAS will include a microscope, microscope mounted camera, an analog to digital converter, a Macintosh computer and 2D-DIAS software.
4. When using water or oil immersion objectives for high-resolution microscopy, the movement of the objective lens is coupled to the imaging chamber coverslip by the immersion medium. When the objective is brought thru the z-series sequence, it can increase or decrease the pressure within the chamber, causing the focal plane to shift with the motion of the z-motor. The use of quartz coverslips can solve this issue.
5. When acquiring a z-series scan of a specimen, certain caveats can arise. Oscillations in Z motor speed, movement of the imaging chamber due to heat, and motion due to the perfusion system in use, all reduce the accuracy and reproducibility of the z-series acquisition. Steps should be taken to mitigate as many of these issues as possible ,before attempting to image specimens in three dimensions.
6. Motor oscillations can reduce the accuracy and reproducibility of a z-series acquisition. By utilizing a higher torque motor one can alleviate this issue to some degree. Motor oscillations can also be caused by mid-range resonance. This may cause variations in motor speed and induce motor stall at certain rotation speeds. This can be addressed by employing a more sophisticated bipolar motor driver that suppresses midrange resonance.
7. When reconstructing a z-stack of images into a three-dimensional object, it is necessary to separate and discard either the up-scan or the down-scan of the acquisition. 3D-DIAS incorporates a character generator to imprint the up-scans and a software detection method that retains only the imprinted frames during post processing. There are alternatives to a

character generator, such as utilizing third-party acquisition software that simply does not record the down-scan, or by employing a shutter in the light path of the camera synchronized with the z-motor to omit the redundant data. However, at present, these systems are difficult to assemble with commercially available products due to the need for synchronization of camera, motor and software at high acquisition rates.

8. When recording time lapse microscopy, it is essential to continuously refresh the microenvironment so that metabolites released by the cells will be rapidly removed and not affect basic motile behavior. It is desirable to replace the full volume of the perfusion chamber at least every 15 s to avoid the buildup of these chemicals.
9. 2D- and 3D-DIAS have the ability to automatically outline a cell based on pixel intensity. Ideally, a background containing no or very few artifacts creates the most reproducible and accurate outline. If the microscopy is not ideal, manually editing the outlines to reflect the true shape of the cell is desirable.
10. When pouring off the supernatant during the wash step of preparation of the polystyrene microspheres and Concanavalin A, it is desirable to use a pipet aid to gently siphon off the supernatant, as the pellet of microspheres is very easily poured off by standard means.
11. The polystyrene microspheres and Concanavalin A solution can be stored at 4°C for up to 2 months. After that period of time, it becomes necessary to re-wash and re-suspend the beads in fresh BSS. This should be done only once.

Acknowledgments

The development of 2D- and 3D-DIAS was supported in part by grants HD18577 and AI40040 from the National Institutes of Health and a generous facility grant from the W.M. Keck Foundation.

References

1. Ridley, A., Schwartz, M., Burridge, K., Firtel, R., Ginsberg, M., Borisy, G., Parsons, J., and Horwitz, A. (2003) Cell migration: integrating signals from front to back. *Science* **302**, 1704–1709.
2. Affolter, M. and Weijer, C. (2005) Signaling to cytoskeletal dynamics during chemotaxis. *Dev. Cell* **9**, 19–34.
3. Janetopoulos, C. and Firtel, R. (2008) Directional sensing during chemotaxis. *FEBS Lett.* **582**, 2075–2085.
4. Soll, D.R., Wessels, D., Zhang, H., and Heid, P. (2002) A contextual framework for interpreting the roles of proteins in motility and chemotaxis in *Dictyostelium discoideum*. *J. Musc. Res. Cell Motil.* **23**, 659–672.

5. Geiger, J., Wessels, D., and Soll, D.R. (2003) Human polymorphonuclear leukocytes respond to waves of chemoattractant, like *Dictyostelium*. *Cell Motil. Cytoskeleton* **56**, 27–44.
6. Kolsch, V., Charest, P., and Firtel, R. (2007) The regulation of cell motility and chemotaxis by phospholipid signaling. *J. Cell Sci.* **121**, 551–559.
7. Wyckoff, J., Wang, W., Lin, E., Wang, Y., Pixley, F., Stanley, E., Graf, T., Pollard, J., Segall, J., and Condeelis, J. (2004) A paracrine loop between tumor cells and macrophages is required for tumor cell migration in mammary tumors. *Cancer Res.* **64**, 7002–7009.
8. Dumstrei, K., Mennecke, R., and Raz, E. (2004) Signaling pathways controlling primordial germ cell migration in zebrafish. *J. Cell Sci.* **117**, 4787–4795.
9. Wessels, D., Lusche, D., Kuhl, S., Heid, P., and Soll, D.R. (2007) PTEN plays a role in the suppression of lateral pseudopod formation during *Dictyostelium* motility and chemotaxis. *J. Cell Sci.* **120**, 2517–2531.
10. Stepanovic, V., Wessels, D., Goldman, F., Geiger, G., and Soll, D.R. (2004) The chemotaxis defect of Shwachman-Diamond syndrome leukocytes. *Cell Motil. Cytoskeleton* **57**, 158–174.
11. Williams, R., Boeckeler, K., Graf, R., Taubenberger, A., Li, Z., Isberg, R., Wessels, D., Soll, D.R., Alexander, H., and Alexander, S. (2006) Towards a molecular understanding of human diseases using *Dictyostelium discoideum*. *Trends Mol. Med.* **12**, 416–422.
12. Galli, E., Rossi, P., Fiore, L., Perlini, R., Celibon, F., Betti, P., and Businco, L. (1983) IgE levels and PMN chemotaxis in atopic dermatitis. *Allergol. Immunopathol. (Madr).* **11**, 189–194.
13. Soll, D.R. (1995) The use of computers in understanding how cells crawl. *Int. Rev. Cytol.* **163**, 43–104.
14. Soll, D.R. and Voss, E. (1998) Two and three dimensional computer systems for analyzing how cells crawl. In: *Motion Analysis of Living Cells* (Soll, D.R. and Wessels, D., eds.), Wiley, New York, pp. 25–52.
15. Soll, D.R., Voss, E., Johnson, O., and Wessels, D.J. (2000) Three-dimensional reconstruction and motion analysis of living crawling cells. *Scanning* **22**, 249–257.
16. Wessels, D., Kuhl, S., Soll, D.R. (2006) Application of 2D and 3D DIAS to motion analysis of live cells in transmission and confocal microcopy imaging. In: *Methods in Molecular Biology* (Eichinger, L. and Rivero, F., eds.), Humana, Totowa, NJ, pp. 261–279.
17. Soll, D.R., Voss, E., Wessels, D., and Kuhl, S. (2007) Computer-assisted systems for dynamic 3D reconstruction and motion analysis of living cells. In: *Cell Motility* (Shorte, S., ed), Springer, Germany, pp. 365–384.
18. Wessels, D. and Soll, D.R. (1998) Computer-assisted analysis of cytoskeleton mutants of *Dictyostelium*. In: *Motion Analysis of Living Cells* (Soll, D.R. and Wessels, D., eds.), Wiley, New York, pp. 101–140.
19. Kumar, A., Wessels, D., Daniels, K., Alexander, S., Alexander, H., and Soll, D.R. 2004. Sphingosine-1-phosphate plays a role in the suppression of lateral pseudopod formation during *Dictyostelium discoideum* cell migration and chemotaxis. *Cell Motil. Cytoskeleton* **59**, 227–241.
20. Stepanovic, V., Wessels, D., Loomis, W.F., and Soll, D.R. (2005) Adenylyl cyclase plays an intracellular role in the suppression of lateral pseudopod formation during *Dictyostelium* chemotaxis. *Eukaryot. Cell* **4**, 775–786.
21. Cocucci, S. and Sussman, M. (1970) RNA in cytoplasmic and nuclear fractions of cellular slime mold amebas. *J. Cell Biol.* **4**, 399–407.
22. Varnum, B. and Soll, D.R. (1984) Effect of cAMP on single cell motility in *Dictyostelium*. *J. Cell Biol.* **99**, 1151–1155.
23. Varnum, B., Edwards, K., and Soll, D.R. (1985) *Dictyostelium* amoebae alter motility differently in response to increasing versus decreasing temporal gradients of cAMP. *J. Cell Biol.* **101**, 1–5.
24. Wells, C. and Ridley, A. (2005) Analysis of cell migration using the Dunn chemotaxis chamber and time-lapse microscopy. *Methods Mol. Biol.* **294**, 31–41.
25. Zigmond, S.H. (1978) A new visual assay of leukocyte chemotaxis. In: *Leukocyte Chemotaxis: Methods, Physiology and Clinical Implication* (Gallin, J.I. and Quie, P.G., eds.), Raven Press, New York, NY, pp. 57–66.
26. Varnum-Finney, B., Voss, E., and Soll, D.R. (1987) Frequency and orientation of pseudopod formation of *Dictyostelium discoideum* amoebae chemotaxing in a spatial gradient: further evidence for a temporal mechanism. *Cell Motil. Cytoskeleton* **8**, 18–26.
27. Shutt, D., Jenkins, L., Carolan, E., Stapleton, J., Daniels, K., Kennedy, R., and Soll, D.R. (1998) T cell syncytia induced by HIV release T cell chemoattractants: demonstration with a newly developed single cell chemotaxis chamber. *J. Cell Sci.* **111**, 99–109.
28. Varnum, B., Edwards, K., and Soll, D.R. (1986) The developmental regulation of single

cell motility in *Dictyostelium discoideum*. *Dev. Biol.***113**, 218–227.

29. Wessels, D., Brincks, R., Kuhl, S., Stepanovic, S., Daniels, K.J., Weeks, G., Lim, C.J., Fuller, D., Loomis, W.F., and Soll, D.R. (2004) RasC plays a selective role in the transduction of temporal gradient information in the cAMP wave of *Dictyostelium*. *Eukaryot. Cell* **3**, 646–662.
30. Lokuta, M., Nuzzi, P., and Huttenlocher, A. (2007) Analysis of neutrophil polarization and chemotaxis. *Methods Mol. Biol.* **412**, 211–229.
31. Sidani, M., Wessels, D., Mouneimne, G., Ghosh, M., Goswami, S., Sarnuebtim C., Wang, W., Kuhl, S., El-Sibai, M., Backer, J., Eddy, R., Soll, D., and Condeelis, J. (2007) Cofilin determines the migration behavior and turning frequency of metastatic cancer cells. *J. Cell Biol.* **179**, 777–791.
32. Wong, K., Wessels, D., Krob, S., Matveia, A.R., Lin, J.L.-C., Soll, D.R., and Lin, J.J.-C. (2000) Forced expression of dominant-negative chimeric tropomyosin causes abnormal motile behavior during cell division. *Cell Motil. Cytoskeleton* **45**, 121–132.
33. Li, Y., Wessels, D., Wang, T., Lin, J.L.-C., Soll, D.R., and Lin, J.J-C. (2003) Regulation of caldesmon activity Cdc2 kinase plays an important role in maintaining membrane cortex integrity during cell division. *CMLS* **60**, 198–211.
34. Volk, P., Heise, C., Hougen, J., Artman, C., Volk, K., Wessels, D., Soll, D., Nauseef, W., Lamb, F., and Moreland, J. (2008) CLC-3 and ICL_{swell} are required for normal neutrophil chemotaxis and shape change. *J. Biol. Chem.*
35. Wessels, D., Soll, D.R., Knecht, D., Loomis, W.F., DeLozanne, A., and Spudich, J. (1988) Cell motility and chemotaxis in *Dictyostelium* amoebae lacking myosin heavy chain. *Dev. Biol.* **128**, 164–177.
36. Wessels, D., Murray, J., Jung, G., Hammer, J., and Soll, D.R. (1991) Myosin IB null mutant of *Dictyostelium* exhibits abnormalities in motility. *Cell Motil. Cytoskeleton* **20**, 301–315.
37. Cox, D., Condeelis, J., Wessels, D., Doll, D., Kern, H., and Knecht, D. (1992) Targeted disruption of the ABP-120 gene leads to cells with altered motility. *J. Cell Biol.* **116**, 943–955.
38. Titus, M., Wessels, D., Spudich, J., and Soll, D.R. (1992) The unconventional myosin encoded by the myo A gene plays a role in *Dictyostelium* motility. *Mol. Biol. Cell* **4**, 233–246.
39. Wessels, D. and Soll, D.R. (1998) Computer-assisted characterization of the behavioral defects of cytoskeletal mutants of *Dictyostelium discoideum*. In: *Motion Analysis of Living Cells* (Soll, D.R. and Wessels, D., eds.), Wiley, New York, pp. 101–140.
40. Wessels, D., Voss, E., Von Bergen, N., Burns, R., Stites, J., and Soll, D.R. (1998) A computer-assisted system for reconstructing and interpreting in three dimensions the relationships of the cell surface, the nucleus and pseudopods in living cells. *Cell Motil. Cytoskeleton* **41**, 225–246.
41. Heid, P., Voss, E., and Soll, D.R. (2002) 3D-DIASemb: a computer-assisted system for reconstructing and motion analyzing in 4D every cell and nucleus in a developing embryo. *Dev. Biol.* **245**, 329–347.
42. Pang, K., Lee, E., and Knecht, D. (1998) Use of a fusion protein between GFP and an actin-binding domain to visualize transient filamentous actin structures. *Curr. Biol.* **8**, 405–408.

Chapter 19

Detergent-Extracted Models for the Study of Cilia or Flagella

Charles B. Lindemann and Kathleen A. Lesich

Summary

Methods for using non-ionic detergents to produce demembranated and reactivated cilia and flagella are described in detail. Demembranated and reactivated cell models are useful as a research tool for studying motility function in flagella and cilia. When the plasma membrane is removed, the factors regulating motility can be studied under standardized experimental conditions that otherwise would be impossible. Practical insight is provided to understand the important factors in producing stable reactivated models. In addition, several useful variations of the method are presented for different types of mammalian and non-mammalian flagellar and ciliary systems.

Key words: Triton X-100, Sperm, Method, Axoneme, Sliding, Dynein, *Chlamydomonas*

1. Introduction

The plasma membrane of the living cell is designed to regulate the internal composition of the cytosol and protect the interior of the cell from oxidative and enzymatic damage. It performs its role so well in these respects that it presents a major obstacle to the study of intracellular processes. Recognizing this problem, Szent-Gyorgyi *(1)* used high concentrations of glycerol to increase the permeability of the membrane. This allowed him to carry out his now famous studies of skeletal muscle physiology that demonstrated the central role of ATP and Ca^{2+} in muscle contraction. Adopting essentially the same approach, Hoffman-Berling and Bishop *(2, 3)* applied the glycerination method to mammalian sperm cells and reported a limited success in inducing

R.H. Gavin (ed.), *Cytoskeleton Methods and Protocols,* Methods in Molecular Biology, vol. 586
DOI 10.1007/978-1-60761-376-3_19,
© Humana Press, a part of Springer Science + Business Media, LLC 2009

motion but not coordinated swimming. Applying the glycerination technique to sea urchin sperm, Brokaw and Benedict *(4)* successfully restored coordinated beating of the flagellum and progressive swimming. Using the nonionic detergent Triton X-100, Gibbons and Gibbons *(5)* showed that normal flagellar motility could be reactivated in the absence of the plasma membrane. This result made it clear that the flagellar axoneme is a self-contained machine, which only requires a suitable medium and a supply of Mg-ATP to function.

The adaptation and application of the detergent-extraction technique to a great diversity of cilia and flagella followed the initial development of a workable reactivation method by the Gibbons' laboratory. Tryptic digests of demembranated sea urchin sperm flagella provided the first dynamic observations of microtubule sliding *(6)*. Subsequent application of the technique to *Tetrahymena* allowed the polarity of action of the dynein arms to be determined *(7)*. The detergent-extraction technique was partially responsible for identifying the cyclic AMP mediated control of the axoneme *(8)*. This powerful technique has also permitted the discoveries of vanadate as a specific inhibitor of dynein *(9, 10)*, the role of Ca^{2+} in the symmetry of the flagellar beat *(11)*, and determining the force generated per dynein head *(12)*.

The challenges that remain in the understanding of cilia and flagella are centered around two major areas of exploration. The first involves the molecular construction of the axoneme. Modern molecular genetics provides the means to explore the function of individual components of the axoneme by targeted mutagenesis. In this endeavor, *Chlamydomonas* is the leading model system, as an extensive library of mutations affecting flagellar proteins is readily available. Demembranated models represent the best hope for quantitatively documenting differences in functional performance of the flagellum under standardized assay conditions. Unless axonemal function is assayed under conditions where Mg-ATP, Ca^{2+}, cAMP and pH are rigidly controlled, too many confounding variables can obscure the true effect of a single mutation. For this reason, membrane permeabilized models are possibly the best assay for determining gene function of flagellar proteins.

The second challenge is in the arena of theory development. Working hypotheses that are advanced on the basis of the available experimental data must be subjected to tests that confirm or reject their validity. Controlled experiments that test a specific hypothesis are often only possible without the interference of the membrane *(13)*.

In the remainder of this report a general method will be presented for reactivation of detergent-extracted models. Variations that have been developed to facilitate working with specific systems will be considered, and the special problems inherent in working with demembranated cilia and flagella will be discussed.

2. Materials

2.1. Reagents and Solutions

Demembranated cells are extremely sensitive to contaminants that would be excluded from the cell interior in a live, intact cell. For this reason, it is very important to start with the highest purity ingredients when making solutions for reactivating membrane-extracted cilia and flagella.

1. Detergents: Triton X-100 or Nonidet P-40 (IGEPAL CA-630). These are the most widely employed detergents for membrane extraction, although many available detergents can give a satisfactory result. Nonidet P-40 is no longer commercially available under that name but many companies still supply a chemically equivalent detergent. It is best to stay with a source that has worked in your own trials. We have had good results with MP Biomedical's (Solon, OH) Nonidet P-40 (IGEPAL® CA-630). For well over a decade we have used Pierce's (Rockford, IL) Surfact-Amps® X-100 10% (w/v) aqueous solution of Triton X-100 supplied in 10-mL ampules. For short term storage, each ampule is transferred into black microtubes (USA Scientific, Ocala, FL) in 0.5-mL aliquots and stored at 4°C, although the manufacturer states it may be stored at room temperature. We bring it to room temperature before use. Due to the susceptibility of these detergents to oxidation when exposed to air, we limit the number of times we use each microtube to four.
2. Reducing agents: Dithiothreitol (DTT) or Glutathione. These are excellent reducing agents and antioxidants. They must be stored dessicated and refrigerated and are critical ingredients in a successful reactivation. It is good to stay with a supplier that has given good results. Sigma-Aldrich (St. Louis, MO) is our supplier for DTT (D5545). The DTT should be made up as a 0.1 M stock solution and then stored frozen (–20°C) for up to 1 year, in small aliquots (<1 mL) in sealed 1.5-mL microfuge tubes. Once a lot has proven itself in use, it is good to have fresh microfuge tubes of the same batch to work with. It is best in practice to freeze and thaw the same microfuge tube no more than four times. Keep the tube sealed and on ice during experiments. In its proper, reduced form, it is a smelly (skunky) compound; if it doesn't stink, don't use it. Glutathione will also give excellent results as an antioxidant. It can be treated much the same as DTT and may be substituted if preferred. Glutathione is the natural antioxidant of the cell interior. Therefore, if your goal is to duplicate the natural interior condition of the cell, glutathione may be an attractive option.

3. Buffers: Tris, HEPES or PIPES. Tris (Tris[hydroxymethyl] aminomethane) is a suitable buffer for reactivating demembranated flagella at the more alkaline range of pH (7.4–8.0). HEPES (*N*-(2-hydroxyethyl)-1-piperazine-*N*′-ethansulfonic acid) and PIPES (piperazine-*N*, *N*′-bis[2-ethanesulfonic acid]) are more widely used for reactivation protocols in the pH range of 6.6–7.4. All are widely available. We have a lot of experience with Sigma-Aldrich's Tris (T6791), preferring to work from the free base and titrating to neutral (pH 6.8–7.2) with HCl to make up the stock solution. Store refrigerated for no longer than 2 weeks.
4. Organic Salts: Potassium glutamate or potassium acetate. Optimizing the reactivation of a flagellum or cilium depends, to some extent, on the ionic strength of the mixture. Potassium salts give better results than sodium salts and organic anions are greatly superior to inorganic anions. Bull sperm will not reactivate satisfactorily with Mg-ATP in a potassium chloride solution. Glutamate eliminates this problem when used as the predominant anion *(14)*. Subsequent studies have confirmed that organic anions generally give superior results *(15)*, acetate being particularly effective. We have had the best results titrating l-glutamic acid supplied by Sigma-Aldrich (#49449) to neutral (pH 6.8–7.2) with KOH. These salts in solution grow bacteria extremely well. Store refrigerated and inspect for cloudiness before each use. Discard after 2 weeks.
5. Nucleotides: Adenosine-5′-triphosphate (ATP) and adenosine-5′-diphosphate (ADP), used in reactivations, should always be the highest purity available and certified vanadate free, if possible. Stock solutions should be titrated to the final working pH and frozen (−20°C) in small (<1 mL) aliquots in sealed microfuge tubes. ATP and ADP are strong buffers and can significantly change the working pH of the final reactivation solution if not pre-titrated to the working pH. Also, if they are left at their initial acid pH they hydrolyze rapidly, decreasing their storage time. ADP is the more unstable of the two compounds in storage. While it is best to make up a fresh stock solution every 6 months, we have successfully used nucleotide stock solutions for up to 1 year after preparation. Adenosine 3′:5′-cyclic monophosphate (cAMP): Stock solution (0.001 M) should be stored frozen (−20°C) in small aliquots (<1 mL) in sealed microfuge tubes. We currently obtain all of the nucleotides from Sigma-Aldrich, but have had equally good results with other suppliers.
6. Chelators: EGTA or EDTA: It is best made up as a stock solution (0.1 M) titrated to neutral (pH 6.8–7.2) or slightly above using KOH. It should be remade every 2 weeks, or less, and stored refrigerated. We use Sigma-Aldrich's EGTA (E0396) and EDTA (E9884) both titrated to pH 7.5.

7. Inorganic salts: $MgSO_4$, $CaCl_2$. Use the best grades available of analyzed reagents. Store stock solutions refrigerated and use within 2 weeks.
8. Water: The higher the purity of your water supply, the more likely reactivations will work consistently. If your water supply is rated ultrapure (18 MΩ) and stored in a sterilized polycarbonate carboy, it will be satisfactory. If you do not have access to ultrapure water, it will be necessary to use a deionizing column to pre-treat all the water for your reagent stock solutions. The value of high quality water can not be overemphasized. Countless hours of time can be lost in the lab due to poor water quality.
9. Glassware: Clean glassware is absolutely critical to achieving a satisfactory experimental result when working with demembranated cells. We use LiquiNox detergent (Alconox, White Plains, NY) for soaking and washing our glassware. We achieve the best results when multiple (at least 4) small volume rinses in regular tap water are followed by multiple rinses in deionized or ultrapure water. We use Alconox's Alcotabs for cleaning reusable pipettes. Visually inspect each piece before use to verify cleanliness.
10. Stock solutions: 10, 5, and 1 M KOH; 5 and 1 M HCl are used for titrating pH. Be sure to start with the highest purity grade reagent, especially for the KOH, as it will be used in many of the solutions. These stock solutions are stored refrigerated:
    - 0.6 M potassium glutamate
    - 0.3 M sucrose
    - 0.1 M MgSO4
    - 0.1 M CaCl2 (optional)
    - 0.1 M EGTA
    - 0.1 M fructose

    10% Triton X-100 (w/w). One gram weighed into 9 g of water. Mix with a magnetic stir bar to dissolve. Triton X-100 is available pre-diluted to 10% in 10-mL ampules from Pierce. These stock solutions are stored frozen:
    - 0.1 M DTT
    - 0.1 M ATP - Titrate to pH 7.8
    - 0.1 M ADP - Titrate to pH 7.8
    - 0.001 M cAMP
11. GRM (glutamate–Tris reactivation medium): Mix 6.0 mL of potassium glutamate stock with 70 mL of sucrose stock and 0.36 g of Trizma base. Stir to dissolve and then adjust pH to 7.8 with HCl. Adjust final volume to 100 mL with ultrapure water. This GRM mixture is isotonic to mammalian sperm. Sperm suspended in it will stay alive. This feature is occasionally very useful, so the final dilution to optimal reactiva-

tion ionic strength is deferred to the time of use. GRM is an excellent growth medium for bacteria; it must be remade at least every 2 weeks, and checked for cloudiness before each use. Store refrigerated and keep on ice during experiments.

12. Sodium citrate buffer: Dissolve 2.85 g of sodium citrate in 50 mL of ultrapure water; add 2 mL of fructose stock solution and 5 mL of $MgSO_4$ stock solution and 1 mL $CaCl_2$ stock solution (optional). Mix and adjust pH to 7.4, then adjust final volume to 100 mL with ultrapure water. If you plan to explore the role of Ca^{2+} in the flagellar/ciliary reactivation, it is necessary to leave $CaCl_2$ out of the citrate buffer.
13. Specialty medium: Modified Krebs-Ringer bicarbonate medium (mKRB) formulated by Neill and Olds-Clarke *(16)* or Hanks Balanced Salt Solution (HBSS) (*see* **Subheadings 3.1**, **3.3**, **3.5**, and **3.6**).
14. Bull semen, diluted in a milk-based extender, from Genex Cooperative Inc. (Tiffin, OH).

2.2. Preparation of the Biological Sample

The main concern when introducing the biological sample into the membrane-extraction medium is the inadvertent introduction of contaminants that will interfere with reactivation of motility. In the case of bull sperm, three low speed centrifugations followed by resuspension in a well-defined medium rather easily resolves this problem. For this, we have used sodium citrate (0.105 M) with 5 mM $MgSO_4$, 2 mM fructose and 1 mM $CaCl_2$ (optional). This is a good choice for our purposes as the sperm, and most other cells, tolerate it for short exposures (up to 4 h at room temperature and longer on ice). The citrate chelates heavy metals and is an organic anion. This simple mixture avoids addition of compounds that will affect the reactivation of the sperm. Unfortunately, every system will have somewhat different requirements to sustain the living cells prior to demembranation. As a general guide, simple is better as long as the viability of the sample is not compromised. In addition, organic anions are better suited to be the principal ionic component. When attempting to reactivate a sample for the first time, plastic petri dishes are a better choice than glass slides or vessels. Glass and glass cleaning methods will sometimes foul a reactivation. Once the method is working on plastic it can usually be duplicated on clean glass especially if the glass has been used for this purpose repeatedly.

2.3. Oxidation and Proteolysis

Oxidation and proteolysis were recognized as the main destroyers of axonemal function since the detergent-extracted models were first produced in the Gibbons lab *(5)*. DTT and EGTA, commonly used in most reactivation methods, are the ingredients that protect against these spoilers. DTT competes with protein as a sink for oxygen free radicals. EGTA chelates contaminating

divalent cations to a level that interferes with calcium-dependent proteases. It also inhibits the creation of free radicals via the Fenton reactions (which require Fe^{3+} or Cu^{2+} ions). In this way, EGTA (and also EDTA) can mask a multitude of sins. If the reactivation method is clean, and the reagents and water are pure, good reactivations can be produced without EGTA or EDTA. We are in the habit of routinely including 0.5–1.0 mM EGTA. Hypothetically, if oxidation and enzymatic degradation could be stopped completely, then reactivated motility should continue indefinitely. In practice this is not true. The average reactivation looks good for 20–30 min maximum. If your reactivations start out looking good and degrade rapidly then contamination may be the culprit.

3. Methods

The following protocol is the one used in our laboratory for reactivating bull sperm samples. It works as well for sea urchin sperm, and was easily adapted for a widely used laboratory exercise to reactivate *Tetrahymena* cilia. With some modification it will also reactivate *Chlamydomonas* flagella (These variations are discussed in **Subheading 3.2**).

3.1. Basic Protocol (See Notes 1–3)

1. Pre-warm, to room temperature, 30 mL of the citrate buffer described above. If you are not using bull sperm you may need to substitute a suspension medium that is better suited to the specific cells you are using. For instance, rat and mouse sperm typically do better in Hank's balanced salt solution (HBSS) or best in a modified Krebs–Ringer bicarbonate medium (mKRB), with or without Ca^{2+} *(16)*.
2. Gently mix the starting sample of suspended cells in their own storage or growth medium. We use Holstein bull semen, diluted in a milk-based extender and shipped overnight on ice, from Genex Inc. (Tiffin, OH). Combine 4 mL of the semen solution with 6 mL of the citrate buffer.
3. Centrifuge the cells at 1,000 × *g* for 10 min. Decant the supernatant after the spin and add citrate buffer (or your substitute) to bring the total volume up to 10 mL.
4. Allow the pellet 2 min to "melt" before actively mixing the sample. Repeat the centrifugation process two additional times, resuspending the final pellet in 4 mL of citrate buffer. The purpose of this step is to transfer the living sample into a defined medium. Adapt this step to your sample density and the nature of the cell preparation. Protozoa and algae

will tend to be more dilute to begin with and may require a larger volume to be processed on the first washing (*see* **Subheading 3.2**). Solid tissues (e.g. Clam gill cilia) can be simply transferred instead of centrifuged. If centrifugation is used, you may need to determine the best speed and time needed to form a loose pellet.

5. Pipette 2 mL of the GRM mixture into a plastic petri dish. For bull sperm and other mammalian tissues, add 1 mL of high purity water to the mixture. For algae and fresh water protozoa, it may be necessary to increase the ratio of water to GRM for optimal results (try 1.5:1.5 or 2:1 mL).
6. Add the following solutions to the GRM-water mixture: 30 μL of 0.1 M DTT from a thawed microfuge tube stored on ice, 30 μL of 0.1 M $MgSO_4$, 15 μL of 0.1 M EGTA and 30 μL of 10% Triton X-100 (*see* **Note 3**). Swirl to mix.
7. Add 20 μL of the biological sample to the dish containing the GRM mixture. Trial and error will determine if the amount needs to be raised or lowered. Gently swirl.
8. Observe the cells in the dish at low power (10× or 20×) using phase contrast optics. There should be no motility, and if the washing procedure is suitable there should be intact flagella or cilia.
9. Add 30 μL of the thawed 0.1 M ATP stock solution from a microfuge tube stored on ice.
10. Observe again for motility. If the procedure has been successful some motility of the cells should be obvious (*see* **Note 2**).
11. If **step 9** did not produce a positive result add 10 μL of 0.001 M cAMP and observe the sample again for a minimum of 10 min. Some cilia and flagella are inactive without cAMP.
12. If both **steps 9** and **11** yielded no motility, repeat **steps 5** through **11** in a second dish but include 15 μL of 0.1 M ADP at **step 9** in addition to ATP. All flagella will reactivate more easily if ADP is present with ATP [(for review *see(17)*]. When reactivation can only be obtained with ADP present, it may be an indication of a contamination problem (*see* **Note 2**).

3.2. Optimization of the Protocol

Once the general method has worked for you, even marginally, it can then be optimized for your system. Virtually all cilia and flagella will do something at low ATP, especially if some ADP is also present (*see* **Note 2**). After reactivation has been achieved, try the following for optimization:

1. Work up to higher ATP concentrations in 10 μL increments to find an optimum concentration. Remember, it is necessary to add more Mg^{2+} if utilizing higher concentrations of nucleotides as they need to be maintained at a 1:1 ratio.

2. Explore the response to cAMP by leaving it out or adding more in 3 μL increments.
3. Try different dilutions of the stock GRM media with water, keeping the total volume at 3 mL so that you don't have to change the rest of the protocol (i.e. try ratios of 1.5:1.5 and 2:1 mL).
4. Vary the washing procedure to see that the damage to the cilia or flagella is minimized.
5. Lower the pH. You may find that a lower pH works better for the cells you are using and you may want to vary the buffer accordingly.
6. Adjust the amount of the biological sample added; a greater number of cells present typically enhance motility.

Using this systematic approach, it is possible to customize the working conditions to your own needs.

3.3. Variations for Specific Systems

The basic protocol in **Subheading 3.1**. will reactivate bull sperm, mouse sperm, human sperm, rat sperm, sea urchin sperm, freshwater clam gill cilia, *Tetrahymena*, and *Chlamydomonas*. However, each system does require some fine-tuning to get the best results.

1. *Rodent sperm*: Use mKRB or HBSS instead of citrate buffer. In our experience, rodent sperm give good progressive motility in a reactivation only if the live sperm in solution exhibits progressive motility. The simple citrate buffer will not suffice for this purpose. We also know that substituting 0.3 M HEPES for Tris in the GRM, high levels of nucleotides (5 mM ATP, 5 mM ADP and 20 μM cAMP) and Mg^{2+} (10 mM) and a lower pH (6.9–7.0) in a mouse sperm reactivation result in more life-like motility.
2. *Ciliates and algae*: Do not use **step 2** of the basic protocol **(Subheading 3.1)** for ciliates and alga because starting samples of them are more dilute than sperm samples. In addition, ciliated protozoa typically yield a better reactivation at a lower optimal pH (7.0–7.4) *(7, 18)* than the various sperm cells *(5, 14)*. At pH lower than 7.4, Tris is not the optimal buffer for the job; HEPES or PIPES is preferable.
3. *Tetrahymena*: A method to prepare *Tetrahymena* for reactivation has been worked out and is readily accessible as part of the "Exercises in Cell Biology for the Undergraduate Laboratory" manual. The manual is available from the American Society for Cell Biology via the Educational Resources link on their website (http://www.ascb.org). It is alternately available directly at: http://www.ascb.org/newsfiles/exercises_cell_bio.pdf.
4. *Chlamydomonas*: Refer to **Note 4** and make the following substitutions in the basic protocol described in **Subheading 3.1**:

(a) Centrifuge 10 mL of *Chlamydomonas* in TAP culture medium (described in (*19*)) at 1,000 × g for 10 min to form a loose pellet. Decant the supernatant and resuspend the cells in the small amount of residual fluid that remains.

(b) Pipet 1.5 mL of the GRM mixture into a plastic petri dish. Add 1.5 mL ultrapure water to the mixture.

(c) Add the following solutions to the GRM-water mixture: 30 μL of 0.1 M DTT from a thawed microfuge tube stored on ice, 60 μL of 0.1 M $MgSO_4$, 30 μL of 0.1 M EGTA, 3 μL of 0.001 M cAMP and 30 μL of 1.0% Nonidet P-40. Swirl to mix.

(d) Add 20 μL of the biological sample to the reactivation mixture from **step c**.

(e) Rapidly draw the sample into and out of a Pasteur pipette repetitively ten times. This mechanically aids in the disruption of the membrane at the very low (0.01%) detergent concentration.

(f) Follow **steps 8–12** in the basic protocol described in **Subheading 3.1**.

3.4. Capabilities and Limitations

There are two important advantages to demembranated-reactivated models. The first is that the investigator has almost complete control of the composition of the solution pervading the axoneme. The second is that a reactivated flagellum can be positioned, poked, probed, enzymatically digested or cut without the complications of a membrane. These advantages give the investigator fantastic control of the experimental conditions both mechanically and chemically.

The limitations of the reactivated state are largely related to the stability of the reactivated models. The working time is limited for most samples to less than 30 min before there is substantial loss of function and loss of structural integrity.

3.5. Removal of the Cytosol

The method as described in **Subheading 3.1**. must be modified if the endogenous cytosolic factors and the detergent are to be eliminated from the final reaction mixture. Rat sperm can be successfully separated from their cytosolic fraction by a slight modification of the basic protocol detailed in **Subheading 3.1**. The method described below works well for rat sperm and may be adapted to other samples as well. We found less than 0.01% carry over of the original mixture into the final reactivation dish, using a tritium labeled cAMP tracer *(20)*.

1. Nick rat sperm epididymides with a razor blade. Gently express the sperm onto a plastic culture dish and immediately cover with a few drops of HBSS at room temperature. Allow the

sperm to disperse into the medium for 5–10 min and then gently pipette to mix.

2. Dilute the sample to 2 mL total volume with the same solution used in **step 1** above.
3. Place 200 μL of the sperm suspension into 3 mL of the demembranation mixture with 0.1% Triton X-100 from **step 4** of the basic protocol in **Subheading 3.1**.
4. Layer half (1.5 mL) of the total volume of demembranated sperm on top of 3 mL undiluted GRM solution in a 16 × 100 mm test tube with the same ingredients as in **step 4** of the basic protocol (1 mM $MgSO_4$, 1 mM DTT, and 0.5 mM EGTA) but without the Triton X-100. A visible meniscus should be present between the two layers. Immediately chill on ice.
5. Centrifuge the layered mixture in a swinging bucket rotor at 160 × *g* in a cold room for 10 min. The centrifuge must be regulated to spin up slowly and to slow down without braking. If successful, two layers separated by a visible meniscus should still be present at the end of the run.
6. Decant and discard the supernatant from the top down to the visible loose pellet of cells.
7. Use the re-suspended pellet as the stock suspension for a new reactivation as in **step 4** of the basic protocol described in **Subheading 3.1**. However, omit Triton X-100.

3.6. Disintegrating the Axoneme

Summers and Gibbons *(6)* showed with sea urchin sperm that a brief tryptic digestion would allow sonicated fragments of the axoneme to slide apart. Our work is chiefly centered on mammalian sperm which will not disintegrate using their method. Thus, we developed two methods that are applicable to mammalian sperm which have larger supporting structures (outer dense fibers) that result in a greater resistance to disintegration.

1. Bull sperm:
   (a) Use the basic protocol in **Subheading 3.1**. except warm 60 mL of citrate buffer and use 15 mL of the semen in the milk-based extender and divide into two tubes of equal volume and wash with citrate buffer following the protocol. Final volume of washed sperm in citrate equals 4 mL.
   (b) Prepare ten dishes as in **steps 5** and **6** of the basic protocol.
   (c) Add 10 μL of 0.001 M cAMP to each dish.
   (d) To each dish, add 250 μL of the washed sperm solution from **step a**.
   (e) Freeze at −20°C for 48 h.

(f) Thaw a preparation and add 1 mM ATP to induce sliding/disintegration.

(g) Unused preparations may be stored as small volume aliquots in liquid nitrogen for use at a later time. It is best if the preparations are thawed for a minimum amount of time and kept at 0° before long term storage.

2. Mouse sperm:

(a) Prepare 10 mL of disintegration buffer by combining 5 mL ultrapure H_2O, 2 mL 0.1 M Tris, 1.7 mL 0.6 M potassium glutamate, 0.5 mL 0.1 M $MgCl_2$, 0.5 mL 10% Triton X-100, 200 μL 0.1 M DTT and 50 μL 0.1 M EGTA.

(b) Adjust pH to 9.4–9.5 by adding ~70 μL of 5 M KOH.

(c) Add 100 μL of 0.1 M ATP.

(d) Store this solution in a 34°C water bath until needed.

(e) Prepare sperm sample by nicking fresh mouse epididymides with a razor blade. Cells can be collected by one of two ways: Gently express sperm onto a plastic petri dish and immediately cover with mKRB medium or place nicked whole epididymides into a microfuge tube filled with mKRB medium. Allow sperm to "swim up" into the medium for 10–15 min. Store this sperm stock solution at room temperature.

(f) Prepare the reactivation mixture following **steps 5** and **6** of the basic protocol except substitute 60 μL of 0.1 M $MgCl_2$ for the $MgSO_4$.

(g) Add 10 μL of 0.1 M ATP and 10 μL of 0.001 M cAMP to the reactivation mixture.

(h) Centrifuge the mouse sperm for 10 min at 400 × *g*. Decant the supernatant.

(i) Add 0.5 mL of the complete reactivation mixture from **step g** to the sperm pellet and view for motility.

(j) If sufficient motility is achieved, add 4.5 mL of the disintegration buffer prepared in **steps a–d** and incubate in a 34°C water bath for 5 min to remove the mitochondrial sheath and initiate sliding.

3.7. Disabling Dynein

Vanadate is a known powerful inhibitor of dynein activity *(9, 10)*. If one desires to create demembranated sperm models without the interference of dynein, the addition of 50 μM or more of sodium metavanadate effectively disables all dynein activity. Even very low concentrations of vanadate can inhibit motility, so in practice we label our imaging chambers that contained any amount of vanadate and purposely use them only for vanadate experiments. Vanadate solutions oxidize quickly and turn yellow,

so it is important to make up a fresh stock solution the day of experiments.

4. Notes

1. The general utility of membrane extracted models often depends on being able to manipulate them or immobilize them, which in turn often depends on making them adhere or keeping them from sticking to various objects and surfaces. Once the flagellum is demembranated the exposed microtubules carry a net negative charge. It is sometimes possible to make use of this property to either enhance or reduce sticking. The sperm preparations used in our lab will stick readily to coated culture dishes (Falcon 3802, Becton Dickinson, Lincoln Park, NJ) but stay more mobile on uncoated plastic petri dishes (Falcon 351007, Becton Dickinson). We produce our own Plexiglas imaging chambers with coverslip bottoms. To facilitate the adhesion of sperm, we pre-treat the glass coverslips prior to use. This is done by washing with 0.05–0.5 M KOH, rinsing with ultrapure water, washing with 100% acetone and lastly rinsing with ultrapure water. Poly-lysine coated surfaces, which impart a positive coating and attract negatively charge proteins, work well to promote sticking, but sometimes too well. Glass coverslips can be treated with 0.1% (w/v) poly-lysine solution (MW 70,000–150,000). Silanization is equally effective. We have had good results in preventing non-specific adhesion of sperm to glass microprobes by dipping the probe in a 1 *N* HCl solution and drying it just prior to use. We have also treated viewing chambers in the same manner. This may work by imparting a negative surface charge to the glass.
2. The most problematic aspect of working with demembranated models arises from the very thing that makes them attractive: the investigator is in complete control of the conditions. Complete control comes with a lot of headaches. The larger the number of ingredients that must be prepared and certified "safe" for use in an experiment, the greater the possibility for an error. In the case of reactivating motility to flagella and cilia, the biological specimen lets you know you've made a mistake by refusing to do anything. This can be humbling and also very frustrating. The following are the most common headaches:
   (a) The biological starting material is defective. If your "live" preparation is old (we use sperm within 4 h), dead, or has been seriously injured, it is unreasonable to expect good

reactivations. For example, cold shock is a problem with mammalian sperm; inadvertently chilling them from 23 to 5°C will render them useless. Check on the condition of the live material at the step before detergent extraction (**step 2** of the basic protocol). Obviously, the best cells are obtained from the most robust, sexually-mature animals.

(b) The water is not an ultrapure grade. "Bad", or even slightly bad, water can literally make it impossible to do any work with reactivated models. Never underestimate the importance of water quality. Be sure to rinse all of the glassware with "good" water before preparing solutions.

(c) If the water and the starting material are in good shape, the antioxidant components of the mixture (DTT or glutathione and EGTA) are very often the culprits of a failed reactivation. Don't let the EGTA stock solution get old and make sure it has been properly titrated (pH 6.8–7.2) with a high quality KOH. DTT is the most erratic ingredient of the mixture because it tends to oxidize. When a lot is giving stable reactivations, stay with that lot using the suggestions given in **Subheading 2**. The telltale sign that oxidation is your problem is when the sample shows some or even good initial motility and rapidly loses it by degenerating to a jittering, vibration-like residual motion.

(d) Contamination contributed by a specific ingredient. This was once a major problem back in the days when some sources of ATP where contaminated with vanadate. It is less of a problem now, if the highest grades of nucleotides and salts are used, but it can still happen. It is informative to look at the manufacturer's analysis of the reagents. You will quickly see that some things you really don't want in a reactivation dish (e.g. Ni^{2+}, Cu^{2+}, $Fe^{3+}$and Hg^{2+}) are common contaminants. Also things you may think you didn't have, like Ca^{2+}, may actually be present at physiologically active concentrations. By consistently using reagents of the purest quality available (e.g. SigmaUltra products) we have been able to greatly minimize the impact of contamination.

(e) The pH of the final mixture is in error. When everything else seems to be right, it is often useful to check the pH of the completed mixture. Cells not at the optimal pH will exhibit a lopsided beat and cease moving sooner than normal.

3. Detergent extraction of sperm releases the acrosomal contents, including acrosin, a Ca^{2+}-dependent serine protease. Most detergent extractions of other cell types will similarly mobilize lysosomal enzymes. To see if this problem could be minimized we have used organic solvents instead of detergent

to permeablize the membranes of bull and rat sperm. Acetone and the lower molecular weights of polyethylene glycol (PEG 400) will permeabilize cells allowing reactivation with exogenous Mg-ATP. These solvents must be used at much higher concentrations than detergent (0.7 mL GRM to 0.3 mL acetone or 0.5 mL GRM to 0.5 mL PEG 400) but we have observed the resulting reactivated motility last up to 2 h, rather than the usual 30 min. It also takes longer for the initial motility to begin. To extract the cells, 200 μL of the sperm stock suspension in citrate buffer (as in **step 2** of the basic protocol) is added to 1 mL of the acetone or PEG 400-extraction mixture with 1 mM DTT present. The sperm are incubated in the extraction mixture for 10 min in acetone or 4 min in PEG 400. After extracting for the required amount of time, the treated cells are used as the starting material for a reactivation, as in the basic protocol although no detergent is required. Transmission electron microscopy revealed that the acrosomal contents had not dispersed in the acetone or PEG treated samples (unpublished results). Such alternate methods of permeablizing the membrane have not been extensively utilized. It was reported that a bacterial pore-forming toxin, Streptolysin O, can be used to yield partially permeablized sperm cells *(21)*. This is a very exciting alternative to detergent, as it may allow size-selective retention of some of the natural internal milieu.

4. The green alga *Chlamydomonas* is the dominant model system for the study of flagellar motility. This is owing to the genetic tractability of *Chlamydomonas* and the well-kept depository of mutant strains that is maintained for this organism at the *Chlamydomonas* Center, Duke University, Durham, NC (http://www.chlamy.org). The irony is that the *Chlamydomonas* flagellum is hardly the ideal choice to typify a "standard" flagellum. *Chlamydomonas* re-grows its flagellum daily and drops them at the slightest affront. Therefore, they are kind of Nature's entry into the disposable organelle market. *Chlamydomonas* also use their flagellum for mating and gliding motility, necessitating a sophisticated membrane-associated transport system. These adaptations make the organism interesting for a number of kinds of research. The downside is that a disposable flagellum is more fragile than one built to last. *Chlamydomonas* flagella are difficult to work with because the demembranation conditions destabilize the axoneme, which then tends to fall apart or lose function. However, because of the intense interest in *Chlamydomonas* there are already good published methods available to use as a template to find a method that is suitable for a given experimental circumstance *(22, 23)*. There is also a cell wall defective strain (cw92)

that allows the flagellar apparatus to be isolated in functional condition after detergent extraction *(24)*. Nonidet P-40 is less disruptive to the axoneme of *Chlamydomonas* than Triton X-100.

Acknowledgments

Thanks to Danial J. Oberski for testing the adaptation of the method to *Chlamydomonas*, Lisa J. Macauley for optimizing the mouse sperm reactivation protocol and Kristen C. Ponichter for refining the method of mouse sperm axoneme disintegration. Supported by N.S.F. Grant MCB-0516181.

References

1. Szent-Györgyi, A. (1949) Free-energy relations and contraction of actomyosin. *Biol. Bull.* **96**, 140–161.
2. Hoffman-Berling, H. (1955) Geiselmodelle und Adenosintriphosphat. *Biochim. Biophys. Acta* **16**, 146–154.
3. Bishop, D.W. and Hoffman-Berling, H. (1959) Extracted mammalian sperm models. I. Preparation and reactivation with adenosine triphosphate. *J. Cell Comp. Physiol.* **53**, 445–466.
4. Brokaw, C.J. and Benedict, B. (1968) Mechanochemical coupling in flagella. I. Movement dependent dephosphorylation of ATP by glycerinated spermatozoa. *Arch. Biochem. Biophys.* **125**, 770–778.
5. Gibbons, B.H. and Gibbons, I.R. (1972) Flagellar movement and adenosine triphosphate activity in sea urchin sperm extracted with Triton X-100. *J. Cell Biol.* **54**, 75–97.
6. Summers, K.E. and Gibbons, I.R. (1973) Effects of trypsin digestion on flagellar structures and their relationship to cell motility. *J. Cell Biol.* **58**, 618–628.
7. Sale, W.S. and Satir, P. (1977) Direction of active sliding or microtubules in *Tetrahymena* cilia. *Proc. Natl Acad. Sci. U. S. A.* **74**, 2045–2049.
8. Lindemann, C.B. (1978) A cAMP induced increase in the motility of demembranated bull sperm models. *Cell* **13**, 9–18.
9. Kobayashi, T., Martensen, T., Nath, J., and Flavin, M. (1978) Inhibition of dynein ATPase by vanadate, and its possible use as a probe for the role of dynein in cytoplasmic motility. *Biochem. Biophys. Res. Commun.* **81**, 1313–1318.
10. Gibbons, I.R., Cosson, M.P., Evans, J.A., Gibbons, B.H., Houck, B., Martinson, K.H., Sale, W.S., and Tang, W.J. (1978) Potent inhibition of dynein adenosinetriphosphatase and of the motility of cilia and sperm flagella by vanadate. *Proc. Natl Acad. Sci. U. S. A.***75**, 2220–2224.
11. Brokaw, C.J. (1979) Calcium-induced asymmetrical beating of Triton-demembranated sea urchin sperm flagella. *J. Cell Biol.* **82**, 401–411.
12. Schmitz, K.A., Holcomb-Wygle, D.L., Oberski, D.J., and Lindemann, C.B. (2000) Measurement of the force produced by an intact bull sperm flagellum in isometric arrest and estimation of the dynein stall force. *Biophys. J.* **79**, 468–478.
13. Lindemann, C.B. and Kanous, K.S. (1995) "Geometric Clutch" Hypothesis of axonemal function: key issues and testable predictions. *Cell Motil. Cytoskeleton* **31**, 1–8.
14. Lindemann, C.B. and Gibbons, I.R. (1975) Adenosine triphosphate-induced motility and sliding of filaments in mammalian sperm extracted with Triton X-100. *J. Cell Biol.* **65**, 147–162.
15. Gibbons, I.R., Evans, J.A., and Gibbons, B.H. (1982) Acetate anions stabilize the latency of dynein 1 ATPase and increase the velocity of tubule sliding in reactivated sperm flagella. *Cell Motil.* **1**(Suppl.), 181–184.
16. Neill, J.M. and Olds-Clarke, P. (1987) A computer-assisted assay for mouse sperm hyperactivation demonstrates that bicarbonate but not bovine serum albumin is required. *Gamete Res.* **18**, 121–140.

17. Lesich, K.A., Pelle, D.W., and Lindemann, C.B. (2008) Insights into the mechanism of ADP action on flagellar motility derived from studies on bull sperm. *Biophys. J.* **95**, 472–482.
18. Hamasaki, T., Murtaugh, T.J., Satir, B.H., and Satir, P. (1989) In vitro phosphorylation of *Paramecium* axonemes and permeabilized cells. *Cell Motil. Cytoskeleton* **12**, 1–11.
19. Harris, E.H. (1989) The *Chlamydomonas* sourcebook: a comprehensive guide to biology and laboratory use. Academic, San Diego, CA.
20. Lindemann, C.B., Gardner, T.K., Westbrook, E., and Kanous, K.S. (1991) The calcium-induced curvature reversal of rat sperm is potentiated by cAMP and inhibited by anti-calmodulin. *Cell Motil. Cytoskeleton* **20**, 316–324.
21. Johnson, L.R., Moss, S.B., and Gerton, G.L. (1999) Maintenance of motility in mouse sperm permeabilized with Streptolysin O. *Biol. Reprod.* **60**, 683–690.
22. Goodenough, U.W. (1983) Motile detergent-extracted cells of *Tetrahymena* and *Chlamydomonas*. *J. Cell Biol.* **96**, 1610–1621.
23. Horst, C.J. and Witman, G.B. (1995) Reactivation of *Chlamydomonas* cell models. *Methods Cell Biol.* **47**, 207–210.
24. Hyams, J.S. and Borisy, G.G. (1978) Isolated flagellar apparatus of *Chlamydomonas*: characterization of forward swimming and alteration of waveform and reversal of motion by calcium ions *in vitro*. *J. Cell Sci.***33**, 235–253.

Part VI

Genetic and Proteomics Approaches for Cytoskeleton Protein Function

Chapter 20

The Analysis of Intermediate Filament Dynamics Using Transfections and Cell Fusions

Jesús M. Paramio

Summary

The intermediate filament (IF) proteins have been recently found as dynamic structures that influence several aspects of cell homeostasis. Here, two alternative approaches to study the dynamics of IF proteins are described: the formation of cell hybrids by the fusion of different parental cells, and the transfection of keratin genes in cultured cells. In the first case, the selection of parental cell lines and the use of specific antibodies allow us to study how IF proteins recombine and copolymerize to form the heterokaryon cytoskeleton by immunofluorescence. In the second approach, some modifications of conventional transfection protocols allow the synchronized expression conditions, making it suitable for the analysis of the incorporation of a newly synthesized IF protein into the preexisting IF cytoskeleton of transfected cells.

Key words: Keratins, Vimentin, Immunofluorescence, Transfection, Cell hybrids, Cell fusion

1. Introduction

Cell cytoskeleton plays fundamental roles in almost all aspects of cell physiology. Many of these functions depend on the dynamic changes that this fibrous structure suffers during the different cellular events. While a large body of evidence has demonstrated the roles of microfilament and microtubule dynamics in cell homeostasis, less is known about the possible role of IF proteins in similar processes. The IF superfamily is the largest among other cytoskeletal protein families and display a carefully regulated tissue-and differentiation-specific pattern of expression, which is also modulated by cell culture procedures *(1)*. Due to their

R.H. Gavin (ed.), *Cytoskeleton Methods and Protocols,* Methods in Molecular Biology, vol. 586
DOI 10.1007/978-1-60761-376-20,
© Humana Press, a part of Springer Science + Business Media, LLC 2009

in vitro biochemical properties, IF proteins have long been considered to be poor dynamic components of the cell cytoskeleton. However, recent evidences have changed this point of view and IF proteins, and, in particular the dynamic changes that these proteins undergo during multiple cell processes, have been considered as essential modulators of cell events *(2–6)*. However, the analysis of IF dynamics is not an easy task. Indeed, the majority of the dynamic studies have been performed by microinjecting the proteins under study after their in vitro labeling *(7)*. This approach has been used with keratins, but still displays some limitations due to specific solubility procedures *(8)*. In addition, this technique could lead to alteration in the dynamic process due to the large amount of protein injected into the cells *(8)* and because the incorporation of new molecules into IF structures also differs between pre-existing and newly assembling filaments *(9)*. As an alternative to microinjection, transfection can also be used. However, although this technique is very useful for investigating the behavior of mutated genes *(10–12)*, the expression of the transgene takes place during a broad range of time (12–96 h), making it difficult to determine the precise moment at which the expression started in any particular cell. Here are two alternative approaches to study the dynamics of IF proteins in general, and keratins in particular: and the transfection of keratin genes under synchronized expression conditions.

The formation of cell hybrids is a possible alternative approach to study the dynamics of IF proteins. Two different parental cell lines, which can be chosen according to their IF expression pattern, are fused and the IF proteins recombine and copolymerize to form the heterokaryon cytoskeleton. Thus, the dynamics of different proteins during the process can be followed by immunofluorescence using specific antibodies. This approach provides a tool for studying the dynamic properties of individual polypeptides in vivo without alterations of their endogenous amounts. The use of appropriate specific antibodies allows the simultaneous observation of the temporal evolution of individual keratins and of the keratin cytoskeleton as a whole **(Fig. 1)**, see also *(13)*. As an alternative approach, transient transfection under synchronized expression conditions, can also be used to study the dynamic incorporation of a newly synthesized keratin into the preexisting keratin cytoskeleton, and has been successfully used to analyze the precise mechanism of keratins K1 and K10 assembly into epithelial and non-epithelial cells **(Fig. 2)**, see also *(14)*.

Finally, both approaches are suitable for analyzing the possible effects of other cellular processes, such as phosphorylation or dephosphorylation, on the dynamic behavior of keratins by adding drugs that inhibit or activate these processes during the temporal evolution of the experiments *(14)*.

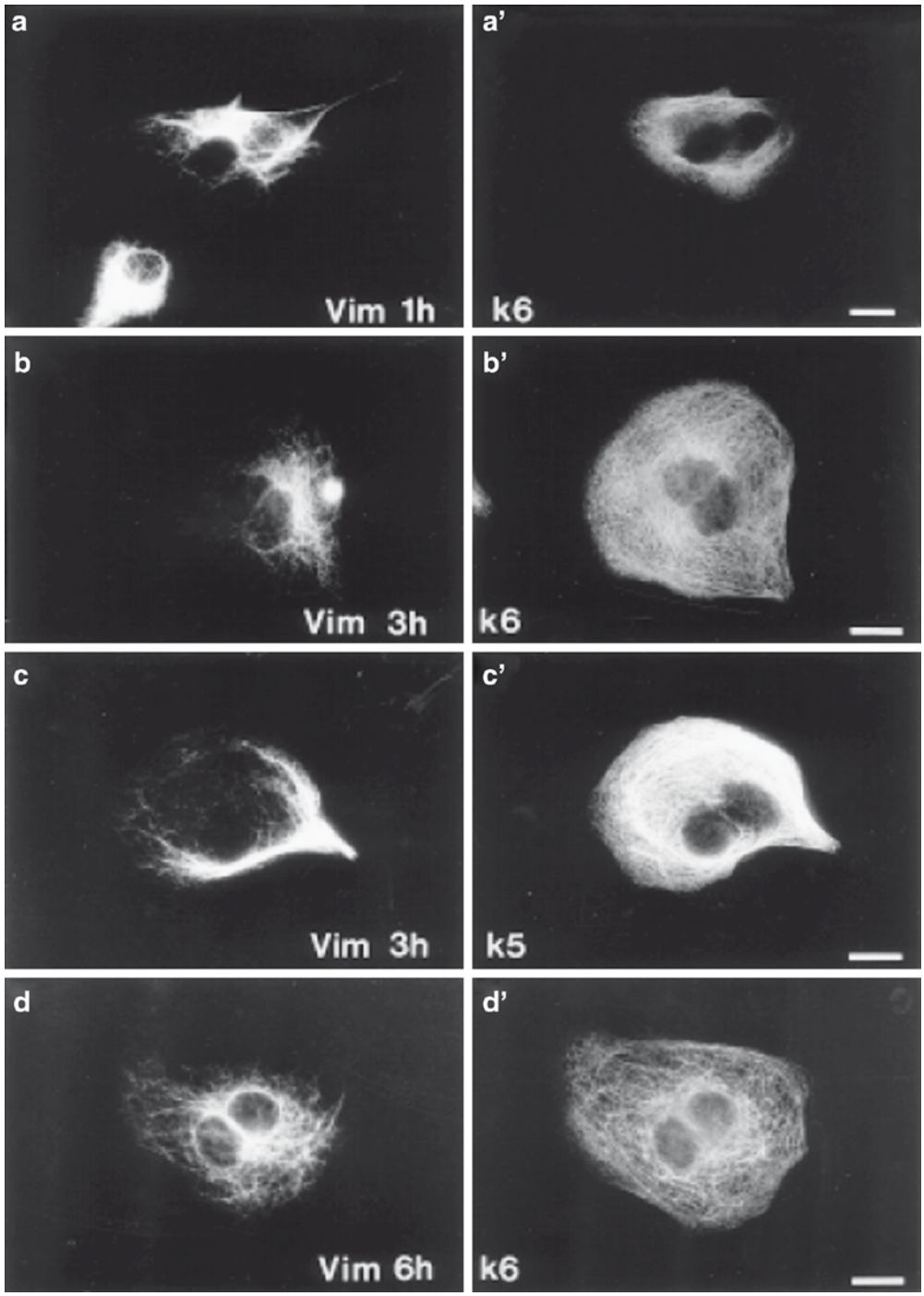

Fig. 1. Example of the dynamics of vimentin (**a**, **b**, **c**, **d**) versus keratin K6 (**a'**, **b'**,**d'**) or K5 (**c'**) upon the fusion between PtK2 (simple epithelial cells, which also express vimentin) and MCA3D (non-transformed murine keratinocyte) cells. Note that keratins spread much faster than vimentin and by 3 h after fusion, K6 (**b'**) and K5 (**c'**) are distributed throughout the heterokaryon cytoplasm, while vimentin (**b**,**c**) appears restricted to filament bundles localized around the parental PtK2 nuclei. At 6 h postfusion, the process is completed for both vimentin (**d**) and keratins K6 (**d'**) and K5 (not shown) which appear redistributed throughout the entire heterokaryon cytoplasm.Antibodies used were mouse mAb V9 against vimentin (Roche) and rabbit polyclonals against K6 (**a'**, **b'**, **d'**) or K5 (**c'**), both purchased from Covance. Bars represent 10 μm.

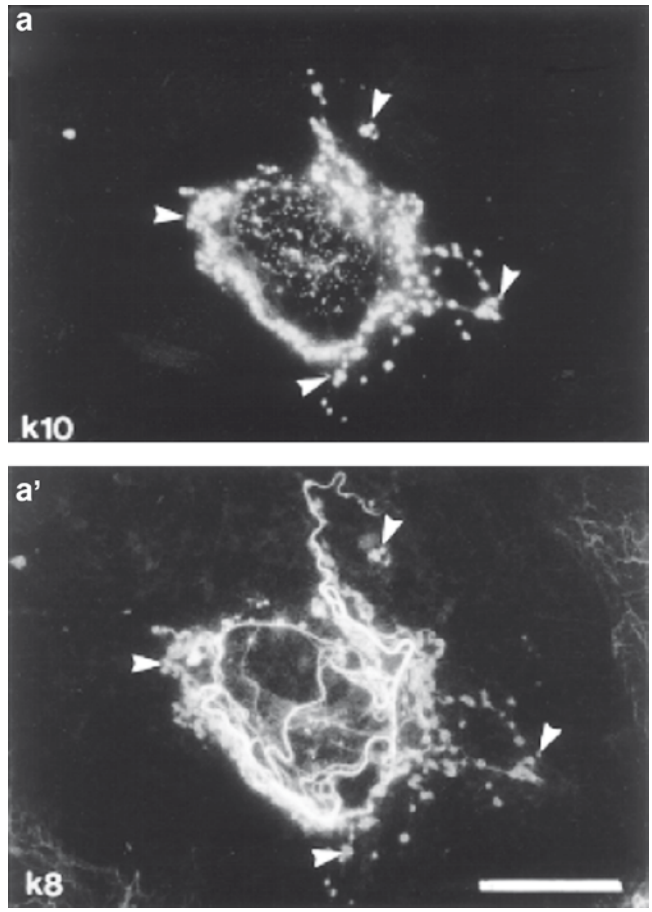

Fig. 2. Example of the interaction between keratin K10 (**a**) and endogenous keratin K8 (**a'**) upon transfection of K10 gene under cytomegalovirus promoter ***(14)*** into PtK2 cells at early time upon synthesis and chase experiment (3 h). Note that at this early time, K10 (**a**) forms round aggregates that display an almost exclusive perinuclear localization and does not integrate into the endogenous keratin filaments. In addition, these aggregates led to the collapse of the endogenous keratins (**a'**) and also tubulin, vimentin and actin cytoskeletal structures ***(14)***. The endogenous keratins remain in some perinuclear filaments and also appear colocalized in aggregates with transfected K10 (***arrowheads***). Later on in these experiments, the vast majority of the transfected cells displayed K10 forming a well developed and organized IF network together with the endogenous keratins (not shown, see also ***(14, 15)***). Antibodies used were mouse mAb K8.60 (Sigma) against K10, and rat mAb Troma 1 (kindly provided by Dr. R.Kemler) against K8. Bar represents 10 μm

2. Materials

2.1. Cell Lines

In order to perform cell hybrid experiments, the different cells to be used should be selected according to their distinct keratin expression pattern, so they differ at least in the two polypeptides to be simultaneously analyzed. Usually, a simple epithelium derived

cell line can be used. However, other possibilities are fibroblasts, that can be detected using anti vimentin antibodies, or different epithelial cells, which can be detected with species specific keratin antibodies. Another important factor to take into account is the similarity of the different culture media for growing the parental cells. It is often advantageous to select cells that grow on similar types of media and at similar serum concentrations. It is important to note that immortalized human keratinocytes or Ha-ras transformed murine keratinocytes express keratins K8 and K18, thus making it very difficult to follow keratin dynamics upon their fusion with simple epithelial cells, which are normally followed using antibodies against these proteins.

For transfection studies, it is important to take into account transfection as a crucial parameter, because under the modifications described here, there is a substantial decrease in the number of efficiently transfected cells.

Another aspect, although less relevant, is the endogenous composition of the IF cytoskeleton, which must allow detection of the transfected protein.

This possible problem can be partially alleviated using tagged constructs *(10, 11)*.

2.2. Chemical

1. Polyethilenglycol (PEG) 1500 (Roche), purchased ready to use and stored at 4 °C for several months.
2. Cycloheximide (Sigma). Stocks (100×; 5 mM) can be made in 70% ethanol and stored at –20°C for at least 1 year.
3. PBS: 137 mM NaCl, 2.7 mM KCl, 4.3 mM $Na_2HPO_4 \cdot 7H2O$, 1.4 mM KH_2PO_4, pH 7.5.
4. PBS-T: PBS containing 0.1% Tween 20.
5. BSA: bovine serum albumin.
6. Methanol fixative for immunofluorescence: cold methanol/acetone (2:1).
7. DAPI (4′ 6-diamidino-2phenylindole).
8. Mowiol or similar aqueous mounting medium.

2.3. Other

2.3.1. Immunofluorescence

2.3.2. Antibodies

For the immunofluorescence analysis, either after cell fusion or transfection, cells are grown onto glass coverslips that were previously washed with 70% ethanol and subsequently sterilized overnight. If the cells do not adhere properly, coverslips can be incubated for 30 min to 1 h in fetal calf serum prior to seeding cells.

The different antibodies against specific keratin polypeptides, can be purchased from different sources: Sigma, Roche, Covance, Abcam and others. Secondary antibodies raised for multiple labeling purposes can also be obtained from different sources. We currently use those from Jackson Immunoresearch Labs.

3. Methods

3.1. Cell Fusion Protocol

1. The day before fusion, trypsinize parental cell cultures and plate an appropriate number of each cell type together onto glass coverslips. The critical aspect is that sufficient numbers of cells are plated. Plating too many cells will lead to confluent growth with polykaryon formation (*see* **Note 1**). Typically, 5–6 × 10^4 cells should be used for a 6 cm diameter petri dish, which can accommodate up to 11 glass coverslips (round 11 mm diameter).
2. Incubate cells in the appropriate medium containing serum at least 12–16 h at 37°C in 5% CO2 atmosphere. Check to determine whether the cells are properly attached and in an appropriate number.
3. Wash the cells three times with prewarmed serum-free medium.
4. Aspirate the medium carefully and add PEG (1 mL per p60 petri dish).
5. Incubate at room temperature for 1 min gently rotating the plate to cover all the glass coverslips.
6. Wash the cells 3–4 times as in **step 3**.
7. Add normal medium containing serum and incubate for different periods of time, for example, a typical experiment must include: 0, 15 min, 30 min, 1 h, 2 h, 3 h, 6 h, 12 h, and 24 h.
8. Collect coverslips for each period of time and process for conventional immunofluorescence analysis.

3.2. Transient Transfection Under Synchronized Expression Conditions

1. The day before transfection, \trypsinize parental cells and plate appropriate number onto glass coverslips. For a conventional calcium phosphate protocol, 5 × 10^5 cells per p60 petri dish.
2. Two hours before transfection change the medium to remove non attached cells and add 50 μM cycloheximide to inhibit protein synthesis (*see***Note 2**).
3. Incubate the cells in the presence of DNA-calcium phosphate precipitates for 12 h.
4. Wash the cells carefully with prewarmed PBS to remove the precipitates. Incubate the cells for 24 h in the presence of complete medium containing cycloheximide. This allows the transgene mRNA expression, but precludes its translation into protein.
5. Wash the cells 3–4 times with prewarmed serum-free medium to remove the cycloheximide.
6. Incubate in complete medium for 12 h to allow the translation of the mRNA of the transfected gene.

7. Add cycloheximide again and incubate the cells for different periods of time (for example: 0, 3, 6, 9, 12 h). This procedure allows the analysis of the assembly of the protein translated during the period of culture in the absence of cycloheximide, without the effect of newly synthesized subunits.
8. At each time point, collect coverslips and process for immunofluorescence staining.

3.3. Indirect Immunofluorescence Analysis

1. Wash coverslips with PBS.
2. Fix the cells by incubation in cold methanol/acetone for 10 min at –20°C (alternative protocols for fixation can be followed).
3. Wash with PBS to rehydrate. Under these conditions the coverslips can be stored up to a week at 4°C. For longer storage do not rehydrate and store dry at –20°C (up to 2 months).
4. Wash the coverslips with PBS-T. Wipe out the excess of liquid.
5. Put the coverslips, cells face up, onto a parafilm foil in a humid chamber.
6. Add the appropriate dilution of primary antibodies. Be sure that they can be analyzed separately, i.e., they must come from different species. Normally, 10–13 μL of the mixture of primary antibodies is enough for a 11 mm diameter round coverslip. For initial tests, mouse or rat monoclonal supernatants can be diluted 1/5 to 1/20, ascites 1/100 to 1/500, rabbit, goat or sheep polyclonals 1/200 to 1/1,000. Dilutions should be prepared in PBS-T (in some cases BSA can be added, up to 1%, to reduce background).
7. Incubate for 1 h at room temperature in a humid chamber.
8. Wash three times (10 min each) in PBS-T. Wipe out excess liquid.
9. Add the secondary antibodies diluted in PBS-T. Be sure that they are suited for multiple labeling purposes, i.e., raised in the same animal and preabsorbed against other animal serum proteins, and labeled with different fluorochromes. Usually manufacturers provide information to achieve appropriate dilution (*see* **Note 3**).
10. Incubate for 30 min to 1 h as in **step 7**.
11. Wash three times with PBS.
12. Mount with Mowiol or similar aqueous mounting media with the cells face down onto glass slides. If required, DAPI (Boehringer Mannheim) can be added to the mounting media to counterstain the nuclei.
13. Allow to dry for at least 2 h.
14. Analyze under epifluorescence microscope equipped with appropriate filters to avoid cross channel light contamination.

4. Notes

1. Sometimes in cell hybrid experiments a different number of each parental cell type fuse forming polykaryons. In these, the speed of the dynamic process can be different because the distinct initial amounts of each polypeptide, depends on the number of each parental type forming the polykaryon, and also on the volume of the cytoplasm in which the preexisting filaments or soluble proteins are spreading. The conditions of each experiment must be adjusted so the number of polykaryons is reduced as low as possible.
2. In cell fusion experiments, protein synthesis can be inhibited to follow the dynamics in the absence of newly synthesized keratins *(13, 15)*. In this case, incubate the cells in the presence of 50 μM cycloheximide for at least 2 h before the fusion and afterwards. Other drugs that activate or inhibit different enzymes, which can be involved in IF dynamics, must be adjusted for each requirement *(15)*. Not all the cell lines can be efficiently transfected by conventional calcium phosphate protocols, and in some cases other methods should be followed. In these cases, the incubation times must be varied and adjusted for each precise requirement. The cycloheximide concentration provided here allows the transcription of transfected gene in PtK2 cells but precludes its translation into protein. In case of using a different cell line, check carefully the mRNA and protein expression at different drug concentrations.
3. Appropriate immunofluorescence controls must be performed by omitting primary antibodies, or/and by preincubation of the primary antibodies with the corresponding immunizing peptides if available. In addition, whenever possible, different antibodies against the same protein must be used to avoid the possible crossreactivity observed with certain antibodies when the antigens used in immunization are closely related, as in the case of keratins.

Acknowledgements

This work is partially supported by Grants: SAF2005–00033 (MEC), Oncocycle (S2006/BIO-0232 from CAM) and ISCIII-RETIC RD06/0020 (MSC) to JMP.

References

1. Moll, R., Franke, W. W., Schiller, D. L., Geiger, B., and Krepler, R. (1982) The catalog of human cytokeratins: patterns of expression in normal epithelia, tumors and cultured cells *Cell* **31**, 11–24.
2. Godsel, L. M., Hobbs, R. P., and Green, K. J. (2008) Intermediate filament assembly: dynamics to disease *Trends Cell Biol* **18**, 28–37.
3. Hyder, C. L., Pallari, H. M., Kochin, V., and Eriksson, J. E. (2008) Providing cellular signposts-post-translational modifications of intermediate filaments *FEBS Lett* **582**, 2140–2148.
4. Oshima, R. G. (2002) Apoptosis and keratin intermediate filaments *Cell Death Differ* **9**, 486–492.
5. Paramio, J. M. and Jorcano, J. L. (2002) Beyond structure: do intermediate filaments modulate cell signalling? *Bioessays* **24**, 836–844.
6. Eriksson, J. E., Opal, P., and Goldman, R. D. (1992) Intermediate filament dynamics *Curr Opin Cell Biol* **4**, 99–104.
7. Joshi, H. C. (1998) Microtubule dynamics in living cells *Curr Opin Cell Biol* **10**, 35–44.
8. Miller, R. K., Khuon, S., and Goldman, R. D. (1993) Dynamics of keratin assembly: exogenous type I keratin rapidly associates with type II keratin in vivo *J Cell Biol* **122**, 123–135.
9. Lu, X., Quinlan, R. A., Steel, J. B., and Lane, E. B. (1993) Network incorporation of intermediate filament molecules differs between preexisting and newly assembling filaments. *Exp Cell Res* **208**, 218–225.
10. Albers, K. and Fuchs, E. (1987) The expression of mutant epidermal keratin cDNAs transfected in simple epithelial and squamous cell carcinoma lines. *J Cell Biol* **105**, 791–806.
11. Albers, K. and Fuchs, E. (1989) Expression of mutant keratin cDNAs in epithelial cells reveals possible mechanisms for initiation and assembly of intermediate filaments. *J Cell Biol* **108**, 1477–1493.
12. Lu, X. and Lane, E. B. (1990) Retrovirus-mediated transgenic keratin expression in cultured fibroblasts: specific domain functions in keratin stabilization and filament formation. *Cell* **62**, 681–696.
13. Paramio, J. M., Casanova, M. L., Alonso, A., and Jorcano, J. L. (1997) Keratin intermediate filament dynamics in cell heterokaryons reveals diverse behaviour of different keratins. *J Cell Sci* **110**, 1099–111.
14. Paramio, J. M. and Jorcano, J. L. (1994) Assembly dynamics of epidermal keratins K1 and K10 in transfected cells. *Exp Cell Res* **215**, 319–331.
15. Paramio, J. M. (1999) A role for phosphorylation in the dynamics of keratin intermediate filaments. *Eur J Cell Biol* **78**, 33–43.

Chapter 21

Functional Analysis of Actin-Binding Proteins in the Central Nervous System of *Drosophila*

Qi He

Summary

Using ***Drosophila*** actin-binding protein Dunc-115 as an example, this chapter describes an MARCM based method for analyzing cytoskeletal components for their functions in the nervous system. Following a concise description about the principle, a step-by-step protocol is provided for generating the needed stocks and for histological analysis. Additional details and explanations have been given in the accompanying notes. With the two together, it should provide a practical and comprehensive recipe for performing at the single cell level loss-of-function and gain-of-function analyses of proteins associated with the cytoskeleton.

Key words: ***Drosophila***, Dunc-115, Actin-binding protein, MARCM, Confocal microscopy

1. Introduction

It is well known that the growth cone, a highly sensitive and motile structure at the leading edge of a growing axon, receives and transduces guidance signals through its surface receptors to regulate actin cytoskeleton *(1)*. Consequently, actin-binding proteins form a critical linkage to the cytoskeleton during the process of relaying guidance signals, and studying the functional roles of these proteins holds promises of revealing the molecular underpinning of axon pathfinding. This chapter describes methods for generating genotypes, dissecting and staining the visual system, and analyzing the function of a ***Drosophila*** actin-binding protein Dunc-115. Other cytoskeletal components can be analyzed similarly.

R.H. Gavin (ed.), *Cytoskeleton Methods and Protocols,* Methods in Molecular Biology, vol. 586
DOI 10.1007/978-1-60761-376-3_21,
© Humana Press, a part of Springer Science + Business Media, LLC 2009

A major step is to analyze axon pathfinding using a powerful technique, MARCM (mosaic analysis with a repressible cell marker) developed in ***Drosophila*** *(2)*. As shown in **Fig. 1**, MARCM utilizes recombination mediated by the FLP/FRT system (***see*** Fig. 1 legend) to generate homozygous mutant clones for a gene of interest such as Dunc-115. Defects of Dunc-115 mutation in these clones during axon projection can then be analyzed by confocal microscopy. By creating the UAS-Dunc115 construct, ectopic Dunc-115 expression can be achieved in homozygous clones **(Fig. 1)**, and thus gain-of-function of Dunc-115 can be analyzed. This approach will also allow the analysis of genes that generate lethality if mutated in the whole animal; it thus provides a practical method for studying axon pathfinding functions of both viable and lethal genes.

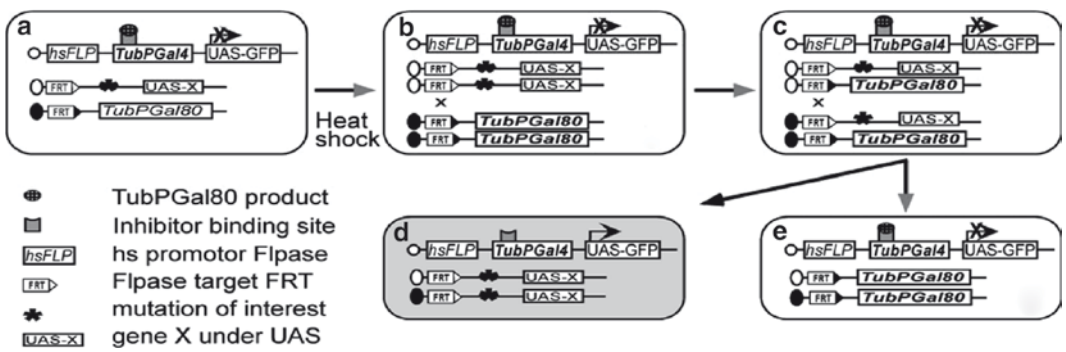

Fig. 1. The MARCM Method. ***Rectangles*** represent individual cells. (**a**) Flippase (FLP) recombinase is under the control of a heat-shock promoter (hs), and both Gal4 and Gal80 are controlled by a universal tubulin 1 promoter (TubP). Transcription factor Gal4 binds to its unique upstream activator sequence (UAS) to drive the expression of GFP or gene X. Gal80 functions as a repressor of Gal4 activity and thus when Gal80 and Gal4 are coexpressed in the same cell, Gal80 ***(hatched oval)*** binds to a site on Gal4 to repress its activity. As a result, both GFP and gene X cannot be expressed in such a cell ***(white cross*** over ***black arrow,*** shown only for GFP). (**b**) A heat-shock activates FLP that catalyzes the exchange of two FRT targets during mitotic cell division after DNA duplication (***black*** X), resulting in the exchange of chromosome arms distal to the FRT sites shown in (**c**). Following the completion of cell division, one daughter cell (**d**) did not inherit Gal80 gene and is also homozygous for the mutant (***black star***, Dunc-115 mutation in this chapter) or a transgene X under UAS control (UAS-X). To express transgene X, UAS-X can be on any chromosome arm, and for simplicity, it has been depicted on the same chromosome as the mutant. In daughter cell (**d**) (and its offspring), Gal4 is active and drives the expression of GFP (and UAS-X). The other daughter cell inherited two copies of Gal80 and thus, has no Gal4 activity or GFP expression, while the background will be cells that did not undergo recombination as in (**b**), and thus, they will be like the cell in (**a**), also without Gal4 activity or GFP expression. Thus, the only cells expressing GFP will be from (**d**). For simplicity, gene X (UAS-X) is depicted as on the same chromosome arm as the mutant (***black star***). In reality, the scheme can be used with a wild-type arm or with a mutant carrying arm, and the UAS-X transgene can be on any chromosome arm except the one carrying Gal80. Heat-shock is carried out at 37°C for a desired period of time and by controlling heat-shock time, it is possible to generate single neuron clones. UAS-GFP is UAS-mCD8-GFP fusion protein (where mCD8 is mouse T cell surface protein CD8) that will be anchored in the plasma membrane. TubP is fused with Gal4 or Gal80 coding sequence. Schematics were based on Lee and Luo (*2*).

2. Materials

2.1. Equipment

1. Standard incubator for culturing ***Drosophila***.
2. Orbital shaker platform.
3. Dissecting microscope.
4. Confocal microscope.

2.2. Reagents

1. Standard cornmeal medium: Mix 850 mL of water with 7.9 g of agar, 27.5 g of torula yeast, 52 g of cornmeal, and 110 g of dextrose. Heat to a boil and cool to 80°C. Add 2.4 g of tegosept dissolved in 92 mL ethanol and pour into culture vials and bottles (***see*** **Note 1**).
2. G418 medium: Prepare standard cornmeal medium and cool to 50°C. Add G418 (Fisher Scientific) to 1 mg/mL final concentration.
3. PBT: Add 0.3% Triton X-100 to 1× PBS.
4. PBTN: Add 5% normal goat serum to PBT.
5. 4% formaldehyde: To make 1 mL stock, mix 0.792 mL H_2O, 0.1 mL 10× PBS and 0.108 mL of 37% formaldehyde stock. The solution should be made fresh daily, and the unused portion should be discarded at the end of the day.
6. Antibodies: mouse anti-24B10, rat anti-N cadherin (both from Developmental Studies Hybridoma Bank), rabbit anti-GFP (Molecular Probes), FITC-conjugated goat anti-mouse, Cy5-conjugated goat anti-rat (both from Jackson Lab), and Alexa647 conjugated donkey anti-rabbit (Molecular Probes).

2.3. Drosophila Strains and Culture

1. A Dunc-115 mutant ***dunc-115^{KG03651}*** (85E4) has been isolated and analyzed *(3)*.
2. The following strains are used and they are available at the Bloomington stock center:
   yw/Y; P[ry, FRT]82B
   yw/Y; TM2/TM6B
   yw hsFlp UAS-mCD8-GFP; Sp/CyO; TM2 Ubx/TM6B Hu
   yw/Y; TubPGal4; FRT82B TubPGal80

3. Methods

3.1. MARCM Analysis

3.1.1. Preparation of FRT dunc-115^{KG03651}, Gal4 and Gal80 strains

1. ***FRT dunc-115*** strain (***see*** **Note 2**):

Set up the following cross:

yw; dunc-115^{KG03651} X ***yw/Y; P[ry, FRT]82B***

Collect females and mate with ***yw/Y; TM2/TM6B***:

yw; dunc-115^{KG03651}/P[ry, FRT]82B X ***yw/Y; TM2/TM6B***

Culture this cross in ***neomycin*** (G418) media and select ***w^{+}*** and cross to ***yw/Y; TM2/TM6B*** (single animal cross) (***see*** **Note 3**):

yw; P[ry, FRT]82B dunc-115^{KG03651}/TM6B X ***yw/Y; TM2/TM6B***

Collect both males and females to establish the following stock:

yw; P[ry, FRT]82B dunc-115^{KG03651} or ***yw; FRT82B dunc-115^{KG03651}***

2. Gal4 and Gal80 strains (***see*** **Note 4**):

   Set up the following cross:

   yw hsFlp UAS-mCD8-GFP; Sp/CyO; TM2 Ubx/TM6B Hu X ***yw/Y; TubPGal4; FRT82B TubPGal80***

   Collect males of ***Sp*** and ***Hu*** and set up:

   yw hsFlp UAS-mCD8-GFP/Y; TubPGal4/Sp; FRT82B TubPGal80/TM6B Hu X ***yw hsFlp UAS-mCD8-GFP; Sp/CyO; TM2 Ubx/TM6B Hu***

   Select both males and females of ***Cy*** and ***Hu^{+}*** and set up the following cross:

   yw hsFlp UAS-mCD8-GFP/Y; TubPGal4/CyO; FRT82B TubPGal80/TM2 Ubx X ***yw hsFlp UAS-mCD8-GFP/yw hsFlp UAS-mCD8-GFP; TubPGal4/CyO; FRT82B TubPGal80/TM2 Ubx***

   Select both males and females of ***Cy^{+}*** and ***Ubx^{+}*** to establish the following stock:

   yw hsFlp UAS-mCD8-GFP; TubPGal4; FRT82B TubPGal80

*3.1.2. Generation of MARCM Clones (*See **Note 5***)*

To generate MARCM clones, strains created in **Subheading 3.1.1** will be crossed to generate the needed genotype subject to heat-shock to induce mitotic recombination.

1. Set up the following cross:
   yw/Y; FRT82B dunc-115^{KG03651} X ***yw hsFlp UAS-mCD8-GFP; TubPGal4; FRT82B TubPGal80***
2. Collect eggs during a window of every 2 h, i.e. switch the animals to a new vial every 2 h. Animals with the following genotype will be the target of analysis: ***yw hsFlp UAS-mCD8-GFP/Y*** or ***yw; TubPGal4/+; FRT82B dunc-115^{KG03651}/FRT82B TubPGal80***
3. Leave the collected eggs at 25°C for 96 h.
4. Heat-shock at 37°C for 1 h.
5. Dissect third instar larvae and stain with antibodies as described below.

3.2. Histology

Dissect the visual system of the third instar larvae in PBS *(3, 4)* and fix in 4% formaldehyde for 40 min at room temperature (RT) (***see*** **Note 6**).

3.2.1. Larval Eye Disc/Brain Specimen Preparation

3.2.2. Antibody Staining

1. Following fixation, wash the specimens three times for 5 min each time with PBT. Make sure all the specimens have sunk to the bottom of the tube.
2. Block nonspecific binding sites on the specimens by incubating with PBTN for 30 min at RT.
3. Following the blocking step, primary antibody is added and the incubation is at 4°C overnight (O/N). Typically, three primary antibodies are used in this analysis: (a) anti-24B10 labels photoreceptor neurons, (b) anti-N cadherin stains neuropils in the optic lobes, and (c) anti-GFP labels GFP expressed in the MARCM clones (***see*** **Fig.1**). These antibodies need to be diluted with PBTN; the folds of dilution depend on the nature of the antibody and will have to be determined empirically.
4. Wash three times for 15 min each with PBT.
5. Add second antibodies. The dilution will be decided experimentally, but it is typically around 200–500 times and is done with PBTN. The three secondary antibodies are tagged with green (FITC-conjugated goat anti-mouse), red (Cy5-conjugated goat anti-rat) and blue (Alexa647 conjugated donkey anti-rabbit) and can be separately detected by confocal miroscopy. The incubation is as described in **Step 3**.
6. Wash as described in **Step 4**.
7. Go through 5-min serial washes with 25, 50, and 75% glycerol in PBS with the 75% glycerol containing 0.1% ***p***-phenylenediamine (anti-quenching agent to prolong the fluorescent intensity).
8. Mount the specimens on glass slides (***see*** **Note** 7) and examine under a confocal microscope.

4. Notes

1. Pre-made fly food mix such as Jazzmix from Applied Scientific can be used according to the manufacturer's instruction, while 10× PBS can be purchased from many vendors, such as Fisher Scientific.
2. This procedure is for loss-of-function analysis (***dunc-115*** mutant) using MARCM. For gain-of-function analysis (ectopic expression), a UAS construct (UAS-Dunc-115 fusion) will need to be built first, using standard molecular biology methods and transgenic animals produced by embryo injection. The resulted UAS-Dunc-115 transgenic flies will be prepared for MARCM in the same way as with the FRT strain. Similar

analysis will reveal the effect of overexpressing Dunc-115 in an MARCM clone.

3. The structure P[ry FRT] carries two copies of the ***neomycin*** gene controlled by the heat-shock promoter (***hs-neo***), and thus confers the ***neomycin*** resistance, *(5)*, while the ***dunc-115^{KG03651}*** strain carries the ***mini-white*** gene and thus has the ***w^{+}*** phenotype. By selecting ***neomycin*** resistance and ***w^{+}***, the only possible genotype is FRT ***dunc-115^{KG03651}***. The chromosomal location of ***dunc-115^{KG03651}*** is 85E4, and the FRT used is at 82B. Given that the distance between the two is not long, it is necessary to set up several vials to increase the chances of recombination. For genes that have greater distances from the FRT site, the number of vials can be reduced. It would be informative to set up a pilot test to see the frequency of a given recombination.
4. The general principle behind MARCM is to bring all the elements into the same animal after a final cross. Thus, it is often necessary to prepare the two stocks needed for the final cross, so that the needed constructs will be in place. For the FRT, it is required to have the Gal80 construct on the same chromosomal arm distal to the FRT site **(Fig. 1)**, while for the other elements such as Gal4 or UAS-mCD8-GFP can be on any chromosomes. Traditionally, heat-shock controlled flippase (hs Flp in **Fig. 1**) is linked with UAS-mCD8-GFP and located on the first chromosome. For a more detailed discussion, ***see*** **ref.** *6*.
5. It is preferable to use females from the UAS-mCD8-GFP strain in the cross as both male and female offspring will have one copy of the GFP fusion protein and thus will be usable. Heat-shock time may vary depending on the actual set up. It is, therefore, highly recommended to test the time first to ensure a desired result. The clone size in MARCM depends on the developmental stage when the heat-shock is given and its duration. A condition can be determined for the generation of single cell clones (see for example *(7)*).
6. It is important to have all the specimens submerged in the fixative to ensure proper fixation. Fixation and other incubation steps should be carried out on an orbital shaker platform.
7. For examination along the dorsal-ventral axis, the visual system needs to be cleaned so that mouth hooks and other accessories are removed, and the whole specimen sits on its ventral base. For a lateral view, the two optic lobes need to be separated with the use of a surgical knife, and each lobe should rest on the cut-phase. Finally, one piece of a cover slip should be placed on each side of the prepared specimen, and a third cover slip should be placed on top of the first two so as to prevent the specimen being squashed by the cover slip and to preserve its morphology.

Acknowledgments

I would like to thank the Bloomington Stock Center for providing fly strains, and Ray Gavin for reviewing the manuscript. This work was supported in part by a PSC-CUNY grant.

References

1. Huber, A.B., Kolodkin, A.L., Ginty, D.D., and Cloutier, J.F. (2003) Signaling at the growth cone: ligand-receptor complexes and the control of axon growth and guidance. Annu. Rev. Neurosci. 26, 509–563.
2. Lee, T. and Luo, L. (1999) Mosaic analysis with a repressible cell marker for studies of gene function in neuronal morphogenesis. Neuron 22, 451–461.
3. Garcia, M.C., Abbasi, M., Singh, S., and He, Q. (2007) Role of ***Drosophila*** gene ***dunc-115*** in nervous system. Invert. Neurosci. 7, 119–128.
4. Kunes, s., Wilson, C., and Steller, H. (1993) Independent guidance of retinal axons in the developing visual system of ***Drosophila*** J. Neurosci. 13, 752–767.
5. Xu, T. and Rubin, G.M. (1993) Analysis of genetic mosaics in developing and adult ***Drosophila*** tissues. Development 117, 1223–1237.
6. Wu, J.S. and Luo, L. (2006) A protocol for mosaic analysis with a repressible cell marker (MARCM) in ***Drosophila***. Nat. Protoc. 1, 2583–2589.
7. Morante, J. and Desplan, C. (2008) The color-vision circuit in the medulla of ***Drosophila***. Curr. Biol. 18, 553–565.

Chapter 22

Proteomic Tools for the Analysis of Cytoskeleton Proteins

Ewa Wywial, Vishnubhat Nataraj Dongre, and Shaneen M. Singh

Summary

Proteomic tools have become an essential part of the tool kit of the molecular biologist, and provide techniques for detecting homologous sequences, recognizing functional domains, modeling, and analyzing the three-dimensional structure for any given protein sequence. Although a wealth of structural and functional information is available for a large number of members of the various classes of cytoskeletal proteins, many more members remain uncharacterized. These computational tools that are freely and easily accessible to the scientific community provide an excellent starting point to predict the structural and functional properties of such partially or fully uncharacterized protein sequences, and can lead to elegantly designed experiments to probe the hypothesized function. This chapter discusses various proteomic analysis tools with a focus on protein structure and function predictions.

Key words: Proteomics, Sequence similarity, Multiple sequence alignment, Protein domains, Secondary structure prediction, Homology modeling, Structure analysis

1. Introduction

The cytoskeleton is made up of a diverse family of structural proteins that together with their interacting partners provide a conspicuous and dynamic internal reinforcement in the cytoplasm of a cell. These proteins comprising the cytoskeletal system in any particular cell type are a bewildering array of distinct molecular architectures – combinations of various modular domains, the function of which may or may not be known. Although a wealth of structural and functional information is available for a large number of members of the various classes of cytoskeletal proteins, many more members remain partially or fully uncharacterized. Computational tools that are freely and easily accessible

R.H. Gavin (ed.), *Cytoskeleton Methods and Protocols,* Methods in Molecular Biology, vol. 586
DOI 10.1007/978-1-60761-376-22,
© Humana Press, a part of Springer Science + Business Media, LLC 2009

to the scientific community currently provide an excellent starting point to predict the structural and functional properties of such uncharacterized protein sequences. The predictions in turn can lead to well-designed experiments that can further probe the hypothesized function.

Proteomic tools provide facility for finding similarities and inferring homologies, recognizing functional domains, modeling three-dimensional structure, and mapping biophysical properties onto the modeled structure for any given protein sequence.

This chapter discusses various proteomic analysis tools with a focus on protein structure and function predictions. These in silico experiments are designed to begin with a raw sequence, which may have no functional annotation associated with it, and in a step-wise manner derive sequence and structural information leading up to a three-dimensional model of the sequence or its constituent domain(s), which can be analyzed for its biophysical properties.

2. Materials

2.1. Computer with Internet Access

A computer with any underlying operating system and access to the internet is required for the computational analysis described in the methods.

2.2. Visualization Software

Swiss-PdbViewer *(1, 2)* is a freely available visualization tool that was originally developed by Nicolas Guex in 1994. The newest version, 4.0, was released on June 27th, 2008.

1. Download your own copy of Swiss-PdbViewer from http://spdbv.vital-it.ch/disclaim.html and save the compressed file on your computer.
2. Unzip the file and choose the location on your computer where you want to extract and install the program (*see* **Note 1**).
3. To access the program, locate the program executable on your computer and run it.

3. Methods

3.1. Retrieval of Protein Sequences

The Universal Protein Resource (UniProt) *(3)* is a comprehensive resource for protein sequence and annotation data, providing high-quality and freely accessible protein sequence and functional information. Protein sequence data are available in several formats including the complete protein record that includes available

functional annotation as well as sequence information (*see* **Note 2**). Steps to obtain a specific protein sequence from the database:

1. Point your browser to UniProt: http://www.uniprot.org/.
2. You can query the database by keyword(s) (*see* **Note 3**) or by an input sequence to retrieve related sequences using the BLAST algorithm (*see* **Subheading 3.2.**)
3. Select the sequence(s) of interest by clicking on the check-box next to the sequence and clicking on 'Retrieve' pop-up frame on the bottom of the page.
4. Choose the format in which you want to download the sequence, e.g. FASTA, and click on the 'Download' button under the chosen format.
5. When a new window appears, select the 'save' option.
6. Select directory to save the file, e.g. C:\Documents and Settings\Authorized User\Desktop\cytoskeleton\tutorial, and then click 'save'.

3.2. Searching for Similarities and Inferring Homologies

The BLAST algorithm *(4, 5)* is used to search the sequence database to find related sequences (*see* **Note 4**). BLAST can be used to infer functional and evolutionary relationships between sequences as well as help identify members of protein families.

1. Point your browser to the NCBI BLAST page: http://blast.ncbi.nlm.nih.gov/Blast.cgi.
2. Select 'protein blast' by clicking on its hyperlink.
   (a) Cut and paste your sequence (in FASTA format) in the 'query sequence' textbox (*see* **Note 5**).
   (b) In the databases select Non-redundant protein sequences (nr) from the pull-down list (*see* **Note 6**).
   (c) In the program selection window select 'blastp' (*see* **Note 7**).
   (d) Click on 'BLAST' and wait for the results page to load. The Blast output has graphics on the top and textual details at the bottom. On the top of the result page you will see the blast program details like the version of the program used, the reference for BLAST, the name and length of the query sequence, the database searched, and contact information (*see* **Note 8**). In the graphical output the horizontal lines represent the closest hits in descending order of sequence similarity with the query sequence. If you mouse-over the lines, you can see the summary information of the sequence. The section below the graphical overview ranks the hits by score. For each hit it gives a link by the accession number to the hit sequence in the database, the name of the sequence, the BLAST score, and *E*-value (*see* **Note 9**). The next section of the results gives a pair-wise alignment of the query sequence and similar

regions in the related sequence and the details of the alignment such as the score, *E*-value, percentage of residues that are identical, and the percentages that are chemically similar (positives).

(e) Select the related proteins of interest by clicking on the checkbox next to each sequence.

(f) Click on 'Get selected sequences' to download them.

3.3. Multiple Sequence Alignment

Multiple sequence alignments (MSA) assist in identifying evolutionary relationships between members of a set of sequences descended from a common ancestor. From the resulting MSA, sequence homology can be inferred and phylogenetic analysis can be conducted to assess the sequences' shared evolutionary origins. MSAs also assist in identifying sequence conservation of protein sequence motifs and patterns, structural and functional domains, and secondary structures elements. Steps to create a MSA of your set of protein sequences are:

1. Point your browser to CLUSTALW *(6–8)*: http://www.ebi.ac.uk/Tools/clustalw2/index.html.
2. Paste your sequences in FASTA format in the text box or upload a file containing your set of sequences (*see* **Note 10**).
3. Click on 'Run' and wait for the results page to load.

The MSA is displayed on the results page and it displays a consensus line below the alignment to indicate residue positions that are invariant, conserved, or semi-conserved (*see* **Note 11**).

4. To view the MSA interactively click on 'Start Jalview' (*see* **Note 12**).
5. To download the MSA click on the hyperlink next to 'Alignment File' with a '.aln' extension. This will display the MSA in a simple text page and it can be saved as a flat file.

3.4. Protein Motifs, Patterns and Domains

3.4.1. Prosite

PROSITE is a database of protein motifs, patterns, and profiles that represent known protein functional sites, families, and domains *(9)*. Steps to identify these in a given protein sequence are:

1. Point your browser to PROSITE: http://expasy.org/prosite/.
2. Paste your protein sequence in the text box provided under 'Prosite Tools'.
3. Click 'Scan' (*see* **Note 13**).

The results page will show you the textual and graphical output, which has details of protein domains and families identified in your target sequence.

3.4.2. Smart

Simple Modular Architecture Research Tool (SMART) is a database of protein domains that allows for the analysis of protein domain architectures by providing identification and annotation tools for the constituent domains in protein sequences *(10, 11)*.

Steps to analyze the domain architecture of your protein sequence are:

1. Point your browser to SMART: http://smart.embl-heidelberg.de/help/smart_about.shtml (*see* **Note 14**).
2. Paste your protein sequence in the 'Sequence' text box or provide the UniProt accession number of your sequence.
3. Click on 'Sequence SMART' The results page shows you the domain architecture of your sequence in cartoon form.
4. Click on any of the identified domain to get the sequence details and functional annotation ascribed to that domain.
5. Click on 'Display all proteins with similar domain ORGANISATION' to retrieve all other proteins that share the same domain architecture as your sequence.

3.5. Protein Secondary Structure Prediction

SSpro is a server for protein secondary structure prediction that allows for a 3-state prediction (helix, strand, and the rest) and a more sophisticated 8-state prediction (alpha-helix, 3–10-helix, pi-helix, extended strand, beta-bridge, turn, bend, and the rest) *(12)*. Steps to predict the secondary structure of your protein sequence are:

1. Point your browser to SSPro: http://scratch.proteomics.ics.uci.edu/.
2. Provide your email address and name of your protein sequence (optional).
3. Paste your protein sequence in the 'Sequence' text box.
4. Select SSPro and/or SSPro8 by selecting the appropriate checkbox(es).
5. Click on 'Submit Query' and wait for your results to be sent to you via e-mail.

The results show the most favorable secondary structure assignment for each amino acid in your sequence (*see* **Note 15**).

3.6. Retrieval of Three-Dimensional Coordinates of known Protein Structures

The column-based PDB file format or the newer chemical-based formats, the macromolecular chemical interchange format (mmCIF) and molecular modeling database format (MMDB), are different ways of encoding the atomic coordinates of amino acid chains in three-dimensional space so that this information can be stored or manipulated in a computer file. Solved coordinates, obtained from the x-ray crystallography and NMR spectrometry, can be downloaded from the protein structure database, the Protein Data Bank (PDB), or built using molecular modeling software (*see* **Subheading 3.7**). In the PDB repository *(13)*, each structure file has a unique four-character alphanumeric code, called a PDB ID code; for example, the PH domain of Drosophila β-spectrin has a PDB ID code 1DRO. Steps to obtain a coordinate file from the PDB are:

1. Point your browser to the PDB repository: http://www.rcsb.org/.
2. You can query the repository by keyword, e.g. cytoskeleton or PDB ID, e.g. 1DRO or author (*see* **Note 16**).
3. Click 'Site Search' button.
4. When the results page appears, look for various icons on the left hand side. Mouse over them to read the description of each link.
5. To view the record click on the 'View PDB file' icon.
6. To visualize the structure click on the 'Structure Visualization with Jmol Viewer' icon (*see* **Note 12**).
7. To download the record, click the 'Download PDB file'.
8. When a new window appears, select the 'save' option.
9. Select directory to save the file, e.g. C:\Documents and Settings\Authorized User\Desktop\cytoskeleton\tutorial, and then click 'save.'

3.7. Modeling the Three-Dimensional Structure of a Protein/ Protein Domain Sequence

Currently, the best route to create a three-dimensional model for a given protein sequence or its constituent domain is by 'comparative' or 'homology' modeling using a template structure with a known fold that displays significant identity to the sequence being modeled. The quality of comparative models depends on the closeness of the evolutionary relationship on which they are based (*14*). The pair wise sequence identity of the protein sequence with its known template has to be greater than 30% and more than 80 residues long for the homology approach to perform with good or high accuracy *(15)*. In cases with low sequence identity to known proteins, homology modeling may need to be coupled with fold recognition methods, which identify the likely protein fold even in cases where there is no clear sequence homology. Homology modeling involves the use of four basic steps: (1) identification of a suitable structural template, (2) alignment of the template and target sequences, (3) model building, and (4) model evaluation (*see* **Note 17**). The following example uses a web-based program called HHpred *(16)*, which performs all of the mentioned **steps 1–4**. However, it is possible to perform each step using separate software tools (*see* **Note 18**).

1. Point your browser to HHpred: http://toolkit.tuebingen.mpg.de/hhpred.
2. Paste your protein sequence in the designated window (*see* **Note 19**).
3. Select the format of your sequence, e.g. FASTA.
4. Click 'Submit job' button and wait for the results.
5. When the results appear in the browser window, click on 'Create model' in the 'Results' panel.

6. Select the box next to the top structure (or any listed structure, or multiple structures) to choose that structure, which will serve as the template for the modeling building steps, which are to follow.
7. Click 'Create single-template model' button and wait for the results.
8. When the results appear in the browser window, enter your MODELLER license key (*see* **Note 20**).
9. Click 'Submit job' button and wait for your results.
10. When the results appear in the browser window, click 'Save' button in the 'PDB-file' panel to save the model on your local computer.
11. When the 'File Download' window appears, click 'save' and search for the directory, in which you want to store the file.
12. Click 'Save.'
13. Click 'View 3D structure' to obtain a quick cartoon rendition of the model.
14. Click 'Quality by VERIFY3D' to assess the quality of the model.

3.8. Tools for Analyzing Structures

3.8.1. Visualization of Protein Structure

1. Open Swiss-PdbViewer.
2. From the menu bar, select 'File', then 'open PDB file,' and search for the directory, in which the file was stored, e.g. C:\Documents and Settings\cytoskeleton\tutorial.
3. Select the desired file, e.g. 1DRO *(17)* or your modeled protein (*see* **Subheading 3.7.**) and then click 'open.'
4. To manipulate a coordinate file use the row of buttons in the Tool Bar above the window that contains the tool buttons and menus of the program (*see* **Note 21**). Below are two examples:
   - You can look at the distribution of surface exposed vs. non-accessible amino acids within your structure.
     - Click 'Window'
     - Click 'Control Panel' to open up Control Panel
     - Click 'Select'
     - Click 'Accessible aa' to select residues with an accessible surface area higher than a given percentage, e.g. 30%
     - The accessible residues will be colored red in the Control Panel window (you can also color them on the structure using the 'Color' menu)
   - You can look for specific sites such as active sites, glycosylation sites, etc.
     - Click 'Edit'

- Click 'Find Sequence…'
- Enter your choice of an amino acid sequence or a PROSITE pattern
- Hit 'OK' to search your molecule for the provided sequence or pattern
- If found, the sequence/pattern residues will be selected and colored red in the Control Panel window (you can also color them on the structure using the 'Color' menu)

5. Steps to save a coordinate file:
   - Select 'File'
   - Click 'Save'
   - Choose 'Layer' to save the currently active layer in PDB format or 'Project' to save all layers in a single PDB file

3.8.2. Electrostatic Potentials, Cavity Identification, and Amino Acid Conservation Profile

1. Point your browser to Mark-Us: http://luna.bioc.columbia.edu/honiglab/mark-us/cgi-bin/submit.pl.
2. Click 'browse' to locate your structure.
3. Click 'upload' to upload your structure onto the server for functional analysis.
4. Select the chain to be analyzed.
5. Enter your e-mail address and the title of your submission (optional).
6. Click 'Mark Us' button and wait for your results to be sent to you via e-mail (*see* **Note 22**).
7. When the results come back, open a window in your browser and point your browser to the link provided in the received e-mail.
8. When your structure appears in the window, click on 'D' button to display the electrostatic potential mapped on the protein structure. The colors blue and red represent positive and negative potentials, respectively.
9. Click on 'C' button to display the amino acid conservation profile mapped on the entire protein structure or individual cavity. The colors spectrum from red to cyan represents decreasing conservation scores as calculated by the program Consurf ***(18)***.
10. Select the box next to each surface accessible cavity to see the cavity location within the structure (*see* **Note 23**).

3.8.3. Ligand Binding Site Prediction

1. Point your browser to Q-SiteFinder ***(19)***. http://www.modelling.leeds.ac.uk/qsitefinder.
2. Enter the PDB ID code in the first box, e.g. 1DRO, or upload a pdb file from your own computer in the second box by clicking on the browse button.

3. Click 'submit' button and wait for the prediction to finish to reveal potential binding sites in the uploaded coordinate file.

4. Notes

1. You will need separate software to unzip the zipped file, if you do not already have one. For PC users, try WinZip. You can download and install a free evaluation version of WinZip at http://www.winzip.com/ddchomea.htm. Newer versions of Windows (Vista and beyond) and Linux come with built-in decompressing utilities to handle .zip files. For Mac (also PC and even Linux) you can download StuffIt expander at http://www.stuffit.com.
2. FASTA is the most popular format for protein sequence data and is widely used in most sequence based proteomic software tools. It is characterized by a comment line, which is a single-line description, followed by lines of sequence data. The description line is distinguished from the sequence data by a greater-than ('>') symbol in the first column. It is recommended that all lines of text be shorter than 80 characters in length. The sequence data is single letter codes in uppercase with no white spaces between them. An example sequence in FASTA format:

```
>gi|5031877|ref|NP_005564.1| lamin B1 [Homo sapiens]
MATATPVPPRMGSRAGGPTTPLSPTRLSRLQEKEELRELNDRLAVYIDKVRSLETENSALQLQVTEREEV
RGRELTGLKALYETELADARRALDDTARERAKLQIELGKCKAEHDQLLLNYAKKESDLNGAQIKLREYEA
ALNSKDAALATALGDKKSLEGDLEDLKDQIAQLEASLAAAKKQLADETLLKVDLENRCQSLTEDLEFRKS
MYEEEINETRRKHETRLVEVDSGRQIEYEYKLAQALHEMREQHDAQVRLYKEELEQTYHAKLENARLSSE
MNTSTVNSAREELMESRMRIESLSSQLSNLQKESRACLERIQELEDLLAKEKDNSRRMLTDKEREMAEIR
DQMQQQLNDYEQLLDVKLALDMEISAYRKLLEGEEERLKLSPSPSSRVTVSRASSSRSVRTTRGKRKRVD
VEESEASSSVSISHSASATGNVCIEEIDVDGKFIRLKNTSEQDQPMGGWEMIRKIGDTSVSYKYTSRYVL
KAGQTVTIWAANAGVTASPPTDLIWKNQNSWGTGEDVKVILKNSQGEEVAQRSTVFKTTIPEEEEEEEEA
AGVVVEEELFHQQGTPRASNRSCAIM
```

3. Use the 'Field' link to limit retrieval of sequences of interest only by combining keywords using the Boolean operators 'AND', 'OR', and 'NOT' and by restricting the field against which the keyword will be searched.
4. BLAST is a heuristic algorithm that uses approximations to add speed to the search. Although it is a popular tool, various implementations of the Smith-Waterman algorithm *(20)* provide optimal solutions to sequence alignment but at the cost of time.

5. As an alternative option you can paste the accession number of your protein sequence or limit the search to a sub-sequence of your provided sequence.
6. You can select 'PDB' as the database of choice if you are looking for only those related sequences that have solved structures associated with the protein sequence.
7. Psi-BLAST *(5)* provides an alternative to the regular BLAST search when the goal is to detect weak relationships and remote homologues for your query sequence. It is a modified BLAST algorithm that runs iteratively by creating position-specific scoring matrices (PSSM) generated by each BLAST run and searches the database using this PSSM instead of a protein sequence.
8. This information is useful to check that the proper query, database, and program were run.
9. The *E*-value gives a statistical measure of the significance of the alignment and describes the number of hits that would be 'expected' to occur by chance when searching a sequence database of a particular size; the lower the *E*-value, the more significant the match. An *E*-value of 1 means that it would be expected to find one match with a similar score simply by chance in a database of the same size. Exact and closely matched hits will have *E*-values of 0. If the query sequence is short (less than 100 nucleotides or amino acids long), the top *E*-values may be larger than 10^{-50} even if there is an exact match. Therefore it is a good idea to check the percentage identity for the alignment, as well as the *E*-value.
10. Make sure that your sequences have different names as the first 30 characters of the name are significant and if they are not unique, the program will fail. Also, remove any white space or empty lines from the beginning of your input.
11. '*' denotes identity, ':' denotes a conserved residue, and '.' denotes a semi-conserved residue in the MSA.
12. You will need a Java-enabled browser for this step.
13. The default scan excludes patterns with a high probability of occurrence to reduce the number of false positive hits. You can uncheck this option if you are interested in doing a more complete but less stringent scan of your sequence. The 'ScanProsite' advanced form allows you to further tweak the scan.
14. When your browser first encounters the SMART website, you will be asked to choose between the 'normal' and 'genomic' modes, after which the mode setting will be saved for future visits. The models differ in the underlying protein database used and only the proteomes of completely sequenced genomes are used in the genomic mode. For most routine

purposes 'normal' mode is chosen but the mode can be changed by accessing the 'Setup' link on the top of the page at any time.

15. The nomenclature for the prediction is:
    - H: alpha-helix
    - G: 3–10-helix
    - I: pi-helix (extremely rare)
    - E: extended strand
    - B: beta-bridge
    - T: turn
    - S: bend
    - C: the rest
16. Use the advance search form if you are looking for very specific information and do not know the PDB ID for that data record.
17. These steps often need to be repeated and tweaked until a satisfactory model is obtained. The second step is crucial to making a reliable model because the alignment dictates the relationship between your protein sequence and the template sequence.
18. All analyses described can be carried out using more than one program. Listed below are some alternative software choices for each type of analysis described earlier. *Note*: This is not an all-comprehensive list but refers the reader to some of the popular tools available.

	Program	URL	References
Sequence similarity	FASTA	http://www.ebi.ac.uk/Tools/fasta33/index.html	*(21, 22)*
	MPsrch	http://www.ebi.ac.uk/Tools/MPsrch/	*(23)*
Multiple sequence alignment	MUSCLE	http://www.ebi.ac.uk/Tools/muscle/	*(24, 25)*
	T-Coffee	http://www.ebi.ac.uk/Tools/t-coffee/	*(26–28)*
Secondary structure prediction	SAM-T06	http://compbio.soe.ucsc.edu/SAM_T06/T06-query.html	*(29–32)*
	PSIPRED	http://bioinf.cs.ucl.ac.uk/psipred/psiform.html	*(33)*
	PROF	http://www.aber.ac.uk/~phiwww/prof/	*(34)*
	JPRED 3	http://www.compbio.dundee.ac.uk/~www-jpred/	*(35)*

	Program	URL	References
Domain databases	ProDom	http://prodom.prabi.fr/prodom/current/html/home.php	(36)
	CDD	http://www.ncbi.nlm.nih.gov/Structure/cdd/cdd.shtml	(37)
	PFAM	http://pfam.sanger.ac.uk/	(38)
Fold recognition and molecular modeling	LOOPP	http://cbsuapps.tc.cornell.edu/loopp.aspx	(39–41)
	FUGUE	http://tardis.nibio.go.jp/fugue/prfsearch.html	(42)
	SAM-T06	http://compbio.soe.ucsc.edu/SAM_T06/T06-query.html	(29–32)
	Gen-Threader	http://bioinf.cs.ucl.ac.uk/psipred/psiform.html	(43)
Structure evaluation	PROSA	https://prosa.services.came.sbg.ac.at/prosa.php	(44, 45)

19. You may want to parse your sequence into its constituent domains and submit each domain sequence individually as structural templates will be identified in most cases separately for each domain. Rarely, there will be structural templates that can be used to model entire multi-domain proteins.
20. This key is freely available for academic users (with academic e-mail accounts) and easily obtainable at: http://salilab.org/modeller/registration.shtml.
21. To learn basic and advanced Swiss-PdbViewer features beyond what is described here, follow the tutorials available at http://spdbv.vital-it.ch/main_tut.html and http://www.usm.maine.edu/~rhodes/SPVTut/index.html. The user guide is available at http://spdbv.vital-it.ch/main_guide.html.
22. This step could take a long time.
23. You can also display the electrostatic, conservation, and cavities reports by selecting options in the 'structure analysis panel' located in the lower left corner of your screen.

References

1. Guex N, Diemand A, Peitsch MC. Protein modelling for all. Trends Biochem Sci. (1999) 24:364–367.
2. Guex N, Peitsch MC. SWISS-MODEL and the Swiss-PdbViewer: an environment for comparative protein modeling. Electrophoresis. (1997) 18:2714–2723.
3. Consortium TU. The Universal Protein Resource (UniProt). Nucleic Acids Res. (2008) 36:D190–D195.
4. Altschul SF, Gish W, Miller W, Myers EW, Lipman DJ. Basic local alignment search tool. J Mol Biol. (1990) 215:403–410.
5. Altschul SF, Madden TL, Schaffer AA, Zhang J, Zhang Z, Miller W et al. Gapped BLAST and PSI-BLAST: a new generation of protein database search programs. Nucleic Acids Res. (1997) 25:3389–3402.
6. Larkin MA, Blackshields G, Brown NP, Chenna R, McGettigan PA, McWilliam H et al.

Clustal W and Clustal X version 2.0. Bioinformatics. (2007) 23:2947–2948.

7. Thompson JD, Higgins DG, Gibson TJ. CLUSTAL W: improving the sensitivity of progressive multiple sequence alignment through sequence weighting, position-specific gap penalties and weight matrix choice. Nucleic Acids Res. (1994) 22:4673–4680.
8. Thompson JD, Higgins DG, Gibson TJ. Improved sensitivity of profile searches through the use of sequence weights and gap excision. Comput Appl Biosci. (1994) 10:19–29.
9. Hulo N, Bairoch A, Bulliard V, Cerutti L, Cuche BA, de Castro E et al. The 20 years of PROSITE. Nucleic Acids Res. (2008) 36:D245–D249.
10. Schultz J, Milpetz F, Bork P, Ponting CP. SMART, a simple modular architecture research tool: identification of signaling domains. Proc Natl Acad Sci U S A. (1998) 95:5857–5864.
11. Letunic I, Copley RR, Pils B, Pinkert S, Schultz J, Bork P. SMART 5: domains in the context of genomes and networks. Nucleic Acids Res. (2006) 34:D257–D260.
12. Cheng J, Randall AZ, Sweredoski MJ, Baldi P. SCRATCH: a protein structure and structural feature prediction server. Nucleic Acids Res. (2005) 33:W72–W76.
13. Berman HM, Westbrook J, Feng Z, Gilliland G, Bhat TN, Weissig H et al. The Protein Data Bank. Nucleic Acids Res. (2000) 28:235–242.
14. Moult, J. (2005) A decade of CASP: progress, bottlenecks and prognosis in protein structure prediction. Curr. Opin. Struct. Biol. 15, 285–289.
15. Baker D, Sali A. Protein structure prediction and structural genomics. Science. (2001) 294:93–96.
16. Soding J, Biegert A, Lupas AN. The HHpred interactive server for protein homology detection and structure prediction. Nucleic Acids Res. (2005) 33:W244–W248.
17. Zhang P, Talluri S, Deng H, Branton D, Wagner G. Solution structure of the pleckstrin homology domain of Drosophila beta-spectrin. Structure. (1995) 3:1185–1195.
18. Landau M, Mayrose I, Rosenberg Y, Glaser F, Martz E, Pupko T et al. ConSurf 2005: the projection of evolutionary conservation scores of residues on protein structures. Nucleic Acids Res. (2005) 33:W299–W302.
19. Laurie AT, Jackson RM. Q-SiteFinder: an energy-based method for the prediction of protein-ligand binding sites. Bioinformatics. (2005) 21:1908–1916.
20. Smith TF, Waterman MS. Identification of common molecular subsequences. J Mol Biol. (1981) 147:195–197.
21. Mackey AJ, Haystead TA, Pearson WR. Getting more from less: algorithms for rapid protein identification with multiple short peptide sequences. Mol Cell Proteomics. (2002) 1:139–147.
22. Pearson WR. Rapid and sensitive sequence comparison with FASTP and FASTA. Methods Enzymol. (1990) 183:63–98.
23. Sturrock S, Collins J. MPsrch version 1.3. Biocomputing Research (1993). Unit University of Edinburgh, Edinburgh.
24. Edgar RC. MUSCLE: a multiple sequence alignment method with reduced time and space complexity. BMC Bioinformatics. (2004) 5:113.
25. Edgar RC. MUSCLE: multiple sequence alignment with high accuracy and high throughput. Nucleic Acids Res. (2004) 32:1792–1797.
26. O'Sullivan O, Suhre K, Abergel C, Higgins DG, Notredame C. 3DCoffee: combining protein sequences and structures within multiple sequence alignments. J Mol Biol. (2004) 340:385–395.
27. Notredame C, Holm L, Higgins DG. COFFEE: an objective function for multiple sequence alignments. Bioinformatics. (1998) 14:407–422.
28. Notredame C, Higgins DG, Heringa J. T-Coffee: A novel method for fast and accurate multiple sequence alignment. J Mol Biol. (2000) 302:205–217.
29. Karplus K, Barrett C, Hughey R. Hidden Markov models for detecting remote protein homologies. Bioinformatics. (1998) 14:846–856.
30. Karplus K, Karchin R, Barrett C, Tu S, Cline M, Diekhans M et al. What is the value added by human intervention in protein structure prediction? Proteins. (2001) Suppl 5:86–91.
31. Karplus K, Karchin R, Draper J, Casper J, Mandel-Gutfreund Y, Diekhans M et al. Combining local-structure, fold-recognition, and new fold methods for protein structure prediction. Proteins. (2003) 53 Suppl 6:491–496.
32. Karplus K, Katzman S, Shackleford G, Koeva M, Draper J, Barnes B et al. SAM-T04: what is new in protein-structure prediction for CASP6. Proteins. (2005) 61 Suppl 7:135–142.
33. McGuffin LJ, Bryson K, Jones DT. The PSIPRED protein structure prediction server. Bioinformatics. (2000) 16:404–405.
34. Ouali M, King RD. Cascaded multiple classifiers for secondary structure prediction. Protein Sci. (2000) 9:1162–1176.

35. Cole C, Barber JD, Barton GJ. The Jpred 3 secondary structure prediction server. Nucleic Acids Res. (2008) 36:W197–W201.
36. Servant F, Bru C, Carrere S, Courcelle E, Gouzy J, Peyruc D et al. ProDom: automated clustering of homologous domains. Brief Bioinform. (2002) 3:246–251.
37. Marchler-Bauer A, Anderson JB, Derbyshire MK, DeWeese-Scott C, Gonzales NR, Gwadz M et al. CDD: a conserved domain database for interactive domain family analysis. Nucleic Acids Res. (2007) 35:D237–D240.
38. Finn RD, Tate J, Mistry J, Coggill PC, Sammut SJ, Hotz HR et al. The Pfam protein families database. Nucleic Acids Res. (2008) 36:D281–D288.
39. Teodorescu O, Galor T, Pillardy J, Elber R. Enriching the sequence substitution matrix by structural information. Proteins. (2004) 54:41–48.
40. Meller J, Elber R. Linear programming optimization and a double statistical filter for protein threading protocols. Proteins. (2001) 45:241–261.
41. Tobi D, Elber R. Distance-dependent, pair potential for protein folding: results from linear optimization. Proteins. (2000) 41:40–46.
42. Shi J, Blundell TL, Mizuguchi K. FUGUE: sequence-structure homology recognition using environment-specific substitution tables and structure-dependent gap penalties. J Mol Biol. (2001) 310:243–257.
43. McGuffin LJ, Jones DT. Improvement of the GenTHREADER method for genomic fold recognition. Bioinformatics. (2003) 19: 874–881.
44. Wiederstein M, Sippl MJ. ProSA-web: interactive web service for the recognition of errors in three-dimensional structures of proteins. Nucleic Acids Res. (2007) 35:W407–W410.
45. Sippl MJ. Recognition of errors in three-dimensional structures of proteins. Proteins. (1993) 17:355–362.

INDEX

A

Actin..... 4, 23, 41, 71, 118, 143, 157, 171, 188, 244, 266, 276, 302, 329, 360, 367
Actin-binding.....42, 82, 144, 267, 270, 271, 367–373
Actin-binding protein 42, 267, 270, 271, 367–373
Actin-cytoskeleton 4, 42, 72, 74, 144, 172, 178, 182, 183, 266, 302, 367
Alexa fluor reagents..... 95, 163
Arabidopsis.....158, 159, 162–166, 245–249, 255–257, 266, 267, 271, 272
Aster..... 103, 106
Axoneme 90, 215, 219–222, 283, 284, 338, 346, 347, 351, 352

B

Basal bodies..... 227–240
Basic motile behavior.....315, 316, 318–321, 326, 327, 333
Bioimaging..... 117

C

Cell
- fusion..... 357–364
- hybrids.....358, 360, 364
- imaging..... 3–66, 121, 158, 159, 163, 165, 193, 244, 247, 249, 250, 257, 306, 320, 323
- migration 3–20, 301, 302, 307
- motility..... 13, 315–333

Centrosome..... 89–112
Chemotaxis..... 9, 315–317, 320, 321, 326
Chlamydomonas.....207, 208, 213, 221, 230, 236, 338, 343, 345, 346, 351, 352
Chondramides..... 71
Cilia.....207, 227, 229, 236, 237, 240, 283–298, 337–352
Ciliary reversal.....285, 287, 296
Critical point drying (CPD)..... 189–192, 195–197, 200, 201, 203
Cytochalasins.....72, 93, 94, 99, 101, 110, 270
Cytoplasm 43, 45, 72, 73, 75, 99, 105, 107, 110, 119, 120, 127, 128, 165, 201, 228, 239, 240, 266–270, 272, 290, 359, 364, 375
Cytoskeleton.....4, 23, 41, 72, 108, 118, 144, 157, 171, 187, 244, 266, 283, 302, 357, 367, 375

D

Deciliation.....284, 285, 287, 288, 290
Deconvolution..... 5, 10, 20, 53, 61, 179
Depsipeptide 72
Drosophila.....367–373, 379
Dunc-115..... 367–373
Dynamic instability 89
Dynein..... 119, 215, 284, 290, 338, 348

E

EB1..... 246, 247, 249, 252, 256, 257
Egg extract 89–112
Embryos 23–38

F

Fibroblast 73, 120, 193, 306–309, 361
Fixed plant material..... 157
Flagella 207, 208, 214, 215, 219, 221, 283, 337–352
Flagellar isolation 210, 214–215
Fluorescent beads 295, 296, 303–307, 311
Fluorescent proteins (FP)..... 23, 25, 36, 41, 42, 44, 46, 47, 53, 57, 58, 96, 103, 124, 136, 138, 139, 144, 158, 173, 228, 246, 251, 252, 255, 257

G

Gel electrophoresis 26, 28, 52, 210, 215–217
Green fluorescent protein (GFP) 42–44, 46, 47, 51, 54–58, 62, 64, 96, 103, 104, 130–133, 147, 151, 158, 163, 165, 208, 228, 230, 232, 236, 238, 245–247, 249, 252, 255–258, 267, 269–272, 317, 329, 330, 368–372
- GFP-labeled cells 208

H

High pressure freezing (HPF)..... 80, 83, 227–240, 247, 254, 259
Homology modeling 380

I

Immunoblotting 211, 217–219, 223
Immunodepletion 99, 103, 104
In vitro assay.....96–98, 104–107
Intraflagellar transport..... 207–224

K

Keratinocytes 4, 11–13, 15, 17–19, 359, 361
Keratins 358–361, 364
Kinesin 119, 208, 222, 248, 250, 254, 255

L

Labeled protein 38, 103, 104
Live imaging 24, 27, 33–35, 37, 108, 158, 199, 251
Live-cell imaging 41–66

M

MAP4 ..... 249, 258
Melanosomes 275–281
Merlin 144–148, 153, 154
Micropatterning 309, 310
Microscopy
  cell traction force (CTF) 301–312
  confocal 4, 25, 27, 34, 61, 82, 105, 118, 124, 157, 158, 162–165, 168, 295, 317, 320, 329, 368, 369, 371
  correlative 189, 190, 192, 193, 199
  DIC 13, 15, 19, 208, 214, 268, 287, 319
  electron 74–77, 79–81, 158, 159, 175, 187–205, 208, 211, 212, 220, 222, 227–240, 244, 247, 249, 250, 252, 253, 276, 281, 351
  FLAP 118, 119, 131–134
  FLIM 118–120, 126–129, 138
  FLIP 118, 119, 130–134, 137–139
  FRET 118–127, 129, 134, 136–138
  immuno-electron 76, 227–240
  immunofluorescence 81, 211–212, 244, 245, 309
  immunogold 191–193, 199, 220, 222
  immunogold scanning electron 220–222
  immunogold TEM
  phase contrast 14–16, 310
  time-lapse 89–112, 302, 333
Microtubules 10, 16, 23–25, 36, 41–44, 75, 89–112, 119, 130, 133, 157, 162–167, 171, 172, 175, 188, 202, 208, 215, 222, 229, 239, 243–260, 266, 276, 277, 284, 338, 349, 357
Migration 3–20, 216, 275, 277, 301, 302, 307
Mitochondria 16, 41–66, 110, 171–183, 272, 348
Motion analysis
  motility assays
  2D 316
  3D 316
Motor proteins 42, 119, 208, 215, 248, 266, 302
Multiple sequence alignment 378, 384
Myofibroblast 308, 309
Myosin 143, 266, 267, 270, 271, 302

N

Neurofibromatosis type 2 (NF2) 144

O

Organelle transport 277

P

Phagocytosis 285, 287, 295
Phalloidin 58, 60, 72, 74, 75, 78, 82, 84, 120, 167, 172, 175, 178, 179, 183, 190, 202
Polyacrylamide gel (PAG) 215–217, 302–307, 310, 311
Protein domains 36, 378, 380
Protein conformation 144, 147, 150, 153
Proteins 4, 23, 41, 72, 89, 118, 143, 158, 171, 188, 207, 228, 243, 266, 284, 301, 315, 338, 357, 367, 375
Proteomics 90, 375–386

R

Roots..... ..... 73, 157–168, 243–245, 255–257, 268
Rotary shadowing 189

S

Secondary structure prediction 379
Sectioning 59, 61, 158–160, 166, 188, 232, 235, 238–240, 326, 331
Sequence similarity 377
Sliding. 57, 284, 338, 348
Sperm.. ..... 90–92, 94, 100, 101, 103, 104, 110, 111, 337, 338, 340–352
Streaming 72, 73, 265–272
Structure analysis 386

T

Tetrahymena thermophila 227–240, 283–298
Transfection 11–13, 19, 25, 121, 135, 145, 150, 153, 357–364
Triton X-100 ..... 46, 78, 95, 97, 103, 107, 110, 135, 146, 158, 159, 161, 162, 174, 190, 202, 204, 250, 251, 338, 339, 341, 344, 347, 348, 352, 369

V

Vimentin 359–361
Vital staining 41, 42, 45, 53, 58, 64, 65

X

Xenopus laevis 23–38, 90, 91, 94

Y

Yeast 41–66, 73, 167, 171–183, 230, 285–287, 369